# A double-stranded DNA rotaxane

D. Ackermann[1], M. Famulok[1]

[1] *LIMES Institute, University of Bonn, Bonn, Germany.*

**INTRODUCTION:** Mechanically interlocked DNA-architectures are an unrealised goal towards the construction of synthetic nanomechanical devices. The prototype of interlocked architectures in which individual components can be set in motion in a controlled manner are rotaxanes. They consist of a dumbbell-shaped molecule encircled by a macrocycle that can move unhindered along the axle, trapped by bulky stoppers. Various examples of interlocked molecular structures with ingenious functions have been realized in organic synthesis. Analogous architectures made from DNA are unprecedented, but would be highly desirable since they represent attractive devices for nanorobotics and synthetic biology. Here, we report the design, assembly and characterization of rotaxanes in which both the dumbbell-shaped molecule and the macrocycle are made of double-stranded DNA, and in which the axle of the dumbbell is threaded through the macrocycle by base pairing [l].

**METHODS:** DNA architectures were assembled from commercially available, 5' phosphorylated DNA sequences by T4 DNA ligation. The design of the DNA nanorings required the incorporation of intrinsically bent AT-tracts that cooperatively result in the overall circular shape. The stopper and macrocycle subunits were purified by weak anion exchange (WAX) chromatography using a TSKgel DEAE-NPR column from TOSOH. Atomic force microscopy (AFM) scans of the dumbbell, the pseudorotaxane, and the rotaxane were performed with WAX purified products adsorbed on polyornithin coated mica surfaces in liquid cell.

**RESULTS:** We have previously described the efficient synthesis of double-stranded (ds) DNA nanorings containing single-stranded (ss) gap regions. These gap rings turned out as versatile building blocks in DNA nanotechnology due to their ease of hybridization with a variety of functional oligonucleotide motifs like chemically modified ssDNA [2], RNA hairpins[3], or dsDNA struts [4].

In the assembly of DNA rotaxanes these gap rings assume a key function as template in the threading process [l]. Hybridizing a DNA rod with a single stranded region of 13 base pairs (bp) and a DNA gap ring with a complementary single stranded

region of 8 bp leads to almost quantitative threading. Subsequent ligation of simple 168 bp ring stoppers on both sides of the DNA rod produced dsDNA pseudorotaxanes. AFM scans of the purified pseudorotaxanes proved the correct constitution of the interlocked architecture. When the macrocycle was released from the rod by adding short complementary oligonucleotides the pseudorotaxane disassembled to the dumbbell and the free macrocycle via slippage mechanism. However, when spherical stoppers composed of two intertwined crossover rings were used, the pseudorotaxane was converted into a genuine dsDNA rotaxane (Fig. 1). The integrity of the rotaxane structure was verified by AFM and the free mobility of the macrocycle was demonstrated by fluorescence spectroscopy [l].

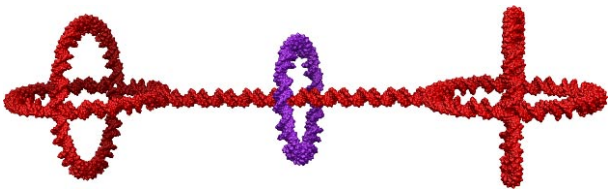

*Fig. 1: Molecular model of a dsDNA rotaxane assembled from 168 bp spherical stoppers and a 126 bp DNA macrocycle.*

**DISCUSSION & CONCLUSIONS:** The rotaxanes we obtained have the potential to be applied as versatile components in nanomechanics and nanorobotics. Moreover, our efficient method for the construction of interlocked dsDNA architectures, which is broadly applicable in DNA nanotechnology, opens new possibilities for research into DNA based molecular machines.

**REFERENCES:** [1] D. Ackermann, T.L. Schmidt, J.S. Hannam, C.S. Purohit, A. Heckel, M. Famulok (2010) *Nature Nanotechnol* **5**:436-42. [2] G. Rasched, D. Ackermann, T. L. Schmidt, P. Broekmann, A. Heckel, M. Famulok (2008) *Angew Chem Int Ed* **47**:967-70. [3] G. Mayer, D. Ackermann, N. Kuhn, M. Famulok (2008) *Angew Chem Int Ed* **47**:971-3. [4] D. Ackermann, G. Rasched, S. Verma, T. Schmidt, A. Heckel, M. Famulok (2010) *Chem Commun* **46**:4154-6.

**ACKNOWLEDGEMENTS:** This work was supported by grants from the Deutsche Forschungsgemeinschaft, the SFB 624, the Fonds der Chemischen Industrie.

# Complexes of polyelectrolytes with quantum dots

M. Adamczak[1], H. J. Hoel[2], J. Barbasz[1], P. Warszyński[1]

[1] *Instititute of Catalysis and Surface Chemistry, Polish Academy of Sciences, st. Niezapominajek 8, Cracow, Poland*

[2]*2Institute for Cancer Research, Norvegian Radium Hospital, Oslo, Norway.*

**INTRODUCTION:** Nanocapsules are ideal candidates for drug delivery systems as their small size facilitate drug targeting and reduce side effects of the treatment [1]. Capsules containing quantum dots (QDs) as fluorescent imaging agents can be tracked in a tissue by luminescence. The advantage of QDs over traditional organic dyes consists in their stability and intensive fluorescence [2]. The negative feature of QDs is their *in vivo* toxicity, however, that can be avoided by encapsulation of QDs in a stable polymer coating.

**METHODS:** Sequential adsorption of oppositely charged polyelectrolytes [3] was applied for the formation of complexes. As components of the shell, two different polyelectrolyte couples were used: cationic poly(allyamine hydrochloride) (PAH) together with anionic poly(sodium styrene sulfonate) (PSS), and biocompatible poly-L-lysine hydrobromide (PLL) as polycation in a pair with biocompatible, anionic poly-D-glutamic acid sodium salt (PGA). Also, complexes of negatively charged CdTe quantum dots with polyelectrolytes (PAH/CdTe, PSS/PAH/CdTe, PLL/CdTe, PGA/PLL/CdTe) were fabricated. The size and zeta potential of obtained complexes were examined by dynamic light scattering, while luminescent properties of the capsules with QDs were characterized with spectrofluorimeter. Later on, complexes were deposited on negatively charged mica surface and studied by atomic force microscope. In order to estimate the cytotoxicity of the QDs containing capsules, some of them were examined by flow cytometry in respect of their influence on B-LCL cell line proliferation and unspecific binding to PBMC cells.

**RESULTS:** We obtained stable complexes of polyelectrolytes in sizes up to 150 nm. Fluorescent nanocapsules of polyelectrolytes with QDs were smaller (approx. 20 nm for positively charged PAH/CdTe and PLL/CdTe complexes, 50 – 70 nm for negatively charged PSS/PAH/CdTe and PGA/PLL/CdTe). Fig. 1 shows an exemplary AFM image of PLL/CdTe complex deposited on mica.

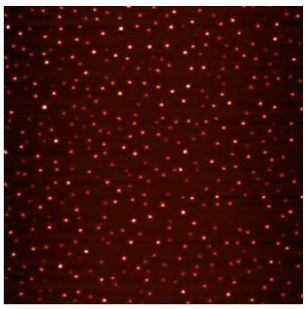

*Fig. 1: AFM image (10 x 10 μm; vertical scale = 30 nm) of PLL/CdTe complex deposited on mica.The picture was obtained in tapping mode.*

The results obtained from a flow cytometer indicate that CdTe quantum dots were toxic at all concentrations tested. After encapsulation of QDs in polyelectrolytes (complex of 25% PGA/26 % PLL/49% CdTe, initial concentrations of solutions: 1000 ppm for polyelectrolytes, 200 ppm for CdTe), a sample has stopped affecting the B-LCL cell proliferation at a 1:400 dilution. Test of unspecific binding to PBMC cells showed no fluorescence in the lymphocytes incubated with the nanocapsules (no presence of unspecific binding), while after incubation with monocytes there was a slight increase in the fluorescence.

**DISCUSSION & CONCLUSIONS:**
Encapsulation of CdTe quantum dots in polyelectrolytes has reduced their cytotoxicity, which allows to consider their application for medical purposes.

**REFERENCES:** [1] A.P.R. Johnston, C. Cortez, A.S. Angelatos, and F. Caruso; *Current Opinion in Colloid and Interface Science*, **2006,** *11*, 203–209;
[2] P.R. Gil, L.L. del Mercato, P. del Pino, A.M. Javier, and W.J. Parak: *Nano Today*, **2008**, *3-4*, 12–21; [3] G. Decher, *Science*, **1997**, *277*, 1232–1237

**ACKNOWLEDGEMENTS:** This work was supported by the "Krakow Interdisciplinary PhD-Project in Nanoscience and Advanced Nanostructures" operated within the Foundation for Polish Science MPD Programme co-financed by the EU European Regional Development Fund and ERA-NET MATERA « NANOMEDPART » project.

# Integrated optical biosensor based on organic optoelectronic components

M. Ramuz[2], D. Leuenberger[1], N. Adsul.[1]

[1] *CSEM SA, Basel, Switzerland.* [2], *Stanford University, USA.*

**INTRODUCTION:** We present a proof of concept of a novel biosensor based on polymer opto-electronic components.

**METHODS:** Figure 1 shows the schematic of the integrated biosensor chip. A polymer light emitting diode (PLED) deposited with ink-jet printing pumps a photoluminescent (PL) layer located directly on top of the Ta2O5 waveguide. The PL emission is coupled into a single mode waveguide. At the out-coupling grating stage, a fully organic mini-spectrometer1 with spectral resolution of 5 nm is used. It consists of a single-mode waveguide with integrated diffraction grating and a dense array of polymer photodiodes (PPDs) as sensing element.

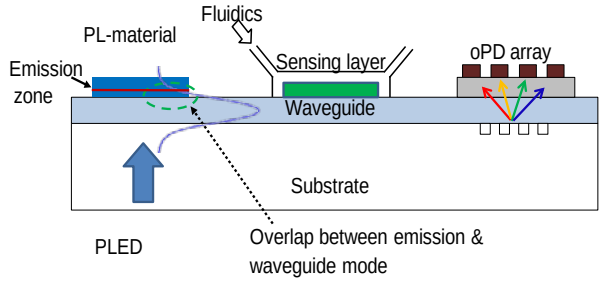


*Figure 1- Integrated optoelectronic biosensor*

Proof of concept of the biosensor was performed by optical absorption tests. A simple micro-fluidic system consisting of a channel of 1mm width and 200µm height is used on the top of the sensing area. First the waveguide surface is functionalized by a mouse IgG (mIgG). The analyte, anti-mouse IgG labelled with Cy5 (amIgG-Cy5). The amIgG-Cy5 was injected into the fluidics which links to mIgG already attached to the waveguide surface. Cy5 has very strong absorption (peak at 650 nm) which overlaps with the PL of the guided light. Here, Cy5 is used as strong absorptive element rather than for its fluorescence property.

**RESULTS:** Figure 2 compares performance of organic spectrometer with inorganic counterpart. The spectrum of out-coupled light measured with mini-spectrometer after each injection is showed in figure 3. After injection of mIgG (t2) we observe absorption in the green-orange part of spectrum (brown). Injection of amIgG-Cy5 (t3) induced almost total absorption of the guided spectrum (red). After washing steps (t4 and t5) the spectra regain their originals shape (t2 and t1) with a slight reduction in absorption.

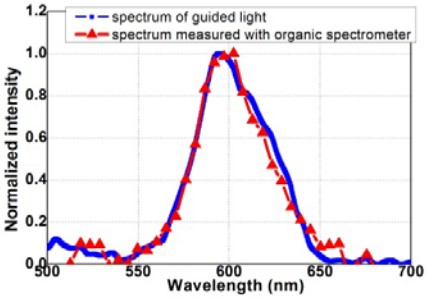


*Figure 2-Comparison of the spectrum measured by inorganic and organic spectrometer*

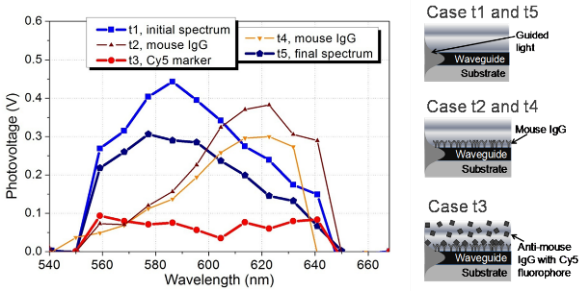


*Figure 3- Absorption biotest spectra (t1):spectrum without biomolecule (t2):mIgG functionalization on surface (t3):amIgG-Cy5 linked to mIgG on the waveguide surface (t4):cleaning amIgG-Cy5 ( t5):removed mIgG by cleaning waveguide surface*

**DISCUSSION & CONCLUSIONS:** The demonstrated sensing scheme can be used as biosensor. Indirect coupling of light using PL into the waveguide makes sensor chip very compact. PLEDs and PPDs facilitate monolithic integration. Sensitivity could be further improved by optimizing the spectral resolution of the mini-spectrometer with improved signal-to-noise ratio and by adding resonant structures in the sensing area. By replacing the $Ta_2O_5$ waveguide by polymer waveguides and incorporating integrated micro-fluidics, the sensor chip potentially leads to a truly low cost lab-on-chip biosensor.

**REFERENCES:** 1. M. Ramuz et al., *EPJAP*, 46 (2009).

**ACKNOWLEDGEMENTS:** This work was partially supported by the European project SEMOFS, Project Nr. IST-FP6-016768. Very helpful discussions with R. Stanley, G. Voirin, S. Pasche and C. Winnewisser of CSEM Neuchatel are gratefully acknowledged.

# Development of a spectroscopic probe to assess the structure of new hybrid silica-based biomaterials

C. Aimé, T. Coradin

*Laboratoire de Chimie de la Matiere Condensee, College de France*
*11 Place Marcelin Berthelot – 75005 Paris, France*

**INTRODUCTION:** Self-assembly is the driving force for nanostructure formation from a broad diversity of building blocks. Therefore, this phenomenon is of particular interest for the elaboration of biomolecular materials. Nowadays, many developments in nanotechnology attempt to exploit self-assembling properties of biomolecules. In combination with biomolecules such as collagen and nucleic acids, we use silica nanoparticles in order to control the structuration of biomaterials at the nanometric scale.

**METHODS: S**ilica is a highly tunable matrix of well known surface chemistry. This allows to synthesized sulfonate-grafted silica nanoparticles, for further collagen grafting, or thiol-grafted particles for the covalent coupling of nucleic acids.

In parallel, we develop a new spectroscopic probe to rapidly assess the structure of the gel: we propose to incorporate a secondary system within the hybrid gel. This new system must exhibit different properties depending on the gel structure (e.g. gel/solution state). To this aim, we investigate the aggregation properties of metal nanoparticles (gold or silver) in model gelatin biogels. Because of plasmon localized effects, gold/silver nanoparticles exhibit optical properties related to their aggregation state allowing the *gel* (aggregated) to *solution* (dispersed) transition to be monitored spectrophotometrically. The characterization of the self-assembled hybrid gels, and the investigation of metallic particles aggregation requires the combination of multiple characterization techniques (such as TEM, SEM, WAXS, DLS, and UV).

**RESULTS:** Our strategy combines organic and inorganic materials in order to take advantage of both building blocks in terms of self-assembly and materials structuration respectively. Using collagen-functionalized silica particles, we have succeeded in engineering new hybrid gels. Indeed, collagen-silica interactions cooperatively trigger the reversible formation of hybrid gels with original structure and properties.

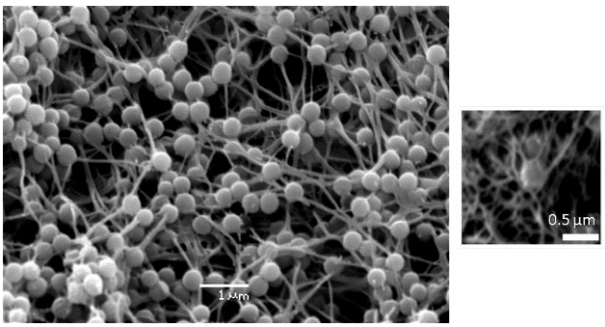


*Fig. 1: Functionalization & Self-assembly. SEM image of silica nanoparticles-collagen hybrid gels.*

In parallel, we show that plasmon absorption band of metallic nanoparticles could be tuned with respect to gel structure. Thus the incorporation of the detection system (gold-silver particles) could provide a rapid and easy-to-read assessment of the responsiveness of the gel.

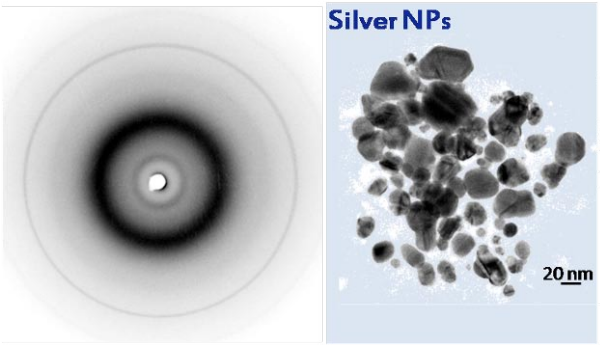


*Fig. 2: WAXS and TEM micrographs of silver particles confined within gelatin biogels.*

**DISCUSSION & CONCLUSIONS:** We have designed new hybrid gels based on the use of biomolecules. In response to a specific stimulus (change in temperature or pH), we could reversibly assemble this gel. We aim at designing hybrid systems that could undergo *gel-to-solution* transition in a reversible and bio-inspired way to elaborate gel-carriers for specific drug delivery.

**REFERENCES:** [1] M.F. Desimone, C. Hélary, I.B. Rietvel, I. Bataille, G. Mosser, M.M. Giraud-Guille, J. Livage, T. Coradin (2010) *Acat Biomater.* **ASAP**.

**ACKNOWLEDGEMENTS:** We thank the Agence National pour la Recherche (ANR-09-RPDOC-023-01), France, for funding.

# Free standing layer-by-layer films of biopolymers for cornea engineering

G. Altay[1], A. Khademhosseini[3], V. Hasirci[1, 2]

*METU, BIOMAT, Departments of [1]Biomedical Engineering, and [2]Biological Sciences, Biotechnology Research Unit, 06531, Ankara, Turkey. [3]Harvard–Massachusetts Institute of Technology Division of Health Sciences and Technology, Cambridge, MA 0213,USA.*

**INTRODUCTION:** Layer-by-layer self assembly is a facile technique emerged as a surface modification of materials in the last decade [1]. The method is based on alternating deposition of polyanions and polycations onto an active surface exploiting the physical adsorption forces [1]. Multilayer film builds up from monomolecular layers and grows up to micron scale thicknesses [2]. The technique is very suitable for bottom up design applications in tissue engineering. Cornea has a highly stratified, hierarchical molecular organization where collagen lamellae are around 2 microns in thickness and is in proteoglycans such as hyaluronic acid [3]. In this study, layer-by-layer self assembly method was adopted for bottom up design of tissue engineered corneal stroma, where polyethyleneimine (PEI) is used as the model polycation and methacrylated hyaluronic acid (MA-HA) as the major anionic constituent.

**METHODS:** Polyelectrolyte multilayer films were fabricated simply by dipping oxygen plasma cleaned glass slides alternatively into PEI and MA-HA solutions (1% MA-HA and 1% PEI in NaCl solution; MA-HA having 0.5% Irgacure 2959 as photoinitiator), for 5 min with rinsing steps of NaCl solution in between. Then films were cured under UV. Films were stained with propidium iodide for CLSM analysis and SEM micrographs of various bilayers (BL) were obtained. Thicknesses were calculated from CLSM and SEM data. Finally films were seeded with human keratocytes that are native to corneal stroma.

**RESULTS:**

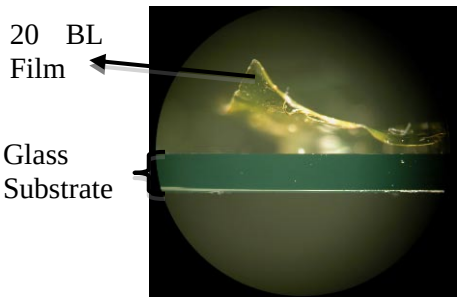


*Fig. 1: Stereomicrograph of 20 BL film lifted off the surface.*

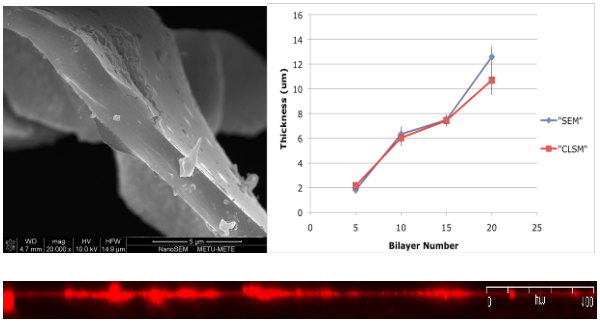


*Fig. 2: SEM micrograph of 5 BL film (top left), thickness growth with increasing bilayer number (top right), CLSM z-section of 5 BL film.*

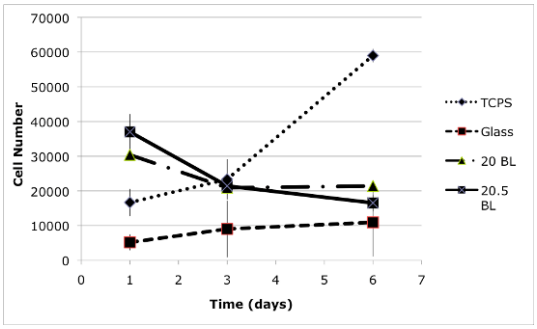


*Fig. 3: Keratocyte proliferation on 20 BL (MA-HA top) and 20.5 BL (PEI top) films.*

**DISCUSSION & CONCLUSIONS:** Free standing polyelectrolyte multilayer films of PEI and MA-HA were obtained. Film thicknesses are tuneable by the BL number. Five BL films are appropriate for stromal lamellae because of their thicknesses. Keratocytes appeared to prefer the films for initial attachment; however, they do not proliferate with time. Optimization of cell proliferation on the films is under investigation.

**REFERENCES:** [1]I. L. Radtchenko, G. B. Sukhorukov, S. Leporatti, et al. (2000) *J Colloid Interface Sci.* **15;230(2)**:272-280. [2]L. Richert, A. J. Engler, D. E. Discher, et al. (2004) *Biomacromolecules* **5:** 1908-1916. [3]B. D. Lawrence, J. K. Marchant, M. A. Pindrus, et al. (2009) *Biomaterials* **30(7):** 1299-1308.

**ACKNOWLEDGEMENTS**: This project is conducted within the scope of TUBITAK METUNANOBIOMAT, 105T508.

# Plasma treated and nano/micro-structured PEEK substrates for adipose tissue-derived stem cell studies

Jasmin Althaus[1,2,4], Stefanie Adam[3], Helmut Schift [4], Jens Gobrecht[4], Uwe Pieles[2], Bert Müller[1] and Kirsten Peters[3]

[1]*Biomaterials Science Center, University of Basel.* [2]*Institute for Chemistry and Bioanalytics, University of Applied Sciences, Northwestern Switzerland.* [3]*Department of Cell Biology (Junior Research Group), University of Rostock.* [4]*LMN, Paul Scherrer Institute, Villigen.*

**INTRODUCTION:** Polyetheretherketone (PEEK) gains increasing interest as biomaterial for trauma, orthopaedic and spinal implants.[1] Since cell shape is known to regulate different-tiation of human mesenchymal stem cells[2]. Our aim is to develop surfaces that induce alterations in stem cell shape and thus a specific stem cell differentiation. By means of plasma treatment and micro-structuring we modified PEEK foils and characterized adipose tissue-derived stem cells (ASC) in direct material contact.

**METHODS:** APTIV PEEK foils were hot embossed from a silicon master (150°C, 100kN, structure depth 1µm). The foils were ammonia or oxygen/argon plasma treated (10 to 100 W, 5min, 30 sccm) before cell seeding (2* $10^4$ cells/$cm^2$). ASC were isolated from lipo-suction-derived adipose tissue. Cell cultivation was under standard conditions (i.e. 37°C, 5% $CO_2$). Cells were cultivated 48 h on the PEEK substrates and subsequently depicted by the fluorescence staining Calcein-AM.

**RESULTS:** Plasma treatment and micro-structuring clearly influenced phenotype and proliferation of ASC. On untreated PEEK foils (fig b), the cells grew heterogeneous and at low densities compared to TCPS controls (fig a). Both oxygen and ammonia plasma treatment increased cell number, similar to TCPS controls. Interestingly, strong oxygen plasma treatment (100 W) resulted in cell aggregation rather than a dense cell layer.

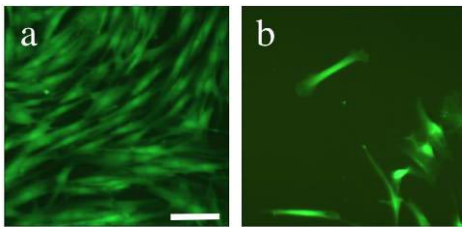


*ASC on a) TCPS and b) untreated PEEK. Scale bar: 100 µm.*

Notably, plasma treatment induced nano-structuring on the PEEK surface. The pillar-like features increased in size (10 nm to 200 nm) with increasing intensity of the plasma treatment (10 W to 100 W).

Regarding micro-structuring by hot embossing, ASC clearly aligned on grooved substrates (fig c-f), independent of groove width (2-20 nm). Again, untreated surfaces induced heterogeneous cell spreading (fig d). Mild oxygen plasma treatment (fig e) resulted in homogenously distributed and aligned cells, whereas harsh oxygen plasma treatment (fig f) clearly showed ASC aggregation in combination with alignment.

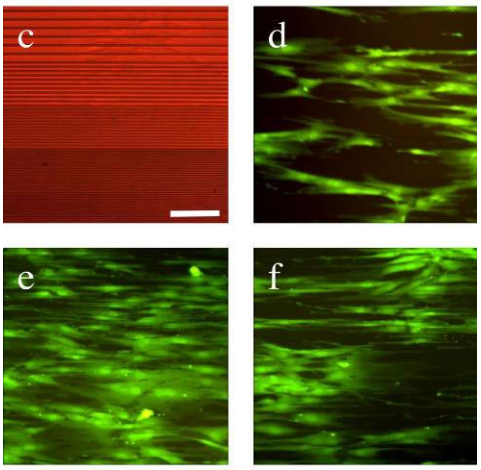


*ASC on grooved PEEK substrates (width 2-20 nm). c) empty, d) untreated, e) $O_2$ plasma 10 W, f) $O_2$ plasma 100 W. Scale bar: 100 µm.*

**DISCUSSION & CONCLUSIONS:** Our still preliminary results demonstrated that ASC reacted to micro-structuring and plasma treatment of PEEK foils with different phenotypes. The aim is to investigate the stem cell differentiation potential of thus induced phenotypes into osteogenic and adipogenic lineage. Furthermore, we are going to analyze the nano-structuring effect of plasma treatment in more detail[3].

**REFERENCES**: [1] S.M. Kurtz and J.N. Devine (2007) *Biomaterials* **28**:4845-69. [2] R. McBeath et al. (2004) *Developmental Cell* **6**:483-95. [3] M.S. Lord et al. (2010) *Nano Today* **5:**66-78.

**ACKNOWLEDGEMENTS:** The presented research activity belongs to the project 'DICANS', funded by the Swiss Nanoscience Institute at the University of Basel. Further financing was by the EU and the Federal State of Mecklenburg-Vorpommern, Germany.

# Plasma treated and nano/micro-structured PEEK substrates for adipose tissue-derived stem cell studies

Jasmin Althaus[1,2,4], Stefanie Adam[3], Helmut Schift [4], Jens Gobrecht[4], Uwe Pieles[2], Bert Müller[1] and Kirsten Peters[3]

[1]*Biomaterials Science Center, University of Basel.* [2]*Institute for Chemistry and Bioanalytics, University of Applied Sciences, Northwestern Switzerland.* [3]*Department of Cell Biology (Junior Research Group), University of Rostock.* [4]*LMN, Paul Scherrer Institute, Villigen.*

**INTRODUCTION:** Polyetheretherketone (PEEK) gains increasing interest as biomaterial for trauma, orthopaedic and spinal implants.[1] Since cell shape is known to regulate different-tiation of human mesenchymal stem cells[2]. Our aim is to develop surfaces that induce alterations in stem cell shape and thus a specific stem cell differentiation. By means of plasma treatment and micro-structuring we modified PEEK foils and characterized adipose tissue-derived stem cells (ASC) in direct material contact.

**METHODS:** APTIV PEEK foils were hot embossed from a silicon master (150°C, 100kN, structure depth 1µm). The foils were ammonia or oxygen/argon plasma treated (10 to 100 W, 5min, 30 sccm) before cell seeding (2* $10^4$ cells/$cm^2$). ASC were isolated from lipo-suction-derived adipose tissue. Cell cultivation was under standard conditions (i.e. 37°C, 5% $CO_2$). Cells were cultivated 48 h on the PEEK substrates and subsequently depicted by the fluorescence staining Calcein-AM.

**RESULTS:** Plasma treatment and micro-structuring clearly influenced phenotype and proliferation of ASC. On untreated PEEK foils (fig b), the cells grew heterogeneous and at low densities compared to TCPS controls (fig a). Both oxygen and ammonia plasma treatment increased cell number, similar to TCPS controls. Interestingly, strong oxygen plasma treatment (100 W) resulted in cell aggregation rather than a dense cell layer.

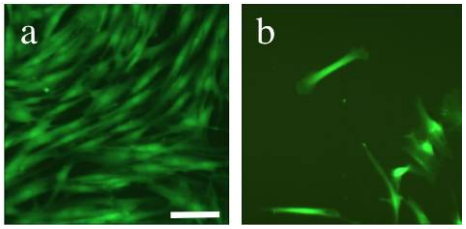


*ASC on a) TCPS and b) untreated PEEK. Scale bar: 100 µm.*

Notably, plasma treatment induced nano-structuring on the PEEK surface. The pillar-like features increased in size (10 nm to 200 nm) with increasing intensity of the plasma treatment (10 W to 100 W).

Regarding micro-structuring by hot embossing, ASC clearly aligned on grooved substrates (fig c-f), independent of groove width (2-20 nm). Again, untreated surfaces induced heterogeneous cell spreading (fig d). Mild oxygen plasma treatment (fig e) resulted in homogenously distributed and aligned cells, whereas harsh oxygen plasma treatment (fig f) clearly showed ASC aggregation in combination with alignment.

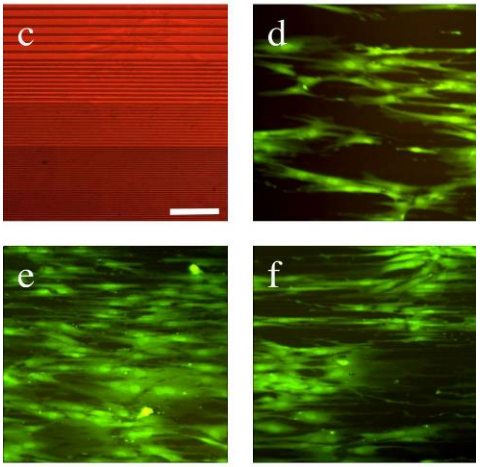


*ASC on grooved PEEK substrates (width 2-20 nm). c) empty, d) untreated, e) $O_2$ plasma 10 W, f) $O_2$ plasma 100 W. Scale bar: 100 µm.*

**DISCUSSION & CONCLUSIONS:** Our still preliminary results demonstrated that ASC reacted to micro-structuring and plasma treatment of PEEK foils with different phenotypes. The aim is to investigate the stem cell differentiation potential of thus induced phenotypes into osteogenic and adipogenic lineage. Furthermore, we are going to analyze the nano-structuring effect of plasma treatment in more detail[3].

**REFERENCES**: [1] S.M. Kurtz and J.N. Devine (2007) *Biomaterials* **28**:4845-69. [2] R. McBeath et al. (2004) *Developmental Cell* **6**:483-95. [3] M.S. Lord et al. (2010) *Nano Today* **5:**66-78.

**ACKNOWLEDGEMENTS:** The presented research activity belongs to the project 'DICANS', funded by the Swiss Nanoscience Institute at the University of Basel. Further financing was by the EU and the Federal State of Mecklenburg-Vorpommern, Germany.

# Use of plant pathogenic fungi *Fusarium moniliforme* for biosynthesis of silver nano particles with emphasis to time

S. J. Ashrafi [1*] ,M. F. Rastegar [1], B. jafarpour [1], S. A. Kumar [2]

[1]-*Plant protection, Ferdowsi university of Mashhad, Mashhad, Iran.,* jamal.ashrafi@stu-mail.um.ac.ir

[2]- *Biomedical Engineering, McGill University, Montreal, Canada*

**INTRODUCTION:** One approach that shows immense potential is based on the biosynthesis of nanoparticles using biological micro-organisms such as fungi. While a number of chemical methods are available and are extensively used, they are often energy intensive, employ toxic chemicals, and require higher temperatures. At There Synthesis of silver nanoparticles using plant pathogenic fungus Fusarium moniliforme demonstrated.

**METHODS:** Fungi extract prepare with culturing a 5mm disc of fungus at PGB (juice of 200 g boiled potato, 15 g glucose /1 liter sterile water) media in vial glass at 21-27 ºC with shaking (180 rpm) for 4 weeks. After the incubation, the biomass was filtered (Whatman filter paper No. 1). AgNO3 (1 mM of final concentration) was mixed with cell-free filtrate in a 100 ml glass vial and agitated at 28□C. Control ((without silver ions) was also run along with the experimental glass vial. The absorbance was measured at the resolution of 1 nm using a UV-visible spectrophotometer (Uv/vis 2100-PC, Japan). Energy-dispersive X-ray spectroscopy was done (Leo 1450VP, Germany). Stub covered with aluminum foil and one drop of Samples were poured on it, allowed to dry in room temperature and coated with very thin layer of gold.

**RESULTS:** Upon addition of Ag+ ions into the filtered cell-free culture, samples Changed in color from almost colorless to brown, with intensity increasing during the period of incubation (Fig 1b). Control (without silver ions) showed no change in color of the cell filtrates when incubated in the same conditions(not shown). Formation of colloidal silver particles can be easily followed by changes of UV-Vis absorption, that at here we showed this variation during the synthesis and 7 month after it (Fig.1).

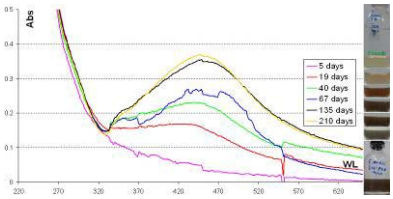


*Fig.1: UV–Visible absorption spectra of silver nanoparticles during 7month of reaction (first 5 days reaction was don at 28C and 180 rpm). b: color changes during these times.*

In EDS analysis shows the peak in silver region confirming presence of elemental silver (Fig 2)

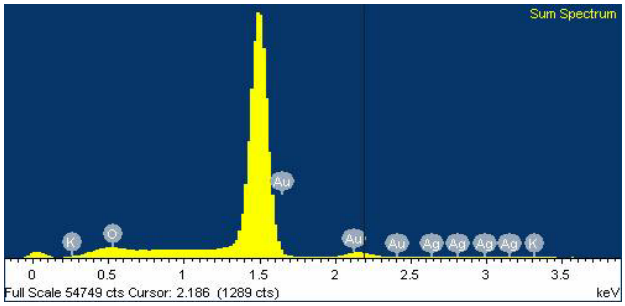


*Fig 2: DifferentX-ray emission peaks showing Signals from the atoms in the silver nanoparticles are observed, whereas strong signals from Au atoms are also visible (related to used coat).*

**DISCUSSION:** We demonstrated simple, stable and efficient biological method for synthesis of silver nanoparticles using fungus, F. moniliforme. The synthesis nano particle monitoring with use of Uv/vis spectrophotometer methods for measurement the stability and changes of this particle during the time. importance result of our work is, for investigate the potential of an fungus in biological synthesis some time need more than five days, with attention to papers we could observe that they note to first five days after incubation. Or other fungi at first days showed good result but after some weeks quickly aggregate and precipitate in media (not reported our data). However the fungal biosynthesis is dynamic and during the time will be result to better or worst, particularly in light vessels. Duran and co-workers.[1]reported in same study F. oxysporum could synthesis silver nano particle but F. moniliform could not synthesis it. Although we use three forme special of F. oxyspourum with F.moniliforme at this study and observed all of them could synthesisi with some variation in speed of synthesis, size and shape of nano particles. (Did not show).

**REFERENCES**:N. Duran, P.D Marcato, et al (2005). Mechanistic aspects of biosynthesis of silver nanoparticles by several Fusarium oxysporum strains. *J nano bio* **3**:8.

# Hydroxyapatite - biopolymer mats by electrospinning

G. Gergely, I. E. Lukács, M. Tóth, L. Illés, F. Wéber, Cs. Balázsi

*Research Institute for Technical Physics and Materials Science, Hungarian Academy of Sciences*

**INTRODUCTION:** Hydroxyapatite (HAp) is the main inorganic component of mammal bone and teeth. It is one of the few bioactive materials, which helps cell growing. The objective of this study was to fabricate hydroxyapatite-biopolimer nanofiber mats [1,2]. To achieve this goal, two different suspensions were used. Approximately 1 μm diameter size fibers with big HAp agglomerates were fabricated using acetone and acetic acid. Fibers with a bigger diameter size and homogenous distributed HAp particles were produced applying acetone and isopropanol. During the experiment the effect of the processing parameters: applied voltage, diameter of needle, the distance of the needle tip and the collector, flow rate was analyzed.

**METHOD:**Samples are made by KDScientific KDS202-CE electrospinnig device with high voltage supply. The needles were common medical needles, which ending-points were polished perpendicular to the direction of the flow. The polymer was cellulose-acetate (CA) (22188; $M_r$~29000 {9004-35-7}; Fluka/Sigma-Aldrich), the applied solvents were acetone (Spektrum3D), isopropanol (Reanal), and acetic-acid (Spektrum3D). Hydroxyapatite (HAP) prepared from eggshell by mechanochemical milling in our department (Hungarian Academy of Sciences, Researc Institute for Technical Physics and Materials Science, Department of Ceramics and Nanocomposites). The samples were analyzed by Jeol JSM-25-SIII scanning electron microscope with attached Bruker Quantax EDS.

**RESULTS:** In the case of acetone-acetic acid solution, the applied concentration was 80 w/w % acetone, 20 w/w % acetic-acid as solvent. The solution included 0,8g HAp, 1,2g CA, 8g acetone, 2g acetic-acid. During the preparation the HAp was treated with ultrasonicator to destroy coagulations. SEM images show that the diameter of the fibers were nearly uniform, about 500-1000 nm. Isopropanol's dielectric constant, viscosity and conductivity have an effect to the bead formation. The samples contain 0,9 g CA, 0,6 g HAp, 1 g isopropanol and 4 g acetone. The parameters of the process: 15 cm target-needle distance, 10 kV voltage, 0,8 mm needle diameter and 0,10 ml/min flow rate. SEM images show that the distribution of the HAp was homogenous and the average fiber diameter was very uniform: 1000±150 nm. According to the EDS spectrum the presence of C (CA), O (CA and HAp), P (HAp), Mg, S (HAp-eggshell trace element) Si (sample holder) and Al (sample cover) were observed. Element mapping based on EDS confirmed that nanosized HAp distributed in the fibers homogenously (Fig. 1 a), b), c), d)).

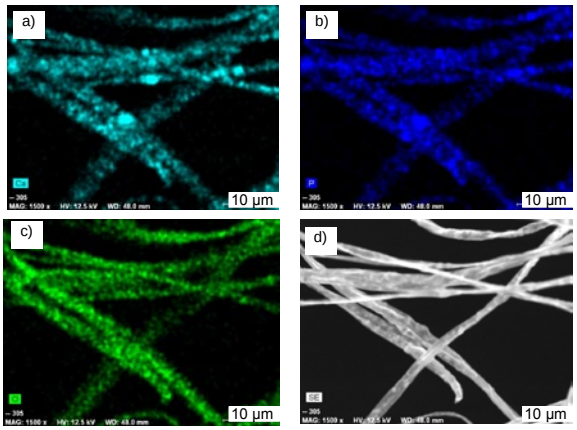


*Fig. 1. Element mapping of the acetone-propanol samples: a) Ca, b) P, c) O and d) the general view (SEM image)*

**CONCLUSION:** Cellulose-acetate nanofibers have been produced from two different solutions. The applied solutions were: Acetone-acetic acid and acetone-isopropanol. The hydroxyapatite has been dispersed in both solutions. It has been found that the acetone – isopropanol samples surpass the acetone – acetic-acid samples in every regard. The average fiber diameter was bigger than that of acetone - acetic-acid samples and the dispersion of HAp was more efficient and homogenous.

**ACKNOWLEDGEMENT:**Thanks to OTKA grant 76181, NKTH Öveges József Grant, MTA-NSF-OTKA bilateral grant and the Hungarian – South-Korea bilateral TéT project.

**REFERENCES:** [1] K.C.B. Yeong, J. Wang, S.C. Ng: Mechanochemical synthesis of nanocrystalline hydroxyapatite from CaO and $CaHPO_4$. *Biomaterials* **22** (2001) 2705-2712. [2] Cs. Balázsi, A. Bishop, J. Yang, K. Sedlácková, F. Wéber, P. Gouma:Biopolymer-Hydroxyapatite Nanocomposite from Eggshell for Prospective Surgical Applications, *Materials Science Forum* Vol. **589** (2008) 61-65.

# What the "cell" sees in Bionanoscience

Francesca Baldelli Bombelli, Dorota, Walczyk, Marco Monopoli, Iseult Lynch, Kenneth A. Dawson.

*Centre for BioNano Interactions, School of Chemistry and Chemical Biology, University College Dublin, Belfield, Dublin 4, Ireland.*

Nanoparticles in contact with biological fluids interact with a range of biomolecules in a quite specific manner. The biomolecules form a corona around the nanoparticles; it might be this corona of biomolecules that determine the fate of the biomolecule-nanoparticle complex as it interacts with cells rather than the "bare" nanoparticle. We have shown that for particles of the same material, differences in size and surface charge alter the composition of the corona significantly. This implies that extreme care must be taken in the development of nanomedicine and nanotherapeutics in terms of controlling the manufacturing process of nanoparticles and control of the surface properties of the final product.

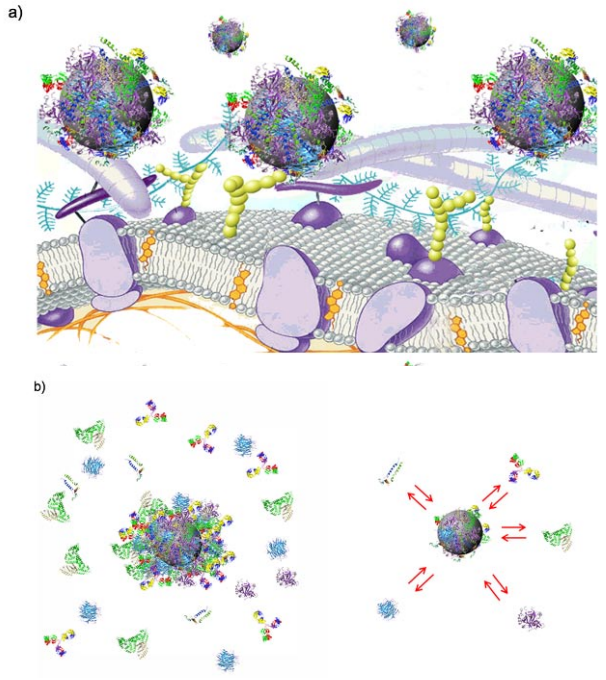


*Figure 1. (a) Cartoon representation of the possible exchange/interaction scenarios at the bio-nanointerface at cellular level. (b) Schematic drawing of the structure of NP-protein complexes in plasma: the 'core' nanoparticle is surrounded by the protein corona composed of an outer weakly interacting layer of protein rapidly exchanging with a collection of free proteins (left) and a 'hard' slowly exchanging corona of proteins (right). Diagram is not to scale in representing the proportions of the different objects. (Copyright Walczyk, D. et al., J. Am. Chem. Soc. **2010**, 132, 5761–5768)*

We hypothesize that the cell 'sees' a system in which the core nanoparticles (and other multi-particle assemblies) are surrounded by a 'hard' slowly exchanging corona of proteins, and an outer (weakly interacting, and rapidly exchanging) collection of proteins (Figure 1). Other forms of multimeric particle-protein complexes may also be present, depending on the dispersion. Collectively these particle-protein complexes constitute 'what the cell sees'. If the slowly exchanging proteins have sufficiently long residence times, then *de facto* the effective unit of bionanoscience is a nanoparticulate core and an associated biomolecule corona that is so strongly bound that the particle itself is merely the scaffold for the proteins. We emphasize that our interest is to understand these questions for complex biological media (such as plasma, tissue culture serum and organ derived fluids). Moreover, the nanoparticle-protein complex changes and evolves depending on the nanomaterial composition, the plasma concentration, and the time of incubation, making understanding of the manifold processes that occur at the nano-bio interface extremely important. Here, we apply several different methodologies, in a time resolved manner, to follow the lifetime of such biomolecular 'coronas'. For several nanomaterial types we find that blood plasma-derived coronas are sufficiently long lived that they, rather than the nanomaterial surface, are likely to be what the cell sees [1]. Such particle-corona complexes can be physically isolated from the surrounding medium, and studied in some detail. From fundamental science to regulatory safety, current efforts to classify the biological impacts of nanomaterials (currently according to bare material type and bare surface properties) may be assisted by the methodology and understanding reported here.

**REFERENCES:** [1] Walczyk, D. et al., *J. Am. Chem. Soc.* **2010**, 132, 5761–5768

# Self-assembled protein Nanocapsules in Ionic Liquids as Templating Nanoreactors for enzyme-encapsulated Hollow Nanocontainers

V. Bansal,[1] S. K. Soni,[1] S. K. Bhargava[1]

*E-mail: vipul.bansal@rmit.edu.au*

[1] *School of Applied Sciences, RMIT University, GPO Box 2476V, Melbourne 3001 (VIC) Australia.*

**INTRODUCTION:** Self-assembly is one of the most important strategies used within biological systems for the development of complex and functional macromolecular superstructures such as nucleic acids, proteins, and lipopolysaccharides. Taking inspiration from naturally occurring self-assembled structures, there have been a myriad of efforts towards controlled self-assembly under laboratory conditions [1]. Notably, most of the self-assembly studies have hitherto explored the aqueous media as fluid phase for self-assembly of amphiphilic biomacromolecules, wherein architectural modification of biomolecules is generally a pre-requisite. Ionic liquids (ILs) have recently become attractive solvents for nanomaterials synthesis due to their unique physico-chemical properties such as high viscosity, high ionic conductivity, high thermal and chemical stability, and negligible volatility, with some interesting applications recently demonstrated in Bioscience [2]. However applicability of ILs in self-assembly of biomacromolecules has not been explored previously, which is the scope of our study.

**METHODS:** Enzymes (e.g. phytase, lipase, etc) of appropriate concentration were added to different ionic liquids (e.g. [BMIM][$BF_4$], [BMIM][$PF_6$], etc.) and allowed to self-assemble for 24 hours. Following self-assembly of enzymes in ILs, an appropriate metal or metal oxide precursor (e.g. TEOS, $HAuCl_4$, $AgNO_3$, $K_2PtCl_6$) was added to IL, and reaction was further pursued for 24 h. This resulted in hollow metal or metal oxide nanocontainers with encapsulated enzyme during their syntheses [3].

**RESULTS:** We demonstrate for the first time that ILs can act as non-aqueous designer solvents for self-assembly of amphiphilic biomacromolecules (e.g. enzymes) without requiring their prior modification. Furthermore, we have used these self-assembled enzyme nanocapsules as templating nanoreactors for *in situ* synthesis of silica, titania, gold, silver, platinum and palladium nanocontainers, and proposed the most plausible synthesis mechanism. These enzyme-loaded nanocontainers were further utilized for

applications in enzyme reusability, drug-delivery and bio-catalysis.

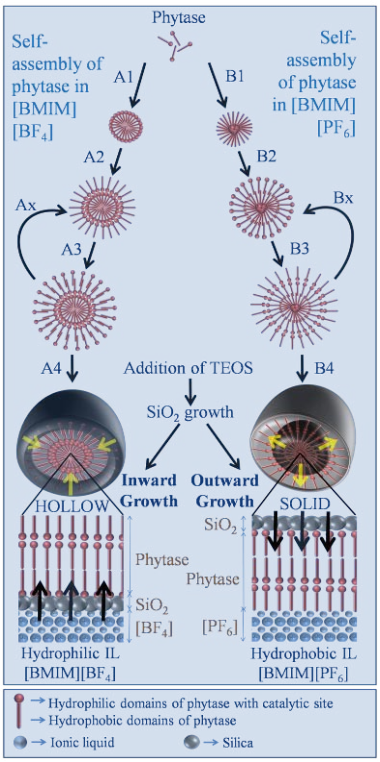


*Scheme 1: Schematic illustration for self-assembly of phytase enzyme in hydrophilic vs. hydrophobic ionic liquids viz. [BMIM][$BF_4$] and [BMIM][$PF_6$] respectively.*

**DISCUSSION & CONCLUSIONS:** As a representative case, synthesis of hollow silica nanocontainers using phytase enzyme is illustrated using schematic, and mechanism is shown (Scheme 1). The generality of our approach for synthesis of metal and metal oxide nanocontainers will be shown during oral presentation.

**REFERENCES:** [1] Hartgerink, J. D.; Beniash, E; Stupp, S.I. *Science* **2001**, *294*, 1684. [2] Greaves, T. L.; Drummond, C. J. *Chem. Soc. Rev.* **2008**, *37*, 1709. [3] Pearson, A.; O'Mullane, A. P.; Bansal, V.; Bhargava, S. K. *Chem. Commun.* **2010**, *46*, 731.

**ACKNOWLEDGEMENTS:** VB thanks Australian Research Council (ARC) for funding through ARC-Discovery Project DP0988099.

# Understanding the Assembly of a Novel Protein Nanotube

E.F. Banwel1[1], J.G. Heddle[2]

*[1] Global Edge Institute, Tokyo Institute of Technology, Nagatsuta, Yokohama, Japan. [2] Heddle Initiative Research Unit, Advanced Science Institute RIKEN, Wako, Saitama, Japan.*

**INTRODUCTION:** The design of novel nanoscale machines and devices is a rapidly growing field and bionanotechnology is an exciting source of structures and materials. As protein sequence-to-structure relationships are better understood we are increasingly able to design proteins and peptides for the bottom-up assembly of such components. Nanotubes are likely to be useful building blocks for future nanotechnologies and have potential uses in therapeutics, microelectronics and sensors. The 11mer ring protein trp RNA-binding attenuation protein (TRAP) is of interest in the design and building of nanotubes because of its small size (comparable with that of carbon nanotubes) and because of the comparative ease of functionalization. Previously, production of a self-assembled protein nanotube has been achieved through the mutation of TRAP[1]. Mutated rings stack head-to-head and tail-to-tail in solution to produce an extremely narrow, uniform nanotube. The precise mechanism of assembly was unknown but was thought to be a mixture of disulphide bonds and hydrophobic interactions.

**METHODS:** Plasmids containing the gene for *B. stearothermophilus* TRAP were mutated to the required sequences and transformed into *E. coli*. The various TRAP mutants were expressed and purified following standard protocols [1]. Once pure, 20 µl samples containing 20 mg/ml TRAP and 30 mM dimercaptopropanol (DMP) were incubated overnight at 4 °C. 6 µl aliquots were applied to carbon coated and hydrophylized copper TEM grids for 30 secs and then excess moisture was wicked away using filter paper. Grids were stained with 2 % phosphotungstic acid using the same method. .

**RESULTS:** Here we present a series of TRAP point mutations designed to further explore the interactions on either face of the ring. Mutations were made to the tube forming TRAP[1] that replaced the Cys residues on each face with either hydrophobic or wild-type or Gly residues, Table 1. Mutants were then reacted with DMP and tube formation investigated. In each case, mutations made to the wide face (residue 69) prevented tube assembly while those made to the narrow face

(residue 50) did not, Figure 1. Mutant 50C 69V produced hexagonally close-packed arrays of rings.

*Table 1.TRAP mutants.*

| Protein Name | Mutation | |
|---|---|---|
| | Residue 50 | Residue69 |
| Wild type | Glu | Val |
| Tube | Cys | Cys |
| 50G 69C | Gly | Cys |
| 50L 69C | Leu | Cys |
| 50C 69V | Cys | Val |
| 50C 69L | Cys | Leu |
| 50L 69V | Leu | Val |

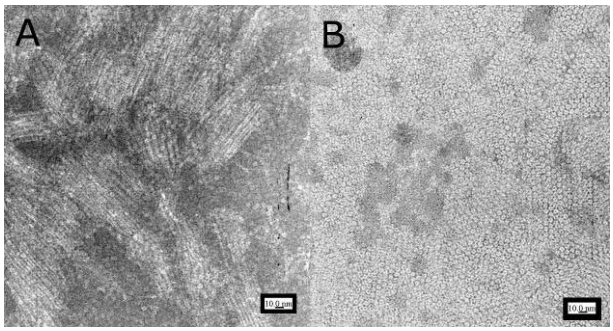


*Fig. 1: A) TRAP mutant 50L 69C is still able to undergo assembly into tubes while 50C 69V (B) is not.*

**DISCUSSION & CONCLUSIONS:** This research gives a very clear understanding of the mechanisms of tube TRAP assembly; it shows the requirement for Cys at position 69, but demonstrates that all that is required for assembly on the opposite face is removal of the negatively-charged wild-type Glu residue.

**REFERENCES:** [1] F.F. Miranda, K. Iwasaki, S. Akashi, K. Sumitomo, M. Kobayashi, I. Yamashita, J.R.Tame, J.G. Heddle (2009) *Small* **5**: 2077-84.

**ACKNOWLEDGEMENTS:** Funding kindly supplied by the Japan Society for the Promotion of Science (JSPS) and the MEXT Special Coordination Funds for Promoting Science and Technology and Grant-in-Aid for Young Scientists.

# Enhanced cellulose degradation by nano-complexed enzymes

Y. Barak[1], S. Moraïs[2,3], A. Heyman[3], O. Shoseyov[3], E. A. Bayer[2]

*[1] Chemical Research Support, [2] Department of Biological Chemistry, The Weizmann Institute of Science, Rehovot, Israel. [3] The Robert H. Smith Faculty of Agriculture, Food and Environment, The Hebrew University of Jerusalem, Rehovot, Israel.*

**INTRODUCTION:** Self-assembly of protein scaffolds into multi-component structures has been studied extensively. A major example of such a complex is the bacterial cellulosome that is responsible for the synergistic degradation of recalcitrant cellulosic substrates. We have designed a fusion protein between stable protein 1 (SP1) from *Populus tremula* and a cohesin from the cellulosome of *Clostridium thermocellum* (Coh-SP1). This construct comprises a ring-shaped thermostable protein scaffold, which bears 12 cohesin units displayed on the SP1 protein [1]. Coh-SP1 can interact with a chimaeric dockerin-containing form of the exoglucanase Cel6B from *Thermobifida fusca* (*t*-6B) forming a 12 exoglucanase-bearing scaffold [2].

**METHODS: Cellulase activity assay:** Phosphoric acid swollen cellulose (PASC) or discs of filter paper were incubated (20 min or overnight respectively) at 50°C with enzyme mixtures, and production of soluble sugars was assayed using the dinitrosalicylic acid method. **Calculation of synergism:** The synergistic effects for each exo-endo ratio were calculated using the activity of the mixture divided by the sum of the individual activities, for the free and/or complexed enzymes.

**RESULTS & DISCUSSION:** In order to determine whether cellulose degradation by the *t*-6B exoglucanase chimaera is enhanced when complexed with the Coh-SP1 scaffold, several enzymatic mixtures were assayed on PASC, a non-crystalline substrate (Fig. 1A). Incorporation of *t*-6B on Coh-SP1 resulted in a decrease in enzymatic activity. However, when the complexed exoglucanase was combined with 1:20 molar ratio of *T. fusca* Cel5A endoglucanase, a 12-fold enhancement of cellulolytic activity (over the sum of the free enzymes) was observed (Fig. 1A). These results may indicate that the activity of the endoglucanase creates additional free ends that are now more available for degradation by the exoglucanases, and that the complex acts with greater facility on the cellulosic substrate, compared with the free exoglucanase. In order to determine whether or not this synergistic phenomenon can be observed on more recalcitrant substrates, similar experiments were conducted using filter paper as a substrate, at an optimal exo-

to-endo ratio of 25:1 (Fig. 1B). The much reduced activity on filter paper suggests that the complexity of the substrate represents a major barrier for degradation. In this case adding Cel5A to the complexed *t*-6B led to a 6-fold enhancement of cellulolytic activity.

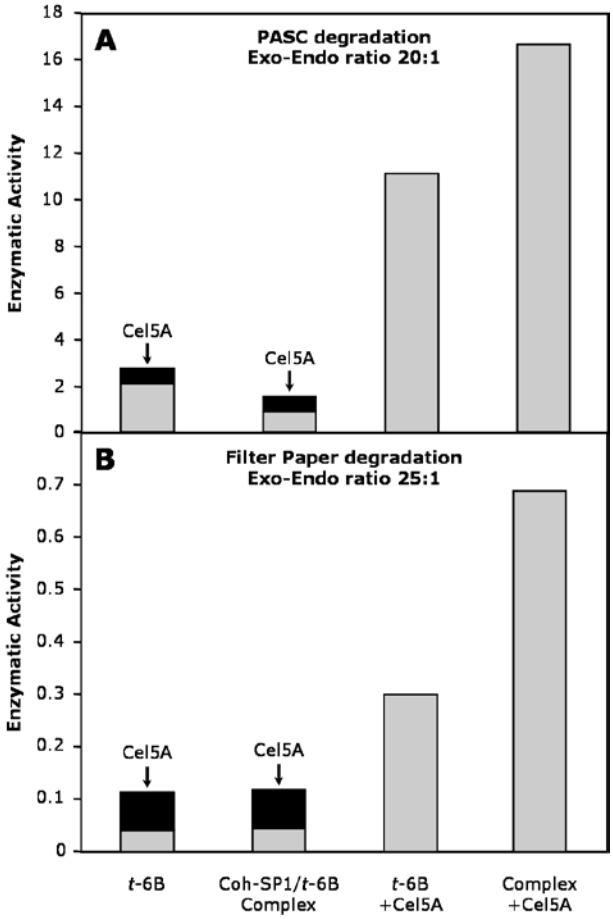


*Fig. 1: A) Degradation of phosphoric acid-swollen cellulose by different enzyme compositions at the optimal 20:1 exo-to-endo ratio (0.6:0.03 μM). B) Degradation of filter paper by different enzyme compositions at the optimal 25:1 exo-to-endo ratio (0.75:0.03 μM). Grey bars indicate activity of different t-6B mixtures. Black bars indicate activity of free Cel5A. Enzymatic activity is defined as the release of soluble reducing sugar (μM) per min.*

**REFERENCES:** [1] A. Heyman, Y. Barak, J. Caspi, et al (2007) *J. Biotechnol*. **131**: 433-439. [2] S. Moraïs, A. Heyman, Y. Barak, et al (in press) *J. Biotechnol*.

# Synthesis and *in vitro* Functional Characterization of Peptide Conjugates that Inhibit the Growth of *Mycobacterium tuberculosis* $H_{37}Rv$

Zs. Baranyai[1], K. Horváti[1], G. Mező[1], Sz. Bősze[1]

*1 Research Group of Peptide Chemistry, Hungarian Academy of Sciences, Eötvös Loránd University, Budapest, Hungary.*

**INTRODUCTION:** Tuberculosis is a serious infectious disease; these days more than two billions people are infected with *Mycobacterium tuberculosis*, which is an intracellular, slow growing pathogen. The cellular uptake of the recently used antituberculotics by infected macrophages is limited. It is a new approach to enhance the efficacy of the antituberculars with receptor mediated targeting. The host cell specific delivery of the active compounds to the infected macrophages can decrease the side effects and shorten the length of the therapy. In this study scavenger [1] and tuftsin receptor [2] specific conjugates were synthesised and functionally characterised.

**METHODS:** Peptide spacer (GFLGC) and a tuftsin derivative (TKPKGTKPKGC (OT10C)) was synthesised manually using Fmoc/*t*Bu strategy on Rink-amide MBHA resin. The peptides and peptide derivatives were characterised by analytical RP-HPLC, mass spectrometry and amino acid analysis. New, *in silico* identified antitubercular compounds (TB803, TB852) were conjugated to the spacer and the carrier peptide through oxime bond [3]. The peptide conjugates were coupled to chloroacetylated branched chain polypeptide with poly-*L*-lysine backbone (SAK; poly[Lys($Ser_{0.90}$-*DL*-$Ala_{2.60}$)]) [4] via thioether bond in 0.1M TRIS buffer (pH 8.12). The substitution degree of the SAK-conjugates was determined by amino acid analysis. Minimal inhibitory concentration (MIC) of the new compounds was measured on *M. tuberculosis* $H_{37}Rv$ culture in Sula liquid media (pH 6.5). The sterility was confirmed using Löweinstein-Jensen solid media and the colony forming unit (CFU) was determined. 5(6)-carboxyfluorescein (**Cf**) labelled conjugates were prepared in order to study the cellular uptake by flow cytometry (BD LSRII) on MonoMac6 human monocytic cell line.

**RESULTS:** Chemically carefully characterized conjugates of *in silico* identified drug candidates and **Cf**-labelled compounds were prepared. The MIC value of the conjugates was in the same concentration range as the free drug moiety. The intracellularly detected fluorescence intensity of the **Cf**-labelled compounds was concentration dependent on monocytes after one hour treatment. Higher cellular uptake was measured in the case of SAK-conjugates.

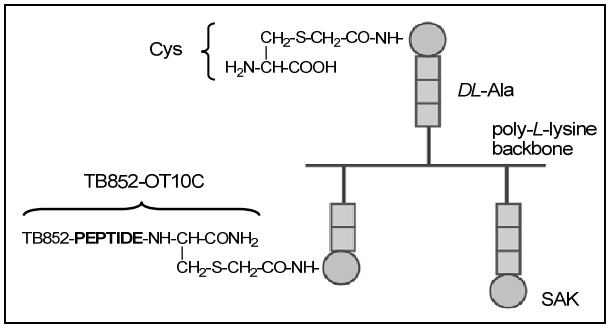


*Fig. 1: The schematic figure of the TB852-OT10C-SAK conjugate*

**DISCUSSION & CONCLUSIONS:** The optimization of the cellular uptake by drug delivery systems can decrease the used dosage and the length of the therapy and it can also enhance the bioavailability of the drug molecules. Receptor specific peptide conjugates were prepared and characterized. The antimicrobial activity of the drug candidates was preserved after conjugation to peptide carriers through oxime bond. The conjugation to poly-*L*-lysine backboned branched chain polypeptide (SAK) dramatically enhanced the cellular uptake.

**REFERENCES:** [1] R. Szabó et al (2005) *Bioconjugate Chemistry*, **16** (6), 1442-1450. [2] G. Mező et al (2004) *Journal of Peptide Science*, **10** (12), 701-713. [3] J. Shao, J. P. Tam (1995) *Journal of the American Chemical Society*, **117** (14), 3893–3899. [4] G. Mező et al (1997) *Biopolymers*, **42**, 719-730.

**ACKNOWLEDGEMENTS:** This work was supported by grants from the Hungarian National Science Fund (OTKA 68358) and National Office for Research and Technology (NKFP_07_1-TB_INTER-HU, NKTH BIOSURF_OM-00146/2008, GVOP-3.2.1-2004-04-0005/3.0; GVOP-3.2.1-2004-04-0352/3.0.).

# A novel platform for surface investigation of bio-conjugated ligands

E. Battista[1], F.Causa[1], R. Della Moglie and P.A. Netti[1]

[1] *Interdisciplinary Research Center on Biomaterials, University "Federico II" and Centre for Advanced Biomaterials for Healthcare, IIT Italian Institute of Technology*

**INTRODUCTION:** In nano-bio-technolgy pivotal role is played by bio-conjugated interfaces interacting with cells or soluble signals. Surface conjugation with control, at the nanoscale, of ligands density and spatial distribution represents a crosswise topic in many fields from biochemistry to nanomedicine. Here, we present a platform to study the distribution and assess, at the nanoscale, the presentation of immobilized ligands on a polymeric surface. As proof of principle, we used as immobilized ligand a RGD peptide (a well known cell adhesive motif), a fluorescent tag on RGD to map ligand distribution and fluorescent microspheres (MS) (endowed with specific peptide against RGD) to probe ligand accessibility on the surface.

**METHODS:** Bioactivation of surfaces with GRGDY were performed tethering with glutaraldehyde in a two step by reductive amination with $NaCNBH_3$. Previously, poly-epsilon-caprolatone surfaces were functionalized by means aminolysis in a 10% IPA solution of 1,6-hexandiamine. MicroBCA (Aldrich) was used to quantify the RGD-peptide density. Surface physico-chemical properties were studied by PM-IRRAS, Contact Angle, SFE, CLSM and AFM[1]. Small cyclic biotinilated peptide[2] highly specific in recognition of RGD-like sequences were conjugated to streptavidinated fluorescent MS (2µm, Polyscience). The MS were imaged by fluorescence microscope; a set of 30 images were processed while counted particles were related to the total surface for MS density evaluation. Bioactivity tests were performed by seeding NIH3T3 and evaluated by CLSM and SEM.

**RESULTS:** A density of about 3 nmol/cm$^2$ of RGD on the surface was evaluated. PM-IRRAS showed diagnostic peaks relative to the peptide covalently bound near 1600 cm$^{-1}$. By using Good-van Oss model, contact angle measurements and SFE evaluation showed a variation in the acid and base polar components as the polymer bioactivation advance. By comparison of AFM and CLSM images (fig.1) is possible to map the peptides groups immobilized along the surfaces in correspondence of amorphous phase of crystallites. The imaging of MS allows to study the ligand distribution, while the analysis of MS binding to the RGD-modified surfaces showed a 30 fold increase attachment with respect to control surface. Biological tests, carried out with NIH3T3 cells,

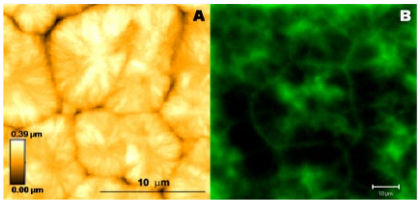


*Fig. 1: Topological mapping of treated surface and spatial distribution of conjugated molecules.*

confirmed that the immobilized RGD presented to cell integrins capable to cell adhesion (fig.2).

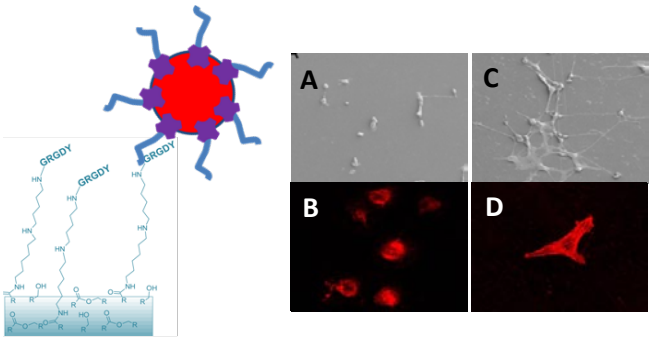


*Fig.2. Scheme of bio-recognition at polymer surface by means peptide epitope mimicking $\beta_3$ integrin subunit with RGD immobilized onto the surface. Adhesion tests with NIH3T3 cells: A,B control ;C,D RGD-modified surface*

**DISCUSSION & CONCLUSIONS:** A methods of surface bioconjugation and the platform to visualize and map the distribution of immobilized ligand is proposed. In addition, a practical approach to study the accessibility of the surface signals allows to scale down the effective amount of molecules capable to interact with cells or soluble signals at the interface. Proposed platform can be useful in the case of cell-materials interaction investigation and all bio-functional assays based on solid support.

**REFERENCES:** [1] Causa F., Battista E. et al, Langmuir. (2010) *in press*; [2] A.W. Morgan et al., Biomaterials **29** (2008) 2556-2563.

**ACKNOWLEDGEMENTS:** Authors would like to thank Dr. D.Guarnieri and M.Iannone for the biological tests

# $TiO_2$ nanotubes for stimulated cell response: Control of cell-surface interactions at the nanoscale

S. Bauer[1], J. Park[2], K. von der Mark[2], P. Schmuki[1]

[1] *University of Erlangen-Nuremberg, Department of Materials Science, Institute for Surface Science and Corrosion, Erlangen, Germany.* [2] *University of Erlangen-Nuremberg, Nikolaus Fiebiger Centre of Molecular Medicine, Institute of Experimental Medicine I, Erlangen, Germany.*

**INTRODUCTION:** During several decades biomedically driven studies in medicine and biomaterial fields have explored how the topography of surfaces can direct cell behavior. Recently nanoscale environments have received considerable attention as a critical factor affecting cell behavior. For many years a satisfying surface structuring technique for biorelevant materials with high lateral resolution in the sub-100 nm range was not available. The present work however, shows the preparation of self-organized nanotubular $TiO_2$ layers to study cell interactions. Highly ordered $TiO_2$ nanotube arrays can be produced on titanium surfaces by anodization in various electrolytes containing fluorides [1]. These surfaces can ideally be used as nanoscale spacing model for cellular response testing of a clinically relevant surface. We demonstrate that 15 nm nanotubes provide a substantially stronger stimulation of vitality and differentiation of mesenchymal than 70 to 100 nm nanotubes, while high rates of apoptosis were seen on 100 nm nanotubes.

**METHODS:** $TiO_2$ nanotubes of different diameters in a wide range between 15 and 100 nm were formed by varying the applied potential [2]. GFP-labeled mesenchymal stem cells as well as hematopoietic stem cells were plated on $TiO_2$ nanotube surfaces with cell densities of 5000/cm$^2$. Cell adhesion and growth was evaluated after 24 hours and 3 days, proliferation was quantified after 6 days using cell proliferation reagent WST-1 (Roche). Cell migration, motility, osteogenic differentiation and apoptosis were monitored and measured as described elsewhere [3-5].

**RESULTS:** Figure 1 shows the dramatic influence of different nanotube diameters in the sub-100 nm scale on the vitality of rat mesenchymal stem cells. Cell adhesion and spreading are enhanced for nanotube diameters of ~ 15-30 nm while a strong decay in cell activity is observed for diameters > 50 nm. It can be shown that 15 nm nanotube diameters induce a highest activation of the cells, whereas 100 nm lead to a significantly increased cell death rate (apoptosis).

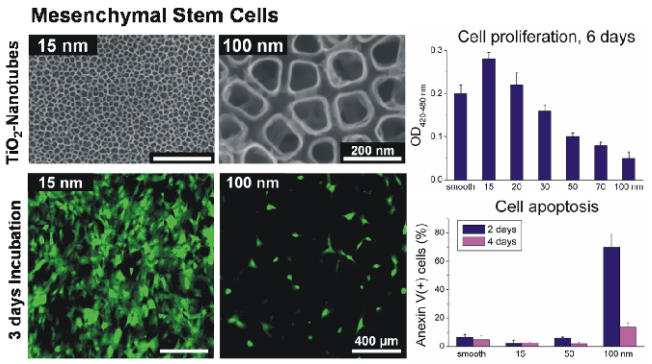


*Fig. 1: SEM images of self-assembled layers of vertically oriented $TiO_2$ nanotubes with diameters of 15 and 100 nm. Fluorescence microscopy images of GFP-labelled mesenchymal stem cells after 3 days incubation on 15 nm and 100 nm samples. Cell proliferation rates measured after 6 days by WST-1 assay as well as cell apoptosis show a strong dependency on nanotube diameter.*

**DISCUSSION & CONCLUSIONS:** We show the first studies demonstrating that the cell-life behavior (including cell growth, migration, differentiation and cell death) indeed is determined by sub-100 nm surface geometry environmental features using $TiO_2$ nanotubes [3-6]. By comparison with other oxide nanostructures we show how strongly the pure nano-geometric dependence dominates over other possible effects on cell activity [5-6]. The presented concept of size-induced cell fate provides important scientific implications and affects a broad range of issues in medical technology.

**REFERENCES:** [1] A. Ghicov, P. Schmuki (2009) *ChemComm* 2791-808. [2] S. Bauer, S. Kleber, P. Schmuki (2006) *Electrochem. Commun.* **8**:1321-5. [3] J. Park, S. Bauer, K. v.d. Mark, et al (2007) *Nano Letters* **7(6)**:1686-91. [4] J. Park, S. Bauer, K. v.d. Mark, et al (2009) *Small* **5(6)**:666-71. [5] J. Park, S. Bauer, P. Schmuki, et al (2009) *Nano Letters* **9(9)**:3157-64. [6] S. Bauer, J. Park, K. v.d. Mark, et al (2009) *Integrative Biology* **1(8-9)**:525-32.

**ACKNOWLEDGEMENTS:** This work was supported by the Deutsche Forschungs-gemeinschaft (SCHM1597/9-1 MA534/20-1).

# Requirements to structure, material components and surface properties of implantable brain-computer interface for cortical vision prosthesis

M.Ivanova, S.Gordeyev, B.Baziyan

*Neurocybernetics laboratory, brain research dept, Science Centre of Neurology RAMS, Moscow, Russia.*

**INTRODUCTION:** One of the most important questions in cortical visual prosthesis development is to create microelectrode array, so called brain-computer interface (BCI), which would stimulate neurons of visual cortex with determined pattern of impulses that will mould the shape that is captured and contrasted by video camera in front of the completely blind prosthesis's user eyes. There are several requirements for the implanted BCI, such as longevity, biocompatibility and stability in the aggressive ion environment of brain liquor. For this reason new techniques and approaches are being developed to reach the maximum of noninvasive and atraumatic functioning of such prosthesis, for example nanocarbon tubes or optoaxon usage instead of implanted microelectrodes. In this abstract we present the results of our research in detecting the range of safe but effective parameters of neural stimulation in laboratory animal and our research in different material of BCI application.

**METHODS:** 13 felines were tested for their ability to develop conditional food-obtaining reflex in response to "phosphene model". 11 of the 13 tested animals qualified for the experiment and were implanted with either subdural/intracortical iridium-oxide microelectrode array or a single aureated silver electrode, in V1 primary visual cortex. Animals were divided into 4 groups based on the localization of the implant and the diameter of the electrodes (0.05, 0.2, or 1.0 mm). Implantations were controlled using stereotaxic atlas and visual evoked potentials. At the end of surgeries, cranium bones were sealed with acryl oxide adhesive. Follow-up period was 8-12 months. Three categories of parameters affecting phosphene perception were measured: 1) brain-computer interface parameters: position of microelectrode tip, diameter of electrodes, and number of stimulated electrodes (1-8); 2) major phosphene-evoking parameters: current strength, pulse duration and impedance for stimulated electrodes; 3) variables: frequency of stimulation, impulse polarity, and duration of train impulses.

**RESULTS:** Preferable position of microelectrode tip was in 3rd-4th intracortical layers. Less current strength was needed with decrease in electrode diameter. Phosphene perception appeared when 3

or more electrodes were stimulated. Preferable frequency of stimulation was 25-100 Hz with bipolar -/+ impulses, at train duration of 1-2 s. Pulse duration was 0.3-1.0 ms for subdural and 0.1-0.5 for intracortical prostheses. Optimal intracortical current strength was 0.1-0.4 mA for 0.2-mm electrodes, and 0.02-0.1 mA for 0.05-mm electrodes. Subdural current strength was 1-4 mA for 1.0 mm electrodes, and 0.8-1.5 mA for 0.05-mm electrodes. Impedance for 0.05-mm electrodes achieved 50 kOm in 8 months after implantation, increasing a risk of neural cell damage.

**DISCUSSION & CONCLUSIONS:** Obtained results let us assume that such material as iridium oxide or aureated silver during intracortical implantation show good results in effectiveness of phosphene induction in cortical visual prosthesis development. But with time impedance increases tremendously, what makes difficult to use this prosthesis for a long time. New approach in biocompatibility, longevity and stability achievement is needed, and one of possible ways we see in nanosputtering or carbon nanotubes usage. So, the major requirements to structure of BCI for cortical visual prosthesis are hypoallergenicity and high level of biocimpatibility of the implanted material in aggregate with good electroconductivity and stability in ion environment of brain liquor.

**REFERENCES:** [1]B. Kh. Baziyan, S. A. Gordeev, M. E. Ivanova et al. (2008) *Bulletin of Experimental Biology and Medicine*, **145**: 4-6., Parameters of Phosphene-Inducing Electric Stimulation of the Cat Visual Cortex via Implanted Surface and Intracortical Electrodes. [2]M.E. Ivanova, S.A. Gordeev, B.Kh Baziyan et al (2008) *Abstr. book IEEE EMBS Conference* P.3371-3374 Evaluation of cortical visual prostheses microelectrode array function. Description of behavioral feline model. [3]W.H.Dobelle, M.G.Mladejovsky, J.R.Evans, et al. (1976) *Nature* **259:**111-112 “Braille” reading by a blind volunteer by visual cortex stimulation.

**ACKNOWLEDGEMENTS:** This research was funded by Russian Humanitarian Scientific Fund, Grant # 08-06-00401a.

# Combining AFM with hollow cantilevers towards electrophysiological measurements

P. Behr[1,2], D. Ossola[1], P. Dörig[1], M. Gabi[1,2], E. Sarajlic[3], M. Bijl[3], J. Vörös[1], T. Zambelli[1]

[1]Laboratory of Biosensors and Bioelectronics, ETH Zurich, Switzerland;
[2]Cytosurge GmbH, Zurich, Switzerland [3] SmartTip B.V., Enschede, The Netherlands

**INTRODUCTION:** Biomedical studies on living cells such as intracellular injections, patch clamping or extracellular deposition of liquids are typically carried out manually using tapered glass micro pipettes. The micro pipette is thereby slowly approached to the cell using micro manipulators under optical control. During this process - even when carried out by skilled operators - the cell is often mechanically injured which frequently leads to cell death and failure of the experiment. To overcome these drawbacks we propose a technique based on a combination of micro fluidics and atomic force microscopy known as FluidFM technology [1]. This approach is further motivated by the fact that AFM techniques are already widely used in the field of nano-biotechnology [2] as well as for the direct manipulation of single living cells [3,4].

**METHODS:** Our instrument is composed of custom micro-fabricated AFM cantilevers with different tip geometries and opening sizes encompassing an integrated micro-fluidic channel. The channel ends at a well-defined aperture located at or in the vicinity of the apex of the AFM probe tip while the other end is connected to a pressure controlled reservoir. The force control system of the AFM microscope allows a very precise regulation of the force applied by the probe tip to any surface while preserving the liquid dispensing capabilities of the probe. In particular, it for a controlled approach onto a cell membrane which in turn allows the discrimination between a "gentle contact" on the membrane or a controlled membrane perforation. Highly localized biochemical stimulation or direct manipulation of single living cells under physiological conditions becomes essentially practicable with the FluidFM technology.

**RESULTS:** The feasibility of our approach has been demonstrated earlier by selectively injecting single living cells in vitro with a membrane impermeable dye [1].
In this work we present how standard AFM microscopy in combination with hollow cantilevers can be used for electrophysiological

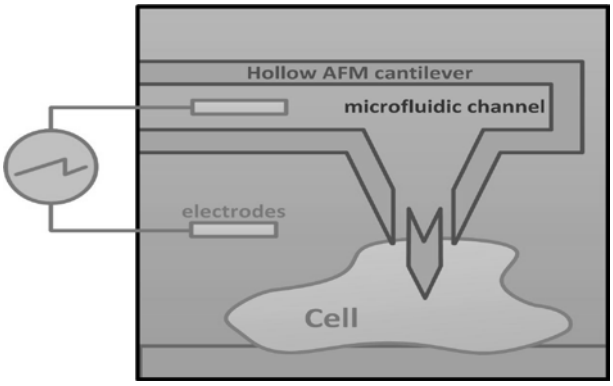


*Fig. 1: Schematics of a combined AFM-patch-clamp experiment. Using hollow cantilevers it is possible to use the same probe for acquiring AFM images and measuring ion channel activities.*

experiments (see figure 1). Thanks to the high resolution imaging capabilities and the force feedback of the AFM such an approach opens the door to numerous new experiments such as spatially correlated patch clamping while at the same time minimizing the overall impact on the investigated cells.

**REFERENCES:** [1]A. Meister, M. Gabi, P. Behr, P. Studer, J. Vörös, P. Niedermann, J. Bitterli, J. Polesel-Maris, M. Liley, H. Heinzelmann, T. Zambelli, *Nano Letters* **2009** 9 (6): 2501-2507 [2] D. J. Müller et al., *Nature Nanotechnology* **2008** 3: 261-269 [3] M. Currie et al., *Biochem. and Biophys. Research Comm.* **2007** 355 (3): 632-636 [4] P. Dörig, P. Stiefel, E. Sarajlic, D. Bijl, P. Behr, M. Gabi, J. Vörös, J. Vorholt, T. Zambelli, *Appl. Phys. Lett.* **2010**, in press.

**ACKNOWLEDGEMENTS:** We would like to thank Stephen Wheeler from the LBB Workshop for technical help. Furthermore, we are indebted to Martin Lanz from the LBB cleanroom facilities for his support in micro-processing related questions.

# Nanobioparticles Interactions: On-line Optical Evidence/Control

A. Bezrukova bezr@PB1097.spb.edu

*Faculty of Medical Physics and Bioengineering, St.Petersburg State Polytechnical University, St.Petersburg, 195 251, Russia*

**INTRODUCTION:** Proteins, nucleoproteids, lipoproteids, liposomes, viruses, virosomes, lipid emulsions, blood substitutes and other nanoparticle systems can be considered as biomedical *3D* disperse systems (DS) with nanoparticles as disperse phase in dispersive medium. The experience [1-4] suggests that the set of optical parameters of so called "second class" is unique for each *3D* DS [1, 4]. In another words each *3D* DS can be characterized by *N*-dimensional vector in *N*-dimensional space of optical parameters [1, 4]. Such presentation can serve as sensing platform and can provide further progress in biomedical *3D* DS characterization and "on-line" or "in-situ" control in nanobiotechnology.

**METHODS:** Multiparametric optical analysis of *3D* DS includes: a) simultaneous measurements of *3D* DS by different compatible non-destructive optical methods such as refractometry, absorbency, fluorescence, light scattering (integral and differential, static and dynamic, unpolarized and polarized); and b) solution of inverse optical problem by different methods including technologies of data interpretation by information-statistical theory. For the last purpose it is necessary to collect information about optical properties of different *3D* DS.

**RESULTS:** Fig. 1 demonstrates one of the examples of nanoparticle interaction evidence at the process of anthracene inclusion into β-cyclodextrin cavity [3, 4]: optical parameter vectors $P_{\text{3D DS state}}\{P_i, P_k, P_l, P_m\}$ present on plane for nanoparticle dispersions of anthracene (A) with concentration $1{,}4 \times 10^{-4}$ M/l (at all studied dispersions), β-cyclodextrin with concentration $8{,}75 \times 10^{-3}$ M/l (CD) and their mixtures. Concentrations of β-cyclodextrin in mixtures are the following: 1) $1{,}75 \times 10^{-6}$; 2) $8{,}75 \times 10^{-6}$; 3) $1{,}75 \times 10^{-5}$; 4) $8{,}75 \times 10^{-5}$; 5) $1{,}75 \times 10^{-4}$; 6) $8{,}75 \times 10^{-4}$; 7) $1{,}75 \times 10^{-3}$; 8) $8{,}75 \times 10^{-3}$ in M/l (number of mixture corresponds to number near point). Point for latex dispersion (L) presents optical parameter vector $\mathbf{P}_{\text{3D DS state}}\{P_i, P_k, P_l, P_m\}$ for latex *3D* DS with mean effective diameter of particles 150 nm (measured at the same conditions and studied in details by static and dynamic light scattering [2]). Uncertainty of parameters is about 5-10 %. Analysis [4] based on data [3].

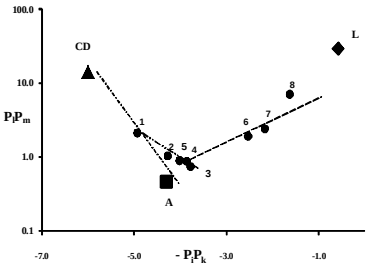


*Fig. 1: One of the examples of nanoparticles interaction evidence at the process of anthracene inclusion into β-cyclodextrin cavity [4]. Explanation is in the text.*

**DISCUSSION & CONCLUSIONS:** Inclusions of A into CD can be considered as the new nanoparticles [4], which share increases with concentration of CD (points 6, 7 and 8 in Fig.1). Such pictures obtained for proteins and viruses aggregations, differentiation of viruses and coli bacillus, differentiation of coli bacillus strains, for clay nanoparticles interaction with coli bacillus, etc. *3D* DS can be characterized and compared with another *3D* DS by means of the second class optical parameter vectors which can reflect the most changes in the state of *3D* DS and their mixtures.

**REFERENCES:** [1]A.G. Bezrukova (2006) *Proceedings of SPIE* **6253**:62530C1-4. [2]A. Bezrukova, M. Lubomska, P. Magri, M. Rogalski (2007) *Proceedings of SPIE*, **6597**: 65970M1-5. [3]A. Bezrukova, M. Lubomska, M. Rogalski (2009) *Rev Adv Mater Sci* **20**: 70-76. [4]A.G. Bezrukova (2009) *Proceedings of SPIE* **7377:**73770B1-6.

**ACKNOWLEDGEMENTS:** Author would like to thank Prof. Dr. M. Rogalski (University of Metz, France) and Prof. Dr. M. Textor (Swiss Federal Institute of Technology, ETHZ) for the help in research and useful discussions.

# Tuning the mechanical properties of bioreducible multilayer films for improved cell adhesion and transfection activity

J. Blacklock[1], A.Vetter[2], D.Oupický[3], H. Mohwald[1]

[1] *Department of Colloids and Interfaces, Max Planck Institute, Potsdam, Germany.*

[2] *Biomaterials Department, Max Planck Institute, Potsdam, Germany.*

[3] *Wayne State University, Department of Pharmaceutical Sciences, Detroit, MI, U.S.A.*

**INTRODUCTION:** A simple approach to the mechanical modulation of layer-by-layer (LbL) films is through manipulation of the film assembly. Here, we report results based on altering the salt concentration during film assembly and its effect on film rigidity. Based on changes in film rigidity, cell adhesion characteristics and transfection activity were investigated *in vitro*. LbL films consisting of reducible hyperbranched poly(amide amine) (RHB)[1] have been implemented along with DNA for investigating fibroblast adhesion on $[RHB/DNA]_{n/2}$ films with varying rigidities. Film mechanical properties along with cell adhesion, stress fiber orientation and transfection activity were investigated with regards to changes in the film rigidity.

**METHODS:** Molecular force probe (MFP) measurements were performed to measure the apparent Young's modulus, $E_{APP}$, of the films *in situ*. Cell adhesion and stress-fiber characteristics were investigated using total internal reflectance microscopy (TIRF-M). The average cell peripheral area, fiber density and average fiber length during 5 days of cell growth were investigated using either low-$E_{APP}$ (below 2.0 MPa) or high-$E_{APP}$ (above 2.0 MPa) films. Transfection studies were performed using gfpDNA and SEAP-DNA to investigate if changes in cell adhesion affect transfection activity. Cell proliferation and cytotoxicity studies were used to investigate cellular viability over a week.

**RESULTS:** These studies have shown that altering the salt concentration during film assembly of bioreducible LbL films can change the film modulus by 2 orders of magnitude, affecting both film thickness and roughness. Additionally, two different growth characteristics have been observed for films assembled in low or high salt concentration.[2] AFM images show that film assembly within these two salt ranges has an effect on surface characteristics as well. Significant differences in cell attachment, growth and transfection activity are seen with film rigidities either < 2 MPa (low-$E_{APP}$) or > 2 MPa (high-$E_{APP}$). During cellular growth and proliferation, it is found that cells grown on high-$E_{APP}$ films have

increased peripheral areas and stress-fiber density compared to cells grown on low-$E_{APP}$ films. These growth characteristics also have an effect on transfection activity which is found to be significantly higher for cells grown on high-$E_{APP}$ films compared to low-$E_{APP}$ films.

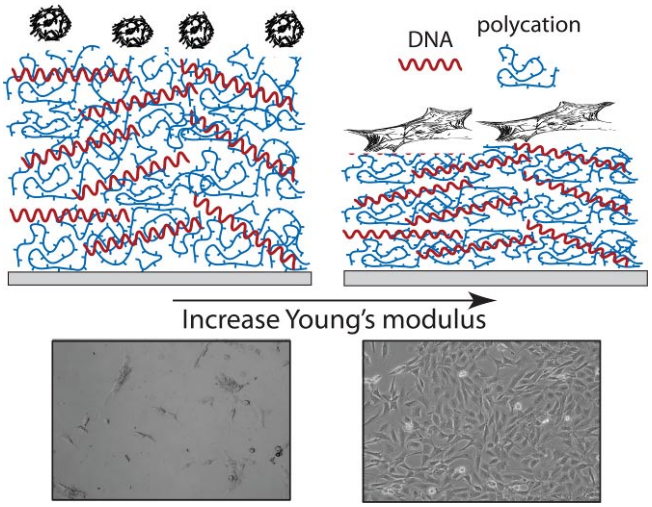


*Fig. 1: Affect of changing film rigidity with regards to cell adhesion. Fibroblast cells are grown on RHB/DNA films having a modulus of either 1.2 MPa(left) or 8.0 MPa (right).*

**DISCUSSION & CONCLUSIONS:** The results have shown that surface modification of bioreducible LbL films of controlled thickness and roughness promotes cellular adhesion, stress-fiber growth and increased transfection activity without the need for an additional adhesive protein pre-coating of the surface or chemical cross-linking of the film. In particular, it has been found that bioreducible LbL films with an apparent elastic modulus greater than 2.0 MPa have increased cell adhesion, cell spreading and transfection activity compared to films with low modulus.

**REFERENCES:** [1] J. Blacklock, Y.Z. You, Q.H. Zhou, G.Z. Mao, D. Oupickỳ (2009) *Biomaterials* **30**:939-50. [2] L. Lee, F. Cavalieri, A.P.R. Johnston, et al (2010) *Langmuir* **26**:3415-22.

**ACKNOWLEDGEMENTS:** The authors would like to acknowledge the Max Planck Society and the Fulbright Fellowship organization.

# Nanodefects to tune the chemical and biological Properties of calcium phosphate biomaterials

M. Bohner[1], S. Gruenenfelder[1], N. Doebelin[1], W. Hofstetter[2], R. Luginbuehl[1], R. J. Egli[1,2]

[1] *RMS Foundation, Bettlach, CH,* [2] *Group for Bone Biology and Orthopaedic Research, Department Clinical Research, University of Bern, CH*

**INTRODUCTION:** Calcium phosphates are amongst the most powerful bone graft substitutes. Especially, hydraulic cements have received much attention in filling and reinforcing poorly accessible bone defects. However, their handling properties need further improvement. Recently, we showed that the start of hydraulic cement reaction of α-tricalcium phosphate (TCP) can be delayed for few hours by treating the cement powder at 500ºC for 24 h [1]. The aims of this study were (i) to elaborate the potential of this treatment to control the onset of the setting reaction, and thus handling of a cement paste, and (ii) to test the response of bone cells cultured on granules subjected to the same treatment.

**METHODS:** Calcium phosphate powders (mean diameter 9 μm) and granules (diameter 125-180 μm) were produced and treated at 500°C for 1-24 h (=calcination). Energy release of powders reacting in water was measured by isothermal calorimetry at 37ºC. Murine calvarial osteoblasts (OB) and bone marrow derived CSF-1 dependent osteoclast precursor cells (OC) were cultured on granules and analyzed for growth and differentiation.

**RESULTS:** Blends of calcined and native α-TCP powders revealed a deferral of the reaction onset from 6 min to 2.5 h with an increasing calcined fraction (Fig.1). In addition, the reaction kinetics was modulated by the liquid component (200 mM $NaxH(3-x)PO_4$ buffer) used for the cement reaction with a delay of the reaction start from a few minutes at pH 4.6 to almost 4 h at pH 10.5. OB growth (XTT assay) and differentiation (ALP activity; expression levels of 85 bone specific genes) was not affected by calcination. The development of OC (TRAP activity) was significantly delayed in cultures on uncalcined α-TCP after 3-5 days. However, TRAP activity significantly increased after 8-9 days, probably due to calcium depletion of the culture medium (favouring osteoclast development) through apatite formation on the granules beyond 8 days, as visualized with SEM. The changes in chemical and biological reactivity due to calcination were not limited to α-TCP but also affected other common calcium phosphates, namely β-TCP and hydroxyapatite (not shown).

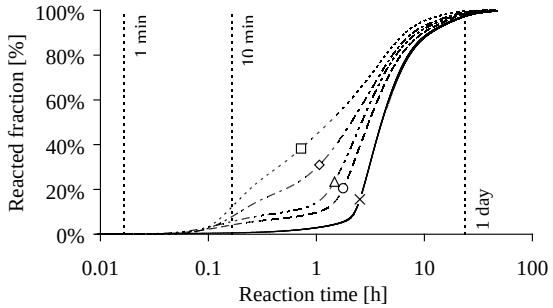


*Fig. 1: Reactivity of uncalcined/calcined (1h or 24h at 500ºC) α-TCP powder blends. (□) 100/0; (◊) 50/50 (1h); (Δ) 10/90 (1h); (o) 0/100 (1h); (x) 0/100 (24h). Hardening of the cement generally occurs close to 10% reacted fraction.*

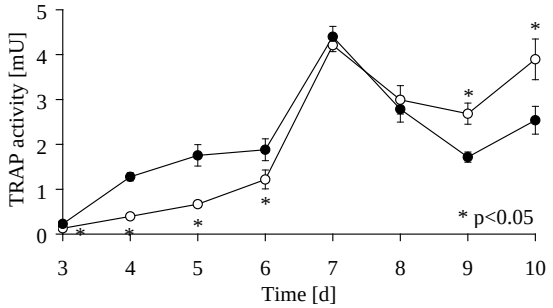


*Fig. 2: TRAP activity of OCs cultured on (o) uncalcined and (●) calcined α-TCP granules.*

**DISCUSSION & CONCLUSIONS:** A simple thermal treatment at 500ºC can be used to tune chemical and biological properties of calcium phosphate bone graft substitutes which opens up new perspectives in the control of the handling properties of calcium phosphate cements. We propose that the different surface dissolution capacities of the calcined and uncalcined materials lead to this effect.

**REFERENCES:** [1] Bohner M. et al., Acta *Biomater*. 2009 Nov;**5**(9):3524-35.

# Second Harmonic Imaging Probes for Bio-Labeling

L. Bonacina[1], J. Extermann[1], C. Kasparian[1], Y. Mugnier[2], R. Le Dantec[2], J.-P. Wolf[1]

[1] *Gap-Biophotonics, University of Geneva, Switzerland.*

[2] *SYMME, Université de Savoie, France.*

**INTRODUCTION:** In the quest for the next generation of imaging bio-markers, successful probes have to prove to be non toxic, bright, stable against long term excitation, and able to generate a sharp contrast against background fluorescence. In all these respects, Second Harmonic Radiation Imaging Probes (SHRIMPs) are receiving an increasing attention as they also open a series of alternative detection possibilities simply not accessible with the present generation of fluorescent dyes and quantum dots.

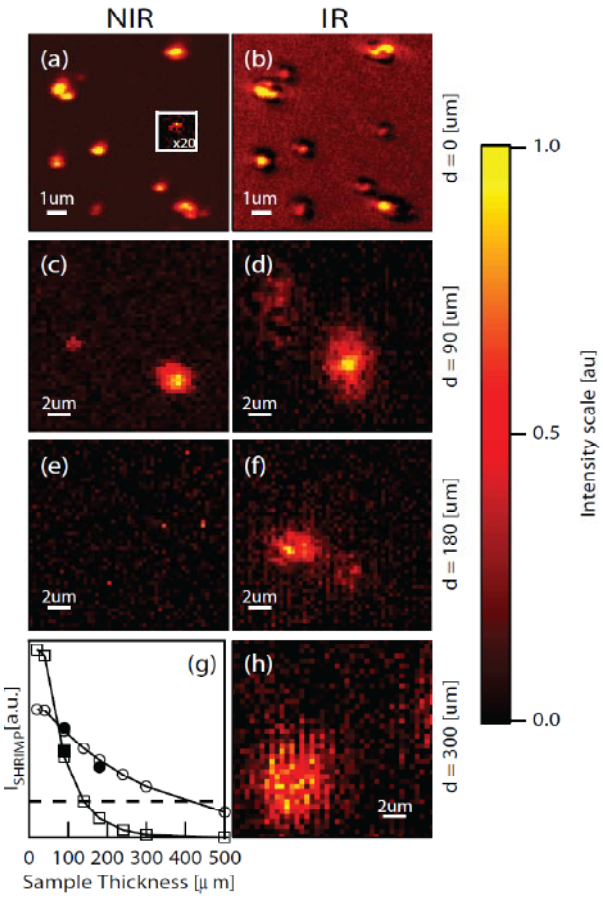


*Fig. 1: The $Fe(IO_3)_3$ SHRIMPs sample is excited at 800 nm (left) and 1.5 um (right), through a diffusive layer of increasing thickness. The bottom left panel compares experimental results (filled datapoints) and Monte Carlo predictions (open datapoints ).*

**RESULTS:** The extreme wavelength flexibility, enabled by the non-resonant nature of the second harmonic process, has been demonstrated by using laser sources in the near- (800 nm) and short-wavelength-infrared (1.55 μm) regions. The latter allow deeper penetration through tissue-phantoms and murine excised samples. An *ad hoc* radiative-transport Monte Carlo code, taking into account the nonlinearity of the interaction, was developed to rationalize these observations and define the best excitation strategy at the light of the spectral and diffusive properties of the specimen[1].

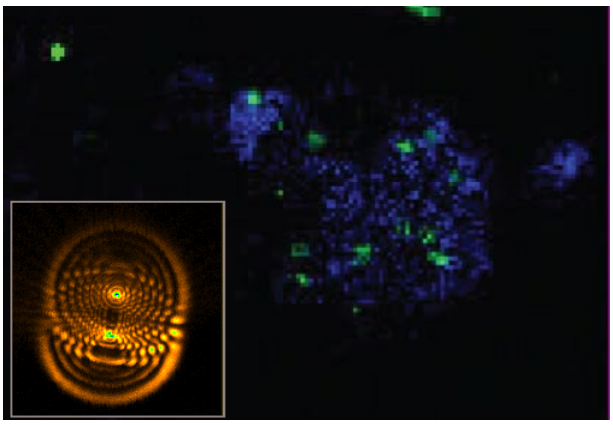

*Fig. 2: Ovcar-3 cell labelled with ZnO SHRIMPs. Cell autofluorescence (blue), SHG signal (green). Inset: defocused image of the second harmonic interference pattern generated by two SHRIMPs 5 μm apart.*

The phase-coherent optical response of the SHRIMPs was exploited to fully characterize the excitation laser pulse in the focal spot of a high-NA objective with nanometric resolution[2]. This proof-of-principle experiment sets the ground for further phase-sensitive self-referenced applications, after the recent demonstration of harmonic holography and heterodyne detection with external references. Finally, we showed that individual SHRIMPs spatial orientation can be retrieved by polarization-microscopy[3], opening the possibility of optically monitoring the local electric field surrounding the nanoprobes.

**REFERENCES:** [1] J. Extermann, L. Bonacina, et al (2009) *Opt Express* **17**(17): 15342-15349. [2] J. Extermann, L. Bonacina, et al (2009) *Opt Express* **16**(14): 10405-10411. [3]. L. Bonacina, Y. Mugnier, et al (2007) *Appl Phys B* **87** (3): 399-403.

**ACKNOWLEDGEMENTS:** Swiss SER (COST MP0604); M. Birkgit fund Geneva; NAOMI (Interreg IV A).

# Novel self assembled conjugation chemistry based nanoparticle system as an effective nano bullets for cancer

D. K. Bora [1] *, N. Kasoju [1], R. R. Bhonde [2], U. Bora[1]

[1] *Biomaterials and Tissue Engineering Laboratory, Department of Biotechnology, Indian Institute of Technology Guwahati, , India.*

[2] *Tissue Engineering and Banking Laboratory, National Centre for Cell Science, Maharashtra , India*

** Currently at Laboratory for High Performance Ceramics, EMPA-Dubendorf, Switzerland.*

**INTRODUCTION:** Cancer, which is a leading cause of death in humans, is caused by an uncontrolled growth and spreading of abnormal cells. In general, a nanoformulation contains a potent anticancer compound and a nanocarrier. However, till now there is no nanoformulation developed for delivery of phthalimide based compounds. Also, to our knowledge, there is no nanoformulation which can directly kill cancer cells, without the need of loading a potent anticancer candidate. The objective of the current study is to synthesize a phthalimide based conjugate which can self assemble to form NPs.

**METHODS:** The synthesis of PHEP-Pal NPs was done in three sequential steps. In the first step, a phthalimide derivative namely N-(2-Hydroxyethyl) phthalimide (HEP) was synthesized. Subsequently, PHEP-Pal conjugate was synthesized by conjugation between HEP and palmitoyl chloride. Finally, the conjugate was allowed to self assemble and form NPs in an aqueous environment.

The anticancer activity of self-assembled PHEPPal NPs in comparison to HEP derivative alone was assessed by MTT assay (Mosmann 1983). Cells (HeLa and A 549) were grown in T-25 culture flasks (Cell Bind, Corning). At sub-confluent stage the were harvested by trypsinization, plated approximately at a rate of 1 9 104 cells per well in a 96 well culture plate (Corning) and cultured for 24 h in a CO2 incubator. The medium from each well was removed and the cells were washed twice with Dulbecco's phosphate buffered saline without $Ca^{2+}$ and $Mg^{2+}$. The cells were then exposed to different concentrations (ranging from 1 to 100 lM in serumfree DMEM) of HEP and PHEP-Pal NPs to study the dose dependent action and to calculate the IC50 values.

**RESULTS:** As shown in Scheme 1, in the first instance, we have reacted phthalic anhydride with ethanolamine, using dried DMF at high temperature, in order to synthesize a pthalimide derivative (HEP). Subsequently, HEP was reacted with palmitoyl chloride to synthesize a PHEP-Pal conjugate.

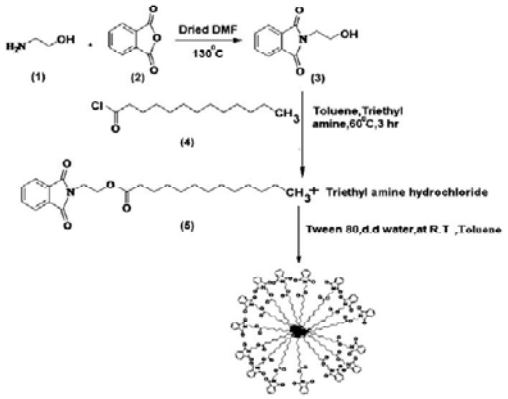


*Fig. 1: Scheme for the synthesis of HEP, PHEPPal conjugate, and subsequent self assembly into PHEP-Pal NPs.*

The application of resultant self-assembled NPs as an anticancer agent was verified with cell culture experiments. We studied the effect of HEP and PHEP-Pal NPs on A549 and HeLa cell lines by MTT assay. Significant difference was observed in the activity of NPs, both in dose and time dependent studies. It needs higher amount of HEP to attain 50% cell mortality (IC50) than PHEP-Pal NPs in case of both A549 and HeLa cells..

**DISCUSSION & CONCLUSIONS:** HEP and PHEP-Pal were subjected to $^{1}H$ NMR spectroscopy, where it was found that, HEP showed signals related to resonances of the ethanolamine methylene protons (d3.82 ppm) and phthalimide protons (d7.69 and d7.81 ppm). Also, in case of PHEP-Pal, a small triplet was found at d 4.41 ppm confirms that conjugation took place through an ester bond. Finally, cell culture studies using A549 and HeLa cells revealed enhanced anticancer effect of PHEP-Pal NPs in comparison to HEP alone.

**REFERENCES:** [1] N. Kasoju, D.K.Bora, R. R. Bhonde and U. Bora, *Journal of Nanoparticle Research*, Volume **12**, Number 3 / March, 2010

**ACKNOWLEDGEMENTS:** This study was accomplished with the financial aid from Government of India organizations, Department of Biotechnology, vide Project Nos. BT/PR6759/BRB/10/446/2005

# Analysis of molecular interactions between focal adhesion proteins talin and vinculin using FRET

A.-K. Born[1], V. Vogel[2], R. Kemkemer[3], K. Maniura-Weber[1]

[1]*Empa, Material-Biology Interactions, St. Gallen, Switzerland*

[2]*ETH Zurich, Biologically Oriented Materials, Zurich, Switzerland*

[3]*Max Planck Institute for Metal Research, Stuttgart, Germany*

**INTRODUCTION:** The development of cell based sensors as well as new material concepts for medical applications will be greatly advanced by tools that allow online life monitoring of cellular processes. Cell adhesion and generation of force on the extracellular matrix (ECM) play an important role for cell viability, migration and differentiation. Primary sites of adhesion are formed between integrin receptors and the underlying substratum. Intracellular, integrin receptors bind to a large number of proteins. Binding of talin to β integrins causes integrin activation followed by accumulation of talin in focal contacts. Recruitment of vinculin to focal adhesions sites is force dependent. Tensile forces that are applied to newly formed adhesion sites cause stretching of the talin rod thereby activating talin's vinculin binding sites that are buried under equilibrium conditions[1]. Vinculin containing focal adhesions are capable of exerting migration forces. Fluorescence resonance energy transfer (FRET) microscopy offers the capability to study the fate and function of biomolecules in living cells[2]. Using CFP and YFP as the donor-acceptor pair for FRET we study the molecular interaction of talin and its binding partner vinculin in focal adhesions.

**METHODS:** For FRET measurements we generated several constructs in which the yellow fluorescent protein is inserted in close proximity to vinculin binding sites of talin rod. As the binding sites for talin are located in the N-terminal vinculin head domain we positioned CFP in front of vinculin. These constructs were used for nucleofection of human fibroblasts. To confirm that mechanosensitivity was unchanged by nucelofection cells adhered on a stretchable substrate were subject to uniaxial strain. FRET efficiency ($E_F$) between talin and vinculin was determined by acceptor photobleaching. Myosin-II inhibitor blebbistatin and Rho-kinase inhibitor Y27632 were used to reduce cell contractility.

**RESULTS:** Human fibroblasts transfected with the fluorescently labelled vinculin or talin showed the expected accumulation of fluorescence signal at focal adhesion sites as confirmed by immunohistochemical staining. Furthermore, mechanosensitivity of transfected cells was comparable to that of non-transfected cells indicating that cellular function is not altered by nucleofection. Cells transfected with control constructs and analysed for FRET efficiency by the acceptor photobleaching method showed that FRET measurements are possible with our setup. Furthermore, FRET efficiencies determined from talin/vinculin co-transfected cells were distinctly increased compared to those efficiencies determined for non-interacting control constructs.

**DISCUSSION & CONCLUSIONS:** Our primary results suggest that transfection of cells with our gene constructs is efficient while the cells mechanosensitivity is not affected. Hence, our approach is qualified for determination of interaction between focal adhesion proteins talin and vinculin in cells. The FRET technique allows testing the ability of cells to form adhesion complexes on a material surface and dynamics associated with this process. It has therefore been chosen as the tool of choice to evaluate cell-material interactions at the molecular level and will be of use especially to study substrates with different mechanical properties.

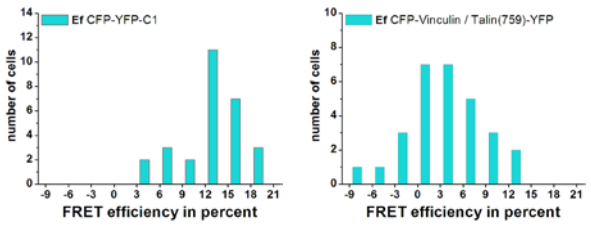


*Fig. 1: FRET efficiency of constructs CFP-YFP-C1 (positive FRET control, $E_F$=13.124±0.804, n=28) and CFP-Vinculin/Talin(759)-YFP ($E_F$=3.897 ± 0.898, n=29) determined by acceptor photobleaching.*

**REFERENCES:** [1] Gingras, A.R., Ziegler, W.H., Frank, R. Barsukov, I.L., Roberts, G.C.K., Critchley, D.R. and Emsley, J. Mapping and Consensus Sequence Identification for Multiple Vinculin Binding Sites within the Talin Rod. *JBC*, **280**, 37217, 2005. [2] Sekar, R.B., and Periasamy, A**.** Fluorescence resonance energy transfer (FRET) microscopy imaging of live cell protein localizations. *JBC*, **160**, 629, 2003

**ACKNOWLEDGEMENTS:** We thank Viola Vogel for stimulating discussion about talin structure and Vesa Hytönen for sharing his ideas for development of talin FRET constructs. The present study is supported by the European Commission through the specific targeted research project CellForce (Contract N°: NMP4-CT-2005-016626) and CCMX Matlife.

# Towards nano-scale controlled actuation of cell membrane receptors

P.J. Bosch[1], A. Ebner[2], P. Hinterdorfer[2], J.S. Kanger[3], V. Subramaniam[1,3]

*[1] Nanobiophysics, MESA+ Institute for Nanotechnology. [2] Institute of Biophysics, University of Linz, Austria. [3] MIRA Institute for Biomedical Technology and Technical Medicine, The Netherlands*

**INTRODUCTION:** We aim to precisely position and control individual ligands onto the cell surface by AFM, while simultaneously following the signalling response of the cell. This response may be followed very specifically by measuring the activation of intracellular signalling and trafficking proteins by FRET-FLIM[1], and by altered receptor dynamics using single molecule tracking methods[2].

We are currently optimising the functionalisation of AFM tips with single epidermal growth factor (EGF) ligands using a long elastic PEG linker. We have performed force interaction measurements with EGF functionalised tips on a model system of antibodies immobilised on a flat surface.

**METHODS:** To attach EGF on an AFM tip, we need to use a distensible heterobifunctional linker. We chose an 8 nm long PEG linker with an NHS ester on one end for covalent linkage to an amino-coated tip, and a less reactive benzaldehyde at the other end to bind to the N-terminus of EGF. As a quantitative test of the binding of EGF onto an aldehyde group, we incubated two different concentrations of EGF on a glutaraldehyde coated gold layer. We then looked at the surface plasmon resonance (SPR) of this gold layer upon exposure to antibodies against EGF.

For AFM force-distance experiments, until now a model system served as the substrate: the same antibodies against EGF were incubated with a small PEG linker on a flat surface. A measurement series consisted of 1,000 force-distance curves, analysed with a non-linear least-squares algorithm, to obtain information from the specific unbinding events only. In control measurements, EGF was added to block the antibodies.

**RESULTS:** Upon a flow of antibodies in the SPR experiment, the EGF incubated gold layer showed a shift in the index of refraction. The binding seems largely specific since washing with buffer did not remove the antibodies. With the known ratio of SPR angle shift to surface coverage for antibodies, the data was rescaled and is shown in figure 1.
In force experiments by AFM, we currently obtain

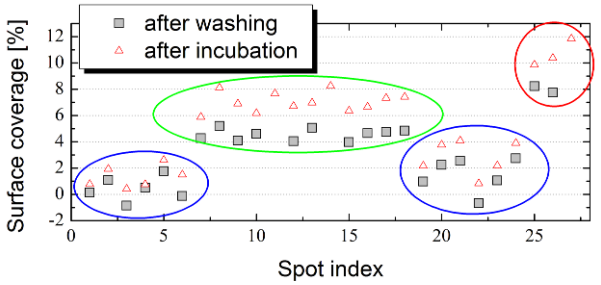


*Fig. 1: Angle shift of the index of refraction of the SPR chip after incubating different concentrations of EGF (blue: 0 μM, green: 0.6μM, red: 6 μM).*

low specific unbinding probabilities of 2 to 6%, consistently distributed around 35 to 50 pN. See figure 2 for an example series. The unspecific adhesion on the tip is more pronounced, but can be distinguished from specific ones due to the typical parabolic shape in the force distance curves caused by the PEG linker. Blocking the antibody whenever tips and samples showed relatively high unbinding probabilities, did reduce the unbinding probability.

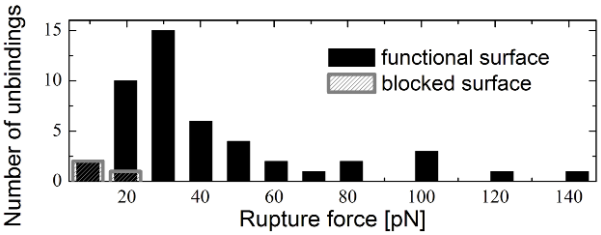


*Fig. 2: Histogram of the rupture force of a single EGF from an antibody in a series of 750 curves.*

**DISCUSSION & CONCLUSIONS:** An SPR measurement proved that we can bind EGF on an amino-coated surface using aldehyde chemistries, while still being recognised by antibodies for EGF. Initial AFM force-distance curves of the interaction between a single EGF protein and an antibody are consistent, but (un)binding probabilities need to be improved before pursuing measurements on the much more complex system of a living cell.

**REFERENCES:** [1] Verveer, P. et al. (2000) *Science* **290**, 1567-1570. [2] Sergé, A. et al. (2008) *Nature methods* **Vol.5 No.8** 687-694

**ACKNOWLEDGEMENTS:** This project is funded by an EU NanoScience E+ grant.

European Cells and Materials Vol. 20. Suppl. 3, 2010 (page 26) ISSN 1473-2262

# Building a model 3D immunosensor on gold nanoparticle monolayers

S. Boujday, A.L. Morel and C.M. Pradier

*Université Pierre et Marie Curie- Paris 6, UMR CNRS 7197, Laboratoire de Réactivité de Surface, F75005 Paris, France*

**INTRODUCTION:** The sensitivity of immunosensors may be significantly improved by building gold nanoparticles (AuNPs) ordered layers on which the IgG receptors are immobilised; both for geometric reason and thanks to the sensitivity of some optical detection techniques, a significant enhancement of the sensor sensitivity is expected on such 3D layers. The challenge is to build an ordered layer of optimal size nanoparticles, and of doing the right chemistry to functionalise them.

Here we built such gold Np layers and evaluated the increase of the number of receptors and of their accessibility brought by such a construction.

**METHODS:** Planar gold chips have been functionalised by amine-terminated self assembled monolayer (SAMs) on which gold NP of 15 or 60 nm diameter were immobilised. Two routes were explored: in a 1st series of experiments, they were grafted right after their synthesis, followed by their functionalisation ; the latter consisted in a covalent binding of protein A to an acid-terminated thiol layer (PrA allows the grafting of antibodies in a well oriented manner); in a second set of experiments, gold Nps were functionalised before their grafting.

The synthesis and deposition of gold nanoparticles, 15 and 60 nm size, were characterised by combining Polarisation Modulation InfraRed Reflexion Absorption Spectroscopy (PM-IRRAS), Photo electron Spectroscopy (XPS) and Surface Enhanced Raman Scattering (SERS), as well as Atomic Force Microscopy (AFM), which all proved the formation of a well dispersed layers of nanoparticles, but with significantly different coverages. The elaboration and bioactivity of the so-built 3D immunosensors were monitored by PM-IRRAS [1], a technique that, in the present case, strictly measures the number of immobilised probes or target molecules, without any optical or electrical enhancement effect.

**RESULTS and DISCUSSION**: Compared to PrA and rIgG immobilised on planar gold samples, the construction of 3D immunosensors increases the number of PrA by a factor of 2 on 60 nm AuNPs, but almost no incresa was observed on 15nm AuNPs. The latter result is explained by the little increase of the available gold area. However, the number of IgG probes was increased whatever the AuNPs size, likely thanks to a decrease of the PrA layer rigidity; overall, the anti-rIgG/rIgG ratio, stating the probe accessibility, was increased by a factor 2 on the larger nanoparticles. The important result is that nanoparticles of 60 nm are preferable for the following reason: they enable to build a denser and well dispersed layer and they increase both the number of receptors (IgGs) and their accessibility.

In the case of gold Np functionalisation in the liquid phase, before immobilisation, similar interesting improvements were observed but with the adventitious formation of AuNPs aggregates on the surface.

**CONCLUSIONS:** This work demonstrates the key role of the number, and of the accessibility of the molecular receptors, which both may be improved by building immunosensors on gold nanoparticles, and choosing the optimal functionalisation method.

Measurements are currently done to test the sensitivity of the anti rIgG detection by Surface Plasmon Resonance on these 3D immunosensors.

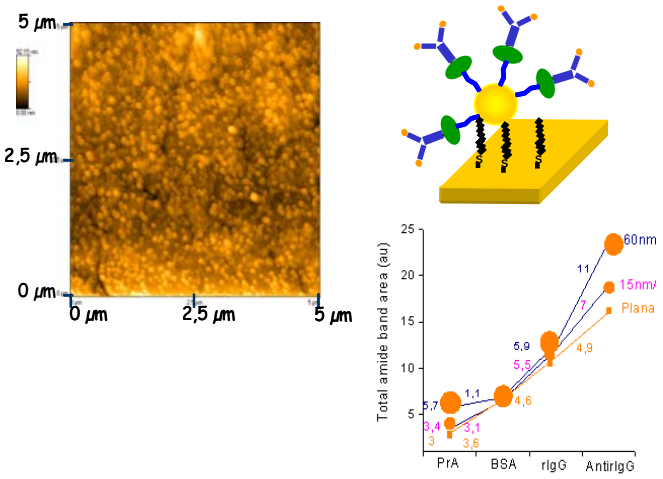


*Fig. 1: A well dispersed layer of 15 nm size gold nanoparticles (left); the scheme of a 3D immunosensor and, amount of grafted proteins, at the successive steps of immunosensor elaboration, on the planar gold , and on 15 and 60nm Np immunosensors.*

**REFERENCES:** [1]S. Boujday, C. Gu, M. Girardot, M. Salmain, and, C.M. Pradier, *Talanta, 78,* 2009, *165-170.*

# Human Elastin-like Polypeptides: Recombinant Biopolymers for Regenerative Medicine

S.Bozzini1, S.Farè1, L.Altomare1, P.Petrini1, A.Bandiera2, M.C.Tanzi1

[1]*Bioengineering Department, Politecnico di Milano, P.zza L. da Vinci 32, 20133 Milan (Italy).*
[2]*Department of Life Sciences, University of Trieste, via Giorgieri 1, 34127 Trieste (Italy)*

**INTRODUCTION:** The use of polymers naturally occurring in the extracellular matrix (ECM) is considered very promising for application in regenerative medicine. Recombinant elastin-like polypeptides (ELPs) represent one of the most fascinating example of this new generation of ECM-mimicking materials, due to their unique biochemical and physical properties. In fact these polypeptides, derived from the most common repeating (VPGXG) motif, typical of the mammalian protein, exhibit rubber-like elasticity reminiscent of the native elastin and can undergo to a reversible, inverse temperature phase transition. Elastin-like polypeptides (ELPs) have been proposed for drug delivery applications [1] and, in general, for repair of damaged elastic tissues [2]. Our work aims at evaluating the potentiality of a human elastin-like artificial protein (HELP) as base material of self-assembled or crosslinked matrices for regenerative medicine applications.

**METHODS:** *HELP production*. The elastin like polypeptides were produced by a synthetic gene expressed in Escherichia coli as described in [3]. *HELP matrices*. HELP protein was crosslinked with bacterial transglutaminase, TGase (N Zyme, BioTec GmbH). To optimize the crosslinking reaction, experimental parameters (protein concentration, pH and temperature) have been properly varied. The matrices, produced by using the best reaction conditions- 5%$w_{HELP}$/v in 10 mM TRIS/HCl, pH 8, 6% (w/v buffer solution) enzyme aqueous solution, room temperature- were freeze-dried, after cooling at -20°C and characterized by comparing with air-dried (37°C) matrices. The samples were observed at SEM (Stereo Scan 360 Cambridge Instruments) and characterized by ATR-FTIR (Nicolet 6700), compression mechanical tests (DMA, 2980 model, TA Instruments) and measurements of swelling ratio.

**RESULTS:** The crosslinking was confirmed by infrared spectroscopy, by evaluating the peak area ratio (v(C-N)/v(C-H)), where v(C-N) is attributed to the primary C-N stretching band and v(C-H) to the C-H stretching (Fig. 1). After crosslinking, an increase of one order of magnitudo of the area ratio occurred in HELP matrices, compared to HELP, because of the decrease of the primary amine groups amount.

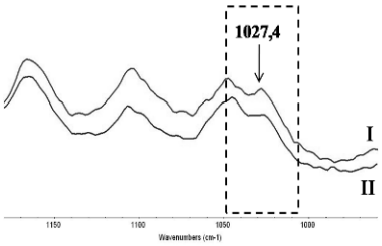


*Fig. 1. ATR-FTIR region of primary amine C-N stretching peak; HELP (I) and cross-linked HELP matrix (II)*

Compression mechanical tests (37°C, frequency sweep 0,5-5 Hz, 10 cycles) has indicated no change in the contribution of the elastic component (E'=2±0,5 KPa) to the mechanical behaviour of the air-dried matrices.

**DISCUSSION & CONCLUSIONS:**

Through incorporation of lysine and glutamine crosslinking domains in the recombinant elastin, cross-linked HELP-based matrices have been produced with bacterial transglutaminase, which catalyzes the reaction between these two amino acids. Our results suggest the produced HELP-based materials could be proposed as non-conventional candidate for regenerative medicine constructs. Additional experimental investigation on preparation of HELP-PEG containing matrices (Fig. 2) is now in progress.

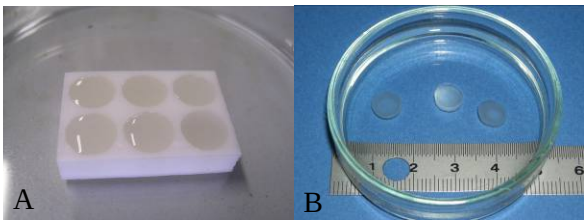


*Fig. 2:Images of TGase crosslinked HELP(A) and HELP-PEG matrices (B)*

**REFERENCES:** 1 E. R. Wright et al, Advanced *Drug Delivery Reviews* **54**, 1057-1073 (2002). 2 S. M. Mithieux et al, *Biomaterials* **25**, 4921-4927 (2004). 3 A. Bandiera et al, *Biotechnol. Appl. Biochem.* (2005) **42**, 247-256

**ACKNOWLEDGEMENTS:** Financed by PRIN Program 2007 (Italy) to M.C. Tanzi

# Interaction between tethered supported lipid bilayers and a glycodendrimeric porphyrin studied by combined QCM-D and EIS

E. Briand, P. Maillard, V. Rosilio

[1] *UMR 8612 CNRS/Univ. Paris-Sud, Châtenay-Mallabry, France*

[2] *UMR 176 CNRS/Institut Curie, Univ. Paris-Sud, Orsay, France.*

**INTRODUCTION:** A set-up combining the quartz crystal microbalance with dissipation monitoring technique (QCM-D) and electrochemical impedance spectroscopy (EIS) was successfully used to follow the interaction between an oligodendrimeric porphyrin and tethered supported lipid bilayers (thSLB). This approach enables to characterize simultaneously the modifications in the electrical and structural properties of the thSLB [1] while interacting with the water-soluble porphyrin. In a first step, the formation of the thSLB on $SiO_2$ coated quartz crystals has been studied and once this achieved, the influence of porphyrin molecules on the properties of the model membranes was assessed. This approach is aimed at understanding and optimizing the chemical structure and pharmacological properties of porphyrins usable in the photodynamic therapy of retinoblastoma.

**METHODS:**

*Tethered supported lipid bilayer assembly:* The thSLB was formed in two steps, with first, the formation of a lipid monolayer containing a low molar ratio of a PEGylated phospholipid via Langmuir-Blodgett (LB) transfer, followed by the fusion of liposomes in the QCM-D/EIS measuring chamber. The formation of the thSLB was followed as a function of time by EIS and QCM-D.

*Interaction with the glycodendromeric porphyrin*: the dendrimeric porphyrin bearing 9 α-mannose moieties was synthesized at the UMR 176 CNRS/Institut Curie laboratory. Aqueous solutions with various concentrations were tested and their influence on the thSLB properties followed by QCM-D (QCM-D E1 with Echem cell from Q-sense) and EIS (SP-150 from BioLogic) as a function of time and porphyrin concentration.

**RESULTS:** Surface pressure-area isotherms were performed prior to LB transfer to determine the structure of the lipid film containing the PEGylated phospholipid. As shown by EIS, the resistivity of the membrane after liposomes rupture on top of the LB transferred monolayer was dependent of the polymer structure of the proximal monolayer. QCM-D analysis of the layer displayed various thicknesses of the polymer cushion according to the length of the polymer chains of the PEGylated lipid. The introduction of the water-soluble porphyrin into the measuring chamber after thSLB completion induced mass increases depending on porphyrin concentration, while no modification of the viscoelastic properties was observed. This adsorption induced a decrease in the resistivity of the SLB. Rinsing the membranes after porphyrin molecules adsorption induced a decrease in the amount of material bound to the surface, while the resistivity of the membranes increased again, to reach *ca* its initial value (*Fig.1*).

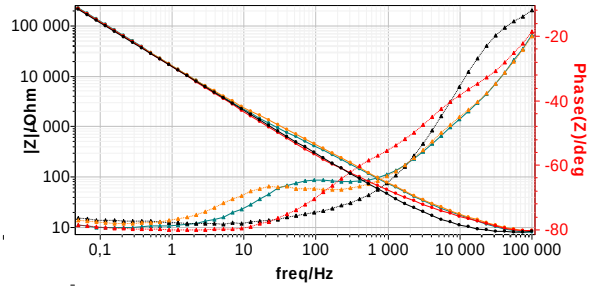


*Fig. 1: EIS phase (dotted lines) and amplitude (straight lines) spectra of bare crystal (black) after thSLB completion (blue), interaction with the porphyrin (red), and rinsing with buffer (yellow).*

**DISCUSSION & CONCLUSIONS:** The results showed that the quality of the thSLB depends dramatically on the structure of the polymer film that will stand as a cushion for the phospholipid monolayer during the LB transfer. The use of different polymers enables to modify the thickness of the polymer layer underneath. The water-soluble glycodendrimeric porphyrin adsorbs to the lipid membrane, disturbing the structure of at least the distal lipid leaflet. The absence of modification in the viscoelastic properties is likely explained by a close interaction between the mannose moieties and the phospholipids polar head groups through H bonds. The partial desorption of porphyrin molecules following rinsing tends to indicate that the hydrophobic core is not deeply inserted within the lipid bilayer.

**REFERENCES:** [1] E. Briand, M. Zäch, S. Svedhem, et al (2010) *Analyst* **135**:343–350

**ACKNOWLEDGEMENTS:** The CNRS is acknowledged for financial support.

# New antibacterial coated surfaces for self-protecting implants

P.S.Brunetto1, K.M.Fromm[1]

[1] *Department of Chemistry, University of Fribourg, Fribourg, Switzerland.*

**INTRODUCTION:** All commonly used implant materials, metals and polymers, seem to present a common problem: bacterial adhesion on their surfaces, mainly S*taphylococci*. The resultant biofilm is resistant to aggressive pharmacological agents as well as host defences [1].

One way to prevent the establishment of infection is to render the implant surface bactericidal, creating a stable environment with a spectrum similar to the soluble antibiotics [2]. The current revival of silver chemistry in this context initiated us to use this metal ion for coating purposes.

We hypothesize that the combination of molecules derived from antibiotics and silver compounds would provide additive, synergic activity against most micro-organisms, and thus the desired protection.

We chose the well-studied antibiotic vancomycin, and silver ions as targets to be bonded to the surface of implant materials. On one hand, vancomycin is the drug of last resort for treating Gram-positive bacterial infections. On the other hand, silver ions are the most powerful antimicrobial and antibacterial inorganic agents used safely in medicine, and this already for many years [3].

Therefore, we propose to avoid or at least strongly reduce bacterial adhesion to implant surfaces using a series of newly developed Ag-antibiotic combinations on implant surfaces.

**METHODS:** We use titanium, activated by a hydroxide surface layer (Ti-OH) to attach our compounds because of its excellent biocompatibility, and, as model surface, self-assembles monolayers (SAMs) on gold (111) to permit permanent attachment of our antibiotic derivative molecules. To extend the antibiotic from the surface, we chose a flexible hydrophilic linker, 8-amino-3,6-dioxaoctanoate (AEEA) and we add a pyridinyl group that may bind silver ions [4]. The new combinations of compounds are characterized by mass spectrometry, NMR, and single crystal x-ray analysis before being attached to the surface device. After being linked to the surface of the substrates by chemical and/or physical techniques, these new modified surfaces are characterized by using different microscopy techniques, Scanning Electron Microscopy (SEM), Atomic Force Microscopy (AFM), surface immunofluorescence detection. The vapour diffusion technique is used for the crystallisation of the antibiotic derivative with silver ions.

**RESULTS:** The surface coatings show typical surface chemical composition. In addition to this, the surface topology is studied as a function of various effects, such as deposition technique, concentrations, and chemical composition. Furthermore, solubility of the new compounds, silver ion release, antibiotic stability biocompatibility studies, soft and hard tissue integration and toxicity studies will be discussed.

.**DISCUSSION & CONCLUSIONS:** The results of in vitro studies of the antimicrobial activity and soft-tissue integration of our new compounds used as surface coatings show promising results and will be presented. This may be an efficient solution conquering bacterial adhesion and biofilm formation

**REFERENCES:** [1]P.S. Stewart, J.W. Costerton (2001) *Lancet* **358**: 135-138. [2]B. Jose, V. Antoci, A.R. Zeiger, E. Wickstrom, N.J. Hickok (2005) *Chemistry & Biology* **12**: 1041-1048. [3]J.L. Clement, P.S. Jarret (1994) *Metal Based Drugs*, 467-482. [4]J. Rao, G.M. Whitesides (1997) *Journal of the American Chemistry Society*, **119**: 10286-10290.

**ACKNOWLEDGEMENTS:** The authors thank the Swiss National Science Foundation for most generous support.

# Characterization and *in vitro* evaluation of antimalarial oligonucleotides adsorbed to cationic nanoemulsions

F. Bruxel[1,2,3], S. Cojean[3], A. Bochot[1], H. Teixeira[1,2], P. M. Loiseau[3], E. Fattal[1*]

[1]*Univ Paris-Sud, UMR 8612 CNRS, France.* [2] *PPGCF, Univ Fed do Rio Grande do Sul (UFRGS), Brazil.* [3] *Univ Paris-Sud, UMR 8076 CNRS, France.*

**INTRODUCTION:** Malaria is one of the most widespread parasitic diseases, endemic in more than 100 countries. The malaria mortality has increased, most likely due to parasite drug resistance [1]. A promising strategy based on the antisense oligonucleotides (ON) against the enzyme topoisomerase II of *Plasmodium falciparum* has been considered, by interfering in protein synthesis and inhibiting parasite growth [2, 3]. However, due to their low stability and cellular penetration, cationic nanoemulsions (NE) have been proposed as carriers for these systems [4]. The aim of this study was to characterize ON/NE complexes and to evaluate *in vitro* their capacity to inhibit red blood cells reinfection by parasites.

**METHODS:** The cationic nanoemulsions were composed by medium chain triglycerides, egg lecithin, glycerol, DOTAP, and MilliQ® water. The ζ-potential (electrophoretic mobility), the mean droplet size (photon correlation spectroscopy) and the morphology of the droplets (transmission electron microscopy - TEM) were determined before and after the addition of the ON. The quantification of ON adsorption was evaluated by an ultrafiltration/centrifugation method. The hemolytic potential of the NE was evaluated in infected and non infected red blood cells.

For the determination of red blood cells reinfection, 10 µM ON solutions or ON/NE complexes were added to early stages parasites, at 0.5% parasitemia at 5% hematocrit. *P. falciparum* 3D7 strain was maintained in O+ human erythrocytes in RPMI 1640 medium supplemented with albumin, 25mM Hepes and 32mM NaHCO3 under continuous culture at 37 °C using the candle-jar method. A NE control (without ON) was also tested. Blood smears were prepared after 24 and 44 hours after treatment, by Giemsa staining. Parasite stages and parasitemia were determined by microscopic examination of at least 5000 erythrocytes under oil immersion.

**RESULTS:** The ON adsorption to NE was evidenced by the inversion of the zeta potential, from positive values (+55mV) to negative ones (-20mV). No significant differences in morphology and size of NE droplets were detected before and after ON adsorption. In contrast, a high electronic density at the interface was observed by TEM after ON addition, suggesting the adsorption of ON at the emulsion interface. The adsorption of progressive ON concentrations showed a progressive ON adsorption until it reached a plateau at approximately 60 mg of ON per g of internal phase of NE. Consequently, the concentration of ON corresponding to 100% of association was chosed for the *in vitro* evaluation.

The hemolytic effect of the cationic NE was lower than 10% for the [+/-] charge ratios until 4. After 24 hours of treatment, there was a significant reduction of total parasitemia, especially for ON/NE complexes whereas after 44 hours, no more differences between treatments were observed. The parasites could still infect new red blood cell, although a delay in the *P. falciparum* life cycle was observed for ON solution and complexes.

**DISCUSSION & CONCLUSIONS:** The overall results showed that ON against *P. falciparum* topoisomerase II gene can be efficiently adsorbed to the cationic nanoemulsions and are probably located at the interface of the oil droplets with the aqueous phase. In addition, these systems didn't show high hemolytic potential, even at final positive charge ratio. Considering the delay in the parasites life cycle and the parasitemia reduction, these systems could be interesting for further studies, which are already in progress.

**REFERENCES:** [1] WHO (2008). http://www.who.int/malaria/wmr2008/malaria2008.pdf. [2] W. Noonpakdee, J. Pothikasikorn, W. Nimitsantiwong et al. (2003) *Biochem Biophys Res Commun* **302**:659-664. [3] F. Föger, W. Noonpakdee, B. Loretz et al. (2006) *Int J Pharm* **319**:139-146. [4] H. Teixeira, C. Dubernet, F. Puisieux et al. (1999) *Pharm. Res.* **16:**30-36.

**ACKNOWLEDGEMENTS:** To CAPES/ COFECUB for the financial support.

# Gold Nanoparticles as Actuators for Biomolecular Reactions

A. Buchkremer[1], J. Bretschneider[1], M. Reismann[2], G. von Plessen[2], U. Simon[1]

[1]*RWTH Aachen University, Institute of Inorganic Chemistry, Germany.*

[2] *RWTH Aachen University, Institute of Physics (1A), Germany.*

**INTRODUCTION:** Recently the application of gold nanoparticles (AuNP) as actuators for the photothermal control of biomolecular reactions including conformational changes of peptides [1] or DNA hybridisation/dehybridisation [2, 3] was demonstrated. In these experiments electro-magnetic radiation was converted into heat, which was then transferred to surface bound peptides, DNA-oligomers or proteins. Here, we present the use of remotely controllable and spatially confined photothermal heating to control the reversible disassembly of networks consisting of DNA-functionalised AuNP [4]. Further, the catalytic activity of the enzyme horseradish peroxidase (HRP) bound to the gold nanoparticle surface is controlled photothermally [5].

**METHODS:** AuNP were prepared by the Turkevich method and further functionalized with ssDNA or HRP, respectively [4, 5]. For photothermal melting experiments, a 100 µm-wide CW-laser beam at a wavelength of 532 nm was chosen as irradiation source due to its spectral proximity to the plasmon resonance of functionalised AuNP. A grating spectrometer (L.O.T.-Oriel, MSI 260i) was used in combination with a Peltier-cooled CCD-chip (Andor Techn.). The cuvette holder was designed to allow conven-tional temperature control of the sample solution via an external thermostat.

**RESULTS:** DNA-AuNP network suspensions irradiated with laser light experienced a network disassembly evidenced by a sigmoidal decay of the plasmon peak. The disassembly process resulted in a spectral blueshift (Fig 1, left). A subsequent redshift shows that the DNA-AuNP are intact as the networks grow steadily. Thus, the disassembly process induced by the laser irradiation is fully reversible [4]. With laser irradiation a temporally broader, reversible transition and an apparent temperature difference $\Delta\Theta_{melt}$ of the melting point compared to conventional heating is observed form the inflection point of the decay.

The enzyme HRP catalyses the reaction of ABTS to $ABTS^+$, which can be detected spectroscopi-cally. The rate of catalytic reaction is determined by temperature and is thus photothermally controllable. The amount of converted $ABTS^+$ rises steadily with time up to the saturation value $\Delta n_{ABTS+}(t = \infty, \Theta)$, which decreases with increa-sing temperature. $\Delta n_{ABTS+}(t = \infty, \Theta)$ exhibits a linear temperature dependence for thermal and photothermal melting processes, but with different slopes. This indicates that the laser-irradiated sample volume has a temperature that is higher by $\Delta\Theta$. This difference scales with the intensity of the applied laser irradiation [5].

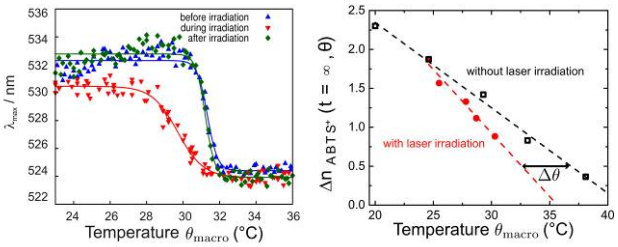


*Fig. 1: Sigmoidal melting curves of DNA-AuNP aggregates (left) and temperature dependence of $\Delta n_{ABTS+}(t = \infty, \Theta)$ (right) for conventional heating and laser irradiation.*

**DISCUSSION & CONCLUSIONS:** The self assembly due to biomolecular recognition of DNA-AuNP can be manipulated in a contactless, locally confined and reversible manner by means of photothermia. Further, the first photothermal manipulation that involves enzymatic conversion on the surface of gold nanoparticles is shown. Both processes were observed in situ using UV/Vis spectroscopy and following the plasmon resonance peak position.

**REFERENCES:** [1] J.M. Slocik, F. Tam, N.J. Halas, R.R. Naik (2007) *Nano Lett.* **7**:1054-1058. [2] K. Hamad-Schifferli, J.J. Schwartz, A.T.Santos, S.G. Zhang, J.M. Jacobson (2002) *Nature* **415**:152-155. [3] J. Stehr, C. Hrelescu, R.A. Sperling, G. Raschke, M. Wunderlich, A. Nichtl, D. Heindl, K. Kurzinger, W.J. Parak, T.A. Klar, J. Feldmann (2008) *Nano Lett.* **8**:619-623. [4] M. Reismann, J. Bretschneider, G. von Plessen, U. Simon (2008) *Small* **4**: 604-610. [5] J.C. Bretschneider, M. Reismann, G. von Plessen, U. Simon (2009) *Small* **5**:2549-2553.

**ACKNOWLEDGEMENTS:** We would like to thank the DFG-Graduiertenkolleg “Biointerface” (No. 1035) for financial support.

# Hierarchical Self-Assembly of One and Two Dimensional Protein Networks

S.Burazerovic, T.R.Ward

*University of Basel, Switzerland*

**INTRODUCTION:** With the aim of creating Protein Organo-Metallic Frameworks (POMF), we have used streptavidin combined with bis-biotinylated anchors (BBAs) (*Fig. 1*). Initial studies allowed us to create one-dimensional collagen mimetics using a linear linker. These were used for biomineralization of calcite [1]. Introduction of a trifurcated BBA in the presence of streptavidin produces dendrimer-like structures (*Fig. 2*). Our goal is to produce and characterize monodisperse dendrimer structures. For this purpose, a bis-biotinylated thiol (BBA-PEG-SH) is currently used for immobilization of the protein networks via self-assembled monolayers (SAMs) on gold surfaces.
Sequential addition of streptavidin followed by the BBAs linkers, allows us to create well defined structures of increasing size. SPR, AFM and TEM are currently used to characterize these protein nano-objects. In parallel to the stepwise assembly process, the self-assembly in bulk solution is investigated.

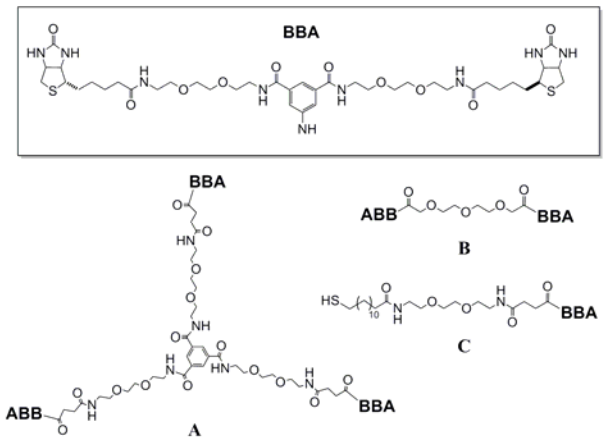


*Fig. 1: Stepwise assembly of Streptavidin tested with BBA-tripod **A** and $(BBA)_2PEG$ **B**. BBA-PEG-SH **C** used for SAMs preparation.*

**METHODS:** Biotinylated SAMs using BBA-PEG-SH in EtOH were produced on gold sensor chips. Stepwise assembly of streptavidin polymer was recorded in real-time with SPR (Biacore X). Successive immobilization of streptavidin followed by BBAs linker **A** or **B** were recorded using different mixtures of buffers and organic solvents. AFM and TEM were then used to characterize the self-assembly of streptavidin in bulk solution using those solvent mixtures.

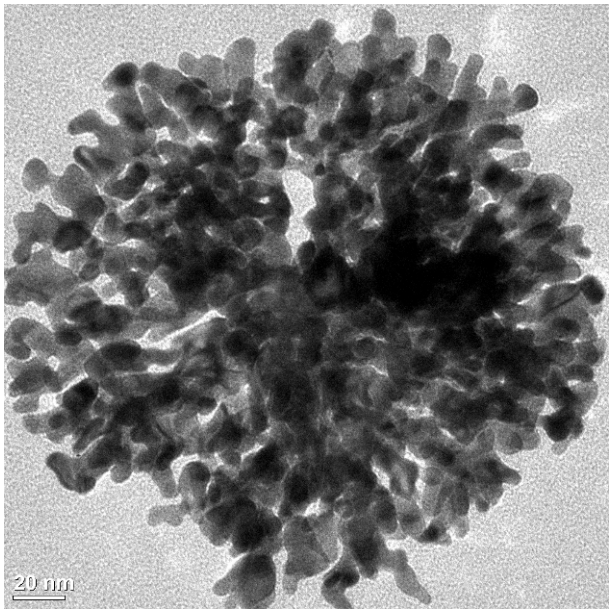


*Fig. 2: TEM micrograph of dendritic structures obtained upon mixing stochiometric amount of streptavidin to BBA-tripod **A**.*

**RESULTS:** Stepwise construction of streptavidin 1D polymer using $(BBA)_2PEG$ was observed by SPR. A regular increase of the SPR signal was obtained by using a 70% EtOH solution (HBS-P Buffer). AFM images on HOPG from $(BBA)_2PEG$ and streptavidin self-assembled in bulk solution (70% EtOH) shows linear streptavidin polymer reaching 100 μm in length.

**DISCUSSION & CONCLUSIONS:** According to the results obtained by SPR, using a solvent system affording good ligand solubility and preventing the protein denaturation allows us to obtain the desired self-assembled nanostructures. We are currently improving the stepwise assembly of streptavidin dendrimers using (BBA)-tripod on biotinylated SAMs.

**REFERENCES:** [1] S. Burazerovic, J. Gradinaru, J. Pierron, T. R. Ward, *Angew. Chem. Int. Ed.* (2007), **46**, 5510 –5514.

**ACKNOWLEDGEMENTS:** This work was supported by the Swiss National Science Foundation (Grants FN 200021-105192 and 200020-113348).

# Multifunctional polymeric nanoparticles prepared from O/W nano-emulsions by a low-energy method

G. Calderó[1,2], C. Bouaoud[2], M.J. García-Celma[3,2], C. Solans[2,1]

*[1] CIBER-BBN, Barcelona, Spain. [2] Institut de Química Avançada de Catalunya, IQAC/CSIC, Barcelona, Spain. [3] Facultat de Farmacia. Universitat de Barcelona, Spain.*

**INTRODUCTION:** Multifunctional nanoparticles are solid materials useful for biomedical applications, designed to fulfil several specific demands at a time. Multiple functionality enable the nanoparticles to reach selectively the disease site at therapeutic concentrations improving efficacy and decreasing adverse effects [1]. Polymeric nanoparticles can be obtained in O/W nano-emulsions by incorporating preformed hydrophobic polymers in the oily dispersed phase followed by solvent evaporation [2]. Although this method has been known for some time, few research has been devoted to the preparation of polymer in water nano-emulsions by low-energy methods [3] and using non-toxic solvents. In this study polymeric nano-emulsions have been prepared by condensation or low-energy methods and used for the preparation of nanoparticles, which have been functionalized for biomedical applications.

**METHODS:** A hydrophobically modified polysaccharide and a polyester were used as preformed polymers. Technical grade nonionic surfactants were used. Ethyl acetate was the organic solvent and water was MilliQ™filtered. Pyrene and Coumarin-6 were used as the fluorescent labels and folic acid as the targeting moiety.

Nano-emulsions were obtained by the phase inversion composition (PIC) emulsification method at constant temperature. The fluorescent label was incorporated in the oil component before nano-emulsion preparation.. Nano-emulsions were characterized by dynamic light scattering and their stability was assessed by light backscattering at 25ºC using a Turbiscan Lab Expert. Nanoparticles were obtained from the nano-emulsions by evaporating the solvent under reduced pressure at room temperature. Nanoparticles were characterized by transmission (TEM) and scanning (SEM) electron microscopy. The amount of fluorescent marker encapsulated in the nanoparticles was determined by spectrofluorometry. Functionalization with folic acid was assessed by FTIR.

**RESULTS:** Nano-emulsions were obtained in water / nonionic surfactant / [Ethyl acetate +

polymer] systems at 25ºC at oil/surfactant ratios higher than 50/50 by the PIC method. The phase inversion taking place along the emulsification path was determined by conductivity. Light scattering measurements revealed that nano-emulsions obtained showed droplet sizes typically around 200nm. Assessment of the stability of the nano-emulsions by backscattering analysis showed that transmission data taken during a period of 24 hours at 25ºC increased uniformly along the whole sample height, suggesting a droplet size decrease, due to the fact that ethyl acetate is partially soluble in water. Besides, no destabilization phenomena due to creaming, sedimentation, flocculation or coalescence were detected. Fluorescent markers were successufully incorporated in the model nano-emulsions. Nanoparticles were obtained from the nano-emulsions by the solvent evaporation method. Characterization of the nanoparticles by TEM image analysis indicated that the hard sphere size was around 50 nm. Nanoparticles were functionalized with folic acid by using coarbodiimide chemistry. Folic acid coupling was evidenced by FTIR

**DISCUSSION & CONCLUSIONS:** Multifunctional polymeric nanoparticles with fluorescent markers and folic acid have been obtained by a low-energy method using oil-in-water (O/W) nano-emulsions as templates. These nanoparticles may be suitable for targeting tumor cells, as folate receptors are overexpressed in the membrane of many kinds of human cancer cells.

**REFERENCES:** [1] VP Torchilin. Adv Drug Delivery Rev 58 (2006) 1532–1555; [2]Desgouilles S., etal. Langmuir 19: 9504-9510, 2003 ; [3] Solans C., Et al. Current Opinion in Colloid and Interface Science 10, 102-110, 2005

**ACKNOWLEDGEMENTS:** CIBER-BBN is an initiative funded by the VI National R&D&i Plan 2008-2011, Iniciativa Ingenio 2010, Consolider Program, CIBER Actions and financed by the Instituto de Salud Carlos III with assistance from the European Regional Development Fund. Financial support from MEC (grant CTQ2008-06892-CO3-O1) and the Generalitat de Catalunya (grant 2009-SGR-961) is acknowledged.

# Dextrin nanoparticles as a protein delivery system: The Interleukin-10 case study

V. Carvalho[1], P. Castanheira[2], C. Gonçalves[1], P. Madureira[3,4], C. Faro[2,5], L. Domingues[1], M. Vilanova[3,4], F.M. Gama[1]

*[1]IBB, Centre of Biological Engineering, Universidade do Minho, Portugal, [2]Biocant, Cantanhede, Portugal, [3]ICBAS, Universidade do Porto, Portugal, [4]IBMC, Universidade do Porto, Portugal, [5]Department of Life Sciences, Universidade de Coimbra, Portugal*

**INTRODUCTION:** Interleukin-10 (IL-10) is an anti-inflammatory cytokine, which active form is a non-covalent homodimer with two intramolecular disulphide bonds that are essential to its biological activity, which includes reduction of tumor necrosis factor α (TNF-α) synthesis and down-regulation of class II major histocompatibility complex (MCH-II) molecules on monocytes/macrophages [1]. Due to IL-10 potential applications in various medical fields, it is essential to develop systems that can effectively deliver the protein. A promising system is protein encapsulation by polymeric nanopartices (NPs), which minimize denaturation, and enables slow-release, while maintaining an effective concentration for the necessary period of time. In previous work, we have developed and characterized NPs obtained by self-assembling of hydrophobized dextrin [2] whose properties makes them promising for IL-10 delivery.

**METHODS:** The recombinant mutated (C149Y) murine IL-10 (rIL-10) was expressed, in form of inclusion bodies, in *E. coli* BL21 star. rIL-10 was recovered by a process of solubilization in 6M guanidine, renaturation and re-oxidation of disulphides. The dimeric form of rIL-10 was collected by gel filtration and further purified by ion-exchange chromatography. SDS-PAGE analysis was used to confirm molecular weight and purity. The amount of rIL-10 obtained was quantified by ELISA.

rIL-10 bioactivity was assayed by its ability to inhibit the production of TNF-α, quantified by ELISA, and the surface expression of MHC-II molecules, monitorized by FACS analysis, in lipopolysacharide (LPS) and IFN-γ activated bone marrow derived macrophages (BMDM).

To form the self-assembled NPs, lyophilized dextrin-VMA-$SC_{16}$ was resuspended in culture medium, at room temperature. NPs formation was confirmed by dynamic light scattering. The complex NPs/rIL-10 was formed by dissolving rIL-10 in culture medium and then by mixing lyophilized dextrin-VMA-$SC_{16}$. rIL-10 incorporation into NPs was verified quantifying the amount of rIL-10 free in solution by ELISA. The release of rIL-10 from the complex NPs/rIL-10 was assessed in a BMDM culture, by measuring free rIL-10 by ELISA. Bioactivity of rIL-10 released form the NPs/rIL-10 complex was assayed as described previously.

**RESULTS:** SDS-PAGE confirmed the expression and molecular weight (18 kDa) of the rIL-10 as well as their purity. Total recovery of dimeric rIL-10 was about 1-1.5 mg/L culture, quantified by ELISA. rIL-10 (in the range of 0.1 to 250 ng/mL) shown the ability to inhibit the TNF-α production and to reduce MHC-II expression on stimulated BMDM. rIL-10 incorporation by NPs was confirmed by quantifying, the amount of rIL-10 in free in solution, that was negligible. In the presence of 20% serum, rIL-10 is being released over time in a BMDM culture. After two hours of incubation with the NPs/rIL-10 complex, the rIL-10 reaches a maximum concentration; a stable value of about 35 ng/mL rIL-10 being estimated after twenty-four hours. The rIL-10 released from the NPs/rIL-10 complex was able to inhibit TNF-α production and MHC-II expression at the same level as the soluble rIL-10.

**DISCUSSION & CONCLUSIONS:**

IL-10 is a cytokine with a strong anti-inflammatory activity. A mutated form of murine IL-10 was successfully expressed in *E. coli*, recovered and purified from inclusion bodies. Its ability to reduce TNF-α synthesis and down-regulate MHCII molecules expression on activated BMDM was confirmed. Due to IL-10 potential applications in various medical fields, it is essential to develop systems that can effectively deliver the protein. For this purpose, dextrin NPs have been used and this work shows that dextrin NPs effectively incorporate IL-10 and enable the slow release of biologically active IL-10 over time. Altogether, these results demonstrate the suitability of dextrin NPs to be used as a system for the controlled release of IL-10.

**REFERENCES:**[1] R. de Waal Malefyt, et al (1991) *J Exp Med* **174**:1209-20. [2] G. Gonçalves, et al (2007) *Biomacromolecules* **8**:392-8.

**ACKNOWLEDGEMENTS:** Vera Carvalho was supppoted by the grant SFRH/BD/27359/2006 from Fundação para a Ciência e Tecnologia (FCT), Portugal. This study was financially supported by FCT through the project PTDC/BIO/67160/2006.

# Studies of Encapsulation of a New Potential Antitumoral Indole Derivative in Nanoliposomes for Drug Delivery Applications

E.M.S. Castanheira[1], A.S. Abreu[1,2], M.J.R.P. Queiroz[2], P.M.T. Ferreira[2]

*[1]Centre of Physics (CFUM) and [2]Centre of Chemistry (CQ-UM), University of Minho, Campus de Gualtar, 4710-057 Braga, Portugal*

**INTRODUCTION:** Nanosized liposomes are among nanotechnological delivery methods for chemotherapeutic drugs in the treatment of cancer. This technique can potentially overcome many common pharmacologic problems, such as those involving solubility, pharmacokinetics, *in vivo* stability and toxicity. Liposomes are closed spherical vesicles consisting of a lipid bilayer that encapsulates an aqueous phase in which hydrophilic drugs can be stored, while water insoluble compounds can be incorporated in the hydrophobic region of the lipid bilayer [1,2]. In this work, a potential antitumoral fluorescent indole derivative **1**, previously synthesized by us [3], has been encapsulated in nanoliposomes of DPPC (dipalmitoyl phosphatidylcholine), egg-yolk phosphatidylcholine (Egg-PC) and dioctadecyl-dimethylammonium bromide (DODAB).

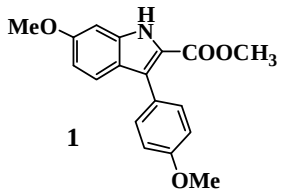


**1**

Methyl 6-methoxy-3-(4-methoxyphenyl)-1*H*-indole-2-carboxylate

**METHODS:** Nanoliposomes were prepared by injection of an ethanolic solution of the lipid in an aqueous media under vigorous stirring, above the lipid melting transition temperature. Mean liposome size was measured by dynamic light scattering (DLS). The encapsulation of compound **1** in the nanoliposomes was assessed by fluorescence resonance energy transfer (FRET) between the fluorescent compound **1** and the fluorescent labelled phosphatidylethanolamine NBD-PE, included in the liposome formulation (with NBD-PE/lipid ratio of 1:250).

**RESULTS:** The nanoliposome hydrodynamic diameters, obtained by DLS, are 87 ± 11 nm for DPPC, 51 ± 2 nm for Egg-PC and 268 ± 37 nm for DODAB. All samples are monodisperse.

*Antitumoral evaluation:* The effect of compound **1** on the *in vitro* growth of three human tumor cell lines, breast adenocarcinoma (MCF-7), non-small cell lung cancer (NCI-H460) and a melanoma cell line (A375-C5), was evaluated after a continuous exposure of 48 h (Table 1).

*Table 1. Values of compound **1** concentration needed for 50% of cell growth inhibition ($GI_{50}$)*

| | $GI_{50}$ (μM) | | |
|---|---|---|---|
| | **MCF-7** | **NCI-H460** | **A375-C5** |
| **1** | 0.37 ± 0.02 | 0.33 ± 0.03 | 0.25 ± 0.02 |

Fluorescence measurements showed the possibility of FRET between the electronic excited compound (acting as donor) and the labelled lipid NBD-PE (with NBD acting as energy acceptor). In Figure 1 it is possible to observe a strong NBD emission upon excitation of compound **1** incorporated in nanoliposomes.

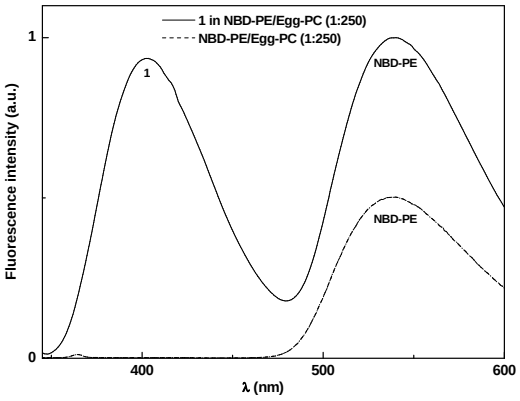


*Fig. 1: Fluorescence spectra of compound **1** in Egg-PC liposomes labelled with NBD-PE and labelled Egg-PC liposomes alone ($\lambda_{exc}$=325 nm).*

**DISCUSSION & CONCLUSIONS:** Compound **1** shows excellent antitumoral properties, exhibiting very low $GI_{50}$ values in the three tumor cell lines. FRET assays indicate that compound **1** molecules and the NBD-labelled lipids are in close proximity in nanoliposomes. These results are important for drug delivery purposes, considering the antitumoral properties of compound **1**.

**REFERENCES:** [1] T.L. Andresen et al (2005) *Prog Lipid Res* **44**:68-97. [2] Y. Malam et al (2009) *Trends Pharmacol Sci* **30**:592-599. [3] M.-J.R.P. Queiroz et al (2007) *Tetrahedron* **63**:2215-2222.

**ACKNOWLEDGEMENTS:** This work was funded by FCT-Portugal and FEDER through CFUM, CQ-UM, Project PTDC/QUI/81238/2006 and Post-doc. grant of A.S. Abreu (SFRH/BPD/ /24548/2005).

# Real Time Monitoring of a Calcium Carbonate Biomineralization Process on a Silk Fibroin via QCM and AFM

Woo-Sik Kim[1], SeungHun Kim[2], Sang-Mok Chang[2], JongMin Kim[2]

[1]*Department of Chemical Engineering, KyungHee University, Korea*

[2]*Department of Chemical Engineering, Dong-A University, Korea*

**INTRODUCTION:** A quartz crystal microbalance (QCM) is well-known for its remarkable mass sensitivity and low cost in analytical applications. As material is adsorbed on the surface of QCM , the resonant frequency is reduced due to an increase in the mass on the quartz crystal[1, 2]. This simple relation makes possible to fabricate a number of mass sensing systems. Biomineralization is a phenomenon related to a mass interaction between a biopolymer and dissolved mineral. Unfortunately, the real time monitoring of the phenomena has several difficulties. In this study, we will show a novel approach to monitor the biomineralization process with the real time using QCM and a chemical force microscopy technique.

**METHODS:** The experimental system is showed as Fig 1. All the experiments were conducted at 25°C±1°C. Immobilization of silk fibroin on QCM gold electrode as selective receptor and biomineralization of calcium carbonate on the silk fibroin were monitored on line by QCA917 (EG&G, Tokyo, Japan). In addition, we used a chemical force microscopy technique to give some evidences for the interpretation of the QCM result related to the CaCO3 biomineralization process.

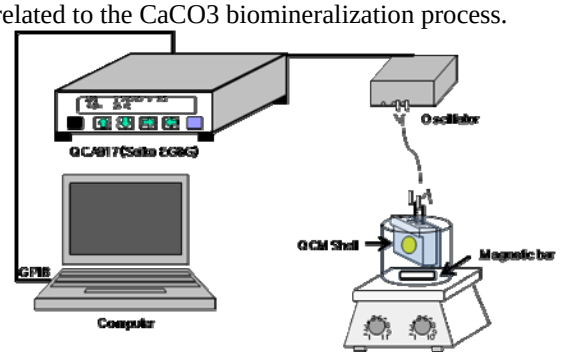


*Fig. 1 Schematic diagram of QCM detection.*

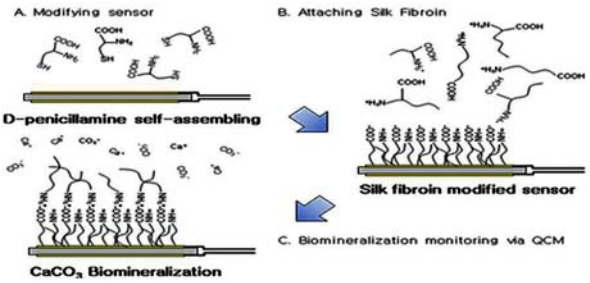


*Fig. 2:Monitoring Procedure of biomineralization.*

The monitoring experiment was performed according to the Fig. 2 procedure.

**RESULTS:** The biomineralization process is normally occurred with a long reaction time, and this property requires a well-prepared real time monitoring technique. In addition, the mass change of QCM itself does not reveal the complicated biomineralization process. Thus, AFM images were used to monitor the biomineralization process. Fig. 3 is QCM response for biomineralization of $CaCO_3$ (0.3mM)without stirring and these results were evaluated by the chemically modified AFM images .

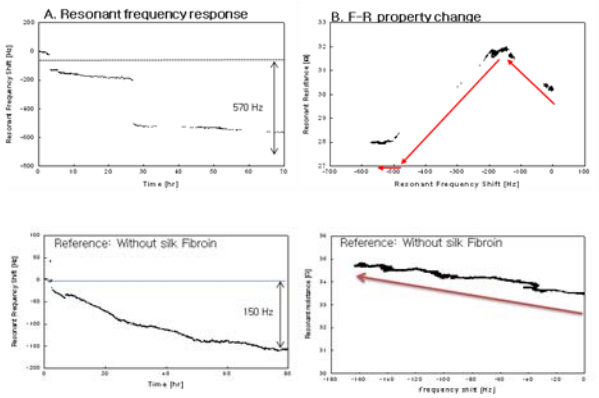


*Fig. 3: QCM response for biomineralization of CaCO3.*

**DISCUSSION & CONCLUSIONS:** The results showed that the properties of obtained biomineral of $CaCO_3$ are different with stirring rate and the biomineralization of $CaCO_3$ quantity increases in proportion as stirring rate. Similar results are obtained with a different solution concentration. It is expected the future QCM experiments will reveal the nature of biomineralization.

**REFERENCES:** [1]WS. Kim et al (2008) *J. Physics and Chemistry of solids.* **69**, 1422-1427, [2]JM. Kim et al (2010) *Bioprocess Biosyst Eng.* **33**, 39-43

**ACKNOWLEDGEMENTS:** This research was supported by Basic Science Research Program through the National Research Foundation of Korea (NRF) funded by the Ministry of Education, Science and Technology (KOSEF, 2009-0064245).

# Enhanced Induction of MSCs to Cardiomyocytes by 5-Azacytidine/Nano-sized Collagen I Molecules

SJ. Chang[1], PL. Kang[2], CH. Yao[3], WT. Liu[1], Shyh Ming Kuo[1]

*[1]Dept. Biomedical Engineering, I-Shou University, Kaohsiung, Taiwan. [2]Dept. of Cardiovascular Surgery, Kaohsiung Veterans General Hospital, Kaohsiung, Taiwan. [3]Dept. Biomedical Imaging and Radiological Science, China Medical University, Taichung, Taiwan.*

**INTRODUCTION:** Many reports have shown that the mesenchymal stem cells (MSCs) obtained from bone marrow were easily differentiated into bone, cartilage, nerves, and cardiomyocytes (CMC) [1]. Several studies have revealed that MSCs could be inducted and differentiated into cardiomyocytes under the stimulus of 5-azacytidine[2]. However, the inducted ratio was low and still needed to improve. Collagen is one of the most commonly used biomaterials in scaffold construction for tissue engineering. The influence of differently organized collagen structures on cellular fates and behaviors is an exciting and interesting area that remains to be explored. The objective of this study was to evaluate the effects of addition of nano-sized type I collagen molecules (particles or fibers) onto the culture medium containing 5-azacytidine on MSCs differentiation.

**METHODS:** Nano-particle collagen was prepared by a high-voltage electrostatic field system which was constructed by two parallel plate electrodes. 1 ml of iced type I collagen solution (0.1 mg/ml) was poured into a plastic petri-dish and then placed at the center point of the two parallel electrodes. The temperature of the chamber was set and kept constant at 7°C for preparing particles.[3] The reaction time was set to 1 h. Collagen fibrils were assembled from collagen monomers (0.1mg/ml) at 37C for 4 hr.

The MSCs from the bone marrow were isolated by selective adhesion procedure. After a series of passages, the cells were treated with 10 μM 5-azacytidine for 24h. After the respective incubation periods, the cells were washed with PBS and culture in DMEM with 10% FBS. The medium was changed once every in 3 days.

| | |
|---|---|
| C | 5-azacytidine |
| P | 5-azacytidine+ nano-sized collagen I molecules |
| F | 5-azacytidine+collagen I fiber |

Primary antibody was Troponin-I(C-19). Secondary antibody used was donkey anti-goat IgG-FITC. DNA-specific fluorescent dye DAPI counterstain was used to detect cell nuclei.

**RESULTS:**

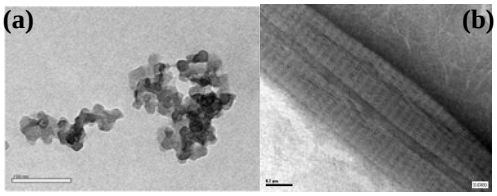


*Fig.1: Transmission electron micrograph of nano-sized type I collagen molecules: (a) particle form; (b) fibrillar form.*

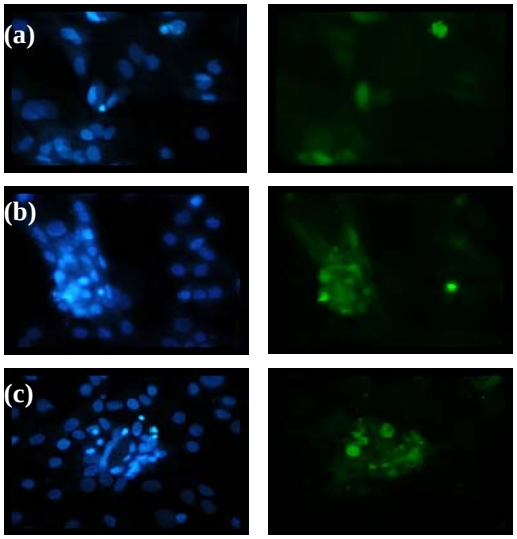


*Fig.2: Immunofluorescence staining of Troponin I (green) and DAPI (blue). MSCs induced with 10 μM 5-azacytidine concentration for 14 days. (a)group C; (b)group P; (c)group F.*

**DISCUSSION & CONCLUSIONS:** The primarily results revealed that more MSCs could be induced into cardiomyocytes which expressed high levels of Troponin-I after addition of nano-sized collagen I molecules.

**REFERENCES:** [1]S. Bajada, I. Mazakova, J.B. Richardson, et al (2008) *J Tissue Eng Regen Med* **2**(4):169–183. [2] S. Wakitani, T. Saito, A.I. Caplan, (1995) *Muscle & Nerve* **18**(12): 1417-1426. [3]S.J. Chang, G.C.C. Niu, S. M. Kuo, et al (2006) *IEE Proc Nanobiotechnol* **153**: 1-6.

**ACKNOWLEDGEMENTS:** This work was supported by grants from the National Science Council, ROC (95-2221-E-214-052-MY3 and 97-2815-C-214 -024 -E).

# Gallium-64 labeled Gold nanoparticles with gadolinium-dtpa coating as a PET/CT/MRI triple contrast Agent

Yongmin Chang[1,2], Hee-Kyung Kim[2], Jeong-Chan Park[1], Jeongsoo Yoo[1]

[1]*Department of Molecular Medicine, Kyungpook National University, Daegu, Korea.*

[2]*Department of Medical & Biological Engineering, Kyungpook National University, Daegu, Korea*

**INTRODUCTION:** Positron emission tomography (PET) imaging has many advantages in terms of its very high sensitivity and excellent quantification while suffers from low spatial resolution and poor image quality. Therefore, recent PET imager is combined with computer tomography (CT), which provides high resolution images. While CT has excellent hard tissue contrast, magnetic resonance imaging (MRI) provides superb soft tissue contrast[1]. PET-CT imager is now introduced in clinical setting and more recently PET-MRI system becomes available. Herein we report the synthesis and *in vivo* application of AuNPs coated with gadolinium-DTPA conjugate and gallium (Ga)-64 radioisotope ($^{64}$Ga-Au@GdL) as a new class of a PET/CT/MRI triple contrast agent.

**METHODS: (1) Functionalized AuNPs with Gd-DTPA conjugate**: Citrate-coated gold nanoparticles of ~12 nm were first prepared. The coating of AuNPs with GdL was accomplished typically as follows: To an aqueous suspension of AuNPs as-prepared (100 mL), L (150 mg) or GdL (150 mg) was added, and the mixture stirred for 20 h. Acetone (100 mL) was then added, and the stirring continued further for 4 h. The nanoparticles were collected by centrifugation and washed successively with water, acetone, and ether. TEM analyses were performed by Center for Instrumental Analysis, KNU **(2) Radio labeling of Au@GdL with $^{64}$Ga**: AuNP with GdL was radiolabeled with $^{64}$Ga and purified with Microcon YM-50. The radiochemical purity was 92% after purification. **(3) In vivo MRI, micro CT, micro PET studies:** ICR mice (n=6) were anesthetized and measurements were made before and after injection of $^{64}$Ga-Au@GdL via tail vein. CT images were obtained using a micro-CT scanner with 120 kVp and 80 mA. PET images were obtained using small animal dedicated micro-PET system for one hour. MR images were taken with a 1.5 Tesla (T) MR unit equipped with a home-made small animal RF coil.

**RESULTS:** Fig. 1 shows the TEM image of well-dispersed spherical particles of $^{64}$Ga-Au@GdL. The particles have an average size of 12 nm with a

narrow size distribution measured by DLS. CT image of $^{64}$Ga-Au@GdL is demonstrated in Fig. 2. After injection, $^{64}$Ga-Au@GdL shows significant liver enhancement with high X-ray attenuation of Au nanoparticles. Fig. 3 shows *in vivo* MR coronal images, which again shows a strong signal enhancement in liver. These observations are in line with those made with PET image (Fig. 4).

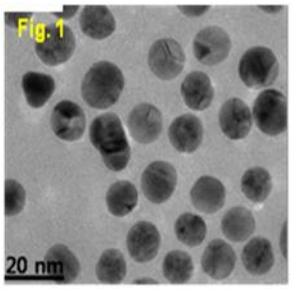


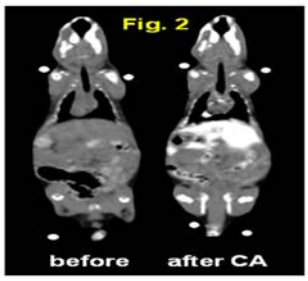


*Fig 1. TEM images of AuNP radiolebed with $^{64}$Ga. The mean size was 12 nm. Fig 2. In vivo CT coronal images of mice obtained with $^{64}$Ga- Au@GdL.*

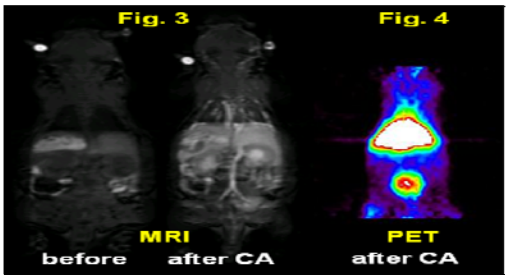


*Fig 3. In vivo MR coronal images of mice obtained by tail vein injection with $^{64}$Ga- Au@GdL. Fig 4. In vivo PET coronal image of the same mice with $^{64}$Ga-Au@GdL.*

**DISCUSSION & CONCLUSIONS:** $^{64}$Ga-Au@GdL exhibits homogeneous size distribution of 12 nm with high loading of GdL on AuNPs ($3.0 \times 10^3$ GdL per AuNPs). A synergistic effect of gadolinium in Au@GdL on X-ray attenuation has been confirmed. PET image well demonstrated the higher signal sensitivity of $^{64}$Ga compared to GdL. In summary, $^{64}$Ga-Au@GdL may put a new entry into multifunctional PET/CT/MR contrast agent.

**REFERENCES:** 1.Jennings LE et al. (2009). “Two is better than one” -probe for dual-modality molecular imaging. *Chem. Commun*. 3511-24.

# Cell Patterning and Alignment on Nanostructured Isotropic and Anisotropic Carbon Nanotubes Substrates

C.A. Che Abdullah[1], P. Asanithi[1], E.W. Brunner[1], C. Lewis Azad[2], R. Ovalle-Robles[2], M.D. Lima[2], X. Lepro[2], S. Collins[2], R.H. Baughman[2], R. P. Sear[1], and A.B. Dalton[1].

[1]*Department of Physics and Surrey Materials Institute, University of Surrey, Guildford, Surrey, United Kingdom GU2 7XH, UK*

[2]*The Alan G MacDiarmid NanoTech Institute, The University of Texas at Dallas, Richardson, TX 75080-3021, USA*

**INTRODUCTION:** Cells sense and respond to the substrate they grown on, thus engineering the substrate is one method to achieve control over cell growth, which is required for tissue engineering. The nanoscale substrate surface patterning can regulate cell behavior and thus, play a vital role in tissue engineering. Cell-culture substrates with subcellular patterns have been fabricated via different methods and have been extensively used to investigate how cells respond to surface topography[1]. Herein we present results for Chinese Hamster Ovary (CHO) cells on both isotropic and anisotropic substrates based on carbon nanotubes with varying nanoscale roughness. We find that both cell morphology and orientation are controllable by modifying the nanoscale surface topography of the substrates. Our substrates offer control over topography on both the micro and the nanoscale.

**METHODS:** The aligned substrates are sheets drawn via compression and drag of the forest sidewall, utilizing an angled razor blade which generated a homogenous and transparent sheet of highly aligned MWNTs which were synthesized via catalytic chemical vapour deposition[2]. The diameters of MWNTs are approximately 10 nm and the heights are about 70 to 300 mm. Chinese Hamster Ovary (CHO) cells were plated at a density 1000-1500 cells/mm$^2$ in 6 well plates containing the substrates. After 20 hours, the cells were fixed and stained with DRAQ5 and Alexa Fluor 488 Phalloidin.

**RESULTS:** CHO cells adhered to and proliferated on both the isotropic buckypaper and anisotropic sheet based MWNTs substrates. Cells were concentrated distinctly with the alignment of the nanoscale grooves of the aligned MWNT bundles on the anisotropic MWNTs sheets [Fig. 1]. Confocal microscopy determines the findings that CHO cells preferably attach to the grooves and thus become linearly aligned within these spaces, a phenomenon called contact guidance.

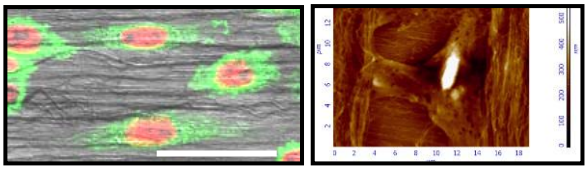

*Fig.1: Confocal images of CHO cells on anisotropic and control substrates (left and middle panel). The images are each merged images of actin staining (green), nucleus staining (red), and a DIC image. AFM height image showing cells bridging between two areas covered with carbon nanotubes (right panel).Scale bar is 20 µm.*

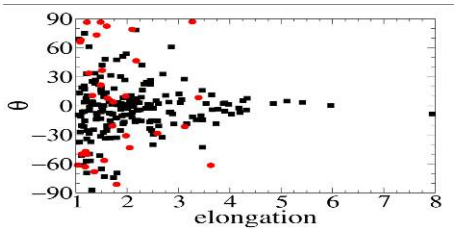


*Fig. 2: A scatter plot for cells on the aligned substrates (black squares) and control surfaces (red circles).*

**DISCUSSION & CONCLUSIONS:** We have proven that nanoscale topographical features significantly influence CHO cell attachment, proliferation, morphology and alignment. The bridging of the gap by cells found in our patterned substrates shows that larger scale (~10µm) features also influence cell behaviour and morphology. Our findings substantiate how future tissue scaffolds can be further engineered with a variety of modifications from structural to biochemical alterations and additions to direct cell behaviour.

**REFERENCES:** [1] Marcus, T. E., Erik, O. S., et al. (2008) *Journal of Biomedical Materials Research Part A* **86 A** (4): 996-1001. [2] Zhang, M., Fang, S. L., Zakhidov, A. A., et al. (2005) *Science* **309** (1): 1215-1219.

**ACKNOWLEDGEMENTS:** C.A Che Abdullah acknowledges MOHE and the Universiti Putra Malaysia for providing financial support for her Phd studies. P. Asanithi acknowledges the Royal Thai Goverment for his PhD funding.

# Self-microemulsifying Premicroemulsion Systems (SMEPMSs) As the Template for Preparing Nanodrugs and Nanoparticles

Ying-Chen Chen, Wei-Yu Huang, Hsiu-O Ho, Ming-Thau Sheu

*School of Pharmacy, College of Pharmacy, Taipei Medical University, Taipei, Taiwan*

**INTRODUCTION:** One important application for microemulsion systems is the utilization as template allowing one to obtain monodispersed size of the nanoparticles (inorganic or organic) by variation of the size of microemulsion droplet radius. Furthermore, the concept of diluting microemulsion system with water (continuous phase) to produce nanoparticles of mitotane by diffusion technique has been introduced by Trotta et al.[1] and the same technique was further applied to prepare griseofulvin nanoparticles[2]. This indicates that optimized dilutable SMEPMSs based on these partially water miscible solvents to form microemulsions are potentially workable as the template for preparaing nanodrugs and nanoparticles.

**METHODS:** The pseudo-ternary phase diagrams forming fenofibrate (FFB) SMEPMSs were constructed with respect to n-Butyl lactate (saturated with FFB) and the surfactant mixture (Tween 20/ethanol, 1-propanol, PEG 600 = 1/4, w/w) at a weight ratio from 1:9 to 9:1 by identifying the clear isotropic self-microemulsifying regions after dilution with 500 times volume of water.

One gram of optimal formulations selected in SMEPMSs regions was dropwise added with 10 ml of various kinds of saccharide solutions (lactose, mannitol, glucose, sucrose, or trehalose at a concentration of either 5 or 10%) at a rate of 3.3 ml/min. After vortexing for 3 min, the mixture was kept steady for 30 min and then the size and distribution of particles in-situ formed were measured. After then, the mixture was sonicated for 10 min and then freezing-dried (FD). The morphology of FD powder was observed by scanning electron microscope (SEM). The crystallinity of FD powder was characterized with X-ray powder diffraction. The particle size and distribution of FD powder was also measured at 30 and 90 min after resuspending in aqueous solution or 0.5% w/w sodium lauryl sulfate (SLS) solution of 50 times its weight with vortexing for 3 min.

**RESULTS:** The pseudo-ternary phase diagrams forming fenofibrate (FFB) SMEPMSs were constructed with respect to n-Butyl lactate (saturated with FFB) and several surfactant mixtures were constructed. Figure 1 shows a typical phase diagram for SMEPMSs and five formulations were selected for characterization of formation of FFB nanodrug with respect to several processing variables.

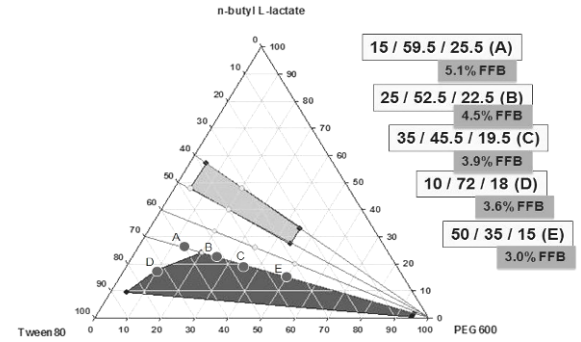


*Fig. 1: Phase diagram of Butyl Lactate/ Tween80/ PEG600 with FFB 100% loaded and five formulation points selected. (Black region: ME; Gray region: E)*

Figure 2 displays that before freeze-drying either in water or saccharide solution, the formation of FFB nanodrugs in amorphous form (confirmed by SEM and *x*-ray powder diffraction) was apparent. However, redispersion of those nanodrugs in water caused only a short time of solubilisation. Then precipitation of microsized particles was observed within 30 min, which of the time lag and the final size of precipitated particles were dependent on addition of SLS as dispersant and the kind of saccharide that codried with.

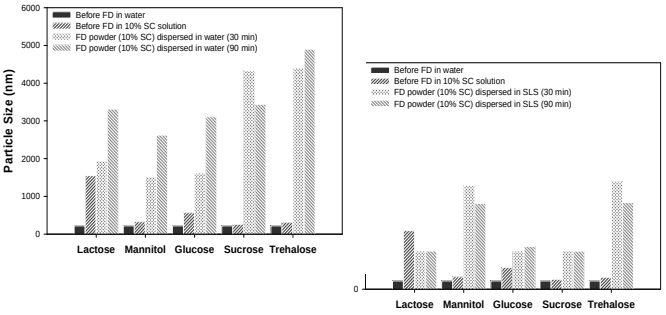


*Fig. 2: Mean particle diameter of the formula $A_e$ to $E_e$ at different treatment group before/after freeze-drying.*

**DISCUSSION & CONCLUSIONS:** Results demonstrated that using SMEPMSs as template could in-situ produce FFB nanodrugs after dilution with either water or saccharide solution. Although those nano-sized drug particles could be collected after freeze-drying, it precipitated in varying time lag (<30min) sooner after those nanodrugs were dispersed in aqueous medium. The addition of SLS as dispersant and lactose as cryoprotectant could reduce agglomeration tendency. It was concluded that using SMEPMSs as template is a practical and workable method for production of nanodrugs.

**REFERENCES:** [1]M. Trotta, M. Gallarate, F. Pattarino, S. Morel (2001) *J Controlled Release* **76**:119-128. [2] M. Trotta, M. Gallarate, ME Carlotti, S. Morel (2003) *Int J Pharm* **254**:235-42.

# Comparison of the effects of TEMPO, Radical containing Nanoparticle and Radical containing Nanoparticle combination Piperine on Aβ Amyloid Toxicity

P.Chonpathompikunlert[1]*, T.Yoshitomi[1], J.Han[2], K.Toh[1], H.Isoda[2], Y.Nagasaki[1]

*[1] Department of Materials Science, Graduate School of Pure and Applied Sciences, Tsukuba Research Center for Interdisciplinary Materials Science (TIMS), Center for Tsukuba Advanced Research Alliance (TARA), Graduate School of Comprehensive Human Science, International Center for Materials Nanoarchitectonics Satellite (MANA), National Institute for Materials Science (NIMS) and University of Tsukuba, Tsukuba, Ibaraki 305-8503, Japan. [2] Graduate School of Life and Environmental Sciences and The Alliance for Research on North Africa, University of Tsukuba, Tennoudai 1-1-1, Tsukuba, Ibaraki 305-8572, Japan*

**INTRODUCTION:** A β-amyloid-induced neurotoxicity involves several brain area caused by reactive oxygen species (ROS), specifically via increasing concentration of superoxide anion and hydroxyl radical in the brain. Recently, numerous researches have been done to find new drug for treatment this pathway[1]. We have been investigating stable nitroxyl radical compounds such as TEMPO, as a potential ROS scavenger. TEMPO, however, shows toxic effect at high concentration. In order to utilize nitroxyl radical in vivo, we have recently designed novel radical containing nanoparticle (RNP), which shows fairly low toxicity due to the compartmentalization of the nitroxyl radicals in the core. Thus, the antioxidant effect and potential mechanism of TEMPO, RNP and combination treatment with RNP and piperine (PI) in human neuroblastoma SH-SY5Y cells against β-Amyloid-induced cell toxicity should be investigated.

**METHODS:** Preparation of radical nanoparticle (RNP) was carried out by our original technique[2]. PEG-b-polystyrene (PSt) possessing TEMPO moiety as a side chain of PSt was prepared by conventional radical telomerization. (MW(PEG)=5000; MW (PCTEMPO =7600) The obtained block copolymer was dialyzed in aqueous media to form self-assembled core-shell type polymer micelle (RNP). The effects of TEMPO, RNP and RNP/PI on neuroblastoma SH-SY5Y cell lines were determined by WST assay for cell viability, nitroblue tetrazolium (NBT) and deoxyribose assay for reactive oxygen species (ROS) generation, ELISA assay for ROS product and apoptotic cell death, biochemical technique for catalase and glutathione peroxidase activity.

**RESULTS:** The combination of TEMPOL, RNP and RNP/PI significantly reduced the ROS level, ROS product and apoptotic cell death compared with control (untreated) group but free TEMPO and RNP attenuated toxic effect of Aβ though its extent is not as high as those of RNP/PI. Moreover, The RNP/PI treatment enhance catalase and glutathione peroxidase activity whereas free TEMPOL and RNP did not show these effect.

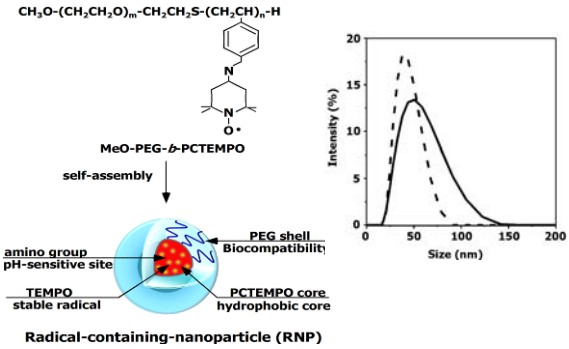


*Fig. 1: Radical-containing Nanoparticle (RNP)and Size distribution of nanoparticles before and after concentrated by a centrifugal evaporator*

**DISCUSSION & CONCLUSIONS:** Combination therapy with RNP and PI has an augmented high antioxidant effect on Alzheimer's model *in vitro*, which provides a novel promising approach in the treatment of Alzheimer's disease. The mechanism of protective effect of combination therapy was correlated with its ability to reduced reactive oxygen species generation and apoptosis via the scavenging enzyme action pathway.

**REFERENCES:** [1]Rutten, B.P., Steinbusch, H.W., Korr, H., Schmitz, C., 2002. Antioxidants and Alzheimer's disease: from bench to bedside (and back again). Curr Opin Clin Nutr Metab Care. 5, 645-651. [2]Yoshitomi, T., Miyamoto, D., and Nagasaki, Y., 2009. Design of Core-Shell-Type Nanoparticles Carrying Stable Radicals in the Core. Biomacromolecules 10, 596–601.

**ACKNOWLEDGEMENTS:** A part of this study was supported by a Grant-in-Aid for Scientific Research (#21240050) from the Ministry of Education, Culture, Sports, Science and Technology of Japan (MEXT).

# Shortening blood clots formation using ADP decorating chitosan nanoparticles

T.W.Chung, Y.F.Chen, H.S.Chen

*Department of chemical & Materials Engineering*

*National Yunlin University of Science & Technology, Taiwan, R.O.C.*

**INTRODUCTION:** Nanoparticles (NPs) have been widely reported as drug carriers in many research fields including in enhancing the rates and amounts of blood clot lysis [1-2]. Among many kinds of NPs, chitosan (CS) based NPs fabricated by using ionic gelation technique are simple and have been widely adopted by many researchers [1-3]. In this study, CS NPs with or without surface decoration with ADP (ACNP) or fibrinogen (FCNP) were fabricated for enhancing hemostasis or clot formations to stop large amount blood losses in medical operations.

**METHODS:** CSNP were prepared by an ionic gelation procedure. For fabricating NPs of ACNP I and II, 0.25% and 1.0 % of ADP solution, respectively, were slowly injected into CSNP solutions, and gently stirred for 20 min for coating process. The NPs were centrifuged, washed and re-suspended in PBS for further studies. The mean particle sizes and zeta potential value of NPs were measured using a DLS. For clotting 0.5 ml blood at 37 $^0$C, an adequate amount of $CaCl_2$ solutions and NPs (in $CaCl_2$ solutions, 6 % in final solutions) were added with mildly stirring. The clotting time is defined the time when plasma or blood was fully clotted to form a gel.

**RESULTS & DISCUSSION:** The characteristics of various NPs fabricated for this study were shown (Table 1). Mean particle size and zeta potential of FCNP were significantly large ($P<0.01$) and lower ($P<0.01$) , respectively, than others which might be due to that NP surface was coated by a high molecular weight and negative charges of fibrinogen [2]. Fig. 1 showed that the photograph of blood clot. In this work, the mean of blood clotting times (n=4) for $CaCl_2$ solution, CS NPs, ACNPs I, ACNP II and FCNP were 177.6±11.9s, 149.0±7.9s, 143.3±2.6s, 134.0±2.5s, 138.3±5.2s, respectively. Of interesting, the times of blood clots were significantly shorten by adding various NPs into blood solutions. The concentrations of ADP for coating CSNP also influenced blood coating times. In addition, among those adding various NPs, the rate of shortening blood clotting times for ACNP II was the highest (43.8 % of $CaCl_2$) while those for CS and FCNP were about 59.9 % (Fig. 2).

*Table 1 Mean particle sizes, zeta potential, and poly-dispersity (PDI) of NPs (n=4).*

| | mean particle size (nm) | zeta potential (mV) | PDI |
|---|---|---|---|
| NP | 251.0±9.8 * | 24.1±0.5 * | 0.15±0.02 |
| ACNP | 245.3±13.9 | 20.6±1.9 | 0.19±0.04 |
| FCNP | 326.5±14.5 * | 15.3±1.5 * | 0.24±0.01 |

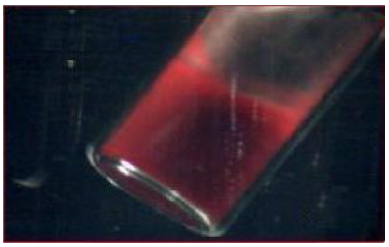

*Fig. 1: The phase change of blood from solutio*

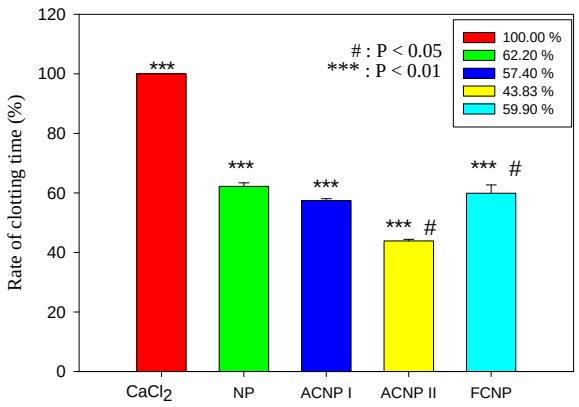


*Fig 2: Blood clotting tims (%) (n=4).*

**CONCLUSIONS:** According to this investigation, blood clotting times can be highly shorted by adding CS based NPs. Moreover, ACNP II has the highest shortening blood clotting time among the tested NPs which has a potential for medical applications.

**REFERENCES:** [1]R. Mehravar, M. Jahanshahi et al (2010) Afr. J. Biotechnol. **8**:6822-27. [2]T.W. Chung, S.S. Wang, W.J. Tsai, et al (2008) *Biomaterials* **29**:228-37. [3]Grenha, A., Remuñán-López, C., Carvalho, E.L.S., Seijo, B.,et al (2008) *Eur. J. Pharm. Biopharm.* **69**:83-93.

**ACKNOWLEDGEMENTS:** This work was supported by a grant from the National Science Council, NSC 96-2221-E-224-007-MY3), Taiwan, Republic of China.

# Vesicle adsorption on mesoporous silica and titania

M. Claesson[1], N-J. Cho[2], C. Frank[2], M. Andersson[1]

*1Department of Chemical and Biological Engineering, Chalmers University of Technology, Gothenburg, Sweden,*

*2Department of Chemical Engineering, Stanford University, Palo Alto, CA, USA*

**INTRODUCTION:** Lipid bilayers are essential in the development of novel biosensing devises since it can serve as a host for transmembrane proteins, such as ion channels, which can be utilized as sensing elements[1]. Traditionally, transmembrane-based bio-sensors are either constructed using a solid supported lipid bilayer (SLBs) or on an aperture spanning membrane. A successful design should provide high mechanical robustness to the membrane as has been shown for SLBs[1], and at the same time provide a suitable environment for transmembrane proteins, as has been shown for aperture spanning membranes[2]. In order to form a functional biosensor, having both these before mentioned qualities, we propose to use mesoporous supported lipid bilayers. The porous structure would result in a stable support due to the pore walls and at the same time provide adequate environments below and above the membrane for the pore spanning part of the membrane. The properties of mesoporous materials, such as, the pore sizes, pore geometry and surface chemistry can be tailored, which allows us to precisely design the support.

**METHODS:** Vesicles, consisting of phospholipids (POPC), were adsorbed on mesoporous and on non-porous silica and titania. The adsorption process was studied by quartz crystal microbalance with dissipation monitoring (QCM-D) and the fluidity of lipids was investigated by fluorescent recovery after photo bleaching (FRAP). Mesoporous materials were prepared according to the sol gel-gel process, which involved self-assembly of silica or titania species together with a triblock copolymer template (P123)[3].

**RESULTS:** We observed SLB formation on mesoporous (pore size roughly 4 nm) and non-porous silica, and intact vesicle adsorption on mesoporous and non-porous titania. This can be seen in the obtained QCM-D results presented in Fig.1. The QCM-D results show a more rapid lipid bilayer formation on the mesoporous silica compared to on non-porous silica. The FRAP analyses (not shown here) showed that the diffusivity of the lipids on silica was decreased by the presence of the mesopores.

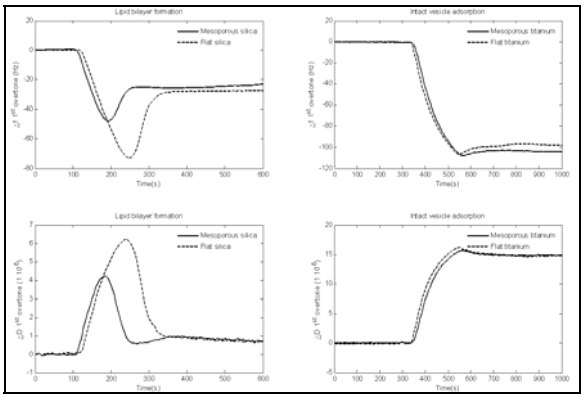


*Fig. 1: QCM-D results showing that lipid bilayers were formed on both silica surfaces. The lipid bilayer was formed more rapidly on mesoporous silica compared to on non-porous silica. Vesicles adsorbed intact on all titanium surfaces regardless of the porosity.*

**DISCUSSION & CONCLUSIONS:** The results showed that lipid bilayers were formed on both mesoporous and non porous silica and that intact vesicle adsorption was obtained on titania, regardless of porosity. This difference is probably due to that the vesicle-surface interaction is stronger on silica, due to its low isoelectrical point (IP ≈2), compared to titania (IP ≈4). The more rapid formation of lipid bilayers on mesoporous silica is suggested to be due to stronger vesicle deformation caused by the porous structure. According to the results obtained by the FRAP measurements, it could be concluded that the mesoporous supported membrane is fluidic. Mesoporous silica is considered to be a promising support for lipid bilayers, to be used in bio sensing devises.

**REFERENCES:**[1]Sackmann.,E (1996), *Science*, **271**:43-48. [2]Schmitt, E. K. Weichbrodt, C.; Steinem, C., (2009) *Soft Matter*, **5**:3347-3353. [3]Alberius P. C. A.; Frindell, K. L.; Hayward, R. C.; Kramer, E. J.; Stucky, G. D.; Chmelka, B. F., (2002) *Chem. Mat.*, **14**:3284-3294.

# Consideration of aggregation processes for nanoparticle exposure assessment

C.Conteduca[1], N. von Goetz[1], K.Hungerbühler1

[1] *ETH* Zürich, *Safety and Environmental Technology Group, Switzerland.*

**INTRODUCTION:** Engineered nanoparticles (ENP) play an important role in a wide variety of industrial products due to their unique physical and chemical properties. Consumers therefore are more and more exposed to ENP of different size, shape and speciation that are contained in these products. For nanoparticles size and shape also influence their uptake rates into the body and, as ENP tend to agglomerate faster than the bulk material, size and shape can change after incorporation into the product. Therefore, for modelling consumer exposure, the aggregation dynamics after product formulation should be known and taken into account.
Currently, two mechanisms of colloid aggregation due to Brownian motion are described in the scientific literature: diffusion-limited colloid aggregation (DLCA), occurring when the aggregation is limited only by the time it takes for a particle to collide with another, and the reaction-limited colloid aggregation (RCLA), which takes place when the repulsion energy between two particles is higher than the kinetic energy. More generally the DLCA is a rapid aggregation process compared to the RLCA that is a slow process.
The two processes cannot be associated with specific nanoparticles, but depend on several parameters, like e.g. charge of the ENP, pH of the solution or the coating. By modeling aggregation and subsequent flocculation of bigger particles in different solvents it is possible to estimate the aggregate distribution in the solution at different times and use this in exposure assessment, without the need of specific experiments for every single combination of parameters.

**METHODS:** In this work we investigate the formation of ENP aggregates at different ENP concentrations and solvents by taking into account agglomeration, diffusion and flocculation processes. We have evaluated the shape of aggregates formed by RCLA and DCLA by using different stochastic models and a simplified Boltzmann-Lattice model to simulate the distribution of the nanoparticle aggregates at a given time. [1] We refined the model to account for different aggregate sizes and different solvents.

**RESULTS:** The aggregates modelled by assuming two different aggregation mechanisms, RCLA and the DCLA, have different structures (see Figure 1).

As also shown by Moncho-Jorda et al.[1] the DLCA clusters are more open and their fractal dimension is lower than 2. The RCLA clusters are comparatively more compact and have a dimension higher than 2.

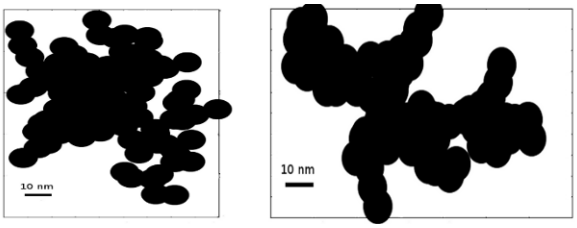


*Fig. 1: Aggregate structures simulated assuming RCLA (left) and DCLA (right)*

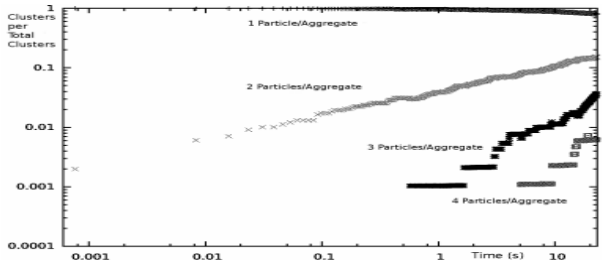


Fig. 2: *Time evolution of the normalized aggregate-size distribution.*

For modelling the distribution of aggregates of different sizes at different times we used a Lattice-Boltzmann simplified model [2] that was modified to account for different aggregate sizes and gives the distribution of the nanoparticle aggregates in the solution for each time t after the incorporation of the nanoparticles into a solvent (see Figure 2).

**DISCUSSION & CONCLUSIONS:** By using different stochastic models it is possible to model the time evolution of shape (Fig:1) and size of aggregates (Fig:2) in consumer products on the basis of the fundamental colloid aggregation processes. This important information can directly be used in exposure and subsequent risk assessment.

**REFERENCES:**[1] Moncho-Jorda et al. (2001) The DLCA-RLCA transition arising in 2D-aggregation: simulation and mean field theory, *The European Physical Journal E* **5** 471-480. [2]Augustin E. Gonzales and Guillermo Ramirez-Santiago (1996) Scaling of the Structure Factor in Fractal Aggregation of Colloids: Computer Simulation, *Journal of Colloid and Interface Science* **182**, 254-267.

**ACKNOWLEDGEMENTS:** Funding of this work by the *Swiss Federal Office of Public Health (*FOPH) is gratefully acknowledged.

# Nanomedicines: a new approach for the treatment of severe diseases

P.Couvreur1

[1] *Université Paris-Sud, UMR CNRS 8612, Chatenay-Malabry, France*

The major obstacle to drug efficacy is the non-specific distribution of the biologically active compound after administration. This is generally due to the fact that the drug distributes according to its physico-chemical properties which makes that diffusion through biological barriers may be limited. Also, certain chemical entities are either rapidly degraded and/or metabolized after administration (peptides, proteins, nucleic acids). This is the reason why the idea has emerged that nanotechnologies may be employed to modify or even to control the drug distribution at the tissular, cellular or subcellular level.

The huge progresses done in material sciences as well as a better knowledge of the physio-pathological disorders of the diseased areas in the body has allowed to construct “smart” nanodevices to perform temporal and spatial site specific delivery. Nanosystems may also be useful to improve the performance of imaging techniques applied for the in vivo diagnosis. Thus, although we are still far from the ideal “magic bullet” proposed a century ago by the immunologist Nobel laureate Paul Ehrlich, today nanotechnology has already completed several key achievements to reach this goal.

In general, “smart” nanocarriers may be equipped with a “core” and a “corona” able to confer to the resulting supramolecular assemblies following functionalities:

Protection of the drug from the recognition by the various detoxification processes of the organism (ie. degradative enzymes or efflux proteins)

Combination of various biologically active compounds acting on complementary biological targets (ie. antiangiogenic and DNA intercalating agents)

Release of the drug content in a controlled manner in response to an external stimuli (ie. pH, temperature or magnetic responsive nanocarriers)

Camouflage towards the recognition by the immunological self-defense mechanisms of the body (ie. “stealth” nanocarriers)

Targeting of specific tissues, cells or even sub-cellular compartments which is attainable by decorating these nanodevices with molecular

ligands (ie. monoclonal antibodies, hormones, peptides, vitamins etc.)

Ability to deliver intra-cellularly drugs which don’t diffuse spontaneously into cells

Combination of a pharmacological and an imaging agent to get simultaneously personalized patient treatment and diagnosis (“Nanotheranostics”)

Although the introduction of nanotechnology has obviously permitted to step over numerous milestones towards the development of the above mentioned “Magic Bullet”, a lot of work remains, however, to be done. Next improvements will certainly come from the introduction of new materials including better stimuli responsive polymers or lipids to elicit the challenge of targeting the drug to its specific site of action, to retain it for the desired duration and to release it according to the correct time schedule. It may also be expected that more sophisticated and multifunctional systems will be conceived allowing with a single system to perform in vivo diagnostic and to release the targeted drug on demand. Finally, the development of strategies aiming to develop entities existing in Mother Nature and based on biomimetism should also participate to major progresses in the next few years.

**ACKNOWLEDGEMENTS:** Some results presented in this lecture were financially supported by ERC Advanced Grant n°249835 TERNANOMED

# Nanostructures for biological investigations

H. G. Craighead

*School of Applied & Engineering Physics, Cornell University, Ithaca, NY USA*

We have explored a variety of lithographic and non-lithographic methods to engineer structures of controlled geometry for integration into new types of analytical systems. In one approach we have used high resolution lithography to pattern a bio-compatible sacrificial polymer layer in order to form surface chemical patterns with minimum feature sizes as small as tens of nanometers. This has been useful for investigating the response of individual cells to spatially well-defined stimuli. We have used similar approaches to create organized cell cultures and to guide the attachment and growth of cells on surfaces. These are building blocks for investigations of cells in engineered microenvironments.

For some time we have been interested in exploring a new paradigm of molecular analysis based on isolation, control and interrogation of many individual molecules. We have studied, for example, the use of nanostructures for manipulating the confirmation and position of DNA molecules and for isolating individual nucleic acid fragments for analysis. The systems involve the integration of nano-scale fluidics and optics. One target for the molecular isolation has been sequence and genetic information, but we also have been targeting individual chromatin molecules for epigenetic analysis. By identification of one or more labelled epigenetic marks on individual chromatin fragments we are quantifying the occurrence of epigenetic features. In addition to identification and quantification of the presence of labelled marks, we are attempting to automatically sort and recover selected fragments for subsequent analysis.

We have recently explored the utilization graphene sheets down to single atom thickness as mechanical components in systems of potential use for molecular sensing and detection. The talk will address the fabrication approaches used for creating these structures and devices.

# Interaction of Oxide Nanoparticles with Bone Cells

T.Daberkow[1], F.Meder[1], L.Treccani[1], K.Rezwan[1]

[1] *Advanced Ceramics Group, Universität Bremen, Am Biologischen Garten 2, Bremen Germany.*

**INTRODUCTION:** The understanding of the interaction between nanoparticles and biological systems is of increasing interest as the application of new materials in the biomedical sector is steadily growing. An example for the release of nanoparticles into the human body is abrasive wear of e.g. hip joint replacement, where oxide materials are typically used such as $Al_2O_3$, $ZrO_2$, and $TiO_2$. The effects of these types of nanoparticles are still unclear and have not been elucidated in depth yet [1].

**METHODS:** As core particles for the coating we used $SiO_2$ nanoparticles (Fibre Optics Centre, US), ~150nm in diameter. These were coated with alumina (as described in [2]), titania, and zirconia by sol gel processes followed by a calcination step (700°C, 5h). Quality of the coatings was characterized by zeta-potential measurements, electron microscopy (HR-TEM, including element mapping), and measurement of specific surface area (BET). Crystallinity of the coatings was determined by X-ray diffraction (XRD). For the cell test human tumorous bone cells (osteosarcoma, MG-63 for details see [3]) were used, culture medium was Dulbecco's Modified Eagle Medium (DMEM) including 10% Fetal Calf Serum (FCS), and 1% antibiotics/antimycotics, substrate for cell culture was a polyester film surface modified to be hydrophilic for cell adherence (Thermanox®). Cells were exposed to uncoated and coated nanoparticles. Nanoparticles were added as an aqueous suspension after cell seeding, the final concentration of nanoparticles in the cell medium was 0.2 %wt, cells were stained with 4′,6-Diamidin-2-phenylindol (DAPI) and Phalloidin (Alexa Fluor 488) for nucleus and cytoskeleton respectively.

**RESULTS:** A well defined complete coating of different metal oxide types ($Al_2O_3$, $TiO_2$, $ZrO_2$) on silica substrate nanoparticles was applied. As shown in Fig.1 the isoelectric point (IEP, pH where the zetapotential is zero) after coating shifted from 2.8 for silica to values expected from the respective ceramic: 9.4 for $Al_2O_3$, 5.2 for $TiO_2$, and 6.4 for $ZrO_2$,. The cells exposed to nanoparticles showed considerably lower cell numbers than cells without nanoparticles exposition (control) as shown in Fig.2.

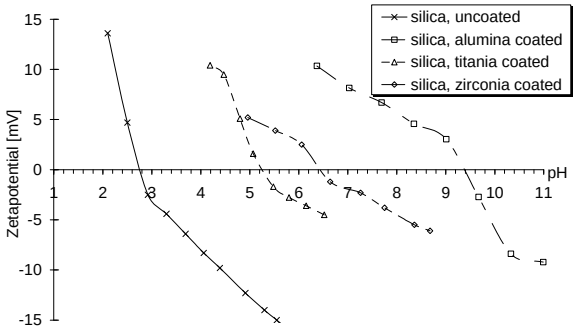


*Fig. 1: Zetapotential of nanoparticles (uncoated and coated with different metal oxides).*

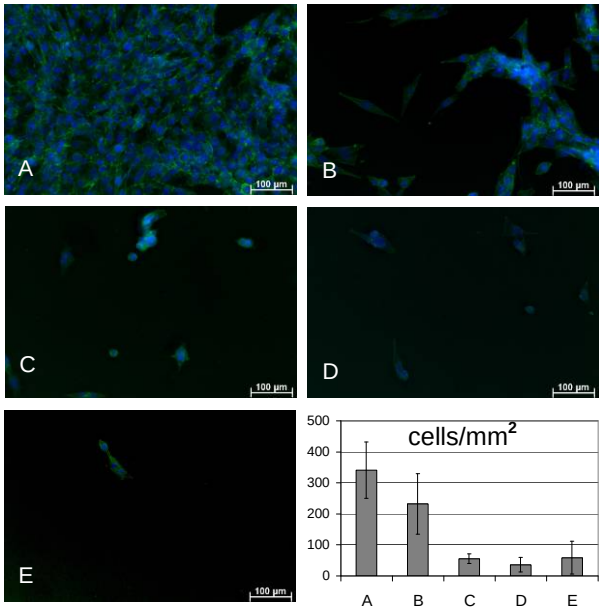


*Fig. 2: Cell numbers after 72h of exposition to control (A), uncoated $SiO_2$ (B), $Al_2O_3$ coated (C), $TiO_2$ coated (D) and $ZrO_2$ coated (E) nanoparticles respectively.*

**DISCUSSION & CONCLUSIONS:** The strong decrease of cell number compared to the control for samples exposed to coated nanoparticles indicates a material depending influence of interaction between nanoparticles and cells. The fabricated particles could be used as a model system to describe the cytotoxicity as a function of material, as the change of size and morphology of the coated nanoparticles was minimal.

**REFERENCES:** [1]S.M. Hussain et al (2009) *Advanced Materials* **21**(16): 1549-1559. [2]K. Rezwan, L.P. Meier, L.J. Gauckler (2005) *Biomaterials* **26**(21):4351-4357. [3]A. Biliau, V.G. Edy et al (1977) *Antimicrobial Agents and Chemotherapy* **12**(1): 11-15.

# Electrochemical Processes in Plasmonic Nanostructures

A.B. Dahlin, T. Sannomiya, R. MacKenzie, B. Dielacher, J. Vörös.

*Swiss Federal Institute of Technology, Zürich, Switzerland.*

**INTRODUCTION:** Electrochemistry and plasmonics both present ways to "play with" free electrons. Our combinations of these techniques are shown to provide new insights into the underlying physical mechanisms. We show how optical spectroscopy of localized and propagating plasmons in gold nanostructures can be used to monitor electrochemical processes that occur on or inside the metal. A variety if conductive gold nanostructures with plasmonic resonances are utilized, such as nanoparticles on indium tin oxide, nanowire arrays or nanoholes in a thin gold film.

**METHODS:** Colloidal lithography was used to produce large areas covered with short-range ordered disks or holes, essentially free of defects. Optical spectroscopy was performed with high resolution, tracking resonance wavelength shifts with a resolution of $10^{-3}$nm at 1s temporal resolution, even on micrometer spots. Electrochemical potentials were applied using a three electrode setup with the plasmonic nanostructures as working electrode, a silver reference electrode and a platinum counter electrode. A simple flow cell was used and measurements were performed at room temperature with 100mM salt concentration.

**RESULTS:** We have studied the influence of electrochemical potentials on e.g. gold nanoparticles by cyclic voltammetry scans. Together with the electrochemical current we acquire synchronized data of plasmon resonance peak position, magnitude and linewidth. In the capacitive charging regime (-200mV to +500mV), a linear and reversible signal is observed when measuring e.g. peak position vs applied potential. Also, a clear damping of the plasmon resonance is observed for positive potentials.

When the potential is increased (up to 800mV), electrochemical reactions can be observed in the current data, corresponding primarily to formation of goldchloride. This is accompanied by large changes in the optical spectrum. When the potential is reversed to negative values, goldchloride is dissolved again, resulting in a hysteresis loop in the peak position vs potential graph.

At higher potentials (>1V) gold starts to dissolve and irreversible changes in the optical spectrum can be observed.

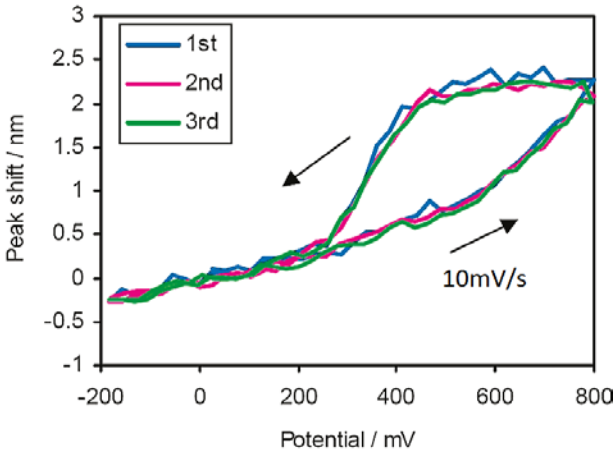


*Fig. 1: Nanoparticle plasmon resonance wavelength shift as a function of applied potential (vs Ag/AgCl) scanned three cycles. A linear relation is observed up to +500mV, after which a reversible hysteresis loop occurs.*

**DISCUSSION & CONCLUSIONS:** As we have discussed on the basis of theoretical models, the plasmon response is dominated by the charges in the metal, which alter the electron density locally close to the surface. In principle, a layer with new material properties is created on the gold surface. Even if only around 20% of the surface atoms carry a charge at +500mV, which can be calculated by integrating the current, this leads to major changes in the spectrum. In fact, the nanoplasmonic sensors are almost as sensitive to a single electron as a single biomolecule binding to the surface.

We also show that the refractive index increase from attracted ions is relatively small and should not lead to any major changes in the optical signal.

**REFERENCES:** [1] T. Sannomiya, H. Dermutz, C. Hafner, J. Vörös and A.B. Dahlin (2010) *Langmuir* **in press**. [2] M.P. Jonsson, A.B. Dahlin, P. Jönsson and F. Höök (2009) *Biointerphases* **3**: Fd30-Fd40. [3] A.B. Dahlin, S. Chen, M.P. Jonsson, L. Gunnarsson, M. Käll and F. Höök (2009) *Analytical Chemistry* **80**: 6572-6580. [4] V. Auzelyte, H.H. Solak, Y. Ekinci, R. MacKenzie, J. Vörös, S. Olliges, R. Spolenak (2008) *Microelectronic Engineering* **85**: 1131-1134.

**ACKNOWLEDGEMENTS:** This work was funded by ETH Zürich and the Swedish Research Council.

European Cells and Materials Vol. 20. Suppl. 3, 2010 (page 49) ISSN 1473-2262

# Compartmentalization by directional gene expression

SS. Daube[1], D. Bracha[2], A. Buxboim[2], RH. Bar-Ziv[2]

*[1]Chemical Research Support, [2]Department of Materials and Interfaces*

*The Weizmann Institute of Science, Rehovot, Israel, 76100*

**INTRODUCTION**: Gene expression in the nucleus takes place in highly concentrated compartments of macromolecules and solutes, with order and orientation of genes, in contact with a feeding reservoir. Our understanding of the effect of density, spatial heterogeneity, and order on gene expression has been limited by the difficulty to experimentally reproduce in vitro the crowded and compartmentalized nature of the cellular DNA environment. We propose an *in vitro* methodology to emulate gene expression in a boundary-free compartment. The approach is based on a photolithographic biochip for fabricating dense phases of surface-bound DNA, thus forming DNA brushes [(1)] (Fig. 1A). The dense brush creates order since sequences align along vertical layers, with well-defined mean distances and orientation relative to the surface (Fig. 1B, C).

**METHODS: Light-directed localization of genes:** Exposure of 'daisy' monolayer to 365nm UV light through a mask de-protects the surface amines allowing conjugation of biotin. Biotinilated long dsDNA molecules are conjugated to SA in solution and are then patterned on the surface biotins to form density-controlled extended DNA brushes (Fig. 1A).

**RESULTS & CONCLUSIONS**: By immobilizing DNA in a dense and ordered fashion and using it as a template for a directional process such RNA transcription [(1,2)], we were able to observe the formation of a segregated environment with characteristically different biochemical activity than the surrounding bulk solution. In the brush, transcription rate was sensitive to the density of the brush, was robust to DNA condensation, and responsive to the position and direction of the promoter, as well as transcript length. The alignment of promoters and terminators all in the same direction and distance from the surface produced a sink and source, respectively, for RNAP, resulting in concentration gradients within the brush [(2)]. Towards the construction of a synthetic cell, we hypothesize that several patterned directional reaction centers on surfaces, each specifying a distinct biochemical activity, could form an interacting network of activities responding to gradients of concentrations according to their direction and spatial localization, all in the absence of a physical barrier [(3)].

A

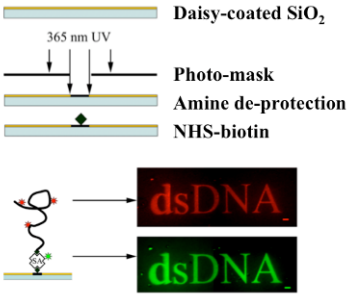


B

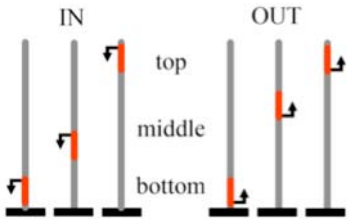


C

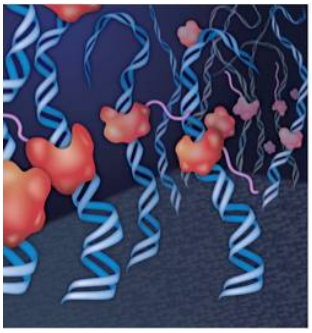

*Fig. 1: (A) DNA brushes are photo-lithographed on a silicon platform. (B) DNA brushes can assemble with a transcription unit facing either away or into the surface and at different distances, forming layers of RNA polymerase perpendicular to the surface (C).*

**REFERENCES:** [1] A. Buxboim, S. S. Daube, R. H. Bar-ziv (2008) Mol Sys Biol **4**: 181.[2] S. S. Daube, D. Bracha, A. Buxboim, R. H. Bzr-Ziv (2010) Proc. Natl. Acad. Sci., USA **107**: 2836-2841.[3] Research highlights (2010) Biopolymers 93: iii.

**ACKNOWLEDGEMENTS:** This work was supported by the Israel Science Foundation and the Minerva Foundation

# Monitoring the adsorption of monoclonal IgGs by QCM-D

P. de Thier and C.C. Dupont-Gillain

*Université catholique de Louvain, Institute of Condensed Matter and Nanosciences Bio- & Soft Matter, Croix du Sud 2/18, 1348 Louvain-la-Neuve, Belgium*

**INTRODUCTION:** ELISA (Enzyme Linked ImmunoSorbent Assay) tests represent one of the most important applications of monoclonal antibodies (IgGs). For ELISA tests, IgGs are adsorbed on a surface and serve as receptors for antigens in solution. Polystyrene (PS) is a widely use sorbent owing to its low cost and hydrophobic character which improves protein adsorption. When IgGs adsorb on PS, they undergo conformational changes to maximize interactions with the hydrophobic sorbent surface. These conformational changes may affect the constant domain as well as the variable ones. While this may promote adsorption [1], it may also affect antigen recognition [2]. Moreover, adsorption in "end-on" orientation with the constant domain in contact with the sorbent surface is also preferred, in such a way that the variable domains are available for antigen binding, thereby increasing the efficiency of ELISA detection kits [3].

The aim of this work is to monitor the adsorption of IgGs on PS. Attention will be paid to adsorption kinetics, adsorbed amount, orientation and conformation of adsorbed monoclonal IgGs. In a first step of this research, the adsorption of different isotypes of IgGs (1, 2a, 2b and 3) from different species (mouse, rat and human) was compared using quartz crystal microbalance (QCM-D). This very sensitive technique allows adsorption to be monitored in real time and in situ.

**METHODS:** The QCM-D system (E4 from Q-Sense) was equipped with flow cells. IgGs were adsorbed on a PS thin film spin-coated onto quartz crystals. The adsorption protocol was inspired by ELISA tests. Different IgG concentrations were tested, ranging from 1 to 20 µg/ml. After IgG adsorption, followed by surface saturation with bovine serum albumin (BSA), the antigen (2,4-dinitrophenol-albumin (DNP) for murine IgGs and cachectin (TNFα) for human IgGs) solution was brought in contact with the surface.

**RESULTS and DISCUSSION:** As expected, the IgG adsorbed amount was shown to increase with concentration in solution. BSA adsorbed amount was inversely correlated with IgG adsorbed amount, reflecting the fact that BSA molecules adsorb on the interfacial domains not covered by IgGs. In a particular case (mouse $IgG_{2a}$), BSA was shown to displace adsorbed IgGs, which may point to a weaker IgG-substrate interaction. Antigen binding globally increased with IgG adsorbed amount. However, depending on IgG isotype and species of origin, antigen/IgG ratio varied, indicating differences in orientation and/or conformation of adsorbed IgGs (see Fig. 1, inset). For a given IgG concentration, adsorption kinetics and adsorbed amount at the plateau strongly differed depending on IgG type (see Fig. 1), giving indications on the affinity of IgGs for the surface. The differences between initial slopes could be explained by deformability of IgGs [4]. Mouse $IgG_{2a}$ could be more subject to conformational changes compared to $IgG_{2a}$ from rat and human.

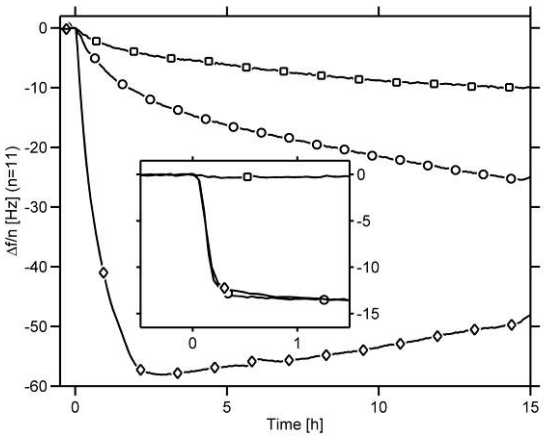


*Fig. 1: Adsorption kinetics of $IgG_{2a}$ (4 µg/ml) from human (square), rat (circle) and mouse (diamond). Inset: corresponding antigen binding.*

**CONCLUSION and PERSPECTIVES:** These first results show the wide variability of adsorption behaviours depending on IgG isotype and species of origin. Antigen-IgG recognition will now be probed by single-molecule force spectroscopy to further explain these results.

**REFERENCES:** [1]J. Buijs, W. Norde, and J.W.Th Lichtenbelt (1996) *Langmuir*, **12(6)**: 1605-13. [2]M. Torres, N. Fernández-Fuentes, A. Fiser, and A. Casadevall (2007) *J. Biol. Chem.* **282(18)**, 13917-27. [3]J. Buijs, D.D. White, and W. Norde (1997) *Colloids Surf. B* **8**: 239-49. [4]V. Hlady (1991) *Appl. Spectrosc.* **45(2)**:246-52.

**ACKNOWLEDGEMENTS:** This work was supported by Région Wallonne (AMOVIM project).

# Self-Assembled Peptide Microspheres

D. de Bruyn Ouboter[1], Th. B. Schuster[1], Ch. Dittrich[1, 2], W. P. Meier[1]

[1] *Department of Chemistry, University of Basel, Basel, Switzerland.*

[2] *Current Affiliation: Harvard Medical School/Children's Hospital Boston, Boston, USA.*

**INTRODUCTION:** In recent years, bottom-up strategies such as self-assembly have found great appeal in the construction of functional nano-sized materials. Whereas lipid and polymeric systems have been widely used, purely peptidic systems are still rare, even though they can offer the advantages of being biocompatible and synthetically well-controllable regarding their amino acid sequence.

**METHODS:** *Synthesis* implemented Fmoc-based solid-phase peptide synthesis on Rink Amide AM resin and HCTU/DIPEA in DMF as the coupling reagent. *Purification* was performed on C18e HPLC with 0.1% TFA and 2% AcOH-buffered acetonitrile:water gradients, followed by desalting and lyophilisation. *Self-assembly* was induced by dissolving the peptide in ethanol followed by exchange of the solvent with water (dialysis). *Characterisation:* Transmission- and scanning electron microscopy (TEM, SEM), atomic force microscopy (AFM), confocal laser scanning microscopy (CLSM), dynamic and static light scattering (DLS, SLS), and small angle X-ray scattering (SAXS) using synchrotron source.

**RESULTS:** We synthesized and purified gT-$X_3$-Ac, a short amphiphilic decapeptide (Ac-[LK(Ac)]$_3$-[LW-DL]$_3$-LW-$NH_2$), with the hydrophobic part consisting of a truncated gramicidin sequence and the hydrophilic part of acetylated lysines. The peptide self-assembles to spherical objects with radii in the 50 − 500 nm range depending on the peptide concentration[1]. Microscopic- and scattering-techniques at different stages of the self-assembly process revealed that the microspheres are solid and hierarchically self-assemble by aggregation of primary micelles[2].

Experiments in which a C-terminal cysteine functionalized analogue of the peptide (C-gT-$X_3$-Ac) was coupled to gold-nanoparticles (5 nm) prior to microsphere formation yielded composite peptide-gold microspheres with a regular inner order after the self-assembly.

Embedding experiments showed that hydrophilic as well as hydrophobic guest molecules (dyes, drugs, siRNA) can be hosted and enriched in our peptide microspheres. Preliminary experiments on THP-1 cells indicated that the microspheres were non toxic and possess the capacity to deliver guest molecules to the cells.

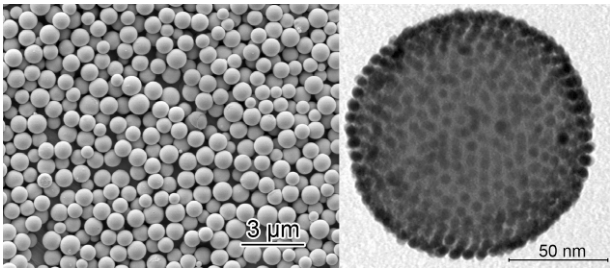


*Fig. 1: Peptide microspheres, SEM (left) and composite peptide-gold microsphere, TEM (right).*

**DISCUSSION & CONCLUSIONS:** Based on our experiments, we suggest a hierarchical self-assembly of the amphiphilic peptide into micelles, followed by aggregation of the micelles, and maturation of the resulting multicompartment micelles into solid spheres. SAXS data confirm that the microspheres consist of nanometer-sized building blocks with diameters corresponding to the primary micelles. Additionally, gold-nanoparticle loaded micelles form closely packed spherical multicompartment micelles. The fact that we can embed hydrophilic and hydrophobic guest molecules additionally indicates compartments with different polarities within the microspheres. Noteworthy are the capacity to embed guest molecules and the biocompatible nature of the material, strongly implying application as a drug delivery system. In addition, the composite peptide-metal microspheres are expected to show exceptional optical and electronic properties (quantum size effect)[3].

**REFERENCES:** [1] Ch. Dittrich, D. de Bruyn Ouboter, Th. B. Schuster, W. P. Meier (2010), *Biomaterials*, submitted. [2] Th. B. Schuster, D. de Bruyn Ouboter, E. Bordignon, Ch. Dittrich, G. Jeschke, W. P. Meier (2010), *Soft Matter*, submitted. [3] M.-C. Daniel, D. Astruc (2004) *Chem. Rev.*, **104***:* 293–346.

**ACKNOWLEDGEMENTS:** Financial support by the SNSF and the NCCR Nanosciences is gratefully acknowledged. The authors thank the Zentrum für Mikroskopie Basel (ZMB), Dr. M. Kümin and R. Erdmann (Prof. H. Wennemers), Dr. A. Mantion (BAM/BESSY), Dr. B. Fischer, Dr. N. Bruns, and M. Inglin.

European Cells and Materials Vol. 20. Suppl. 3, 2010 (page 52) ISSN 1473-2262

# Patterning Proteins on Surfaces: at What scales and What for?

E. Delamarche[1], S.R. Coyer[1,2], D.J. Solis[1], A.J. García[2]

*[1] IBM Research GmbH, Rueschlikon, Switzerland. [2] Woodruff School of Mechanical Engineering, Petit Institute for Bioengineering and Bioscience, Georgia Institute of Technology, Atlanta, USA.*

The involvement of nanotechnology in biology, biomedical devices, and analytical sciences provides tantalizing opportunities to miniaturize biosensing platforms for applications in diagnostics, biotechnology, environmental monitoring, pharmaceutical research, and research in life sciences at large. Key for realizing these opportunities is the accurate patterning of protein receptors on surfaces and the development of new bio-analytical methods

The immobilization of receptors for analytes on surfaces is a first step in many bioassays, a prerequisite for the design of bioelectronic devices, and valuable in certain combinatorial screening strategies. In biosensors, molecules are often immobilized on a solid surface, where they function as specific ligands for biomolecules such as enzymes, antigens, antibodies, and DNA. Therefore, biopatterning receptors on surfaces with great accuracy might be helpful for realizing demanding bioanalytical applications as well as for investigating the role of proteins, or, more generally, the role of complex protein architectures, in biological events that occur on surfaces.

Microcontact printing and structured elastomeric poly(dimethylsiloxane) stamps can be used to decorate surfaces with proteins down to the nanometer scale – even attaining individual proteins. All applications of microcontact printing proteins however do not require the same degree of protein patterning accuracy and technical implementation. Both the critical dimensions of the protein patterns and their pitch (distance of repetition of identical motives) are important and may determine which patterning method should be used. For example, the patterning of proteins on surfaces at lengthscales of 100 nm for cell research (pitch of tens of micrometers) and 100 nm for arraying biological libraries (pitch of approx. 1 micrometer) is highly challenged by the limited mechanical stability of structured stamps.

Using planar stamps that have a layer of protein everywhere and structured nanotemplates for selectively removing proteins from the planar stamp, we are now able to easily pattern proteins on surfaces with sub-100-nm resolution and arbitrary patterns. This method is also applicable

to the simultaneous patterning of multiple proteins into complex architectures with high resolution, high contrast, and self-alignment.

# Mixed PEO/PAA brushes for the control of protein adsorption

M.F. Delcroix[1], W. Van Camp[2], F.E. Du Prez[2], C.C. Dupont-Gillain[1]

[1]*Université catholique de Louvain, Institute of Condensed Matter and Nanosciences, Bio & Soft Matter, Croix du Sud 2/18, 1348 Louvain-la-Neuve, Belgium*

[2]*Ghent University, Department of Organic Chemistry, Polymer Chemistry Research Group, Krijgslaan 281 S4-bis, 9000 Gent, Belgium*

**INTRODUCTION:** The creation of smart surfaces with designed functionalities is currently of growing interest in the field of biomaterials. Polymer material presents a large variety of properties which can be tuned to create such smart surfaces. Mixed polymer brushes are of particular interest since they offer the possibility to combine different properties on a same material.

This study aims at creating surfaces showing tunable properties with respect to protein adsorption, using the combination of a protein-repellent polymer and of a polymer which adopts different behaviours towards proteins depending on the environment. Brushes of poly(ethylene oxide) (PEO) are known to prevent protein adsorption. Brushes of poly(acrylic acid) (PAA), a weak polyelectrolyte, are able to swell or shrink according to the pH and the ionic strength (I) of the solution. Using an appropriate combination of these two parameters, mixed PEO/PAA brushes are expected to either repel proteins, or allow their immobilization.

**METHODS:** The adopted strategy is the "grafting to" approach with thiol-functionalised polymers which self-assemble on gold surfaces. PEO-SH had a $M_w$ of 2,000 and was provided by Polymer Source (Dorval, Quebec, Canada). PAA with a midchain disulfide bond PAA-S-S-PAA ($M_n$=6,500) was synthesized as described previously [1]. These polymers were immobilised on gold from ethanol, water, or 50:50 solution of these solvents. The created surfaces were then submitted to human serum albumin (HSA) adsorption (concentration 200µg/ml, pH adjusted with HCl and NaOH, I adjusted with NaCl).

Polymer assembly was assessed by means of contact angle measurements, atomic force microscopy (AFM) and X-ray photoelectron spectroscopy (XPS). Polymer assembly and protein adsorption were monitored in situ by means of quartz crystal microbalance with dissipation monitoring (QCM-D).

**RESULTS & DISCUSSION:** Exploratory experiments have been performed on homogeneous PEO or PAA brushes in order to study the assembly process as well as HSA adsorption from solutions with different pH and I.

$M_w$ of the thiol-functionalized polymers was adjusted according to the obtained results.

The successful assembly of both polymers on gold could be observed by contact angle measurements, AFM and XPS. Brush thicknesses of about 1 nm for PEO and about 3 nm for PAA were measured by AFM. These results are compatible with the level of Au signal detected by XPS. QCM-D measurements performed in real time show the swelling or shrinking of PAA depending on pH and I. These observed effects are in agreement with those obtained previously by means of other techniques by other groups.

QCM-D monitoring of HSA adsorption allowed conditions of PEO assembly to be identified for which HSA adsorption was nearly totally prevented. On PAA, adsorption could be prevented at high pH while it was enhanced when pH was lowered. These effects were modulated by I. Other groups have shown that when protein adsorption occurs on PAA, proteins are adsorbed deeply inside the brush and retain their secondary structure as well as their activity [2-4].

**CONCLUSIONS & PERSPECTIVES:** Assembly conditions leading to prevention of protein adsorption on PEO and PAA homobrushes were identified, as well as conditions which provide a mild environment for proteins on PAA. Experiments of protein adsorption on mixed brushes of these polymers are in progress, with the aim to develop surfaces showing tunable properties with respect to protein adsorption.

**REFERENCES:** [1]W. Van Camp, F.E. Du Prez, H. Alem, et al (2010) *Eur Polym J* **46**:195-201. [2]C. Czeslik, G. Jackler, T. Hazlett et al (2004) *Phys. Chem. Chem. Phys.* **6**:5557-63. [3]O. Hollmann, R. Steitz, and C. Czeslik (2008) *Phys. Chem. Chem. Phys.* **10**:1448-56. [4]B. Haupt, T. Neumann, A. Wittemann, et al (2005) *Biomacromolecules* **6**:948-955.

**ACKNOWLEDGEMENTS:** M.F. Delcroix is a Research Fellow of the Belgian National Foundation for Scientific Research (FNRS). W. Van Camp thanks the Fund for Scientific Research – Flanders (FWO) for a postdoctoral fellowship.

# Free-Standing lipid bilayers in porous supports for investigating ion Channels

S. Demarche, A. Studer, D. Langenegger[1], J. Vörös[2], L. Tiefenauer[1]

[1] *Laboratory for Biomolecular Research, Paul Scherrer Institut, Villigen PSI, Switzerland*
[2] *Laboratory of Biosensors and Bioelectronics, ETHZ, Zürich, Switzerland*

**INTRODUCTION:** The stability of artificial bilayers suspended in nanopores is higher by at least one order of magnitude in comparison to bilayer suspended in micrometer pores [1;2]. However, the insertion of a membrane protein in the nanopores is a critical step: A technique allowing the fusion of proteoliposomes in order to insert the protein of interest into a preformed lipid bilayer has recently been established. We report here investigations of insertion and functional data of the voltage-gated sodium channel from *Bacillus halodurans* (NaChBac) [3].

**METHODS:** *Materials and electrochemical measurements:* Chip fabrication has been previously reported [1]. Two buffer-filled compartments in a four-electrode setup [3] are separated by a nanoporous or microporous silicon chip; alternatively a polypropylene foil in which a single micropore is present is used. Lipid bilayers are formed on these supports by painting.

*Ion Channel preparation and reconstitution:* The bacterial sodium channel NaChBac is over-expressed in E. coli C43(DE3), purified by affinity chromatography and gel filtration and reconstituted by dialysis in POPC/POPE/ergosterol (4/4/2, molar ratio) proteoliposomes, resulting in a 10 mg $mL^{-1}$ suspension of 200nm diameter proteoliposomes.

*Integration of the protein:* First, a bilayer is painted using a POPC/POPE (7:3 w/w) mixture in decane (10 mg $mL^{-1}$). Integration of NaChBac is then achieved by fusion of ergosterol containing proteoliposomes by the help of the nystatin peptides which generate an osmotic pressure (Fig. 1, A-B) [3].

**RESULTS:** We identified, from the transient current peaks, the integration of the reconstituted NaChBac ion channel using the nystatin/ergosterol fusion system. Fusion occurs more frequently in larger pores [3]. The opening and closing of individual sodium channels at an applied voltage could be monitored on polypropylene foil by means of a continuous current measurement. The specificity of the signal was demonstrated using the blocker nimodipine. A conductance of 120pS per channel and an opening time in the range of seconds have been observed (Fig. 1, C).

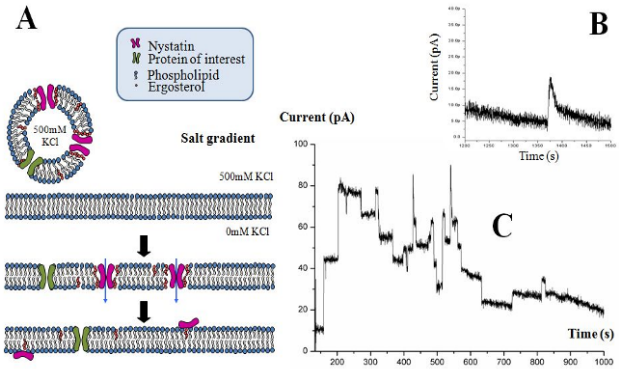


*Fig. 1: Nystatin/ergosterol fusion A) Liposomes with ergosterol and nystatin are added to a free-standing planar lipid bilayer and integrated therein. B) Fusion event is identified as a transient peak at 100 mV. Upon dilution of ergosterol the nystatin channels decay within about 1 min. C) Fusion experiment on a polypropylene foil: At 166 and 201 sec after proteoliposomes addition, fusions deliver ion channels into the preformed bilayer. NaChBac activity results in stepwise current changes of 12 ± 3 pA [3].*

**DISCUSSION & CONCLUSIONS:** We demonstrated that functional ion channels can be integrated by fusion of proteoliposomes to preformed bilayers. However the probability of fusion decreases when using smaller pores, in which bilayers are more stable. Other methods for protein insertion are thus being investigated, such as the direct formation of proteobilayers over nanopores.

**REFERENCES:** [1] Han X., Studer A., and Tiefenauer L. (2007) Nanopore arrays for stable and functional free-standing lipid bilayers. *Advanced Materials* **19**, 4466-4470. [2] Studer A., Han X., Winkler F., and Tiefenauer L. X. (2009) Formation of individual protein channels in lipid bilayers suspended in nanopores. *Colloids & Surfaces B: Biointerfaces* **73**, 325-331. [3] Studer A., Demarche S., Langenegger D., and Tiefenauer L. Integration and recording of a reconstituted voltage-gated sodium channel in planar lipid bilayer. *Biosensors and Bioelectronics*, submitted.

**ACKNOWLEDGEMENTS:** This work is financially supported by the EU project ASMENA-214666.

# Cell labelling with functionalised nano-beads

K. Demeter[1], K. Kenesei[1,2], A. Czeh[2], L. Török[2], B. Orsolits[1], G. Lustyik[2], E. Madarász[1]

[1] *Inst. of Experimental Medicine, Budapest, Hungary*, [2] *Softflow Hungary Inc. Pécs, Hungary*

**INTRODUCTION:** Neural stem cells and committed progenies display distinct sets of cell surface adhesion molecules and adhere to different extracellular matrix assemblies. While mature neurons can not attach to cyclic RGD pentapeptide motifs known as high-affinity ligands to $\alpha_v\beta_3/\alpha_5\beta_1$ integrins, neural stem cells adhere preferentially to the synthetic AK-c(RGDfC) peptide-conjugate (1). In recent studies, novel peptide conjugates recognizing different adhesion receptors were covalently coupled to fluorescent nano-beads and were used for in vitro labelling of different types of tissue cells. Here we present results and new approaches to develop methods for finding and labelling living stem cells among isolated/cultivated cells and in tissue slices.

**METHODS:** *Cell suspensions and cultures:* Cell suspensions were prepared by mechanic dissociation from embryonic (E14-16) mouse forebrains, and by combined enzymatic (Acutase, Milltenyi neurodissociation kit) procedures from early postnatal (P0-P3) and adult mouse forebrains. Cells were used for direct labelling in suspension or were plated onto poly-L-lysine-coated plastic surfaces at a cell density of 3–4 $*10^5$ cell/$cm^2$ and grown in MEM supplemented with 5% FCS, 4 mM glutamine, and 40 μg/ml gentamycin at 5% $CO_2$ containing humidified air atmosphere, at 37°C. Cultured cells were exposed to various bead-preparations (see below) for 1 - 24 hours to distinguish surface attachment, endocytosis and clearance of various beads by living cells.

*Functionalization of nano-beads*: Red and yellow SPHERO™ (Kisker) beads (0.04-0.11μm) were functionalised with poly-lysine/poly-alanine (AK) backbone carrying the specific ligand motifs by carbo-diimide conjugation.

*Immunocytochemistry:* Cells grown on poly-L-lysine-coated glass coverslips were washed free from non-attached beads with PBS and fixed with 4% paraformaldehyde (in PBS) for 20 min, at room temperature. For visualization of intracellular antigen epitopes, the cells were permeabilized with Triton X-100 (10 min, 0.1% v/v in PBS). Non-specific antibody binding was blocked by incubation with 2% BSA in PBS at room temperature, for 1 h. Primary antibodies were used overnight, at +4°C. Second-layer

fluorescent antibodies were added for 1.5 h at room temperature.

*Microscopic evaluation*: Immun-stained and bead-labelled preparations were evaluated by using multicolour fluorescence (Zeiss Axiovert 200M) and confocal (Olympus Fluoview, FV1000) microscopes. The cell surface or intracellular location of the beads was investigated by optical sectioning either by ApoTome (Zeiss) or by confocal techniques.

*FACS analysis*: The amount of non-washable beads, and their distribution among different cell-types was analysed by fluorescence aided cell sorting (FACS Vantage; BD Biosciences).

**RESULTS:** Beads with different fluorescence and functionalised with adhesion ligands recognizing different cell-adhesion receptors, provided a tool to i) compare in semi-quantitative terms the functional sets of adhesion molecules of different types of cells; ii) isolate defined groups of cells by selective adhesive behaviour. Microscopic studies also revealed a cell-type specific kinetics of adhesion-receptor initiated endocytosis. Optimization of the size and surface coverage of beads for microscopic and FACS investigations are in progress.

**DISCUSSION & CONCLUSIONS:** The results indicate that adhesion-based bead labelling provides a promising experimental tool for laboratory analyses of cell surface characteristics, endocytosis triggering and phagosome-cycling. As a technical innovation, it can serve a base for adhesion-selective cell sorting, and distinguishing cell populations with distinct adhesion preferences.

**REFERENCES:** 1. Markó K, Ligeti M, Mezo G, Mihala N, Kutnyánszky E, Kiss E, Hudecz F, Madarász E. A novel synthetic peptide polymer with cyclic RGD motifs supports serum-free attachment of anchorage-dependent cells. (2008) *Bioconjug Chem*. **19(9):**1757-66.

**ACKNOWLEDGEMENTS:** This work has supported by the "Bio-Surf" National Technology Program provided by the Hungarian National Office for Research and Technology.

European Cells and Materials Vol. 20. Suppl. 3, 2010 (page 56) ISSN 1473-2262

# Sub-diffusion in Nanochannels by Fluorescence Correlation Spectroscopy

I.De Santo[1], F.Causa[1], P.A. Netti[1]

[1] *Interdisciplinary Research Center on Biomaterials, University "Federico II" and Advanced Biomaterials for Healthcare, IIT Italian Institute of Technology*

**INTRODUCTION:** The understanding of molecular motion in nanoconfined space is a fundamental issue for developing nanosystems in biomedical and bioanalytic applications and for the design of drug delivery devices. In fact, integration of nano-engineered materials into useful bioactive based devices has been hampered by lack of understanding of the mechanisms of molecular trafficking occurring in nano-confined spaces. Here the influence of topological confinement on molecular motion is investigated through a single molecule technique, Fluorescence Correlation Spectroscopy (FCS). FCS is performed on both rigid probes and flexible macromolecules diffusing in glass channels of nanometric height.

**METHODS:** In order to understand the diffusion mechanism under topological confinement, FCS was performed in borosilicate nanochannels of nanometric depths of 10, 20 and 30 nm and micrometric width of 10 or 30 μm widths with constant length of 500 μm on Rhodamine6G, Polyethylene glycol (PEG) 20kDa and Dextran 40kDa molecules. Nanochannels filled by PEEK connectors with a nanomolar molecule solution were first imaged on a confocal microscope, then at equilibrium the fluorescence emission time course was collected and correlated. Data obtained were analyzed to derive diffusion time and the anomalous parameter.

**RESULTS:** Rhodamine6G ($r_g$ of 0.8nm) is almost unaffected from confinement whereas PEG20kDa ($r_g$ 4.7 nm) and Dextran40kDa ($r_g$ 5.8 nm) Auto Correlation Functions (ACF) have different shapes in nanoslits. In Figure 1, in particular, the ACF of PEG are shown in bulk, 10, 20 and 30 nm channel heights. ACFs have a diverse shape in each channel, revealing a dependence of molecular motion on the degree of confinement. In fact curves from smaller nanoslit heights are shifted toward longer decorrelation times. Moreover macromolecules ACFs fitted with the anomalous diffusion model give an anomalous parameter close to 0.5 with decreasing channel height. The anomaly parameter α in fact, follows a decreasing trend in narrow channels, suggesting that the anomaly grade is related to system size. In order to interpret the anomalous behavior the mobility reduction was ascribed both to conformational changes and to adsorption-desorption phenomena. Dextrans and PEG showed positive partitioning. This correspond to attractive surface interactions. The measured increase in partition can be addressed to a shift from the critical to the adsorption regime [1].

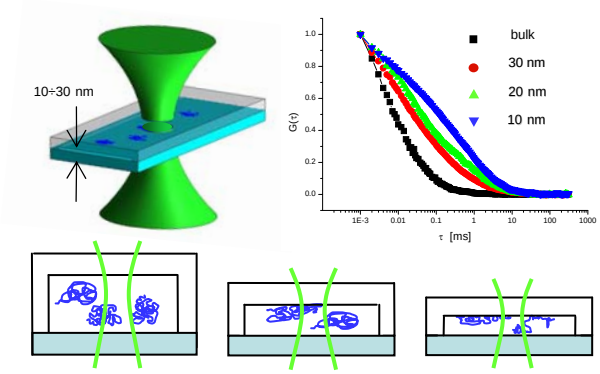


*Fig. 1: Left high_ Experimental set-up. Right high_ ACF for PEG20kDa registered in bulk, 30nm, 20 nm and 10 nm channel. Below sketch of flexible molecules in nanochannels going from the critical regime (left) to the adsorption regime (right).*

**DISCUSSION & CONCLUSIONS:** Anomalous diffusion is demonstrated in nanochannels for flexible molecules diffusion and a square root dependence with time is shown for strong confinement. Molecule flexibility and adsorption-desorption phenomena were considered to interpret the anomalous behavior and their influence was estimated as a function of molecular confinement [2].

**REFERENCES:** [1]A. Gorbunov, A. M. Skvortsov, *Adv. Colloid Interface Sci.* (1995), 62 ,1,31-108. [2]I.De Santo, F. Causa. P.A. Netti, (2010) *Anal Chem* 82 (3), pp 997–1005.

**ACKNOWLEDGEMENTS:** Authors are indebt with Dr. Wachsmuth for the fluctuation analyzer software and for valuable discussions and suggestions.

European Cells and Materials Vol. 20. Suppl. 3, 2010 (page 57) ISSN 1473-2262

# Actin Self-Assembly: A Microfluidic Approach

S. Deshpande[1], D. Steinhauser[2], S. Arnold[1], T. Pfohl[1,2]

*[1] Chemistry Department, University of Basel, Basel, Switzerland. [2] Max Planck Institute for Dynamics and Self Organization, Göttingen*

**INTRODUCTION:** Many biomolecules such as actin, collagen and fibrin show hierarchical self-assembly; from monomers to polymers and finally forming complex three-dimensional networks. We study these hierarchical self-assemblies and the involved processes with microfluidic setups using a bottom up approach. Using microfluidics, we are able to analyze every consecutive step of the reaction, generate gradients (salt, ATP, reactants), add or dilute the reaction compounds. In this work, we focus on the formation of actin filaments, networks and bundles.

**METHODS:** *Microfluidic devices*: Silicon wafer masters were fabricated with the help of soft lithography using a negative photoresist SU8 and a negative chromium mask. PDMS devices were further prepared using the silicon wafer masters[1]. A typical microfluidic device consists of microchambers attached to the main channel through narrow connecting channels. Also, a gradient can be established within a microchamber by connecting it to two parallel channels through narrow connecting channels. Typical heights of the channels and the chambers are 2-3 μm. Microchambers of different shapes and sizes are designed and the typical volume a chamber holds ranges from 0.2 pL to 20 pL.

*Fluorescence Microscopy*: Rhodamine labelled actin monomers were used to perform the experiments. The actin filaments were stabilized by phalloidin, which prevents depolymerization. Actin bundles were formed in the presence of multivalent $Ca^{2+}$ ions by counter-ion condensation. Since actin filaments are overall negatively charged polyelectrolytes, they attract cations from the solution which results in closely bundled actin filaments at high ionic strength.

*FEM simulations*: Finite Element Modelling was done with COMSOL software in order to simulate the flow velocity distributions and the concentration profiles inside the microchannel devices.

**RESULTS:** Due to the designed geometry of the devices, the transport and exchange of materials inside the microchambers are governed by diffusion and can be controlled by changing the flow velocities, concentration profiles and compound compositions in the main channel. Experimental measurements of the flow profiles as well as the concentration profiles within the microdevices are in good agreement with the FEM-simulations.

The time evolution of the bundling process in the presence of divalent cations using a microfluidic quasi-2D system can be seen in Figure 1. We analyzed the contour of bundles by image processing and determined the persistence lengths by calculating the tangent correlation function along the filaments[2]. It was found that the persistence length of actin bundles ($L_p$) increases proportionally with the number of filaments present in a bundle ($n$) as: $L_p \propto n^{1.3}$. Thus, the measured values lie in an intermediate region reflecting that the filaments are neither decoupled (independent bending of individual filaments inside the bundle, $L_p \propto n$) nor fully coupled ($L_p \propto n^2$).

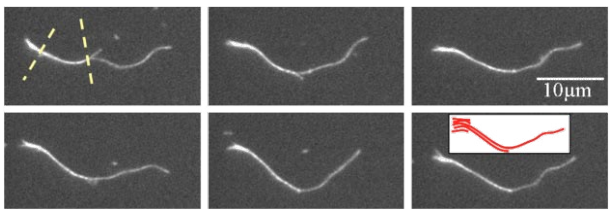


*Fig. 1: Fluctuating actin bundle ($\Delta t$ = 240 ms) consisting of three parts; a thin end consisting of a single filament, middle part with two filaments and a thick end consisting of many filaments.*

**DISCUSSION & CONCLUSIONS:** The bundled actin filaments are held together by electrostatic interactions. In bent bundles, a redistribution of the charges i.e. additional stretching or compression is necessary which can explain the partly coupled case. Further experiments with proteins as the cross-linking agents using FRET microscopy can help us understand the interactions within bundles and networks.

**REFERENCES:** [1] S. Köster and T. Pfohl (2009) *Cell Motility and the Cytoskeleton* **66**: 771-776 [2] S. Köster, D. Steinhauser and T. Pfohl (2005) *J. Phys.: Condens. Matter* **17**: S4091-S4104

**ACKNOWLEDGEMENTS:** We gratefully acknowledge SNF (NCCR Nano) and DFG (Pf 375/4, SPP1164) for financial support.

# Towards nanowire sensors on a microfluidic platform: In-situ formation, positioning and sizing of nanowire bundles

Phillip Kuhn[1], Josep Puigmartí-Luis[1], Inhar Imaz [2], Daniel Maspoch[2] and Petra S. Dittrich[1]

[1]*Department of Chemistry and Applied Biosciences, ETH Zurich, Switzerland*

[2] *Centre d'Investigacions en Nanociencia i Nanotecnologia (ICN-CSIC), Barcelona, Spain*

**INTRODUCTION:** Progress in microelectronics, sensors and optics is strongly dependent on further miniaturization of components. However, the resolution of top-down technologies based on lithography has limits concerning the dimensions and the choice of material. Hence, several bottom-up approaches have been investigated to satisfy the need for structures with large aspect ratios in the nanometer regime [1]. Unfortunately, most of the methods described up to now either use expensive instruments or involve tedious procedures. Previously, it has been shown that microfluidic devices can support the formation of nanometer-sized structures, such as metal wires and hybrid fibers [2]. In these approaches, those nanostructures are formed at the interface of two reagent streams. We have advanced this method by developing a smart chip design that facilitates the *in-situ* formation, as well as the positioning of nanowires with controllable lengths

**METHODS:** We employ a multilayered microfluidic chip made of PDMS [3], which comprehends a fluid layer and a control layer, filled with nitrogen gas and separated by a thin, flexible PDMS membrane. Application of pressure to the gas inlets actuates the freestanding membrane and results in deflection of the predefined donut-shaped features into the fluid layer, thereby encapsulating a volume inside the fluid channel. The fluid channel is utilized to form nanowires by co-flowing aspartic acid (10 mM) and $CuNO_3 \cdot 6H_2O$ (15 mM) [4].

**RESULTS:** Nearly immediately, we can observe the formation of metal-organic wires at the interface where both reactants meet. Changing the flow rate of one reactant stream allows to induce the wire formation at different positions in the channel, e.g. directly under a donut structure. Hence, upon pressurization (3 bar) of the donut structure, the wire underneath is encapsulated and simultaneously fixed in position. Due to the continuous flow inside the channel, the nanowire bundles break at the edge of the donut trap so that their length is defined by the size of the donut (Fig. 1). Nanowires of various lengths between 50 and 250 µm have been created within a few minutes.

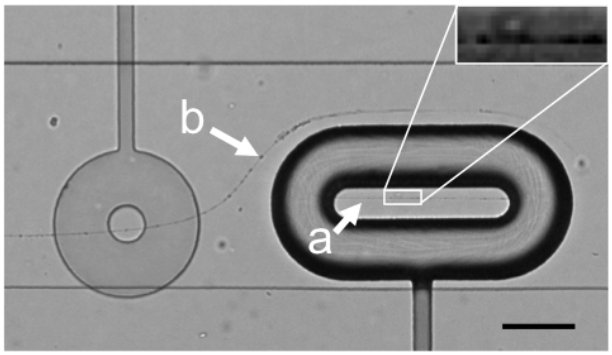


*Fig. 1: Optical microscope image showing the encapsulation of a wire bundle by actuation of the right donut (arrow a). Reagent streams are still flowing through the channel, but are now partly deflected by the closed donut feature (arrow b). The black interface due to ongoing nanowire formation can be clearly seen (b). Inset (brightness adjusted) shows a magnification of the trapped wire. Scale bar: 100 µm.*

**DISCUSSION & CONCLUSIONS:** The here-described approach accomplishes different intriguing goals of nanotechnology; it facilitates a defined and reproducible formation pathway, localization and control over the assembly process and capability to decide the length of an anisotropic structure. It is generally applicable, and we envision that the presented method will lead to easier integration of fully functional systems by bridging nano-, micro- and macroscopic dimensions. Our future work focuses on the construction of nanowire-based sensing devices made of conductive metal-organic materials.

**REFERENCES:** [1] Y. Xia, P. Yang, Y. Sun, Y. Wu, B. Mayers, B. Gates, Y. Yin, F. Kim, and H. Yan, *Advanced Materials*, **5**, 15 (2003). [2] J. Puigmarti-Luis, D. Schaffhauser, B.R. Burg and P.S. Dittrich, *Advanced Materials*, **22**, 1-5 (2010). [3] C-H. Hsu and A. Folch, *Aplied Physics Letters*, **86**, 023508 (2005). [4] I. Imaz, M. Rubio-Martinez, W.J. Saltera, D.B. Amabilino, and D. Maspoch, *JACS*, **131**, 18222-18223 (2009).

**ACKNOWLEDGEMENTS:** Funding from the European Research Council under the 7th Framework Programme (ERC Strating Grant no. 203428 nµLIPIDS) is gratefully acknowledged.

European Cells and Materials Vol. 20. Suppl. 3, 2010 (page 59) ISSN 1473-2262

# Modeling of peptide binding to polar surfaces OF ZnO by molecular dynamics simulations

T.A.Do, J.Pleiss

*Institute of Technical Biochemistry, University of Stuttgart, Germany*

**INTRODUCTION:** Zinc oxide (ZnO) is a versatile material in a variety of applications, ranging from electronics to catalysis, that depend critically on its defect and surface properties. Specifically, ZnO (0001) orientation has two distinct polar surfaces: a positive Zn-terminated and a negative O-terminated surface. Over the last ten years, several peptides with affinity for ZnO surfaces have been discovered by phage display or cell surface display methods. These ZnO-binding peptides are known to have the potential for biomineralization and many others in the field of bio-nanotechnology. However, a fundamental theoretical understanding of the peptide-ZnO interactions is still lacking. Here we report for the first time a modeling of the adsorption of peptides on the polar ZnO surfaces at an atomic level by using molecular dynamics (MD) simulation.

**METHODS:** Peptides with high and low affinity for ZnO were modeled by MD simulations [1]. ZnO slab models (ideal and reconstructed surfaces) were built from a wurtzite type crystal structure with the atomic charges provided by the Mulliken analysis [2]. The peptide and the ZnO slab model were solvated in a periodic simulation box of water molecules (*Fig. 1*). All the simulations utilized the GROMACS package and the AMBER force-field. A near-equilibrium pulling simulation (steered MD simulation) was used to attach the peptide onto the ZnO surface, followed by a production MD simulation for a minimum of 5 ns to fully equilibrate the system. Simulation trajectories were analyzed by using tools in the GROMACS package.

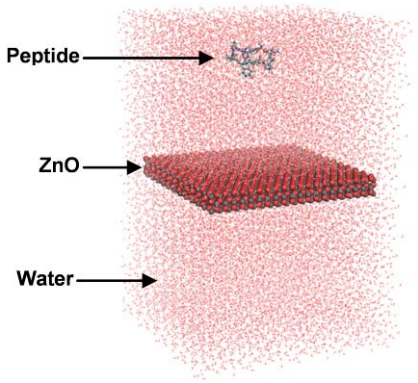


*Fig. 1: Model of the periodic simulation box with the ZnO slab and the peptide in waters.*

**RESULTS:** Simulations showed that the peptides bound to both polar ZnO surfaces only at a few charge points by electrostatics interactions within 2.5–4 Å. The binding conformation of the peptides therefore depended on number of charged residues and their position in the sequence (*Fig. 2*). However, good binders preferred the negatively charged O-terminated to the positively charged Zn-terminated surface. The interaction of a single peptide molecule with a ZnO surface depended on the surface morphology and was mediated by the adsorbed water layers. In fact, a reduction of the surface charge for polar stabilization rearranged water molecules at the interface, and hence the water molecules also influenced the interaction energies between the peptide and the ZnO surface.

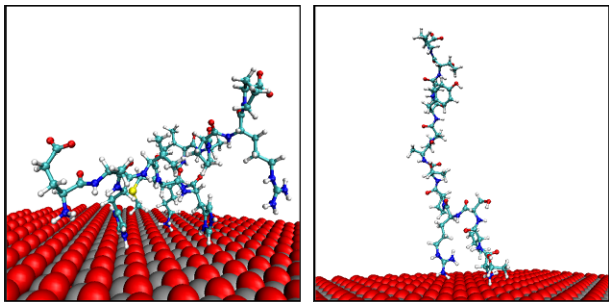

*Fig. 2: The binding conformation of a good (left) and a bad (right) binder peptide on the O-terminated ZnO surface.*

**DISCUSSION & CONCLUSIONS:** Electrostatic attraction between opposite charges is likely to dominate the adsorption process. Specifically, the attraction between positively charged peptide groups and the negatively charged surface seems to drive the adsorption of peptides on the polar ZnO surfaces. Our observations also suggest that the charged amino acid composition of a peptide as well as its amino acid sequence can be used to predict high or low affinity for ZnO.

**REFERENCES:** [1] M. Umetsu, et al. (2005) *Advanced Materials*, **17**(21):2571-2575. [2] D. Raymand, et al. (2008) *Surface Science* **602**(5):1020-31.

**ACKNOWLEDGEMENTS:** This work is funded by the Deutsche Forschungsgemeinschaft.

European Cells and Materials Vol. 20. Suppl. 3, 2010 (page 60) ISSN 1473-2262

# Controlled Displacement of Single Mammalian and Microorganism Cells by FluidFM Technology

Pablo Dörig,[1] Philipp Stiefel,[2] Pascal Behr,[1,3] Michael Gabi,[1,3] János Vörös,[1] Julia Vorholt,[2] Tomaso Zambelli[1]

[1] Laboratory of Biosensors and Bioelectronics, D-ITET, ETH Zurich, Switzerland [2] Institute of Microbiology, D-BIOL, ETH Zurich, Switzerland [3] Cytosurge LLC, Zurich, Switzerland.

**INTRODUCTION:** The FluidFM technology uses micro-channeled AFM cantilevers that are fixed to a channeled AFM probeholder.[1] A continuous fluidic circuit is thereby achieved extending from an external liquid reservoir, through the probeholder and the hollow cantilever to the tip aperture. In this way, both overpressure and an underpressure can be applied to the liquid reservoir and hence to the built-in fluidic circuit. The setup is able to operate in liquid environment, therefore in physiological conditions of microorganisms.

**METHODS:** We take advantage of the principal features of the FluidFM technology, the force feedback, for a safe and quick approach onto the biological objects and the possibility to apply an underpressure to "grasp" the cells, whereby different tip apertures can be used. The object is then lifted and moved to a new position where the force feedback is activated again to approach the surface and a short overpressure pulse is administered to release the object.

Two different hollow-cantilever designs were used for these experiments, one having a blunt and the other a tube shaped tip. Manipulations were carried out with a low cost, custom BioAFM and custom LabView software.

**RESULTS:** Saccharomyces cerevisiae (budding yeasts) were picked up from a Petri dish filled with buffer solution and relocated in the patter shown in figure 1. Negative pressures of 50mbar were used to lift up the cells. No impact onto the viability of the displaced yeasts was observed. The same procedure was used to detach adherent, spread mammalian cells like neurons, and to transfer cells from one glass slide to another medium e.g. agar medium for further cultivation or analysis.

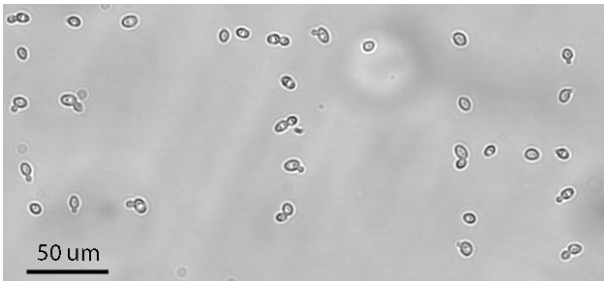


*Fig. 1: S. cerevisiae after spatial manipulation by FluidFM, displaying the letters ETH*

**DISCUSSION & CONCLUSIONS:** The operation under physiological conditions allowed the displacement of viable organisms with micrometric precision in a non-destructive way.[2] The protocol is applicable to both eukaryotic and prokaryotic cells. Moreover, we could think of using this procedure on all kinds of microscopic entities, such as nanoparticles and viruses.

**REFERENCES:** [1]A. Meister, M. Gabi, P. Behr, P. Studer, J. Vörös, P. Niedermann, J. Bitterli, J. Polesel-Maris, M. Liley, H. Heinzelmann, T. Zambelli, Nano Letters **9** (2009) 2501. [2]P. Dörig, P. Stiefel, E. Sarajlic, D. Bijl, P. Behr, M. Gabi, J. Vörös, J. Vorholt, T. Zambelli, Appl. Phys. Lett. (2010) in press.

**ACKNOWLEDGEMENTS:** We would like to thank Stephen Wheeler from the LBB Workshop for technical help.

European Cells and Materials Vol. 20. Suppl. 3, 2010 (page 61) ISSN 1473-2262

# Preparation and Physico-Chemical Characterization of Bioactive Glass Nano Particles

A Doostmohammadi[1], A Monshi[1], MH Fathi[1], U Pieles[2], AU Daniels[3]

*[1] Isfahan University of Technology, Isfahan, Iran. [2] University of Applied Sciences Northwestern Switzerland (FHNW), Muttenz, Switzerland. [3] Laboratory of Biomechanics and Biocalorimetry,Clinical Morphology & Biomedical Engineering, University Basel, Basel, Switzerland.*

**INTRODUCTION:** Bioactive glasses (SiO2 glasses containing Ca and P) are well-known materials for use in implant applications, and have been shown to augment formation of bone and other tissues [1]. Compared to particle of µm or larger sizes, bioactive glass nano particles may provide a means for more rapid release of Ca and P where this is desired [2]. The aim of this work was preparation and characterization of bioactive glass particles of a specific mol % target composition 63 SiO2, 28% CaO and 9% P2O5 (short name 63S), with a nominal largest dimension below 100 nm (nano particles).

**METHODS:** The particles were produced using a sol-gel process followed by drying of the gel at 60ºC for 10 hours, heat treatment at 600ºC for 10 hours and milling to reduce aggregation. SEM images were made for qualitative assessment of particle morphology. X-ray fluorescence spectroscopy (XRF) and dispersive X-ray analysis (EDX) were used to confirm the bioactive glass composition. The structure (glassy vs. crystalline) nature of the particles was evaluated by X-ray diffraction (XRD). The intended presence of a potentially bioactive surface layer of hydroxyapatite was investigated by Fourier transform infrared spectroscopy (FTIR) before and after immersion in a buffered ionic solution (simulated body fluid = SBF) [3] at 37 ˚C for 30 days. Particle surface area was analyzed by BET gas surface adsorption. Particle size and size distribution were assessed with laser dynamic light scattering (DLS). Finally, to indicate the stability of particle suspensions, the zeta potential of the particles was measured by laser Doppler electrophoresis (LDE) in water and at three different pH values in physiological saline.

**RESULTS:** XRF and EDX results showed that the mol % composition of the 63S bioactive glass was on target: 62.17% $SiO_2$, 28.47% CaO and 9.25% $P_2O_5$ and XRD showed confirmed that the particles were amorphous. FTIR confirmed the formation of an apatite surface layer on the particles after 30 days in SBF, suggesting they will readily release Ca and P ions and thus be biologically active and possibly promote tissue formation by cells. The BET surface area of the particles was ~223 m²/g. Assuming uniform spherical particles, this yields a calculated particle size of ~24 nm. SEM confirmed particles in this range (<50 nm) but showed the particles were agglomerated (Fig. 1). Agglomerate size range measured by DLS was 100-500 nm. LDE showed the particles had a low negative zeta potential in water (~5 mV) and in physiological saline: ~7 mV at pH 5, ~16 mV at pH 7.4 and ~14 mV at pH 9.

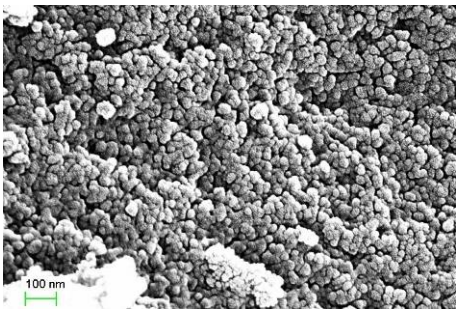


*Fig.1: Ag-glomerated bioactive glass nano particles.*

**DISCUSSION & CONCLUSIONS:** 63S bioactive glass nano (< 50 nm) particles can be produced by a sol-gel method. These particles form an apatite surface layer over time in SBF. The small particle size (high surface area) and appatite surface layer suggest that a given mass of these particles will release Ca and P ions faster than the same mass of larger bioactive glass particles. This may be an advantage in some implant coating and tissue engineering applications. The particles have a rather low negative zeta potential in water and physiological saline solution, and this may explain their tendency to form 100-500 nm aggregates**.**

**REFERENCES:** [1] L.L. Hench (2006) *J Mater. Sci. Mater. Med* **17**:967. [2] P. Sepulveda, J. R. Jones, L. L. Hench (2002) *J Biomed Mater Res* **61**: 301-11. [3] T. Kokubo, Z. Huang, T. Hayashi, S. Sakka, T. Kitsugi, T. Yamamuro (1990) *Biomed Mater Res* **2**4:331-43.

**ACKNOWLEDGEMENTS:** Hardy & Otto Frey-Zünd Foundation, Basel CH; Helmut Fally (FHNW, Muttenz) for superb technical assistance.

# Engineering of Quantum Dot Pattern Luminescence via Energy Transfer for Sensing Applications

D.Dorokhin[1,2], S.H.Hsu[2,3], N.Tomczak[4], C.Blum[5], V.Subramaniam[5], J.Huskens[3], D.N.Reinhoudt[2], A.H.Velders[2], G.J.Vancso[1]

*[1] Materials Science and Technology of Polymers, [2] Supramolecular Chemistry and Technology, [3] Molecular NanoFabrication, [5] Biophysical Engineering, Faculty of Science and Technology and MESA+ Institute for Nanotechnology, University of Twente, Enschede, The Netherlands.*

*[4] Institute of Materials Research and Engineering, A*STAR Singapore.*

**INTRODUCTION:** Semiconductor quantum dots (QD) belong to a novel class of highly stable, optically bright nanoscale emitters, which are subject of extensive research due to scientific interests in quantum confinement effects, and to promising applications in biolabeling and (bio)sensing.[1] Energy or electron transfer processes are often utilized as the signal transduction mechanisms in the sensing schemes involving QDs.[2] Robust platforms for luminescence sensing can be fabricated using supramolecular assemblies of QDs. Multivalent binding of QDs *via* host-guest complexes can yield stable, well define structures at susbtrate surfaces.[3] QD patterns can thus provide spatially defined luminescence regions and display molecular recognition ability for sensing applications.

**METHODS:** Water-soluble, carboxylated core-shell CdSe/ZnS QDs (eBioscience, San Diego, US) were functionalized with β-cyclodextrin heptamine (β-CD$(NH_2)_7$) and immobilized on β-CD modified glass slides via multivalent host-guest interactions with microcontact printed adamantyl-terminated poly(propylene imine) (2nd generation, G2-PPI-$(Ad)_8$) dendrimers.[3] Lissamine rhodamine divalent adamantyl (LR-$(Ad)_2$) moleucles were printed across the QDs patterns using PDMS stamps. A UV-Vis spectrophotometer Varian Cary 300 and an Edinburgh XE-900 spectrofluorometer were used to record spectra. Fluorescence imaging was occurred using a Olympus IX71 inverted microscope. A custom-built scanning confocal microscope was used to perform fluorescence lifetime imaging (FLIM).[4]

**RESULTS:** FRET was shown to occur between CdSe/ZnS QD donors functionalized with β-cyclodextrin incorporated into supramolecular multilayer structures and functionalized lissamine rhodamine dyes microcontact printed on top of the QD layer.

**DISCUSSION & CONCLUSIONS:** Vacant β-CD formed host-guest supramolecular complexes with dye molecules functionalized with adamantyl groups. Fluorescence microscopy, spectroscopy and FLIM proved that a FRET process occurred in the regions where the dye was bound to the β-CD functionalized QD (Figure 1 and 2).

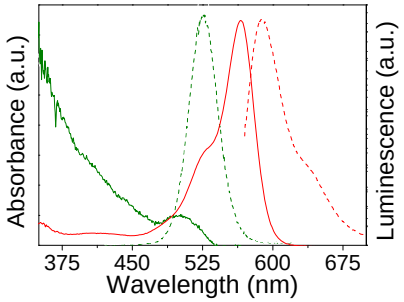


*Fig 1. Absorption (solid) and emission (dashed) spectra of CdSe/ZnS QDs (green) and LR-$(Ad)_2$ in water. Excitation wavelength is 450nm and 550nm respectively.Fig 2. Fluorescence images (a,b) and*

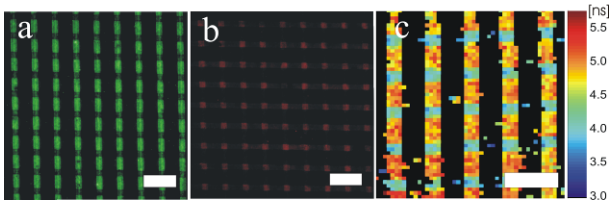


*lifetime image (c) of QDs/β-CD cross-printed with LR-$(Ad)_2$. The scale bars are 25 μm and 20 μm.*

A FRET efficiency of 18% was obtained for the supramolecular patterns. The QDs patterns provide very promising molecular recognition platforms due to the FRET signal transduction mechanism.

**REFERENCES:** [1] A.P. Alivisatos (1996) *Science* **271**:933-937. [2] R.C. Somers et al (2007) *Chem. Soc. Rev.* **36** :579-591. [3] D. Dorokhin et al (2010) *ACS Nano* **1**:137-142. [4] C. Blum et al (2009) *J. R. Soc. Interface* **6**:S35-S43.

**ACKNOWLEDGEMENTS:** The MESA+ Institute for Nanotechnology and the nanotechnology program NanoNed of the Dutch Ministry of Economic Affairs are highly appreciated for financial support.

# ELECTROSPUN MATERIALS WITH CELL ADHESION AND PROLIFERATION PROMOTING SURFACES

A. dos Santos[1], M. Cornelissen[2], E. Schacht[1], P. Dubruel[1]

*[1]Polymer Chemistry & Biomaterials Research Group, Department of Organic Chemistry, Ghent University, Krijgslaan 281 – B-9000 Ghent-Belgium 2Department of Basic Medical Sciences, Ghent University, De Pintelaan 185, 6B3 B-9000 Ghent- Belgium*

**INTRODUCTION:** Electrospun architectures offer important advantages in tissue engineering since it mimics the ECM. In addition, properties such as high surface to volume ratios and high porosity facilitate cell migration across the implant and greatly reduce diffusion limitations to wastes and toxic products. Also, the high surface/volume ratio allows a higher density of surface binding sites and thus, a more intense cell stimulation[1, 2].The addition of tissue-specific proteins or peptides to the surface of biomaterials can strongly enhance the desired cell response. The objective of this work was to prove that the cell interaction and proliferation on nanofibres can be enhanced by surface modification of the fibres surface with adhesion and proliferation peptides

**METHODS:** Starting from stable electrospun materials based on a polymer with poor cell interaction, PCL, the fibre surface (*Figure 1*) was modified with two peptides (Cyclic RGD and FHRIKA) by two different strategies: post-modification and co-electrospinning in blend. To allow the coupling of the peptides to the fibre surface and ensure the presence of the peptides on the surface, a disulphide pyridine derivative of PCL was previously synthesized (*Figure 2*).

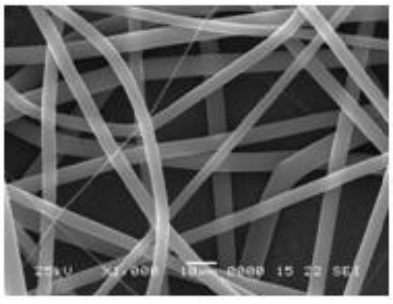

*Fig 1: Electrospun PCL fibres.*

**RESULTS:** The tests clearly show an increase in cell adhesion and proliferation when the peptides are present. The most consistent growth after 2 weeks is obtained for the equimolar mixture of both peptides, cyclic RGD+ FHRRIKA, (*Figure3*).

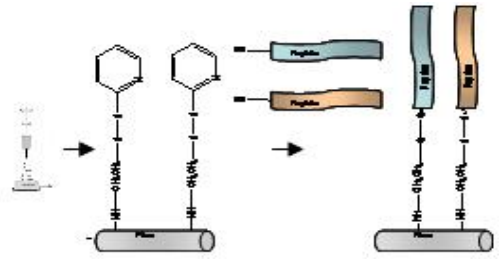

*Fig 2: Strategy of polyvalente surface modification with PCL-S-S-Pyr derivative allowing the conjugation of different peptides on the electrospun fibres surface. The PCL/PCL-S-S-Pyr blend was electrospun first and the fibres were subsequently modified with the peptides.*

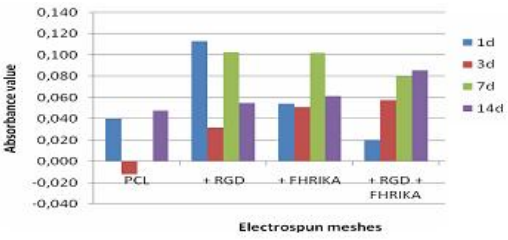


*Fig 3: MTS test results of MC3T3-E1 cells plated in PCL mats containing 9 nmol of surface peptides/g of polymer.*

**DISCUSSION & CONCLUSIONS:** This work proves that is possible to improve the bioactivity of electrospun materials based on materials characterized with poor surface properties to be used in tissue engineering. In this way, in addition to the mechanical properties of an electrospun polymer material, cell adhesion and proliferation potentialities can be imparted. The versatility of this method will certaily lead to further applications using other peptides or other polymer fibres.

**REFERENCES:**[1] Agarwal, S.; Wendorff, J. H.; Greiner, A., Use of electrospinning technique for biomedical applications. *Polymer* **2008,** 49, (26), 5603-562, [2] Nisbet, D. R.; Forsythe, J. S.; Shen, W.; Finkelstein, D. I.; Horne, M. K., A Review of the Cellular Response on Electrospun Nanofibers for Tissue Engineering. *Journal of Biomaterials Applications* **2009,** 24, (1), 7-29

**ACKNOWLEDGEMENTS:** EU funding (Flexifunbar, project number 505864).

# Investigation of cytotoxicity of silica nanoparticles using viability tests and surface-enhanced Raman spectroscopy

D. Drescher[1,2], G. Orts-Gil[1], W. Österle[1], J. Kneipp[1,2]

[1] *BAM Federal Institute for Materials Research and Testing, Berlin, Germany*

[2] *Humboldt-Universität zu Berlin, Department of Chemistry, Berlin, Germany*

**INTRODUCTION:** Due to their extraordinary properties, nanoparticles have found multiple applications in various fields of today's life, such as pharmaceuticals and cosmetics, materials science, optics, and catalysis. Although systematic toxicological studies have been performed on a multiplicity of different nanoparticles and cell types, a large number of uncertainties concerning toxicological effects and in particular the associated mechanisms still remain. By combination of Raman spectroscopy and standard assays we are able to get insight into biological reaction pathways and the fate of the nanoparticles in the cells.

**METHODS:** The aggregation behaviour of silica nanoparticles in DMEM (Ludox TM50, particle size 35 nm, *Sigma-Aldrich*) has been investigated using dynamic light scattering techniques, SAXS and TEM.[1] Cytotoxicity of these particles on 3T3 cells was determined by XTT assay. SERS experiments were conducted after incubation of silver or gold nanoparticles.

**RESULTS:** Since agglomeration of nanoparticles has a significant influence on cytotoxicity, DLS measurements were conducted to prove the stability of the silica dispersion in cell culture relevant media. In all investigated concentrations, the hydrodynamic diameter of silica in DMEM is approximately 35 nm.[1] Determination of cytotoxicity of silica nanoparticles using the XTT assay shows a strong decrease of cell viability with rising concentration after 24 hours. At a concentration of 100 µg/ml, cell viability is decreased to about 20% in comparison to unexposed cells.

The uptake of silver or gold nanoparticles enables sensitive detection of Raman spectra from different compartments inside the living cell, based on surface enhanced Raman spectroscopy (SERS).[2] We have been developing SERS as a tool for cytotoxicity investigations on different kinds of nanoparticle interaction with cellular systems. Figure 2 shows selected SERS spectra from a 3T3 cell, incubated with gold nanoparticles. Bands can be allocated to different cell constituents, giving information about the intracellular environment and nanoparticle influence.

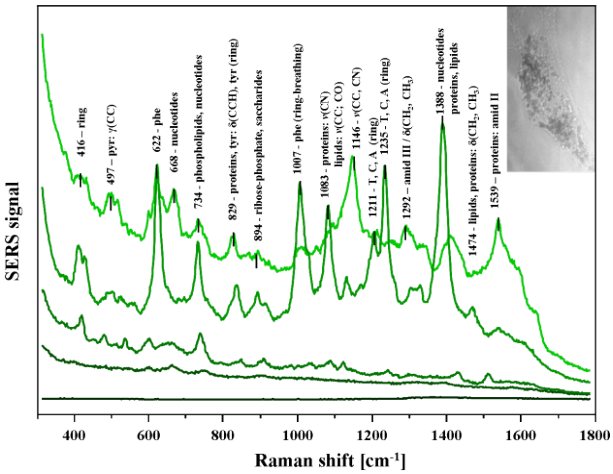


*Fig. 2: Selected SERS spectra from a 3T3 fibroblast cell after 24h-incubation with gold nanoparticles in $10^{-10}$ M (excitation wavelength 785 nm; $5 \cdot 10^4$ W/cm$^2$, 1s accumulation time). Abbreviations: tyr, tyrosine; phe, phenylalanine; A, adenine; T, thymine; C, cytosine.*

**DISCUSSION & CONCLUSIONS:** The combination of Raman spectroscopy and standard assays has shown to be a powerful instrument for investigation of cytotoxicity of nanoparticles and the processes involved, such as endocytosis, vesicular transport, accumulation, and apoptosis. Future investigations aim at tracking intracellular changes after incubation of silica nanoparticles, related to cytotoxicity.

**REFERENCES:** [1] G. Orts-Gil, K. Natte, D. Drescher, H. Bresch, A. Mantion, J. Kneipp, W. Österle (2010) *Journal of Nanoparticle Research* DOI 10.1007/s11051-010-9910-9. [2] A. Matschulat, D. Drescher, J. Kneipp (2010) *ACS Nano* **4**:3259-3269.

European Cells and Materials Vol. 20. Suppl. 3, 2010 (page 65) ISSN 1473-2262

# Oriented cellulose nanowhiskers guide Myoblast fusion to produce highly aligned Myotubes

J M Dugan, J E Gough and S J Eichhorn

*School of Materials, The University of Manchester, UK*

**INTRODUCTION:** The morphology, differentiation and gene expression of various cell types have been modulated using different model materials with nanoscale topographies [1]. Materials that can impose a degree of organisation on cultured tissue may find applications in regenerative medicine and tissue engineering [2]. Here we show that features of only ~10nm in height induce contact guidance in proliferating myoblasts, directing subsequent differentiation. We have produced radially oriented surfaces of tunicin cellulose nanowhiskers (CNWs) by spin coating. The initial response of C2C12 myoblasts (C2C12s) was determined using AFM and image analysis. Upon differentiation the myoblasts fused to form myotubes which exhibited striking radial orientation in line with the oriented CNWs.

**METHODS:** CNWs were prepared from the tests of *Halocynthia roretzi* tunicates by partial hydrolysis with sulfuric acid to yield a stable aqueous suspension of whisker-like nanoparticles with net anionic surface charge [3]. Surfaces of CNWs were prepared by spin coating. Pieces of glass were cleaned and treated with 0.6% (w/v) polyallylamine hydrochloride. An aqueous suspension of CNWs (0.5% w/w) was then spin coated onto the clean cationic glass. A high spin speed of 6000 RPM achieved an extremely high degree of orientation whereas slower speeds gave surfaces with a much lower degree of orientation. The surfaces were characterised by atomic force microscopy (AFM).

Cell culture was carried out using standard methods [2]. For AFM imaging of cells on CNW substrates, the cells were fixed after 4 hours in glutaraldehyde and air dried. All AFM imaging was carried out in tapping mode. Differentiation was induced, and myotubes were stained for myosin using immunocytochemistry. Large scale tile scans were captured using a Leica SP5 confocal microscope with a motorised stage.

**RESULTS:** Homogeneous and uniform arrays of CNWs were prepared with a high degree of radial orientation as shown in Fig.1A. C2C12s were observed to “sense” their surrounding topography using extremely fine filopodia (Fig.1B) and to adopt elongated morphologies in line with the radial axes of the samples. Upon differentiation the

C2C12s fused to form extensive elongated myotubes that expressed fast myosin. The myotubes were oriented in a striking radial pattern that reflected the arrangement of the underlying CNWs (Fig. 1C).

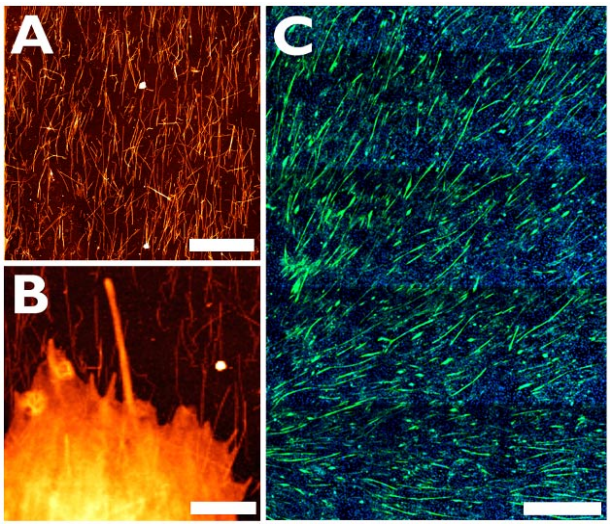


*Fig. 1: (A) AFM topography image of a highly oriented CNW surface (bar=5 μm). (B) AFM topography image of the leading edge of a myoblast on a CNW surface (bar=2 μm). (C) Large area tile scan of differentiated myotubes (green) and nuclei (blue) on a CNW surface (bar=1 mm).*

**DISCUSSION & CONCLUSIONS:** We have shown that CNWs of only ~10nm diameter support the attachment and differentiation of myoblasts and that the spatial arrangement of the CNWs directs the morphology and arrangement of the myoblasts and differentiated myotubes. We propose that myoblasts are a particularly sensitive cell type to topographical control and that cellulose may be an important material for engineering bioactive surfaces.

**REFERENCES:** [1]Biggs et al. (2008) *J.R.Soc.Interface*, **5**, 1231. [2]Huang et al. (2006), **6,** 3, 537. [3]Van den Berg et al. (2007), *Biomacromolecules* (2007), **8**, 1353.

**ACKNOWLEDGEMENTS:** Tunicin CNWs were kindly donated by Dr Laurent Heux, CERMAV, Grenoble, France.

# Polymer Therapeutics Containing Coiled-Coils: New Therapeutics and Linkers

S.P.E Deacon[1], B. Apostolovic[2], A.K. Schott[3], R.J. Carbajo[3], M.J. Vicent[3], A. Pineda-Lucena[3], H-A. Klok[2], R. Duncan[1] mail to:profruthduncan@btinternet.com

*[1]Centre for Polymer Therapeutics, Welsh School of Pharmacy, Redwood Building, King Edward VII Avenue, Cardiff, CF10 3XF, UK, [2]Ecole Polytechnique Fédérale de Lausanne (EPFL), Institut des Matériaux, Laboratoire des Polymères, Bâtiment MX-D, Lausanne, Switzerland, and [3]Centro de Investigación Príncipe Felipe, Av. Autopista del Saler 16, E-46012 Valencia, Spain.*

An increasing number of "polymer therapeu-tics" [1,2] have been approved for routine clinical use as 1st generation "nanomedicines". Importantly they have shown that they are able to satisfy the stringent requirements of industrial development and Regulatory Authority Approval. Our early studies developed a series of HPMA copolymer-based anticancer conjugates that have progressed into clinical trials [1,2]. Recently we have begun to explore polymer therapeutics designed to promote tissue repair, deliver combination chemotherapy, and to design conjugates that localise to newly emerging molecular targets. The main goal has been to capitalise on lessons learnt during transfer of the first polymeric anticancer conjugates into clinical development (reviewed in [1,2]), and combine with the increasing understanding of the molecular basis of diseases.

PEG-peptide and PEG-protein conjugates are now well-established nanomedicines [3]. Thus, knowing that the coiled-coil peptide motif is fundamentally important in the regulation of many cellular and pathological processes (of all naturally occurring amino acids, approximately 3-5 % are predicted to form α-helical coiled-coils), we initiated a project to test the feasibility of designing PEG conjugates containing the coiled-coil motif as a putative therapeutic "molecular switch". Two targets were chosen to establish establish proof of concept; the AP-1 (fos-jun) transcription factor that is important in cancer progression, and also the GP2 Ebola virus protein important for cellular entry. In the case of AP-1, an mPEG-Fos$W_C$ conjugate was prepared by reacting mPEG-maleimide (Mw 5,522 g $mol^{-1}$, Mw/Mn 1.1) with an FosW peptide synthesized to contain a terminal cysteine residue (Fos$W_C$). Its ability to form a stable coil-coil heterodimer with the target c-Jun sequence of the oncogenic AP-1 transcription factor was confirmed using 2D $^{15}$N-HSQC NMR and a $^{15}$N-labelled c-Jun peptide. Preliminary studies on cellular uptake and cytotoxicity have been conducted [4].

An exciting opportunity for exploitation of this concept is the design of conjugates as fusion inhibitors for the treatment of Ebola [4]., and an mPEG-EBGP2$_{609-630}$ conjugate was synthesised with this goal in mind.

In parallel studies we have been exploring the possibility of designing polymeric carriers containing coiled coil linkers as a new platform for drug delivery [4]. Such non covalent polymer conjugates can theoretically be used to create an easier to assemble polymer platform for combination therapy, be synthesised to contain peptides able to promote cytosolic access of the payload being carried, and finally might be designed to include the above-mentioned concept of a conjugate also able to act as a therapeutic molecular switch in its own right.

This presentation will review these new concepts and their current status.

**REFERENCES :**

[1] (a) Duncan, R. *Nature Rev. Drug Discov*. 2003, **2***(5)*, 347-360. (b) Duncan, R. *Nature Rev. Cancer* 2006, **6**, 688-701. (c) Vicent, M.J.; Duncan, R. (Eds.) *Adv. Drug Del Rev.* 2009, **61** *(13)*, 1117-1232 (whole volume).

[2] (a) Duncan, R. *Adv. Drug Del. Rev.* 2009, *61*, 1131-1148. (b) Duncan, R.; Vicent, M. J. *Adv. Drug Del. Rev.* 2010, **62**, 262-272.

[3] Veronese, F. M., Harris, J. M.; *Adv. Drug Deliv. Rev.* 2008, 60(1), whole issue.

[4] (a) Deacon, *et al. Control. Rel. Soc. 35th Ann. Mtg., New York*, July 2008; (b) Deacon *et al. 7th Intl Symp Polymer Therapeutics, Valencia, May* 2008; (c) *Deacon et al. Biomacromolecules*, 2010 submitted.

[5] Apostolovic, *et al. Biomacromolecules*, 2010, **11** (5), pp 1187–1195.

**ACKNOWLEDGEMENTS**

BBSRC, EPSRC Platform Grant (EP/C 013220/1) (SD, RD), the Ramón y Cajal programme, the Swiss National Science Foundation and the NCCR Nanoscale Science and the Spanish Ministerio de Ciencia e Innovación are acknowledged for financial support.

# Incorporation of collagen in LbL assemblies: mechanism and synthesis of size-controlled nanotubes

C.C. Dupont-Gillain, J. Landoulsi, S. Demoustier-Champagne

*Université catholique de Louvain, Institute of condensed matter and nanosciences, Bio and Soft Matter, Croix du Sud 2/18, 1348 Louvain-la-Neuve, Belgium.*

**INTRODUCTION:** The extracellular matrix (ECM), which regulates cell behaviour, presents a complex structure on the micro- and nanoscales. The creation of environments mimicking the ECM is a challenge of importance in biomaterials science and tissue engineering. Layer-by-layer (LbL) assembly is an attractive method to incorporate ECM proteins into nano-objects. However, while the LbL assembly of synthetic polyelectrolytes is well known, the build-up of multilayers using proteins is not trivial in reason of the particular structure and charge distribution of protein molecules. The aim of this study is to incorporate collagen, the most abundant ECM protein, into LbL assemblies, and to synthesize collagen-containing nanotubes using LbL assembly within the pores of a membrane (template method). Since collagen denaturation may facilitate diffusion inside the pores, the assembly of native (COL) and denatured (dCOL) type I collagen will be compared.

**METHODS:** LbL assembly was performed at pH 4.7 by successive adsorption steps of poly(styrene sulfonate) (PSS) and COL or dCOL. A layer of poly(allyl amine) (PAH) was used to ensure positive charging of the surface prior to LbL assembly. Assembly was first investigated on flat silicon substrates. The obtained multilayers were examined by X-ray photoelectron spectroscopy (XPS), ellipsometry, quartz crystal microbalance (QCM-D), atomic force microscopy (AFM) and force spectroscopy. Templates used for nanotube synthesis were polycarbonate track-etched membranes with pore diameters of 200 or 500 nm. Build-up of the multilayers inside the pores was monitored by gas flow porometry. The nanotubes, freed from the template, were imaged by scanning (SEM) and transmission electron microscopies.

**RESULTS and DISCUSSION:** In situ (QCM-D) and ex situ (ellipsometry) monitoring of LbL build-up showed a progressive increase of multilayer thickness for COL, demonstrating that COL can be used as a polycation for LbL assembly. Multilayers were also obtained using dCOL. However, their thickness decreased after each PSS adsorption step while it increased after each dCOL adsorption step, to finally reach a dry thickness of 18 nm after deposition of 6 bilayers, which is similar to the thickness obtained with COL (Fig. 1a). This behaviour is attributed to the formation of a soluble PSS-dCOL complex. XPS and AFM results confirmed the occurrence of assembly and indicated that a more dense coating was formed with COL compared to dCOL. Measurement of interactions between COL or dCOL-modified probes and PSS-treated substrate demonstrated that dCOL-PSS interaction is stronger than COL-PSS interaction. This may explain the similar build-up of multilayers with COL and dCOL despite the loss of soluble dCOL-PSS complexes. Gas flow porometry showed that multilayer thickness was higher inside pores compared to flat substrates, owing to confinement effect, and increased with dCOL compared to COL in 200 nm pores, owing to better diffusion. Nanotubes with controlled dimensions could be obtained using COL (Fig. 1b) [1] as well as dCOL.

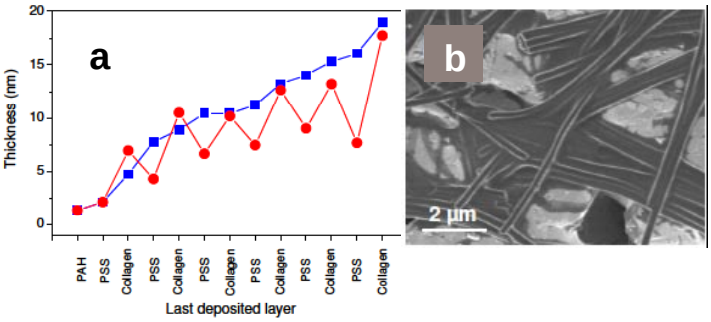


*Fig. 1: (a) ellipsometry measurement of the thickness of PAH/(PSS/COL)$_n$ (■) and PAH/(PSS/dCOL)$_n$ (●) multilayers; (b) SEM image of PAH/(PSS/COL)$_6$ nanotubes obtained in a template with a pore diameter of 200 nm.*

**CONCLUSIONS and PERSPECTIVES:** Collagen was successfully incorporated into LbL assemblies, allowing size-controlled collagen-containing nanotubes to be obtained by the template method. These nanotubes will now be used to design substrates for cell culture.

**REFERENCES:** [1] J. Landoulsi, C.J. Roy, C.C. Dupont-Gillain, S. Demoustier-Champagne (2009) *Biomacromolecules* **10**:1021-4.

**ACKNOWLEDGEMENTS:** This work was funded by BELSPO (IAP network 6/27).

# Bactericidal Coatings with Silver Nanoparticles

B.S. Necula[1], L.E. Fratila-Apachitei[1], S.A.J. Zaat[2], I. Apachitei[1], J. Duszczyk[1]

[1] *Delft University of Technology, Department of Materials Science and Engineering, Group of Biomaterials Technology, Mekelweg 2, 2628 CD Delft, The Netherlands*

[2] *Academic Medical Center, Department of Medical Microbiology and Center for Infection and Immunity Amsterdam (CINIMA), Meibergdreef 15, 1105 AZ Amsterdam, The Netherlands*

**INTRODUCTION:** Peri-implant infection remains one of the most common complications associated with surgical procedures aimed to restore the function of the joints or to heal bone fractures by using implantable devices. Next to the prevention through control of environmental and personnel contamination, additional strategies that can minimize the incidence of implant associated infections are explored, e.g. surface modification of implantable devices to confer them antibacterial activity [1]. The plasma electrolytic oxidation (PEO) process is used in our laboratory to produce biofunctional coatings on Mg and Ti alloys [2]. The aim of this work was the synthesis and evaluation of the *in-vitro* antibacterial activity of a $TiO_2$ porous coating bearing Ag nanoparticles. The bactericidal activity was assessed against methicillin-resistant *Staphylococcus aureus* (MRSA) using a novel direct contact assay.

**MATERIALS & METHODS:** The Ti6Al7Nb medical alloy has been oxidized under galvanostatic conditions in an electrolyte based on calcium glycerophosphate and calcium acetate salts to which 3.0 g/L Ag nanoparticles was added as bactericidal agent. For the assessment of bactericidal activity, a modified version of the JIS Z 2801 standard was used [3]. The assay was adjusted to better reproduce the scenario of an implant associated infection during surgery. The antibacterial activity against MRSA was evaluated in three different culture media, i.e. 1% TSB in 10 mM phosphate, 1% TSB in 10mM phosphate with 10% serum and 1% TSB in 10 mM phosphate containing 50% serum. Three different types of specimens were included for investigations, i.e. ground titanium disks (TG), oxidized titanium disks without the embedded Ag nanoparticles (TO) and oxidized titanium bearing Ag nanoparticles (TO-Ag).

**RESULTS & DISSCUSION:** The bactericidal coatings showed interconnected porosity, with pores size up to 3 µm. Next to Ag nanoparticles distributed within the oxide matrix, Al and Nb species from the titanium substrate and Ca and P species from the electrolyte were detected in the coatings. The thickness of the oxide layers was 12 ± 2 µm. Quantitative cultures after 24 hours of incubation clearly evidenced the bactericidal activity of the oxide coatings bearing Ag nanoparticles as no MRSA colonies were present on the blood agar plates at any dilution. The number of CFU/disk calculated from the quantitative culture results are included in Fig. 1. On the ground titanium disks and oxidized disks bearing no particles a 1000 fold increase in CFU/disk numbers relative to the inoculum at t = 0 (i.e. 2 x $10^5$ CFU per disk) was recorded.

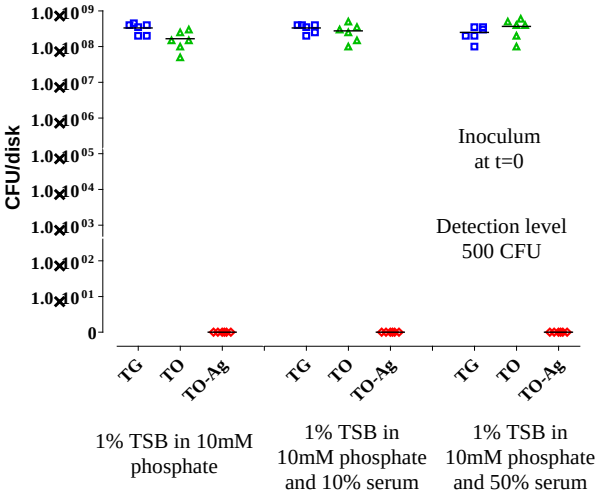


*Fig. 1. Antibacterial effect of TO-Ag coatings against MRSA compared with TG and TO disks*

**SUMMARY:**

- The novel assay allowed reliable quantitative assessment of the *in-vitro* antibacterial activity of the coatings.
- The results revealed complete killing of MRSA inocula within 24 hours, even in the presence of 50% human serum, while ground and oxidized titanium in the absence of Ag nanoparticles showed a 1000 fold increase in bacteria CFU.
- This highly bactericidal coating shows potential in lowering the incidence of implant related infections in orthopedic applications such as cementless hip implants based on titanium alloys.

**REFERENCES:** [1]E.M. Hetrick, H. Mark Schoenfisch (2006), *Chem Soc Rev* **35**:780-789. [2]B.S. Necula, I. Apachitei, L.E. Fratila-Apachitei, A. Berkani, J. Duszczyk (2009), *J Mat Sci: Materials in Medicine* **20**:339-345. [3]Anon (2000). *Antimicrobial Products - Test for antimicrobial activity and efficacy*, JIS Z 2801:2000.

European Cells and Materials Vol. 20. Suppl. 3, 2010 (page 69) ISSN 1473-2262

# Synthesis and Characterization of Self-organized Cross-linked Nanoparticle Sensors for Intracellular pH Measurements

Pramod Kumar E.K., Nynne M.Christensen, Rikke V. Benjaminsen, Thomas L. Andresen

*Technical University of Denmark, Department of Micro- and Nanotechnology, Frederiksborgvej 399, 4000 Roskilde, Denmark.*

**INTRODUCTION:** Nanosensor technology offer new possibilities for obtaining reliable measurements of key metabolites (including pH and ions) at cellular and sub-cellular level. In order to use the sensors in cells, it is necessary to develop improved sensor systems[1] that are surface functionalized for spontaneous cell internalization and targeting of specific compartments in cells. If sensors that target specific sub-cellular compartments are constructed, it will not only provide new knowledge about cell biology but will furthermore give insight into how we can utilize pH changes in cellular compartments after endocytosis, to release drugs from engineered drug delivery systems.

**METHODS:** Polymeric micelle based pH nanosensors were synthesized by spontaneous self assembly[2] of amphiphilic triblock copolymers, functionalized with fluorophores, in water. Amphiphilic triblock copolymers were synthesized by ATRP (Scheme1). The pH sensitive fluorophores (Fluorescein and Oregon Green), the pH insensitive reference fluorophore (Rhodamine B) and click reactive cross-linkers (Azido- and alkynyl-) were introduced in to the hydrophilic-hydrophobic interface of the triblock copolymers. A targeting ligand (Peptide) was bound to the hydrophilic block of Boc-NH-PEG-b-PHEMA-b-PMMA polymer. All monomers in suitable ratio were dissolved in DMF and dialysis against MilliQ water for five days. The obtained polymer micells were hereafter cross-linked by "click" chemistry and further dialysis gave the desired cross-linked and cell targeting pH nanosensors.

**RESULTS:** The pH Nanosensors were characterized by DLS, AFM, CryoTEM and Zeta potential measurements. It was found that the self-organization resulted in nanoparticles that were ~45 nm in size and furthermore highly uniform. In Vitro fluorescence measurements were used to construct pH calibration curve based on ratiometric measurements showing that functional nanosensors had been obtained. Reversibility and time of response to changes in pH was also confirmed. cryoTEM and DLS showed that the cross-linking was occurring giving a nanosensor system that can no longer dissociate, even though it was formed by an advantageous self-organization process. Cell uptake studies of pH nanosensors were carried out in HeLa cells and it was found that the nanoparticles are internalized by the cells.

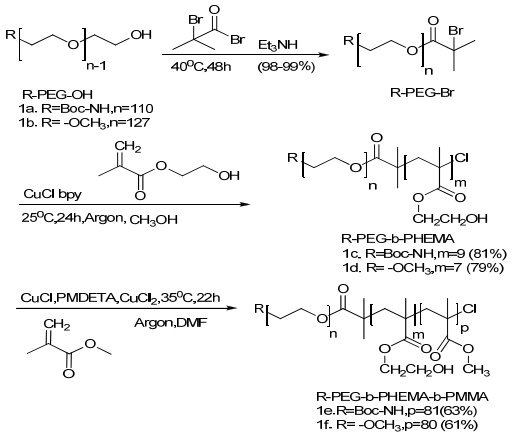


*Scheme 1.Synthesis of triblock copolymers using ATRP*

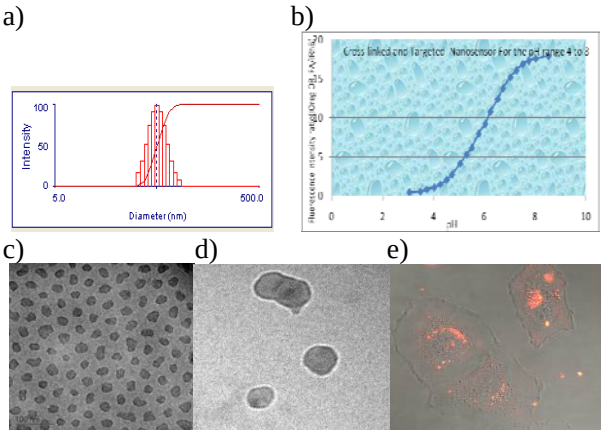


*Fig. 1: a) dynamic light scattering measurement, b) pH calibration curve, c) CryoTEM before cross-linking, d) after cross-linking, e) cell uptake study in HeLa cells.*

**CONCLUSIONS**: A nanosensor has been constructed that with a pH measurement range from 4 to 8, thus covering the full range of pH in endosomes/lysosomes. Sensors are sensitive towards the pH changes within microseconds.

**REFERENCES:** [1] Sun H, Scharff-Poulsen AM, Gu H, Almdal K.(2006) *Chem. Mater.* **18**:3381-3384.[2] Zhibo Li, Ellina Kesselman, Yeshayahu Talmon,Marc A. Hillmyer,Timothy P. Lodge (2004)*Science*,**306**:98-101

**ACKNOWLEDGEMENT:** The Danish Strategic Research Council (NABIIT) is gratefully acknowledged.

# General supramolecular approach for ATP sensing and surface bound alkaline Phosphatase kinetics using microfluidic platform

B.Eker1, M.D.Yilmaz2, A. Gonzalez-Campo2, P.Jonkheijm2, J. Huskens2, H. Gardeniers[1]

*[1] Mesoscale Chemical Systems. [2] Molecular Nanofabrication Group*

*MESA+ Institute for Nanotechnology, University of Twente, Enschede, The Netherlands*

**INTRODUCTION:** A general supramolecular platform has been developed by using self-assembled monolayers (SAMs) for two different studies; developing an ATP selective anion sensor and investigating the kinetics and reusability of surface bound biotinylated alkaline phosphatase (AP). The ATP sensing and AP platform have been implemented using microfluidics. The microfluidic approach has attracted significant attention in the last decades for chemical and biological assays because of faster detection time, low consumption of analyte and reagents, and the possibility of integrated continuous monitoring of analyte solutions.

**METHODS:** An on-chip assay was performed to develop a sensing system for biologically relevant phosphate ions and an AP platform via surface chemistry. The microchannel surface was functionalized with βCD SAMs by following three-step reaction, as described by Manon et al [1]. For ATP sensor, Eu(III)- cyclen complex was incorporated into β-cyclodextrin monolayers via orthogonal supramolecular host-guest interactions. The self-assembly of the Eu(III)-cyclen conjugate and naphthalene β-diketone as an antenna resulted in the formation of a highly luminescent lanthanide system on the microchannel surface. For AP platform, streptavidin (Sav) was attached to β-cyclodextrin SAMs via orthogonal host guest and Sav-biotin interactions, and biotinylated AP was incorporated into β-cyclodextrin monolayers through Sav-biotin interactions.

**RESULTS:** For ATP sensor, detection of different phosphate anions was demonstrated by monitoring the decrease in red emission, whereby among various phosphate anions only ATP displaced the antenna, resulting in quenching of the Eu(III) emission (Fig 1). Parallel synthesis of five sensing SAMs in a single multichannel chip was performed, as a first demonstration of anion screening in a high-throughput format that allows detection of different phosphate anions in a single test run. For AP platform, the enzymatic chip showed high enzyme activity, and reusability upon reaction of biotinylated AP with a highly sensitive fluorescent AP substrate (Fig 2) while no reaction was observed with nonbiotinylated AP, indicating that enzyme attachment on the surface is highly specific.

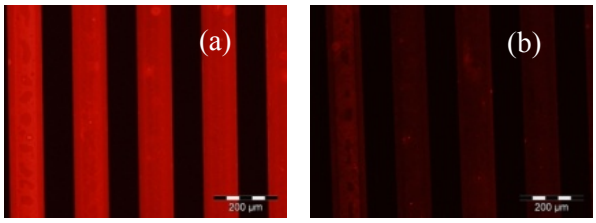


*Fig. 1: (a) Eu(III)-cyclen and β-diketone complex on the microchip surface (b) Eu(III)-cyclen and β-diketone complex after 1 mM ATP*

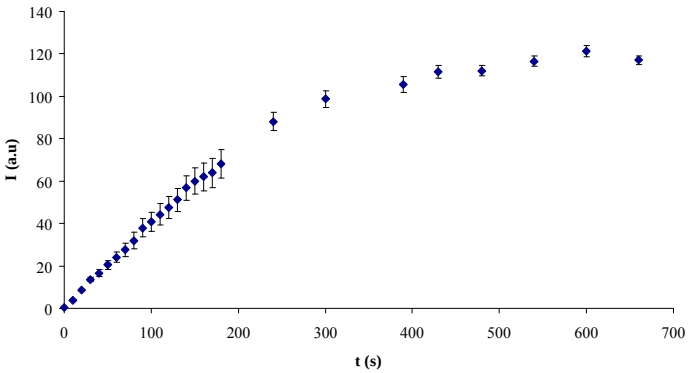


*Fig. 2: Fluorescence Intensity-Time Profile of the reaction with 1 mM AP substrate in the presence of biotinylated AP*

**DISCUSSION & CONCLUSIONS:** In this course of work, ATP selective sensor and highly active and reusable AP microchip platform was developed by modifying βCD SAMs with orthogonal host guest interactions. Thereby, such supramolecular microfluidic platform provides promising applications for different purposes such as in biological, biomedical and metabolic studies for ATP sensing and in immunoassays for AP platform.

**REFERENCES:** [1] M. J. W. Ludden et al (2006) *Small* **2**:1192-1202.

**ACKNOWLEDGEMENTS:** We thank to STW,

WO, The technology program of the Ministry of Economical Affairs, and NWO-CW, Netherlands.

European Cells and Materials Vol. 20. Suppl. 3, 2010 (page 71) ISSN 1473-2262

# Photochemical fabrication of a highly elastic and adhesive surgical tissue sealant

Christopher M Elvin[1], Tony Vuocolo[1], Alan G Brownlee[1], Mickey Huson[3], Misook Kim[1], Russell E Lyons1, Lillian Sando[1], Glenn A Edwards[4], Nancy E Liyou[1], John AM Ramshaw[2] and Jerome A Werkmeister[2]

*[1]CSIRO Livestock Industries, St. Lucia 4067, Australia, [2]CSIRO Molecular & Health Technologies, Clayton 3169, Australia, [3]CSIRO Materials Science & Engineering, Geelong, Australia and [4]Faculty of Veterinary Science, Werribee 3030, Australia*

**INTRODUCTION:** We recently reported the preparation of a highly elastic, dityrosine-crosslinked protein biomaterial via a rapid photochemical method using visible light and a ruthenium metal ligand catalyst [1]. We predicted that other tyrosine-rich proteins, that assemble at the nano-scale, might also be susceptible to covalent crosslinking via this approach. We subsequently showed that unmodified native fibrinogen could be photochemically crosslinked to form an adhesive hydrogel [2, 3]. Here we show that high Bloom, unmodified gelatins (either type A or type B) can also form highly elastic protein hydrogels displaying high adhesive strength and serve as rapidly-curing surgical tissue adhesives.

**METHODS:** Fibrinogen was from Sigma or prepared from bovine plasma [3]. Gelatin was bovine type B, or porcine type A (Sigma), 300 Bloom and used as 15% solutions in PBS. Ruthenium trisbipyridyl chloride, $[RuII(bpy)_3]^{2+}Cl_2$, and sodium persulphate (SPS) were from Sigma. Photo-crosslinking was carried out with 1mM $[RuII(bpy)_3]^{2+}Cl_2$ and 10mM SPS by illumination for 20 s with a 300W xenon lamp. Adhesive strength was assessed using an Instron 5544 using a bovine amnion membrane model. Dumbbells of photo-crosslinked proteins were cast in a PTFE moulds and assessed for mechanical properties. *In vivo* studies using canine and porcine surgical models were carried out according to CSIRO/University of Melbourne Animal Ethics procedures.

**RESULTS:** Dityrosine crosslinks were readily formed by photochemical curing of fibrinogen and gelatin as shown by the presence of high molecular weight protein polymers formed after crosslinking by SDS-PAGE analysis. The presence of dityrosine can be shown by its fluorescence and by LC/MS analysis following acid hydrolysis.
The adhesive strength of gelatin was determined by photo-crosslinking of 2 bovine amnion sheets. The adhesive strength of photo-crosslinked mammalian gelatin was at least 5-fold higher than a commercial fibrin adhesive (Fig 1B). Cold-water

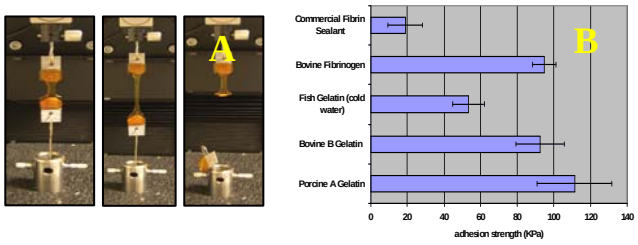


*Figure 1: (A) Photocrosslinked gelatin is highly extensible. (B) Comparison of adhesion strengths (kPa) of various photo crosslinked protein formulations compared to fibrin adhesive using bovine amnion.*

fish gelatin, showed lower adhesion strength, but this was still considerably higher than that of the fibrin adhesive. For photo-crosslinking, the time of illumination was 30s, whereas for the commercial fibrin based sealant, at least 15 min elapsed before measurement.

**DISCUSSION & CONCLUSIONS:** Photo-crosslinking of unstructured gelatin is very rapid and gives a highly elastic and strong tissue adhesive. Despite its highly defined structure, fibrinogen also self-associates at the nano-scale and forms an effective tissue adhesive via interaction with tissue ECM proteins. These protein-based nanomaterials have potential for use in surgical applications where high adhesive strength and elasticity is required, (eg. gastrointestinal, vascular and lung applications). This system is also compatible with cells, so has potential as a vehicle for cell delivery in tissue engineering and cell therapy applications

**REFERENCES:** [1] Elvin et al. (2005) Synthesis and properties of crosslinked recombinant pro-resilin. *Nature*, **437**: 999-1002. [2] Elvin et al. (2009 ) Evaluation of photo-crosslinked fibrinogen as a rapid and strong tissue adhesive. *J Biomed Mater Res A.* in press, epub. [3] Elvin et al. (2009) The development of photochemically crosslinked native fibrinogen as a rapidly formed and mechanically strong surgical tissue sealant. *Biomaterials*. **30**: 2059-2065.

# Controlled Production of Uniform Vesicles by Shear-Enhanced Pore Extrusion

H. Engel[1] and E. J. Windhab[1]

[1] *Institute of Food, Nutrition and Health, ETH Zurich, 8092 Zurich, Switzerland*

**INTRODUCTION:** Vesicles are nanometer- to micrometer-sized compartments consisting of an aqueous core and one or more self-closed bilayer membranes of amphiphiles, which may be low molar mass compounds (lipids, surfactants) or block copolymers. The spontaneous formation of vesicles by simple swelling of an initially dried lamellar film or by directly dispersing the amphi-philes in excess water results in a polydisperse vesicle suspension with mainly large, multilamellar vesicles (MLV). The most common method for the reproducible preparation of homogeneous, uni-lamellar vesicles consists of repetitively forcing a MLV suspension through polycarbonate membra-nes with defined pore sizes, however, this requires at least 10 recirculation cycles [l]. The aim of the current project is to provide the biomedical, cosmetic and food industries with new processing technologies for the controlled large scale production of uniform, application-tailored vesicles from conventional biomembrane phospho-lipids and block copolymers.

**METHODS:** Based on the principle of membrane emulsification [2], a shear-enhanced nano membrane pore extruder (NAMPEX) has been constructed which combines the conventional process for vesicle extrusion with tailored flow stresses at the pore exit (Figure 1). The shear field induced above the membrane is expected to detach bilayer fragments of the emerging vesicles which immediately self-close to form small unilamellar vesicles. The influence of shear rate on vesicle size reduction has been studied by extruding MLV suspensions from purified soy phosphatidylcholine (PC) and a novel food grade block copolymer at controlled flow rates, i. e. transmembrane pressu-res, through track-etched PET membranes with mean pore diameters of 400 nm and 200 nm. Dynamic light scattering (DLS) and cryo transmission electron microscopy (cryo-TEM) were used for morphological characterizations.

**RESULTS:** Compared to conventional extrusion, a significant decrease in mean hydrodynamic diameters of soy PC vesicle suspensions was observed after one extrusion cycle using the NAMPEX device and applying high shear forces. Vesicle size reduction with increasing shear rate was more pronounced upon extrusion through 200

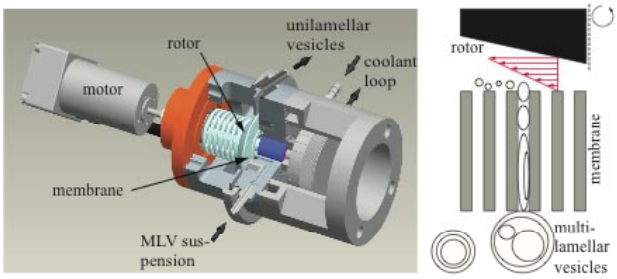


*Fig. 1: Technical drawing of the shear-enhanced nano membrane pore extruder (left) and schematic representation of its principle to reduce size and lamellarity of MLVs in one step (right).*

nm pores rather than trough 400 nm pores. For both membrane types used, the size of vesicles prepared from block copolymers was hardly affected by the presence of the shear field.

**DISCUSSION & CONCLUSIONS:** The performance of nano membrane pore extrusion in homogenizing MLV suspensions can be increased by inducing a strong shear field at the membrane outlet. Mechanical properties of the vesicle membrane were observed to have a big influence on the effectivity of the flow stresses. In future investigations, they will be adjusted by using appropriate mixtures of vesicle forming amphi-philes and by taking advantage of the versatility of block copolymer chemistry. The shear forces seem to primarily act on the leading edges of deformed vesicles emerging from small pores rather than on intact vesicles traveling through larger pore channels and finally through the shear gap itself. The suggested mechanism of vesicle size reduction in shear-enhanced pore extrusion will be investi-gated by directly observing an electroformed giant unilamellar vesicle passing through a microfluidic cross-flow channel.

**REFERENCES:** [1] P. Walde (2004) Preparation of vesicles (liposomes) in *Encyclopedia of Nano-science and Nanotechnology*, Vol. **9** (ed H. S. Nalwa) American Scientific Publishers, pp 43-79. [2]V. Schadler and E. J. Windhab (2006) *Desalination* **189**:130-135.

**ACKNOWLEDGEMENTS:** This project is in collaboration with Prof. Wolfgang Meier (Univer-sity of Basel, Switzerland) and Bühler AG (Uzwil, Switzerland) and is supported by the Commission of Technology and Innovation (CTI, Bern, Switzerland).

# Uptake and transfection efficiency of peptide modified and unmodified PLL-g-PEG-DNA nanocondensates in dependence to the cell cycle

T. von Erlach, T. Lühmann, H. Hall

*Cells and BioMaterials, Department of Materials, ETH Zurich, Switzerland*

**INTRODUCTION:** Polycationic polymers form condensates with plasmid DNA and are used for gene therapy as an alternative to viral vectors. Poly-L-lysine (PLL) grafted with poly(ethylene glycol) (PEG) has already been extensively studied and shows high transfection efficiency combined with low cytotoxicity in COS-7 cells [1,3].

In this study cell cycle dependence of the uptake and transfection efficiency of PLL-g-PEG-plasmid DNA condensates is analysed. Several studies reported a difference of efficacy of gene transfer into cells depending on the cell cycle phase [2]. As uptake and transfection depend on cell type and of size, shape, charge and chemistry of the delivery system, cell cycle dependence was analysed in different cell types and with different peptide modifications of PLL-g-PEG co-polymers.

**METHODS:** Cells were either synchronized by serum depletion or thymidine excess**.** Synchronization by serum depletion was done by incubation in 0.1% FBS containing tissue culture medium with 1 mg/mL glucose for 72h in the case of COS-7 and for 24h when using human foreskin fibroblasts. Synchronization by thymidine excess was achieved by two times 16h incubation with 40 mM tymidine with 9h incubation in 480 µM deoxycytidine in between all in normal tissue culture medium. For the subsequent proliferation analysis WST-1 proliferation assay (Roche) was used. Analysis of the cell cycle phases of propidium iodide-stained cells was done by FACS analysis. The polymers used in this study were PLL(20kDa)-g5-PEG(5kDa) or PLL(20kDa)-g3-PEG(5kDa) with a viral dynein binding peptide sequence or a poly(Arg) sequence attached [4]. The nanoparticles were analyzed after condensation with pEGFP-N1 plasmid DNA for transfection. The uptake of PLL-g-PEG was analysed after condensation with Cy3-labelled pEGFP-N1 plasmid DNA by FACS analysis as described previously [3].

**RESULTS:** The synchronization protocols resulted in a significant but reversible reduction of proliferation compared to untreated cells and a significant increase of the whole cell population in the particular cell phase (data not shown). The synchronized cells showed lower transfection

efficiency compared to normal growing non-synchronized cells in both cell types (data not shown). The uptake of the polymer-DNA condensates was significantly higher in G2 phase compared to G1 phase synchronized cells and also to non-synchronized cells in both cell types (Fig. 1).

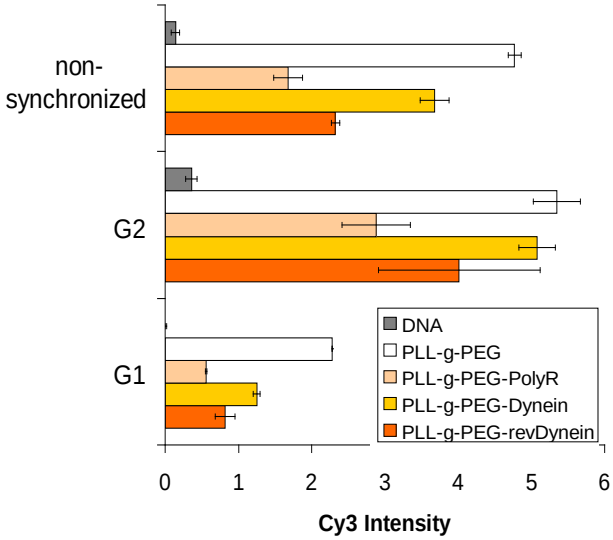


*Fig.1: Uptake of different PLL-g-PEG co-polymers condensated with -Cy3-labelled DNA in G1 or G2 cell cycle phase synchronized COS-7 cells compared to non-synchronized cells.*

**DISCUSSION & CONCLUSIONS:** The lower transfection efficiency in synchronized cells compared to untreated cells is in line with prior studies and underlines the requirement of mitosis and the associated transient rupture of the nuclear envelope for efficient plasmid DNA delivery into the nucleus. The cell cycle dependent uptake of the polymer-plasmid DNA nanoparticles seems to correlate with cell cycle dependent differences in endocytotic activity, which is highest in G2 phase [2].

**REFERENCES:** [1] Rimann et al. *Bioconjug Chem* 2008, **19**, (2), 548-57. [2] Männistö et al. *J Gene Med* 2005; **7**: 466–476 [3]Lühmann et al. *Bioconjug Chem* 2008, **19**, (9), 1907-16. [4] T. Lühmann, DISS ETH NO. 18717, 2009.

**ACKNOWLEDGEMENTS:** We want to thank M. Kisielow and A. Schütz from the Flow Cytometry Laboratory ETHZ for all their help and support with the FACS experiments.

# Interactions of Engineered Nanomaterials with the Immune System

B. Fadeel[1], A. Shvedova[2], V. Kagan[3]

*[1]Division of Molecular Toxicology, Institute of Environmental Medicine, Karolinska Institutet, Stockholm, Sweden; [2]Pathology and Physiology Research Branch, Health Effects Laboratory Division, National Institute for Occupational Safety and Health, and West Virginia University, Morgantown, West Virginia; [3]Department of Environmental and Occupational Health, and Center for Free Radical and Antioxidant Health, Graduate School of Public Health, University of Pittsburgh, Pittsburgh, Pennsylvania.*

Engineered nanomaterials present tremendous opportunities for industrial growth and development, and hold great promise for the enrichment of the lives of citizens in medicine, electronics, and numerous other areas. However, there are considerable gaps in our knowledge concerning the potential hazardous effects of nanomaterials on human health and the environment.

Our research focuses on effects of engineered nanomaterials on the immune system, the body's primary defense system against foreign intrusion. One of the underlying postulates guiding our work is that the recognition or non-recognition of engineered nanoparticles by professional phagocytes of the immune system will determine not only the distribution of these materials in the body but also their toxic potential. Our recent studies have focused on single-walled carbon nanotubes (SWCNT).

Functionalization of SWCNT with the phospholipid, phosphatidylserine (PS), a known recognition signal for macrophages, makes them recognizable *in vitro* and *in vivo* by professional phagocytes and reduces macrophage secretion of pro-inflammatory cytokines. PS functionalization could be exploited for targeted delivery of SWCNT with specified cargoes into professional phagocytes. Our proof-of-principle studies demonstrate that PS-coated SWCNT are able to ferry cytochrome c into the RAW264.7 macrophage cell line resulting in activation of the cytochrome c-dependent caspase cascade in these cells.

In addition, our recent work shows that hypochlorite and reactive radical intermediates of the human neutrophil enzyme myeloperoxidase (hMPO) catalyse the biodegradation of SWCNT *in vitro*, in neutrophils and to a lesser degree in macrophages. Cellular uptake and subsequent biodegradation was enhanced by coating of the carbon nanotubes with immunoglobulin (IgG). Importantly, the biodegraded SWCNT do not

generate an inflammatory response when aspirated into the lungs of mice. These findings suggest that the extent to which SWCNT are biodegraded may be a major determinant of the scale and severity of the associated inflammatory responses in exposed individuals.

Overall, these studies shed light on how professional phagocytes of the immune system (macrophages, neutrophils) recognize and react to carbon nanotubes, and point to strategies for the mitigation of adverse outcomes of exposure to these materials. A detailed understanding of interactions of engineered nanomaterials with the immune system is important for the safe development of such materials for biomedical and other applications.

Supported by the Swedish Research Council, National Institutes of Health (NIH) (grants to Prof. Kagan, Prof. Shvedova) and Seventh Framework Programme of the European Commission (FP7-NANOMMUNE-Grant Agreement No. 214281) (project coordinator: B. Fadeel).

**SUGGESTED READING:**

Fadeel B, Garcia-Bennett AE. Better safe than sorry: understanding the toxicological properties of inorganic nanoparticles manufactured for biomedical applications. *Adv. Drug Deliv. Rev.* 2010;**62**:362-374.

Shvedova AA, Kagan VE, Fadeel B. Close encounters of the small kind: adverse effects of man-made materials interfacing with the nano-cosmos of biological systems. *Annu. Rev. Pharmacol. Toxicol.* 2010;**50** 63-88.

Kunzmann A, Andersson B, Thurnherr T, Krug H, Scheynius A, Fadeel B. Toxicology of engineered nanomaterials: focus on biocompatibility, biodistribution and biodegradation. Biochim. *Biophys. Acta* 2010; May 8 [Epub ahead of print].

# Microalgal Synthesis of Gold Nanoparticles by *Tetraselmis suecica*

*Faramarzi M.A., Forootanfar H., Shakibaei M., Shahverdi A.R.*

*Department of Pharmaceutical Biotechnology, Faculty of Pharmacy, Tehran University of Medical Sciences, P.O. Box 14155-6451, Tehran, 14174, Iran*

**INTRODUCTION:** Metal nanoparticles have wide-ranging applications in diverse areas such as chemistry, physics, biomedical and material sciences. Gold nanoparticles (AuNPs) absorb light in the visible region of electromagnetic spectrum due to their surface plasmon resonance and convert it to heat. Therefore, AuNPs could be used for photothermal therapy and imaging. Leukemia therapy, biomolecular immobilization and labeling for the contrast enhancement in cryoelectron microscopy are other AuNPs applications. Some microorganisms such as *Actinobacter* sp., *Rhodopseudomonase capsulata*, and methanol extracts of some medicinal plants have been used as nanofactories for green synthesis of AuNPs. Microalgae, the photosynthetic pro- and/ or eukaryotes, proved to have a potential talent for conducting the safe reactions in biotransformation processes and the removal of heavy metals from the environment. The exposure of the aqueous $HAucl_4$ to a powder prepared from a marine alga, *Sargassum wightii*, resulted in the conversion of $Au^{3+}$ to $Au^0$ after 12 h. The present study showed the capability of *Tetraselmis suecica* for rapid synthesis AuNPs following the incubation of $HAucl_4$ solution with the fresh algal cell extract

**METHODS:** The biomass of *Tetraselmis suecica* was harvested by centrifugation at 4000 g for 10 min after culturing in f/2 Guillard medium followed by washing them three times. The biomass was disrupted by liquid nitrogen and the cell extract was prepared after removing of cell debris by centrifugation at 4000 g for 10 min. after adding the cell extract of *Tetraselmis suecica* to 1 mM $HAuCl_4$, formation of gold nanoparticles was investigated under different temperatures (30-90 °C). The UV/Vis-spectrum, TEM analysis and X ray diffraction (XRD) analysis as well as Fourier transform infrared (FTIR) spectroscopy analysis were performed to characterize the formed AuNPs.

**RESULTS:** Comparison of the UV/Vis-spectrum of treated $HAuCl_4$ to untreated solution represents an absorption peak around 530 nm typical for formation of gold nanoparticles observed only in a mixture containing 1 mL of cell extract after 5 min incubation at 90°C. AuNPs were not synthesized in other mixtures and thermal conditions. Transmission electron micrograph of AuNPs showed well-separated and spherical shapes nanoparticles without any aggregation. Particle size distribution pattern of AuNPs were in a range between 51-120 nm. The XRD pattern (four peaks positioned at $2\theta = 38.2°$ ,44.6°, 63.1° and 76.6° due to (111), (200), (220), and (222) lattice planes, respectively) was agreed with Bragg's reflection related to Au nanoparticles. FTIR measurements of AuNPs show main peaks at 3431.58 and 1675.11, $cm^{-1}$. Strong peak at 3431.58 $cm^{-1}$ could be corresponded to O-H or N-H and this indicated an alcohol or N-H containing amide. Although the carbonyl absorption always observed at 1690-1760 $cm^{-1}$ but the strong peak at 1675.11 $cm^{-1}$ at Fig. 6 could be related to a carbonyl group. Each of the mentioned functional groups existed on the surface of the gold nanoparticles could be used for the formation of covalent binding between the various active compounds and nanoparticles or bioconjugation and immobilization of enzymes on the surface of the AuNPs.

**DISCUSSION & CONCLUSIONS:** Nano-gold formation was taken place after 5 min incubation of *Tetraselmis suecica* cell extract at 90°C. This green, easy and low cost method for production of AuNPs is more preferable to the most of nanoparticles synthesis methods for example the application of organic solvents and toxic reagents caused environment pollution problems.

**REFERENCES**: [1] Faramarzi M.A., Adrangi S., Tabatabaei Yazdi M., (2008) *J. Phycol.* 44: 27-37 [2] Aveendran P., Fu J., Wallen S.L., (2006) Green Chem. 8: 34-38 [3] Kojima C., Hirano Y., Yuba E., Harada A., Kono K., (2008) *Colloid Surf. B: Biointerfaces*. 66: 246-252 [4] Podsiadlo P., Sinani V.A., Bahng J.H., Kam N.W., Lee J., Kotov, N.A. (2008) Langmuir. 24: 568-744 [5]Huang H., Liu Z., Yang X. (2006) *Analyt. Biochem.* 356: 208-214

**ACKNOWLEDGEMENTS:** This work was financially supported by the grant No. 88-02-90-8747 from Biotechnology Research Center, Tehran University of Medical Sciences, Tehran, Iran.

# Physical characterization methods for nanomedicine: structure-function relationships

N. Farkas[1], J.A. Dagata[1], C. Yang[2], A. Rait[2], K.F. Pirollo[2] and E.H. Chang[2]

[1] *National Institute of Standards & Technology, Gaithersburg, MD 20899, USA*
[2] *Department of Oncology, Georgetown University Medical Center, 2700 Reservoir Road, Washington, DC 20017, USA.*

**INTRODUCTION:** There are increasing needs for new measurement methodologies in such fields as drug delivery and nanomedicine. Manufacturing of targeted nanoparticle delivery systems (NDS) is often realized through self-assembly where a slight change in the process can significantly alter the structural-functional properties and with that the efficacy of the formulation toward early detection and treatment of cancer. A proper characterization must reveal these dimensional changes at both the elementary particle and average distribution level and provide quality control during production. When a nanoparticle system is composed of soft, bio-mimetic materials and consequently prone to deformation, physical characterization becomes even more challenging, requiring controlled surface attachment and biologically relevant measurement conditions.

**METHODS:** NDS preparation: Cationic liposomes consisting of 1:1 DOPE:DOTAP were prepared by the ethanol injection method. The targeting protein used in these studies is an anti-transferrin receptor single-chain antibody fragment [1]. Encapsulation of a payload, including p53 gene therapy, small interfering RNA, Magnavist or SPIO magnetic resonance imaging contrast agents, was done by simple mixing of the components.

NDS characterization: From metrology and manufacturing viewpoints, the ability to measure size, which is highly interdependent with stability and functionality, is essential to assure potency and manufacturability of a specific drug formulation. Fluid scanning probe microscopy (SPM) is a powerful imaging tool to monitor dimensional and organizational changes of NDS as they undergo multiple stages of self-assembly (Figure 1). In particular, reproducible and quantitative size analysis by fluid SPM is possible by using a novel tunable surface preparation method, which allows controlled attachment of soft NDS [2]. Our approach to physical characterization of multi-component NDS is to integrate SPM and dynamic light scattering (DLS) methods. Combination of the two techniques provides us with a comprehensive measurement solution to obtain understanding of the NDS self-

assembly process and how it affects transfection efficiency of the resulting NDS population.

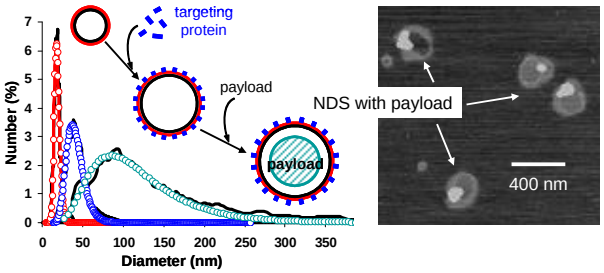


*Figure 1: Self-assembly of NDS and its size distribution after each self-assembly step (left). High-resolution SPM image of NDS with superparamagnetic iron oxide (SPIO) (right).*

**RESULTS:** We find that self-assembly induces substantial reorganization of the components manifested by changes in NDS size, stability and functionality. In addition, this dynamic interaction between individual constituents increases polydispersity, and leads to the formation of a heterogeneous population, i.e. only fraction of the NDS is capable of targeted delivery of a payload. The transfection efficiency of a NDS solution therefore is determined by the relative ratio and interaction of the components during self-assembly and sensitive to processing conditions. Consequently biological measures of efficacy and manufacturing measurement of size and stability must be viewed as highly interdependent. We illustrate this point through a specific example, where implementation of the integrated SPM and DLS measurement methods enables development and optimization of the self-assembly process of a NDS with SPIO payload.

**DISCUSSION & CONCLUSIONS:** Our results show that understanding of structure-function relationships in NDS and establishing correlation between physical and biological measurements are imperative to rational drug design, optimization and manufacturing of formulations and to the advancement of nanomedicine.

**REFERENCES:** [1] L. Xu, et al (2002) *Mol. Cancer Ther.* **1**:337-46. [2] J.A. Dagata, et al (2008) *Nanotechnology* **19**:305101.

# Exploiting Biological Diversity

Christof Fattinger

*F. Hoffmann-La Roche Ltd, Basel, Switzerland*

In the last decade ingenious methodologies for high-throughput and high-content analysis of biological samples have evolved. Within this progress the proficient design and application of miniaturized *in vitro* assays have become indispensible for exploiting the enormous breadth of biological diversity in modern drug discovery in particular and in the life sciences in general.

Miniaturized high-throughput technologies for *in vitro* biology assays rely on “miniaturization” and “parallel processing” of the samples to be analyzed. The arrangement of samples in a linear or planar array allows for parallel implementation of process steps in the assay, such as sample handling, sample preparation, liquid handling, incubation, molecular recognition, hybridization, signal amplification, and readout of the analytical results.

However, the paradigm “miniaturization and parallel processing of molecular entities by integrated devices” is not sufficient for the concept of “efficient state-of-the-art assays”!

To investigate the breadth of biological diversity in the pharmaceutical sciences we need to observe large numbers of parameters and conditions, while keeping the number of individual sample handling and sample preparation steps low. We need to break down the different process steps for the assay into optimized subprocesses in order to work efficiently. Each subprocess benefits from different strategies for miniaturization and parallelization while keeping the subprocesses and the main process fairly simple. In this way we generate a vast diversity of information by intelligent nesting of the different subprocesses.

The essence of efficient assays is intelligent nesting of subprocesses. This fundamental concept will be exemplified and discussed for three novel assay methodologies, namely: protein arrays devised for drug discovery and clinical research, high-density oligonucleotide probe arrays, and deep sequencing of genomes.

This presentation discusses the conceptual design, the operational advances, and the

interplay of modern miniaturized high-throughput assays. It illustrates the remarkable improvements of these analytical methods in recent years and reflects on how this rapidly advancing field might evolve in the future.

# Parallel AFM imaging and force spectroscopy using 2-dimensional probe arrays for applications in cell biology

M.Favre[1], A.Meister[1], S.Dasen[1], G.Gruener[1], R.Ischer[1], T.Overstolz[1], J.Bitterli[1], P.Vettiger[1], M.Liley[1], H.Heinzelmann[1]

[1] *CSEM, Centre Suisse d'Electronique et de Microtechnique SA, Neuchâtel, Switzerland.*

**INTRODUCTION:** Atomic force microscopy (AFM) is increasingly used in cell biology to study individual cells: to characterize a cell's morphology or to measure its mechanical or adherence properties using force spectroscopy. Today's commercial AFMs use single cantilevers to probe the sample surface. However, AFM based analyses involving living cells are usually extremely time consuming [1], due to cell dynamics and the need for a large number of identical experiments for statistical reasons. In order to be routinely utilized in R&D e.g. for cell based screening, the method has to become faster and easier to use. We describe here an instrument to manipulate 2-dimensional cantilever arrays.

**METHODS:** The deflections of all cantilevers in the array are measured in parallel using a Michelson interferometer. An interferogram captured by a CMOS camera is analyzed using dedicated software to determine the deflection of each cantilever. A special instrumental platform has been developed, that includes the optical read-out, micro- and nanopositioning stages, as well as a fluid chamber to keep the cells in a liquid environment at 37°C. The 2-dimensional AFM arrays were developed and fabricated at CSEM. Cantilevers with and without tips were fabricated: the former to analyze the topography and mechanical properties of cells, and the latter to measure intercellular interaction forces.

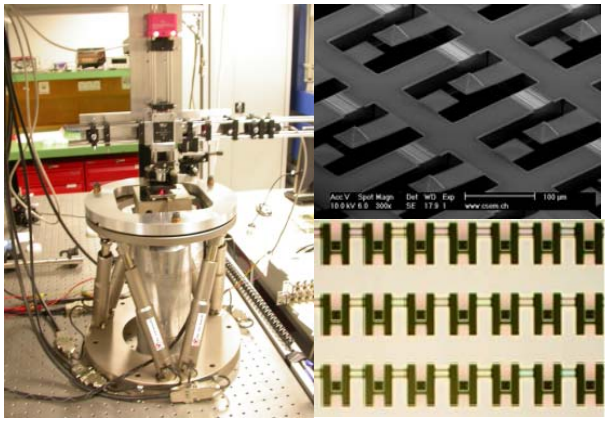

*Fig. 1: Instrumental platform and AFM probe arrays (SEM image (top) and optical image (bottom)).*

**RESULTS:** First experimental measurements have demonstrated the use of the platform to operate 2D cantilever arrays in air and in liquid. The system was first tested by parallel topographical imaging on fixed and dehydrated cells in air. The 35 topography images shown in the *Fig. 2 (left)* were taken simultaneously by the cantilever array. The platform was then tested for parallel force spectroscopy on living 3T3 cells in a liquid environment. All force curves of *Fig. 2 (right)* were taken simultaneously.

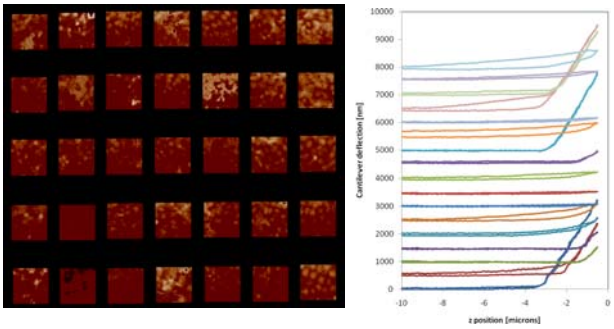

*Fig. 2: Parallel imaging on fixed cells and parallel force spectroscopy on living cells.*

**DISCUSSION & CONCLUSIONS:** One targeted application of the new system is in oncology, especially research into cancer metastasis. Analysis of intracellular adhesion is relevant to the release of metastatic cells from the primary tumor. Studies of mechanical cell stiffness allow to analyze how reagents can affect the softness of the metastatic cells, the softness of metastatic cells being related to their invasive character [2]. These developments aim to open new research possibilities in the field of metastasis, from fundamental cancer research to pharmacology.

**REFERENCES:** [1] G. Weder (2009) *Langmuir*, DOI: 10.1021/la904526u. [2] M. Lekka (1999) *Eur. Biophys. J.* **28**:312-316.

**ACKNOWLEDGEMENTS:** The partial financial support of the European Territorial Cooperation Program INTERREG IV A France-Suisse 2007-2013 in the frame of the project OSCAR, and of the NANOTERA Swiss federal program through the project PATLiSci is gratefully acknowledged.

# Smart pH-responsive Nanocarriers for Nucleic Acid Drug Delivery

A. Felber, B. Castagner, J.-C. Leroux

*Institute of Pharmaceutical Sciences, ETH Zurich, Zurich, Switzerland*

**INTRODUCTION:** The therapeutic value of RNAi-based treatments offers exciting potential, but still faces important issues, mainly i) low stability against enzymatic degradation, ii) lack of tissue or organ specificity, iii) rapid renal clearance, and iv) poor cellular uptake. The objective of our research is the design of polyion complex micelles (PICMs), which could circumvent, at least partly, the aforementioned limitations. The selected approach relies on the combined efficiency of cationic condensing agents with anionic diblock copolymers. We recently reported that poly(ethylene glycol)-*block*-poly(propyl methacrylate-*co*-methacrylic acid) (PEG-*b*-P(PrMA-*co*-MAA)) could interact with poly(amido amine) (PAMAM) dendrimers to form 50-70 nm sized PICMs, and accommodate nucleic acids drug in their inner core (Fig. 1) [1]. These nanocarriers present noteworthy features such as pH-responsiveness and potential targeting abilities. In this work, PICMs bearing antibody fragments on their surface were prepared by a new optimized approach, and silencing of the targeted mRNA was observed upon nanocomplex transfection.

**METHODS:** $PEG_{115}$-*b*-P($PrMA_{21}$-*co*-$MAA_{45}$) was synthesized as previously reported [1]. Fab'-maleimide-$PEG_{169}$-*b*-P($PrMA_{31}$-*co*-$MAA_{62}$) was prepared by conjugating fragmented and freshly reduced anti-transferrin receptor (CD71) antibody (Fab'-SH) to $H_2N$- $PEG_{169}$-*b*-P($PrMA_{31}$-*co*-$MAA_{62}$) *via* a maleimide-NHS linker (Fig. 2A). PEG-copolymer solutions, typically containing 2.5 mol% Fab'-PEG-*b*-P(PrMA-*co*-MAA), and siRNA were mixed with PAMAM G5 at increasing N/(P + COOH) ratios in Tris buffer (10mM, pH 7.4).

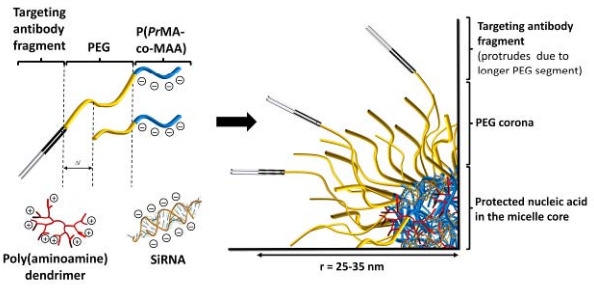


*Fig. 1: Schematic illustration of PICMs formation.*

PICMs size distribution and zeta-potential were determined by dynamic light scattering and laser Doppler anemometry, respectively. Cellular uptake of the PICMs was assessed by flow cytometry. Interference activity of siRNAs loaded nanocarriers was studied at the mRNA and protein level via qPCR and western blot respectively.

**RESULTS:** Reduced Fab'-SH coupling to maleimide-terminated PEG copolymer yielded up to 80% functionalization, and the final product was characterized by gel electrophoresis (Fig. 2B). PICMs bearing anti-CD71 Fab' had a mean hydrodynamic diameter of around 52 nm, a narrow size distribution and a near-neutral zeta potential at an optimal N/(P+COOH) molar ratio of 1.4. Increased cellular uptake was observed for PICMs presenting anti-transferrin receptor *versus* non-specific MOPC21 antibody fragments control. Preliminary studies showed that Bcl-2 mRNA levels 24 h post antiCD71-PICMs transfection was similar to positive control lipofectamine-transfected cells.

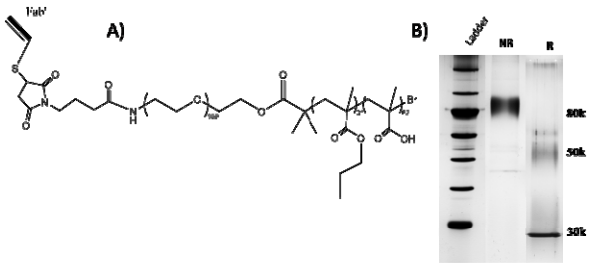


*Fig. 2: (A) Structure of Fab'-PEG-b-P(PrMA-co-MAA). The fab' is linked to the polymer via a stable thioether bond. (B) SDS-PAGE of the copolymer under non-reducing and reducing conditions.*

**DISCUSSION & CONCLUSIONS:** Stable PICMs bearing anti-transferrin receptor antibody fragments were prepared and showed transfection efficacy. The receptor-mediated endocytosis of the nanocomplexes will allow the specific delivery of their nucleic acid cargo. Their small size and PEGylated surface should provide the PICMs an extended biological half-life *in-vivo*.

**REFERENCES:** [1] M. Elsabahy *et al.* (2009) *Adv Func Mater* **19**, 1-6.

**ACKNOWLEDGEMENTS:** This work is financially supported by an ETH Research Grant (ID ETH-0209-3).

# NanoLock Polypeptide for the Permanent Immobilization of Recombinant Proteins on SNAP25 Functionalized Supports

E.Ferrari[1], F.Darios[1], M.Soloviev[2], B.Davletov[1]

[1] *MRC Laboratory of Molecular Biology, Cambridge, UK.* [2] *School of Biological Sciences, Royal Holloway University of London, Egham, UK.*

**INTRODUCTION:** Many techniques in molecular biology, clinical diagnostics and biotechnology rely on binary affinity tags [1]. The existing tags are based on either small molecules or peptide tags. Among these, the biotin-streptavidin system is most popular due to the nearly irreversible interaction of biotin with the tetrameric protein, streptavidin. The major drawback of the stable biotin-streptavidin system, however, is that neither of the two tags can be added to a protein of interest via recombinant means leading to the requirement for chemical coupling. Here we report a new immobilization system which utilizes two monomeric polypeptides which self-assemble to produce non-covalent yet nearly irreversible complex which is stable in strong detergents, chaotropic agents, as well as in acids and alkali.

**METHODS:** Our system is based on the core region of the tetra-helical bundle known as the SNARE (soluble N-ethylmaleimide-sensitive factor attachment protein receptor) complex [2]. We designed a pair of self assembling polypeptides mimicking the neuronal SNARE complex: the first element is represented by the SNAP25 protein and the second is a 17 kDa fusion of syntaxin SNARE motif and synaptobrevin (Fig.1A) which we called NanoLock (NL). To test the capability of the NL to bind SNAP25 and resist harsh treatments we produced: 1) a functional immobilization matrix made by SNAP25 cross-linked to activated BrCN-Sepharose beads, 2) a SNAP25-tagged Biacore chip for Surface Plasmon Resonance (SPR) assays and 3) SNAP25 functionalized gold nanoparticles for Localized SPR (LSPR) experiments.

**RESULTS:** We first show the capability of SNAP25 and NL to self assemble. As shown in the SDS-PAGE gel in Fig. 1B, the SNARE complex, which is known to be SDS resistant, is completely formed after 30' reaction. We then report the permanent immobilization on the SNAP25 sepharose matrix of an enzyme, glutathione-S-transferase (GST), fused to the NL by recombinant means. The enzyme retains activity after its bio-conjugation and cannot be eluted after washing the matrix using harsh conditions (Fig.1C), although the combination of acidic buffer and detergents allows the complete regeneration of the support for further use. The same results are confirmed by

SPR assays where SNAP25 is immobilized on the chip, while the NL flows in the microfluidic chamber. Finally, we show the bio-conjugation of GST fused to NL to gold nanoparticles derivatized with SNAP25. We also report LSPR data suggesting the use of the SNARE tags as a practical platform for nanoparticle-based bio-sensors.

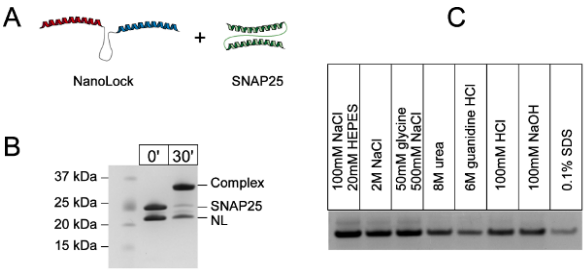


*Fig. 1: (A) A schematic showing the NL and SNAP25; (B) Coomassie stained SDS-PAGE gel showing that NL and SNAP25 assemble into a SDS-resistant complex within 30'. Molecular weights are indicated on the left; (C) Coomassie stained SDS-PAGE gel showing retention of GST-NL on the SNAP25 matrix following washes with the indicated eluants.*

**DISCUSSION & CONCLUSIONS:** The emerging field of nanotechnology increases the demand for tailored conjugation methods for the development of nanochips, bio-sensors, microarrays and nanodevices for drug delivery [3]. Biomaterial and tissue engineering can also benefit from the presented conjugation method for decoration of inert fibrous scaffolds with biologically active molecules. Finally, industrial processes involving immobilized enzymes could require non-covalent yet stable conjugation specifically designed to be resistant to harsh treatments.

**REFERENCES:** [1] K. Terpe (2003) *Appl Microbiol Biotechnol* **60**:523-33. [2] R.B. Sutton, D. Fasshauer, R. Jahn, and A.T. Brunger (1998) *Nature* **395**:347-53. [3] Y. Astier, H. Bayley, S. Howorka (2005) *Curr Opin Chem Biol* **9**:576-84.

European Cells and Materials Vol. 20. Suppl. 3, 2010 (page 81) ISSN 1473-2262

# A Simple Nanoplasmonic Sensor with Microliter Sample Handling

L.Feuz[1], H.Agheli[1], A.Gunnarsson[1], F.Höök[1]

[1] *Department of Applied Physics, Chalmers University of Technology, Gothenburg, Sweden*

**INTRODUCTION:** Liquid handling in biosensing applications is a crucial factor both with respect to sample consumption and sensor design. The possibility to perform experiments with μL sample volumes is of interest when investigating e.g. interaction kinetics of costly antibodies. Simple liquid handling is attractive when developing e.g. point-of-care devices.

We present a simple, label-free biosensor based on nanoplasmonics and capillary flow. Liquid exchange is controlled through a filter paper thereby omitting the integration of pumps and complex microfluidics. Specific biomolecular interactions using μL sample volumes are demonstrated.

**METHODS:** Nanoplasmonic sensing is based on scattering and absorption of light on metallic nanofeatures. This manifests as an extinction peak in the transmission spectrum. The peak position is sensitive to changes in the interfacial refractive index (as it occurs when molecules adsorb on a surface) and can be tracked with high precision (< 0.002 nm) [1].

We use colloidal lithography combined with dry etching to produce short-range ordered gold nanodisks with diameters of 100 nm and heights of 30 nm on a glass slide (Fig. 1a). This structure exhibits an extinction peak around 700 nm and has a bulk sensitivity of 225 nm/refractive index unit.

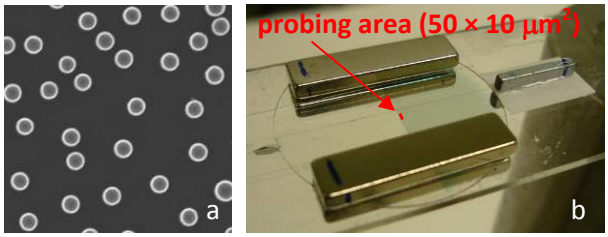


*Fig. 1: a) SEM top view image (2 × 2 μm²) of gold nanodisks with diameters of 100 nm. b) Micro-fluidic cell with nanoplasmonic active area on the right. The filter paper further right draws the droplet on the left into the channel.*

The microfluidic cell consists of an open PDMS channel (800 μm wide, 30 μm high) on a glass slide with the nanoplasmonic substrate clamped with magnets as a cover (Fig. 1b). The channel is filled by means of capillary forces and liquid is exchanged by applying a droplet on one side of the channel and sucking the liquid on the other side

with a filter paper. By drying the filter paper with a stream of nitrogen, constant flows from 0.5 to 10 μL/min can be established.

**RESULTS:** The efficiency in liquid exchange is shown by injecting 5 μL glycerol containing solutions of increasing concentration leading to exchange times below one second (Fig. 2a). Orthogonal (material specific) surface functionalization as shown in a previous study [2] is performed under constant flow conditions (5 μL/min) using a total volume of 50 μL (Fig. 2b). This platform with bioactive areas on the gold disks can be used for specific binding of analytes to the sensitive gold regions only (Fig. 2c).

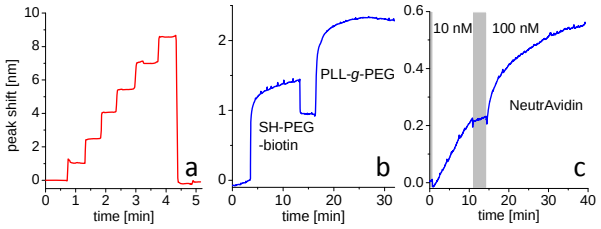


*Fig. 2: a) Sensor response upon 5 μL injections of glycerol solutions with increasing concentration. b) Binding of SH-PEG-biotin on gold, followed by adsorption of PLL-g-PEG on $SiO_2$. c) NeutrAvidin binding to biotin.*

**DISCUSSION & CONCLUSIONS:** The proposed setup provides a simple solution for sensor assembly and minute liquid handling. Magnetic clamping permits the reuse of the substrates. Liquid exchange by virtue of a filter paper allows for operation under stagnant conditions or constant flow. This approach can easily be applied to other types of sensing structures, e.g. nanoplasmonic active flow-through pores [3].

**REFERENCES:** [1] A.B. Dahlin, J.O. Tegenfeldt, F. Höök (2006) *Anal Chem*, **78**:4416-23. [2] L. Feuz, P. Jönsson, M.P. Jonsson, F. Höök (2010) *ACS Nano*, **4**:2167-77. [3] M.P. Jonsson, A.B. Dahlin, L. Feuz, S. Petronis, F. Höök (2010) *Anal Chem*, **82**:2087-94.

**ACKNOWLEDGEMENTS:** This work was supported by the Swedish Foundation for Strategic Research (SSF) funded Ingvar program.

# *In Vitro* Optimization of Injectable Nanovesicles to Treat Drug Overdose

V. Forster, P. Luciani, J.-C. Leroux

*Institute of Pharmaceutical Sciences, ETH Zürich, Zürich, Switzerland.*

**INTRODUCTION:** With an ever growing number of people taking various medications, acute drug intoxications represent a serious public health problem. In 2008, more than 3000 cases of drug intoxications were reported in Switzerland among which almost 5% involved cardiovascular drugs [1]. In particular, calcium channel blockers (CCBs), such as diltiazem (DTZ) or verapamil (VP), may lead to serious morbidity when taken in excess. To this date, no specific treatments or antidotes are available and management of CCBs toxicity remains empirical. To mitigate the adverse effects of over-exposure to these drugs, we propose to design a detoxifying system consisting of nanovesicles that can extract CBBs from organs and relocate them into the bloodstream. Based on the ion trapping capacity of transmembrane pH-gradient liposomes, DTZ and VP can be encapsulated with high efficiencies [2]. In this research, we have studied *in vitro* the properties influencing drug uptake kinetics and have developed an optimized detoxifying agent for both model CBBs, DTZ and VP.

**METHODS:** Liposomes composed of egg phosphatidylcholine, cholesterol (CHOL), dipalmitoyl phosphatidylcholine (DPPC), and 5 mol% of 1,2-distearoyl-*sn*-glycero-3-phospho-ethanolamine-*N*-[carbonyl(methoxypoly-ethylene glycol)$_{2000}$] (P) were prepared by the film-hydration/extrusion method. Their diameter was comprised between 120 and 160 nm to allow a long biological half-life *in vivo*. The lipids were hydrated with citrate buffers of different pHs and molarity. The pH-gradient was established by size-exclusion chromatography columns using Sephadex G-25 equilibrated and eluted with isotonic HEPES buffered saline (HBS) at pH 7.4. The final phospholipid concentration was determined by a phosphate colorimetric assay. Drug uptake kinetics were measured with horizontal diffusion cells in HBS in the presence or absence of 50% (*v/v*) fetal bovine serum (FBS). DTZ and VP were extracted from FBS with solid-phase extraction columns, and the drugs concentrations were then assessed by high-performance liquid chromatography.

**RESULTS:** Liposome membrane composition greatly influenced uptake capacity. Vesicles made from DPPC with 45 mol% CHOL (D50:C45:P5) exhibited the optimal DTZ capture capacity. The internal buffer had a strong impact on DTZ uptake (Fig. 1). Citrate buffer 250 mM pH 3 proved to be the optimal inner medium: the uptake was the highest and the drug remained stably encapsulated for up to 8 h. The uptake of VP was found to be superior to that of DTZ in the buffer (data not shown) (due to higher $pK_a$), but inferior in 50% FBS (higher biding to serum proteins) (Fig. 2) [3].

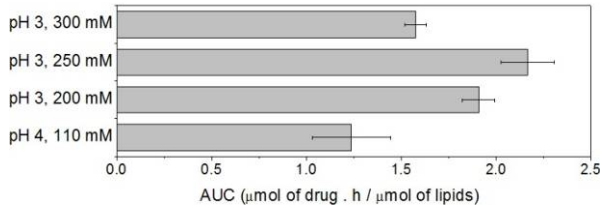


*Fig. 1: Capture capacity of D50:C45:P5 liposomes in 50% FBS. Inner buffers specifications are shown on the left hand-side. The areas under the curve (AUCs) represent integrations of the uptake curves during the first 8 h.*

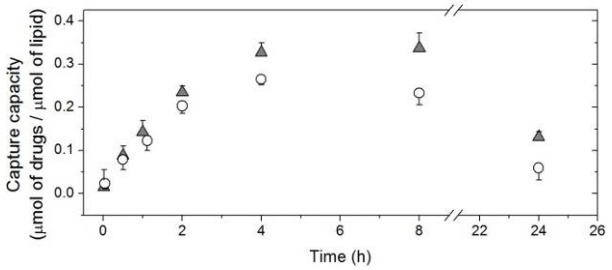


*Fig.2: Capture capacity in 50% FBS of D50:C45:P5 liposomes for DTZ (▲) and VP (○).*

**DISCUSSION & CONCLUSIONS:** With a DTZ and VP capture lasting stably over 8 h, the present work demonstrates the potential of transmembrane pH-gradient liposomes as nanovectors for biodetoxification. Moreover, these novel vesicles should be viewed as a versatile model for prevention and/or treatment of a wide range of drug intoxications and other hazardous chemicals, such as pesticides or chemical weapons.

**REFERENCES:** [1]Swiss Toxicological Informa-tion Centre (2009) *Anhang zum Jahresbericht 2008* pp 2-5. [2]J.-C. Leroux (2007) Injectable nanocarriers for biodetoxification *Nat. Nanotechnol* **2**:679-684. [3]P.D. Henry (1980) Comparative pharmacology of calcium antagonists: Nifedipine, verapamil and diltiazem *Am J Cardiol* **46**: 1047-1058.

**ACKNOWLEDGEMENTS:** This work was financially supported by the Swiss National Science Foundation (ID 31003A_124882).

# Uptake of gold nanoparticles of different sizes, shapes and coatings in human endothelial cells

C.Freese1, R. E. Unger1, C. J.. Kirkpatrick1, M.I. Gibson2, H.-A. Klok2

[1] *Institute of Pathology, REPAIR Lab, University medical centre Mainz, Johannes-Gutenberg University, Mainz, Germany.* [2] *EPF Lausanne, Lausanne, Switzerland.*

**INTRODUCTION:** A big challenge for all biomedical applications with nanoparticles (NPs) to specific targeting organs (especially the brain) is to cross the biological barriers built by endothelial cells. For the treatment of diseases using NPs it is therefore very important to synthesize NPs which overcome this barrier and get into the cells of interest. Gold nanoparticles (Au-NPs) are being developed for many applications in human such as diagnostic purposes (e.g. labeling[1]). Since NPs have to be internalized and transcytosed by endothelial cells we have analyzed the uptake behavior and the fate of the Au-NPs which differ in sizes, shapes and coatings, in endothelial cells (primary human dermal and brain microvascular endothelial cells) by fluorescence, light and transmission electron microscopy and quantified the uptake of specific Au-NPs by spectroscopy (ICP-AES).

**METHODS:** Different human microvascular endothelial cells were incubated with nanoparticles for 4h and 24h. To visualize the uptake of internalized Au-NPs we examined the NP-exposed cells by light and fluorescence microscopy after antibody staining of the endothelial membrane marker PECAM. The confirmation of the uptake was done by transmission electron microscopy. To quantify the amount of internalized Au-NPs we used inductively coupled photon and atomic emission spectroscopy (ICP-AES).

**RESULTS:** The well characterized Au-NPs have no influence on cell viability (MTS-test), cell morphology and cell toxicity (LDH-test). We are able to detect the internalized Au-NPs by light microscopy and can visualize the cell borders by antibody staining at the same time (Fig.1). Therefore, we can demonstrate differences in the amount of internalized NPs which differ in shape, size and coating. Additionally, we can detect different uptake behavior of Au-NPs in dermal and brain endothelial cells. Most of the NPs are stored in the perinuclear region even after 4h of NP-

treatment. Transmission electron microscopy confirms the results of light/fluorescence microscopy. The quantification of the amount of internalized Au-NPs by spectroscopy (ICP-AES) confirms the observation by the microscopic techniques.

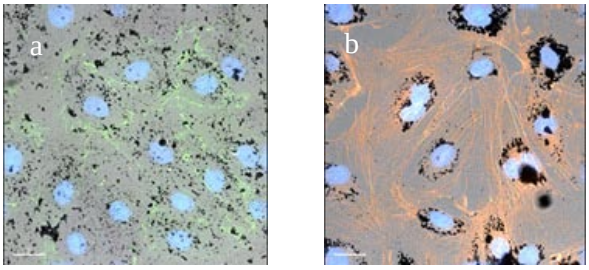


*Fig. 1: Fluorescent images of gold nanoparticles in HDMEC cells showing broad distribution in cells (a, nuclei blue, gold nanoparticles black) or localized and concentrated near nuclei (b).*

**DISCUSSION & CONCLUSIONS:**

These results may lead to the conclusion that different Au-NPs are internalized in differing amounts depending on size, shape and coating. These observations are interesting for creating new applications for drug and gene delivery strategies with Au-NPs. Further studies may reveal if the nanoparticles can cross the endothelial barrier via transcytosis and if there are differences of the transcytosis in the different cell types.

**REFERENCES:** [1] R. A. Sperling et al (2008) *Chem. Soc. Rev*, **37,** pp. 1896-1908, Biological applications of gold nanoparticles.

**ACKNOWLEDGEMENTS:** This study has been funded by European Commission (NanoBioPharmaceutics and CellNanoTox projects). The authors acknowledge the team of Dr. Christoph Brochhausen (J.-G. University, Mainz, Germany) for technical assistance in the TEM analysis.

# Responsive insulin-loaded polymeric nanoparticles interacting with model lipid membranes

R.Frost[1], G. Coué[2], J.F.J. Engbersen[2], B. Kasemo[1] and S. Svedhem[1]

*[1] Chalmers University of Technology, Göteborg, Sweden. [2] University of Twente, Enschede, The Netherlands.*

**INTRODUCTION:** As an increasing number of drugs are administered using nano-sized drug carriers, there is an emerging need for tools to evaluate and optimize the properties of these assemblies. Our approach to this field is the study of nanodrug interactions with model lipid membranes, using a platform based on surface sensitive techniques.[1] Here, we report on the study of the interaction between pH-responsive insulin-loaded nanoparticles and supported lipid bilayers of different charge. The studied nanoparticle is a spontaneously assembled complex between a polymer and human insulin. The nanoparticle has been developed for alternative delivery of human insulin. The quartz crystal microbalance with dissipation monitoring (QCM-D) technique allows for real-time monitoring of these interactions through the detection of the amount of mass adsorbed to the surface, together with its viscoelastic properties, and thus structural arrangement. The result is supported by complementary AFM data. Furthermore, the dissolution of the nanoparticles, by addition of a reducing agent, has been monitored.

**METHODS:** Nanoparticle characterization was performed by dynamic and electrophoretic light scattering measurements using a Zetasizer Nano (Malvern Instruments Ltd, UK). The model lipid membranes were prepared by liposome rupture and subsequent fusion on a $SiO_2$-coated QCM-D sensor surface.[2] Two different lipid compositions were used, POPC and POPC:POPS (3:1). QCM-D real time interaction studies were performed in flow mode using an E4 instrument (Q-Sense, Sweden).

**RESULTS:** The positively charged insulin-loaded nanoparticles (d = 160 nm) adsorb to both the plain POPC and to the more negatively charged POPC:POPS (3:1) model membrane. However, the relationship between the adsorbed mass ($\Delta f$) and its viscoelasticity ($\Delta D$) differs significantly between the two membranes (Figure 1). The adsorbed nanoparticles form a more rigid structure (low $\Delta D$) on the more negatively charged POPC:POPS (3:1) membrane than on the POPC membrane.

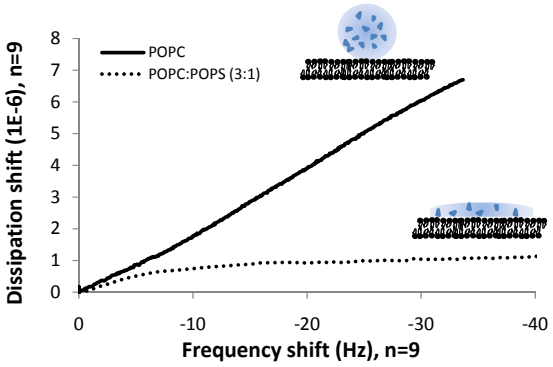


*Fig. 1: Dissipation shift vs. Frequency shift for the adsorption of insulin-loaded polymeric nanoparticles on two different model membranes.*

**DISCUSSION & CONCLUSIONS:** The presented results show that the nanoparticles collapse upon adsorption to a POPC:POPS (3:1) membrane. Possibly, structural rearrangements also occur, although to a lesser extent, when the nanoparticles adsorb to a POPC membrane. The collapse of the nanoparticles could be associated with the release of insulin. One advantage of the real-time monitoring is that effects of the nanoassemblies caused by changes the environmental conditions (*e.g.* pH or temperature) can be studied. The nanoparticle in this study was designed to disintegrate when exposed to a reducing agent, a property that has been clearly demonstrated in our system.

**REFERENCES:** [1]R. Frost, C. Grandfils, B. Cerda, B. Kasemo and S. Svedhem, *Real-time interactions between polymeric insulin-loaded nanoparticles and surface-supported lipid bilayers*, submitted to Langmuir. [2]Keller, C. A.; Kasemo, B., *Surface specific kinetics of lipid vesicle adsorption measured with a quartz crystal microbalance.* Biophysical Journal **1998,** 75, (3), 1397-1402.

**ACKNOWLEDGEMENTS:** Financial support from the EU FP6 IP NanoBioPharmaceutics is gratefully acknowledged. Novo Nordisk is acknowledged for supplying human insulin.

European Cells and Materials Vol. 20. Suppl. 3, 2010 (page 85) ISSN 1473-2262

# Cross-linking Polymers For Nanocrystal Stabilization

K. Fuhrmann, M. A. Gauthier, and J.-C. Leroux

*Institute of Pharmaceutical Sciences, Department of Chemistry and Applied Biosciences, ETH Zurich, Zurich, Switzerland*

**INTRODUCTION:** Nanosizing drugs is a useful method for the formulation of hydrophobic drugs. However, size reduction often results in unwanted aggregation and/or uncontrolled dissolution. Herein, we present functional copolymers bearing either alkynyl or azido groups which may prevent aggregation and alter the circulation time of drug nanocrystals by "click-chemistry"-mediated cross-linking. We show monomer and polymer synthesis and 1,3-dipolar cycloaddition of the polymers in solution and on the surface of nanocrystals.

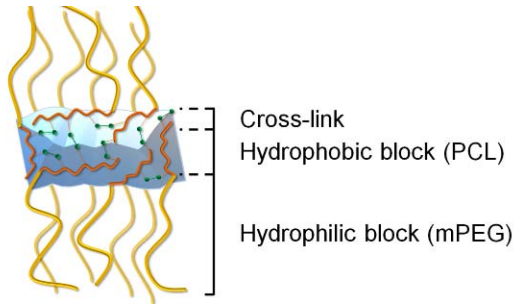


*Scheme 1: Drug nanocrystal (blue) stabilized by cross-linked polymer.*

**METHODS:** Functional monomers (**1** and **2**, Scheme 1) were synthesized as described elsewhere[1,2]. Copolymerization of the functional monomers with ε-caprolactone (CL) from ω-methoxy poly(ethylene glycol) (mPEG) was achieved via cationic ring-opening polymerization (CROP) catalyzed by HCl[3].

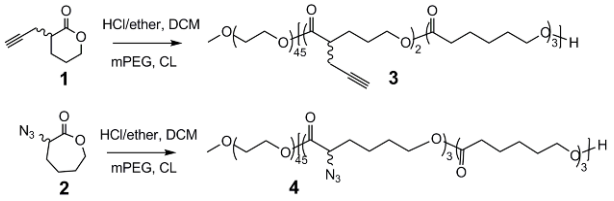


*Scheme 2: Synthesized monomers: α-propargyl-δ-valerolactone (**1**), α-azido-CL (**2**), and corresponding copolymers with CL (**3** and **4**).*

Wet milling was performed in a cylindrical glass vessel containing an aqueous suspension of the dissolved polymer (**3**:**4**, 1:1 *w/w*) and solid drug (polymer:drug, 1:2 *w/w*) with 0.3-mm zirconium oxide beads. The vessel was placed on a roller mill and rotated at 220 rpm for 18 h. After milling and removal of milling beads, polymer-stabilized drug nanoparticles were separated from free polymer by size-exclusion chromatography (SEC). Catalyst ($CuSO_4$ / ascorbic acid) was added to this colloidal dispersion and agitated for 10 min at room temperature. The cross-linking reaction was stopped by catalyst removal through SEC. DLS and FTIR spectroscopy were used to evaluate the outcome of this reaction.

**RESULTS:** Functional polymers with low polydispersity (1.1 – 1.2) were obtained according to Scheme 2. These polymers displayed characteristic peaks for the alkynyl and azido groups in their FTIR spectra (Figure 1). Particle sizes of about 120 nm were prepared by the wet milling process. Cross-linking was confirmed qualitatively by the disappearance of the alkynyl groups (strong ≡C–H stretch at 3270 $cm^{-1}$) in the presence of excess azide (2100 $cm^{-1}$) as observed by FTIR spectroscopy.

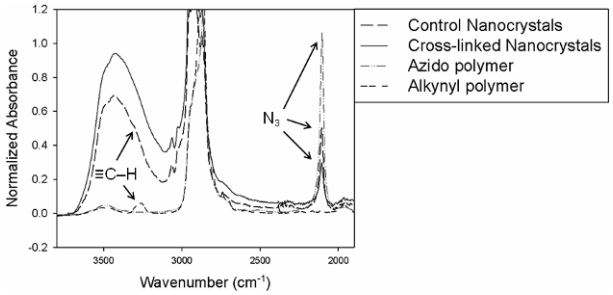


*Figure 1: FTIR spectra of nanocrystals and controls.*

**DISCUSSION & CONCLUSIONS:** In this work, functional copolymers were successfully prepared by transition-metal free CROP. The polymers maintained their functional groups following wet milling with paclitaxel and reacted succesfully in the presence of nanocrystals. This may serve as a powerful tool to control dissolution rate and thereby circulation time in the body. In future work we will test this and also append a targeting moiety such as an antibody (or fragment thereof) to improve cellular uptake following passive accumulation in tumoral tissues.

**REFERENCES:** [1] Parrish B, Breitenkamp RB, Emrick T (2005) *J Am Chem Soc,* **127**:7404-10. [2] Lenoir S, Riva R, Lou X, et al. (2004) *Macromolecules,* **37**:4055-61. [3] Kim MS, Seo KS, Khang G, et al. (2005) *Macromol Rapid Commun,* **26**:643-48.

# molecular-NANOintegrated surface for selective protein recognition by molecular imprinting concept

Kyoko Fukazawa[1], Qiang Li[5], Stefan Seeger[5], Kazuhiko Ishihara[1,2,3,4]

[1]*Department of Materials Engineering,* [2] *Department of Bioengineering*
[3] *Center for Medical System Innovation, The University of Tokyo, Tokyo, Japan.*

[4] *Core Research for Evolutional Science and Technology, JST, Tokyo, Japan.*
[5]*Institute of Physical Chemistry, University of Zurich, Zurich, Switzerland*

**INTRODUCTION:** The selective recognition and detection of proteins are highly desirable in the fields of bioscience and bioengineering. In this study, we tried to construct the specific recognition sites of proteins by a new molecular imprinting method based on molecular nanointegration (Fig.1). To achieve the selective recognition of target proteins, it is necessary to suppress the nonspecific adsorption of them to the non-recognition sites. Therefore we used the phospholipid polymer including 2-methacryloyloxyethyl phosphorylcholine (MPC) unit which is well known to suppress the nonspecific absorption of proteins as a matrix [1]. The recognition sites were constructed by integrating a surfactant as the ligand and immobilized it with new biocompatible photoreactive phospholipid polymer (PMPAz) (Fig. 2). First, we selected the cell-adhesive protein fibronectin (FN) as the imprinting protein for preparing templates and evaluated selective cell adhesion on the FN imprinting substrate. Furthermore, the recognition sites were confirmed by deep-UV laser-based fluorescence lifetime imaging microscopy directly [2].

**METHODS:**. The FN imprinting substrate, the non-imprinting substrate and the BSA imprinting substrate were placed in the 24-well plate. The fibroblast cells (L929) were cultured in Dulbecco's modified eagle medium (DMEM) containing 10% fetal bovine serum (FBS) at 37 °C. After 24 hours, DMEM was aspirated, and the plate was rinsed the PBS. The number and shape of the L929 cells were observed using a phase contrast microscope, and the amount of rebound FN from DMEM were evaluated by ELISA. On the other

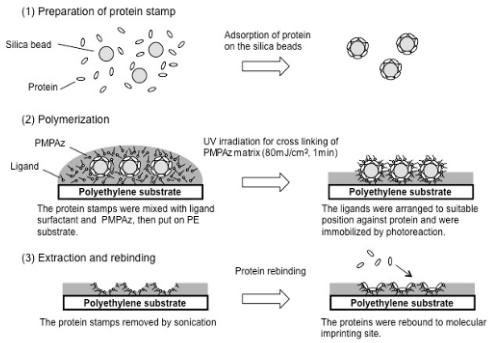


*Fig. 1. Preparation for molecular nano-integration for selective protein recognition*

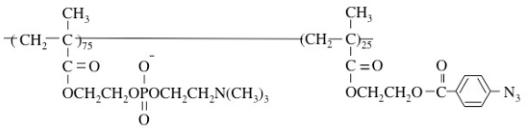

*Fig. 2. Chemical structure of PMPAz*

hand, the quartz glass slides were pretreated with buthyltrichlorosilane and the BSA was imprinted for the deep-UV laser-based fluorescence lifetime imaging microscopy.

**RESULTS AND DISCUSSION:** On the FN imprinting substrate, the cells adhered only in the place where the FN was imprinted. However, on the non-imprinting substrate and the BSA imprinting substrate, the cells did not adhere at all.

The cell adhesion on the surface occurs after adsorption of cell-adhesion protein, FN. On the FN imprinting substrate, the FN in the cell culture medium was adsorbed on the surface selectively, and cell adhesion was induced. On the other hand, on the non-imprinting substrate and the BSA substrate, the protein adsorption from cell culture medium was prevented completely. These results indicate that the FN binding sites were well constructed by arranging the ligand surfactant to a suitable position and immobilized by the photoreactive MPC polymer. And the MPC polymer prevented the nonspecific adsorption of proteins from the cell culture medium. The amount of rebound protein on the surface is few. Furthermore, it was confirmed that the BSA was rebound only in the place where the BSA was imprinted by deep-UV laser-based fluorescence lifetime imaging microscopy directly. We concluded that this procedure can apply to various substrates and biomolecules, and lead to a highly convenient analytical method of biomolecules.

**REFERENCES:** [1] K. Ishihara, et al. (1999) *J.Biomater.Sci.*, **10**(10):1047-1061. [2] K. Fukazawa, et al. (2009) *Biosens. Bioelectron.*,**25**:609-614. [3] Q. Li, et al. (2004) *J. Phys. Chem. B*, **108**:8324-8329.

# Controlling the loading number and orientation of Immunoglobin G on gold nanoparticles and the induced formation of nano-assemblies

L.García-Fernández[1], R.Sperling[1], J. Arbiol[2], V. Puntes[1]

[1] *Institut Català de Nanotecnologia, ICN, Barcelona, Spain.* [2]*ICREA and Institut de Ciència de Materials de Barcelona, CSIC, Barcelona, Spain.*

**INTRODUCTION:** The ability to create physicochemically well-defined gold nanoparticle-antibody conjugates is important to facilitate their advanced application in biology and medicine [1]. With this aim, we have developed an optimal bioconjugation methodology to achieve the control of the number of antibodies and their orientation on gold nanoparticles (NPs) which, in turn, enables a maximum functional availability of the antibody for targeting. The control of both, the number of antibodies and their orientation, have been demonstrated by the design of architectures created by molecular recognition events between the antibody-functionalized NPs.

**METHODS:** The directional and covalent linkage between antibodies and the NPs surface was achieved by first synthesizing thiol-derivatized antibodies [2,3] with subsequent addition to the "bare" NPs. The methodology of conjugation was consisted on the periodate-oxidation of the carbohydrate on the Fc portion of the antibody to form an aldehyde, which was immediately reacted with a heterobifunctional linker containing hydrazide and thiol-end groups. The aldehyde and hydrazide groups reacted spontaneously to form a hydrazone bond, which was further stabilized by cyanoborohydride reduction. The binding process of the linker-antibody complex and gold NPs was monitored by DLS and UV-visible spectroscopy techniques. This enabled to form conjugates with different controlled amount of antibodies (Au 16 nm-anti-rabbit IgG produced in goat). The loading of these conjugates was confirmed by mixing the NPs together with the anti-antibody-loaded NPs (Au 9 nm-anti-BSA IgG produced in rabbit) at controlled composition and different ratios, resulting in different groupings of particles with a desired connectivity.

**RESULTS:** According to DLS measurements, the average diameter of gold NPs increased gradually after systematic additions of linker-modified antibodies until it reached a maximum value which corresponds to a maximum loading. A maximum particle size increase of ~ 18 nm in diameter (volume-average) was observed for different sized-NPs, however non-covalent and non-oriented attachment of antibodies showed an increase in

NPs diameter up to 100 nm, leading in most cases to aggregation. Surface Plasmon Resonance (SPR) of the conjugates exhibited a characteristic red shifted plasmon peak during thiol-gold bond until it reached a constant value of ~ 8 nm at the saturation point that matched the DLS maximum diameter. Control of the loading of antibodies and their orientation made the targeting of structures possible by mixing different ratios of nano-conjugates with controlled composition (*Fig.1*).

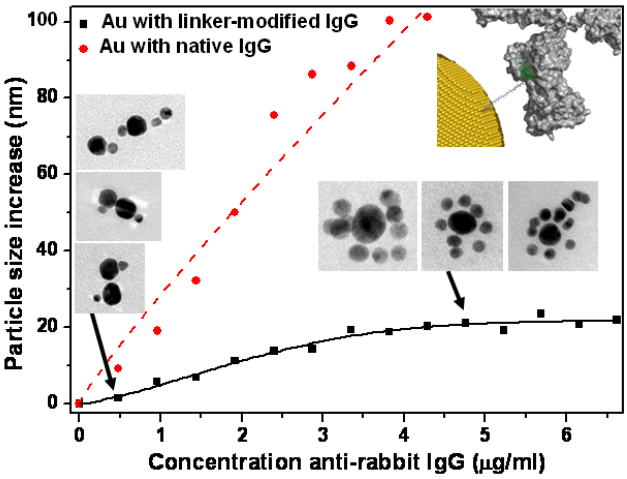


*Fig. 1: Binding study of the native vs the linker-modified anti-rabbit IgG with gold NPs (16 nm) at increasing antibody concentration. TEM images of the nano-assemblies formed by 9- and 16-nm-sized NPs loaded with controlled amounts of anti-BSA and anti-rabbit IgG molecules, respectively.*

**DISCUSSION & CONCLUSIONS:** The loading of antibodies and their orientation on gold NPs can be conveniently monitored by DLS and UV-Visible spectroscopy. Indeed, self-assembly of inorganic NPs using the specific recognition properties of surface-attached antibodies proved the control on number and orientation of the conjugated antibodies.

**REFERENCES:** [1] P. Alivisatos (2004) Nat Biotechnol **22**:47-52. [2] G. T. Hermanson (2008) *Bioconjugate Techniques*, Elsevier Inc. [3] S. Kumar, N. Harrison, R. Richards-Kortum (2007) Nano Lett **7**: 1338-1343.

# Force and function: Probing proteins with single molecule force spectroscopy

Hermann E. Gaub

*University of Munich and Center for Nanoscience, Amalienstr. 54, 80799 Munich, Germany*

Forces play a pivotal role in life, and the response of live systems to forces requires molecules and molecular interactions with adequate properties to counteract both in a passive but also, if needed, in an active, dynamic manner. However at the level of individual molecules these forces are so minute, that the development of sophisticated experiments to measure and control them was required. With the maturation of these techniques, particularly the AFM-based single molecule force spectroscopy into commercial instruments, the scope has widened considerably and more and more studies shed light onto the different aspects of biomolecular mechanics. This talk will highlight recent advances in elucidating the force-sensing mechanisms of Titin Kinase and the mechanical activation of the lipase CalB. It will also report recent advancements in the development of a DNA-based parallel format force assays for the label-free detection of binding forces in biomolecular complexes.

European Cells and Materials Vol. 20. Suppl. 3, 2010 (page 89) ISSN 1473-2262

# Novel nanostructured drug delivery technology to enhance bioavailability, increase solubility and drug loading

G. Heltovics, Zs. Ötvös, G. Filipcsei, F. Darvas
*Nangenex Inc, H-1031 Budapest, Záhony u. 7., Hungary*

**INTRODUCTION:** Nanotechnology provides new innovative solutions for original as well as generic applications in a wide variety of industries including pharmaceuticals, agrochemicals, cosmetics, foods, nutraceuticals and home care[1-3]. Nanoformulation is the reduction of particles size down to below 200 nm. The reduction of particles size leads to significantly increased solubility, bioavailability as well as reduced food and side effects of active pharmaceutical ingredients (API).

Poorly soluble drugs generally have low solubility as well as low dissolution velocity and exhibit a small concentration gradient across the intestinal mucosa, which can result in low, variable absorption and a poor therapeutic response. Not only the solubility but also the rate of drug dissolution are primary driving forces behind improved pharmacokinetic properties the drugs. Novel proprietary nanostructured drug formulations produced by continuous flow nano precipitation technology will be presented.

**METHODS:** Novel bottom-up nanoparticle drug delivery technology that relies on controlled nano precipitation was used for the preparation of unique nanostructured drug delivery systems. The properties of the produced nanostructured particles could be modified during the process by the precise control and optimization of various reaction parameters (e.g. temperature, flow rate, pH and concentration).

**RESULTS:** Comparative solubility ($C_{max}$) and in vitro artificial skin permeability tests of nanosized cGMP specific phosphodiesterase type 5 inhibitor (cGMP5) versus the reference API were performed. The solubility of nanosized cGMP5 was 6.8 times higher than the reference in distillate water. In in vitro experiments, the penetrated amount of nanostructured cGMP5 on artificial skin was 390 % higher compared to the reference after 30 minutes of administration.

The in vivo pharmacokinetic benefit of a nanostructured angiotensin receptor blocker (ARB) over the parent active molecules was also investigated. The reduction in particle size below 200 nm led to 100s fold higher solubility and $10^{3-4}$ fold increased drug concentration in a stable colloid solution by instantaneous redispersibility of nanosized drug.
The bioavailability of reference and nanostructured ARB was determined after oral administration (30 mg/kg) in fasted state in Sprague-Dawley rats.

Nanosized ARB had an $AUC_{15\text{-}360\ min}$ value of 6412 μg·min/ml while this value after reference treatment was 940.1 μg·min/ml. The ratio of the two AUC values ($AUC_{15\text{-}360\ min\ (nanosized)}$ / $AUC_{15\text{-}360\ min\ (reference)}$) was 6.82.

In vivo comparative pharmacokinetic tests of nanosized ARB versus reference marketed drug was also performed, the bioavailability was determined after oral administration of 30 mg/kg active ingredient in physiological saline solution at pH=5 in Sprague-Dawley rats under fed condition using international standard protocols. Nanosized ARB had an $AUC_{15\text{-}360\ min}$ value of 2744 □g·min/ml while this value after reference treatment was 1242 □g·min/ml. The ratio of the two AUC values ($AUC_{15\text{-}360\ min(nanosized)}$ / $AUC_{15\text{-}360\ min\ (reference)}$) was 2.21.

**DISCUSSION & CONCLUSIONS:** The significant benefit that can be achieved by the unique nanostructured particle formation will be applicable for many other established drugs with limited solubility to transform them into instantaneously redispersable form with increased solubility. Moreover, the novel nanoparticle drug delivery technology enables us to design and produce nanostrucured pharmaceutical macromolecules (e.g; polypeptides, polynucleotides) and highly stable nanostructured particles for prolonged release to extend the half life of the drugs.

**References:**

[1] S. Katteboinaa, V.S.R Chandrasekhar, S. Balaji, *International Journal of PharmTech Research* **1**(3), 682, 2009.

[2] J-U.A.H. Junghanns, R.H. Müller, *International Journal of Nanomedicine* **3**(3) 295–309, 2008.

[3] Christoph Schmidt, Alf Lamprecht, Nanocarriers in drug delivery-design, manufacture and physicochemical properties, chapter 1, Nanotherapeutics Drug Delivery Concepts in Nanoscience, Pan Stanford Publishing, 2009.

European Cells and Materials Vol. 20. Suppl. 3, 2010 (page 90) ISSN 1473-2262

# Monitoring Vessel Formation of Endothelial Cells on Micropatterned Biochips

A. Giese[1], C.Padeste[2], K. Ballmer-Hofer[1]

*[1] Molecular Cell Biology, Paul Scherrer Institut, Villigen-PSI, Switzerland. [2] Laboratory for Micro- and Nanotechnology, Paul Scherrer Institut, Villigen-PSI, Switzerland.*

**INTRODUCTION:** Vascular Endothelial Growth Factors (VEGFs) constitute a family of proteins that regulate blood and lymphatic vessel development and homeostasis. In normal, healthy organisms vessel development is tightly regulated to maintain adequate blood supply and lymph drainage. Vessels are aberrantly stimulated in various diseases such as during tumor growth, in atherosclerosis, retinopathies and in lymphoproliferative or rheumatoid disease [1]. We are investigating the mechanisms responsible for vessel formation by VEGF family ligands in vitro using endothelial cells grown on micropatterned substrates. Patterned substrates are generated to mimic the extracellular milieu, in particular the extracellular matrix (ECM), of the cells.

**METHODS:**

**Protein Immobilization:** The 'Molecular Assembly Patterning by Lift-Off (MAPL) technology' developed at ETH Zürich [2] was adapted to the immobilization of VEGF. We use the natural affinity of VEGF-$A_{165}$ to heparin for indirect coupling. For this, we incubated commercially available heparin-biotin with neutravidin and bound the complex to the PLL-g-PEG biotin pattern. Further, VEGF-$A_{165}$ was immobilized via the heparin and visualized with an anti-VEGF antibody.

**Cell assay:** Porcine Aortic Endothelial (PAE) cells expressing the Vascular Endothelial Growth Factor Receptor 2 (VEGFR-2) were grown on VEGF patterns. Cells were fixed and immunostained with an anti-VEGFR-2 antibody.

**RESULTS:** In our study, we successfully immobilized VEGF-$A_{165}$ on patterned glass coverslips. Visualization with an anti-VEGF antibody showed the expected pattern (Fig. 1). Furthermore, we demonstrated that PAE cells are able to migrate and divide on the generated micropatterns (Fig.2).

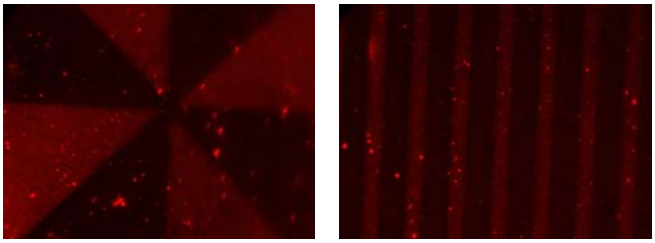

*Fig. 1: VEGF-$A_{165}$ detection on PLL-g-PEG biotin patterns.*

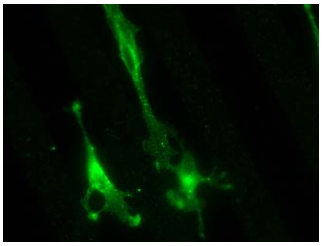

*Fig. 2: PAE-VEGFR-2 cells on VEGF-patterned coverslips, stained with anti-VEGFR-2 antibody.*

**DISCUSSION & CONCLUSIONS:** The purpose of this study was to establish a technology mimicking the extracellular milieu of endothelial cells. We were able to grow PAE cells on the heparin/VEGF-$A_{165}$ coated glass support. In a next step, we will culture pluripotent mouse stem cells and primary endothelial cells derived from human tissues as embryoid bodies [3] on our patterned substrates. Various isoforms of VEGF will be added as either soluble or matrix-bound material on the surface of glass coverslips. Further, we will monitor sprouting angiogenesis and vessel formation by live cell video microscopy and histologically after fixation.

**REFERENCES:** [1] N. Ferrara (2001) *Am. J. Physiol Cell Physiol 280, C1358-C1366.* [2] D. Falconnet, A. Koenig, F. Assi, M. Textor (2004) *Adv. Funct. Mat.* **14**, 749-756. [3] L. Jakobsson, J. Kreuger, L. Claesson-Welsh (2007) *J Cell Biol.* **177**(5):751.

**ACKNOWLEDGEMENTS:** This work is funded by Swiss National Science Foundation (SNSF).

# PEG-bisphosphonate-stabilized calcium phosphate nanoparticles for gene delivery

E.V.Giger, R. Schlatter, B.Castagner, J.-C.Leroux

*Institute of Pharmaceutical Sciences, Department of Chemistry and Applied Biosciences, Swiss Federal Institute of Technology (ETH) Zurich, Switzerland*

**INTRODUCTION:** Gene therapy offers a tremendous potential but its successful use has been hampered so far by the lack of sustained gene expression and major delivery challenges.[1]

Calcium phosphate-DNA co-precipitates have been used for more than 35 years for the *in vitro* delivery of nucleic acids.[2] A drawback of this procedure is the instability of the particles, which creates reproducibility problems and prevents *in vivo* administration.

We present here a new system of delivering nucleic acids using DNA-loaded calcium phosphate nanoparticles stabilized with PEG-bisphosphonate (Fig. 1).

Bisphosphonates are used in the clinic to treat osteoporosis due to their affinity for bone hydroxyapatite (a form of calcium phosphate).

**METHODS:** Green fluorescent protein DNA (6.6 µg/mL) and calcium chloride (250 mM) were added to HEPES buffer containing 1.5 mM phosphate. PEG-bisphosphonate was added immediately afterwards. Particle size was measured over time by dynamic light scattering. HeLa cells were used for transfection. Twenty four hours after seeding, nanoparticles were added to the cells and incubated for 48 h in the presence of 10% serum. Transfection efficiency was determined by flow cytometry.

**RESULTS:** The size of DNA-loaded calcium phosphate nanoparticles prepared with 10 and 25 µM PEG-bisphosphonate was around 220 nm. Nanoparticles stabilized by 25 µM PEG-bisphosphonate stayed stable 48 h after preparation while the ones decorated with 10 µM PEG-bisphosphonate increased in size by ~100 nm. Figure 2 shows that the nanoparticles could transfect 60% of HeLa cells. Calcium phosphate co-precipitate (CP-control) transfected around 40% of the cells when added to the cells directly after preparation. When nanoparticles were incubated for 48 h at room temperature, transfection efficiency of calcium phosphate-DNA co-precipitate decreased to less than 5% while the one of the stabilized nanoparticles remained constant at around 60%.

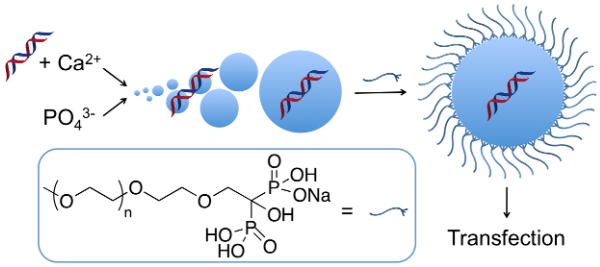


*Fig. 1: Preparation of stabilized calcium phosphate nanoparticles.*

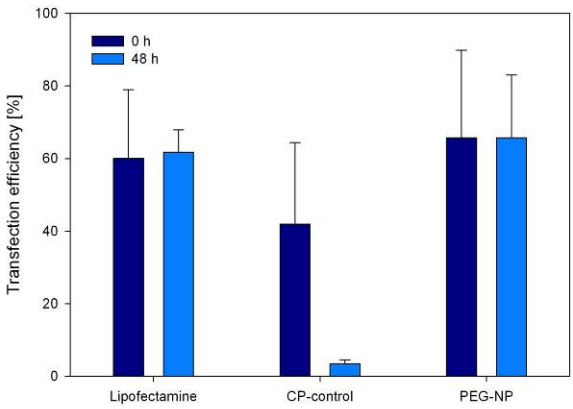


*Fig. 2: Transfection efficiencies directly and 48 h after preparation and lipofectamine control. Mean ± SD, n=3-5.*

**DISCUSSION & CONCLUSIONS:** We showed that calcium phosphate nanoparticles could be stabilized by a PEG-bisphosphonate coating. The nanoparticles were stable for at least 48 h. Transfection efficiencies were similar to CP-control when added to the cells directly after preparation and remained constant after 48 h confirming the stability of the new system.

These nanoparticles are bioresorbable, biocompatible and could eventually be used *in vivo*. The addition of a targeting ligand will be investigated in the future.

**REFERENCES:** [1] Glover, D.J; Lipps, H.J.; Jans, D.A. *Nat Rev Genet* 2005, **6**, 299-310. [2]Graham, F.L.; Van der Erb, A.J. *Virology* 1973, **52**, 456-467.

European Cells and Materials Vol. 20. Suppl. 3, 2010 (page 92) ISSN 1473-2262

# Force spectroscopy study of a nano-patterned organothiol surface fabricated by colloidal lithography

G.Giudetti[1], P.Lisboa[1], L.Sirghi[2], H.Rauscher[1], P.Colpo[1], F.Rossi[1]

[1] *JRC-European Commission, IHCP, NBS, TP203, Via E. Fermi, 2749, 21027 Ispra (VA,) Italy*
[2]*Alexandru Ioan Cuza University , Department of Physics, bd. Carl I, 11, Iasi 700506, Romania*

**INTRODUCTION:** The main challenge to improve the detection performance of label free biosensors consists in the development of advanced bio interfaces that guarantee efficient immobilization of the bio probes on the transducer surfaces. The use of nano-patterned transducer surfaces[1] has lead to an improvement in biorecognition thanks to a better availability of the binding sites and to special physicochemical properties of the nano-patterns[2]. The goal of this work is to study the interaction of the proteins with nanostructures by atomic force spectroscopy to gain information on the mechanism of interactions. The nano-patterned surfaces are produced by colloidal lithography, and are based on organothiols with carboxylic and polyethylene oxide terminations. The study aims at a better characterization of the forces governing the observed preferential bio-interaction that takes place in the bioactive carboxylic nano-areas mostly at the boundary between the two different organothiols[3].

**METHODS:** Smooth gold substrates (roughness of 0.15 nm) were prepared by template stripping of gold layers from glass[3]. The nanoarrays were produced on the smooth gold by colloidal lithography, as described [3], using polystyrene beads (500nm) to protect the bioadhesive layer of mercaptohexadecanoic acid during etching, then backfilling with thiolated PEO. AFM imaging was used to evaluate the quality of the nanopatterned surfaces.

Force spectroscopy experiments were carried out with a commercial AFM in standard setup (SMENA head, Solver electronics from NT-MDT, Russia) equipped with a liquid cell and using commercial gold coated tips (PPP-ContscAu, Nanosensors, Switzerland) that were in-house functionalized with –COOH, $-NH_3$, $-CH_3$ residues.

Force spectroscopy experiments were carried out as arrayed measures and performed in 10mM PBS pH 7.4 at room temperature. The resulting data were normalized to the estimated tip curvature radius for each measurement..

**RESULTS:** Fig. 1 shows an adhesive force map obtained on the nanopatterned surface in PBS and using a –COOH functionalized tip: zones characterized by a high adhesive force are clearly distinguishable and correspond to the single mercaptohexadecanoic bioadhesive regions. The results show that the –COOH functionalized tip interacts with the pattern with large adhesive force on the carboxylic surface of spots and by no adhesive force on the PEO surface. Initial results from the $-NH_3$ functionalized tip show a repulsive kind of interaction; a weak attraction force has been observed all over the pattern when a $-CH_3$ functionalized tip was used to perform the force spectroscopy experiments.

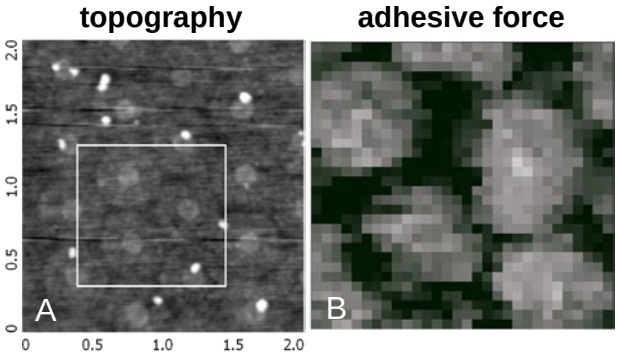


*Fig. 1: topography (A) and force spectroscopy map (B) on nanopatterned surface (lighter regions mark higher adhesive force, range [0, 0.1] nN/nm), obtained with a –COOH functionalized tip.*

**DISCUSSION & CONCLUSIONS:** A clear difference in adhesion forces has been observed throughout the nanopatterned surface when scanned with –COOH functionalized tips, showing a region specific interaction with a specific chemical functional group. This could help to explain the peculiar preferential bio-interaction characteristics that are observed with this nanopatterned surface. To refine results and obtain a higher resolution of the data, more experiments will be carried out in liquid, using in-house produced whole-gold AFM tips that gave encouraging results in terms of tip size and sharpness control.

**REFERENCES:** [1] Agheli,H.; Malmström,J.; Larsson;E. M., Textor,M.; Sutherland,D. S. *Nano Lett*. 2006, **6,** 1165-1171.[2] Krishnamoorthy,S.; Himmelhaus,M. *Adv. Mat.* 2008, **20**, 2782-2788. [3] P.Lisboa, L.Sirghi, G.Giudetti, G.Marchesini, P.Colpo, H. Rauscher, A.Valsesia, F.Rossi (2010) paper in preparation.

European Cells and Materials Vol. 20. Suppl. 3, 2010 (page 93) ISSN 1473-2262

# Delivery of an Anti-Inflammatory Hormone via Layer-by-Layer Assembly of Biomolecules

D.P. Go[1,2], J.A. Palmer[3], S.L. Gras[1,2], A.J. O'Connor[1]

*[1]Particulate Fluids Processing Centre, Department of Chemical and Biomolecular Engineering, The University of Melbourne, Victoria, Australia. [2]Bio21 Molecular Science and Biotechnology Institute, The University of Melbourne, Victoria, Australia. [3]O'Brien Institute, Melbourne, Victoria, Australia.*

**INTRODUCTION:** Many biomaterials used in tissue engineering cause a foreign body response *in vivo* and tissue regeneration can be severely reduced if this response becomes excessive.[1] Our objective was to modulate inflammatory responses by incorporating the anti-inflammatory hormone, α-melanocyte stimulating hormone (α-MSH) on the biomaterial surface via the layer-by-layer (LbL) assembly. Delivery of α-MSH is facilitated using a model biodegradable polymer, poly (lactic-*co*-glycolic) acid (PLGA) microspheres.

**METHODS:** PLGA microspheres were prepared using an oil-in-water emulsion and solvent evaporation technique. Initially, α-MSH was physisorbed on the surface of microspheres. Its bioactivity upon release was assessed *in vitro* using a macrophage inflammation cell assay and *in vivo* with a subcutaneous rat model.

Next, the oppositely charged polyelectrolytes, hyaluronic acid and chitosan, were assembled onto the spheres via LbL assembly after α-MSH was adsorbed. Two alternative strategies were also tested, incorporating different lipids between the α-MSH and the polyelectrolytes. In all cases, the layers were cross-linked using carbodiimide chemistry. Layer growth was assessed by quartz crystal microgravimetry and confocal microscopy. The release profiles of the hormone were established using a micro BCA assay (Thermo Scientific) and high performance liquid chromatography with a C18 column.

**RESULTS:** α-MSH released from microspheres without the polyelectrolyte multilayers was able to reduce the production of an inflammatory cytokine in inflamed macrophages, confirming that its bioactivity was retained. Histological analysis of tissue sections (Fig. 1) indicated the presence of an inflammatory response to the plain PLGA microspheres implanted subcutaneously. Conversely, α-MSH coated PLGA microspheres appeared to reduce the influx of these cells. However, the α-MSH was released quite quickly, showing limited duration effects *in vivo*.

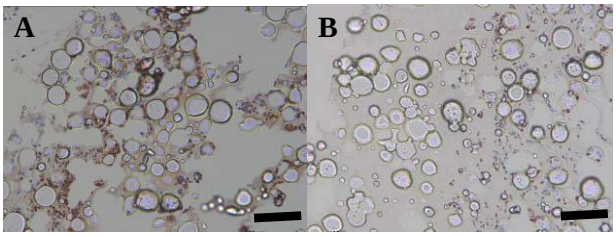


*Fig.1: Myeloperoxidase staining of neutrophils around (A) plain PLGA microspheres and (B) α-MSH coated PLGA microspheres after 3 days' subcutaneous implantation in rats. Scale bar: 100 μm.*

Multilayer assembly was investigated as means to slow the release of α-MSH. QCM analysis showed that α–MSH could not be effectively embedded within the polyelectrolytes due to its hydrophobic nature and small size (1.6kDa). However the addition of lipid layers facilitated the LbL assembly of chitosan and hyaluronic acid via electrostatic interaction. Both QCM and confocal microscopy indicated that the film formed was stable with no loss of polyelectrolytes when the pH was changed from 5.5 to 7.4.

**DISCUSSION & CONCLUSIONS:**

Biomolecular multilayers can be successfully assembled on a hydrophobic polymer surface such as PLGA after adsorption of α-MSH using a switching layer of lipids. Cross-linked polyelectrolytes also provide stability towards fluctuations in the pH of their microenvironment.[2] This multilayered assembly can potentially slow the release of molecules like α-MSH by hindering their diffusion and it can be tuned to vary their release profile over therapeutically relevant time scales.

**REFERENCES:** [1]Anderson, J.M. (2001), *Ann Rev of Mat Res* **31**: p. 81-110. [2] T.I. Croll, A.J. O'Connor, G.W. Stevens et al (2006) *Biomacromolecules* **7**:p. 1610-22.

**ACKNOWLEDGEMENTS:** The authors acknowledge the Particulate Fluids Processing Centre for infrastructure support.

# Direct Cell-Membrane Penetration using Amphipathic Polyphosphobetaines

T. Goda[1], K. Ishihara[2], Y. Miyahara[1]

*[1] NIMS, Ibaraki, Japan, [2] The University of Tokyo, Tokyo, Japan*

**INTRODUCTION:** Nanoscaled materials are normally engulfed in endosomes by energy-dependent endocytosis and fail to access the cytosolic cell machinery [1]. Although some biomolecules may penetrate non-endocytically or fuse with plasma membranes without overt membrane disruption, to date no synthetic macromolecule of comparable size has been shown to exhibit this property. Here we discovered mechanism of direct penetration by bioinspired amphipathic polymer across the plasma membrane of live mammalian cells without cytotoxicity.

**METHODS:** Rhodamine B-tagged random copolymers comprising 2-methacryloyloxyethyl phosphorylcholine (MPC) and *n*-butyl methacrylate (BMA) (rhoPMBs) were synthesized by varying the MPC/BMA compositions (from 30/70 to 70/30) and molecular weights. The polymer uptake by HepG2 cells was visualized by confocal microscopy (LSM-510, Carl-Zeiss) and was quantified by flow cytometry (EPICS XL, Beckman Coulter).

**RESULTS:** The rhoPMBs which formed polymeric aggregates in aqueous media depending on the degree of hydrophobicity and molecular weight were used. Zeta potential was nearly 0 mV.

When rhoPMBs were incubated with cells, it was observed to enter cells very rapidly (within a few minutes) [2]. Surprisingly, substantial amount of rhoPMBs penetrated through the plasma membrane even at 4°C (Fig. 1) or in ATP depletion solution (3 mM sodium azide and 50 mM 2-deoxy-D-glucose in DPBS) at 37°C. Internalized rhoPMBs were able to escape from the cytoplasm when cells were incubated in polymer-free medium. Fluorescence correlation spectroscopy (FCS) confirmed that the fluorescent dyes in the cytosol resulted from the positions of rhoPMBs rather than enzymatically cleaved dye from the polymer. Direct penetration of the rhoPMBs with higher $M_w$ of up to $4 \times 10^6$ was observed. Semi-quantification by flow cytometry revealed that there was no clear relationship between the MPC/BMA ratios and the fluorescence intensities, while rhoPMPC (lack of BMA unit) was unable to penetrate the plasma membrane (Fig. 1). Increased internalization amount of rhoPMB was accompanied by decreased surface tension in the solution, which is caused by

the aggregate formation. In contrast the surface tension of rhoPMPC solution remained unchanged (65–68 mN $m^{-1}$) throughout the concentration range.A high degree of localization of the rhoPMB at mitochondria in the cytosol was observed [2]. Interestingly, Hoechst33258-tagged PMB30 exhibited dominant nuclear localization and FITC-tagged PMB30 distributed throughout the cells. Simultaneous multiple staining of mitochondria, nuclei, and the whole cytosol with these polymers was successful, indicating that the cytosolic distributions are not mutually exclusive events.

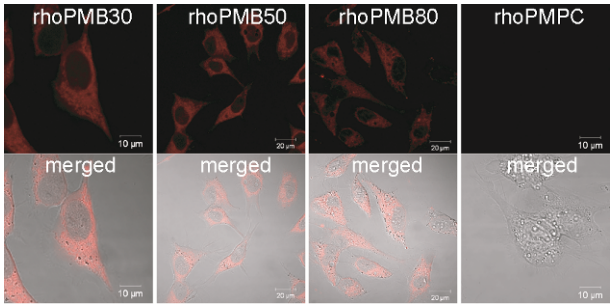


*Fig. 1: Confocal images of cells incubated with 1.0 mg $mL^{-1}$ rhoPMB30, rhoPMB50, rhoPMB80, or rhoPMPC in serum-free medium for 30 min at 4°C. All images were taken after rinsing with DPBS.*

**DISCUSSION & CONCLUSIONS:** Direct penetration could involve the polymeric aggregates forming inverse micelle-like structures containing hydrophobic lipid cores, which eventually collapse back to form a more stable planar bilayer, thereby releasing the polymer into the cytosol. We assume the ability of both MPC units and natural phospholipids to form hydration shells enables them to readily fuse with each other. In summary, amphipathic polyphosphobetaines are capable of providing energy-independent rapid cellular uptake with targeted cytosolic distribution, namely direct penetration. Our results may have relevance for live-cell imaging and delivery of therapeutic agents to specific sites within cells [3] and living organisms without cytotoxicity.

**REFERENCES:** [1] S. D. Conner, et al (2003) *Nature* **422**:37–44, [2] T. Goda, et al (2010) *Biomaterials* **31**:2380-7. [3] R. Miyata, et al (2009) *Int. J. Cancer* **124**:2460-7.

**ACKNOWLEDGEMENTS:** The author (T.G.) is grateful to the JSPS fellowship.

European Cells and Materials Vol. 20. Suppl. 3, 2010 (page 95) ISSN 1473-2262

# PEGylated nanoparticles for cancer detection and treatment

B. Thierry [1], C. Barbe [2], F. Al-Ejeh [3], M. Brown [3], H.J. Griesser [1]

[1] *Ian Wark Research Institute, University of South Australia, Mawson Lakes, SA 5095, Australia.*

[2] *Australian Nuclear Science and Technology Organisation, Private Mail Bag 1, Menai, NSW 2234, Australia, and CeramiSphere Pty Ltd., New Illawarra Road, Menai, NSW 2234, Australia.*

[3] *Royal Adelaide Hospital, Adelaide, SA 5000, Australia.*

The field of nanomedicine encompasses, *inter alia*, the use of nanoparticles for the detection and treatment of tumours. Several classes of nanoparticles have been investigated, and continue to be investigated, intensively for their utility to target tumours and either aid their detection or deliver drugs to combat cancerous tissue.

One common requirement in these studies is the need to ensure efficient utilisation. However, nanoparticles injected into the blood stream are subject to rapid clearance by the process of opsonisation, in which proteins of the immune system mark the nanoparticles for detection and elimination by the reticulo-endothelial system (RES). Minimization of opsonization increases blood residence time and improves the ability to target solid tumors.

Another requirement is that nanoparticles accumulate efficiently at the tumour site. This can be achieved by utilising the leaky nature of the neovasculature of tumours, or by active targeting utilising a suitable antibody to a tumour-specific surface protein.

Thus, clearly, bio-interfacial engineering strategies play a key role in the nanomedicinal application of nanoparticles. Lessons learnt in the design and bio-interfacial engineering of “macroscopic”, two-dimensional biomaterials can greatly assist work on the surface engineering of nanoparticles. Moreover, it is often less challenging to verify by surface analytical techniques the success of intended bio-interface modification approaches on flat 2-D materials surfaces, compared with nanoparticles. Such detailed analyses are essential before proceeding to in vitro and in vivo studies, such as to ensure that the observed biological responses can be interpreted reliably in terms of well-characterised surface chemistries. Yet, there are, in some instances, significant effects arising from the curvature of nanoparticles compared with flat, 2-D surfaces; as a result, one needs to be careful when translating 2-D bio-interfacial engineering approaches to nanoparticles.

This applies particularly to PEGylation of nanoparticles. Some of the approaches that can readily be applied to macroscopic flat surfaces can

be problematic with nanoparticles; for one, the segment density of grafted polymer chains as a function of distance from the solid surface differs between flat and curved surfaces when the same number of chains per surface area is grafted.

This contribution will discuss approaches we have studied for the PEGylation of nanoparticles. Silica nanoparticles (20 and 100 nm diameter) able to encapsulate a wide range of bioactive molecules were PEGylated to improve the bio-availability of these particles by electrostatic self-assembly of PEG-copolymers with polyethyleneimine (PEI). The self-assembly process as well as protein adsorption onto the coated particles were characterized using surface analytical procedures. The nanoparticles achieved substantially increased circulation times; however, though delayed, RES clearance still occurred, pointing to the need for improvement.

An interesting approach to achieving a high density of grafted PEG chains, essential for optimal protein resistance, is the use of a PEG melt. This works well with 2-D surfaces but can be challenging with nanoparticles.

Gold nanorods and noble metal nanoparticles were PEGylated using a different approach, involving ligand exchange with thiolated PEG molecules. A robust method has been developed that prevents aggregation of the nanoparticles.

For active targeting, we have used the approach of using an antibody called 3B9 as an immuno-targeting addition for magnetic nanoparticles. This strategy targets La, a ribonucleoprotein that is abundantly expressed in malignant tumors and during apoptosis, moves from the nucleus to the cytoplasm of cells. As many anti-cancer drugs work by inducing apoptosis in tumor cells, it is useful for clinicians to detect the progress of apoptosis in order to assess how well a treatment is progressing. 3B9 molecules were coupled onto the free end of PEG chains on nanoparticles.

We acknowledge support by the Australian Research Council and the National Health and Medical Research Council.

European Cells and Materials Vol. 20. Suppl. 3, 2010 (page 96) ISSN 1473-2262

# Carbohydrate-modified LSPR Transducers for Protein Recognition

D.Grünstein[1], R.Kikkeri[1], L.H.Hossain[1], G.Bellapadrona[2], A.B.Tesler[2], A.Vaskevich[2], I.Rubinstein[2], P.H.Seeberger[1]

*[1] Max Planck Institute of Colloids and Interfaces, Department of Biomolecular Systems, Am Mühlenberg 1, 14476 Potsdam, Germany & Free University Berlin, Institute of Chemistry and Biochemistry, Arnimalee 22, 14195, Berlin, Germany. [2] Department of Materials and Interfaces, Weizmann Institute of Science, Rehovot 76100, Israel.*

**INTRODUCTION:** Interactions of carbohydrates with proteins are among the most important in living organisms.[1] Study of such interactions is therefore crucial for the understanding of basic biological processes as well as for the development of biosensors, primarily for diagnostics and drug development. In recent years, noble metal nanostructures that support localized surface plasmons (SPs) have been widely applied to sensing the interactions between chemical and biological molecules.[2] Changes in the local refractive index (RI) in the vicinity of the nanostructures affect the intensity and position of the SP extinction band, thus making localized surface plasmon resonance (LSPR) spectroscopy a convenient tool for the study of biological interactions, for biosensing and diagnostics.

**METHODS:** In this work LSPR transducers based on gold island films evaporated on glass were developed for monitoring protein-carbohydrate recognition, comparing the LSPR response of different gold island films to the highly specific interaction between Concanavalin A from *Canavalia ensiformis* and D-(+)-mannose as a model system.

Sensing assays were performed under stationary and dynamic conditions, the latter allowing recording of the kinetics of protein binding and release. To show the applicability of LSPR to sensing of carbohydrate-protein interactions, the sugar mannose **1** and controls galactose **2** and linker **3** were immobilized onto Au island films and exposed to a protein analyte in solution (*Fig 1*).

**RESULTS:** The sensing step of Au island transducers caused a red-shift and an increase in intensity of the LSPR band, characteristic of an increase of the local RI. The results are consistent with specific binding of Con A to **1** but not to **2** and **3**. Ellipsometry and FTIR measurements confirmed theses results.

Determination of Con A – mannose SAM binding affinity was achieved by measuring changes in the extinction at 545 nm in a flow cell as a function of ConA concentration. The LSPR transducer showed sensitivity down to nanomolar concentrations.

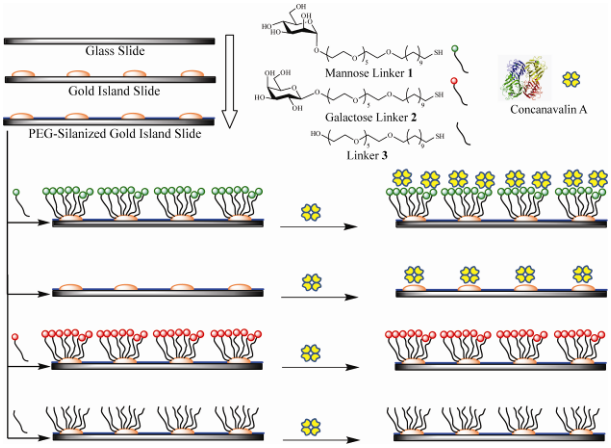


*Fig. 1: Schematic representation of the sensing experiment.*

**DISCUSSION & CONCLUSIONS:** Au nano-island based LSPR transducers can be used effectively to detect binding of proteins to carbohydrates immobilized on the Au island surface, distinguishing between specific and non-specific interactions. The method is simple, low-cost and label-free. The biosensing capability of our method with more relevant sugars involved with disease-causing viruses, parasites or bacteria will be investigated. The development of an automated method for the synthesis of carbohydrates [3] opens new possibilities in this area.

**REFERENCES:** [1] A. Varki, R. Cummings, J.D. Esko, H. Freeze, G. Har, J. Marth (2002) *Essentials in Glycobiology* Cold Spring Harbor Laboratory Press, Plainview, NY. [2] A. Vaskevitch and I. Rubinstein (2007) In *Handbook of Biosensors and Biochips* (eds. Wiley) Vol. 1. [3] P.H. Seeberger, D.B. Werz (2007) *Nature* **446**:1046.

**ACKNOWLEDGMENTS:** We thank the Max-Planck Society, the Israel Science Foundation, the Marie Curie fellowship (CARMUSYS program) and the Faculty of Medicine, "Sapienza" University of Rome, for financial support.

# Probing Molecular Recognition on the Single Molecule Level

A. Gunnarsson[1,2], P. Jönsson[1], P. Sjövall[1,2], F. Höök[1]

[1]*Department of Appleid Physics, Chalmers University of Technology, Göteborg, Sweden.*
[2]*SP Technical Research Institute of Sweden, Borås, Sweden.*

**INTRODUCTION:** Molecular diagnostics, the identification and quantification of genetic and proteomic biomarkers, is a key component for future development in drug discovery, biomedical diagnostics and bioanalytical assays in fundamental research. The last decade has witnessed a rapid development of new detection concepts with high sensitivity and selectivity, demonstrating, in some cases, even single-molecule resolution. In parallel, the need to analyze multiple analytes simultaneously has driven the development of multiplexed assays such as biochip technology or, more recently, bioassays based on target-specific barcodes.

**METHODS:** Total internal reflection fluorescence (TIRF) microscopy and time-of-flight secondary ion mass spectrometry (TOF-SIMS).

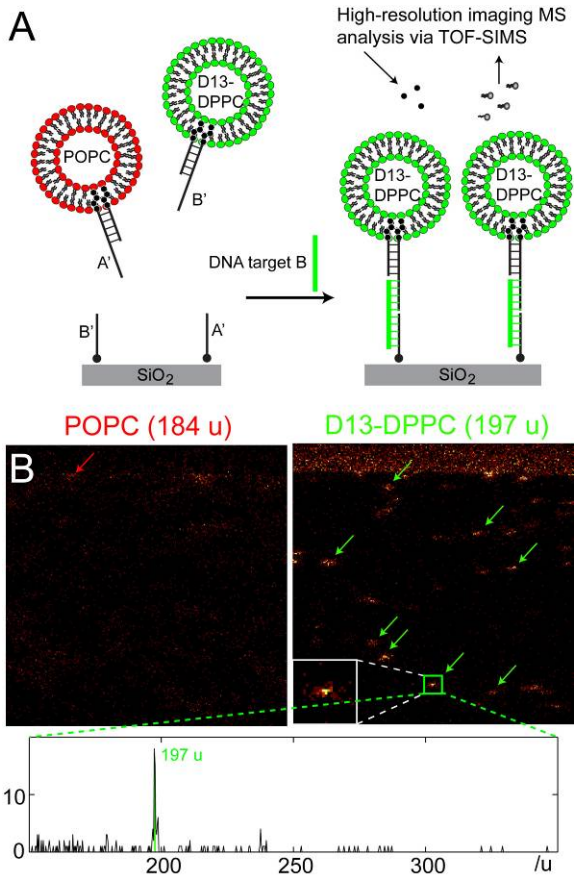


*Fig. 1: (A) Schematic illustration of the sensing template based on DNA-modified liposomes, where the lipid composition of each liposome act as a chemical barcode to identify unique DNA target sequences down to the single molecule level. (B) High-resolution ion images of two different mass peaks (184 u and 197 u) characteristic for POPC and D13-DPPC lipids respectively. Each high intensity spot corresponds to an individual liposome immobilized at the surface mediated by a single DNA target.*

**RESULTS:** We report on a single-molecule assay demonstrating a detection limit in the low fM regime for short unlabeled DNA targets[1]. Furthermore, the assay is shown capable of extracting kinetic data from statistics of the residence time of the binding reaction in equilibrium, i.e. without following neither the rate of binding upon injection nor release upon rinsing. The potential of this feature is demonstrated by discriminating a single mismatch from a fully complementary 30-mer DNA target[2], an important capability for single nucleotide polymorphism (SNP) diagnostics. On top of rapid and sensitive detection, the sensing template can also be combined with high-resolution imaging mass spectrometry (TOF-SIMS) for multiplexed detection on a random array utilizing chemical barcodes[3] (Fig. 1). The exceptionally high image resolution provided by the TOF-SIMS[4] allows for multiplexed DNA detection down to level of single molecules. Finally, the extension towards a membrane protein compatible assay is disclosed.

**DISCUSSION & CONCLUSIONS:** The concept can easily be extended to multiplexed protein analysis by exchanging the capture and probe DNA sequences to suitable antibody pairs, or, as discussed in the final section, membrane residing proteins, which are currently the major targets in drug discovery.

**REFERENCES:** [1]A. Gunnarsson, et al (2008) *Nano Lett.*, 8(1):183-188. [2]A. Gunnarsson, et al *Nucleic Acids Res.*, (2009), 37(14):e99. [3]A. Gunnarsson, et al (2010) *Nano Lett.*, (2010) 10(2):732–737. [4]A. Gunnarsson, et al (2010) *Anal. Chem.*, 82(6):2426–2433.

**ACKNOWLEDGEMENTS:** The authors thank C. Wingren, Lund University for providing cells and antibodies for the membrane protein experiments.

European Cells and Materials Vol. 20. Suppl. 3, 2010 (page 98) ISSN 1473-2262

# Wettability and Protein Adsorption Properties of Biodegradable Polymeric Nanolayers

G. Gyulai[1], Cs. B. Pénzes[1], P. Petrik[2], T. Lohner[2], É. Kiss[1]

*[1]Laboratory of Interfaces and Nanosize Systems, Lorand Eötvös University, Budapest 112, PO Box 32, H-1518, Hungary. [2]Research Institute for Technical Physics and Materials Science, Hungarian Academy of Sciences, Budapest, PO Box 49, H-1525 Budapest, Hungary.*

**INTRODUCTION:** Biodegradable polyesters such as poly(lactic acid) (PLA) and poly(lactic/glycolic) acid copolymers (PLGA) are preferred materials for controlled drug delivery [1]. Their surface hydrophobicity however, triggers the fast clearance of colloidal drug carrier particles from the body [2]. Surface hydrophilization by immobilization of poly(ethylene glycol) (PEG) molecules might prolong their blood circulation time and hence allows the programmed drug release [3].

**METHODS:** In the present work thin polymer films on a solid support were used as a model system to study the interfacial interactions with aqueous media. The polymer films were prepared by spin coating method from PLGA mixed with the modifying PEG-containing compound (Pluronics) at various concentrations. Wettability and surface characterization techniques (XPS, AFM) were applied to study the effect of surface modification on the composition, morphology and hydrophilicity of the polymer nanolayers. The increased hydrophilicity and hence the reduced protein adsorption on the surface is supposed to be in correlation with its biocompatibility. To investigate the bovine serum albumin (BSA) and fibrinogen adsorption *in situ* spectroscopic ellipsometric studies were performed.

**RESULTS:** The measured protein surface concentrations showed a good correlation with the surface hydrophilicity of the samples. Protein adsorption was successfully reduced below the biofouling level (10 ng/cm$^2$).

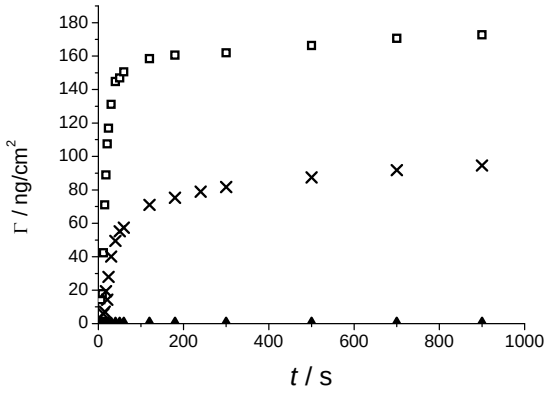


*Fig. 1: Adsorbed protein surface concentrations as a function of time on different surfaces.*
□ *unmodified PLGA,* **x** *PLGA with 4w/w% additive,* ▲ *PLGA with 10w/w% additive*

Interfacial behavior of PLGA and Pluronic blend films were found to be dependent on the type of preparation method: solvent casting / spin coating. The protein adsorptions were compared for three PLGA + Pluronic films at each composition (0w/w%, 4w/w%, 10w/w% additive) with various thicknesses. The differences in adsorbed BSA and fibrinogen obtained from ellipsometric measurements help revealing the mechanics of Pluronic in reducing the adsorption.

**REFERENCES:** [1]R.M. Rasal, A.V. Janorkar, D.E. Hirt (2010) *Progr. Polym. Sci.* **35**: 338-356. [2]Santander-Ortega, A.B. Jódar-Reyes, N. Csaba, D. Bastos-González, J.L. Ortega-Vinuesa (2006) *J. Colloid Interf. Sci.* **302**: 522–529. [3]É. Kiss, I. Bertóti, E. I. Vargha-Butler (2002) *J. Colloid Interf. Sci.* **245**: 91-98.

**ACKNOWLEDGEMENTS:** Financial support of research programmes OTKA K68120, BIOSPONA TeT-08-SG-STAR, GVOP 3.2.1-2004-04-0099/3.0 and NKTH-BIOSURF_OM00146/2008 is acknowledged.

# An *in-vitro* method to study anti-apoptotic signaling from the extracellular environment

M.Håkanson[1], S. Kobel[2], M. Charnley[1], M. Lutolf[2], M. Textor[1]

[1] *Surface Science and Technology, Department of Materials, ETHZ, Zurich, Switzerland.*
[2] *Laboratory of Stem Cell Bioengineering, Inst. of Bioengineering, EPFL, Lausanne, Switzerland*

**INTRODUCTION:** The emergence of acquired multidrug resistance (MDR) remains a major hurdle in the successful treatment of cancer. Signaling from the extracellular environment has shown to induce de novo drug resistance, a pre-state to MDR. [1] Hence, identifying such signaling pathways may pave the way for novel targeted therapies that can prevent the occurance of MDR. This creates a demand for a predictive in vitro method for the study of the dependence of anti-apoptosis signaling on the environment.

So far, in vitro studies of the effect of environmental parameters on drug response have typically focused on one parameter at a time, such as the interaction with matrix proteins [2] or the effect of enhanced cell-cell contacts in 3D organized cells [3]. Therefore we are working on an in vitro platform, with which it is possible to simultaneously study the effect of several extrinsic parameters. This platform consists of a microwell array molded into a polyethylene glycol (PEG) hydrogel. [4] The material properties of this hydrogel make it possible to mimic tissue-like stiffness. This allows us to explore many parameters of the environment, such as dimensionality, composition of the interfacing protein matrix and rigidity.

**METHODS:** Hydrogel microwell arrays were prepared as described previously.[4] Arrays were used for cell experiments one day after preparation. After UV-sterilization, MCF-7 cells were seeded into the wells at a density of 750 000 cells / ml. After 1 hr of adhesion the samples were rinsed to remove cells from the microwell plateau. The cells were pre-cultured in the microwells for 24 hrs. Thereafter 10 nM taxol or vector only were added to the samples for another 24 hrs.To visualize the apoptotic ratio the samples were fixed in paraformaldehyde and stained with Hoechst 33342. Samples were imaged with a Leica confocal microscope equipped with a water objective, 20x magnification and 0.7 NA. For each microwell 3 images separated by 15 um in z-direction were obtained and analyzed for the percentage of fragmented nuclei. The experiment was performed in duplicates and repeated three times.

**RESULTS:** MCF-7 breast cancer cells formed dense clusters similar in size when cultured within 100 µm wide microwells coated with collagen I. It was found that cells organized in clusters were more resistant to treatment with taxol compared to cells cultured on flat substrates. The apoptosis detection on single cell level allows us to measure non-symmetric distributions of cell phenotypes. In this experiment there were no significant difference s in cell death ratios over the clusters.

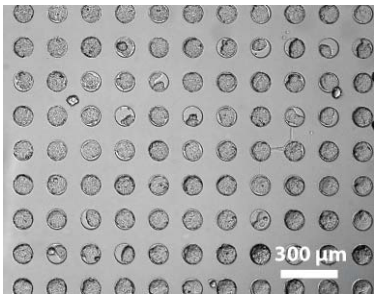


*Fig. 1: MCF-7 cells form cluster in 100 µm wide microwells. This image is from 48 hrs post seeding.*

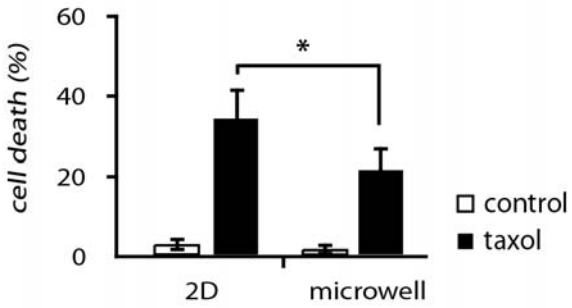


*Fig. 2: The 3D organization of the cells in the microwells provides an anti-apoptotic effect.*

**DISCUSSION & CONCLUSIONS:** This work aims at the development of a tool to study the dependence of drug response on environmental parameters. The preliminary results demonstrate that the 3D organization of cancer cells induce an anti-apoptotic signaling. Understanding and targeting such signaling might help to overcome novel MDR.

**REFERENCES:** [1] Shain *et al*., *Mol Cancer Ther*, **1**, 69, 2001. [2] Aoudjit *et al*., *Oncogene*, **20**, 4995, 2001. [3] St. Croix *et al*., *Nat Med*, **2**, 1204, 1996. [4] Lutolf *et al*., *Intergr Bio*, **1**, 59, 2009.

European Cells and Materials Vol. 20. Suppl. 3, 2010 (page 100) ISSN 1473-2262

# Development of methods for testing the toxicological profile of nanoparticles used in the biomedical field

B.Halamoda-Kenzaoui, C.Chapuis, L.Juillerat-Jeanneret

*University Institute of Pathology CHUV-UNIL, Lausanne Switzerland.*

**INTRODUCTION:** Nanoparticles (NP) are becoming a very interesting option for both medical diagnosis and targeted drug delivery. Their large biomedical application in the future is probable; however detailed studies have to be conducted in order to exclude any potential toxicity to living organisms. Our objectives are to evaluate the interaction of different types of NP with specific cells, their cell uptake and release, their transport across biological barriers and their potential cytotoxic effects. This information will then be useful to design efficient standardized *in vitro* methods for testing various NP of potential future interest.

**MATERIALS & METHODS:** Five different types of NP have been selected for the study: titanium dioxide nanoparticles, iron oxide nanoparticles uncoated and coated with oleic acid, poly(lactic-co-glycolic)acid(PLGA-PEO) nanoparticles and silica fluorescent nanoparticles. The uptake and localisation of NP in cells has been studied using TEM technique (Fig.1) and quantified in case of iron oxide NP with the Prussian blue reaction.

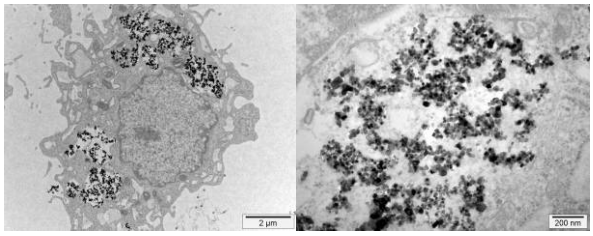


*Fig 1: The uptake and localisalisation of $TiO_2$ NP in cell are visualised by TEM imaging of ECp23 cells after 24h exposure to $TiO_2$ NP.*

Various tests of proliferation and viability such as MTT reduction, WST-1 assay or PI uptake have been performed in order to asses a general toxicological profile of the NP. The mechanism of their eventual toxicity is now being studied focusing on inflammation, immunotoxicity, oxidative stress and genotoxicity as cross- cutting issues. The intracellular fluorescent probes of ROS such as carboxy-dichlorofluorescein (carboxy-DCFH) or dihydroethidium (DHE) have been employed and we measured intracellular thiol level by bromobimane assay. Abiotic production of ROS was examined using DTT assay. An *in vitro* model of the blood – brain barrier has been developed using human brain – derived HCEC endothelial cells in order to study the transport of NP across this barrier in the absence and presence of an external magnetic field. This study was done using the Transwell® inserts and the transported iron oxide NP were detected with the Prussian blue reaction.

**RESULTS & CONCLUSIONS:** The uptake of iron oxide NP was shown to be dependent on their coating: uncoated iron oxide NP, even though they agglomerated quickly in cellular environment, were able to enter the cells, whereas oleic acid coated iron oxide NP were more stable but not taken up by the cells (Fig.2).

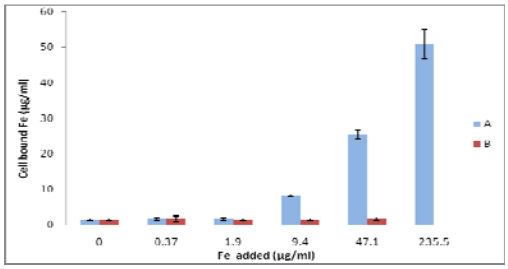


*Fig. 2: The uptake of iron oxide NP uncoated (A) and coated with oleic acid (B) after 24h exposure to HCEC cells.*

The study of the transport of iron oxide NP across the HCEC barrier did not show any transport for both types of NP, even when an external magnetic field was used. Preliminary results of cytotoxicity assays did not show any toxicity of PLGA-PEO NP but did show a significant cytotoxicity of oleic acid coated iron oxide NP at high doses. Interference tests confirmed that most of the examined NP interact with the assay reagents and can significantly modify the assay results (Fig.3), showing the importance of performing these tests each time the cytotoxicity is tested.

**REFERENCES:** M.Dusinska: Testing strategies for the safety of nanoparticles used in medical applications, *Nanomedicine* (2009)**4**, 605-607

**ACKNOWLEDGEMENTS:** This research is funded by the FNRS and the European Commission ECFP7 projects NanoTEST and NanoImpactNet.

European Cells and Materials Vol. 20. Suppl. 3, 2010 (page 101) ISSN 1473-2262

# Cell type specific cell guidance in Wound Healing

H. Hall, T. Lühmann, S. Tang

*Cells and BioMaterials, Department of Materials, ETH Zurich, Switzerland*

**INTRODUCTION:** Wound healing consists of a series of interlinked processes that need to follow each other to result in proper healing. Different cell types need to fulfill different tasks in the wound site including fibroblasts that change the fibrin clot to a more mature collagen-based matrix and endothelial cells (ECs) that provide sufficient vasculature. This study investigated different cell guidance modalities, namely shear forces exerted by fluid flow and covalently–bound guidance cues within 3D-fibrin matrices to determine their effects on guidance of endothelial cells and fibroblasts. In combination with different capabilities to degrade the surrounding matrix (plasmin versus MMP-based matrix degradation), differential cell guidance towards the wound site seems to be important in wound healing.

**METHODS:** HUVECs and hFFs were exposed to 1 and 5.6 ml/min shear for 24 h when cultivated in Ibidi µ-slides. The slides were coated with collagen IV for HUVECs. Then cells were stained with life and dead stain to determine cell viability and alignment microscopically. Both cell types were also cultivated on/in gradient L1Ig6-modified fibrin matrices [1-2] that served as chemical guidance structures. Cell alignment was analyzed after 48 h after DAPI and phalloidin Alexa-488 staining which allowed determination of the contours of the cells and their longest axis [1]. Matrix degradation was analyzed by providing either MMP or plasmin inhibitors to cells cultivated within 3D-fibrin matrices. The number and length of cell processes growing into the matrix was determined after 24 h [3].

**RESULTS and DISCUSSION:** HFFs and endothelial cells respond to different external stimuli. HUVECs align with increase in shear forces applied whereas hFFs do not (Fig. 1). This is interesting in the perspective of wound healing as HUVECs need to follow the shear forces of blood flow in order to form new blood vessels towards the wound site, whereas fibroblasts need to be almost stationary to locally remodel the ECM. However, fibroblasts get attracted by chemical guidance cues that are covalently attached to the 3D-matrix. This feature allows them to follow ECM-guidance to reach their places of action within the wound site. HUVECs do not respond (Fig. 2). HUVECs use MMPs and plasmin to degrade efficiently the fibrin matrix whereas hFFs predominanlty use MMPs (not shown).

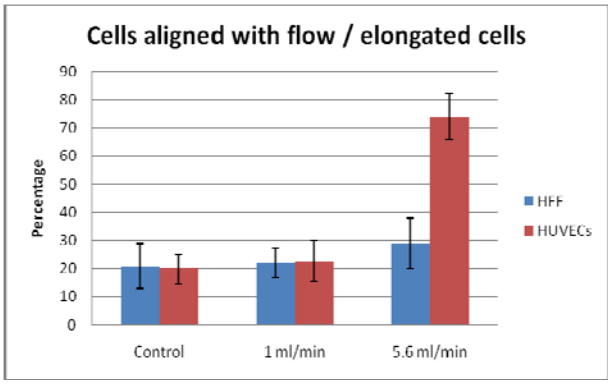


*Fig. 1: Percentage of elongated cells aligned with flow.*

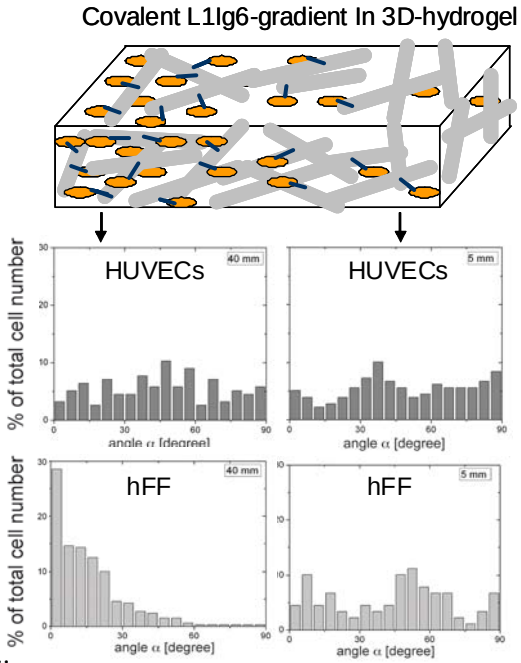


*Fig. 2: Percentage of aligned cells with the covalent gradient of L1Ig6 within 3D matrices.*

**CONCLUSIONS:** Stimulation of wound healing requires different signals addressing different cell types. This information should be placed into a modern wound dressing in order to support e.g. deficient wound healing successfully.

**REFERENCES:** [1]Lühmann et al., *Biomaterials* **30**. 2009, 4503–4512; [2] Lühmann and Hall, 2009, *Materials*, **2**, 1058-1083; [3]Urech et al, 2005, *Biomaterials* 1369–1379.

**ACKNOWLEDGEMENTS:** This study was supported by GRF-Foundation and CCMX (TL).

# LacI search kinetics changes with number of operators

P.Hammar[1], N.Grantcharova[1], P.Leroy[1], J.Elf[1]

[1] *Department of Cell and Molecular Biology, Uppsala University, Uppsala, Sweden*

**INTRODUCTION:** In the early 1980s mathematical modelling predicted facilitated diffusion as the way for DNA binding proteins to find their regulatory operator sites [1]. In essence this refers to the combination of 3D diffusion in the cytoplasm and 1D diffusion (sliding) along the DNA. Since then the theory has been accepted and widely used in new models but also visualized in single molecule *in vitro* experiments [2]. Recent *in vivo* experiments detecting proteins binding on the single molecule level pointed towards a revision of the model [3], and the presence of other DNA binding proteins, roadblocks, has then been suggested as the missing parameter that bridges the early model with the latest data [4].

**METHODS:** We have employed the method described in [3]. The *E.coli* repressor LacI fused to the fluorescent protein Venus binds to its specific operators in glucose rich medium. Binding and un-binding is dictated by the addition of inducer IPTG, that binds LacI and inhibits DNA binding, and anti-inducer ONPF that compete with IPTG and when bound to LacI allows the protein to bind back to its operator. We have measured the time it takes for LacI-Venus to move from a free (Fig. 1, right) to a specifically bound (Fig 1, left) state, in different *E.coli* strains.

The optical setup includes an argon ion laser tuned to 514nm, a Nikon Eclipse Ti microscope (oil immersion lens 100x/1.49, autofocus system and external phase contrast module), with dichroic mirror, excitation filter (514/10), emission filter (550/50) and an Andor Ixon+ EMCCD for detection. The signal from Venus is acquired at 40W/cm$^2$ and a 1s exposure. The automated setup is controlled by the open source software µManager.

**RESULTS:** Our first and preliminary data show how the presence of three operator sites on the DNA result in search kinetics 2-3 times faster compared to that of a single operator (Fig 2).

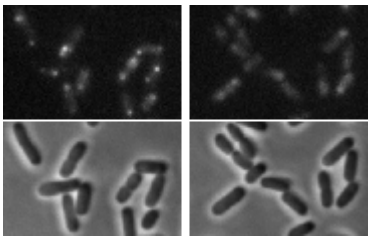

*Fig. 1: Single LacI-Venus proteins, bound to their specific targets and seen as diffraction limited dots over the fluorescent background (top left), or un-bound (top right), visualized over a 1s exposure. At the bottom, same cells imaged with phase contrast.*

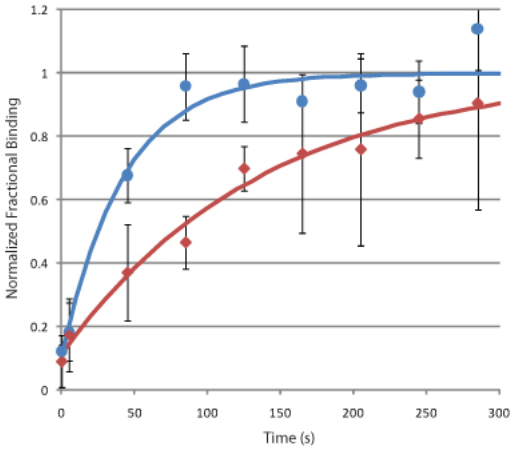


*Fig. 2: Binding kinetics for strains with one LacI binding site (red) or three binding sites (blue).*

**DISCUSSION & CONCLUSIONS:** Our results show that it takes less time for a single LacI-Venus protein to find any of three operators compared to a single operator. In the wild type *lac* operon this is likely to be combined with DNA looping. Here the transcription factor, binding to any of the auxiliary sites, will use its tetramer structure to move on to the regulatory site in an event much faster than the initial search time [4].

**REFERENCES:** [1] O.G. Berg, R.B. Winter and P.H. von Hippel (1981) *Biochemistry* **20(24)**:6929-48. [2] I. Bonnet, A. Biebricher, P.L. Porté, et al (2008) *Nucleic Acids Res* **36(12)**:4118-27. [3] J. Elf, G.W. Li and X.S. Xie (2007) *Science* **316(5828)**:1191-4. [4] G.W. Li and J. Elf (2009) *Nature Physics* **5**:294-297

**ACKNOWLEDGEMENTS:** We thank Gene-Wei Li for helpful discussions and Brian English for help with the optical setup.

# Formation of metal-bioorganic nanofibres on a microchip

Urs Hartfelder[1], J.Puigmartí-Luis[1], Inhar Imaz[2], Daniel Maspoch[2], P.S.Dittrich[1]

[1] *Department of Chemistry and Applied Biosciences, ETH Zürich, Switzerland.*

[2] *Centre d'Investigacions en Nanociencia i Nanotecnologia (ICN-CSIC), Barcelona, Spain*

The past decade has evidenced an explosive growth in research aimed to control and guide the assembly of different molecular building blocks. Among others, normal synthetic procedures are focused in lithographic, vapour deposition and electron-beam based technologies.[1] These processes involve complex, expensive and time consuming techniques. Owing to this fact, much effort has been conducted to find alternative methods. In this sense, microfluidics has emerged as an advanced alternative approach for controlling and guiding large molecular assemblies.[2, 3]

Here we report the microfluidics-guided assembly of a coordination polymer based on copper ions and sodium aspartate (Cu(II)-Asp). This microfluidic approach demonstrates the formation of nanofibres within milliseconds at the interface of the two reactant streams (Fig. 1).

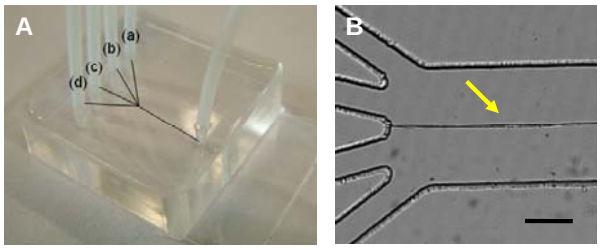


*Fig. 1: (A) Photography of the micro-reactor that has four inlets used for supplying the solution for the sheath flow (a) and (d) and the reactants (b) and (c). (B) Optical microscope image of Cu(II)-Asp wire (yellow arrow) generated on the chip. The scale bar is 100 µm.*

In a typical synthetic procedure two aqueous solutions containing $Cu(NO_3)_2 \cdot 3H_2O$ (1.5 mM) and L- aspartic acid (1 mM) and NaOH (2.5 mM), respectively, were injected via a syringe pump system into a four-channel microfluidic platform. The reactants were applied in the central channels, (Fig. 1, channels (b) and (c)) and guiding of the assembly through the entire chip was accomplished by modifying two aqueous auxiliary streams. (Fig. 1, channels (a) and (d))

We investigated the formation under various conditions, including changes of the volume flow rates of the reagent and auxiliary side streams. Studies of the eluted structures by scanning electron microscopy corroborated the nanowire

morphology described previously in bulk.[4] However, while in bulk synthesis the reaction time last from few hours to a few days, it is reduced to milliseconds in the microfluidic reactor. Moreover, the ease to adjust flow rates on this system leads to control over the reaction zone of the two reactants. Consequently, guiding and positioning of the structures can be addressed just by changing sheath flow or reactants flow rates (Fig. 2).

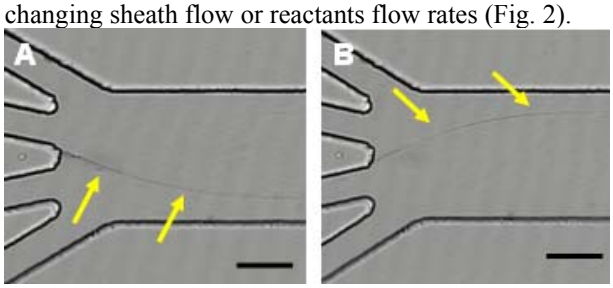


*Fig. 2: Optical microscope images demonstrating the positioning of Cu(II)-Asp wires (yellow arrows) by changing the flow rates of the sheath streams. The scale bars are 100 µm.*

In summary we have presented a new route for a straightforward production of metal-organic frameworks by using microfluidic technologies. We anticipate that this is a general approach enabling fast and well-controlled nanowire formation of other metal organic/bioorganic composite materials and possesses the ability of guiding and tuning the formation pathway of the assembled structures just by varying flow-rate conditions.

**REFERENCES:** [1] Y.N. Xia, P.D. Yang, Y.G. Sun, Y.Y. Wu, B. Mayers, B. Gates, Y.D. Yin, F. Kim, Y.Q. Yan (2003) Adv.Mat. **15**, 353-389. [2] Y. Gao, L. Chen (2008) Lab Chip **8**, 1695–1699. [3] J. Puigmartí-Luis, D. Schaffhauser, B. R. Burg, P. S. Dittrich (2010) Adv. Mat. 10.1002/adma.200903428. [4] I. Imaz, M. Rubio-Martinez, W.J. Saltera, D.B. Amabilino, and D. Maspoch (2009) J. Am. Chem. Soc. **131**, 18222-18223.

**ACKNOWLEDGEMENTS:** Funding from the European Research Council under the 7th Framework Programme (ERC Starting Grant, project no. 203428, "nµ-LIPIDS") and the ETH for the fellowship to J.P.-L. is gratefully acknowledged.

# A New Biomimetic Interface: Liquid Crystal-supported Mixed Phospholipid/Cholesterol Monolayer

D.Hartono, Hody, KL.Yang, LYL.Yung

*Department of Chemical and Biomolecular Engineering, National University of Singapore, Singapore.*

**INTRODUCTION:** Biomimetic cell membranes are widely used to investigate diverse biological phenomena such as association of signalling proteins at cell membranes and binding events that permit penetration of external molecules into cells. An emerging method to create these biomimetic interfaces uses self-assembly of phospholipids (a major constituent of cell membranes) at an interface between aqueous phase and water-immiscible liquid crystals (LCs) [1, 2]. This method offers advantages such as real-time and label-free reporting of biomolecular interactions occur at the interface. However, to date, it is not known if cholesterol (another major constituent of cell membranes) can be self-assembled at aqueous-LC interface. Here we report the formation and characterization of a new biomimetic interface that consists of a mixture of phospholipids and cholesterols at aqueous-LC interface.

**METHODS:** Thin films of LCs as a platform for biomimetic interface formation were prepared following published procedures [2]. Formation of the biomimetic interfaces via self-assembly of either phospholipid, cholesterol or mixed phospholipid/cholesterol monolayer at aqueous–LC interface were accomplished by immersing the LC films into a buffer phase containing 100 μM of either phospholipid, cholesterol or mixed phospholipid/cholesterol for 2 h. At the end of the self-assembly, the LC films laden with the lipids were flushed with fresh buffer. The optical images of LCs were examined under polarizing microscope. The presence of cholesterol at aqueous-LC interface was tested via cholesterol oxidation by cholesterol oxidase. This oxidation generates cholest-4-en-3-one and $H_2O_2$, where the latter can oxidize tetramethyl benzidine (TMB) catalyzed by horseradish peroxidase (HRP) to produce a distinct coloured product [3].

**RESULTS:** In the absence of any lipid, contact of LC films with buffer phase caused the optical image of LCs to appear fully bright (Fig. 1 left). In contrast, in the presence of cholesterols, some dark domains were formed (Fig. 1 middle), reflecting some degree of self-assembly of cholesterols at aqueous-LC interface. Only in the presence of phospholipids or mixed phospholipid/cholesterol, the optical images of LCs turned to completely dark (Fig. 1 right). However, these two latter interfaces gave different responses when they were exposed to cholesterol oxidase. Sample from phospholipid/cholesterol-laden interface, when mixed with TMB and HRP, showed blue colour and absorbance at 650 nm (Fig. 2). In contrast, sample from phospholipid-laden interface was colourless and showed no measurable absorbance (Fig. 2).

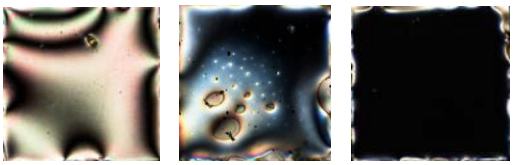

*Fig. 1: Optical images of LCs in contact with buffer solutions containing (left) no lipid, (middle) cholesterol, (right) phospholipid or mixed phospholipid/cholesterol.*

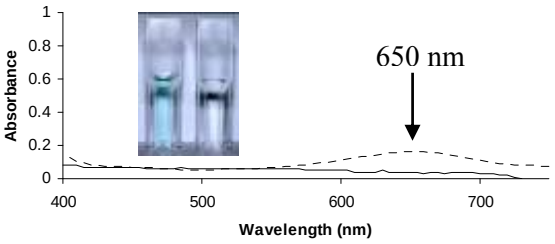


*Fig. 2: Photographs and UV-Vis absorbances of samples from mixed phospholipid/cholesterol (blue vial and dashed line) and phospholipid only (colourless vial and solid line) after being exposed to cholesterol oxidase followed by TMB and HRP.*

**DISCUSSION & CONCLUSIONS:** The results presented here provide evidences that cholesterols can not only be self-assembled but also be co-self-assembled with phospholipids at aqueous-LC interface. This phospholipid/cholesterol monolayer can serve as a new biomimetic cell membrane model to investigate diverse biological phenomena in a simple system.

**REFERENCES:** [1] J.M. Brake, et al. (2003) *Science* **302**:2094-97. [2] D. Hartono, et al. (2009) *Biomaterials* **30**:843-49. [3] P.D. Josephy, et al. (1982) *J Biom Chem* **257**:3669-75.

# Linking cellular and organismal toxicities of silver nanoparticles in the model earthworm *Eisenia fetida*

Y. Hayashi[1,2], P. Engelmann[3], HV. Pedersen[2], J. Wang[1], J. Scott-Fordsmand[2], DS. Sutherland[1], LH. Heckmann[2]

[1] *Interdisciplinary nanoscience center (iNANO), Aarhus University, Denmark.*
[2] *National Environmental Research Institute (NERI), Aarhus University, Denmark.*
[3] *Department of Immunology and Biotechnology, University of Pécs, Hungary.*

**INTRODUCTION:** Silver nanoparticles (Ag-NPs) are amongst the most studied model nanomaterials for their potential toxicity to public health and the environment. Emerging publications on Ag-NP toxicity primarily aim to illuminate the mechanistic view of how NPs interact with biological systems *in vitro*. But only a very limited number of studies have screened the potential toxicity *in vivo*, particularly to ecological key species[1]. The fate and effects of NPs can depend on the physico/biochemical environment that NPs encounter, which makes it difficult to derive causality and to extrapolate. Reported here is our initial assessment on cellular and organismal toxicities of Ag-NPs in the ecotoxicological model earthworm, *Eisenia fetida*.

**METHODS:** PVP-coated Ag-NPs, obtained as powder, have previously been characterised in house[2]. All stock and test conditions (described hereafter) were characterised using a combination of techniques (e.g. Dynamic light scattering). For comparison, the silver salt $AgNO_3$ was used as a dissolved Ag treatment. The earthworm *E. fetida* was used as a test species for both of *in vivo* and *in vitro* studies. In the *in vivo* study, the earthworms were individually exposed in aqueous media and mortality was assessed after 24 h. For the *in vitro* study, a mixed population of immune-competent cells, known as coelomocytes, were extruded for this species and collected prior to each experiment. To improve colloidal stability under physiological conditions, Ag-NPs were pre-treated with bovine serum albumin (BSA) and used as a stock suspension. Several endpoints (e.g. cell viability) were assessed following 24 h exposure.

**RESULTS:** The colloidal suspensions retained good stability for 24 h under the test conditions used both in the *in vivo* and in the *in vitro* tests (Fig. 1) and the hydrodynamic diameters were comparable to the average primary size obtained previously (ca. 80 nm)[2]. Table 1 shows the $LC_{50}$ values estimated in the *in vivo* and *in vitro* studies. The values were relatively similar in the dissolved Ag ion treatments, whereas for Ag-NP treatments the toxicity was lower in the *in vivo* experiment.

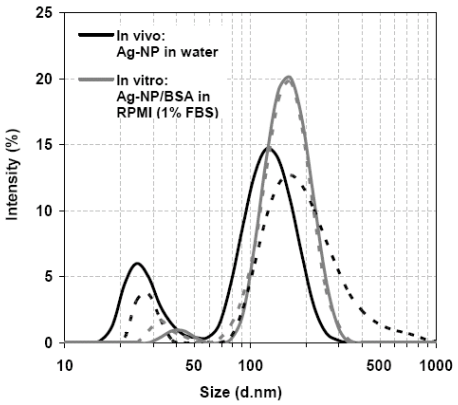


*Fig. 1: Size distributions of Ag-NPs at <1 h (dashed line) after 24 h (solid line) under each test condition.*

*Table 1. Estimated $LC_{50}$s obtained for* E. fetida.

| | Ag-NP | $Ag^+$ ion |
|---|---|---|
| *In vivo* | 67 ppm | 0.3 ppm |
| *In vitro* | 5 ppm | 0.1 ppm |

**DISCUSSION & CONCLUSIONS:** Using coelomocytes as model systems for studying the cellular toxicity, we illustrated an initial approach to linking lower and higher biological responses in *E. fetida* exposed to Ag-NPs. In the present study, the acute effect caused by Ag-NP exposure was lower than caused by the silver salt in both *in vitro* and *in vivo* systems, the latter being the least susceptible. The potential window of toxicity and the mechanistic link to the organismal response await further characterisation of the dynamic nano-bio interplay at the interface of ecotoxicology and bionanoscience.

**REFERENCES:** [1] A. Kahru & HC. Dubourguier (2009) *Toxicology* **33**:105-19. [2] K. Hansen *et al.* (2009) *Aquat Toxicol* **96**:159-65.

**ACKNOWLEDGEMENTS:** This work is financially supported by FUU and the Danish Strategic Research Council (NABIIT project 2006-06-0015 “SUNANO”).

# BIOMIMETIC NANOCRYSTALLINE APATITE RESEMBLING BONE

WX. He[1, 2], J. Bielecki[3], C.S. Knee[4] and M. Andersson[1]

[1]*Dept. Chemical and Biological Engineering,* [3]*Dept. Applied Physics, Chalmers University of Technology, Gothenburg, Sweden*

[2]*Dept. Polymer Science, East China University of Science and Technology, Shanghai, China*

[4]*Dept. Chemistry, University of Gothenburg, Gothenburg, Sweden*

**INTRODUCTION:** Liquid Crystalline Phases (LCP) having water domains in the size range 5-10 nm can be used as templates for the formation of nano-sized Hydroxyapatite (HA).[1] In the present study, LCPs together with Glycosaminoglycans (GAGs) have been utilized for HA synthesis. The GAGs were added since the electrostatic interactions between the anionic sites (carboxyl or sulphate groups) on GAGs and the cationic sites (calcium) on HA have an effect on the HA crystallisation process.[2] The HA formed using LCPs were compared to HA formed using simple water based precipitation.

**METHODS:** All chemicals were purchased from Aldrich (reagent grade). For synthesis using LCP, $Ca(NO_3)_2 \cdot 4H_2O$, 85% $H_3PO_4$ (with a Ca:P ratio of 1.67) and various concentrations of GAGs (Heparin Sodium, Grade 1-A) were dissolved in Milli-Q $H_2O$. Then by mixing the aqueous solution with the surfactant Pluronic® L64 ($EO_{13}PO_{30}EO_{13}$) and *p*-Xylene, a reverse hexagonal liquid crystalline phase (15wt% aqueous solution, 70wt% L64 and 15wt% *p*-Xylene) was formed. After being equilibrated for 24 h, the liquid crystalline phase was placed in an ammonia atmosphere (ammonium hydroxide, 35wt% aqueous solution) to increase the pH, thus to initiate the precipitation of HA. The reaction was completed after 4 days. The formed HA materials were purified using filtration with water and ethanol. For the water-based precipitation (WBP), the aqueous solution was stirred at 500 rpm and directly exposed to an ammonia atmosphere for 4 days. The post process for WBP was the same as for LCP.

**RESULTS:** Fig.1 shows HA particles synthesized using the LCP, which are needle-like crystallites (about 5×35 nm in size) and by WBP, which are more plate-like (width ~15 nm). The addition of GAGs increased the specific surface area in both routes, suggesting its interaction with HA. Furthermore, from Raman spectral analysis, see Fig. 2, sample B (surface area, 277.9m²/g) stands out from other synthetic HA and shows a great resemblance to the mineral found in bone.

*Table 1. Sample information and BET results*

| Sample No. | Synthetic Route | GAGs Conc. | BET Surface Area (m²/g) |
|---|---|---|---|
| A | LCP | 0 | 218.9 |
| B | LCP | 1.54 wt% | 277.9 |
| C | WBP | 0 | 75.9 |
| D | WBP | 1.54 wt% | 85.2 |

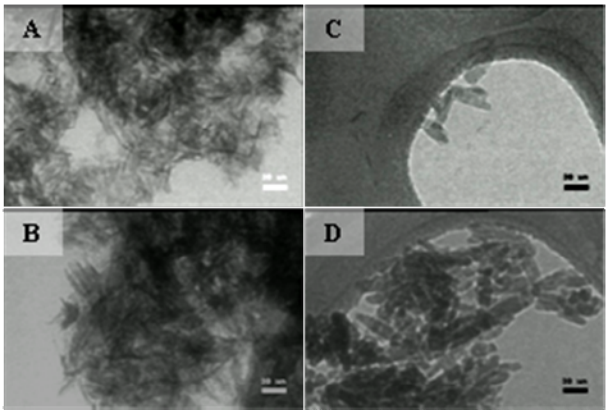


*Fig.1: TEM micrographs of the formed HA*

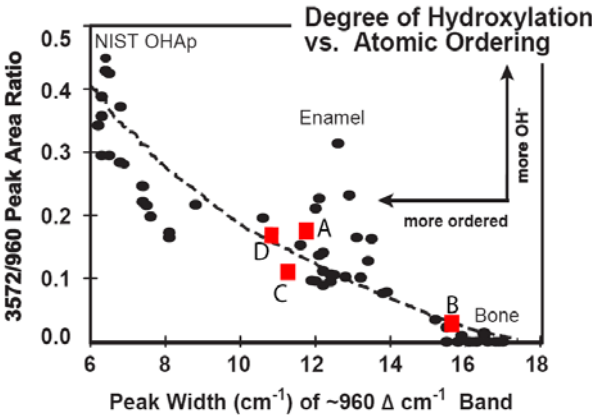


*Fig. 2: Comparison of Raman spectra with data of various synthetic and biological HA samples.*[3]

**CONCLUSIONS:** Combining the size confinement effect of LCP and the structural modulation of GAGs, HA particles with a considerably high surface area can be prepared.

**REFERENCES:** [1]P. Kjellin et al. (2005) *Synthetic nano-sized crystalline calcium phosphate and method of production* Patent WO 2005/123579 A1. [2]S. Chander et al. (1984) Solubility and interfacial properties of hydroxyapatite: A review (eds D.N. Misra) Plenum Press, pp 29-50. [3]J.D. Pasteris et al. (2004) *Biomaterials* **25**:229-238.

# A self-assembled artificial protein nanotube

F. F. Miranda[1], K. Iwasaki[2], S. Akashi1, K. Sumitomo[3], M. Kobayashi[4], I. Yamashita[4], J. R. H. Tame[1], J. G. Heddle[1,5]

[1]*International Graduate School of Arts and Sciences,Yokohama City University,Yokohama, Japan*
[2]*Institute for Protein Research, Osaka University, Osaka, Japan and CREST Japan Science and Technology Agency, Kawaguchi, Japan*
[3]*NTT Basic Research Laboratories 3-1 Morinosato-Wakamiya, Atsugi Kanagawa 243-0198*
[4]*Nara Institute of Science and Technology, Nara. Japan*
[5]*Global Edge Institute Tokyo Institute of Technology Yokohama, Japan and Advanced Science Institute, RIKEN, Wako, Japan*

**INTRODUCTION:** A major goal of nanotechnology is to design and build complex functional devices at the nanoscale. This is achieved routinely in Nature where, for example, functioning nanomachines such as enzymes are assembled in aqueous solution in a "wet nanotechnology" process. Our challenge is to design artificial biological nanostructures (primarily proteins) in order to build up a toolbox of parts which may be of use as components of future nanodevices. *De novo* protein design is not feasible due to the astronomically high number of conformations that amino acids in a typical protein chain can adopt (Levinthal's Paradox [1]). We therefore employ a "semi-synthetic biology" approach whereby existing proteins of a potentially useful structure are used as a start point and engineered so that they self-assemble into the required structure. We have recently applied this technique to engineer an artificial, self-assembled protein nanotube using the ring shaped bacterial protein TRAP [2]. By adding cysteine residues to the two opposing faces of the protein ring, we were able to induce polymerization into a nanotube, which was confirmed via TEM.

**METHODS:** The gene encoding *Bacillus stearothermophilus* TRAP protein was mutated to insert mutations D8H, F32A, E50C, R66H, and V69C using the QuikChange site-directed mutagenesis kit (Stratagene).The protein was purified as previously described [3]. Polymerization of the rings was achieved by increasing the protein concentration to approximately 20 mg/ml and incubating in 50mM Tris-HCl (pH 8.5), 100mM NaCl in the presence of DTT. TEM was carried out using a 200 kV JEM-2200FS (JEOL, Tokyo).

**RESULTS:** Transmission electron microscope analysis showed that the mutant TRAP formed long tubular structures approximately 8 nm in diameter (Figure 1). We have been able to form tubes of over 1 µm in length which, given that a single TRAP ring is approximately 3 nm in length, represents an extremely high aspect ratio. Furthermore, we can "switch" on the self assembly process by the addition of certain agents.

*Figure 1. Docking the atomic structure of TRAP ring (ribbon diagram, pdb 1qaw) into the EM map of TRAP tube (cyan surface)*

**DISCUSSION & CONCLUSIONS:** We have successfully modified TRAP to produce a self assembled protein nanotube and are now investigating the details of the poplymerization reaction. Protein nanotubes have many potential uses in biosensors and as templates in nanoelectronics. We hope that further development of the TRAP nanotube and other proteins will lead to applications in these areas.

**REFERENCES:** [1]C. Levinthal, J. (1968). *Chim. Phys.* PCB **65**, 44–45. [2]F. F. Miranda, K. Iwasaki, S. Akashi, K. Sumitomo, M. Kobayashi, I. Yamashita, J. R. H. Tame, J. G. Heddle (2009), *Small* **5**: 2077-84. [3] J. G. Heddle, T. Yokoyama, I. Yamashita, S.-Y. Park, J. R. H. Tame (2006). *Structure* **14**, 925-33.

**ACKNOWLEDGEMENTS:** J.G.H. was supported by MEXT Special Coordination Funds for Promoting Science and Technology and a Grant-in-Aid for Young Scientists (WAKATE
B-20710083). F.M. was a JSPS Special Research Fellow. J.R.H.T. and S.A. were supported by grants-in-aid from MEXT. M.K. and I.Y. was supported by the Human Frontier Science Program.

European Cells and Materials Vol. 20. Suppl. 3, 2010 (page 108) ISSN 1473-2262

# Real-time Monitoring of Nanostructured Surface Build-up and Function using a novel Micro-Impedance Measurement Instrument (z-LAB)

J. Hedlund[1], A. Lundgren[2], H. Elwing[2]

[1]*Layerlab AB, Gothenburg, Sweden.* [2]*University of Gothenburg, Interface Biophysics, Sweden.*

**INTRODUCTION:** Impedance measurements of biological processes is a well-recognized method that now has been developed into a real-time, compact and user-friendly instrument; z-LAB (*Fig1*). By applying an AC-electric field over a set of functional microelectrodes, the z-LAB instrument gains information about surface charging and conductivity, which is seen as change in surface capacitance and resistance [1]. The capacitance response reflects the real surface area and is therefore ideal for analysis of non-flat surfaces like nanostructured surfaces.

**METHODS:** Gold electrodes are coated by self-assembly with dithiol that forms a homogenous layer. Charge stabilized gold nanoparticles (AuNP) (Ø10nm) are deposited with controlled surface coverage and interparticle distance by altering the ionic strength of the nanoparticle buffer solution [2]. Area between particles were blocked with maleimide conjugated PEG. AuNP surface was charged by adsorption of mercaptopropionic acid (MPA) followed by adsorption of avidin.

**RESULTS:** Manipulation of the Debye-screening between neighbouring particles allows for variation in the surface coverage of AuNP. Increased surface capacitance upon paricle binding is proportional to surface area enhancement (*Fig2A*). Areas in-between particles are isolated by the dithiol layer and appear "invisible" in the capacitance measurements whereas the particle surfaces become charged, probably due to electron tunnelling. Adsorption of mPEG to the AuNP coated surface (*Fig3*) results in an increased capacitance due to change of running buffers (citrate⇒phosphate). Citrate ions associated to the AuNP surface is replaced with phosphate ion, resulting in an increased surface net charge. Adsorption of MPA decreases surface capacitance as the surface becomes more insulating. Avidin adsorption to modified surfaces with varying AuNP coverage is seen as a decrease in surface capacitance.

**DISCUSSION & CONCLUSIONS:** This technique to nanostructure gold electrodes allows control of both the nanostructure and the chemistry on top of and between the bound nanoparticles. In these work, the direct assembly of molecules onto

and between bound particles was investigated using a novel micro-impedance instrument (z-LAB). Impedance measurements goes beyond mass adsorption data, with detection of changes in adsorption of both large molecules like avidin as well as detection of changes in small and charged molecules like MPA and phosphate ion.

*Figure1. The complete z-LAB system. Sensor chips are shown to the right.*

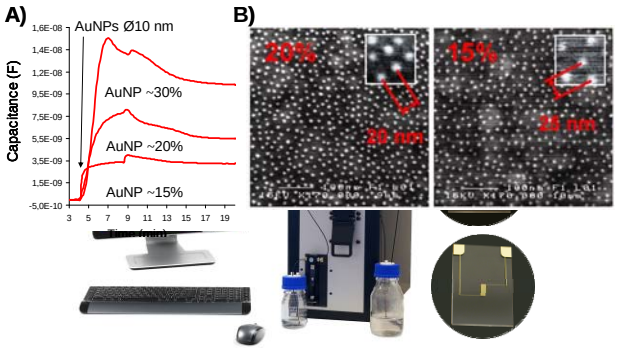


*Figure2. A) AuNP particle density is proportional to increased surface capacitance. B) SEM pictures showing surfaces with different AuNP coverage.*

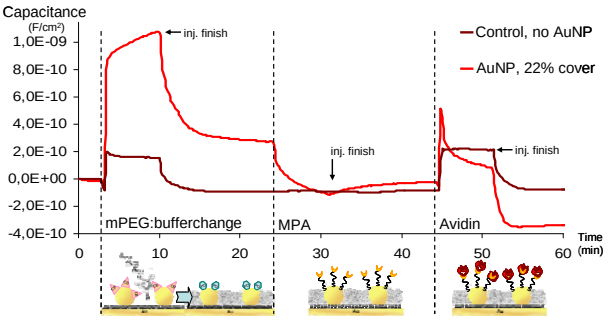


*Figure3.Surface chemistry is controlled by adsorption of mPEG between particles and charging the exposed AuNP surface area with MPA. Avidin adsorption is seen as a decrease in surface capacitance.*

**REFERENCES:** [1]J. Hedlund et al (2009) *Sensors and Actuators B*, **142**:495-501.[2] A. Lundgren et al (2008) *Nano Letters*, **8**:3989-3992.

European Cells and Materials Vol. 20. Suppl. 3, 2010 (page 109) ISSN 1473-2262

# Iron from nanocompounds containing iron and zinc is highly bioavailable in rats without tissue accumulation

FM. Hilty[1], M. Arnold[2], M. Hilbe[3], A. Teleki[4], TJN. Knijnenburg[4], F. Ehrensperger[3], RF. Hurrell[1], SE. Pratsinis[4], W. Langhans[2], MB. Zimmermann[1]

*[1] Human Nutrition Laboratory, ETH Zurich. [2] Physiology and Behaviour Laboratory, ETH Zurich, [3] Institute of Veterinary Pathology, University of Zurich, [4] Particle Technology Laboratory, ETH Zurich*

**INTRODUCTION:** Iron deficiency affects more than two billion people worldwide and can cause anaemia, reduce cognitive development and lower work capacity. Effective iron fortification of foods is difficult because water-soluble compounds that are well absorbed, such as ferrous sulphate ($FeSO_4$), often cause unacceptable colour or taste changes in foods, whereas poorly water-soluble compounds that cause fewer sensory changes but are not well absorbed[1]. Here[2] we show that poorly water-soluble nanosized Fe and Fe/Zinc compounds made by scalable flame aerosol technology[3] have in-vivo iron bioavailability in rats comparable to $FeSO_4$ and cause less colour change in reactive food matrices than conventional iron fortificants.

**METHODS:** Bioavailability of the different compounds (Table 1) was determined in 128 male Sprague-Dawley rats using the haemoglobin repletion bioassay. Relative bioavailability values of each compound relative to $FeSO_4$ were calculated using the slope-ratio method by comparing the change in haemoglobin (g/L) with the measured Fe intake (µg/d). Sensory performance was tested in two sensitive foods (chocolate milk and banana milk).

| Compounds | SSA $m^2/g$ | RBV % |
|---|---|---|
| $FePO_4/Zn_3(PO_4)_2$ | 191 | 96 [a] |
| $Fe_2O_3/ZnO/MgO$ | 192 | 91 [a,b] |
| $Fe_2O_3/ZnO/CaO$ | 105 | 82 [*,a,b] |
| $Fe_2O_3/ZnO$ | 174 | 77 [*,b] |
| $FePO_4/Fe_2O_3$ | 197 | 78[*,b] |
| Electrolytic Fe | 0.35 | 60[*,c] |
| $FeSO_4$ dried | | 100 |

*Table 1. Specific surface area (SSA) and Relative Bioavailability (RBV) compared to $FeSO_4$. RBVs with a common letter (a, b or c) are not statistically different from each other while RBVs labelled with * are statistically different from FeSO4 ($P < 0.05$)*

**RESULTS:** The relative bioavailability values (Table 1) of the $FePO_4/Zn_3(PO_4)_2$ and the $Fe_2O_3/ZnO/MgO$ did not differ significantly from $FeSO_4$, whereas the bioavailability of other compounds tested were significantly lower.

After feeding rats with nanostructured iron-containing compounds, no stainable Fe was detected in their gut wall, gut-associated lymphatics or other tissues, suggesting no adverse effects. As seen in Figure 1, colour change in both reactive matrices was markedly less for the nanostructured compounds than for ferrous sulphate or NaFeEDTA, and was comparable to that of ferrous fumarate.

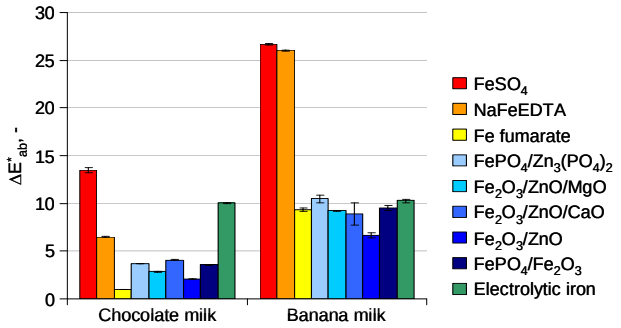


*Fig. 1 Sensory performance of nanostructured iron-containing compounds in comparison with commercially available compounds*

**DISCUSSION & CONCLUSIONS:** The nanostructured compounds show promise for nutritional applications, especially the mixed Fe/Zn compounds could deliver both Fe and Zn to deficient populations, and the ratio of Fe to Zn could be tailored to meet the specific need of the target population.

**REFERENCES:** [1] M. B. Zimmermann, R. F. Hurrell (2007) *Lancet* **370**:511-520. [2] F.M. Hilty, M. Arnold et al (2010) *Nature Nanotech* (published online: April 25, 2010). [3] R.Strobel, S.E. Pratsinis (2007) *J Mater Chem* **45**:4743-4756.

**ACKNOWLEDGEMENTS:** The authors would like to thank L. Berger for her technical assistance. The study was supported by the Swiss National Science Foundation, Bern, Switzerland; the Swiss Commission for Technology and Innovation (KTI Projekt9765.1 PFLS-LS), Bern, Switzerland; IMP (Industrial Metal Powders (India) Pvt Ltd) andETH Zurich, Switzerland.

European Cells and Materials Vol. 20. Suppl. 3, 2010 (page 110) ISSN 1473-2262

# Controlling Orientation and Measuring Length of Lipid Nanotubes Using High-Frequency AC Electric Field

K. Hirano[1], M. Aoyagi[1], T. Ishido[1], T. Ooie[1], H. Frusawa[2], M. Asakawa[1], T. Shimizu[1], M. Ishikawa[1]

*[1] National Institute of Advanced Industrial Science and Technology (AIST), Japan. [2] Kochi University of Technology, Japan.*

**INTRODUCTION:** To make full use of lipid nanotubes (LNTs) in industrial and pharmaceutical applications, their properties must be investigated in detail. However, manipulation techniques for LNTs are not as well developed as for carbon nanotubes. Manipulation techniques using alternating current (ac) electric field that are used for other micrometer-sized rods or spheriods (e.g. bacteria [1] and carbon nanotubes [2]) should be useful for manipulating LNTs. Here, we investigated a technique for controlling the orientation and measuring the length of individual LNTs in aqueous solution.

**METHODS:** Fine-powered and rough-powdered LNTs made of renewable-resource-based GL-AIST, with a hollow cylindrical architecture composed of multiple lipid bilayer membranes (average i.d. and o.d. of 70 nm and 192 nm, respectively), were dissolved in aqueous solution.

For orientation control, 4 aluminium electrodes were arranged in 2 facing pairs on a coverslip and the ac electric field was applied alternatively and orthogonally between the pairs, orientating the individual LNTs synchronously in one direction and then the other direction. The strength of the dc and ac fields was maintained constant, at 2 x $10^4$ V/m and 2 x $10^4$ $V_p$/m, respectively.

To visualize the LNTs in sharp contrast to the aqueous solution, individual LNTs were stained with DAPI and observed under an inverted fluorescence microscope, in order to determine orientation and measure length.

**RESULTS:** Individual LNTs under an ac field were oriented steadily and without displacement at a frequency higher than 1 MHz. This orientation occurred due to an interaction between the external electric field and the induced dipole moment in the LNT because the dipole moment is oriented parallel to the external field lines [1]. In contrast, the use of a dc field generated heat and subsequent turbulence flow and bubbles due to electrolysis (see Fig. 1).

The length of individual LNTs was measured on fluorescence images by rotating the LNT at 4 MHz. The length measurement was limited to single LNTs over 2 µm in length because the spatial resolution of the present measurement system was not able to distinguish particle LNTs from cylinder LNTs at below this length. The length distribution is characterized by one maximum and a trailing

distribution to the longer-length region, both of which depend on the preparation process of the sample. Relaxation length was found to be useful for measuring the length of the longer LNT region; relaxation length of the fine-powdered LNTs was longer than the rough-powdered LNTs by a factor of 2.

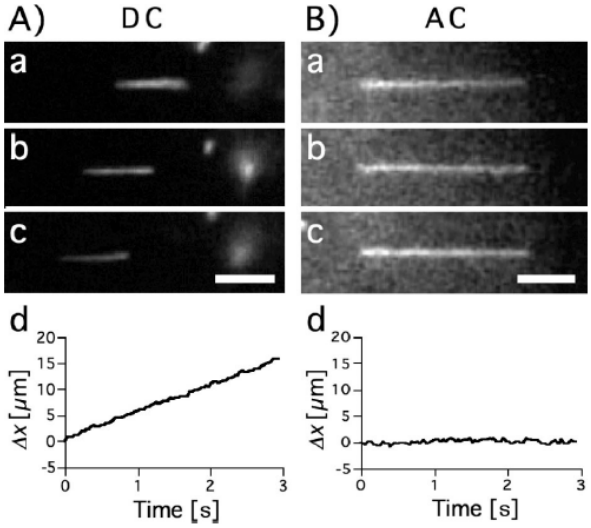


*Fig. 1: Comparison between direction of single LNT under (A) a dc and (B) an ac electric field. (a-c) Fluorescence images of single oriented LNT at 1-s time intervals with a positive electrode placed at the left side of each image. Scale bar is 10 µm. (d) Change in displacement of the center of gravity* Δx *of the single LNT with time.*

**DISCUSSION & CONCLUSIONS:** By using a high-frequency ac electric field, we could quantitatively measure the length distribution for two different types of LNTs.

**REFERENCES:** [1] M. Nishioka, S. Katsura, K. Hirano, et al (1997) *IEEE Trans Ind Appl* **33**:1381-8. [2] R. Krupke, F. Hennrich, H. V. Lohneyson, et al (2003) *Science* **301**:344-7.

**ACKNOWLEDGEMENTS:** This study was supported by a grant form the Industrial Technology Research Program from NEDO.

# Controlled redistribution of blood peptides (BPs) between human serum albumin (HSA) and mesoporous silica (MPS)

H. Kabata, K. Kawasaki, K. Hirai, R. Tsuruoka, H. Takahashi

*The NASCENT group, Central Research Laboratories, Sysmex Corporation, Japan*

**INTRODUCTION:** BPs can serve as an easy-handled, disease-specific, and stage-selective biomarker [1], and have been explored solely by mass spectrometry (MS). Biochemical pretreatment of serum is a key for MS-based mining of BPs [2]. In addition, nanotechnological methods, like inclusion of BP into MPS, have been applied as a new potential pretreatment [3]. BPs however favor nonspecific adsorption onto silica surface. Evidence for the inclusion by MPS (and its practical benefit in the BP mining) remains controversial. Originally, inclusion of BPs is observed for blood circulation, where BPs bind to and are buried in HSA [4]. Most BPs thus exist as a sequestered, inaccessible form rather than a free, available. Biomarker exploration essentially depends on redistribution of BPs from refractory HSA to a controllable tool, like MPS.

**METHODS:** After IRB approval, 103 samples from healthy volunteers and breast cancer patients (in stage I-II) were collected and kindly given by Dr Yoshidome (Osaka Police Hospital). Sera and peptides were analyzed by a modified SDS-PAGE and MALDI-TOF MS. Silica surfaces were characterized by thermoporometry using a conventional differential scanning calorimeter.

**RESULTS:** To demonstrate inclusion of BPs by MPS, we incubated a typical BP (the ACTH 1-24 fragment) in serum (data not shown) or with a large excess amount of proteinase K. The enzyme digested ACTH rapidly (Fig 1). In contrast, the digestion disappeared for ACTH that was once absorbed by capillary action into dry powders of MPS (with pore sizes of 4-7 nm). This observation confirmed that MPS included and moreover preserved BPs, being a clue to an efficient pretreatment. We hereby checked whether or not serum-intrinsic BPs were enzymatically liberated from HSA and then re-included into MPS. When a nonporous silica gel coexisted in a serum mixture containing MPS and trypsin, HSA was fixed on the gel and cleaved (but not "chopped"). BPs were released out, and indeed collected by MPS (Fig. 2).

**DISCUSSION & CONCLUSIONS:** The successful BP redistribution presented here was due to a combination of protease (cutting open of HSA), nonporous silica (removal of the residuals), and MPS (sieving of BPs). The determinant step seems to be a competition between proteases, HSA, and MPS. MPS should mechanically absorb BPs much faster than the proteins equilibrate to associate with. Development using MPS for breast cancer BP test is underway, and will be discussed in the session.

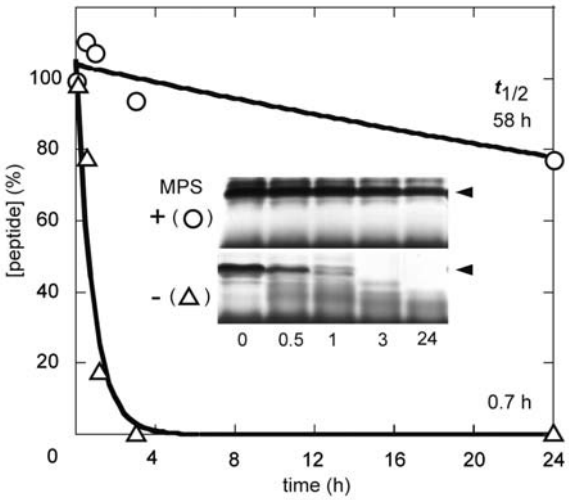


*Fig. 1: MPS with a 7-nm opening protected the ACTH peptide from a harsh proteolysis.*

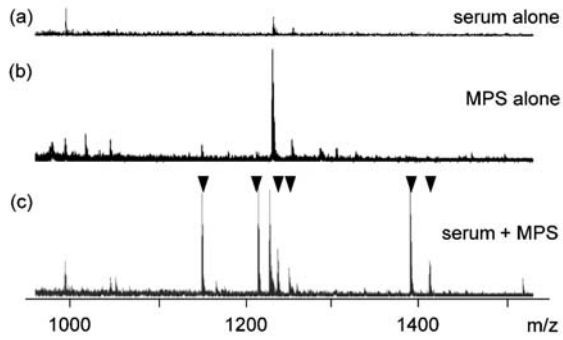


*Fig. 2: MS showed a locally-limited trypsinization of HSA isolated BPs with the assistance of MPS.*

**REFERENCES:** [1] G.L. Hortin (2006) *Clin Chem* **52**:1223-37. [2] S. Radhakrishna et al (2003) *Mol Cell Proteom* 2:1096-1103. [3] R. Tian et al (2007) *J Chromatogr A* 1216:1270-78. [4] M.S.L. Lowenthal (2005) *Clin Chem* **51**:1933-45.

**ACKNOWLEDGEMENTS:** MPS powders were a courtesy of Taiyo Kagaku Co. This research was supported in part by a "Risk-Taking Fund For Technology Development" program (no. D09-01) from Japan Science and Technology Agency (JST).

European Cells and Materials Vol. 20. Suppl. 3, 2010 (page 112) ISSN 1473-2262

# A novel comprehensive evaluation platform to assess nanoparticle toxicity *in vitro*

Cordula Hirsch[1], Florian Wessling[1], Kathrin Fischer[1], Matthias Roesslein[1], Peter Wick[1], Heinrich Hofmann[2], Harald F. Krug[1]

*1Empa - Swiss Federal Laboratories for Materials Testing and Research, St. Gallen, Switzerland*

*2EPFL – Powder Technology Laboratory, Lausanne, Switzerland*

**INTRODUCTION:** The amount of engineered nanomaterials is constantly increasing. Their unique properties, compared to their bulk counterparts, render them suitable for various applications in many areas of life. Hence, nanomaterials appear in a variety of different consumer products leading to the exposure of human beings and the environment during their lifecycle.

Although many studies and results on biological effects of nanomaterials are available, standardized and validated test systems are still missing. Furthermore, interactions of nanomaterials with assay systems or inappropriate suspending methods often lead to false results [1-6]. Summarizing and comparing all available data to obtain an overall evaluation of potential nano-related toxicity is thus virtually impossible.

Since safety and risk assessment become increasingly important for consumers, the lack of toxicological evaluation standards may lead to a loss in acceptance of nanotechnological applications which would especially affect the trading with nano-products. Hence, standardized and robust methods which create a platform of comprehensively validated tools to assess toxicological effects of nanomaterials are urgently needed.

**METHODS & RESULTS:** We currently establish a novel *in vitro* evaluation system based on already existing ISO and OECD guidelines, addressing four key aspects of cytotoxicity: viability of cells, inflammation, genotoxicity and oxidative stress. As various nanomterials interfere with several test systems we will carefully reassess and validate the suitability of at least two independent methods for each of the four parameters and thoroughly characterize the applied nanomaterial samples. Furthermore, the reliability and robustness of the assays will be verified by interlaboratory comparisons. The resulting evaluation platform will comprise reliable, reproducible, robust and sensitive *in vitro* methods validated for different engineered nanomaterials. Successively used, this platform will be able to reduce the currently prevailing ambiguity concerning the toxicity of nanoparticle containing products. This is fundamental not only for consumers but also for authorities and industry.

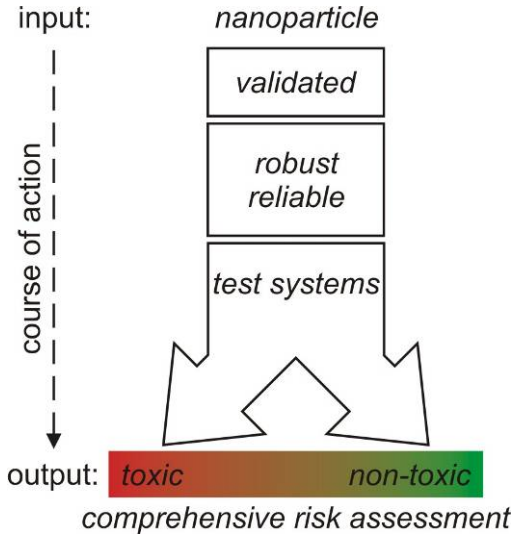


*Fig. 1: Scheme of the in vitro evaluation platform. Validated, robust and reliable test systems allow to comprehensively assess the cytotoxic properties of various nanoparticles.*

Here we present the overall strategy of establishing and using the testing platform, introduce selected methods for each of the four parameters and exemplarily show preliminary results and emerging challenges.

**REFERENCES:** [1]Belyanskaya L. et al. (2007) *Carbon* **45**:2643-2648. [2]Wörle-Knirsch JM et al. (2006) *Nano Lett.* **6**:1261-1268. [3]Casey A et al. (2007) *Carbon* **45**:1425-1432. [4]Guo L. et al. (2008) *Small* **4**:721-727. [5]Monteiro-Riviere NA, Inman AO (2006) *Carbon* **44**:1070-1078. [6]Pulskamp K et al. (2007) *Toxicol. Lett.* **168**:58-74.

**ACKNOWLEDGEMENTS:** This work is funded by the Competence Centre for Materials for Life Sciences (CCMX), the Swiss Federal Offices for Health (FOPH) and environment (FOPH), the Swiss "Interessengemeinschaft Detailhandel" (IG-DHS) and Wessling GmbH (Germany) and is done in cooperation with the Powder Technology Laboratory of the "Ecole Polytechnique Fédérale de Lausanne" (EPFL).

European Cells and Materials Vol. 20. Suppl. 3, 2010 (page 113) ISSN 1473-2262

# Synthesizing bioactive silane layers on nanopatterned stainless steel surfaces

M. Hirsimäki[1], L. Kanninen[1], N. Jokinen[1], P. Jussila[1], K. Lahtonen[1], R. Pärna[2], E. Nõmmiste[2], M. Valden[1]

[1] *Surface Science Laboratory, Tampere University of Technology, Tampere, Finland.*

[2] *Institute of Physics, University of Tartu, Tartu, Estonia.*

**INTRODUCTION:** Biofunctionality of surfaces and surface coatings plays a critical role in biomedical applications involving biomedical implants, biosensors and aerosol based drug delivery techniques. Our goal is to fabricate on stainless steel covalently bound silane layers with functional biotin groups for binding avidin proteins in well-defined manner. Our recent results show that a high quality, monolayer thick silane film can be produced by depositing a high concentration of hydroxyl species on the surface prior to silanization.[1] In the present study, we deposit a mixed (3-mercaptopropyl)trimethoxy-silane (MPS) and (3-aminopropyl)trimethoxysilane (APS) layer on stainless steel at varying mixing ratios. Once an optimal MPS/APS ratio is found, Maleimide-Polyethylene Glycol (Mal-PEG) is deposited on the surface. Only MPS exhibits reactivity towards Mal-PEG, leading to preferential Mal-PEG adsorption at MPS sites. APS sites are deactivated by simultaneous deposition of N-hydroxysuccinimide Polyethylene Glycol (NHS-PEG). Once the adsorption behavior of Mal-PEG on MPS/APS covered stainless steel is known, the surface can be activated for applications in biotin-avidin technologies by replacing Mal-PEG with Mal-PEG-Biotin.

**METHODS:** Our set of substrates consists of high quality stainless steel with a well-defined distribution of nanoscale Cr surface compounds. Each substrate is hydroxylated prior to the deposition of a solution consisting of MPS and APS at varying relative concentrations. The composition, morphology and orientation of silane layers are characterized by surface sensitive x-ray photoelectron spectroscopy (XPS) and x-ray absorption spectroscopy (XAS) techniques by using laboratory and synchrotron radiation (MAX-lab, Lund, Sweden) sources. Mal-PEG/NHS-PEG deposition is carried out on the substrate exhibiting optimal MPS/APS concentration. The surface is subsequently characterized by XPS and XAS.

**RESULTS:** A set of MPS/APS covered stainless steel surfaces were prepared and investigated by XPS and XAS. A selected XPS result is shown in Fig. 1.

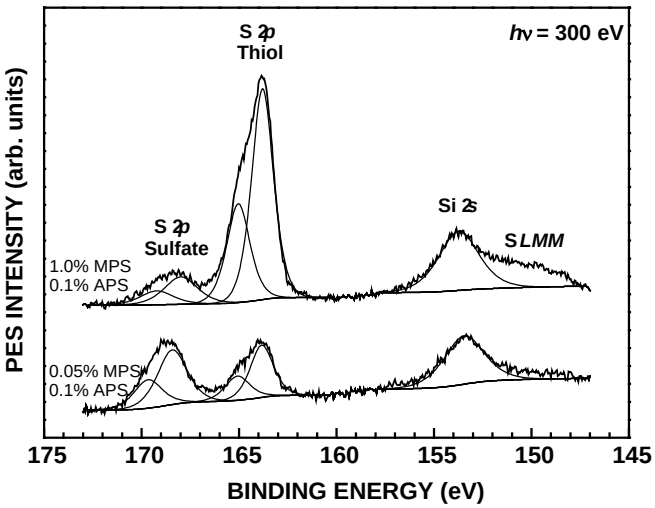


*Fig. 1: S 2p, Si 2s XPS photolines and S LMM Auger signal measured at a synchrotron using 300 eV photon energy. MPS concentration in the solution was 1.0 vol-% (top) and 0.05 vol-% (bottom). The higher binding energy S 2p corres-ponds to sulphate. The lower binding energy photoline indicates the presence of MPS thiol groups. The layer thickness and silane concen-tration were approximately the same, but a clear correlation can be seen between the thiol surface coverage and MPS concentration in the solution.*

**DISCUSSION & CONCLUSIONS:** We have shown that a high quality, monolayer thick silane layers can be fabricated on stainless steel surface and that the properties of bioactive layer can be readily controlled via the properties of the substrate and silane layer.

**REFERENCES:** [1] P. Jussila, H. Ali-Löytty, K. Lahtonen, M. Hirsimäki, and M. Valden, *Surf. Interf. Anal.* **42** (2010) 157-164.

**ACKNOWLEDGEMENTS:** The Academy of Finland (Grant Nos 5205296, 5213914, 5210276, and 5110328) and the National Technology Agency of Finland (Grant Nos 160951, 161035, and 161111) are acknowledged for their financial support. Financial support by the Outokumpu Oyj Foundation, the Vaisala Foundation, and the National Graduate School in Materials Physics is also gratefully acknowledged.

# Glyco-Dendrimers for Lectin-Dimerization

Sung You Hong, Raghavendra Kikkeri, Mayeul Collot, Maha Maglinao, Bernd Lepenies, Peter H. Seeberger*

*Max Planck Institute of Colloids and Interfaces, Department of Biomolecular Systems, Research Campus Golm, 14424 Potsdam, Arnimallee 22, 14195 Berlin, Germany*

**INTRODUCTION:** Protein dimerization plays a fundamental role in cellular control mechanisms such as activation of signal transduction or cell membrane receptors where multiple supramolecular interactions are crucial.[1,2] The groups of Schreiber and Crabtree have shown synthetic chemical tools so-called chemical inducers of dimerization (CIDs), which can promote protein association.[2] Nguyen *et al.* demontrated hetero-/homo-protein dimerizations using supramolecular interactions between cucurbit[8]uril and phenylalanine-glycine-glycine tripeptide motif.[3] Here we report the construction of hetero glyco-dendimers via cyclodextrin and adamantane interaction, which have potential application as CIDs for lectin hetero-dimerization based on carbohydrate-lectin interaction.

**METHODS:** The adamantyl group is known to strongly bind to β-cyclodextrin (β-CD) by the near perfect match between the cavity and guest diameter (~7 Å). The association constant is approximately $3\times10^4$ $M^{-1}$.[4] Galactosyl dendron ($Gal^D$) was prepared from tris(hydroxylmethyl)aminomethanyl core motif. Couping *N*-(Tris[(2-ethylcarboxyl-ethoxy)methyl]) methylamine with NBoc-β-alanine, followed by saponification and esterifcation with pentafluorophenol (PFP) afforded **2** in 52% yield (3 steps). PFP ester was further reacted with 2-aminoethoxy per-acetylated galactose to give **3** in 75% yield. The 2nd generation galactose adamantane dendrimer **6** was obtained by conjugation of PFP ester-adamantane with **4**, followed by Zemplén de-esterification (69%, 2 steps).

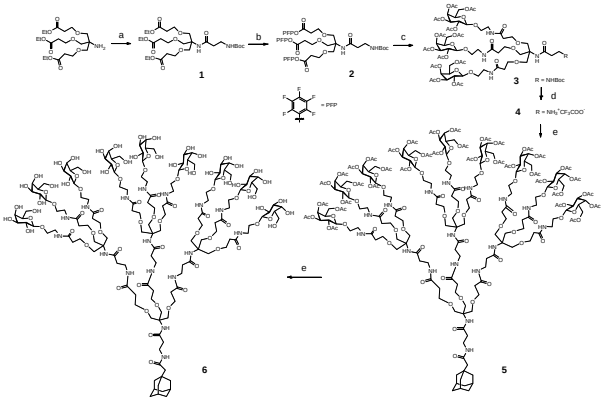

*Figure 1: Synthesis of nonapodal Gal-dendron **6**. (a) NBoc-β-alanine, DIC, HOBt•$H_2O$, DCM, 0 ℃→RT (74%); (b) (i) NaOH, EtOH, RT, (ii) pentafluorophenol, DIC, DCM, 0 ℃→RT, 70% (2 steps); (c) 2-aminoethoxy per-acetylated galactose, TEA, DCM, RT, 75%; (d) TFA, DCM, RT, 100%; (e) tripodal adamantine core, TEA, DCM, RT, 86%; (f) NaOMe, MeOH, RT, 80%.*

**RESULTS:** Nonapodal $Gal^D$-adamantane **6** was complexed with Man-CD in $D_2O$ (the host:guest ratio, 1:1) and measured *in situ* by ROESY and NOESY. Both spectra of the mixture of the $Gal^D$-adamantane **6** (2.8 μmol) and Man-CD (2.8 μmol) showed that the peaks of the adamantyl group correlate well with proton peaks of the β-CD cavity. Hetero lectin dimerization (Man-CD↔$Gal^D$-adamantane or Gal-CD↔$Man^D$-adamantane inclusion complexs) is under investigation with mannose binding ConA and galactose binding RCA.

**DISCUSSION & CONCLUSIONS:** Hetero-lectin dimerization was designed using reversible supramolecular interactions. The 2nd generation nonapodal mannose- and galactose-adamantane dendrimers were prepared bearing a tris(hydroxylmethyl)aminomethane core. Each dendrimer was complexed either with Gal-CD or Man-CD by 'adamantane-CD' host-guest interactions to afford hetero-glycodendrimers, which was checked by ROESY and NOESY spectra.

**REFERENCES:** [1] D. M. Spencer, T. J. Wandless, S. L. Schreiber, G. R. Crabtree, *Science* **1993**, *262*, 1019. [2] J. D. Klemm, S. L. Schreiber, G. R. Crabtree, *Annu. Rev. Immunol.* **1998**, *16*, 569. [3] H. D. Nguyen, D. T. Dang, J. L. J. van Dongen, L. Brunsveld, *Angew. Chem. Int. Ed.* **2010**, *49*, 895. [4] M. R. Eftink, M. L. Andy, K. Bystrom, H. D. Perlmutter, D. S. Kristol, *J. Am. Chem. Soc.* **1989**, *111*, 6765.

**ACKNOWLEDGEMENTS:** S.Y.H., R.K., M.C., M.M., and P.H.S thanks to MPI research funds. This template was modified with kind permission from European cells and Materials Conferences (http://www.ecmjournal.org/journal/meetings.htm).

European Cells and Materials Vol. 20. Suppl. 3, 2010 (page 115) ISSN 1473-2262

# Biodegradable Multilayered Systems with Incorporated siRNA Nanoparticles as a Powerful Technique for Local Drug Delivery

S. Hossfeld[1,*] H. Hartmann[1,*], U. Mittnacht[1,*], H. Oliveira[2], A.P. Pêgo[2], D. Stoll[1], B. Schlosshauer[1], R. Krastev[1]

[*] first three authors contributed equally to this work

[1] *NMI Natural and Medical Sciences Institute at the University of Tübingen, Germany.* [2] *INEB – Instituto de Engenharia Biomédica, Divisão de Biomateriais and Faculdade de Engenharia Universidade do Porto, Portugal.*

**INTRODUCTION:** Gene silencing triggered by small interfering RNA (siRNA) represent a new technology for the therapy of human diseases. RNA interference could be used as a drug that interferes with every desired disease-causing protein and thereby it inhibits the synthesis of designated target proteins[1]. We have developed a drug system for local time specific siRNA delivery. The system is based on biodegradable polyelectrolyte multilayers (PEMs), which have been explored as sophisticated coatings for controlled drug release. These coatings are used especially for biomedical applications such as implants, or targeted drug delivery devices. PEMs are built-up in a layer-by-layer (LbL) technique, which is based on the deposition of polycations and polyanions[2]. The coatings can be functionalized with drugs, proteins or oligonucleotides that are released subsequently from the alternating layers during decomposition of the PEM.

**METHODS:** The biocompatible PEM were formulated from natural polysaccharides. They were loaded with siRNA using siRNA/polymer nanoparticle aggregates (NP). The PEMs were deposited on planar glass substrates using an additional deposition step in the LbL technique. The build up of PEM with incorporated siRNA NP was analyzed by quartz crystal microbalance (QCM) and fluorescence spectroscopy. The size and zeta potential of siRNA NP were analyzed with photon correlation spectroscopy. The sizes of siRNA NPs ranged from 150-350 nm and show positive zeta-potentials. The sustained release of siRNA by erosion of PEMs in different solutions was monitored over time by measuring fluorescence intensity of the released particles in the solution.

**RESULTS:** In cell culture PEMs with incorporated NP show low cytotoxicity with resazurin assay and the cellular uptake of NP resulted in a homogenous distribution in the cell cytoplasm analyzed by microscopy. The use of

PEM have allow for long term controlled release of the incorporated siRNA containing nano particles. The release kinetic was followed for up to two weeks.

**DISCUSSION & CONCLUSIONS:** PEMs with incorporated siRNA nanoparticles are an innovative system which could be used for controlled drug delivery tool. The obtained coatings allow biological functionalization of structural implants and assure controlled and sustained release. The obtained coatings have low toxicity and better patient convenience over conventional formulations.

**REFERENCES:** [1] G. Meister, T. Tuschl (2004), *Nature* **431**: 343. [2] G. Decher, J.B. Schlenoff (2003) *Multilayer Thin Films: Sequential Assembly of Nanocomposite Materials*, Wiley-VCH, Weinheim.

**ACKNOWLEDGEMENTS:** Part of this work was financed by BMBF 13N10023ff, Germany.

# Polymeric nanomaterials in vaccine adjuvancy

Jeffrey A. Hubbell, Melody A. Swartz, Sachiko Hirosue, André J. van der Vlies, Diana Velluto, Conlin P. O'Neil, Eleonora Simeoni, Armando Stano, Chiara Nembrini, Susan N. Thomas, Iraklis Kourtis

*Ecole Polytechnique Fédérale de Lausanne (EPFL), Lausanne, Switzerland.*

**INTRODUCTION:** We present novel block copolymer amphiphiles for formation of subviral sized-nanoparticles bearing protein antigens or antigen-encoding DNA and additionally biomolecular adjuvants. Self-assembly is utilized to control size of the resulting particles in the 20-35 nm range, even with plasmid DNA as the biomolecular payload. These materials, by virtue of their ultrasmall size, can penetrate tissue interstitium and mucosal barriers to access antigen-presenting cells resident in lymph nodes or in mucosal-associated lymphoid tissues. We show that strong Th1 biases in immune response can be induced, much stronger than with co-delivery of antigen and adjuvant not associated to the carrier nanoparticles. Examples in vaccination *vs.* infectious diseases are being pursued.

**METHODS:** Our laboratory has recently described a novel family of AB and ABA block copolymeric amphiphiles that are capable of forming micelles and vesicles, as well as inverse emulsion-polymerized nanoparticles based on the B block using Pluronic emulsifiers. As a hydrophilic block A, we employ polyethylene glycol (PEG), because of its well known toxicological profile and its well-defined and low polydispersity. As a hydrophobic block, we have selected polypropylene sulfide (PPS), a low Tg polymer that can be synthesized by a ring opening living polymerization also with low polydispersity. We have demonstrated that these polymers form mesoscopic aggregates that are sensitive to oxidative environments by conversion of the hydrophobic PPS to the hydrophilic polypropylene sulfone; this provides a route of degradation of the micelle-forming amphiphile into a fully soluble low molecular weight polymer, sufficiently small for clearance by renal filtration. We have also sought to render these same structures sensitive to reduction, to allow destabilization of vesicles within the early endosome after endocytosis by linking the two blocks with a reduction-sensitive disulfide, for use in intracellular delivery, for example of adjuvant molecules targeting intracellular receptors (such as CpG DNA), antigens for targeted MHC 1 presentation, or antigen-encoding DNA. Thus, the redox sensitivity of these materials can be used to enable release of incorporated agents and ultimate elimination of the micelle-forming polymer.

**RESULTS:** Biodistribution studies performed with both PPS nanoparticles and PEG-PPS micelles showed extensive particle uptake in antigen presenting cells in the lymph nodes draining both intradermal and intramuscular injection sites. Surprisingly, antigen presenting cells in the spleen were also major targets by both routes of administration with subviral sized particles. With intranasal administration, nanoparticle presence in M cell and antigen presenting cells in the nasopharynx-associated lymphoid tissues was confirmed. With pulmonary instillation, more than 15% of pulmonary dendritic cells and remarkably 100% of pulmonary macrophages were targeted by the nanoparticles.

When conjugated to antigen in the absence of co-administration of a biomolecular adjuvant, the nanoparticles and micelles were capable of induction of a Th2-biased humoral but not cellular immunity when administered parenterally or intranasally. When co-administered with a biomolecular adjuvant such as CpG or co-conjugated to flagellin, the nanoparticles induced a Th1-biased humoral and cellular immunity by all three routes of administration. Challenge versus influenza and Mycobacterium tuberculosis demonstrated very favorable results.

**DISCUSSION & CONCLUSIONS:** By exploiting materials in the nanodimension, with sizes that are subviral, we were able to very efficiently target antigen presenting cells in the lymph nodes, in the spleen, in the mucosal-associated lymphoid tissues, and in the lung. This efficiency of targeting, along with conjugation of antigen and co-delivery or co-conjugation of biomolecular adjuvants, was able to obtain strong Th1-biased cellular and humoral immunity in mouse models of prophylactic vaccination versus infectious diseases.

**ACKNOWLEDGEMENTS:** This work has been funded by the European Commission (NanoImmune), the Bill and Melinda Gates Foundation, the Swiss National Science Foundation (32003B-120630) and by Mymetics Corp.

# An anisotropic changes in manganese ferrite nanoparticle by proton irradiation

Sung Wook Hyun, Sun Chun Hong, Sam Jin Kim, Chul Sung Kim

*Department of Physics, Kookmin University, Seoul 136-702, Korea*

**INTRODUCTION:** The magnetic nanoparticles (NPs) have been reported by many researchers with its scientific and technological interests [1-2]. Especially, the ferrite NPs have shown the novel magnetic properties caused by its small sizes and studied in the fields of hyperthermia, target drug delivery, and the magnetic resonance imaging (MRI) [3]. They were reported to have enhanced properties suitable for MRI reagents, when their sizes reach in nanometer scale [4]. In this report, we have performed with the magnetic properties and the hyperfine structure of $MnFe_2O_4$ NPs.

**METHODS:** $MnFe_2O_4$ NPs were prepared by a high temperature thermal decomposition (HTTD) way [1]. 1 mmol of manganese(II) acetylacetonate (acac), and 2 mmol of iron(III) acac were used to fabricate uniform NPs. 6 mmol of 1,2-hexadecanediol was mixed with both Mn and Fe acac in 20 ml phenyl ether. The mixture was heated up to 200 $^oC$ to dissolve and uniformly disperse the particles, and maintained for 30 min under Ar atmosphere. It was reheated up to 256 $^oC$ and maintained for 30 min to form the $MnFe_2O_4$. Then, it was cooled down to room temperature (RT) and the black $MnFe_2O_4$ powder was obtained. The obtained NPs, pressed into a pellet form, were irradiated with proton beam (5 MeV, 20 nA). Two irradiations were consecutively applied to the samples with dose of 5 pC/μm$^2$ (5 pC) and 10 pC/μm$^2$ (10 pC).

**RESULTS:** The crystal structure of $MnFe_2O_4$ was cubic spinel with space group of *Fd3m* by x-ray diffraction (XRD). The lattice constants decreased with increasing proton irradiation. The high resolution transmission electron microscopy (HRTEM) was measured to confirm the XRD measurement on the average particle size, which has 4.4 nm with comparatively uniform shapes.

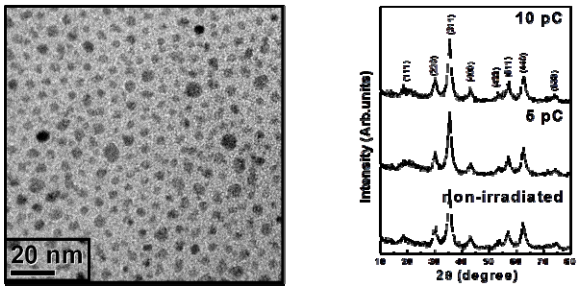


*Fig. 1: HRTEM image of $MnFe_2O_4$ (left) and x-ray patterns of proton irradiated $MnFe_2O_4$ (right).*

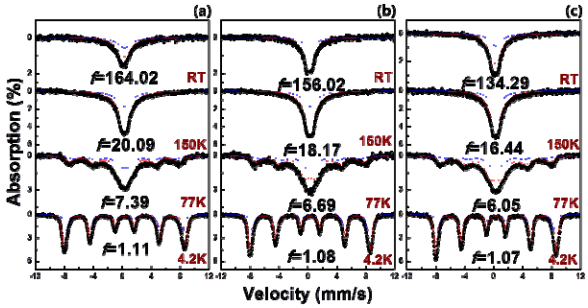


*Fig. 2: Mössbauer spectra of (a) non-irradiated, (b) 5 pC and (c) 10 pC $MnFe_2O_4$ NPs.*

The magnetization measurement was performed with vibrating sample magnetometer (VSM). The proton irradiated samples showed the smaller magnetization than one of non-irradiated sample. The hyperfine interaction between the Fe and its environment in the crystal lattice was characterized by Mössbauer spectroscopy. Mössbauer spectra were taken at various temperatures ranging from 4.2 K to RT. The 4.2 K spectrum presented the conventional $MnFe_2O_4$ material. The drastic line broadening for the temperature dependence was observed with proton irradiation.

**DISCUSSION & CONCLUSIONS:** Here, we have investigated 5 and 10 pC proton irradiated $MnFe_2O_4$ NPs prepared by HTTD. We have observed the decreases of the lattice constants, magnetization and relaxation frequencies. It suggests that the proton irradiation causes the breaking of super-exchange interactions, which leads to decrease of lattice constants. Also, the relaxation frequencies at RT decreased due to the proton irradiation, which leads to increasing of the magnetic anisotropy energy.

**REFERENCES:** [1] Y. Piao, et al (2008) *Nature Mater.* **7:**242-247. [2] D. Zhang, et al (2006) *Chem. Phys. Lett.* **426**:120-123. [3] Q. Song, et al (2007) *Chem. Mater.* **19**:4633-4638. [4] U. I. Tromsdorf, et al (2007) *Nano Lett.* **7**:2422-2427.

**ACKNOWLEDGEMENTS:** This work was supported by Basic Science Research Program through the National Research Foundation of Korea (NRF) grant funded by the Korea government (MEST)(2010-0000851 and 2009-0083645)

European Cells and Materials Vol. 20. Suppl. 3, 2010 (page 118) ISSN 1473-2262

# Biodegradable Ternary Nanocomposites with Improved Mechanical Properties

J. Idaszek [1], A. Bruinink[2] W. Święszkowski[1], K.J. Kurzydłowski[1]

[1] *Warsaw University of Technology, Warsaw, Poland,* [2] *EMPA, Switzerland*

**INTRODUCTION:** Poly(ε-caprolactone), PCL, is a biodegradable, biocompatible and highly processible polyester, therefore it is of great interest for biomaterials.[1] The disadvantage of the polymer is its lack of bioactivity, very slow degradation rate and low mechanical properties. Addition of bioactive inorganic nanoparticles to the polymer matrix leads to an increase of the Young's modulus but at expense of the tensile strength at higher concentration of the filler, thus limiting its concentration.[2] The main reason of weakening of the strength is poor adhesion of the filler particles to the polymeric matrix. Our approach to reinforce the composite was to prepare a ternary composite comprised of PCL blended with poly(D,L-lactide-*co*-glycolide), PLGA, as a polymer matrix, and hydroxyapatite (HA) nanoparticles.

**METHODS:** Four composites were prepared with different concentrations of PLGA (Resomer RG 504 H, i.v. 0.45-0.60 dl/g, Boehringer-Ingelheim, Germany), which was mixed with HA and dissolved in methylene chloride (see *Tab.1*). The nanoparticles were dispersed by means of ultrasonic processor. Subsequently, the PCL ($M_n$=80 kDa, Sigma-Aldrich, USA) was added. The suspension was cast into Petri dishes and dried in the fume hood for 2h and subsequently in vacuum oven (100 mbar, 40 ºC, 48h). Afterwards the membranes were cut into pieces. A solid freeform fabrication device (Bioscaffolder, SYSENG, Germany) was used to form fibres at 90ºC with a volume dispensing speed 200 rpm and dispense pressure 5 bars. The inner diameter of the needle was 330 µm. Tensile test at the fibres were carried out on a MTS Tytron 250, Microforce Testing System (MTS, USA) at a cross-head speed of 15 mm/min. The ultimate strength was calculated from the maximum stress on the strain-stress curve.

**RESULTS:** The maximum elongation of all the fibres exceeded 360%. The mechanical tests showed that all ternary composites had significantly higher values of the Young's modulus than the pure PCL (see *Fig 1).* The highest ultimate strength has been reached for composites with 15 and 25 wt% of PLGA.

| Name | PCL (wt %) | PLGA (wt %) | HA (wt%) |
|---|---|---|---|
| PCL | 100 | 0 | 0 |
| PCL_95 | 95 | 0 | 5 |
| PCL_90 | 90 | 5 | 5 |
| PCL_80 | 80 | 15 | 5 |
| PCL_70 | 70 | 25 | 5 |

*Table 1: Composition of the prepared materials.*

*Fig. 1: Effect of the PLGA concentration on a) the Young's modulus and b) Ultimate strength of the fibres. * p<0.05, ** p<0.01 vs PCL95 (Tukey-Kramer post-hoc ANOVA)*

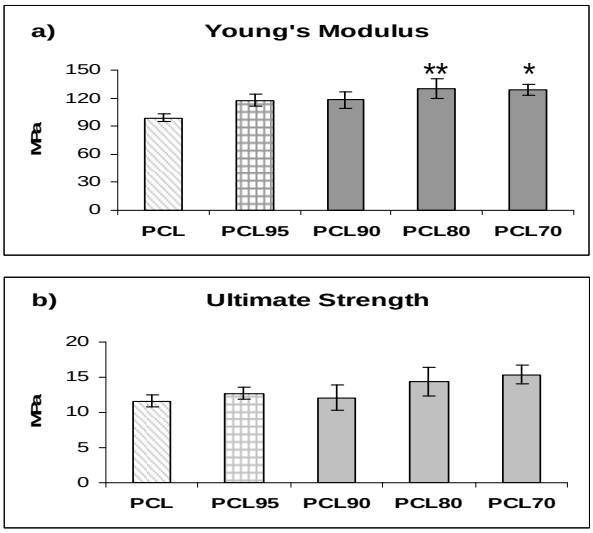


**DISCUSSION & CONCLUSIONS:** Addition of PLGA and HA had a significant positive effect on mechanical properties of the composite. We assume that this was caused by better adhesion of PLGA to HA as well as by stronger interactions between PLGA and PCL than for pure PCL and HA.

**REFERENCES:** [1]L.S. Nair, C. T. Laurencin (2007) *Prog Polym Sci* **32**:762-798. 2M.Z. Rong et al., (2004) *Polym Int* **53**:176–183

**ACKNOWLEDGEMENTS:** This work was supported by the European Regional Development Fund within the Innovative Economy Operational Programme in the frame of project BIO-IMPLANT (Grant No. POIG.01.01.02-00-022/09).

European Cells and Materials Vol. 20. Suppl. 3, 2010 (page 119) ISSN 1473-2262

# Biomolecules Adsorption onto Ordered Mesoporous Carbon

M. Ignat, I. Alexa, E. Popovici

*Department of Chemistry, Laboratory of Material Chemistry, Al. I. Cuza University, Iasi, Romania*

**INTRODUCTION:** The production of mesoporous carbons is extremely important for their applications in the adsorption and separation of biomolecules that are too large to enter micropores[1]. The mesoporous carbons with uniform and tunable mesopore sizes are essential for the adsorption of large bio-molecules. Therefore, the preparation of well ordered large cage type mesoporous carbon with reliable control of textural parameters, such as specific pore volume, specific surface area and pore diameter, is critical for the envisaged applications in the separation and adsorption of giant molecules such as proteins, vitamins and alkaloids. Direct peptide binding on mesoporous carbon materials suggests roles of specific amino acids in direct protein interaction with carbons. For sensing or for any other intended application, a more detailed picture on bridging mesoporous carbon materials with biological systems should be essential in designing life sciences-related tools employing these nanomaterials.

**METHODS:** The first ordered mesoporous carbon that was a faithful replica of the template was synthesized employing SBA-15 as a template[2] and glycerol as carbon precursor[3].

**RESULTS:**

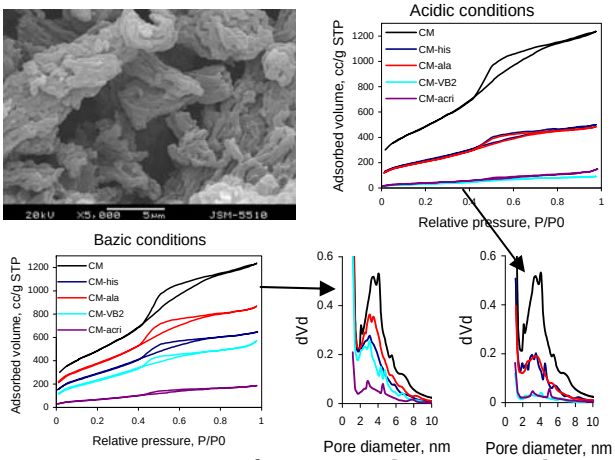


*Fig. 1: SEM image of CM; N2 adsorption isotherms and PSDs of CM before and after adsorption to biomolecules in acidic and basic conditions.*

The carbon material consists of uniformly sized carbon rods arranged in a hexagonal pattern. At first sight, it was rather surprising that SBA-15 leads to the stable carbon replica CMK-3. Unconnected channels should not lead to the formation of a free-standing 3D structure but rather to disconnected carbon rods. However, there is growing evidence since the discovery of SBA-15 that there are micropores connecting the mesoporous channels[4]. Since the connecting micropores are also filled with carbon precursor, they form structure-supporting links between the carbon rods.

*Table 1. Textural properties and adsorbed quantities of biomolecules calculated from TOC results.*

| Sample | | S, $m^2/g$ | $V_p$, cc/g | Pore diam, nm | mg of bio/g of CM |
|---|---|---|---|---|---|
| CM | | 1863 | 1.91 | 3.5 | |
| CM-his | b | 1118 | 1.00 | 3.1 | 339 |
| | a | 813 | 0.77 | 3.5 | 351 |
| CM-ala | b | 1416 | 1.34 | 3.5 | 330 |
| | a | 779 | 0.75 | 3.5 | 358 |
| CM-$VB_2$ | b | 935 | 0.88 | 3.1 | 377 |
| | a | 129 | 0.14 | 3.3 | 459 |
| CM-acri | b | 284 | 0.29 | 3.1;4.5 | 457 |
| | a | 154 | 0.23 | 3.5 | 465 |

**DISCUSSION & CONCLUSIONS:** The adsorption of proteins from solution onto solid surfaces has attracted much attention due to its scientific importance and applications in many areas, such as biology, medicine, biotechnology and food processing[5]. Amino acids are used on a large scale as supplement to stock feed and for the improvement of proteins in food technology. In this context, mesoporous carbons have been tested as adsorbents for the adsorption of amino acids from aqueous solution. The adsorption capacity of mesoporous carbons for vitamin $B_2$ (riboflavin), also studied in this work, was significantly higher than that achieved with mesoporous silica[6]. Synthesized mesoporous carbon was also tested as adsorption and drug delivery systems for the controlled release of acriflavine, an antiseptic drug, being used as well as dye.

**REFERENCES:** [1]A.Vinu, C.Streb, V.Murugesan M.Hartmann, *J. Phys. Chem. B*, **2003**:*107*, 8297. [2]S.Ju, S.H.Joo, R.Ryoo, M.Kruk, M.Jaroniec, Z.Liu, T.Ohsuna, O.Terasaki, *J. Am. Chem. Soc.* **2000**, *122*, 10712. [3]M.Ignat, C.J.Van Oers, J.Vernimmen, M.Mertens, S.Potgieter-Vermaak, V.Meynen, E.Popovici, P.Cool, *Carbon*, **2010**:*48*, 1609. [4]M. Hartmann, A. Vinu, *Langmuir* **2002**:*18*, 8010. [5]T.A. Horbett, J.L. Brash, Proteins at Interfaces II: Fundamentals and Applications, *Am Chem Soc*, Washington, DC, 1995. [6]M.Hartmann, *Chem. Mater.* **2005**, *17*, 4577.

# Highly Non-linear Response of Dipolar Colloidal Gels

Patrick Ilg[1], Emanuela Del Gado[2]

[1] *ETH Zürich, Department of Materials, Polymer Physics, Switzerland.* [2] *ETH Zürich, Department of Civil Engineering, Institute for Building Materials, Switzerland.*

**INTRODUCTION:** Suspensions of dipolar colloids can form not only chain-like aggregates, but show also pseudo-crystalline ordering under certain conditions [1]. Recently, computer simulations of colloids with extended dipoles have shown that a percolating network of cross-linked chains appears at low temperatures [2]. Starting from this model, we here analyze the properties of the network structure in different state points and investigate the response of the system to an external electric field.

**METHODS:** We perform numerical simulations of $N$ interacting, charged soft dumbbells, where each dumbbell carries two opposite point charges $q$ at a fixed distance $d$, forming a finite dipole $p=qd$. Due to the charges, particles interact via (unscreened) Coulomb potential. In addition, particles experience a soft, short-range repulsion, which prevents permanent aggregation. The model system and parameters are taken from [2], where the dumbbells consist of two interpenetrating spheres that are separated by roughly 20% of the particle diameter. Note, that the electric dipoles can also be interpreted as magnetic dipoles. We typically study systems of 1000 dumbbells at different state points. For volume fractions $\varphi$ = 0.033, 0.048, and 0.065, well-equilibrated configurations are prepared by molecular dynamics simulations via slowly cooling statistically independent samples from the high temperature phase.

**RESULTS:** For rather high temperatures, we observe the formation of chain-like aggregates with an exponential distribution of chain lengths as theoretically expected [1]. For lower temperatures, the cluster size distribution shows a power-law decay with an exponent 2.2 that is typical for random percolation. This result indicates a transition from an ensemble of individual chains to a connected, at least instantaneously, percolating network (see Fig. 1, top and Ref. [2]). The network formation is accompanied by a significant change of dynamical behaviour, like the occurrence of anomalous diffusion and stretched exponential relaxation [2,3].

Next, we apply an external electric field $E$, which adds the extra force $qE$ to all charges. In the chain-formation regime, we observe a typical paraelectric (or paramagnetic) behaviour, where

the induced polarisation increases linearly with the strength of the external field before it satures. In the network regime, however, a linear regime seems to be absent since the network suppresses dipole reorientation for small fields. After reaching a critical field strength, the network transforms into a system of bundled chains, such that the induced polarisation increases very steeply.

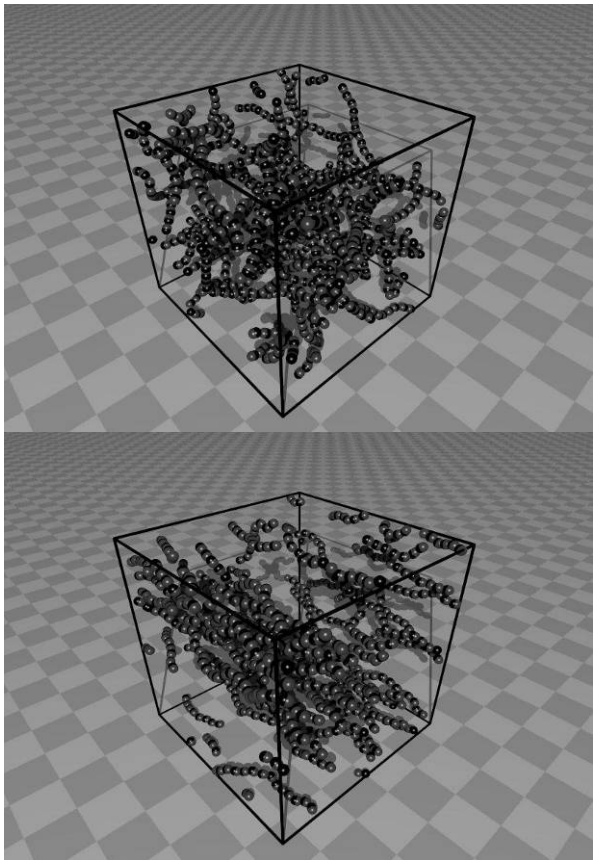

*Fig. 1: Snapshots of particle configuration in the network regime (top) and after applying a strong external field (bottom).*

**DISCUSSION & CONCLUSIONS:** The strong structural changes upon applying an external field allow for direct manipulation of the dielectric and mechanical properties of dipolar colloids, which could lead to interesting applications as smart materials.

**REFERENCES:** [1] S. Odenbach (ed.) (2008) *Colloidal Magnetic Fluids*, Lecture Notes in Physics, Springer. [2] R. Blaak, M.A. Miller, J.-P. Hansen (2007) *EPL* **78**: 26002. [3] E. Del Gado, W. Kob (2010) *Soft Matter* **6**:1547-58.

# A rapid antibody isolation system (RAntIS) based on *in vitro* immunization

T.Inagaki[1], M.Kawahara[2], T.Nagamune[1,2]

[1] *Department of Bioengineering, The University of Tokyo, Tokyo, Japan.* [2]*Department of Chemistry and Biotechnology, The University of Tokyo, Tokyo, Japan.*

**INTRODUCTION:** An *in vitro* approach in immunotechnology for producing monoclonal antibodies, *in vitro* immunization, was proposed in 1980's. [1-2] B lymphocytes are exposed to antigens *in vitro* and are further stimulated by thymocyte-derived lymphokines. However, they are poorly reproducible methods due to lot-to-lot variation of thymocyte-derived lymphokines. Other supportive media including mitogens, adjuvant peptides and a combination of cytokines and mitogens have been used to stimulate antigen-exposed B lymphocytes. However, these studies did not analyze whether such stimuli could trigger various immune responses such as somatic hypermutation (SHM). We focused on both the induction of activation-induced cytidine deaminase (AID) and the formation of germinal center (GC) to induce SHM in antigen-specific immunoglobulin genes.

**METHODS:** A cell suspension of splenocytes was prepared from 4–6-week-old female BALB/c mice. The splenocytes were dispersed through a sterilized nylon mesh (70 μm; Becton Dickinson & Co.). Following lysis of the red blood cells with ACK lysis buffer, the remaining splenocytes were suspended in RPMI 1640 containing 25 mM HEPES. Splenocytes ($1 \times 10^7$ cells) were placed in a 15 ml tube and exposed to the antigen (1 μM) and muramyl dipeptide (50 μg/ml) for 15 min at room temperature. The following stimuli were added to antigen-exposed splenocytes in various combinations: IL-4 (10 ng/ml), IL-5 (10 ng/ml), LPS (40 μg/ml, *Escherichia coli* 0111:B4), anti-CD38 antibody (αCD38, NIMR-5, 10 μg/ml), anti-CD40 antibody (αCD40, 1C10, 10 μg/ml). Cells were resuspended in RPMI 1640 supplemented with 40% FCS ($2–4 \times 10^6$ cells/ml), and cultured for several days. The expression level of activation-induced cytidine deaminase (AID) mRNA was analyzed by Real-time PCR method and the expression of surface markers of germinal center (GC) B cell were analyzed by flowcytometer. The activity of scFv clones were analyzed by ELISA.

**RESULTS:** We identified a combination of T cell-dependent stimuli (IL-4, IL-5, anti-CD38 and anti-

CD40 antibodies) that stimulates antigen-exposed splenocytes followed by induction of germinal center B cells *in vitro*. We also observed that lipopolysaccharides induced high expression levels of AID mRNA. We stimulated antigen-exposed splenocytes, followed by the induction of somatic hypermutation in immunoglobulin genes and selective expansion of antigen-specific antibody producing positive cells. This method enabled quick (~10 days) and efficient (23.3% of randomly selected clones had affinity to antigen peptides) generation of antigen-specific monoclonal scFv clones, even though the antigen was a small peptide (angiotensin I, 10-mer), without conjugation to carrier proteins.

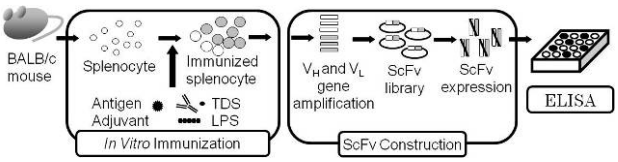


*Fig. 1: Schematic representation of RAntIS .*

**DISCUSSION & CONCLUSIONS:** The GC consists of activated B cells that exhibit rapid proliferation and mutation through SHM and class switch recombination (CSR). A key factor for SHM and CSR is AID. Because RAntIS induced both high expression of AID and formation of GC, we were able to achieve high efficiencies.

Interestingly, B cells were activated even by a small peptide as an antigen, and GC B cells with antigen-specific antibody genes were generated with high efficiency. This is noteworthy because we used only a small peptide that could not cross-link BCRs. Because RAntIS immunized splenocytes with a high concentration of peptide antigen (8 μM) during exposure, RAntIS might induce the enhanced aggregation of antigen/BCR complexes on lipid rafts and achieve stronger induction of BCR signaling than other methods.

**REFERENCES:** [1]Borrebaeck, C.A. (1983) *Scand J Immunol* **18**, 9-12. [2]Boss, B.D. (1984) *Brain Res* **291**, 193-196.

# Measurement of Condensation Speed and Size of Single Globular DNA Molecule by Laser Trapping

T. Ishido[1], M. Ishikawa[1], K. Hirano[1]

[1] *National Institute of Advanced Industrial Science and Technology (AIST), Japan.*

**INTRODUCTION:** Using the process of DNA condensation, a single huge DNA molecule can be trapped and manipulated directly in free solution, avoiding fragmentation [1]. We describe here the measurement of condensation speed in real-time observations of single globular DNA molecules, the direct sizing of the single condensed molecules by laser trapping, and their subsequent reuse in PCR for future single genome molecule analysis.

**METHODS:** The DNA samples used were λ and T4 phage DNA (Nippon Gene, 48.5 and 166 kbp, respectively) and two sections of chromosomal DNA from the yeast *Saccaromyces cerevisiae* (285 and 365 kbp from chromosomes VI and III, respectively).

For measuring condensation speed, one end of a single DNA molecule of λ phage DNA (48.5 kbp) was fixed on the channel surface of a PDMS chip. Condensation was started by exchanging the solution inside the channel with the condensing agents PEG (60 mg/mL) and $MgCl_2$ (30 mM).

For sizing, single globular DNA molecules were trapped optically with a Nd:YAG laser beam. The suitable laser power for trapping the single molecules was determined using various nanospheres of known sizes.

We also investigated the feasibility of reusing the same single (λ phage) DNA molecule condensed by PEG and $MgCl_2$ treatment for subsequent PCR.

**RESULTS:** Figure 1(a) shows the real-time observation of condensation, with the time course of condensation used for calculating the speed shown in Fig. 1(b). The condensed DNAs were categorized as simply condensed DNA or surface interacted DNA. The condensation speed of the former was a very fast 123.4 kbp/s.

For sizing, first, using known-sized nanospheres, critical velocity at a laser power of 800 mW was found to be optimal. By exploring the dependence of critical velocity and trapping force on particle diameter by using the known-sized nanospheres, it was revealed that the use of critical velocity can effectively size single globular huge DNA molecules of unknown radii. As shown in Fig. 2, yeast chromosome III (285 kbp) was sized successfully (281 ± 40 kbp) from a calibration curve scaled using λ, T4 phage, and yeast

chromosome VI (48.5, 166, and 385 kbp, respectively). In addition, PCR efficiency was found not to be deteriorated by the presence of the condensing agents PEG and $MgCl_2$.

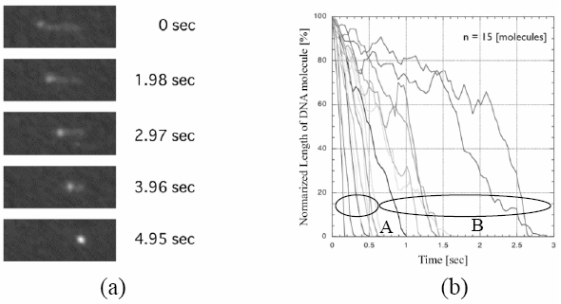


*Fig. 1: (a) Real-time observation of condensation of a single DNA molecule. (b) Time course of change in length of DNA molecules during condensation. The condensed DNAs were categorized as simply condensed DNA (region A) or surface interacted DNA (region B).*

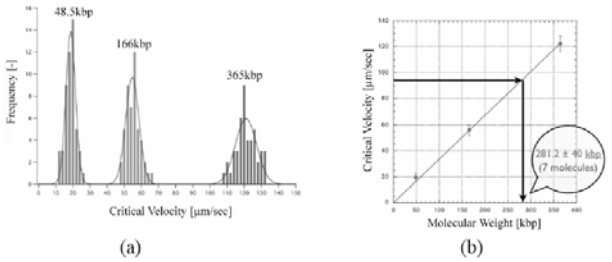


*Fig. 2: (a) Histograms of critical velocities of various sized DNA molecules measured by laser trapping. (b) Calibration curve obtained from (a).*

**DISCUSSION & CONCLUSIONS:** The high-speed PEG and $MgCl_2$ condensation and sizing method allowing direct observation of single DNA molecules of unknown radius is simple and quick to perform. It also allows the molecule to be reused in subsequent biochemical treatments such as PCR. As the PEG-Mg condensation is a reversible reaction, so we are now try to measure the decollapse speed of condensed DNA molecules.

**REFERENCES:** [1] Y. Matsuzawa, K. Hirano, K. Mori, et al (1999) *J Am Chem Soc* **121**:11581-2.

**ACKNOWLEDGEMENTS:** This study was supported by a grant form the Industrial Technology Research Program from NEDO.

European Cells and Materials Vol. 20. Suppl. 3, 2010 (page 123) ISSN 1473-2262

# Nanoforce Measurement During Protein Adsorption to Well-controlled Polymer Brush Surfaces

Kazuhiko Ishihara, Tomoaki Nakanishi, Madoka Takai and Yuuki Inoue

*Department of Materials Engineering, Department of Bioengineering, School of Engineering, The University of Tokyo, Tokyo 113-8656, Japan and Core Research for Evolutional Science and Technology (CREST), Japan Science and Technology Agency, Tokyo 102-0075, Japan.*

**INTRODUCTION:** When the materials get contact with blood, non-specific protein adsorption occurs on the surface and the protein adsorption layer induces much severe biological responses including cellular reactions. Therefore, evaluating the first protein adsorption is important for preparing the nonbiofouling surfaces. To clarify the protein adsorption behavior on polymer brush layers, the precise surface characterizations and contrast of the repellency of protein adsorption on polymer brush layers should be performed[1]. In this study, we notified the chemical structure of the well-defined polymer brush layer with various hydrophilic groups: phosphorylcholine (PC), sulfoxybetaine, carboxybetaine (zwitterionic), and poly(ethylene glycol) chain, and hydroxyl group (nonionic), and examined the effects of the chemical structure of the polymer brush layers on initial protein adsorption behavior.

**RESULTS AND DISCUSSION:** Polymer brush surface was prepared by the method reported previously[1]. The kinetic analysis during the surface-initiated atom transfer radical polymerization represented that the graft polymerization proceeded in a living manner. So, we could obtain polymer brush layer with 1-20 nm in thickness on the substrate. The density of every polymer chains and surface coverage with them were high enough to form dense polymer brush structure. In particular, hydroxyl group bearing polymer brush structure showed highest graft density. Among the zwitterionic polymer brush structures, both of the graft density and surface coverage of sulfoxybetaine group and carboxybetaine group bearing polymer chains were higher compared with those of the PC group bearing polymer chains.

The amount of adsorbed protein from 100 % serum on polymer brush layers was quantified using quartz crystal microbalance with dissipation (QCM-D). Protein adsorption on the every zwitterionic polymer brush layers apparently decreased with the increasing thickness of these grafted polymer layers from 1nm to 10nm in thickness, however, it became almost constant above 10 nm in thickness. For example, it was 17 ng/cm$^2$ on PC group bearing polymer-grafted substrate; however, it was 180 ng/cm$^2$ on nonionic polymer-grafted substrate with the thickness close to 15 nm. That is, the amount of proteins adsorbed on thicker hydroxyl group bearing polymer brush layer was 10 times more than that on PC group bearing polymer brush layer.

Atomic force microscopy (AFM) makes it possible to directly measure the forces generated by protein-surface interaction in aqueous media down to the few piconewtons range. Measurement was performed in contact mode in PBS at room temperature, using bovine serum albumin (BSA)-immobilized AFM cantilever. The scan rate was 1 Hz. In each force measurement, 100 approaching/retracting force-versus-distance curves were collected, and the average value was defined as the adsorption force between the protein and the surfaces. The value of control substrate (Initiator immobilized surface) was 1.3-1.4 nN. On the surface of hydroxyl group bearing polymer brush layer, the adhesion force depended on the thickness of the graft layer very significantly, on the other hand, the dependence was not clear in the case of PC group bearing polymer brush layers and it was quite low (~0.1 nN).

From both observations, amount of protein adsorption and adsorption force of protein, we concluded that the chemical structure of the polymer brush layer was the significant factor for excellent protein adsorption resistance even though it had a dense polymer brush structure. On the surface of hydroxyl group bearing polymer brush layer, adsorption force was almost the same as that on zwitterionic group bearing polymer brush layers; however, the amount of protein was larger. This may be due to conformational change of protein at the surface after first contact to the surface. The zwitterionic group bearing polymer brush layers maintain the natural conformation of proteins even when they contact with the surface.

Finally, we confirmed that the zwitterionic group bearing polymer brush surface is one of the candidate surfaces with nonbiofouling characteristics.

**REFERENCES:** [1] K. Kitano, Y. Inoue, T. Konno, et al. (2009) *Coll Surf. B: Biointerface* **74**: 350-7.

# Self-Assembled Nanostructures from Organic Bolaamphiphiles for Gene Delivery

N. Jain, Y. Arntz, V. Goldschmidt, G. Duportail, Y. Mely, Andrey S. Klymchenko

*LBP, UMR 7213 CNRS, Faculté de Pharmacie, Université de Strasbourg, France*

**INTRODUCTION:** The success in gene therapy relies strongly on new efficient gene delivery vectors. Nonviral vectors based on lipids and polymers constitute an important alternative to the viral vectors. However, the key problem with these vectors is poor structural control of their DNA complexes. Unsymmetrical bolaamphiphiles (bolas) bearing positively charged and neutral head groups could be an attractive alternative. These molecules can generate asymmetric membranes (in form of vesicles or nanotubes) having positively charged inner and neutral outer surfaces, where the inner membrane surface can be used to wrap the DNA molecule. The current work presents new bolaamphiphiles, characterization of their assembly with DNA and application for gene delivery.

**METHODS:** The design methodology is based on bola molecules bearing neutral sugar (gluconic or lactonic) and ornithine di-cationic residues as head groups, connected by a long hydrophobic spacer (Fig. 1). Gel Electrophoresis in 0.9% agarose was used to study interaction of bolas with DNA. DNA condensation within the bola-DNA complexes (bolaplexes) was followed by ethidium bromide (EtBr) exclusion assay. Size and charge of the bolaplexes at different N/P ratios was examined by Dynamic Light Scattering (DLS) and Zetasizer respectively. Atomic Force Microscopy (AFM) in liquid phase with tapping mode was performed to study the morphology of bolaplexes. Transfection efficiency of the bolaplexes was tested for different formulations by luciferase assay. DOPE, a helper lipid, or an endosmolytic reagent chloroquine was used in the formulations. Cytotoxicity of the bolas was analyzed by MTT-based assay.

**RESULTS:** New unsymmetrical bolaamphiphiles were synthesized. Strong interaction of bolas with DNA was observed with particle size of ~200-300 nm. Moreover, an increase in size and surface charge of bolaplexes was noticed at higher N/P ratios. AFM studies reveals nano-structural rod shaped or spherical morphology of bolaplexes. Transfection efficiency of the bolaplexes improves considerably using DOPE or chloroquine, as helping agents. Finally, all bolas showed low cytotoxicity (cell viability >80%).

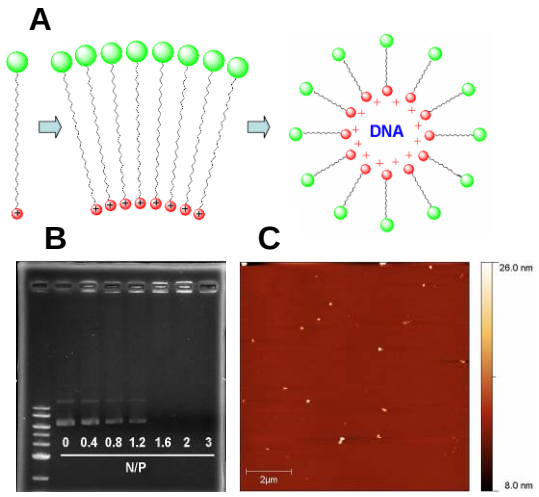


*Fig. 1: Schematic presentation of bolaamphiphile and its assembly with DNA (A). Gel electrophoresis (B) and AFM images (C) of bola-DNA complexes.*

**DISCUSSION & CONCLUSIONS:** Obtained data suggests that the size and shape of the bolaplexes depends on bola structure and the formulation used. The increase in size at higher N/P ratio is probably related to charge neutralization which is in line with zeta potential analysis. Increase in transfection efficiency with the use of DOPE or chloroquine suggests that the key barrier for their internalization can be endosomal escape. Thus, the new bola molecules show the potential for construction of nonviral vectors featuring controlled small size, high efficiency and low cytotoxicity.

**REFERENCES:** [1]Zuber G., Daut, E., Nothisen M., Belguise P. & Behr J.P. Adv Drug Deliv Rev **52**, 245-253 (2001).[2]Shimizu T., Masuda M. & Minamikawa H. Chemical Reviews **105**, 1401-1443 (2005).[3]Fuhrhop J.H. & Tank H. Chemistry and Physics of Lipids **43**, 193-213 (1987). [4]Masuda M. & Shimizu T. *Langmuir* **20**, 5969-5977 (2004).

**ACKNOWLEDGEMENTS:** We acknowledge financial support of FRM. We thank to the groups of J.-S. Remy and B. Frisch for help with luminometry and DLS measurements.

# Can SBF methods be used to predict the bioactivity of different titanium surfaces?

S.Jegou[1], J.Hall[2]

[1] *Nobel Biocare AG, Zurich, Switzerland.* [2] *Nobel Biocare AB, Gothenburg, Sweden.*

**INTRODUCTION:** Simulated Body Fluids (SBF), first introduced by Kokubo in 1991, are aqueous solutions containing ions with concentrations mimicking those found in nature in blood plasma but they are supersaturated with respect to calcium phosphates. These solutions are extensively used today by the scientific community and are believed to reveal the bioactivity of a material, i.e. its ability to bond bone in vivo. This is done by evaluating its ability to spontaneously form an apatite layer on its surface in vitro, in a similar manner that it's been observed in vivo on bioactive materials such as bioglasses. The aim of this study is to evaluate the potential of using several SBF solutions in predicting the bioactivity of two commercial dental implant surfaces, TiUnite® and machined titanium which showed already a different response in vivo.

**METHODS:** Both discs and screw implants with a TiUnite® or a machined titanium surface were used. TiUnite® consists of a thick and porous $TiO_2$ layer that is electrochemically grown on titanium by spark anodization. For the experiments with the discs SBF solutions after the international standard ISO 23317[1] and Bohner (SBF-JL2[2]) were employed. SBF-JL2 is a new solution and should be used in an incubator with controlled $pCO_2$ of 0.05 atm to mimic the physiological conditions. For the screw specimens the same ISO standard and 3 own solutions with 3 different calcium and phosphate ion concentrations were used with 1.5, 2, and 3 times the concentration of the ISO standard. All the implants were attached to a nylon wire and dipped into SBF solutions for 1, 4, and 10 days, 1 to 4 weeks, in an oven regulated at 37°C. For the tests with SBF-JL2, an incubator set at 37°C and $pCO_2$ = 5% was used instead. After dipping, the specimens were removed from the solution and gently rinsed with distilled water and dried. The surfaces of the specimens were analysed by means of XRD, SEM, and FTIR.

**RESULTS:** FTIR, XRD and SEM analyses showed the formation of a continuous layer of nanosized hydroxyapatite (HA) crystals on the surface of both machined titanium and TiUnite® specimens dipped into SBF-JL2, SBFx2, and SBFx3 (Figure 1). The thickness of the HA layer was similar for the machined and TiUnite® implants and increased with increasing dipping time. On the contrary, no HA layer could be observed on the specimens dipped into ISO 23317 whereas only a very thin HA layer could be observed on both titanium surfaces with SBFx1.5.

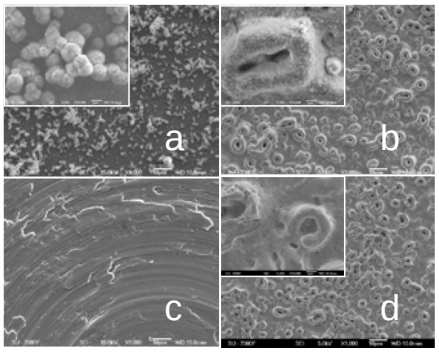


*Fig.1: SEM micrographs of machined titanium and TiUnite® discs dipped for 4 days into SBF-JL2 (a,b), machined titanium and TiUnite® discs dipped for 4 weeks into ISO 23317 (c,d).*

**DISCUSSION & CONCLUSIONS:** The original purpose of using SBF solutions was to have a simple and fast screening tool for the osseointegration potential of a surface without using animal studies. In this study two completely different surface topographies and Titanium dioxide surface compositions were used and tested with several SBF compositions. No influence of the topography or composition could be found, i.e. there was always HA precipitation for the solutions with higher ionic concentrations compared to ISO 23317. Using the SBF composition according to the ISO standard gave no HA precipitation at all. Therefore we question the discriminating power of SBF tests. Alternative in vitro methods, incorporating proteins for instance, should be considered to get a better correlation between the results observed in vivo and better understand the mechanisms of osseointegration.

**REFERENCES:** [1] M. Bohner, J. Lemaitre (2009) *Biomaterials* **30**:2175. [2] Kokubo (2007), ISO 23317.

**ACKNOWLEDGEMENTS:** The authors would like to thank Prof. Shen's group at Stockholm University, Sweden, and C.Combes, I.Demnati, O.Marsan, and C.Rey from CIRIMAT, Toulouse, France, for their precious contribution to this work.

European Cells and Materials Vol. 20. Suppl. 3, 2010 (page 126) ISSN 1473-2262

# Shear-Driven Motion of Supported Lipid Bilayers in Microfluidic Channels

P.Jönsson[1], MP.Jonsson[1], JP.Beech[2], JO.Tegenfeldt[2], F.Höök[1]

[1] *Dept. of Applied Physics, Chalmers University of Technology, Gothenburg Sweden.*
[2] *Div. of Solid State Physics, Lund University, Lund Sweden*

**INTRODUCTION:** Supported lipid bilayers (SLBs) have emerged as one of the most common model systems for studies of cell membranes. We recently discovered that the shear force from a bulk flow of liquid above an SLB can be used to accurately move the lipid bilayer and its constituents in the direction of the bulk flow [1].

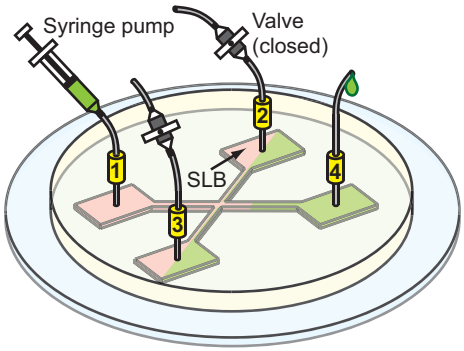


*Fig. 1: Schematic illustration of the microfluidic setup used to form and drive the SLB.*

**METHODS:** The microfluidic setup shown in Fig. 1 was used in our experiments to form and drive the SLB. By flowing lipid vesicles from 1 to 2 and 3 an SLB is formed in the left part of the channel by vesicle fusion to the channel walls. A subsequent flow of buffer solution between 1 and 4 drives the lipid bilayer in the direction of the flow. Depending on the application, the supporting subs-trate was either a glass slide [1-2] or a $SiO_2$-coated substrate with submicrometer sized wells [3].

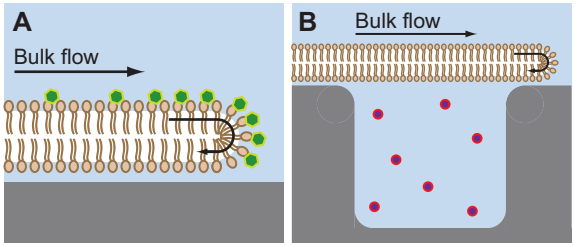


*Fig. 2: (A) The SLB moves in a rolling type of motion under the influence of a bulk flow. (B) Spanning lipid bilayers can be created if the SLB is driven over a surface with embedded wells.*

**RESULTS & DISCUSSION:** The SLB moves in a rolling type of motion, with the lower leaflet of the bilayer being essentially immobilized (see Fig. 2A). This indicates that the frictional coupling between the lipid bilayer and the support is substantially stronger than the frictional coupling

between the bilayer leaflets [2]. If the SLB is driven towards a region with embedded wells (see Fig. 2B), the lipid bilayer either follows the contours of the surface or spans the wells depending on the properties of the bulk solution. By increasing the pH of the bulk solution solvent-free lipid bilayers were made that spanned and sealed the submicrometer sized wells [3].

For some membrane-associated molecules, the lipid bilayer front was observed to act as a molecular sieve [1]. This is illustrated in Fig. 3, which shows the intensity from the fluorescent lipid probe rhodamine-DHPE at the bilayer front. It was furthermore observed that different molecules had different drift velocity in the SLB under the same bulk flow [1], potentially opening up for separation of membrane-associated molecules based on the drift velocity in the SLB.

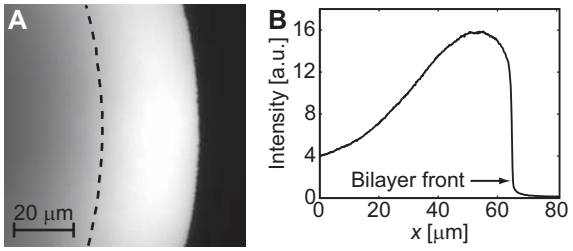


*Fig. 3: (A) A fluorescence micrograph of the SLB. The dashed line corresponds to the position of the bilayer front 150 s before the current frame. (B) A line profile of the intensity through the center of the channel. Data from [1].*

**CONCLUSIONS:** Hydrodynamic forces can be used to move an SLB and its constituents, which makes it possible to concentrate and separate membrane-associated molecules in the SLB. The technique also provides an alternative means of forming lipid bilayers on surfaces where vesicle adsorption and fusion is not applicable.

**REFERENCES:** [1] P. Jönsson et al. (2009) *J Am Chem Soc* **131**:5294-97. [2] P. Jönsson et al. (2009) *Langmuir* **25**:6279-86. [3] P. Jönsson et al. (2010) *Nano Lett*, in press (DOI: 10.1021/nl100779k).

**ACKNOWLEDGEMENTS:** This work was financially supported by the Swedish Research Council for Engineering Sciences, the Swedish Strategic Research Foundation, and the Royal Physiographic Society in Lund.

European Cells and Materials Vol. 20. Suppl. 3, 2010 (page 127) ISSN 1473-2262

# Nanoparticles embedded in Alginate Hydrogels: An Innovative Approach for Sustained Release of Hydrophobic drugs

E. Josef[1], M. Zilberman[2], H. Bianco-Peled[1,3]

*[1]Inter-Departmental Program for Biotechnology, Technion, Israel. [2]Department of Biomedical Engineering, Tel-Aviv University, Israel. [3] Faculty of Chemical Engineering, Technion, Israel.*

**INTRODUCTION:** Over 40% of the drugs developed in the past two decades are extremely hydrophobic [1]. Lipophilic drugs can act as efficient therapeutic agents, since they can penetrate the hydrophobic cell membrane as opposed to hydrophilic drugs. However, their low bioavailability prevents their implementation. We present an innovative methodology for sustained delivery of hydrophobic drugs using composite hydrogels, prepared by embedding oil-in-water microemulsions in hydrophilic hydrogels. The hydrophobic nature of the microemulsion core enhances the solubilization of hydrophobic drugs, while the crosslinked matrix could be readily used as a solid controlled delivery vehicle.

**METHODS:** The microemulsion (ME) was prepared by mixing the surfactants Tween-80 and Span-20 with oil (IPM), followed by dropwise addition of double distilled water. Drug-containing microemulsion was prepared by mixing the drug ketoprofen (KT), the surfactants and the oil prior to water addition. Drug concentrations for release profiles were determined by UV absorbance with Synergy HT microplate reader (Bio-Tek Instruments, Winooski, VT, USA). ME were investigated with dynamic light scattering (DLS), performed in a BI-200SM Research Goniometer System (Brookhaven Instruments Corp.). Diameters of the droplets were calculated by implementing CONTIN model. Small angle X-ray scattering (SAXS) was used to characterize MEs and composite gels, using small-angle diffractometer (Molecular Metrology SAXS system with Cu $K_\alpha$ radiation and pinhole slits).

**RESULTS:** A microemulsion was formulated from pharmaceutical accepted components; the droplets diameter was shown to be about 10 nm by DLS and SAXS. Combining the ME with alginate solution and crosslinking with calcium ions resulted in a clear hydrogel. The model drug, KT, precipitated from the alginate hydrogel, but the drug-containing composite hydrogel was clear and macroscopically homogenous (*Fig. 1*). The nanostructure was investigated by SAXS; scattering plots indicate that oil droplets exist in the composite hydrogel. Release profiles from composite gels exhibit gel-composition dependency (*Fig. 2*).

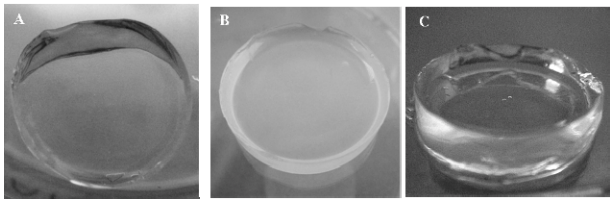


*Fig. 1: Alginate hydrogels, with25 mg/ml alginate and 15 mM Ca-EGTA. (A) No drug, (B) KT 1 mg/ml, (C) Composite gel with 1 mg/ml KT.*

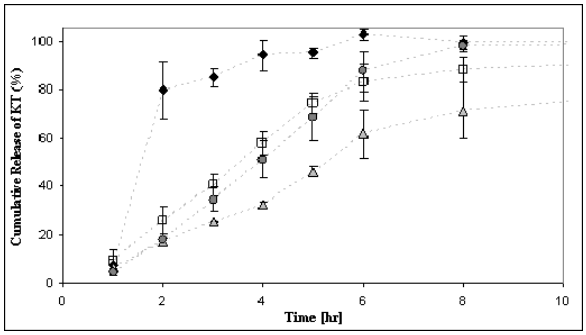


*Fig. 2: Drug release from composite gels with 7.5 mM Ca-EGTA and ◆15 △20 □25 and ●30 mg/ml alginate.*

**DISCUSSION & CONCLUSIONS:** Results suggest that the model drug is more soluble in the ME-composite gel than in the gel alone. Release profiles of the drug from the composite hydrogel demonstrate the applicability of this system as a controlled delivery vehicle. Furthermore, the release rate could be tailored for a specific application utilizing different alginate and calcium concentrations. The methodology of incorporating microemulsion droplets into alginate hydrogels for the purpose of increasing drug solubility could be applied to more drugs. Moreover, other hydrophilic polymers can be utilized to create composite hydrogels. Other systems have to be examined carefully, as the polymer and the drug could affect the stability of the microemulsion. Yet, we believe that composite hydrogels holds great potential for enhancing the solubility of hydrophobic drugs.

**REFERENCES:** [1] C.A. Lipinski, F. Lombardo, B.W. Dominy, et al (2001) *Experimental and computational approaches to estimate solubility and permeability in drug discovery and development settings*, Adv. Drug Delivery Rev., **46:** 3-26.

European Cells and Materials Vol. 20. Suppl. 3, 2010 (page 128) ISSN 1473-2262

# Fluorescent nanoparticles as implantable "Smart Tattoo" biosensors for dissolved oxygen monitoring

A. Joshi[1], R. Srivastava[1,*]

[1] *Department of Biosciences and Bioengineering, IIT Bombay, Mumbai, India*

**INTRODUCTION:** Oxygen ($O_2$) is an important dissolved gas component in the human body which mediates several physiological, pathological, and atmospheric reactions. $O_2$ measurement could serve in determining fate of several processes. Continuous monitoring of $O_2$ is possible with the advent of implantable biosensors. "Smart Tattoo" biosensors allow for minimally invasive method for determination of *in vivo* analytes.

**Smart tattoo concept:** It uses near infra red fluorescene emission scanning in response to reaction with the analyte.

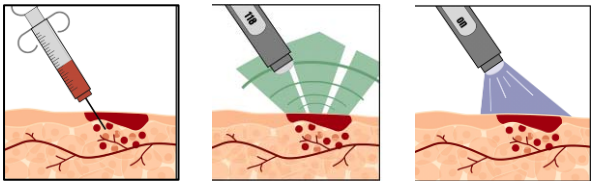

*Fig.1:"Smart tattoo" concept: implantation, interrogation, and readout* [1].

The research aims at developing a "Smart Tattoo biosensor" responsive to dissolved $O_2$ for continuous measurement sensing assay based on near infra red range fluorophores.

**METHODS:** Polymeric nanoparticles of poly lactic acid (PLA) were prepared using conventional emulsification method [2], and Platinum octaethyl porphine (PtOEP) (an oxygen sensitive fluorophore) was loaded in nanoparticles and characterized using DLS, TEM and fluorescence spectroscopy. The response of PtOEP was determined in response to dissolved $O_2$ at different concentrations using fluorescence spectroscopy with excitation and emission maximum of 500 and 640 nm, respectively. The values were then correlated using Orion Oxygen sensing electrode.

**RESULTS:**

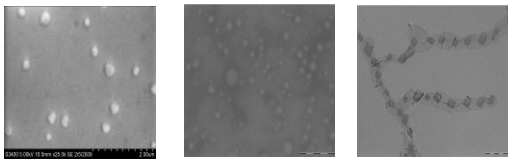

*Fig. 2: SEM image of PLA nanoparticles (left), TEM image of PLA nanoparticles (middle) and dye loaded PLA nanoparticle (right)*

DLS, SEM and TEM measurements show that, PLA nanoparticles and dye loaded PLA nanoparticles showed a particle size of 280 nm and 450 nm with a poly-dispersity of 0.151 and 0.24, respectively. SEM and TEM images showed the presence of nearly spherical nanoparticles with similar sizes of 280 nm and 450 nm for unloaded and loaded nanoparticles.

### Oxygen sensing

The basis of $O_2$ measurement is quenching of intensity due to presence of oxygen.

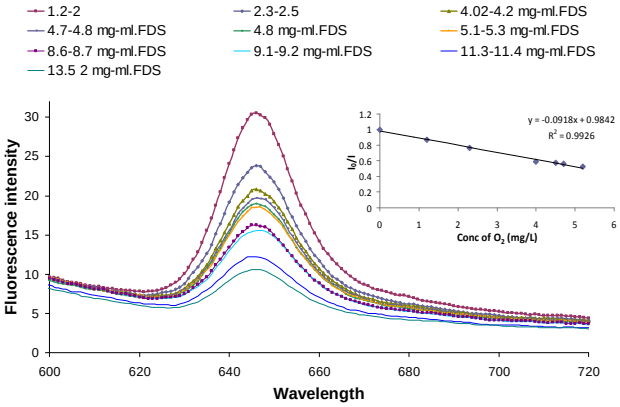


*Fig. 3: Fluorescence emission scans of PtOEP loaded PLA nanoparticles in response to oxygen concentration (Inset shows the stern-volmer plot for oxygen measurement).*

The fluorophore loaded Sensing studies in the concentration range of 0-15 mg % $O_2$.

**DISCUSSION & CONCLUSIONS:** Stern-Volmer plot of linear range was 0-5mg/L in contrast to a logarithmic plot in range 0-14 mg/L. Sensitivity (Ksv) value for oxygen is found to be 0.098/mg/L of oxygen [3]. These polymeric nanoparticles containing oxygen sensitive fluorophores can amplify the prospects of smart tattoo biosensors.

**REFERENCES:** [1]M. McShane Topics in fluorescence spectroscopy, Springer (11) 131-163. [2]S. Desgouilles, C. Vauthier, D. Bazile et al (2003) *Langmuir* **19**: 9504-9510. [3]R. Gillanders, M. Tedford, P. Crilly et al (2004) *Analytica Chimica Acta* **502:** 1–6

**ACKNOWLEDGEMENTS:** This research is supported by CSIR, India.

European Cells and Materials Vol. 20. Suppl. 3, 2010 (page 129) ISSN 1473-2262

# A Versatile Toolset for Nanometer Scale Research in Life Science

G.Kada[1], M. Duman[2], H-P. Huber[2], C. Rankl[1], P. Hinterdorfer[2], F. Kienberger[1]

*[1] Agilent Technologies, Nanomeasurements Division, Linz, Austria. [2] JKU University of Linz, Biophysics Institute, Linz, Austria.*

**INTRODUCTION:** This presentation will focus on key Scanning Probe Microscopy (SPM) technology and introduce new and exciting developments for applications in the life sciences.

**DISCUSSION:** Atomic Force Microscopy (AFM) has been widely used for imaging biological samples down to molecular and subunit resolution under physiological conditions[1]. Moreover, a novel method has been developed for the localization of specific binding sites with nanometer positional accuracy by combining dynamic AFM with single molecule recognition force spectroscopy using functionalized tips, termed Topography and RECognition imaging (TREC).

In addition, optical imaging techniques enable the spectroscopic discrimination of different species in a biological sample. In particular, fluorescence microscopy has proven to be a powerful tool for selective and specific visualization of labeled molecules down to the single molecule level, rendering it possible to follow cellular processes and monitor the dynamics of living cell components. The advantages of AFM and fluorescence microscopy complement each other, and the combination of the two techniques allows a more detailed characterization of cellular structures and processes (Fig. 1).

The ultimate level of measuring structure and organization of membrane receptor proteins can be achieved by combining topography measurements with biological recognition mapping (using TREC) AND recording fluorescence images of the very same area (Fig. 2)[2]. A new way of designing an integrated device which can combine seamlessly all three techniques into a single unit will be discussed.

**OUTLOOK:** This presentation will finish with an introduction of a new technique, called near field Scanning Microwave Microscopy (SMM), with its potential of measuring changes in capacitance and dielectric constant of biological matter, thereby visualizing structures from underneath the surface.

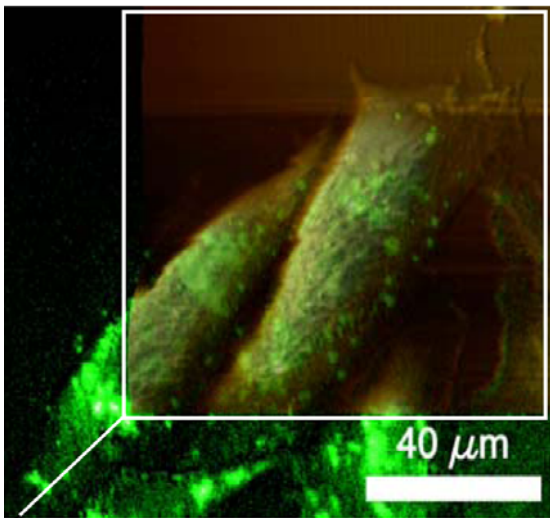


*Fig. 1 Combined AFM/Fluorescence imaging of CHO cells (Chinese Hamster Ovary) expressing GFP-labeled cell receptors[2].*

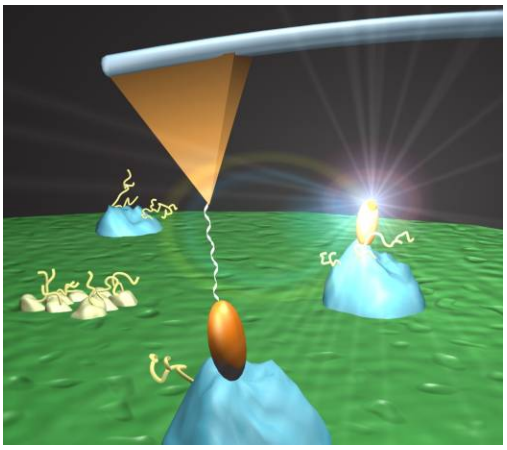

*Fig. 2 Sketch of proteins in a cell membrane which can be detected by using (a) AFM topography imaging, (b) recognition imaging using a ligand on a string bound to the tip, and (c) fluorescence microscopy.*

**REFERENCES:** *[1] G. Kada, P. Hinterdorfer, F. Kienberger (2008)* Nanotoday ***3****:12-19. [1] M. Duman, G. Kada, P. Hinterdorfer, et al (2010)* Nanotechnology ***21****: 115504.*

**ACKNOWLEDGEMENTS:** This work was financially supported by the Austrian Christian Doppler Society and the EC grant SMW ('Single Molecule Workstation', grant number 213717).

European Cells and Materials Vol. 20. Suppl. 3, 2010 (page 130) ISSN 1473-2262

# Nanostructured fluorescent S-layer coatings on silica particles

B.Kainz1, S.Küpcü1, K.Steiner1, U.B. Sleytr1, J.L. Toca-Herrera2, D. Pum[1]

[1] *Department of NanoBiotechnology, BOKU Vienna, Austria.* [2] *CICbiomaGUNE, San Sebastian, Spain.*

**INTRODUCTION:** This work focuses on the design of nanostructured fluorescent surfaces on silica particles by using genetically functionalised fluorescent S-layer fusion proteins (crystalline bacterial cell surface layer proteins [1]), which act as scaffold and as sensing element simultaneously. Therefore, the intrinsic self assembling capability of the S-layer protein SgsE, forming p2 lattices, is combined with the pH-dependent fluorescent properties of fused cyan ECFP, green EGFP, yellow YFP and red mRFP1 proteins in a 1:1 stoichiometry [2,3]. Furthermore, a fluorescence resonance energy transfer system (RET) with molecular precision on silica particles is described by using the bi-fluorescent S-layer tandem fusion protein ECFP-SgsE-YFP where ECFP is acting as donor and YFP as acceptor fluorophore.

**METHODS:** The S-layer protein SgsE from *Geobacillus stearothermophilus* NRS 2004/3a [4] was used to incooperate N- and/or C-terminal fused fluorescent proteins (fusion partners: GFP variants and mRFP1). Molecular cloning procedures were performed using standard protocols for S-layer technology [3]. Fluorescence measurements with proteins in solution were carried out using fluorimetry. Structural investigations were carried out with electron (TEM) and atomic force microscopy (AFM). Zeta-potential measurements were performed to follow the particle coating, to understand their colloidal behaviour and to determine the isoelectric point. Confocal microscopy and flow cytometry were used to monitor the pH-dependence of the fluorescent S-layer biocolloids as well as the resonance energy transfer within the assembled bi-fluorescent tandem fusion protein.

**RESULTS:** Structure investigations of reassembled fluorescent S-layer fusion proteins with TEM (self assembly products) and AFM (particle surface) revealed, that the p2 lattice symmetry (a=11 +/-0.5 nm, b=14 +/- 0.4 nm, γ=80 +/- 1°) of the SgsE-protein is not affected by the fused moieties. At the isoelectric point of the S-layer biocolloids (pH 4.6 +/-0.2) an increase in particle aggregation was detected with flow cytometry. With fluorescent measurements it was found out, that 50% of the initial fluorescence intensities vanished at calculated pKa values of the chromophores. While the fluorescence intensities

of SgsE-ECFP, SgsE-EGFP and SgsE-YFP vanished in decreasing pH solutions, the spectral properties of the red SgsE-mRFP1 were minimally affected in acidic conditions.

Cellular uptake studies of SgsE-YFP biocolloids by HeLa cells was demonstrated.

Within the bi-fluorescent S-layer tandem fusion protein ECFP-SgsE-YFP an energy transfer efficiency of 20 % can take place. The distance between the ECFP donor and YFP acceptor moiety was calculated to be 6 nm.

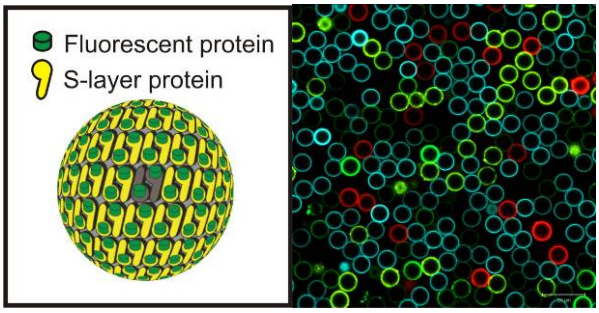


*Fig. 1: left: Schematic representation of the S-layer fusion protein technology on particles with p2 lattice symmetry. Right: Confocal micrograph of fluorescent S-layer coated silica particles.*

**DISCUSSION & CONCLUSIONS:** The combination of the fluorescence and self-assembly properties of genetically engineered fluorescent S-layer fusion proteins makes them to a promising tool to build up novel nanopatterned biofunctional architectures for different applications in nanobiotechnology such as structure investigations, pH-indicators (*in vivo* and *in vitro*), for controlled cellular uptake studies or as fluorescence marker.

**REFERENCES:** [1] U.B. Sleytr et al (2007) *FEBS J* **274**:232-334. [2]B. Kainz et al (2010) *Biomacromolecules* 11:207-14. [3] C. Schäffer et al (2007) *Small* **3**:1549-59. [4]P. Messner (1986) *J Ultrastruct Mol Struct Res* **97**:73-88.

**ACKNOWLEDGEMENTS:** This work was supported by the Austrian NanoInitiative under the project SLAYSENS within the project cluster ISOTEC.

# High Efficiency GaN-Based Platforms for Biology and Medicine

A. Kaminska1 J. Weyher2J. Waluk1 S. Gawinkowski1R. Holyst1

[1] *Institute of Physical Chemistry Polish Academy of Sciences, , Kasprzaka 44/52, 01-224 Warsaw,Poland M*

[2] *Institute of High Pressure Physics, Polish Academy of Sciences, Sokolowska 29/37, 01-142 Warsaw, Poland*

**INTRODUCTION:** In the last decade broad interest was focused on producing and using nano-structural forms (e.g. nano-columns) as active platforms for immobilization and examination of organic substances. Such platforms, covered by nano-size metal layers (e.g. Au, Ag, Cu), constitutes very sensitive bio-sensors on which different individual organic molecules can be examined by surface-enhanced Raman spectroscopy (SERS)[1.].
In this study we disuse the potential of our GaN-based platform in immunoassay SERS spectroscopic detection.

**METHODS:** Si-doped MOCVD-grown GaN on sapphire with carrier concentration 1 x 10E18 $cm^{-2}$, were photo-etched in KSO-D solution (water solution of KOH and $K_2S_2O_8$, according to the procedure described recently[2]. sing optimized photo-etching procedure nano-pillars are formed on threading dislocations in the GaN epitaxial layers. After short etching time the dislocation-related pillars are sticking separately, while prolonged etching results in bunching of long pillars to form “sheafs”. Subsequently the samples were covered by 60 nm Au layer using simple physical evaporation method resulting in formation of very rough cones. In this study we disuse the potential of our GaN- based platform in immunoassay SERS spectroscopic detection. Akt (pan) Mouse mAB antibody were used as the SERS probes on samples. SERS measurements were performed using a Renishaw InVia Raman system equipped with a He-Ne laser emitting a 632,5nm line used as the excitation source.

**RESULTS:** Antibody (Akt (pan) Mouse mAB) was immobilized onto SERS platform, and the SERS spectra before and after treatment with antigen ( Akt (pan) Blocking Peptide) and were recorded to compare Raman signatures of antibody alone versus antibody plus captured antigen (Fig.1). Of the spectral features apparent in the mAB antibody spectrum ( Fig.1a), the most intense bands at 1057and 850 $cm^{-1}$ mostly likely arises from Tyr and Trp residues. Prominent bands are observed in the 1350- 1500$cm^{-1}$ region of Akt (pan) Blocking Peptide and Akt (pan) Mouse mAB antibody complex (Fig. 1b). This is presumably due to selectively enhanced side-chain vibrations, although the amide III protein mode may be observed in both mAB and mAB+ Blocking Peptide spectra. These results show that antibodies or related capture moieties can be used to provide selectivity to SERS biosensing.

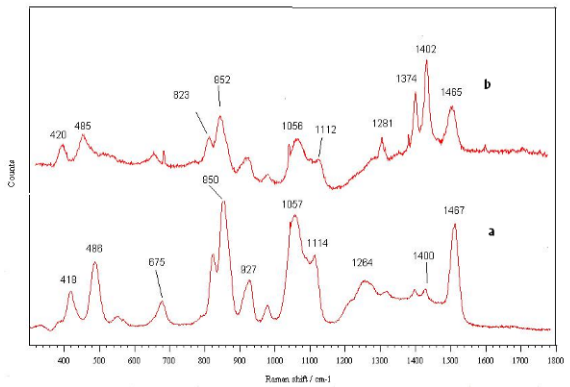


*Fig. 1:SERS spectra of (a) antibody mAb and (b) antibody after interaction with blocking peptide (Akt(pan)) immobilized onto a SERS platform (lexc = 632.5 nm).*

**DISCUSSION & CONCLUSIONS:** In this work, we successfully demonstrated the applicability of SERS spectroscopy using Au-coated GaN platform for the detection of antigen-antibody interaction. In addition, because antibodies to an extensive range of antigens are commercially available, they can be used to perform a broad variety of immunological reaction of clinical importance.

**REFERENCES:** [1] A. Kudelski (2009) *Surface Science* **603** 1328–1334. [3] D.H. van Dorp, J.L. Weyher, M.R. Kooijman and J.J. Kelly (2009) *J. Electrochem. Soc.* **156,** 10 D371-D376

**ACKNOWLEDGEMENTS:**

The research was partially supported by the European Union within European Regional Development Fund, through grant Innovative Economy(POIG.01.01.02-00-008/08).

European Cells and Materials Vol. 20. Suppl. 3, 2010 (page 132) ISSN 1473-2262

# Monitoring for Intra Cellular Cytoskeletal Change by Chemical Stressors Using Quartz Crystal Microbalance

HW.Kang[1,2,3], BJ.Lee[2], SM.Chang[3], YS.Kwon[3], H.Muramatsu[1]

*[1] Tokyo University of Technology, Tokyo Japan. [2] Inje University, Kimhae, Korea.*

*[3] Dong-A University, Busan, Korea.*

**INTRODUCTION:** For cellular analysis, cultured cells are widely used to evaluate cell activities. In these analyses, a study of morphology is fundamental for understanding the effect of chemical stimulations. A thin lipid double layer is formed on the surface of a cell, and a number of proteins are dispersed in the lipid membrane. The cytoskeleton in cells allows the cells to work the spatial and mechanical functions [1]. Integrin links between a cytoskeleton and an extracellular matrix (ECM). The cell shape is mainly depending on the cytoskeleton and the ECM. Thus, the morphology and physical properties reflect a state of the cytoskeleton and activity of cells [2-4].

**METHODS:** An activity of the cultured cell was monitored by the quartz crystal under the chemical stressors. A human hepatoma cell line, HepG2, was cultured on the collagen coated quartz crystal that was mounted in the bottom of the cultured chamber. The quartz crystal is 9 MHz, AT cut type and has ITO electrodes that enable transmission imaging of the cultured cell by a CCD camera in a $CO_2$ incubator during the experiments. The resonance frequency and the resonance resistance of the quartz crystal were measured simultaneously with QCM922 (Seiko EG&G, Japan) for analyzing the mass and viscous changes of the cell. The cytoskeletal change was achieved by staining actin filaments with rhodamine-phalloidin and following observing with a fluorescence microscopy.

**RESULTS & DISCUSSION:** Fig. 1 shows the time course of the resonance frequency and the resonance resistance when glutaraldehyde was injected to the HepG2 cells. After injection, the resonance frequency was decreased and the resonance resistance was increased, and then the signals kept their level respectively. As glutaraldhyde cross-links to the proteins, the mass increased and the viscous also increased [5].

The cross-linking effect was well shown in Fig. 2, which shows the series of optical images after the glutaraldehyde treatment. After 4 hours, there was no change in the cell shape. On the other hand, the cytoskeleton was decreased as shown in Fig. 3, because the cross-linking by glutaraldehyde weakened the cell which could not construct the cytoskeleton any more.

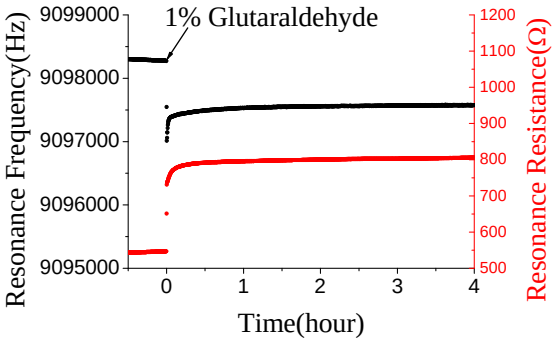


*Fig. 1: Time course of the resonance frequency and the resonance resistance when glutaraldehyde was injected.*

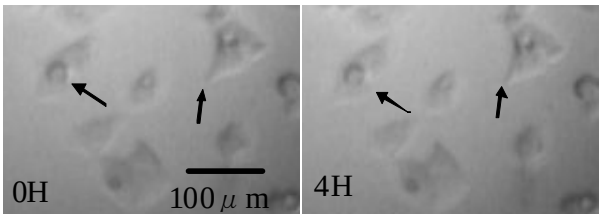


*Fig. 2: Series of optical images after the glutaraldehyde treatment.*

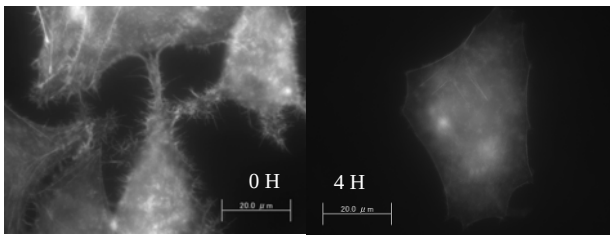


*Fig. 3: Fluorescence images of HepG2 cells after glutaraldehyde treatment.*

**REFERENCES:** [1] B. Alberts, A. Johnson, J. Lewis, M. Raff, K. Roberts, P. Walter (2002) *Molecular Biology of the Cell*, Garland Science. [2] D. Discher, P. Janmey, Y. Wang (2005) *Science* **310**:1139-1143. [3] J. Bercoff et al. (2003) *Ultrasound Med. Biol.* **29**:1387-1396. [4] A.L. McNight et al. (2002) *Am. J. Roentgenol.* **178**:1411-1417. [5] H.W. Kang and H. Muramatsu (2009) *Biosens. Bioelectr.* **24**:1318-1323.

**ACKNOWLEDGEMENTS:** This work is supported by the National Research Foundation of Korea Grant funded by the Korean Government [NRF-2009-351-D00012].

European Cells and Materials Vol. 20. Suppl. 3, 2010 (page 133) ISSN 1473-2262

# Surface Science Analysis and Surface Modification Methods for Biomaterials Research

L. Kanninen[1], N. Jokinen[1], K. Lahtonen[1], P. Jussila[1], H. Ali-Löytty[1], M. Hirsimäki[1], J. Leppiniemi[2], V. Hytönen[2], M. Kulomaa[2], N. Ahola[3], K. Paakinaho[3], M. Kellomäki[3], and M. Valden[1]

*[1] Surface Science Laboratory, Tampere University of Technology, Finland [2] Institute of Medical Technology, University of Tampere and Tampere University Hospital, Finland [3] Department of Biomedical Engineering, Tampere University of Technology, Finland*

**INTRODUCTION:** Although surface properties of biomaterials play an important role in the phenomena occurring at the surface of biomaterial, the chemical composition of the biomaterial surface is often unknown. The chemical composition of the surface may differ significantly from the bulk composition. Thus, a detailed knowledge of the surface properties is essential in order to modify the surface for the enhancement of cell adhesion, proliferation and differentiation for tissue engineering and regenerative medicine, biocompatibility or drug release properties of implants or specific binding of biomolecules for biosensors.

**METHODS:** X-ray Photoelectron Spectroscopy (XPS) is an established surface sensitive analysis method for the determination of the elemental and chemical composition of the sample surface. Detailed information on the differences in in-depth chemical composition can be obtained by experimental and computational methods. By utilizing XPS it is possible to e.g. determine concentration gradients of drugs implanted in biomaterial matrix, analyze proteins on different surfaces and even recognize different types of cells immobilized on solid substrates. The XPS experiments are performed in ultra high vacuum (UHV). Sample surfaces can range from atomary flat to porous.

The research equipment at Surface Science Laboratory (SSL) has many *in situ* surface treatment methods e.g. ion sputtering, physical vapor deposition and electrospray deposition of large molecules. Sample preparation *in situ* in UHV enables nanoscale sample fabrication in ultra pure environment.

MAX-Lab at University of Lund, Sweden is a multidisciplinary synchrotron radiation research centre where tunable and high brightness x-ray and ultraviolet radiation facilitates a variety of unique surface sensitive methods. We have utilized Photoelectron Emission Microscopy (PEEM) for the elemental surface imaging and Near Edge X-ray Absorption Fine Structure (NEXAFS) for the orientation of surface molecules. Tunable photon energy allows us to optimize the elemental sensitivity of high resolution photoelectron spectroscopy.

**RESULTS:** We have studied methods for biofunctionalization of stainless steel surfaces with highly ordered mixtures of silanes with different organofunctional groups. Electrochemical passivation of steel surface prior to silanization leads to stable, reproducible monolayers of (3-aminopropyl)trimethoxysilane (APS) on stainless steel[1]. These monolayers can be biofunctionalized by adding silane molecules with a different organofunctional group. We have used (3-mercaptopropyl)trimethoxysilane (MPS) as a linker silane. Preliminary results of experiments performed at SSL and MAX-Lab indicate that maleimide terminated biomolecules can be covalently bonded to the MPS in APS/MPS monolayers. As the density of the MPS can be varied, the properties of the biomolecule overlayer on silanized stainless steel can be tuned in a bottom-up manner.

Recently, we have also investigated the effect of hydrolysis on surface properties of a composite of poly(lactide-co-caprolactone) polymer with comonomer ratio of 70/30 and β-tricalcium-phosphate (β-TCP). Significant changes of the surface chemical properties are observed in both polymer and β-TCP moieties as a function of hydrolysis time.

**CONCLUSIONS:** We have shown that by surface modification we can introduce biofunctional properties into stainless steel surface. Surface analyses at different stages of biofunctionalization were essential in the process of modifying the surface towards better biofunctionality.

**REFERENCES:** [1] P.Jussila, H. Ali-Löytty, K. Lahtonen, M. Hirsimäki, and M. Valden (2010) *Surface and Interface Analysis* **42** 157-164.

European Cells and Materials Vol. 20. Suppl. 3, 2010 (page 134) ISSN 1473-2262

# Treating "intractable" tumours using nanoDDS and TGF-beta inhibitor

MR. Kano[1,2], H. Nishihara[4], K. Kataoka[3], K. Miyazono[1]

*[1]Dept. Molecular Pathology, Graduate School of Medicine, [2]Medical Scientist Training Program, Faculty of Medicine, [3] Division of Clinical Biotechnology, Center for Disease Biology and Integrative Medicine, Graduate School of Medicine, University of Tokyo, [4]Dept. Translational Pathology, Graduate School of Medicine, Hokkaido University, Sapporo, Japan.*

**INTRODUCTION:** Effective treatment of currently intractable solid tumours is one of important goals of chemotherapy using nanoDDS. To realize this, we need to investigate why intractable tumours, such as pancreatic cancer, are "intractable". Our recent study suggests that the structure of vasculature in those tumours is different from what we observe in popular tumour animal models.

**METHODS:** We used xenografts of BxPC3 cell line derived from human pancreatic cancer as a model of intractable cancer, and those of C26 cell line derived murine colon cancer as an ordinary cancer model. Vascular endothelial cells in the specimens were detected by antibody anti CD31 or CD34, and pericytes by antibody anti smooth muscle actin (SMA). FITC-dextran of 2 MDa was used as a model of nanoparticle for comparison of vascular structure, whereas polymer micelle incorporating adriamycin, EGFP-expressing vector, or magnetite was used where applicable. LY364947 at 1 mg/kg was administered ip for TGF-beta inhibition, and Sorafenib at 40 mg/kg for VEGF inhibition.

**RESULTS:** We compared animal models of pancreatic cancer and diffuse-type gastric cancer, which have rich stromal components, with ordinary model of colon cancer. The stroma rich models have more pericyte-covered vasculature than the colon cancer model. Although nanoparticle accumulated autonomously in the colon cancer model, it accumulated hardly in the stroma rich models.

Use of TGF-beta inhibitor, which reduces pericytes, increased accumulation of nanoparticle in stroma rich models. This increase resulted in significant treatment effect in these models. Yet, use of VEGF inhibitor, reported to normalize vasculature, did not increase accumulation in the stroma rich models. VEGF inhibitor did increase distribution of nanoparticle in the colon cancer model, although TGF-beta inhibitor did not.

The effect of combined use of TGF-beta inhibitor in pancreatic tumour model was shown with nanoparticles incorporating expression vector of GFP or magnetite as contrast medium for MRI.

We further analysed vascular structure in human tissues of pancreatic, gastric, or colon cancer. Vasculature in pancreatic cancer and diffuse-type gastric cancer was covered by pericytes, whereas that in colon cancer and ordinary gastric cancer was not covered by pericytes.

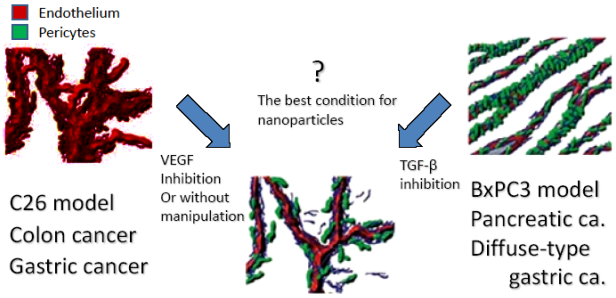


*Fig. 1: Schematic comparison of cancer types depending on vascular structure.*

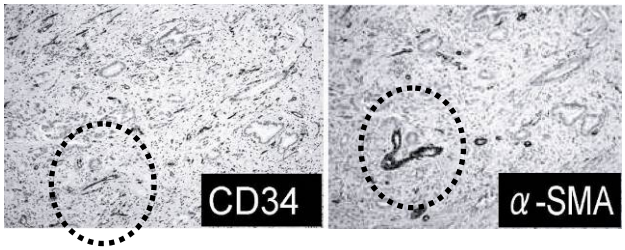


*Fig. 2: Vasculature in human pancreatic cancer. Endothelium (left) is covered by SMA-positive cells (right, a serial section).*

**DISCUSSION & CONCLUSIONS:** Currently intractable solid tumours may have more pericyte-covered, non-leaky vasculature. Therefore, treatment of such tumours could benefit from the combined treatment with TGF-beta inhibitor and nanoparticles.

**REFERENCES:** [1] M.R. Kano et al., (2007) *Proc Natl Acad Sci USA* **104**:3460-3465. [2] MR. Kano et al (2007) *Proc. Natl. Acad. Sci., USA* **104**:3460-3465. [3] K. Miyata, M.R. Kano et al (2009) *Pharm Res* **25**:2924-2936. [4] M.R. Kano et al (2009) *Cancer Sci* **100**:173-180. [5] M. Kumagai, M.R. Kano et al (2009) *J Control Rel* **140**:306-311.

European Cells and Materials Vol. 20. Suppl. 3, 2010 (page 135) ISSN 1473-2262

# Thermal Stabilization of Localized Plasmon Transducers

T. Karakouz, A. B. Tesler, T. A. Bendikov, A. Vaskevich, and I. Rubinstein

*Dept. of Materials & Interfaces, Weizmann Institute of Science, Rehovot 76100, Israel*

**INTRODUCTION:** Nanostructured noble metal (Au, Ag) films support excitation of localized surface plasmon polaritons in the visible to NIR wavelength range. The sensitivity of localized surface plasmon resonance (LSPR) to the dielectric properties of the immediate environment allows detection of analyte binding to the nanostructured films.

Discontinuous noble metal films on transparent substrates (glass, quartz, sapphire) are known to be unstable. This morphological instability is the source of artifacts in measurements of the LSPR response as well as a major drawback for practical applications of LSPR sensors. Stabilization of noble metal layers on oxide surfaces is commonly achieved using adhesive promoters and/or stabilizing overlayers, however, both methods interfere with the performance of LSPR transducers as well as complicate their preparation procedure.

**RESULTS:** We have recently introduced a new approach to the preparation of strongly-bonded and morphologically-stable Au nanostructures on glass substrates for application as LSPR transducers. The new scheme involves high-temperature annealing of nanostructured Au films on glass, carried out in air at temperatures in the vicinity of the glass transition of the substrate (550-600 ºC), leading to partial embedding of the metal nanostructures in the glass (Fig. 1) [1].

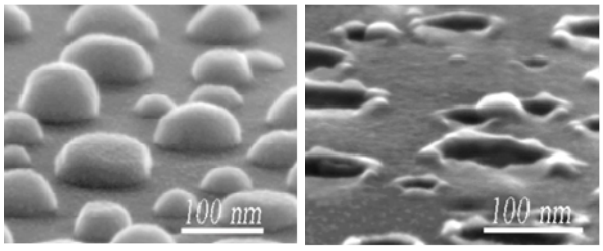


*Fig. 1: HRSEM images of a 10 nm Au island film evaporated on glass, annealed 70 h at 600 ºC (left) and the glass substrate after Au dissolution (right). Samples are covered with a 3 nm Cr layer.*

Using this approach, Au island films prepared by resistive evaporation on glass as well as citrate-stabilized Au nanoparticles immobilized on aminosilane-modified glass were stabilized without the use of adhesion promoters or coating layers.

The kinetics of annealing of percolated Au films as well as temperature and environmental effects were studied using a custom-designed oven enabling in situ optical measurements under controlled atmosphere. During annealing at 600 ºC three main stages were identified: fast formation of a surface plasmon (SP) absorption band (up to 5 minutes), a blue shift of the SP band (3-5 hours), followed by a gradual red shift (tens of hours). These changes were correlated with the Au film morphology, i.e., island formation and separation, and embedding in the glass substrate.

The morphology and optical response of partially embedded Au nanostructured films are exceedingly stable toward immersion in solvents (including phosphate buffer saline, PBS), drying, and self-assembly of biological molecules. Application of Au island films as transducers for LSPR sensing of IgG antigen-antibody interactions was demonstrated [1].

**REFERENCES:** [1] Karakouz, T.; Tesler, A. B.; Bendikov, T. A.; Vaskevich, A.; Rubinstein, I. *Adv. Mater.* **2008**, *20*, 3893-3899.

**ACKNOWLEDGEMENTS:** Support of this work by the Israel Science Foundation, grant No. 672/07, is gratefully acknowledged. This research is made possible in part by the historic generosity of the Harold Perlman family.

European Cells and Materials Vol. 20. Suppl. 3, 2010 (page 136) ISSN 1473-2262

# Electrochemical Impedance Spectroscopy as a Tool for Studying Ion Channels in Tethered Bilayer Lipid Membranes

JKR.Kendall[1], Benjamin R.G. Johnson[1], PH.Symonds[1], G.Imperato[2], RJ.Bushby[3], JD.Gwyer[4], C.van Berkel[4], SD.Evans[1], LJC.Jeuken[2]

[1] *School of Physics & Astronomy, University of Leeds, Leeds, United Kingdom*; [2] *Faculty of Biological Sciences, University of Leeds, Leeds, United Kingdom*; [3] *Centre of Molecular NanoScience, University of Leeds, Leeds, United Kindom*; [4] *Philips Research (UK), Cambridge Science Park, Cambridge, United Kingdom*.

**INTRODUCTION:** A systematic study has conducted into tethered bilayer lipid membranes (tBLMs) and their potential use as platforms for ion-channel based biosensors. Ion channels have a wide range of specificities – detecting stimuli ranging from light and temperature to pH and chemical compounds in the surrounding environment. Highly sensitive gating mechanisms can result in the conductance of large numbers of ions providing natural amplification of the signal. Here, valinomycin and gramicidin are used as model systems.

**METHODS:** Sputtered gold electrodes provided by Philips Research are modified with self-assembled monolayers (SAMs) composed of a cholesterol tether ($EO_3$ cholesterol, $EO_3C$) - either pure or mixed with a diluent molecule (6-mercaptohexanol, 6MH). The latter system is shown schematically in Fig. 1. A tethered bilayer lipid membrane (tBLM) is then formed on top of these SAMs via the fusion of *Escherichia coli* polar lipid extract vesicles. Gramicidin and valinomycin are incorporated into the tBLM from the bulk solution and ion transport is measured using electrochemical impedance spectroscopy (EIS).

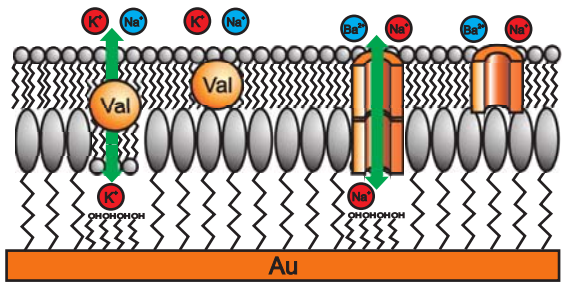


*Fig. 1: Schematic of ionophore-mediated transport in the $EO_3C$:6MH tBLM system*

**RESULTS:** Three main observations were made.[1] (1) EIS spectra of tBLMs formed on pure $EO_3C$ were unaffected by the addition of either gramicidin or valinomycin. (2) Incorporation of valinomycin into the tBLM on mixed SAMs, results in a significant drop in membrane resistance, while tBLM capacitance remains

largely unaffected. This change in resistance is ion specific, only being observed in a $K^+$ solution (Table 1). (3) In contrast, incorporation of gramicidin into tBLMs formed on mixed SAMs increases the double layer capacitance (Table 1). These changes are also ion specific, only being observed in $Na^+$ solutions, yet being reversed when exchanged with $Ba^{2+}$.

*Table 1. Effects of ionophore-mediated transport on mixed $EO_3C$:6MH tBLM*

| | Resistance ($M\Omega.cm^2$) | Capacitance ($\mu F.cm^{-2}$) |
|---|---|---|
| tBLM ($Na^+$) | 1.58 ± 0.52 | 0.75 ± 0.01 |
| Valinomycin ($Na^+$) | 1.00 ± 0.08 | 0.77 ± 0.01 |
| Valinomycin ($K^+$) | **0.006 ± 0.003** | 0.80 ± 0.01 |
| Gramicidin ($Ba^{2+}$) | 0.009 ± 0.004 | 0.73 ± 0.02 |
| Gramicidin ($Na^+$) | 0.38 ± 0.02 | **1.64 ± 0.11** |

**DISCUSSION & CONCLUSIONS:** The work presented here demonstrates that tBLMs are suitable platforms for biosensors, development of which is continued using various bacterial ion channels. The incorporation of ion channels will be of great use in the fields of biosensing and high throughput drug screening.

In the tBLM system perpared using cholesterol-based tethers, the data indicates that ion transport activity is confined to regions of the tBLM overlaying nanoscale domains of 6MH (Figure 1). This is in contrast to previously reported schemes where SAMs of pure thiolipid have been used.[2]

**REFERENCES:** [1] J.K.R. Kendall, B.R.G. Johnson, P.H. Symonds, et al (2010) *ChemPhysChem* (in press). [2] S.R. Jadhav, D. Sui, R.M. Garavito, et al (2008) *J Colloid Interface Sci* **322**:465-72.

**ACKNOWLEDGEMENTS:** Funded by a CASE studentship from the Biotechnology and Biological Sciences Research Council (BB/E527939/1) in conjunction with Philips Research (UK).

# Adaptive Self-Assembly in Coordination Nanoparticles

N. Kimizuka

*Department of Chemistry and Biochemistry, Graduate School of Engineering,*
*The International Research Centre for Molecular Systems, Kyushu University, JST CREST*
*744 Moto-oka, Nishi-ku, Fukuoka 819-0395, Japan.*

**INTRODUCTION:** The ability to encapsulate molecules and nano-scale materials in supramolecular networks holds promise to tailor and improve their functions for technologically important applications. The key feature to encapsulate guest molecules and nanomaterials is adaptability, which has been one of the unexplored functions in supramolecular chemistry. In this talk, we introduce supramolecular nanoparticles which are self-assembled in water from nucleotides and lanthanide ions.[1-4] They are composed of amorphous coordination networks and show adaptive inclusion properties for varied guest materials during their self-assembly. Functional molecules such as dyes, porphyrins and even inorganic nanoparticles are enfolded inside. Possible applications of these self-assembling nanoparticles will be discussed.

**RESULTS & DISCUSSIONS:** Nucleotides are selected as components since they show rich structural diversity. They are composed of nucleobases, ribose or 2'-deoxyribose linkers and phosphate groups, which structures are regarded as bidentate ligands. Lanthanide ions, meanwhile exhibit large coordination numbers with high coordination flexibility. The combination of these components is suitable for making amorphous coordination networks that are self-assembled to accommodate the size and shape of guest materials. Nanoparticles were spontaneously obtained by mixing aqueous $GdCl_3$ with nucleotides in aqueous environment. These nucleotide/lanthanide nanoparticles displayed unique properties such as sensitized lanthanide luminescence and excellent performance as MRI contrast agents, depending on the combination of nucleotides and lanthanide ions.[1] Interestingly, various guest molecules were readily incorporated into the nucleotide/lanthanide self-assemblies.[1-4] Cyanine dye **1** showed very weak fluorescence under UV light ($\Phi_F$ ~ below 1%) due to prevailing nonradiative thermal deactivation of the singlet excited state which is promoted by free conformational rotation around the central methyne moiety. On the other hand, when **1** was incorporated in AMP/$Gd^{3+}$ CNPs, intense blue emission was observed ($\Phi_F$ ~ 49%).

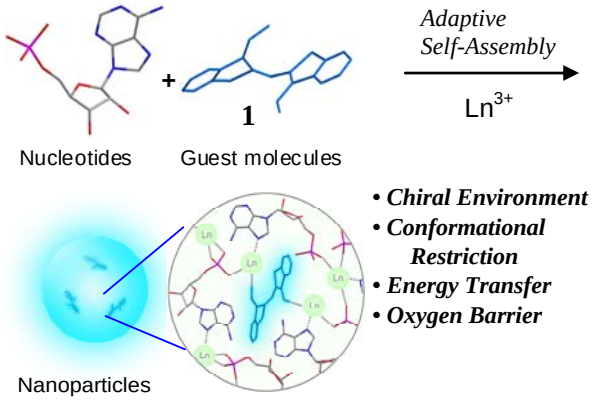


*Fig. 1: Schematic illustration for adaptive inclusion of guest molecules in coordination nanoparticles.*

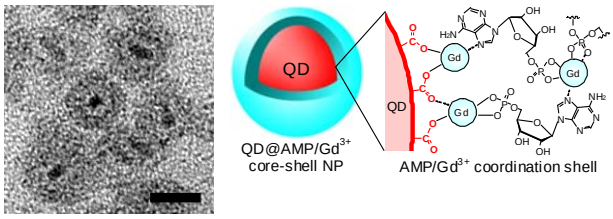


*Fig. 2: A TEM micrograph of CdSe/ZnS QDs wrapped by AMP/$Gd^{3+}$ networks. Scale bar=20 nm.*

It indicates that the conformational freedom of cyanine dye **1** in AMP/$Gd^{3+}$ CNPs is highly restricted by the surrounding coordination networks.[2] The adaptive self-assembly also occurs on the surface of semiconductor nanocrystals (QDs). Anionic CdSe/ZnS QDs were enfolded in the shell of AMP/$Gd^{3+}$ (Figure 2).[4] The adaptive inclusion ability of present supramolecular assemblies allows us to design a variety of nanoparticles with manifold functions. As examples of biological applications, immobilization of enzymes and cellular uptake will be discussed.

**REFERENCES:** [1] R. Nishiyabu and N. Kimizuka et. al. *J. Am. Chem. Soc.*, **131**, 2151-2158 (2009). [2]R. Nishiyabu, C. Aimé and N. Kimizuka et.al, *Angew. Chem. Int. Ed.*, **48**, 9465-9468 (2009). [3]C. Aimé, R. Nishiyabu, R. Gondo and N. Kimizuka, *Chem. Eur. J.* **16**, 3604-3607 (2010). [4]R. Nishiyabu, C. Aimé, R. Gondo, K. Kaneko and N. Kimizuka, *Chem. Commun.*, *in press* (2010).

# Monitoring of Initial Cell Adhesion Process on Nanometer-scaled and Organized Surfaces

Tomomi KITAGAWA[1], Yuuki INOUE[2], Madoka TAKAI[2] and Kazuhiko ISHIHARA[1,2]

*[1]Department of Bioengineering, [2]Department of Materials Engineering, School of Engineering, The University of Tokyo, Tokyo 113-8656, Japan*

**INTRODUCTION:** Control of cell-materials interactions is the most important issue in developing biomedical devices and scaffolds for regenerated medicine. To consider this, we should understand the initial cell adhesion behavior on the materials. The first phase of cell-material interactions is protein adsorption and after that cells start to attach, adhere and spread on the protein adsorption layer [1]. Therefore, analyses of these processes continuously will provide novel knowledge for understanding cell-materials interaction. The aim of this study is the monitoring these processes on various surfaces in real time using quartz crystal microbalance with dissipation (QCM-D). As for surfaces, polymer brush surfaces were prepared by surface-initiated atom transfer radical polymerization (SI-ATRP). The SI-ATRP is an excellent technique for preparing a nanometer-scaled and organized surfaces and control in the thicknesses of the polymer layer.

**METHODS**: Three kinds of polymer brush layers composed of 2-methacryloyloxyethyl phosphorylcholine (PMPC), 2-hydroxyethyl methacrylate (PHEMA) and 2-methacryloyloxyethyl trimethylammonium chloride (PMEMA) were prepared by SI-ATRP on Au substrate of QCM-D. Initiator-immobilized surface (initiator-SAM) and carboxyl-terminated SAM surface (COOH-SAM) were also prepared on Au substrate. The modified Au substrates were mounted in the QCM-D chamber kept at 37□. Fibronectin solution in serum-free D-MEM (10 μg/mL) was injected into the chamber and frequency change (ΔF) was monitored for 1h. After rinse with serum-free D-MEM, HeLa cell suspension (1.0 x $10^4$ cells/$cm^2$) was injected into the chamber and ΔF was monitored for 3h. The morphologies of adherent cells were observed by microscope and the numbers of adherent cells were counted.

**RESULTS:** The polymer graft densities were 0.14 (PMPC), 0.48 (PHEMA), and 0.35 chains/$nm^2$ (PMEMA), respectively. Thus, nanometer-scaled and organized surface could be prepared.

Fig. 1 shows QCM-D charts of ΔF on each surface and morphologies of the adherent cells after incubated for 3h. As in the protein adsorption process, ΔF was almost zero on PMPC brush surface, while ΔF on

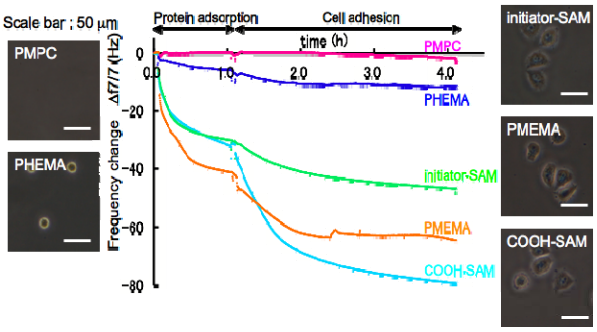


*Fig. 1. Frequency changes (ΔF) on each surface and cell morphologies after incubated for 3h.*

PHEMA brush surface was around 10 Hz. On the other three surfaces, large ΔFs were observed. ΔF, related to cell adhesion process, increased in the following order, PMPC < PHEMA < initiator-SAM < PMEMA < COOH-SAM. From microscope images, cells could not be observed on PMPC surface and small number of cells was observed on PHEMA surface (3.2 x $10^3$ cells/$cm^2$). On the other three surfaces, a lot of cells adhered (8 x $10^3$ cells/$cm^2$). Thus, we could monitor both protein adsorption process and cell adhesion process continuously by one parameter. It is the first report about this subject. On initiator-SAM, PMEMA and COOH-SAM surfaces whose adherent cells number are almost same, ΔF's showed clearly difference. The different QCM-D signals to initial cell adhesion behaviors would be corresponded to the adsorption state of proteins and surface chemical/physical characteristics.

**CONCLUSIONS:** Protein adsorption and following cell adhesion behaviors on the well-defined polymer brush surfaces were monitored continuously with time using QCM-D. It is clear that the initial cell adhesion behaviors were strongly influenced by protein adsorption state induced from surface characteristics. We confirmed that it is applicable to understand initial cell-materials interactions and design of new biomaterials.

**REFERENCES:** [1]N. Faucheux, et al (2004) *Biomaterials* **25**: 2721-30.

# Cationic amphiphilic calixarenes for hierarchical assembly of DNA nanoparticles and gene delivery

A. S. Klymchenko,[1] R.V. Rodik,[2] N. Jain,[1] L. Richert,[1] V.I. Kalchenko,[2] Y. Mely[1]

*[1]LBP, UMR 7213 CNRS, Faculté de Pharmacie, Université de Strasbourg, France. [2]Institute of Organic Chemistry, National Academy of Science of Ukraine, Kiev, Ukraine.*

**INTRODUCTION:** Assembly of small DNA particles constitutes a fundamental problem in the gene delivery research. While viruses are able to compact a single DNA/RNA molecule into nanoscopic objects of 30-100 nm, most of well established nonviral gene delivery vectors, such as cationic lipids and polymers form complexes with multiple DNA molecules of poorly defined architecture and size. The need for supramolecular concepts in the development of nonviral vectors becomes very clear in the recent years.[1] Especially interesting in this respect is an approach of hierarchical self-assembly,[2,3] which could utilize pre-assembled building blocks to construct vectors of controlled architecture. Macrocyclic amphiphilic molecules based on calix[4]arenes are highly attractive in this respect because they present unique pre-organized conical architecture that favors their self-assembly into well-defined cationic micellar building blocks for DNA nanoparticles.[4]

**METHODS:** Synthesis of the target cationic calixarenes was done in several steps from corresponding tetraalkyl-calixarenes. Their self-assembly into micelles was followed by fluorescent probes and fluorescence correlation spectroscopy (FCS). Gel electrophoresis in agarose was used to study interaction of calixarenes with DNA, while DNA condensation was followed by ethidium bromide (EtBr) exclusion assay. Size of the complexes was examined by dynamic light scattering (DLS) and FCS. Atomic force microscopy (AFM) in liquid phase was performed to study their morphology. Transfection efficiency of the DNA-calixarene complexes was tested for different formulations by luciferase assay. Cytotoxicity was analyzed by MTT-based assay.

**RESULTS:** In the present work, new amphiphilic calixarenes bearing cationic groups at the upper rim and alkyl chains at the lower rim were synthesized. It was found that calixarenes bearing long alkyl chains (octyl) self-assemble into micelles of 6 nm diameter at low critical micellar concentration and present unique ability to condense DNA into small nanoparticles of *ca* 50 nm diameter (Fig. 1). In contrast, short-chain (propyl) analogue that cannot form micelles at low concentrations failed to condense well DNA giving large polydisperse DNA complexes. The small particles from the long-chain calixarenes bearing luciferase-encoding DNA plasmid showed much better gene transfection efficiency in cell culture as compared to the large DNA complexes of the short-chain analogue. Helper lipid DOPE improved considerably the efficiency. Moreover, all the studied cationic calixarenes showed low cytotoxicity.

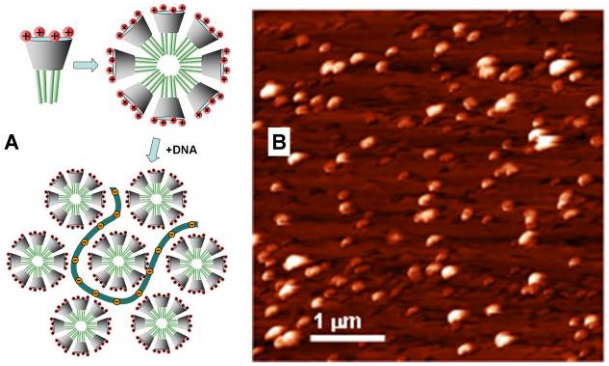


*Fig. 1: Assembly of a cationic calixarene (A) and an AFM image of a DNA-calixarene complex (B).*

**DISCUSSION & CONCLUSIONS:** The obtained results suggest that formation of the small DNA nanoparticles is hierarchical, so that it requires pre-formation of micellar building blocks from calixarenes that further co-assemble with DNA into small virus-like particles (Fig. 1A). This two-step hierarchical concept is promising for development of efficient gene delivery vectors featuring well- organized supramolecular architecture.

**REFERENCES:** [1] E Mastrobattista,.; M.A.E.M. van der Aa, W.E. Hennink, et al (2006) *Nat Rev Drug Discov* ***5***:115-121. [2] H. Wu, V.R. Thalladi, S. Whitesides, et al (2002) *J Am Chem Soc*, **124**: 14495-502. [3] A.S. Klymchenko, S. Furukawa, K. Mullen et al (2007) *Nano Lett* **7**:791-5. [4] Y. Aoyama, T. Kanamori, T. Nakai, et al (2003) *J Am Chem Soc* **125**: 3455-7.

**ACKNOWLEDGEMENTS:** We acknowledge financial support of FRM. We thank to the groups of J.-S. Remy and B. Frisch for help with luminometry and DLS measurements.

European Cells and Materials Vol. 20. Suppl. 3, 2010 (page 140) ISSN 1473-2262

# Sensitivity considerations in dual-gated Si-nanowire FET sensors

O.Knopfmacher, A.Tarasov, W.Fu, M.Calame, C.Schönenberger

*University of Basel, Basel, Switzerland*

**INTRODUCTION:** Field effect transistors (FETs) based on nanowires (NWs) are increasingly used for the label-free detection of analytes in chemical and biological experiments and have been recently applied to nanoscale devices like nanowire (NW) FETs [1]. The detection concept is based on the charge density modulation in the FET channel via a gate electrode. By gating the device, the carrier density of the device channel can be changed. Gating can be realized either through electrostatic potentials $V_{bg}$ or $V_{lg}$ applied respectively to a back gate electrode underneath the channel or to the surrounding liquid containing the analytes. Devices like the ion sensitive FET (ISFET) allows measuring proton concentration (pH) of an electrolyte. We study here silicon-based NW-FETs in a dual-gate approach (Fig. 1a) [2] that allows properly tuning the working point of the NW FET. We measure the conductance map G of the wire vs. $V_{bg}$ and $V_{lg}$ (Fig. 1b) for different pH-values. A change in pH results in a shift of the conductance onset, which we characterize by the threshold shift $V_{th}$, as illustrated in Fig. 1c for pH 4 (dashed line). The maximum threshold shift amounts to 59.5mv/pH, as determined by the Nernst equation. Interestingly, we find that these shifts can take up values exceeding the Nernst limit in certain regime for dual-gated NW-FETs (Fig. 1d).

**METHODS:** Si-nanowire FETs were fabricated following a top-down approach, etching the structures into SOI-wafers [3]. For the operation in electrolyte environments and to prevent leakage currents, we deposited a thin $Al_2O_3$ ALD layer. The electrical characterization of the NW FETs was performed in the linear regime at low source-drain voltage $V_{sd}$ (10 - 100mV). Fig 1a shows a sketch of the measurement setup. The operation point of the FET is adjusted by means of a dual-gate system, where gate voltages are simultaneously applied to the back- and the liquid gate. All measurements were performed in standard pH buffer solutions.

**RESULTS:** The 2d-conductance map G for a NW FET is shown in Fig. 1b as a function of both $V_{bg}$ and $V_{lg}$, measured at pH 6. To analyze the conductance change at different pH values, 2d-maps have been recorded at pH values ranging between 2 and 9. Conductance traces at constant liquid-gate voltage $V_{lg}$ = 0V can be extracted as shown in Fig. 1c. By increasing the pH values the conductance curves and hence the threshold voltages $V_{th}$ shift to more positive gate values. Fig. 1d summarizes the deduced voltage threshold shifts plotted against the pH value. Surprisingly, we found that for fixed liquid gate potentials, the sensitivity (i.e.: the slope of the graph, in mV/pH) can vary from very small values of only a few mV/pH to values that exceed the Nernst limit (dotted line).

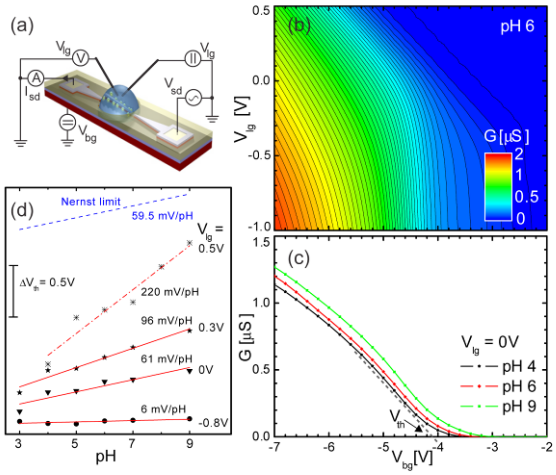


*Fig. 1: (a) Sketch of the measurement setup. (b) 2d-conductance map at pH 6 as function of $V_{lg}$ and $V_{bg}$. (c) Effect of pH change on the transfer characteristics measured at $V_{lg}$ = 0V and different $V_{bg}$ voltages. (d) Measured $V_{th}$ vs. pH at different liquid-gate voltages. Data from two devices [4].*

**DISCUSSION & CONCLUSIONS:** The response of the NW-FET is governed by the ratio of the two gates capacitances. While the back-gate capacitance $C_{bg}$ remains constant throughout the experiment, the liquid gate capacitance $C_{lg}$ depends on the pH. This explains why sensitivities can exceed the Nernst limit in some cases. Taking the pH dependence of the liquid gate capacitance into account, we can normalize the threshold shifts by the capacitance ratio and obtain sensitivities in agreement with the Nernst limit [4].

**REFERENCES:** [1] F. Patolsky et al. (2006) *Nanomedicine* **1**:51. [2] O. Knopfmacher et al. (2009) *Procedia Chemistry* **1**:678. [3] E. Stern et al. (2007) *Nature* **445**:519. [4] O. Knopfmacher et al. submitted.

# From Molecules to Cells: Sensing the Nanomechanical Way

Jochen Köser[1], Jasmin Althaus[2], Bert Müller[2], Felice Battiston[3] and Uwe Pieles[1]

[1] *University of Applied Sciences Muttenz, Switzerland.* [2] *Biomaterials Science Center, University of Basel, Switzerland,* [3]*Concentris GmbH, Basel, Switzerland.*

**INTRODUCTION:** Micromechanical cantilevers are tiny mechanical sensors which bend in response to expansion and contraction reactions on their surface. Such bending responses have been observed upon molecular interactions of various ligands with cantilever immobilized receptor molecules such as ssDNA, antibodies, enzymes and also with synthetic receptor molecules[1]. Here we will present examples for this application of cantilever sensors as biosensors and the recent use as a research tool for surface sciences and cell biomechanics.

**METHODS:** Nanomechanical silicon cantilever sensors with typical dimensions of 500 x 100 x 1 µm, which allow the detection of forces as small as 0.01 mN/m, have been applied for the experiments. Following gold-coating of the top side of the cantilevers molecules can be immobilized selectively on either the top or the bottom side by thiol or silane chemistry. Subsequently cantilever sensors are transferred to the Cantisens Research detecting system (Concentris GmbH, Switzerland) and surface stress induced changes in cantilever bending are monitored via the beam deflection principle (*Fig. 1*).

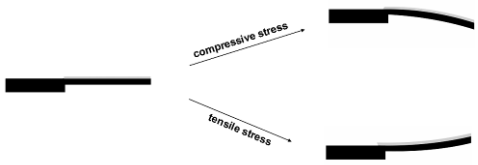


*Fig. 1: Cross section view of the cantilever sensor based surface stress sensing principle.*

**RESULTS:** As an example for the use of cantilevers as biosensors data will be presented for the label free real time detection of DNA using this measurement principle.

Another application of cantilever sensors is the monitoring of layer formation processes such as protein immobilization on a sensor surface or the build-up of multilayered structures (polyelectrolyte multilayers, layer-by-layer, LBL) which can be followed in real time and whose internal stresses can be determined[2]. We will present data on the kinetics of multilayer formation as well as the influence of polyelectrolyte concentrations on the internal stress of such multilayer surface coatings (*Fig. 2*).


*Fig. 2: Surface stress in LBL coatings.*

Recently we have gone one step further in size scale and have applied cantilever sensors for the quantification of forces exerted by whole cells growing on hard surfaces like medical implants or standard tissue culture dishes. To this aim cells are plated on cantilever sensors, are allowed to adhere and develop contractile cell forces which bend the cantilever. Subsequently the cells are enzymatically released and the concomitant relaxation of the support is recorded (*Fig. 3*). Multiplexing this measurement principle will allow in the future the biomechanical characterization of cells growing on surfaces with different molecular and topographical characteristics thus having practical implications for medical implant design.

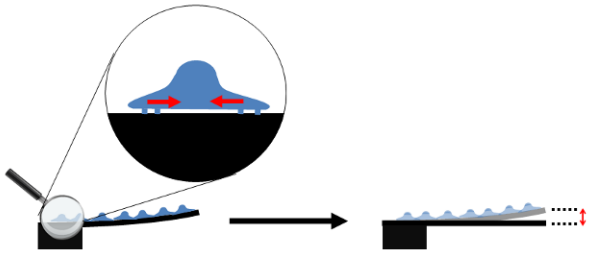

*Fig. 3: Principle of a cantilever sensor based cell force quantification assay.*

**DISCUSSION & CONCLUSIONS:** Sensors based on nanomechanical cantilevers have matured over the years and are now used for a wide range of applications. Their unique mechanical sensing principle makes them a useful tool not only for bio- and chemical sensing but also in the areas of surface sciences and complex cell biological studies.

**REFERENCES:** [1] Vashist, *Journal of Nanotechn. Online* (2007), [2] Koeser *et al.*, *J. Nanoscience and Nanotechnology* **10 (4)**, 2578-82 (2010).

**ACKNOWLEDGEMENT:** We are thankful to funding by the KTI, the Swiss Nanoscience Institute and the EU FP6 programm.

# Preparation of elongated polyelectrolyte particles from particles

Dorothee Kohler[1,2], Marc Schneider[3], Claus-Michael Lehr[2], Michael Krüger[4], Helmuth Möhwald[1] and Dayang Wang[1]

*[1]Max Planck Institute of Colloids and Interfaces, Potsdam, Germany. [2] Helmholtz-Institute for Pharmaceutical Research, Saarland (HIPS) & Saarland University, Germany. [3]Pharmaceutical Nanotechnology, Saarland University, Saarbrücken, Germany. [4] Boehringer Ingelheim Pharma GmBH& Co.KG, Ingelheim, Germany*

**INTRODUCTION:** Drug delivery to the lung gained importance during the past decade. New particulate aerosol drug carriers are needed to improve not only deep lung deposition, but also to overcome rapid pulmonary clearance.

In our study, rods with defined dimensions are prepared by an extended template technique. Polyelectrolyte elongated particles are prepared and loaded with polyelectrolyte capsules resulting in multicompartment structures.

**METHODS:** Polystyrene (PS) and Silica spheres were modified by additional Polyallylamine (PAH)/ Polystyrenesulfonate (PSS) layers. The polyelectrolytes are deposited in a layer by layer (LBL) procedure as described elsewhere [1].

PS or Si spheres, modified or unmodified, are used as colloidal models for particle infiltration into pores of Polycarbonate (PC) membranes with varying pore size (0.2-5µm) by pressure infiltration. The PC membrane is placed on a second PC membrane with a pore size smaller than the infiltrated particles to prevent spheres to be pushed out from the pores.

To interconnect the particles, polyelectrolytes are deposited in a LbL procedure as described previously. The PC membrane is dissolved in CH2Cl2 to liberate the prepared rods.

**RESULTS:** Rods with different aspect ratios were prepared, by using different pore diameters. Particles with aspect ratios ranging from 1:2 to 1:10 are shown in figure 1.

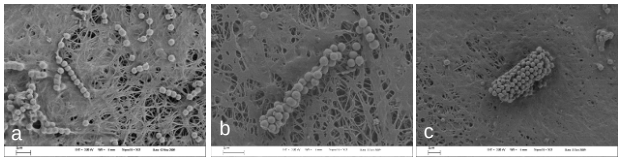


*Figure 1: SEM pictures of a) Si (841nm) in 1µm PC-membrane, b) Si (841nm) in 2µm PC-membrane and c) Si (841nm) in 5µm PC-membrane. All particles are coated with 5 bilayers PAH/PSS and interconnected by 3bilayers PAH/PSS prior to the dissolution of the PC-membrane*

PS particles as infiltrated particles will result in polyelectrolyte rods filled with hollow polyelectrolyte capsules as can be seen in figure 2, as the particles are decomposed during the template decomposition. These resulting hollow capsules can afterwards be loaded with active ingredients as described in literature for polyelectrolyte capsules.

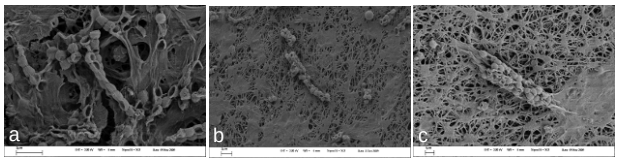


*Figure 2: a) PS (836nm) in 1µm PC membrane, b) PS (836nm) in 2µm PC-membrane and c) PS (836nm) in 5µm PC-membrane. All particles are coated with 5 bilayers PAH/PSS and interconnected by 3bilayers PAH/PSS prior to the dissolution of the PC-membrane.*

**DISCUSSION & CONCLUSIONS:** A new technique was established to produce hollow polyelectrolyte rods with defined length and diameter. Rods with different aspect ratio and porosity could be prepared.

**REFERENCES:** [1]Caruso, F. (2003) Hollow inorganic capsules via colloid-templated layer-by-layer electrostatic assembly in *Colloid Chemistry*, **227**: p. 145-168.

**ACKNOWLEDGEMENTS:** This project is financially supported by Boehringer Ingelheim Pharma GmbH Co.KG. Dr. M. Wolkenhauer and Dr. R. Cartier, (Boehringer Ingelheim, Ingelheim, Germany) are acknowledged for the fruitful scientific discussions.

# Single cell analysis based on functional phospholipid polymers

T.Konno[1], K.Taniguchi[1,2], H.Nishida[1,2], H.Kambara[1,2], K.Ishihara[1]

[1] *Advanced Biodevice Engineering Lab., Department of Bioengineering, School of Engineering, The University of Tokyo, Tokyo, Japan.*

[2] *Central Research Laboratory, Hitachi Ltd., Tokyo, Japan.*

**INTRODUCTION:** The importance of single cell analysis has been increased with a development of regenerative medicine. It has been revealed that the amount of gene expression is different in a single cell level[1]. Therefore, it is important to investigate the cell functions in a single cell level. We develop the single cell analysis device based on cytocompatible phospholipid polymers. The phospholipid polymer, 2-methacryloyloxyethyl phosphorylcholine (MPC) polymer, was synthesized. A photo-reactive MPC polymer was synthesized to prepare a micropattern surface[2]. Mouse embryonic stem (ES) cells were plated on the MPC polymer surface to guide an embryoid body[3]. And, a reversible polymer hydrogel was prepared as cell immobilization platform matrix to manipulate a single cell[4].

**METHODS:** The round bottom surface was coated with water-insoluble MPC polymer. The ES cells were plated on the surface. The cell aggregate (embryoid body, EB) formation was induced on the surface. Photo-reactive MPC polymer was used to prepare micropattern surface. The ES cells were plated on the surface with 100 μm square of adhesive region. The ES cell was cultured, and the formed colony was immunostained (alkaline phosphatase staining) to evaluate their undifferentiation property. Water-soluble MPC polymer containing phenylboronic acid moiety was mixed with poly(vinyl alcohol) to form polymer hydrogel. The cells including ES cells were encapsulated in the hydrogel. The proliferation and differentiation of encapsulated cells were evaluated.

**RESULTS:** The ES cells plated on the MPC polymer surface were aggregated in an each well, and the single EB was formed (Fig. 1).

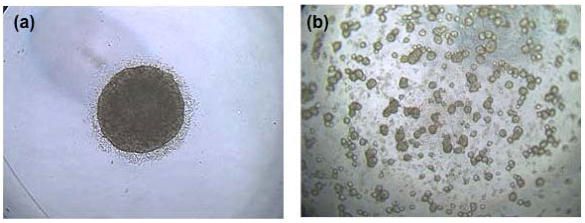


*Fig.1 Phase contrast microscope images of ES cells on MPC polymer (a) and hydrophobic polystyrene (b).*

The size of EB was depended on initial cell number. The ES cells plated on the micropattern surface prepared with photo-reactive MPC polymer were formed ES cell colony. The colonies were well stained by alkaline phosphatase staining which means their undifferentiated property (Fig. 2).

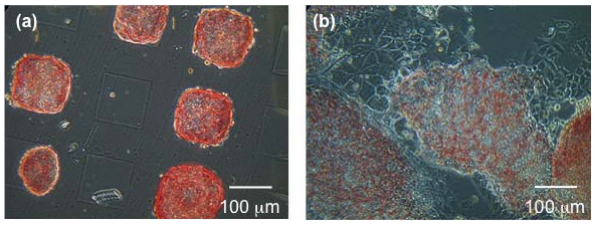


*Fig.2 Alkaline phosphatase staining image of ES cells on micropattern surface (a) and unpatterned surface (b).*

The spontaneously forming hydrogel (PMBV/PVA hydrogel) was used as a 3D cell immobilization matrix. The ES cells immobilized in the hydrogel were maintained their undifferentiated state. In the case of fibroblast cells, the immobilized cell was proliferated from a single cell level, and the homogeneous cell aggregate was formed in the PMBV/PVA hydrogel (Fig. 3).

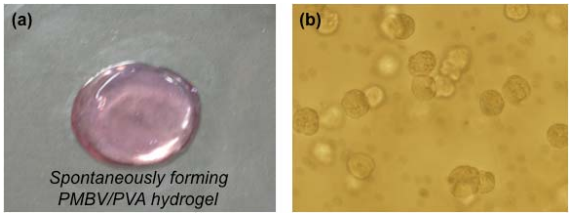


*Fig. 3 Digital photograph of PMBV/PVA hydrogel (a) and cell aggregate derived from encapsulated cell immobilized as single cell in the hydrogel.*

**CONCLUSIONS:** The cytocompatible MPC polymers bearing various functional monomers were useful platform biomaterials to investigate and development for single cell analysis.

**REFERENCES:** [1]K. Taniguchi et al (2009) *Nature Methods* **6**:503-6. [2]T. Konno et al (2005) *Biomaterials* **26**:1381-8. [3]T. Konno et al (2005) *J.Biosci.Bioeng.* **100**:88-93. [4]T. Konno et al (2007) *Biomaterials* **28**:1770-7.

# Optical Biosensing Based on Photonic Crystal Surface Waves

V.N. Konopsky and E.V. Alieva

*Institute of Spectroscopy, Russian Academy of Sciences, Troitsk, Moscow region, 142190, Russia.*

**INTRODUCTION:** We present a new optical biosensing technique based on registration of bounded optical surface waves (SWs) propagating along an external interface of a one-dimensional photonic crystal (1D PC). Unique tunable properties of 1D PCs permit the design of a 1D PC structure with one of surface modes abutting on the angle of the total internal reflection (TIR) [1-3]. This mode, in which the exited angle is infinitesimally close to the angle of TIR from the external medium, has a very large penetration depth in this medium (e.g., water) and may be used as a reference of bulk RI fluctuations. This permits us to segregate the volume and the surface signals from the analyte and increase the sensitivity of the PC SW biosensor.

**METHODS:** For biosensing in a liquid, both *s*- and *p*-polarized PC surface waves (PC SWs) may be employed on a dielectric surface. The liquid RI may be determined by measuring the critical angle for *p*-polarization of the laser beam, while the *s*-polarization is used for the excitation of the adlayer-thickness-sensitive PC SW.

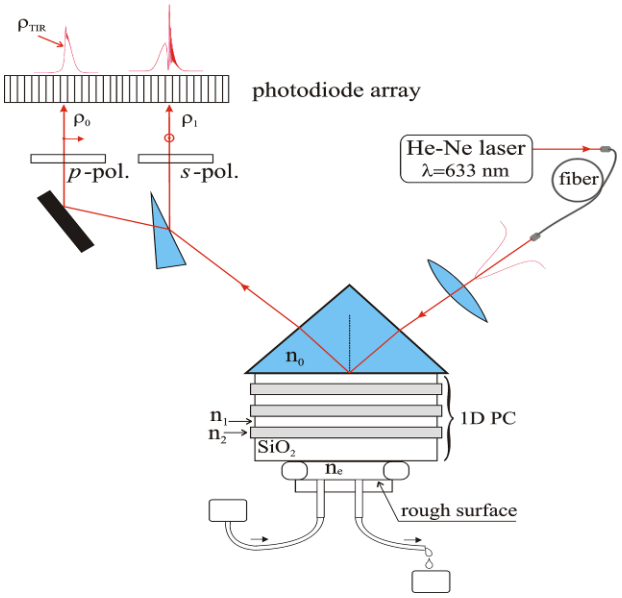


*Fig. 1: A sketch of the biosensor. The typical reflection profiles are shown near the photodiode array.*

The absence of metal damping (in contrast to the SPR technique) leads to increasing of propagation length for the *s*-polarized SW that enhances the sensitivity of this wave to the adlayer deposition. A high sensitivity of the RI detection in the presented technique arises from the fact that the sharpness of the reflection near the critical angle (for *p*-polarization) is much higher in this system than both in SPR-based systems and in standard critical-angle Abbe refractometers with uncoated prisms.

**RESULTS:** To demonstrate the biosensor's sensitivity we present the experimental data of free biotin binding on the streptavidin monolayer [4].

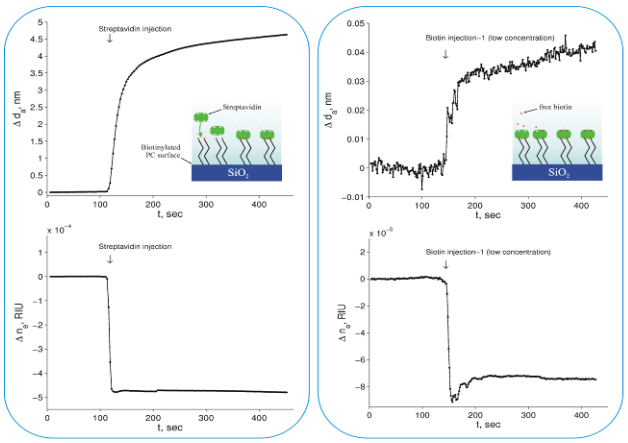


*Fig. 1: Immobilization of streptavidin on a biotinylated surface (top left) with subsequent binding of free biotin to this streptavidin monolayer (top right). Corresponding changes of RI of the buffer during these injections is shown at the bottom. In color inserts the possible corresponding processes are illustrated.*

**CONCLUSIONS:** The exploitation of the 1D PCs as substrates supporting the long-range optical surface wave propagation permits to detect the adsorption of (bio)nanofilms and their thickness variations at the level better than $10^{-3}$ nanometre, segregate surface and volume events in biosensing and improve the RI sensitivity of the Abbe-like refractometer to the level ~$10^{-8}$ RIU.

**REFERENCES:**[1] V.N. Konopsky, and E.V. Alieva (2006) *Phys. Rev. Lett.* **97**: 253904. [2] V.N. Konopsky, and E.V. Alieva (2007) *Anal. Chem.* **79**: 4729–35. [3] V.N. Konopsky, E.V. Alieva (2009) in *Biosensors and Biodetection*, vol. 503 (eds A. Rasooly and K.E. Herold) Humana Press, USA, pp.49-64. [4] V.N. Konopsky, E.V. Alieva, (2010) *Biosens. Bioelectron.* **25**: 1212–16.

**ACKNOWLEDGEMENTS:** This work was financially supported by the Russian Federal Program ''Research and educational personnel of innovative Russia'' and by the Russian Foundation for Fundamental Researches.

European Cells and Materials Vol. 20. Suppl. 3, 2010 (page 145) ISSN 1473-2262

# Rapid Microwave-Assisted Method for Preparation of Magnetic Nanoparticles for Hyperthermia Treatment

Z. Kozakova, V. Babayan, M. Sedlacik, I. Kuritka, V. Pavlinek

*Polymer Centre, Faculty of technology, Tomas Bata University in Zlin, TGM Sq. 275, 762 72 Zlin, Czech Republic*

**INTRODUCTION:** At the present time, magnetic hyperthermia treatment of cancer gets great attention due to its efficiency and harmlessness. The principle of this method is damaging the tumour cells by the heat generated by application of AC magnetic field on magnetic nanoparticles introduced into the diseased tissue.[1, 2] Since the values of strength and frequency of magnetic field are restricted for therapeutic application, the challenge is preparation of particles of suitable size and shape as well as excellent magnetic properties. Therefore many synthetic strategies for preparation of magnetic nanoparticles were published from which solvothermal methods appear to be ones of the most simple and efficient.[3] However, some aspects of these methods, namely the duration of the synthesis and relatively low yields lead us to use microwave pressurized system by which we are able to prepare particles within few minutes in high yields and simple tune particle properties.

**METHODS:** Magnetic nanoparticles were prepared by microwave-assisted solvothermal method using CEM Mars 5 pressurized reactor (CEM Corporation). $FeCl_3.6H_2O$ was used as the source of ferric ions, ethylene glycol as a solvent and reducing agent and aqueous $NH_3$, $(NH_4)_2CO_3$, **$NH_4Ac$** or $NH_4CO_3$ served as nucleating agents. Reactants were mixed together, loaded into Teflon vessels and heated in microwave reactor at the required temperature (200, 210, 220 °C) for 30 minutes. The as-obtained product was filtered off and allowed to dry at room temperature. The particle properties were investigated by X-ray diffraction (XRD), scanning electron microscopy (SEM) and vibrating sample magnetometry (VSM).

**RESULTS:** The XRD analyses confirm that the resulting product is $Fe_3O_4$ (magnetite or maghemite). As can be seen in Figure 1, particles are uniform, nanosized (around 200 nm) with spherical shape. VSM measurements showed that the saturation magnetization values vary from 8 to 76 $emu.g^{-1}$ depending on synthesis conditions.

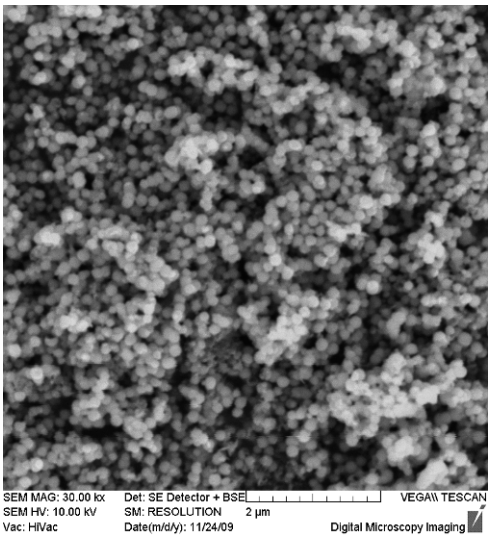


*Fig. 1: SEM image of $Fe_3O_4$ particles prepared with $NH_4Ac$ at 220 °C for 30 minutes.*

**DISCUSSION & CONCLUSIONS:** Microwave-assisted solvothermal synthesis of magnetic nanoparticles presented here is a fast method by which the product can be obtained in 30 minutes with suitable properties. As-prepared particles are uniform in shape, nanosized and exhibit ferromagnetic behaviour. Moreover, particles morphology and magnetic properties can be simply tuned by changing the synthesis conditions, namely, temperature, concentration of ferric ions as well as the type and concentration of nucleating agent. Temperature control of synthesis proved to be appropriate and very sensitive tool for tuning the magnetic properties when $NH_4Ac$ or $(NH_4)_2CO_3$ are used as nucleating agents. However, is not so applicable while using aqueous $NH_3$, although saturation magnetization is higher than in previous two cases.

**REFERENCES:** [1] E. Pollert et al (2009) *Progress in Solid State Chemistry* **37**: 1-14. [2] Q. A. Pankhurst et al (2003) *J. Phys. D: Appl. Phys.*, **36**: R167–R181. [3] H. Peng et al (2009) *Journal of Physical Chemistry C.* **113**: 900-906.

**ACKNOWLEDGEMENTS:** This work was supported by the internal grant of TBU in Zlin No. IGA/25/FT/10/D funded from the resources of specific university research.

# Tailor-made fluorescent nanocrystals for 2-photon in vivo imaging

L. Krapf[1], J. Dimitrijevic[2], A. Schüth[3], J. Niehaus[4], S. Becker[2], C. Schmidkte[2], T. Vossmeyer[2], G. Hüttmann[1], A. Gebert[3], H. Weller[2]

[1] *Institute of Biomedical Optics,University of Lübeck, Peter-Monnik-Weg 4, 23562 Lübeck, Germany*
[2]*Institute of Physical Chemistry, University of Hamburg, Grindelallee117, 20146 Hamburg, Germany*
[3] *Institute of Anatomy, University of Lübeck, Ratzeburger Allee 160, 23538* Lübeck, Germany
[4] *Centrum für Angewandte Nanotechnologie (CAN) GmbH, Grindelallee 117, 20146Hamburg, Germany*

**INTRODUCTION:** Two-photon laser scanning microscopy (TPLSM)[1] is an ideal tool to study the fate of single nanocrystals in vivo, due to the high penetration depth of NIR excitation into tissue and minimization of photodamages. Taking into account the significant autofluorescence background of tissue samples, this task, however, requires the design of nanocrystals with high fluorescence quantum yields (QYs) and exceptionally high two-photon action cross-sections. Moreover, in order to prevent degradation of optical properties in biological media, it is necessary to stabilize the nanocrystals by a suitable ligand shell. Here we describe the design and use of pegylated quantum dots and quantum dots@quantum rods as marker for TPLSM. In vivo imaging was performed by investigating murine intestinal tissue.

**METHODS:** Hot-injection method was used to prepare highly luminescent CdSe/CdS/ZnS-quantum dots (QDs)[2] and CdSe/CdS-quantum dots@ quantum rods (QDs/QRs)[3]. Their optical and structural properties were studied by PL- and UV/vis-spectroscopy, TEM, XRD, and confocal microscopy. We used a PEO polymer with various exo-functional groups (-COOH, -OH, $-NH_2$) to stabilize the nanocrystals in aqueous media. TPLSM was conducted using a DermaInspect Microscope (Jenlab) and a TriMscope (LaVision BioTec), equipped with a tunable fs-NIR laser and multichannel detection systems.

**RESULTS:** Figure 1A shows absorption (red) and photoluminescence (black) spectra of a chloroform solution containing 30 nm long QDs/QRs grown from 4.8 nm CdSe seeds with cubic (zinc-blende) structure. TEM and HRTEM images display a high degree of crystallinity and monodispersity (figure 1B). Measured values of two-photon action-cross sections for QDs/QRs are more than one order of magnitude higher than those of QDs (~$10^5$ vs. ~$10^4$ GM). Spin-coated samples of QDs/QRs were imaged with TPLSM (figure 1C). Blinking behaviour, indicating the presence of single, non-aggregated crystals, was clearly observed. Additionally, single QDs/QRs were observed using polarized fluorescence detection. Figure 1D shows a section through murine intestinal villi recorded in vivo. This result proves the successful application of QDs/QRs as TPLSM marker used in a physiological environment.

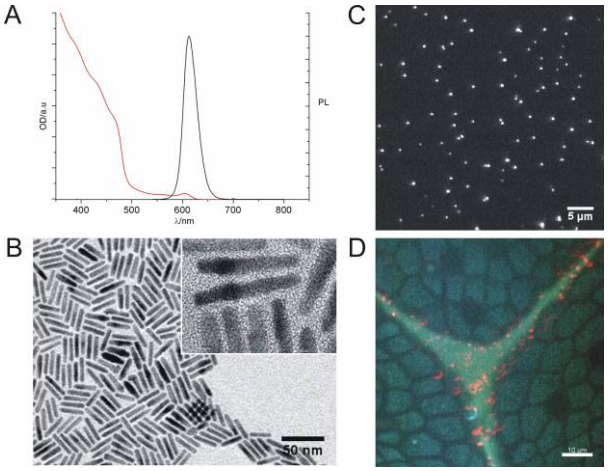


*Fig. 1: A) Absorption (red) and emission (black) spectra of QDs/QRs in $CHCl_3$. B) TEM image of QDs/QRs. C) Single QDs/QRs imaged with TPLSM. D) QDs/QRs between murine intestinal villi imaged in vivo.*

**DISCUSSION & CONCLUSIONS:** High PL QYs (~50%) and excellent photostability make pegylated semiconductor QDs very attractive marker for two-photon imaging and tracking of single particles in vivo. In this study we found that dot@rod-like nanocrystals (QDs/QRs) are especially useful for this purpose, because of their high two-photon action cross section, which results from their relatively large volume and their high quantum yield (>70%). The stability of such hetero-structures in combination with their supperior optical properties makes them promising candidates for studying uptake pathways of nanoparticles through tissue barriers (i.e. the small intestinal epithelium) by TPLSM.

**REFERENCES**. [1]W. Denk, J.H. Strickler, W.W. Webb (1990), *Science* **284**:73. [2]D. Talapin, H. Weller (2004), *J. Phys. Chem. B* **108**:18826. [3]L. Carbone, L.Manna (2007), *NanoLett.* **7**:2942.

**ACKNOWLEDGEMENTS:** This project is supported by the Deutsche Forschungsgemeinschaft, SPP 1313-Programme.

# Passive trapping, levitation and assembly of nanometric objects in a fluid

M.Krishnan, N. Mojarad, V. Sandoghdar

*Laboratory for Phyiscal Chemistry, ETH Zurich, Switzerland.*

The ability to trap an object in space, whether a single atom or a macroscopic entity, is of primary importance in fields ranging from quantum optics to soft condensed matter physics, biophysics, and clinical medicine [1,2]. Many sophisticated methodologies have been developed to counter the randomizing effect of Brownian motion in solution, but stable trapping of nanometric objects remains very challenging [3-5]. For example, optical tweezing requires sufficiently polarizable objects and is therefore unsuitable for manipulating small macromolecules.

Here we present a fluidic trap concept that addresses these issues and provides trapping and levitation of single charged nano-objects such as gold particles, polymer beads, and lipid vesicles for up to several hours. The principle is based on the spatial modulation of the electrostatic potential created in a topographically-tailored fluidic nanoslit. As a result, the trap requires no external intervention and is free of constraints imposed by the object's mass or dielectric function. The stiffness and stability of the trap can be tuned by varying the geometry of the system and the ionic strength of the environment. The technique may be readily integrated with other manipulation mechanisms and holds great promise for contact-free confinement of single proteins and macromolecules, sorting and fractionation of nano-objects, and the assembly of high-density arrays with applications ranging from biophysics to nanophotonics.

The disc-shaped pocket and groove structures investigated in our work can be generalized to a wealth of trap morphologies with different functionalities. In particular, elongated trap geometries could be used to confine and align anisotropic nano-objects such as ellipsoids and nanorod [6]. The inherently compact architecture of the trap described here facilitates high-throughput, parallel processing of a large number of particles. Indeed, our preliminary works have succeeded in assembling rewriteable arrays of nanoparticles at a lattice spacing of 500 nm. The technique may be readily integrated with other manipulation mechanisms and holds great promise for the assembly of high-density arrays for plasmonic and nanophotonic applications. We discuss the prospects of this method in the context of self-assembly of two-dimensional "fluidic metamaterials".

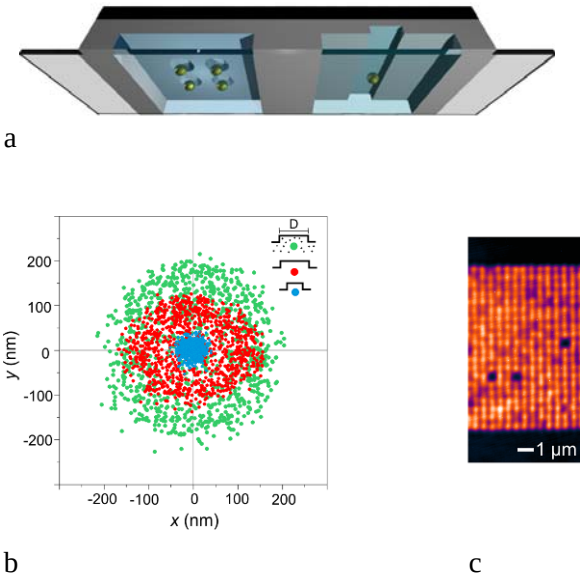


*Fig. 1: (a) A pictorial representation of the fluidic device. (b) Scatter plot of positions of a 100 nm gold particle confined under different conditions: pocket diameter, D= 200 nm (blue), D=500 nm (red) and D= 500 nm with 0.1 mM salt added to the aqueous phase. (c) An array of 100 nm gold particles assembled at a center-to-center spacing of 500 nm.*

**REFERENCES:** [1] S. Chu (2002) Cold atoms and quantum control, *Nature* **416**: 206-210. [2] D. G. Grier (2003) A revolution in optical manipulation, *Nature* **424**: 810-816. [3] A. E. Cohen & W. E. Moerner (2006) Suppressing Brownian motion of individual biomolecules in solution, *Proceedings of the National Academy of Sciences of the United States of America* **103**: 4362-4365. [4] A.H.J. Yang (2009) Optical manipulation of nanoparticles and biomolecules in sub-wavelength slot waveguides, *Nature* **457**: 71-75. [5] M. L. Juan et al (2009) Self-induced back-action optical trapping of dielectric nanoparticles, *Nature Physics* **5**: 915-919. [6] A. Jamshidi *et al.* (2008) Dynamic manipulation and separation of individual semiconducting and metallic nanowires, *Nature Photonics* **2**: 85-89.

# Protein nanopatterning for studying cell adhesion

Stine Kristensen, Jenny Malmström, Jette Lovmand, Mogens Duch and Duncan S. Sutherland

*Interdisciplinary Nanoscience Center(iNANO), Aarhus University, Denmark*

**INTRODUCTION:** Synthetic materials are often used for biomedical applications. Interaction of cells with the interfaces and tissue components determine the biological outcome of the device. Knowledge about the interaction between the cells and biointerfaces is hence of importance in area such as biomaterials, tissue engineering and cell culture. The interaction of the cells with its surroundings is mediated at the molecular and macromolecular level. Specific interaction with the extracellular matrix (ECM) components or macromolecules in the outer membrane of adjacent cells provides signaling and communication pathways.[1, 2] These kinds of interfaces have both topographic nanostructure and chemical interaction site distributed at the nanoscale.[3]

**METHODS:** Protein nanopatterns at the 100-3000 nm scale and with lateral ordering between independent ligands and controlled lateral mobility has been made by using a nanoscale chemical contrast of Au patches in a background of $SiO_2$ by colloidal lithography. The nanostructured surfaces are made by depositing a triple polyelectrolyte layer (PSS/PDDA/Aluminium chloride hydroxide) at Au substrates. Latex particles self assemble at the surface governed by electrostatic forces followed by $SiO_2$ evaporation and removal of the particles.[4] The generated short range ordered arrays were further modified by octadecylmercaptane adsorption (2mM in ethanol). The samples were subsequently treated with PLL(20)-g(3.5)-PEG(2) 0.25/ml in 10mM HEPES buffer pH 7.4 for 30 minutes followed by rinsing. Fibronectin (20 µg/ml) was adsorbed to the substrates from TRIS Buffer (10mM TRIS 2.7mM KCl, 137 mM NaCl pH 7.4 )for 2 hours followed by rinsing.

**RESULTS:** Fibronectin distribution at the nanopatterned surfaces was studied via liquid AFM showing that protein was observed to adsorb preferentially on the methyl terminated thiol films at the gold patches. SEM images showed that protein coating was deposited over large areas. Fibronectin patterns in regions between cells for substrates cultures appeared the same as those for the original deposited protein nanopatterns. Protein patterns of several other proteins such as Osteopontin, Vitronectin and Laminin were also demonstrated.

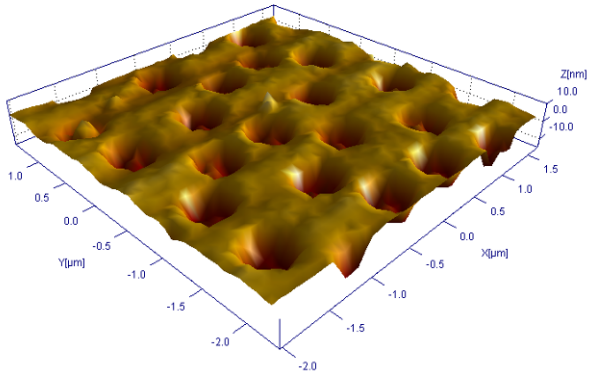


*Fig. 1: Representative TM-AFM combined height and phase image of a nanostructured surface made by colloidal lithograph. The nanopatterned substrate is modified by thiolation (protein adhesive) of the gold holes and PLL-g-PEG (protein repulsive) is adsorbed onto the $SiO_2$ patches to prevent the protein binding. Fibronectin are adsorbed into the modified gold holes.*

**DISCUSSION & CONCLUSIONS:** Colloidal lithography combined with alkanethiol and PLL-g-PEG modification was used to demonstrate protein patterns of different size scale from the nano to the micro scale and from different proteins. The patterns are of a sufficiently large area to carry out large scale cellular characterisation in terms of adhesion, morphology and differentiation.[5]

**REFERENCES:** [1]Geiger, B. et al., *Nature Reviews Molecular Cell Biology* **2001,** 2, (11), 793-805. [2]Geiger, B. et al., *Nature Reviews Molecular Cell Biology* **2009,** 10, (1), 21-33. [3]Teixeira, A. et al, *Journal of Vacuum Science & Technology B: Microelectronics and Nanometer Structures* **2003,** 21, (2), 683-687. [4]Hanarp, P. et al, *Colloids and Surfaces a-Physicochemical and Engineering Aspects* **2003,** 214, (1-3), 23-36. [5]Malmstrom, J. et al, *Nano Letters* 10, (2), 686-694.

**ACKNOWLEDGEMENTS:** This work was supported by funding from the Lundbeck foundation and FTP.

# High-Throughput Analysis of Vesicle Membrane Permeation Using a Droplet-Based Microfluidic System

S. K. Küster, D. Lombardi, P. S. Dittrich

*Department of Chemistry and Applied Biosciences, ETH Zurich, Switzerland*

**INTRODUCTION:** Membrane permeability is an important parameter to predict the adsorption, diffusion, metabolism and elimination (ADME) properties of a drug.

In this contribution, we present a method for studying the kinetics of passive permeation of a drug through a liposome membrane on a microfluidic chip.

**METHODS:** The liposomes enclose the lanthanide europium that becomes highly fluorescent upon complexation with tetracycline (TC) and a number of other similar drug molecules. In order to achieve fast mixing of the suspended liposomes with dissolved TC, we introduce both solutions into microdroplets, generated continuously in a stream of hydrophobic carrier solution on the microfluidic chip (Fig. 1) [1].

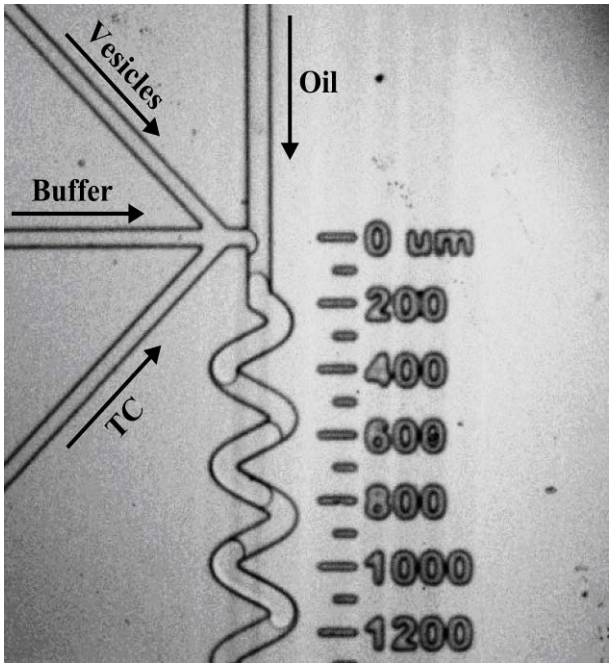


*Fig. 1: Image of the microfluidic device made of poly(dimethyl siloxane). The aqueous solutions (suspended vesicles, buffer, tetracycline (TC)) are introduced through separate input channels and injected into the continuous stream of a hydrophobic carrier (oil).*

These microsized compartments, formed in-situ on the microchip, pass a combination of turns and straight channel sections, which promotes rapid mixing of target molecules and liposomes thereby enabling the evaluation of fast kinetics in the time range of msec up to sec.

Determination of the fluorescence intensity in individual droplets along the microchannel by means of a confocal laser scanning microscope allows us to continuously monitor the permeation process and to determine the permeation rate.

**RESULTS:** Our studies include the uptake of tetracycline into liposomes made of DLPC and furthermore, the influence of cholesterol and membrane rigidity on the permeation rate.

**DISCUSSION & CONCLUSIONS:** With this new tool in hand, we are able to screen membrane permeation of possible drug candidates with high sensitivity. Our ultimate goal is the incorporation of the continuous method in a modularly designed screening device, to systematically determine the ADME/Toxicity potential of a drug candidate.

**REFERENCES:** [1] H. Song and R.F. Ismagilov (2003). *J Am Chem Soc* **125**: 14613-9.

**ACKNOWLEDGEMENTS**: The project was financially supported by the European Research Council under the 7th Framework Programme (ERC Starting Grant, project no. 203428, nμLIPIDS).

# Knowledge-based design of a reagentless protein kinase activity biosensor from designed ankyrin repeat proteins

L.Kummer[1], P.Mittl[1], A.Plückthun[1]

[1] *Department of Biochemistry, University of Zurich, Zurich*

**INTRODUCTION:** Eukaryotic protein kinases are key signaling molecules to orchestrate complex signal transduction and regulatory pathways. Dysregulation of protein kinases is an essential part of a variety of diseases, and consequently underlines the need of selective and sensitive methods for accurate and direct assessment of kinase activities. Affinity probes based on small, organic fluorophores with direct readout fulfill all requirements and are thus ideally suited for high-throughput applications [1]. At present, specific binding probes are often proteins, in most cases antibodies. While antibodies and their engineered derivatives provide great specificity, affinity and variability, they have several intrinsic limitations, mostly due to their insufficient conformational stability and *in vitro* half-lives under harsh conditions, precluding their intracellular use and limiting their use in assays. In an attempt to overcome these obvious limitations, a new binding scaffold based on ankyrin repeat proteins was developed in our laboratory [2]. Combinatorial libraries of designed ankyrin repeat proteins (DARPins) have been generated by randomization of the paratope. DARPins show very favorable biophysical properties and specific high-affinity binders were successfully selected against a variety of protein antigens [2].

**METHODS:** Inactive and active extracellular signal regulated kinase 2 (ERK2), a mitogen-activated protein kinase (MAPK) pivotal for regulation of cell survival and proliferation, were used as targets for selection of binders from combinatorial DARPin libraries. Selections were carried out by ribosome display, a complete *in vitro* selection technology developed in our laboratory [3]. The enriched pools of binders were tested for their specific interaction with ERK2 by enzyme-linked immunosorbent assay (ELISA) and affinity precipitations from eukaryotic cell lysate. The most promising selected DARPins were further characterized by gel-filtration chromatography and affinity measurements. Structural analysis of DARPin/unphosphorylated ERK2 (AR40/ERK2) and DARPin/phosphorylated ERK2 (AR59/pERK2) complexes was carried out to elucidate binding specificity and to identify DARPin residues amenable for site-directed coupling of suitable fluorophores via the introduction of cysteine mutations.

**RESULTS:** Selections were carried out with DARPin libraries consisting of two or three randomized ankyrin repeat modules between an N-terminal and a C-terminal capping repeat [2]. Three to four standard ribosome display selection rounds were sufficient to select for high-affinity binders. Selected DARPins reliably differentiate between the unphosphorylated inactive and phosphorylated active form of the MAPK ERK2 both *in vitro* and in cell lysates. No cross-binding to other MAPK family members was observed. Furthermore, the binders are monomeric and have affinities in the low nM range. Co-crystallization studies of AR40/ERK2 and AR59/pERK2 revealed that both DARPins are in contact to the activation loop and C-terminal lobe of the kinase, regions known to be structurally different in the inactive and active form of ERK2. In order to create fluorescent affinity probes the crystal structures of the DARPin/kinase complexes were used to locate suitable residues as potential coupling sites for different fluorophores.

**DISCUSSION & CONCLUSIONS:** Despite the high similarity of the target proteins, selected DARPin binders were able to recognize specifically small structural differences between the inactive and active form of the MAPK ERK2. In addition, the concept of ankyrin based fluorescent biosensors may be applied to other antigen proteins, even without structural information, because of the conserved geometry of the DARPin paratope. Due to their superior stability DARPin based biosensors could have a major impact in numerous applications ranging from drug discovery to diagnostics.

**REFERENCES:** [1] E. Brient-Litzler, et al. (2010) *PEDS* **23**:229-241. [2] H.K. Binz, et al (2005) *Nat Biotechnol* **23**:1257-1268. [3] J. Hanes, and A. Plückthun (1997) PNAS **94**:4937-4942

European Cells and Materials Vol. 20. Suppl. 3, 2010 (page 151) ISSN 1473-2262

# Silicon Nanowires as Biochemical Sensors

J. Kurz[1], U. Pieles[1], Ch. Schönenberger[2]

[1] *Nanotechnology Group, University of Applied Sciences Northwestern Switzerland, Muttenz, Switzerland.* [2] *Department of Physics, University of Basel, Switzerland.*

**INTRODUCTION:** Recently, intense investigations have been performed for creating and using silicon nanowires (SiNWs) as biochemical sensors [1–3]. The operation principle of such a sensor is based on the modulation of the NW surface potential through a field effect, due to binding of analyte molecules to receptors attached to the sensor surface. NWs, thanks to their large surface to volume ratio, tuneable electrical properties and biocompatibility, have a great potential to become highly sensitive, label-free, electrical sensors.

**METHODS:** The conversion of SiNW transistors into biochemical sensors is performed by linking specific functional groups to the silicon surface. Two methods of surface preparation have been tested: for silicon oxide surface modification, various silanization procedures were used, while hydrosilylation was carried out to functionalize the hydrogen-terminated silicon surface.

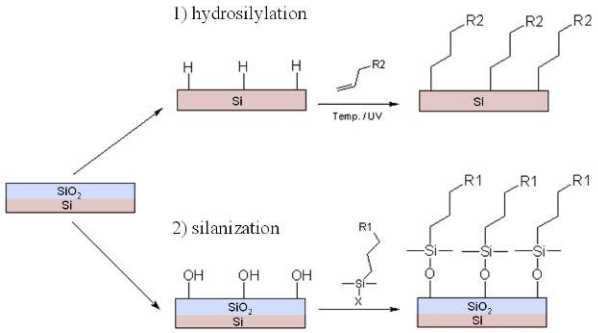


*Fig. 1: The concept of two procedures used to functionalize different SiNWs regions, with and without an oxide layer.*

The efficiency of the functionalization process was evaluated by fluorescent labelling, contact angle and XPS measurements.

**RESULTS:** The possibility of the selective modification of the NW surface offers the promise of enhancing the functionality and sensitivity of the biosensor. Certain layers can act as passivating, antiadhesive and non-fouling coatings, stabilizing the properties of the underlying substrate, whereas others can be used to tailor the specific functional properties of the sensor.

The resistance of the NW surface to unwanted interactions is a critical issue, crucial for biosensor development. Limiting the binding of an analyte to the electronically inactive regions of the nanowire may by achieved with fluoro-compounds, which are known to provide excellent water repellency, while PEG/OEG coatings successfully limit unspecific protein adsorption. Surface hydrophobicity was verified with the contact angle method, whereas protein adsorption was monitored using fluorescent assays.

Functional layers were created using amine- and carboxy-terminated linker molecules. This type of surface modification provides the opportunity for a variety of chemical strategies to immobilize biological receptors on the NW surface. The successful introduction of reactive groups onto the silicon surface was followed by contact angle measurements and confirmed with XPS.

To demonstrate the concept of biosensor development for bacterial detection during a kidney infection a pre-feasibility study of the interaction between a glycoconjugate immobilized to the silicon surface and a lectin-type of protein was undertaken using QCM.

**DISCUSSION & CONCLUSIONS:** In our work, we have established functionalization protocols for both silicon oxide and silicon surfaces and we demonstrate the successful introduction of different functionalities. Our modified surfaces exhibit features which are important for the design of chemical and biological sensors, like functional end-groups for the selective immobilization of various biological receptors, protein-resistivity, hydrophobicity and pH-responsiveness.

**REFERENCES:** [1] G.J. Zhang at al (2009) *Biosens Bioelectron* **24**: 2504-08. [2] C.H. Lin at al (2008) *Chem Commun* **44**: 5749-51. [3] N.N. Mishra at al. (2008) *Lab Chip* **6**: 868-71.

**ACKNOWLEDGEMENTS:** This project is financed with a grant from the Swiss Nano-Tera.ch initiative and evaluated by the Swiss National Science Foundation.

# Hemocompatibility of Liposomes Loaded with Diglyceride Esters of Methotrexate and Melphalan

N. Kuznetsova[1], N. Bovin[1], C. Sevrin[2], D. Lespineux[2], C. Grandfils[2], E. Vodovozova[1]

[1]*Shemyakin and Ovchinnikov Institute of Bioorganic Chemistry, RAS, Moscow, Russia.* [2]*Research Center of Biomaterials, University of Liège, Liège, Belgium.*

**INTRODUCTION:** A variety of nanoscale drug delivery systems, including liposomes, offer promising approaches for disease diagnosis, treatment, and prevention [1]. Since majority of the systems is to be administered systemically, there is no doubt hemocompatibility studies of the formulations are obligatory. Here we report the results of hemocompatibility studies of antitumor liposomes carrying diglyceride esters of well-known anticancers, methotrexate and melphalan (**MTX-DG** and **Mlph-DG**, respectively), in the lipid bilayer. Grafting of carbohydrates of sialyl Lewis (**SiaLe**) family onto the surface of liposomes was used to allow for their active targeting to sites of inflammation and neovascularization [2].

**METHODS:** Liposomes composed of egg phosphatidylcholine (**PC**) – phosphatidylinositol (**PI**) of baker's yeast – **MTX-DG**/**Mlph-DG**, 8:1:1 (by mol), either targeted with 2 mol % of $SiaLe^X$-PEG-DG or not, were prepared by extrusion through polycarbonate membrane filters with mean pore diameter of 100 nm. Liposome size was controlled by methods of dynamic light scattering (**DLS**) and electron microscopy (negative staining and freeze-fracture techniques). Liposome composition was verified with gel chromatography on a Sepharose CL-4B column. Zeta potential was evaluated using a Nano ZS Malvern Zetasizer.

The following panel of hemocompatibility tests was performed according to ISO standards (10993-4). Hemolysis of red blood cells (**RBC**) was assessed by a colorimetric procedure employing Drabkin's reagent. RBC and platelet morphology, counting, and size distribution were analyzed on a Coulter II Multisizer. Beckton Dikinson kit (Human C3a ELISA for quantification of Human C3a-desArg) was used to estimate complement activation in the presence of liposomes. Coagulation cascade functioning was controlled on a Behring Coagulation Timer (Dade Behring).

**RESULTS:** According to DLS, electron microscopy, gel filtration, spectrophotometry, and elemental analysis of phosphorus concentration data, the prodrugs incorporate completely into lipid bilayer of monolamellar liposomes less than 100 nm in diameter [3]. Drug-loaded liposomes were found to be negatively charged, mean zeta potential ranging from –33.9 ± 1.8 through –45.6 ± 0.8 to –52.7 ± 2.5 mV for formulations containing 10 mol % Mlph-DG, 2.5 mol % MTX-DG, and 10 mol % MTX respectively. Liposomes loaded with Mlph-DG, either targeted or not, didn't exhibit any significant hemoreactivity. On the opposite, liposomes containing MTX-DG induced elevated C3a levels and abnormal coagulation times in a concentration dependent manner. The reactivity of liposome surface wasn't influenced by the structure of carbohydrate ligand attached ($SiaLe^X$ versus $SiaLe^A$) or by the presence or absence of PI, an anti-opsonizing component of the formulation. Important is the fact that decrease of liposome loading with MTX-DG from 10 to 2.5% resulted in lower surface charge density, smaller liposome size and thus considerably reduced impact on the complement activation and coagulation cascades.

**DISCUSSION & CONCLUSIONS:** Interference of MTX-liposomes with the processes of blood coagulation and complement activation may be ascribed to physical adsorption of at least one of the protein components involved in the interrelated cascades on the surface of MTX-liposomes.

The hemocompatibility tests are of screening nature, meaning they are designed to distinguish between tolerated and unsustainable candidates for drug delivery systems. The data obtained so far proved the relatively good hemotolerance of the liposomes loaded with lipophilic prodrugs despite of some undesirable yet manageable effects on coagulation and complement activation linked to the nature of the drug.

**REFERENCES:** [1] R. Singh and J.W. Lillard Jr (2009) *Exp Mol Pathol* **86**:215-223. [2] C. Ehrhardt, C. Kneuer, and U. Bakowsky (2004) *Adv Drug Del Rev* **56**:527-549. [3] N. Kuznetsova, A. Kandyba, I. Vostrov, et al (2009) *J Drug Deliv Sci Techn* **17**(1):51-59.

**ACKNOWLEDGEMENTS:** The work was supported by the Russian Foundation for Basic Research (project no. 06-04-49432) and FEBS Collaborative Experimental Scholarships for Central & Eastern Europe.

# Polymer Nanotechnology for Molecular Imaging

Ick Chan Kwon

*Biomedical Research Center, Korea Institute of Science and Technology, Seoul, Korea*

Molecular imaging is recognized as a key technology for theragnosis which is known as an emerging paradigm for future personalized medicine. Polymer nanoparticles which have been used as useful carriers for drug delivery system could also be excellent imaging probes for molecular imaging. Approaches to combine these two important functionalities all together in a polymer nanoparticle are proposed in this presentation.

First, we propose a new drug delivery system for cancer theragnosis based on polymer nano-technology. Nano-sized drug delivery system, such as liposome, micelles, nanoparticles, have been intensively investigated for the application of cancer therapy. The effectiveness of cancer targeting with using polymer nanoparticles can be attributed to their small size, reduced drug toxicity, controlled drug release and modification of drug pharmacokinetics and biodistribution. However, to date, only limited information is available for the evaluation of targeting efficiency of drug carriers. Our new optical imagining probes made with drug loaded polymer nanoparticles allow us providing a whole body biodistribution at a real-time and non-invasive manner in a small animal disease model. Thus, we anticipate that polymer nanoparticles could serve as potential candidate for selective drug carriers as well as a molecular probe for a real-time visualization of biodistribution of drug carriers.

Second, self assembled and near-infrared fluorescence auto-quenched nanoparticular probes have been designed to visualize target molecules, such as proteases and protein kinases, in cellular levels or in small animal. These nanoparticles can serve as useful molecular probes for screening new drug candidates in cellular and in vivo small animal disease model. It might also be possible to use these nanoparticles for the evaluation of therapeutic efficacy of nano-sized drug carriers by visualization of enzyme activities in live animial model.

In vivo NIRF imaging was performed using a Kodak Image Station 4000 MM. The illumination settings (lamp voltage, filter, and exposure time, etc.) used were identical to those in the animal imaging experiments and all the NIRF emission

data were normalized to photons per second per centimeter squared per steradian (p/s/cm2/sr). All fluorescence images were acquired with a ten second exposure time. The tumors and major organs were dissected and imaged again. For quantitative comparison, tumor contrasts were calculated by dividing the NIRF intensities at the tumor area by those of normal tissue areas. All data calculated using the regions of interest (ROIs) were drawn over tumor and normal tissue and the results were presented as mean ± s.e. (n=3). For histological evaluation, excised tumors and other organs were frozen in Cryomatrix (frozen specimen embedding medium) at - 20□C, and sectioned into 6 □m slices. The NIRF image of each tissue section was viewed by fluorescence microscopy (Carl Zeiss, Oberlcochem, Germany) with a Cy5.5 filter set.

In conclusion, polymeric nanoparticle-based theragnostic system showed a real-time and non-invasive evaluation of nanoparticles' biodistribution in vivo and revealed that nanoparticles were localized in tumor site. Furthermore the therapeutic efficacy of nano-sized drug carriers can be visualized and quantified in live animal model.

**REFERENCES:**

1. Park K, Lee S, Kang E, Kim K, Choi K, Kwon IC, New generation of multifunctional nanoparticles for cancer imaging and therapy, *Advanced Functional Materials*, 2009;**19**;1553-1566.

2. Lee S, Ryu JH, Lee A, Park K, Lee SY, Yoon IC, Ahn CH, Yoon SM, Moon DH, Myung SJ, Chen X, Choi K, Kwon, Kim K, Polymeric nanoparticle-based activatable near-infrared nanosensor for protease determination in vivo, *Nano Letters*, 2009;**9**;4412-4416.

European Cells and Materials Vol. 20. Suppl. 3, 2010 (page 154) ISSN 1473-2262

# Influences of Nano-sized Type I Collagen Molecules on Hepatocyte Cultures

MW. Lee[1], CW. Lan[2], YT. Lin[2], TW. Liu[2], SM. Kuo[2]

[1]*School of Medical Laboratory and Biotechnology, Chung Shan Medical University, Taichung, Taiwan.* [2]*Dept. Biomedical Engineering, I-Shou University, Kaohsiung, Taiwan.*

**INTRODUCTION:** Collagen is one of the most commonly used biomaterials in scaffold construction for tissue engineering today. The influence of differently organized collagen structures on cellular fates and behaviors is an exciting and interesting area that remains to be explored[1-2]. The objective of this study was to evaluate the effects of addition of nano-sized type I collagen molecules (particles or fibers), instead of growth factors, into the culture medium on rat hepatocytes grown in the regularly used culture dish (static culture) or bioreactor (dynamic culture). For comparative purposes, the effects of these added molecules on the viability and function of rat hepatocytes were evaluated. The cell morphologies were also observed and examined by scanning electron microscopy.

**METHODS:** Nano-particle collagen was prepared by a high-voltage electrostatic field system which was constructed by two parallel plate electrodes. 1 ml of iced type I collagen solution (0.1 mg/ml) was poured into a plastic petri-dish and then placed at the center point of the two parallel electrodes. The temperature of the chamber was set and kept constant at 7°C for preparing particles.[3] The reaction time was set to 1 h. Collagen fibrils were assembled from collagen monomers (0.1mg/ml) at 37C for 4 hr.

Hepatocytes were isolated from sacrificed Sprague-Dawley rats (250–350 g) using a modified collagenase perfusion protocol. The isolated hepatocytes were mixed with various concentrations of nano-sized type I collagen molecules in a centrifuge tube were initially incubated at 37°C in 5% $CO_2$ incubator for 3 h, allowing for enhanced attachment between hepatocytes and collagen molecules. After that, the cell-collagen I molecules mixture was transferred and poured into a stir bioreactor. This bioreactor was placed inside a 37°C incubator. A culture without addition of type I collagen molecules acted as a control group. After pre-determined culturing periods, the viability and the biochemical function of hepatocytes were evaluated by an MTT assay and histological observations.

**RESULTS:**

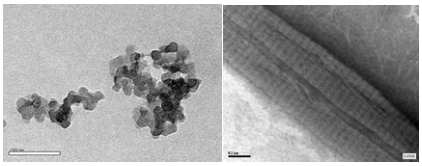

*Fig. 1: TEM of nano-sized type I collagen molecules: (a)particle form; (b)fibrillar form.*

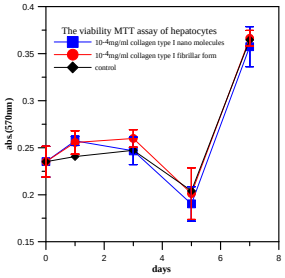


*Fig. 2: The viability MTT assay of hepatocytes.*

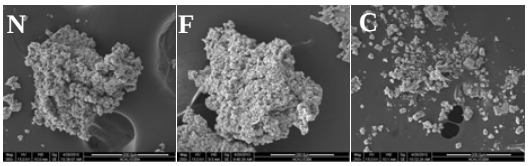


*Fig. 3: SEM of hepatocytes cultured with nano-sized type I collagen molecules after 6 days in vitro static culture. N: nano-particle collagen; F: collagen fibril; C: control.*

**DISCUSSION & CONCLUSIONS:** In this study, we could produce hepatocyte spheroids in short-term bioreactor cultures. However, more data or evidences still need to be examined, such as the interaction mechanism between nano-sized collagen molecules and hepatocytes and the appropriate concentrations of nano-sized type I collagen, before the value of liver spheroids can be fully evaluated.

**REFERENCES:** [1]J.C. Dunn, R.G. Tompkins and M. L. Yarmush (1992) *J Cell Biol* **116**:1043-1053.[2]H. Ouchi, K. Otsu, T. Kuzumaki, et al (1998) *Arch Biochem Biophys* **358**:58-62. [3]S.J. Chang, G.C.C. Niu, S.M. Kuo, et al (2006) *IEE Proc Nanobiotechnol* **153**:1-6.

**ACKNOWLEDGEMENTS:** This work was supported by grants from the National Science Council, ROC (95-2221-E-214-053-MY3 and 95-2221-E-214-086-MY3).

# Size and Ligand Dependent Cytotoxicity of Gold Nanoparticles

A. Leifert[1], Y. Pan[2], D. Ruau[2], S. Neuss[3], J. Bornemann[4], G. Schmid[5], W. Brandau[6], W. Jahnen-Dechent[2], U. Simon[1]

*[1] Inorganic Chemistry, RWTH Aachen University, Germany. [2] Biomedical Engineering, RWTH Aachen University, Germany. [3] Pathology, RWTH Aachen University, Germany. [4] Electron Microscopy Facility (Medical Faculty), RWTH Aachen University, Germany. [5] Inorganic Chemistry, University of Duisburg-Essen, Germany. [6] Radiochemistry, University-Hospital Essen.*

**INTRODUCTION:** Gold nanoparticles (AuNPs) are of great interest for use in biomedicine as imaging tools, phototherapy agents and gene delivery systems. These promising applications are confronted by relatively few studies concerning possible adverse effects on living organisms to date.[1]

Therefore, we chose the size of AuNPs as a variable parameter in a first systematic study to investigate the cell response towards numerous species. We investigated the cytotoxicity of AuNPs with different sizes in a range between 0.8 nm to 15 nm, all stabilized by a water soluble triphenylphosphine ligand (TPPMS).[2] Furthermore, we used 1.1 nm sized, glutathione (GSH) stabilized AuNPs as a reference material and examined oxidative stress levels induced by AuNPs.[3]

**METHODS:** The nanoparticles were characterized by means of UV/Vis, SEM or TEM, elemental analysis and AAS. The cytotoxicity was tested by MTT assay in four different cell lines. Cells were treated with a propidium iodide/annexin V double staining and investigated in a subsequent flow cytometry measurement. Oxidative stress was investigated with CM-$H_2$DCFDA staining. A DNA gene chip analysis was performed. For details, see ref. 2, 3.

**RESULTS:** Phosphine stabilized AuNPs with a mean diameter of 1.4 nm proved to be most toxic (Fig. 1). In contrast, AuNPs with a size of 15 nm were found to be non-toxic at up to a 60-fold higher concentration.

The propidium iodide/Annexin V double staining revealed that 1.4 nm particles caused predominantly necrosis within 48 h while 1.2 nm particles provoked predominantly apoptosis. The CM-$H_2$DCFDA staining showed that the cytotoxicity of 1.4 nm sized AuNPs is related to oxidative stress. The addition of a variety of antioxidants could significantly reduce the toxicity.

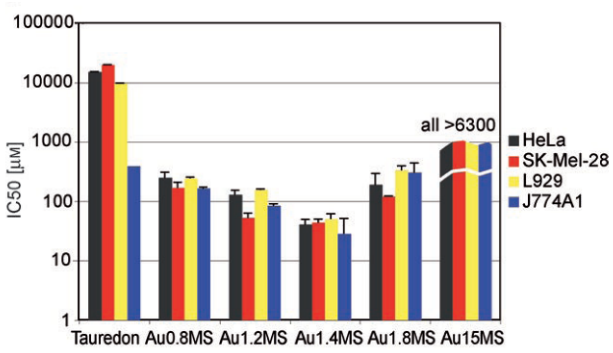


*Fig. 1: $IC_{50}$ values, determined by MTT assay, for different AuNP species and in four different cell lines.*

A DNA gene chip analysis showed an up-regulation of stress-related genes. Furthermore, it was found that size and ligand chemistry of the AuNPs play a crucial role, as 15 nm sized particles (TPPMS stabilized) and GSH stabilized, 1.1 nm sized particles didn't induce the same cell reactions.

**DISCUSSION & CONCLUSIONS:** The size dependent cytotoxicity of AuNPs might be related to the fact that small AuNPs are in the same size regime as biological functionalities/cell organelles, and therefore a specific interaction might trigger the toxicity. On the other hand the fact that the toxicity is linked to oxidative stress could be a hint for a mechanism based on the catalytical activity of AuNPs. Further investigations are ongoing to reveal the mechanism of cell death induced by small, phosphine stabilized AuNPs.

**REFERENCES:** [1] N. Lewinski, V. Colvin, R. Drezek (2008) *Small* **4**:26-49. [2] Y. Pan, S. Neuss, A. Leifert, et al (2007) *Small* **3**:1941-1949. [3] Y. Pan, A. Leifert, D. Ruau, et al (2009) *Small* **5**:2067-2076.

**ACKNOWLEDGEMENTS:** The authors thank the German Science Foundation (DFG) for funding within the Research Training Grant GRK1035, and investigator grants Si609/9, and Ja562/13.

European Cells and Materials Vol. 20. Suppl. 3, 2010 (page 156) ISSN 1473-2262

# Detection of fluorescent silica nanoparticles in cells using confocal microscopy

A.Lemelle, A.Bidus, S.Morgan.

*Cranfield Health, Cranfield University, Bedfordshire MK43 0AL, U.K.*

**INTRODUCTION:** The use of fluorescent silica nanoparticles (FSNPs) is being widely investigated for biological applications such as cellular imaging for the study of cellular processes. The method developed by van Blaaderen is a common way to synthesise FSNPs but it generally produces structures larger than 100 nm and incorporate only a limited number of fluorophores. We have adopted a method using an amino acid-catalysed reaction to produce smaller particles containing three fluorescent dyes: Rhodamine 6G (R6G), Fluorescein isothiocyanate (FITC), and Methylene blue (MB). To determine the potential of these nanoparticles in cellular study, the particles were incubated with two prostate-derived cell lines. Particle uptake and location within these cells was then investigated by confocal microscopy.

**METHODS:** Silica seeds were synthesised using a modified Stöber method, utilising an amino acid route. The three dyes at desired concentrations were incorporated throughout the formation of the particles. Finally, the surface of the FSNPs was coated with amine and phosphonate groups to improve their dispersion.

Nanoparticle size was characterised by both SEM and TEM, whilst their composition was determined by infrared spectroscopy. The optical properties of the particles were assessed by fluorescent spectroscopy.

To assess cellular uptake, two prostate-derived cell lines were employed. PC3 (prostate adenocarcinoma, ECACC: 90112714) and PNT1A (SV40 immortalised normal prostate, ECACC: 95012614) cells were seeded at $9x10^4$ cells/ml in chamber flasks and incubated for 24 hours. fsNPs were then added to the cells at a concentration of 1 mg/ml and these were again incubated for 24 hours. Cells were then fixed in methanol and subsequently counterstained with sytox green (nuclear) and streptavidin, alexa fluor 555 (cytoplasmic). Cells were imaged using a Zeiss LSM 510 Meta inverted confocal microscope at x40, using 488 and 543 nm laser sources.

**RESULTS:** SEM and TEM images indicate that the particles are 15 to 40 nm in diameter and slightly agglomerated. Infrared spectroscopy shows the presence of siloxane bonds, which proves the formation of the silica network. All combinations of the three dyes were tested. Blank nanoparticles do not exhibit any particular signal, but all other samples absorb light at 495 (FITC), 525 (R6G), and 600/660 nm (MB) according to their dye content. R6G and FITC show a strong fluorescence, but MB generates a weaker signal.

Confocal studies demonstrated that both PC3 and PNT1A cells were able to take up the FSNPs, though qualitative differences were noted in uptake between the two cell types. The particles appear as bright spots within the cell cytoplasm and can clearly be distinguished from the sytox green (green) and alexa fluor (red) counterstains. The only exception being MB, which cannot be detected. Upon continuous illumination, the particles do not bleach, contrary to the counterstains.

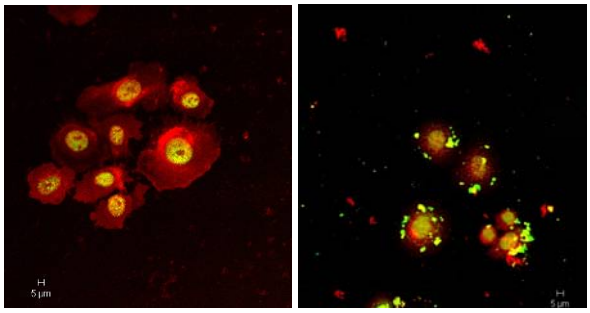

*Fig. 1: Confocal images of unlabelled PC3 cell (left) and PC3 labelled with R6G-FITC-loaded nanoparticles.*

**DISCUSSION & CONCLUSIONS:** Our method yields very small spherical nanoparticles a few tens of nanometres in size. The three dyes used during the synthesis of the nanoparticles were successfully entrapped and exhibit a strong fluorescence.

Both PC3 and PNT1A endocytosed the nanoparticle in spite of their agglomeration. The difference in uptake may be cell- or surface-dependent since the surface of the nanoparticles was modified with phosphonate and amine groups.

Future work will involve the loading of FSNPs with other fluorophores and a more detailed analysis of the cellular fate of the nanoparticles.

**REFERENCES:** [1] A. Van Blaaderen, A. Vrij (1992) *Langmuir*, **8**: 2921-31. [2] K.D. Hartlen, A.P. Athanasopoulos, V. Kitaev, (2008) *Langmuir*, **24**, 1714-20.

European Cells and Materials Vol. 20. Suppl. 3, 2010 (page 157) ISSN 1473-2262

# Cellular Responses To Physically And Mechanically Patterned Biomaterials

V. A. Schulte[1], M. Diez[1], M. Möller[1], M. C. Lensen[1,2]

*[1] DWI an der RWTH Aachen e.V., Aachen, Germany [2] University of Technology, Berlin, Germany.*

**INTRODUCTION:** Tissue cells (e.g. fibroblasts), neurons and macrophages are sensitive to several characteristics of biointerfaces such as the chemistry, topography and elasticity. In order to manipulate the cellular behaviour (e.g. adhesion, migration, proliferation) we have developed several methods to fabricate micro- and nanopatterns of those properties; separately and in combination.

**METHODS:** PEG- hydrogels and PFPE-elastomers were prepared from UV-curable prepolymers, which crosslink under illumination with UV-light (365 nm) in the presence of a photoinitiator (0.5-1% PI) and eventually a low molecular weight crosslinker (up to 10% CL). The PEG-hydrogels are crosslinked from linear or star-shaped poly(ethylene glycol) macromonomers with acrylate end groups, whereas the PFPE-elastomer precursor is a linear macromolecule with 2 methacrylate end groups.[1].

Topographic patterns are made by molding against (silicon) masters bearing µm-sized patterns of grooves or round holes. Hydrogels with binary patterns of elasticity are prepared by a soft lithographic technique adapted from MIMIC.

**RESULTS:** Thin layers or SAMs of PEG are known to suppress non-specific protein adsorption and cell adhesion.[2] The bulk PEG-hydrogels that we have used are also not supportive of cell adhesion and growth. However, when topographic patterns are present, fibroblast do adhere and undergo morphological changes that can be called 'contact guidance'; the cells align along the grooves (Fig. 1).[3]

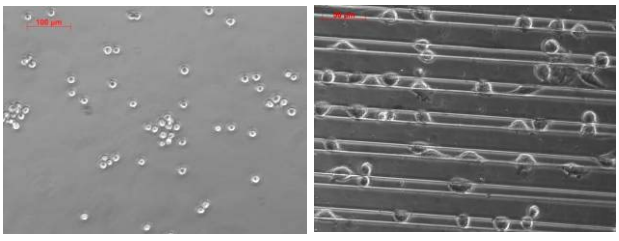

*Fig. 1: Fibroblasts do not adhere on smooth PEG-hydrogels (left) while they do adhere and spread on the same material when it is topographically patterned (right).*

Unexpectedly, considering the hydrophobic nature of the fluoropolymer, the PFPE-elastomer supports cell adhesion and spreading to an extent

comparable to the standard tissue culture plastic TCPS.[4] On topographic patterns cells adhered and spread significantly as well.

The preparation method of the biomaterials, i.e. employing different wt % of PI and CL, allows tuning of the crosslinking density and thus of the stiffness of the gels. In Table 1 the Young's moduli of our 3 most investigated hydrogel formulations are listed. We have observed that - whereas on smooth hydrogels cells cannot adhere let alone spread, regardless of the stiffness – on gels prepared from the same material but with a binary pattern of elasticity, cells selectively adhere to the stiffer areas (results not shown).

*Table 1. Young's moduli of 3 typical hydrogel formulations, measured in dry and swollen state.*

| % PI_CL | Dry (MPa) | Swollen (MPa) |
|---|---|---|
| 0.5_5 | 0.18 | 0.09 |
| 1_5 | 0.85 | 0.35 |
| 1_10 | 2.6 | 1.1 |

**DISCUSSION & CONCLUSIONS:** As PEG is generally well known for its anti-adhesive behaviour and is commonly applied for biomedical applications, our results are remarkable: physical (topography) and mechanical surface patterns and can impede the anti-adhesive characteristics of PEG. This opens new opportunities for biomimetic material design which do not rely on biochemical surface functionalization for manipulating cellular responses.

**REFERENCES:** [1] M.C. Lensen P. Mela, et al. (2007) *Langmuir* **23**:7841-7846. [2] J.H. Harris (1992) in *Poly(ethylene glycol) chemistry: Biotechnical and biomedical applications* New York: Plenum Press. [3] V.A. Schulte, M. Diez, et al. (2009) *Biomacromolecules*;**10**:2795-2801. [4] V.A. Schulte, M. Diez, et al. (2010) *Biomaterials*; accepted.

**ACKNOWLEDGEMENTS:** Financial support in the form of a Sofja Kovalevskaja Award (MCL) from the Alexander von Humboldt Foundation and funded by the federal ministry of education and research (BMBF) and from the Graduiertenkolleg 'Biointerface' (German research association, DFG) is greatly acknowledged.

European Cells and Materials Vol. 20. Suppl. 3, 2010 (page 158) ISSN 1473-2262

# Protein Mechanics: from Single Molecule to Biomaterials

S. Lv[1], DM. Dudek[2], Y. Cao[1], MM. Balamurali[1], J. Gosline[2], H. Li[1]

*[1]Department of Chemistry, [2]Department of Zoology, University of British Columbia, Vancouver, British Columbia, Canada.*

Elastomeric proteins underlie the elasticity of natural adhesives, cell adhesion and muscle proteins. The development of single molecule force spectroscopy techniques has made it possible to directly probe the mechanical properties of elastomeric proteins at the single molecule level. Combining single molecule atomic force microscopy (AFM) and protein engineering techniques, researchers have started to understand the molecular design principles of elastomeric proteins and use such knowledge to engineer novel elastomeric proteins of tailored nanomechanical properties. Here we describe our efforts in using single molecule AFM studies to guide the design of artificial elastomeric proteins to mimic the mechanical properties of the giant muscle protein titin, and employing such miniature titin-mimetic proteins to engineer biomaterials that mimic the passive elastic properties of muscles. The passive elasticity of muscle is largely governed by the I-band part of titin, a complex molecular spring composed of a series of individually folded immunoglobulin-like (Ig) domains as well as largely unstructured unique sequences. These mechanical elements have distinct mechanical properties, and when combined, they provide desired passive elastic properties of muscle, which are a unique combination of strength, extensibility and resilience. Our prior single molecule AFM studies demonstrated that the macroscopic behavior of titin in intact myofibrils can be reconstituted by combining mechanical properties of these mechanical elements measured at the single-molecule level. Based on such insight, we used well-characterized protein domains GB1 and resilin to engineer artificial elastomeric proteins that mimic the molecular architecture of titin. We showed that these artificial elastomeric proteins can be photocrosslinked and cast into solid biomaterials. These biomaterials behave as rubber-like materials showing high resilience at low strain and as shock absorber-like materials at high strain by effectively dissipating energy. These properties are comparable to passive elastic properties of muscles within the physiological range of sarcomere length and thus these materials represent a novel muscle-mimetic biomaterial. The mechanical properties of these biomaterials can be fine-tuned by adjusting the composition of the elastomeric proteins, providing possibilities for molecular level engineering of macroscopic mechanical properties of biomaterials. We anticipate that these novel biomaterials will find applications in tissue engineering as scaffold and matrix for artificial muscles.

# Magneto-Responsive Biomolecular Nanodiscs

M.Liebi[1], J.Kohlbrecher[2], T.Ishikawa[3], P.Fischer[1], P.Walde[4], E.J.Windhab[1]

*[1]Laboratory of Food Process Engineering, ETH Zurich, Switzerland, [2]Laboratory for Neutron Scattering, PSI Villigen, Switzerland, [3]Department of Biology, ETH Zurich, Switzerland, [4]Department of Materials, ETH Zurich, Switzerland*

**INTRODUCTION:** Phospholipids are amphiphilic molecules and main components of biological membranes. Due to their diamagnetic susceptibility anisotropy, phospholipids have a preferred orientation in magnetic fields. For single molecules the disordering thermal fluctuation energy exceeds the magnetic orientation. However for a phospholipid bilayer with parallel aligned molecules the diamagnetic susceptibility becomes additive and an orientation in magnetic field is possible.[1] Anchoring of paramagnetic lanthanide ions to the membrane with the help of a phospholipid-chelator can further increase magnetic orientability.[2]

**METHODS:** A new type of bicellar disks has been developed composed of the phospholipid DMPC (1,2-dimyristoyl-*sn*-glycero-3-phospho-choline) and the phospholipid-chelator DMPE-DTPA (1,2-dimyristoyl-*sn*-phosphatidylethanol-amine-diethylenetriamine-pentaacetate with complexed lanthanides. The system was studied with small angle neutron scattering (SANS) measurements in a magnetic field of 8 T, and cryo-transmission electron microscopy (cryo-TEM). Further information was gained using dynamic light scattering (DLS) and $^{31}$P NMR.

**RESULTS:** Bicelles are disc-shaped aggregates, normally composed of bilayer-forming phospholipids in the center and more wedge-shaped molecules covering the highly curved edge region of the bicelle.

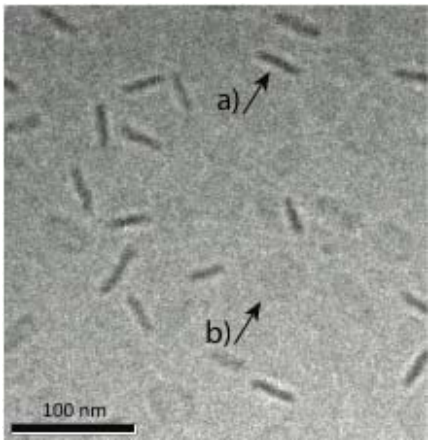


*Fig. 1: Cryo-TEM micrograph of bicelles formed by a mixture of DMPC and DMPE-DTPA with complexed lanthanides in edge-on (a) and face-on view (b).*

We found that from a mixture of DMPC and DMPE-DTPA after appropriate preparations steps, that is, extrusion through a polycarbonate membrane followed by a cooling step, mono-disperse small unilamellar bicelles are formed. The radius depends on the molar ratio of DMPC:DMPE-DTPA. As shown in Fig. 1 for a molar ratio of DMPC:DMPE-DTPA of 4:1 and a total lipid concentration of 15 mM, the resulting bicelles have a radius of 20 nm and a bilayer thickness of about 4 nm. Those bicelles are stable in the investigated temperature range of 2.5 – 30°C. Weak alignability in a magnetic field of 8 T is observed if the paramagnetic lanthanide $Tm^{3+}$ is used as shown with SANS in magnetic fields.[3]

**DISCUSSION & CONCLUSIONS:** We have shown that bicelles can be formed from a mixture of DMPC and DMPE-DTPA with complexed lanthanides. In this mixture, only one type of fatty acid tail, myristoyl, is present, in contrast to conventional bicelles, which consist of a long chain phospholipid plane and short chain lipid, covering the highly curved edges.

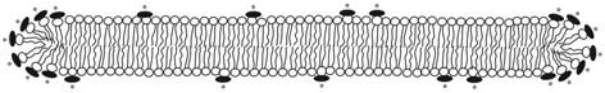

*Fig. 2: Sketch of a bicelle (cross section of a edge-on view) formed by DMPC (white) and DMPE-DTPA (black).*

We assume that partial lipid segregation occurs, due to the large headgroup of the DMPE-DTPA with the complexed lanthanides, accumulating preferably in the edge region of the bicelle as shown in the sketch (Fig. 2). Current research is directed towards an investigation of the complex bicelle formation process and enhancing of stability and magneto-responsiveness of the bicelles. Such magnetic field alignable bicelles could be embedded afterwards into structured matrices in order to create macrostructures with smart properties such as the anisotropic transfer of electromagnetic waves.

**REFERENCES:** [1]K.Binnemans and C.Görller-Walrand (2002) *Chem Rev* **102**:2303-45. [2]R.S.Prosser, V.B.Volkov, and I.V.Shiyanovskaya (1998) *Biophys J* **75**:2163-69. [3]P.Beck, M.Liebi, J.Kohlbrecher, et al. (2010) *Langmuir* **26**:5382-87.

# Significantly Improved Sensitivity of Localized Surface Plasmon Resonance at interstice of Two-dimensional Gold Nanoparticles

Chuen-Yuan Hsu, Jing-Wen Huang, and Kuan-Jiuh Lin*

*Department of Chemistry, National Chung Hsing University, Taichung 402, Taiwan(ROC)*

**INTRODUCTION:** We report that the optical response of localized surface plasmon resonance (LSPR) is strongly dependent on the molecule binding location where the chemical/biological binding events are immobilized at the interstices between interparticles. Two samples of durable Au nanostructures on transparent glasses were fabricated using a microwave plasma oven. The average interparticle gap of one (represented as 11Au-LSPR) was 11 ± 5 and that of the other (represented as 45Au-LSPR) was 45 ± 19 nm. The optical response of the biotin-immobilized 45Au-LSPR chip was found to be insignificant, while that of 11Au-LSPR had a limit of detection (LOD) of 102 pM for detecting streptavidin molecules, based on the optical extinction changes. This strongly indicates that increasing the refractive index of the medium at interstices plays an important role in the creation of an enhanced local electromagnetic field (E-field), resulting in very high sensitivity to binding events.

**METHODS:** The immobilization of Sulfo-NHS-LC-Biotin on the APTMS/Au-LSPR substrates was achieved by standard amine coupling chemistry. Briefly, the surface of APTMS/Au-LSPR substrates was incubated in 1 mg/mL Sulfo-NHS-LC-Biotin in PBS (pH 7.4) for 1 h at 20 °C, rinsed with PBS buffer solution and deionized water, and dried with N2 gas. Streptavidin molecules with precise control of concentration were stepwise introduced onto the biotin-immobilized Au-LSPR chips for periods of 20 min for every concentration, followed by thorough rinsing with PBS buffered solution to remove the nonspecific binding events.

**RESULTS:** The ability of the 11Au-LSPR plasmonic nanostructures was examined. Figure 1 shows a quantitative analysis of the optical extinction response of LSPR as a function of the streptavidin concentration, which varied from 2 ng/mL to 3000 ng/mL. The saturation concentration for 11Au-LSPR chips was evaluated to be approximately 2000 ng/mL as determined by the lack of change in the optical extinction after being exposed to 3000 ng/mL. Within the concentration range of 7 ng/mL ( ~ 102 pM) and 2000 ng/mL ( ~ 29 nM), the response curve indicates that increasing concentrations of streptavidin caused larger optical extinction change. A plot of □Ext as a function of the streptavidin concentration shown in Fig. 5b indicates that the streptavidin detection limit was 7 ng/mL ( 102 pM).

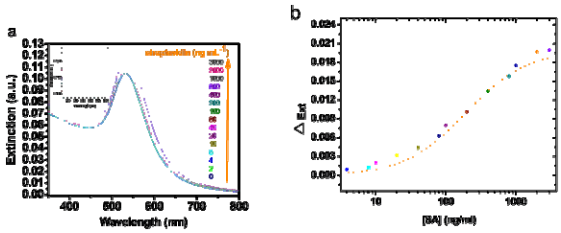


*Fig. 1: a) Observation of optical extinction changes in LSPR spectra for specific biotin-streptavidin detection on interstices for $^{11}$Au-LSPR biochips with varying streptavidin concentrations. b) Concentration dose-response curve for biotin-streptavidin binding for $^{11}$Au-LSPR biochips. The error bars was evaluated by calculating the standard deviation. The detection limit of our chip is defined as the lower concentration that causes the smallest resolvable change from the measuring instrument.*

**DISCUSSION & CONCLUSIONS:** We have demonstrated that our plasmonic Au-patterning substrates could enable significant promise as a label-free, chip-based biosensor because their nanostructures unravel the following drawbacks involving (i) poor adhesion of nanoparticles to the substrate, (ii) plasmonic materials that are prone to oxidation, and (iii) unfavorable sensitivity of LSPR nanosensors and resolution of spectra. The attractive features of substrate-bound plasmonic gold nanostructures include longer operating time in air, reusability, durability, reliability, high sensitivity, and low-cost and time-saving preparation, all of which are suitable for development in the present point-of-care testing stage as prevalent commercial SPR.

**REFERENCES:** Hsu, C.-Y.; Huang, J.-W.; Gwo, S.; Lin, k.-J. *Nanotechnology* **2010,** 21 035302

**ACKNOWLEDGEMENTS:** This work was supported by the National Science Council of Taiwan (NSC-98-2113-M-005-004-MY3).

European Cells and Materials Vol. 20. Suppl. 3, 2010 (page 161) ISSN 1473-2262

# Preparing Bio-Molecule Gradients on PEDOT-$N_3$ using Electro-Click Reactions

JU.Lind1, TS.Hansen1, TL.Andresen1 and NB.Larsen1

[1]*DTU Nanotech, Technical University of Denmark, Frederiksborgvej 399, 4000 Roskilde*

**INTRODUCTION:** The ability to generate surface gradients of biologically active molecules is important in gaining understanding of cell migration and communication, and in advanced cell handling devices. Copper(I)-catalyzed reaction between azide groups and terminal alkynes is one of the most applied "Click chemistry" reactions. In electro-click chemistry, Cu(I) catalyst is generated locally through electrochemical reduction of Cu(II) to Cu(I)1. The electrical conductive polymer poly-3,4-(1-Azidomethylethylene)-dioxythiophene (PEDOT-$N_3$) can be selectively functionalized by this method[2]. The further away from a counter electrode the active PEDOT-$N_3$ surface is located, the slower the catalyst is generated, creating a gradient pattern.

**METHODS:** A copper plate was partially covered with an insulating layer of a transfer adhesive in which a 0.5 mm slit was cut using a $CO_2$ laser. The copper electrode was placed above a PEDOT-$N_3$ film using a 190 µm thick spacer. The functionalization was done using a DMSO solution of 1mM RGD-PEG-alkyne and 1mM CuSO4, and applying a potential of -0.5 V vs. the copper electrode for 5 minutes. Remaining azide groups were reacted for 6hrs in a second clickreaction in a 50mM NaCl aqueous solution containing: 20M PEG-alkyne, 0.67mM $CuSO_4$ and 27mM sodium ascorbate. Steeper and more narrow gradients, has been produced in a similar fashion, using a spincoated COC polymer as thin insulating material, and using shorter reaction times.

**RESULTS:** A gradient of RGD-peptide-alkynes was fabricated. Azides remaining on the PEDOT-$N_3$ substrate after the gradient fabrication were reacted with a PEG-alkyne, using a standard aqueous click reaction. The peptides contain a PEG spacer segment which serves to present the RGD motif to the cells on a PEG background, thus limiting non-specific interaction between cells and substrate. In a homemade microfluidic flow chamber, 3T3 fibroblast cells were allowed to adhere to the surface. Non-attached cells were removed by flowing buffer through the chamber. The remaining cells are displayed in Fig.2. Control experiments using a scrambled peptide sequence showed no ability to induce cellular adhesion, verifying that the cellular adhesion is bio-specific.

**DISCUSSION & CONCLUSIONS**: The fabricated pattern is defined by the geometry of the setup, especially the shape of counter electrode. Therefore this novel method is well-suited for making linear as well as complex 2D gradients of covalently bound molecules, useful in various biological systems.

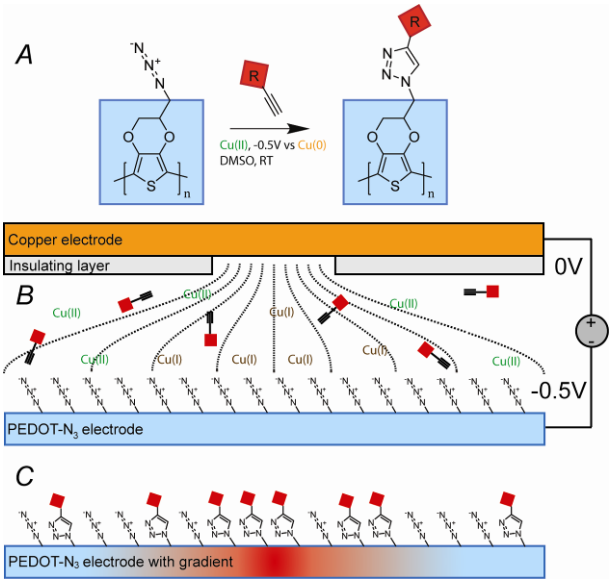


*Fig. 1: Principle of the electrochemical gradient fabrication*

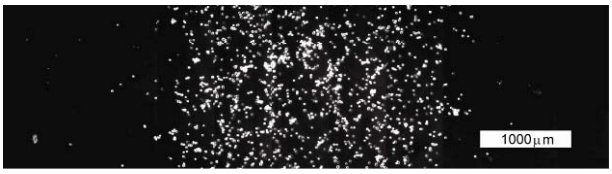


*Fig. 2: 3T3 Fibroblast cells caught on a symmetric PEDOT-$N_3$ RGD-gradient.*

**REFERENCES:** [1]N. K. Devaraj, P. H. Dinolfo, C. E. D. Chidsey, J. P. Collman (2006), *J. Am. Chem. Soc.*, **128**, 1794-1795. [2]T. S. Hansen, A. E. Daugaard, S. Hvilsted, N. B. Larsen (2009), *Adv Mater*, **21**, 4483

**ACKNOWLEDGEMENTS:** The Danish Council for Technology and Innovation and The Danish Council for Independent Research are acknowledged for financial support.

European Cells and Materials Vol. 20. Suppl. 3, 2010 (page 162) ISSN 1473-2262

# Photoreactive Biodegradable Electrospun Fibers

R.Lösel[1], M.Möller[1], D.Klee[1]

[1] *RWTH Aachen, Institute of Technical and Macromolecular Chemistry and DWI an der RWTH Aachen e.V., Aachen, Germany.*

**INTRODUCTION:** Biodegradable amphiphilic block copolymers can be electrospun from a suitable solvent mixture to form hydrophilic fiber structures which are used as scaffolds for tissue engineering applications. Polymers with reactive end-groups can be functionalized with biologically active compounds like adhesion promoting peptide sequences or growth factors to control the interaction of the scaffold with cells. Electrospun fibers prepared from different reactive block copolymers which can covalently bind active compounds, e.g. maleimide terminated PLA-*block*-PEG copolymers, have been described [1]. Novel diazirine-terminated PCL-*block*-PEG copolymers **1** and **2** (fig. 1) have been synthesized. Under long-wavelength UV irradiation, the diazirine group forms reactive carbene intermediates which instantly add to amine groups under physiological conditions [2,3]. The disulfide bond in compound **2** can be reductively cleaved, thus releasing the active compound from the polymer matrix.

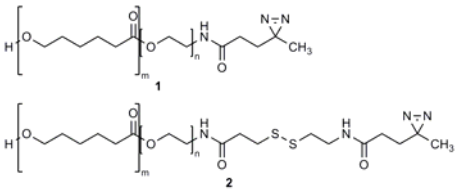

*Fig. 1: Structures of PCL-block-PEG-diazirine (**1**) and PCL-block-PEG-SS-diazirine (**2**).*

**METHODS:** PCL-*block*-PEG-diazirine (**1**) and PCL-*block*-PEG-SS-diazirine (**2**) were prepared by reacting poly(ε-caprolactone)-*block*-ω-aminopoly(ethylene glycol) (PCL-*block*-PEG-$NH_2$) with succinimidyl 4,4'-azipentanoate (SDA) or succinimidyl 2-[(4,4'-azipentanamido)ethyl]-1,3'-dithiopropionate (SDAD), respectively, in presence of DIPEA. Polymers with a 37.0 kDa PCL block and a 5.5 kDa PEG bock were electrospun from a 20% (*m*/*m*) solution in a 3:1 (*V*/*V*) chloroform/methanol mixture using a vertical point-plate geometry setup with a spinneret diameter of 0.8 mm, a flow rate of 0.3 mL/h and a voltage of −20.0 kV. Fibers were collected on 10 mm × 10 mm silicon substrates in a distance of 150 mm from the spinneret. PCL-*block*-PEG-diazirine, PCL-*block*-PEG-SS-diazirine and PCL-*block*-PEG-$NH_2$ fibers were incubated in 500 µL/substrate of a 50 µM solution of Alexa Fluor® 488 cadaverine sodium salt in PBS (pH 7.4) protected from light for 1 h. Identical samples were irradiated with a 4 W UV lamp ($\lambda$ = 365 W) positioned 20 mm above the samples. All samples were washed with PBS and ultrapure water and characterized by fluorescence microscopy.

**RESULTS:** Electrospinning of PCL-*block*-PEG-diazirine (**1**), PCL-*block*-PEG-SS-diazirine (**2**) and PCL-*block*-PEG-$NH_2$ results in formation of homogeneous fibers with an average diameter of 2 µm. Diazirine-terminated fibers show intensive fluorescence after incubation with Alexa Fluor® 488 cadaverine under UV irradiation while virtually no fluorescence can be observed after incubation in the dark or with fibers spun from amine-terminated PCL-*block*-PEG (fig. 2).

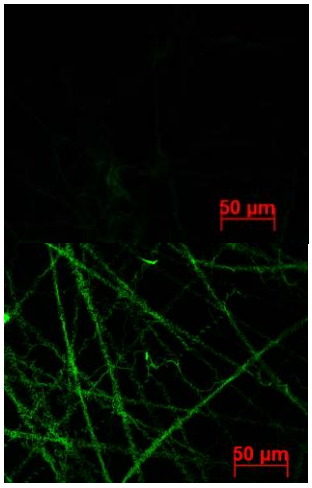


*Fig. 2: Electrospun PCL-block-PEG-diazirine fibers after incubation with Alexa Fluor® 488 cadaverine without (left) and with (right) UV irradiation (fluorescence microscopy, exposure time 200 ms).*

**DISCUSSION & CONCLUSIONS:** Diazirine-terminated PCL-*block*-PEG copolymers react with amines when exposed to long-wavelength UV irradiation. Fibers electrospun from these materials are promising tissue engineering scaffolds after immobilization of biologically active compounds which can be released from the polymer depending on the functional end-group of the polymers.

**REFERENCES:** [1] R. Lösel, D. Grafahrend, M. Möller, D. Klee (2008) *BIOmaterialien* **9**:129. [2] M. Suchanek, A. Radzikowska, C. Thiele (2005) *Nature Methods* **2**:261-8. [3] Y. Tanaka, J. J. Kohler (2008) *J Am Chem Soc* **130**:3278-9.

**ACKNOWLEDGEMENTS:** This work is supported by DGF SFB TR 37 "Mikro- und Nanosysteme in der Medizin – Rekonstruktion biologischer Funktionen".

European Cells and Materials Vol. 20. Suppl. 3, 2010 (page 163) ISSN 1473-2262

# Investigation of Drug-Protein Interactions by Means of Droplet Microfluidics and Magnetic Beads

D. Lombardi, P. S. Dittrich

*Department of Chemistry and Applied Biosciences, ETH Zurich, Switzerland*

**INTRODUCTION:** The absorption and distribution of a drug depend significantly on the extent and kinetics of its interactions with specific components of the organism such as proteins and other biomacromolecules or lipid membranes. In this study we introduce a new method to determine binding constants of two reagents. By implementing a technique based on magnetic beads with a microfluidic device for segmented flow generation, we demonstrate drop-wise fast, robust and complete separation of magnetic beads. We employ the method for characterisation of drug-protein binding, here warfarin to human serum albumin.

**METHOD:** A microfluidic chip is designed and fabricated that facilitates the formation of droplets, the mixing and incubation of the droplet content, and the final splitting at a T-junction into two daughter droplets of equal volume (Fig. 1). Magnetic beads, coated with the target protein and the binding partner (drug) are introduced into the droplets and the reaction equilibrium of binding and dissociation events is reached before the droplets are symmetrically split. Placing a magnet next to one of the two outlet channels results in selectively separation of the beads into one of the daughter droplets (Figure 1). The affinity (binding) constant can be derived from the concentration ratio of the ligand molecules in the two daughter droplets.

**RESULTS:** The key feature of the microdevice is the withdrawal of magnetic beads during droplet splitting from one of the daughter droplets. We achieved this up to nearly 100 % by placing the small magnet in close proximity to one of the microchannel outlets. The applicability of the device for binding studies was proven by determining the affinity constant of warfarin, an anticoagulant drug, to human serum albumin (HSA) that was immobilised on the surface of the magnetic beads (HSA_MBs). After passing the microdevice, the concentration of the radiolabeled warfarin in the two outlet channels was determined by a scintilation counter and the affinity constant were calculated (Table 1).

The result was benchmarked using a conventional bulk method [1].

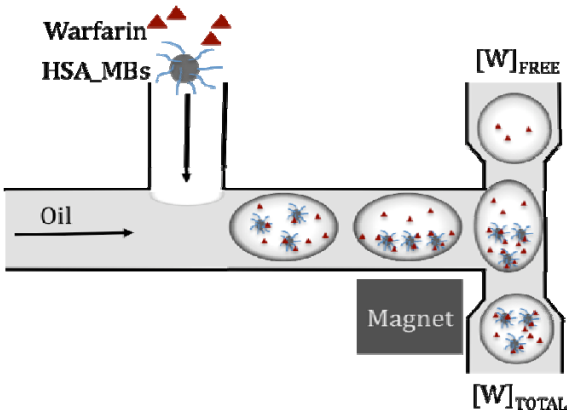


*Fig. 1: Scheme of the method (not to scale) for measuring the affinity constant of warfarin and human serum albumin (HSA).*

*Table 1. Comparison of measured and reported warfarin-HSA association constant, $K_A$.*

| Association constant $K_A$ x $10^{-5}$($M^{-1}$) | Reference |
|---|---|
| 4.74±2.84 (a) | This work, on-chip method |
| 4.93±2.46 (a) | This work, bulk method |
| 2.10±0.2 | Ref. [2] |
| 6.26±0.7 | Ref. [1] |

*(a) Mean of three independent experiments ± standard deviation.*

**DISCUSSION & CONCLUSIONS:** The binding process between warfarin and HSA was investigated implementing a magnetic beads technique with a microfluidic device. The fully continuous method could be employed for various applications, including binding assays, kinetic studies and single cell analysis, in which fast and complete removal of a reactive component is required. Furthermore it can be easily implemented into a modular device with further functionalities as required for pharmacokinetic studies.

**REFERENCES:** [1] M.P. Marszall, and A. Bucinski, (in press) A protein-coated magnetic beads as a tool for the rapid drug-protein binding study. *J Pharm Biomed Anal* **52** 420-4. [2] B. Loun, and D.S. Hage, (1994) Thermodynamic studies of (R)- and (S)-warfarin binding to immobilized human serum albumin. *Anal Chem* **66** 3814-22.

**ACKNOWLEDGEMENTS:** Financial support ERC Starting Grant, project no. 203428, nµLIPIDS.

European Cells and Materials Vol. 20. Suppl. 3, 2010 (page 164) ISSN 1473-2262

# Quantum dot-peptide conjugates for determination of Transferase enzyme activity

S. B. Lowe[1, 2], J. E. Ghadiali[1, 2], M. M. Stevens[1, 2]

[1] *Department of Materials, Imperial College London, UK.* [2] *Institute of Biomedical Engineering, Imperial College London, UK.*

**INTRODUCTION:** Post-transcriptional modification of proteins plays an important role in the regulation of cellular processes. Abnormal activity of p300 histone acetyltransferase (HAT) has been implicated in the progression of prostate cancer[1], the most common cancer in men.

We have developed a quantum dot bionanoconjugate system capable of detecting enzyme activity at sub-nM concentrations. This technology has been previously utilized for detection of Src and Abl kinases[2]: here we demonstrate applicability for a HAT enzyme, p300.

**METHODS:** CdSe/ZnS core/shell quantum dots were decorated with designer peptides used to mimic the natural substrate of p300; detection was achieved with dye-labelled monoclonal antibodies. The sensing mechanism is described in Fig. 1.

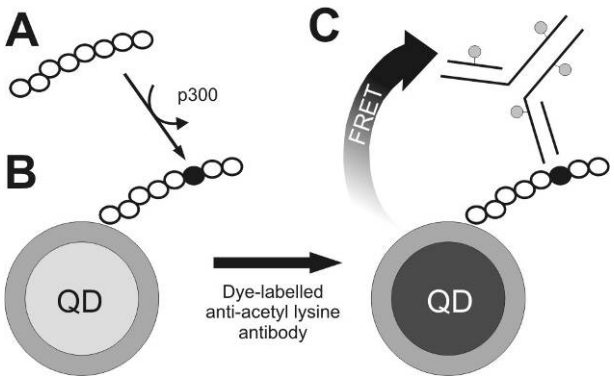


*Fig. 1: A – Peptide substrates incubated with p300 and acetylated. B – Photoluminescent quantum dots (QDs) functionalised with multiple peptides (one peptide shown for clarity). C – Binding by dye-labelled antibodies facilitates Förster Resonant Energy Transfer (FRET).*

**RESULTS:** The spectral response of the p300 assay is illustrated in Figure 2A; Figure 2B shows data from experiments where the p300 is introduced alongside an inhibitor, anacardic acid. The spectra in Fig. 2A show a time-dependent quenching of quantum dot emission and a corresponding enhancement of dye fluorescence, a characteristic FRET response arising from formation of a dye-antibody-peptide-quantum dot complex. The increase in FRET is a function of peptide acetylation due to p300 activity. The ratiometric FRET response data in Fig. 2B shows a typical dose-response curve for enzymatic inhibition. The lower limit of detection of this assay was also investigated, and a response was detected at p300 concentrations as low as 600 pM (Fig. 3).

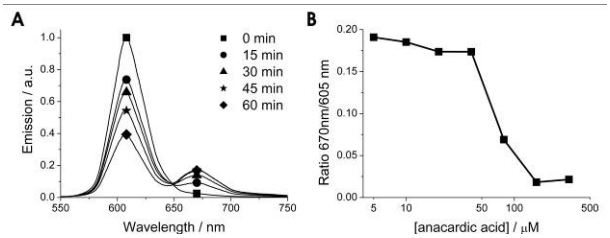


*Fig. 2: A - Photoluminescence spectra taken at 15 min intervals post addition of 320 nM p300. B – Plot of emission peak ratios showing effect of pre-incubation with varying concentrations of p300 inhibitor, anacardic acid.*

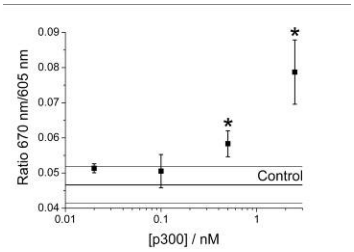


*Fig. 3: Emission peak ratios 6 h post addition of p300. Asterisks indicate significant signal above control range (95% confidence level, n=3).*

**DISCUSSION & CONCLUSIONS:** This quantum dot-based assay presents a rapid, simple alternative to existing enzyme-detection methods. The demonstrated detection sensitivity for p300 is comparable to the current detection standard, radiolabelling. It also provides an excellent response in the biological range and thus has exciting potential applications in medical research and drug discovery.

**REFERENCES:** [1] D. B. Seligson, S. Horvath, T. Shi, H. Yu, S. Tze, M. Grunstein, S. K. Kurdistani (2005) *Nature* **435**:1262-1266. [2] P. Cohen, (2002) *Nat. Rev. Drug Discov.* **1**:309-315. [3] J.E. Ghadiali, B.E. Cohen, M.M Stevens, in preparation.

**ACKNOWLEDGEMENTS:** SBL, JEG, and MMS would like to thank the EPSRC.

European Cells and Materials Vol. 20. Suppl. 3, 2010 (page 165) ISSN 1473-2262

# LSPR-Based Biosensing & Simultaneous Optical-Electrochemical Sensing with Gold Nanowire Arrays

R. MacKenzie, C. Fraschina, B. Dielacher, T. Sannomiya, V. Auzelyte, J. Vörös

*Laboratory of Biosensors & Bioelectronics, ETH Zurich, Zurich Switzerland*

**INTRODUCTION:** Using localized surface plasmon resonance (LSPR) with noble metal nanowire arrays the creation of a combined optical-electrical system offers a unique and powerful new platform for electochemical and biosensing applications. The optical properties of gold nanostructrures and the inherent conductive nature of nanowires also enable new studies of the fundamental *in situ* behaviour of nanowires and surface reactions on the nanoscale.

**METHODS:** Nanoline arrays are created using Extreme Ultraviolet Interference Lithography (EUV-IL). [1] The resulting patterns are converted to two different systems of gold or silver nanowires: Evaporated or particle-based nanowires. The scale and integration of the resulting nanowire arrays is shown in Figure 1.

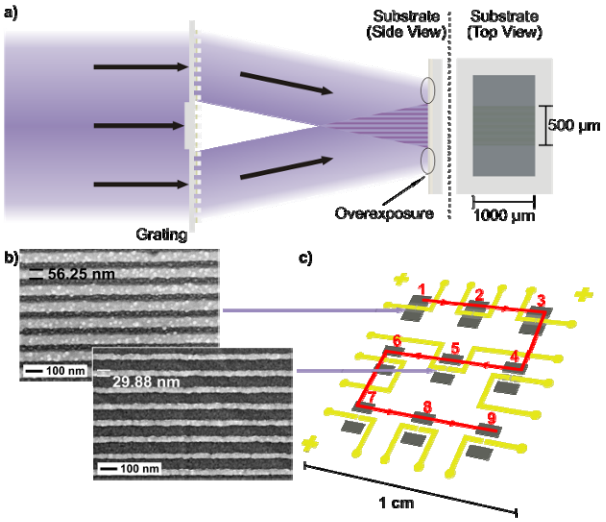


*Fig. 1: EUV-IL and large-scale evaporated nanowire arrays on an optical-electrical chip.*

**RESULTS:** Initial biosensing experiments were performed on Au particle-based nanowire arrays. By capitalizing on the nanogaps in the particle-based nanowire array, it was possible to observe changes in the extinction spectrum as biomolecules adsorbed to the surface of the exposed gold and surrounding $Nb_2O_5$ surface (Figure 2). In an electrochemical flow cell the application of voltages to evaporated gold nanowire arrays attracts and repels ions in a solution of NaCl, thereby changing the local refractive index near the wires, which is observable in the LSPR spectral response (Figure 3). [2]

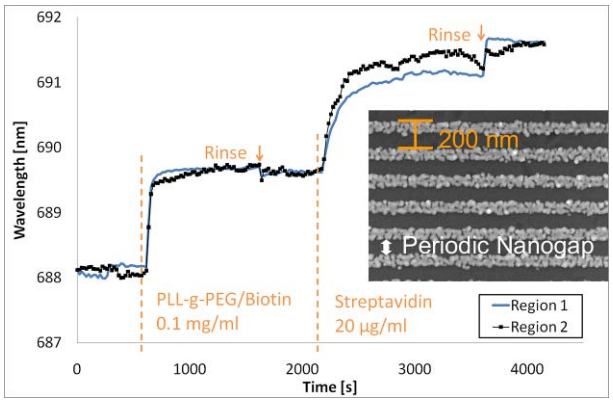


*Fig. 2: Adsorption of streptavidin to PLL-g-PEG/Biotin with particle-based nanowire arrays.*

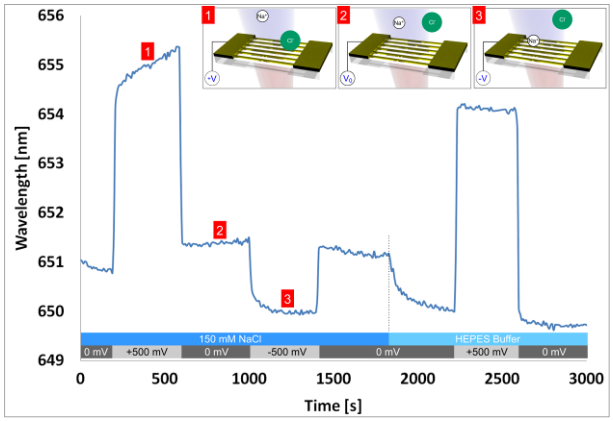


*Fig. 3: Shifts in LSPR peak wavelength upon the application of potentials in 150 mM NaCl solution.*

**DISCUSSION & CONCLUSIONS:** Streptavidin adsorption to PLL-g-PEG/Biotin yielded a 3σ calculated signal-to-noise ratio of 30. The combination of electrical and electrochemical properties of the nanowire arrays with their optical response is unique. LSPR peak shifts of over 4 nm, a system sensitivity up to 114.6 nm/RIU and limits of detection as low as 4.5 x 10-4 RIU have been obtained for evaporated nanowire arrays.

**REFERENCES:** [1]Auzelyte, V., et al., *Extreme ultraviolet interference lithography at the Paul Scherrer Institut.* Journal of Micro-Nanolithography Mems and Moems, 2009. **8**(2): p. 10. [2]MacKenzie, R., et al., *Optical Sensing with Simultaneous Electrochemical Control in Metal Nanowire Arrays.* Acs Nano *Submitted*, 2010.

**ACKNOWLEDGEMENTS:** We appreciate the financial support from CCMX and from the Nano-Tera Initiative, as well as the achievements of Martin Lanz and Stephen Wheeler.

European Cells and Materials Vol. 20. Suppl. 3, 2010 (page 166) ISSN 1473-2262

# A novel synthetic adhesive peptide conjugate supports the xeno-free culturing of embryonic and neural stem cells

K.Markó[1], E.Gócza[2], Á.Apáti[3], T.Kőhidi[1], E.Madarász[1]

[1] *Institute of Experimental Medicine, Hungarian Academy of Sciences, Budapest, Hungary.*

[2] *Agricultural Biotechnology Center, Gödöllő, Hungary.*

[3] *National Blood Center, Hungarian Academy of Sceinces.*

**INTRODUCTION:** Defined and xeno-free conditions are essential for the growth of embryonic and other tissue type stem cells, especially for the potential human therapeutic applications. While soluble xenobiotic factors (as components of sera) are quite easy to be replaced in culturing media, ensuring solid surface that enables proper cell attachment is a much harder issue. Formerly we demonstrated, that AK-cyclo[RGDfC], synthetic polypeptide effectively covers various surfaces used in cell culturing and provides an appropriate surface for many adhesion-dependent cell types[1].

**METHODS:** AK-cyclo[RGDfC] peptide conjugate was synthesized by G. Mező et al, and culturing surfaces were covered by the peptide as described earlier (Markó et al, 2008). R1/E murine and HuES9 human embryonic stem cells were cultured in defined medium (KO-DMEM, 15% SRL, 1000 IU LIF and 15% SRL, 8ng/ml bFGF, respectively). The pluripotency of murine ES cells were demonstrated by in vivo chimaera-assay. Human and murine ES cells were characterized by immunocytochemistry, RT-PCR and FACS-analyses. Radial glia-like neural stem cells were cultured in defined medium: DMEM/F12 (1/1), 1% B27, 20ng/ml and were characterized by immunocytochemistry, RT-PCR and differentiation assays.

**RESULTS:** Here, we show that AK-cyclo[RGDfC] enables the long-term culturing of both murine and human embryonic stem (ES) cells in defined medium. ES cells of different origin cultured on AK-cyclo[RGDfC]-covered surfaces for many passages retained their morphological characteristics, the expression of pluripotency markers and the potential to differentiate. Moreover, murine ES cells cultured on the synthetic polypeptide could integrate into mouse blastocysts and give rise to chimaeric embryos. The same adhesive polypeptide enabled the isolation/adhesion-based selection and long-term adherent maintenance of radial glia-like neural stem cells in defined conditions. These epidermal growth factor-dependent cells showed radial glia-like characteristics, expressed neural stem cell markers and could give rise to neurons, astrocytes and oligodendrocytes.

**DISCUSSION & CONCLUSIONS:** Application of AK-cyclo[RGDfC] enabled the culturing of embryonic and neural stem cells using completely defined conditions. The peptide-conjugate may contribute for platforms that apply such cells for therapeutic applications.

**REFERENCES:** [1] Markó K, Ligeti M, Mező G, Mihala N, Kutnyánszky E, Kiss E, Hudecz F, Madarász E. A novel synthetic peptide polymer with cyclic RGD motifs supports serum-free attachment of anchorage-dependent cells. *Bioconjug. Chem.* 2008 Sep;**19**(9):1757-66

**ACKNOWLEDGEMENTS:** AK-cyclo[RGDfC] was synthesized and kindly provided by Dr. Gábor Mező, Research Group of Peptide Chemistry, Hungarian Academy of Sciences. This work was supported by Bio_Surf National Technology Program (NKTH, Budapest).

European Cells and Materials Vol. 20. Suppl. 3, 2010 (page 167) ISSN 1473-2262

# Hydrogel-based Field Effect Transistor for Lectin Detection

Y.Maeda[1], A.Matsumoto[1], Y.Miura[2], Y.Miyahara[1]

[1] *National Institute for Materials Science, Tsukuba, Japan.* [2] *Kyushu University, Fukuoka, Japan.*

**INTRODUCTION:** We have developed a novel biosensor, which is based on field effect transistor (FET), which, however, doesn't depend only on the direct detection of the intrinsic electrical charge on the target biomolecule. We have previously proposed and demonstrated a unique way of utilization of stimuli-responsive polymer gels, namely "smart gels", as a route to obtain FET-based, but nonetheless virtually "Debye-length-free", universal molecular detection [1-3]. In this configuration, the detection of specific molecule by the smart gel triggers a volume phase transition of the gel accompanied by changes in its physicochemical properties, such as size, charge density, and permittivity, thus accomplishing a conversion of chemical signal into electrical signal.

In this presentation, we will first report on the synthesis of $\alpha$ -mannose-containing gel (αMan gel). This gel responded to the addition of tetrameric Concanavalin A (Con. A), one of the most common lectins. The phenomenon is due to the formation of con A-$\alpha$ Man complex where we found that the molar ratio of mannose determines direction of the gel response (swelling or deswelling). This may provide a new insight into a principle of remarkably sensitive way to detect proteins or other large molecules-involved bio-recognitions.

**METHODS:**

*Preparation of sugar gel and its responsibility to lectin*: Pregel solutions containing *N*,*N*-dimethylacrylamide (DMAAm) and *p*-*N*-acrylamidophenyl α-D-mannoside were prepared. $\alpha$ Man gels synthesized by thermal polymerization in glass capillaries were kept immersed in 20mM HEPES buffer (pH6.9, 4˚C, I=0.3M) containing 1mM $CaCl_2$ and 1mM, $MnCl_2$. The ⟨Man gels were transferred to new buffer solutions, and then Con. A was added to be 10μM. The weight changes of αMan gels were measured as a function of time.

*Preparation of sugar gel-based FET and its electrical characteristics*: The Con. A-responsive αMan gels (50μm thick) were covalently introduced to the surfaces of gold electrodes by photopolymerization and, then, reaction chambers were made on the extended gate electrodes by immobilizing glass tubes onto them. 20mM

HEPES buffer (pH7.0, 25˚C, I=0.3M) containing 1mM $CaCl_2$ and 1mM, $MnCl_2$ was poured into them. Real-time changes in threshold voltage ($V_T$) were recorded with a Ag/AgCl reference electrode after Con. A was added to the solution (5μM).

**RESULTS & DISCUSSION:** The weight measurement showed that the direction of swelling is controllable by molar ratio of αMan to DMAAm: the gel of low molar ratio swells due to the increase of osmotic pressure derived from the formation of Con. A-αMan complex of 1:1, on the other hand, the gel of high molar ratio, although it swells at first, but finally deswells due to the effect of physical crosslinking derived from the multivalent complex formation. Fig. 1 shows a time course of $V_T$ of the FET modified with gel of high molar ratio for addition of 5μM Con. A. The $V_T$ sharply increased at first, then decreased, and finally re-increased. The weight measurement supports this $V_T$ behaviour. The gel, at first, is negatively charged due to the binding to Con. A (pI = ca.6-7), and then, swells due to the increased osmotic pressure. Finally, multivalent Con. A-αMan interaction makes gel deswell.

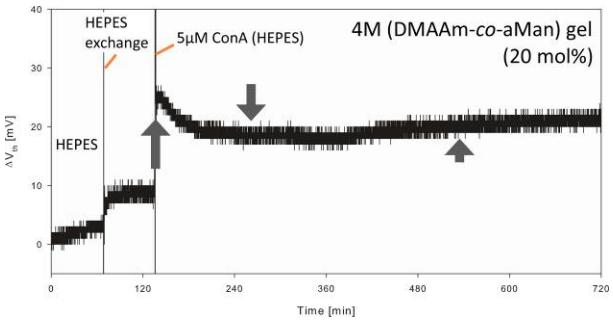


*Fig. 1: Time course changes of threshold voltage ($V_T$) of a Concanavalin A-responsive gel-modified FET.*

**REFERENCES:** [1] A. Matsumoto, Y. Miyahara (2009) *Adv Mater* **21**:4372-78. [2] A. Matsumoto, T. Endo, R. Yoshida, et al (2009) *Chem Commun* **37**:5609-11. [3] A. Matsumoto, N. Sato, Y. Miyahara, et al (2009) *Curr Appl Phys* **9**:214-217.

European Cells and Materials Vol. 20. Suppl. 3, 2010 (page 168) ISSN 1473-2262

# Wrapped up in a circle: Sensing RNA-protein interactions using a FRET-based approach

AD. Malay[1] and JG. Heddle[1]

[1]*RIKEN Advanced Science Institute, Wako, Japan*

**INTRODUCTION:** The bacterial protein **TRAP** (*trp* RNA-binding attenuation protein) folds into an 11-membered ring shaped structure having an external diameter of 9 nm [1]. In the presence of the ligand L-tryptophan, TRAP binds to its target RNA sequence with nanomolar affinity. The crystal structure of the ternary complex reveals that single-stranded RNA having the consensus sequence $(XXXAG)_{11}$ wraps around the perimeter of the activated TRAP ring. In the present investigation we use the TRAP biological system to devise a method to rapidly detect protein-induced RNA circularization using the principle of Förster resonance energy transfer (FRET).

**METHODS:** We have designed an RNA probe consisting of a 55-base target binding sequence flanked by short terminal linkers in the central region, and two covalently attached fluorophores (Fluorescein and a Cy3 analog) at either end of the oligonucleotide, forming the FRET pair. It is predicted that binding should cause the labeled RNA to wrap around the TRAP protein ring into close proximity, thus producing a measurable FRET signal (*Figure 1*).

Binding reactions for making fluorescence scans were carried out at room temperature and typically contained 50 nM refolded TRAP protein from *Bacillus stearothermophilus*, 10 nM double-labeled RNA probe and 0.5 mM L-tryptophan in 10 mM Tris-HCl pH 8.0, 0.5 M NaCl, and 1 mM EDTA. Excitation and emission profiles were measured out using a Hitachi F7000 fluorescence spectrophotometer. Gel shift assays were performed using 4 nM labeled RNA, 0.5 mM L-Trp, and increasing concentrations of TRAP (0-128 nM). Samples were subjected to native PAGE electrophoresis and bands were quantitated using a Typhoon imager.

**RESULTS:** Initial results show that the assay produces a significant FRET signal above the background. Fluorescence emission scans reveal a 13% increase in the signal intensity at 560 nm (FRET peak wavelength) for the TRAP:RNA sample compared to negative controls (*Figure 2*). A significant background emission is also observed however, which could be caused by the partial overlapping of the absorbance spectra for the two dyes, or insufficent physical separation between the two dyes in the labeled RNA probe.

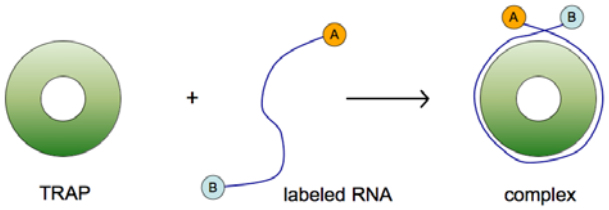


*Fig. 1: Schematic representation of the assay. Binding causes the labeled RNA to wrap around the TRAP protein, bringing the two fluorophores into close proximity and thus producing a FRET signal.*

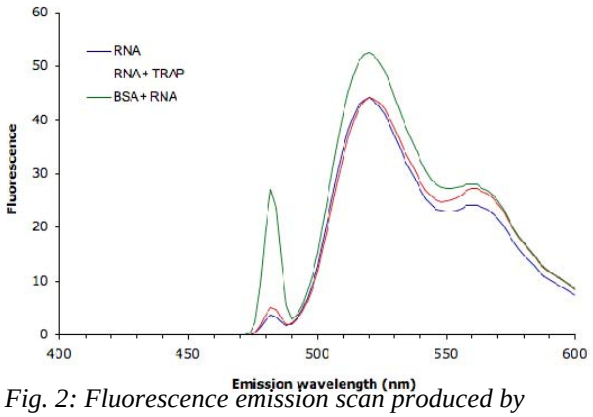


*Fig. 2: Fluorescence emission scan produced by excitation at 480 nm. The FRET signal is emitted with a peak maximum at 560 nm.*

**DISCUSSION & CONCLUSIONS:** We have used a protein-RNA binding phenomenon found in nature as an inspiration to design a biosensor system that can detect the wrapping of a specific oligonucleotide sequence around its interaction partner. This rapid and reproducible FRET-based assay is predicted to be applicable to other DNA- or RNA- protein binding systems with comparable conformational changes, and may have potential applications for nanodevices that feature conformational changes in its component oligonucleotides.

**REFERENCES:** [1]X. Chen, AA. Antson, M. Yang, et al (1999) *J Mol Biol* **289:**1003-16.

**ACKNOWLEDGEMENTS:** J.G.H was supported by MEXT Special Coordination Funds for Promoting Science and Technology and Grant-in-Aid for Young Scientists (WAKATE B-20710083) from the ministry of Education, Culture, Sports, Science and Technology, Japan.

European Cells and Materials Vol. 20. Suppl. 3, 2010 (page 169) ISSN 1473-2262

# Large Area Protein Patterning for Control of Focal Adhesion Development

J. Malmström[1], B. Christensen[2], H. P. Jakobsen[1], J. Lovmand[1,2], R. Foldbjerg[3], S. Kristensen[1], E.S. Sørensen[2], D.S. Sutherland[1]

*[1] Interdisciplinary Nanoscience Center, University of Aarhus, Denmark. [2] Department of Molecular Biology, University of Aarhus, Denmark. [3] Department of Environmental and Occupational Medicine, University of Aarhus, Denmark.*

**INTRODUCTION:** The growth and differentiation of cells are affected by biological cues presented from the extracellular matrix (ECM), other cells and the media. Well controlled and characterized model systems are an important tool to gain insight in protein-surface and cell-protein interactions. Nanoscale organization of adhesion cues (peptides or proteins) has received a lot of interest and is known to influence integrin clustering and focal adhesion formation in cells.[1,2] Here we demonstrate the development of a robust method to pattern protein patches over large areas in the 100-1000nm range and utilize it to study the interaction of cells with ECM components laterally organized on the nanoscale.

**METHODS:** Protein nanopatterns at the 100-1000 nm scale were produced by using a nanoscale chemical contrast of Au patches in a background of $SiO_2$ by colloidal lithography.[3,4] The nanostructured surfaces were made by depositing a triple polyelectrolyte layer onto gold substrates to render the surface positively charged. Negatively charged latex particles self assemble at the surface and is used as an evaporation mask during the deposition of $SiO_2$. After the removal of the particles gold patches in $SiO_2$ was achieved and used to, after chemical modification, preferentially adsorb protein to the gold part of the substrate. The adhesion of MDA-MB-435 cells to fibronectin patterns of 100, 200, 500 or 1000nm was studied and compared to the adhesion to fibronectin adsorbed at the homogenous control. The cells were stained for actin, vinculin and the nucleus and fluorescence microscopy and SEM was used to quantify and evaluate the data.

**RESULTS:** No significant cell binding was seen to the 100nm fibronectin pattern and significantly lower cell adhesion to the 200 nm surface compared to the larger patterns and the homogenous control was seen. The cells on the 200 nm fibronectin patches were in general not very spread and in most cases devoid of well defined vinculin spots or clear actin filaments although some small faint spots were seen in vinculin stained images in the outer region of the membrane and in lamellipodia. The cells on 500 nm fibronectin patches exhibited mainly small less

defined vinculin spots and few actin filaments. For the biggest protein patches (1000 nm) almost all the cells were spread with well-defined vinculin localizations. The cells were still largely devoid of thick actin stress fibers, but a significant number of the vinculin spots were co-localized to the end of thin actin fibers. On the homogeneous control the cells had well defined, comparatively large and rod shaped mature focal adhesions in many cases connected to thick actin stress fibers.[4]

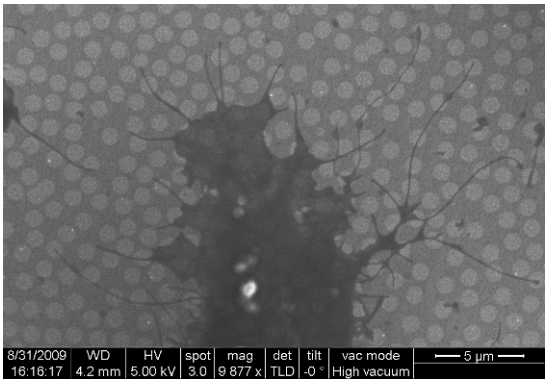


*Fig. 1: Cell spreading on 1000nm fibronectin pattern. Imaged with SEM.*

**DISCUSSION & CONCLUSIONS:** We propose that the size of the protein patches limits the conversion of focal complexes to focal adhesions, perhaps by limiting the force that can be applied, and for the patches of 200-500 nm, leading to the adhesive complexes being arrested at the stage of focal complexes. For 1000 nm patches the formation of larger focal adhesions and connection to actin fibres appears to occur on a regular basis. These results show the potential for giving defined surface cues to cellular systems.

**REFERENCES:** [1]Geiger, B. et al., *Nature Reviews Molecular Cell Biology* **2009**, 10, (1), 21-33. [2]Arnold M et al, *Chemphyschem* **2004**, 5, (3), 383-388. [3]Agheli H et al, *Nano Letters*, **2006**, 6, (6), 1165-1171. [5]Malmstrom, J. et al, *Nano Letters* **2010**, 10, (2), 686-694.

European Cells and Materials Vol. 20. Suppl. 3, 2010 (page 170) ISSN 1473-2262

# A Comparative Atomic Force Microscopy Study on the Interaction between the CD44 Cell Surface Receptor and Different Glucosaminoglycans

AA.Martens[1], M. Bus[1], EJR.Sudhölter[1], LCPM.de Smet[1]

[1] *Chemical Engineering, Delft University of Technology, Delft, The Netherlands.*

**INTRODUCTION:** Hyaluronan (HA), member of the class of glucosaminoglycans (GAGs) is a versatile, linear polysaccharide present in the extracellular matrix and on cell surfaces. Its binding to the CD44 cell surface receptor (a glycoprotein) is among the first adhesive interactions between moving and static cells. Therefore this interaction plays an important role in tissue development, regeneration, wound healing and leukocyte homing, but also in unwanted processes like metastasizing and tumour growth. To deepen our understanding of this interaction, we used Atomic Force Microscopy (AFM) to investigate the affinity of CD44 to HA and other GAGs.

**METHODS:** A silicon AFM tip on the end of a silicon nitride cantilever (spring constant of 0.005 N/m) was functionalised with aminopropyltri-ethylsilane (APTES), covalently bound protein A, and a physically bound fusion protein (IgG-CD44 hyaluronan binding domain), respectively. To avoid possible protein denaturing due to drying, in-situ protein attachment was performed in the AFM setup. (*Fig. 1*) The GAGs: HA, Heparan sulfate, Heparin, and Chondroitin sulfate (ChS) were each covalently bound to a silica wafer. Multiple (8-11) force distance curves were recorded for the CD44 interaction with the listed GAGs. (*Table 1*).

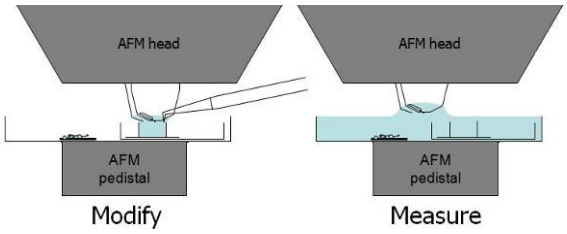


*Fig.1: AFM probe modification in concentric dishes in AFM setup, avoiding drying between modification and measurement.*

**RESULTS:** *Figure 2* is an example of a force distance plot for HA. Every retract curve (blue in *Fig 2.*) is the product of multiple interactions. The area between the retract curve and the baseline (approach curve, red in *Fig 2.*) was integrated, yielding a measure of the affinity between the CD44-modified AFM tip and the different GAGs. Averaged collective affinities are listed in *Table 1.*

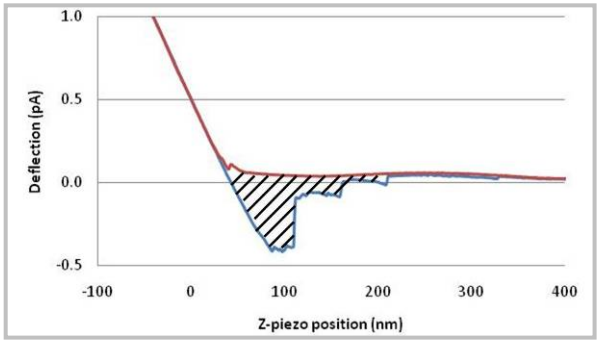


*Fig. 2: Deflection of the cantilever as a function of the Z-piezo position. The shaded area is a measure for the CD44-GAG affinity (HA in this example).*

*Table 1. Average area between the approach and retract curve as a measure of affinity between CD44-modified AFM tip and GAGs.*

| GAG | pA×nm |
|---|---|
| Hyaluronan | 40 |
| Heparan sulphate | 16 |
| Heparin | 11 |
| Chondroitin sulphate | 42 |
| Hyaluronan again (control) | 55 |

CD44 appears to have low affinity to Heparin and Heparan sulfate and high, comparable affinity to HA and ChS. However, the rupture characteristics were found to be different: the HA rupture shows multiple small rupture events over a distance of 400 nm, while ChS releases with a few large jumps within 250 nm.

**DISCUSSION & CONCLUSIONS:** The affinity of CD44 for both HA and ChS indicates that ChS may influence HA binding in CD44 isoforms that contain ChS in the variant domain. The differences in retract curves between HA and ChS suggest that the immobilized ChS is more cross-linked or entangled than the immobilized HA. ChS affinity to CD44 needs to be verified by another technique. The CD44-HA interaction is currently being quantified by single molecule AFM force spectroscopy.

**ACKNOWLEDGEMENTS:** This research was supported by the faculty of Applied Sciences (TU Delft) and by the Netherlands Organization for Scientific Research (NWO-Veni to LCPMdS).

European Cells and Materials Vol. 20. Suppl. 3, 2010 (page 171) ISSN 1473-2262

# Intact mammalian cell function on semiconductor nanowire arrays: new perspectives for cell-based biosensing

Trine Berthing[1], Sara Bonde[1], Claus B. Sørensen[2], Pawel Utko[2], Jesper Nygård[2], and Karen L. Martinez[1].

*[1] Bio-Nanotechnology Laboratory, Department of Neuroscience and Pharmacology & Nano-Science Center, University of Copenhagen, Universitetsparken5, DK-2100, Copenhagen, Denmark.*
*[2] Niels Bohr Institute & Nano-Science Center, University of Copenhagen, Universitetsparken 5, DK-2100, Copenhagen, Denmark.*

**INTRODUCTION:** It is of great interest for fundamental cell biology and for the development of improved cell-based drug screening assays, to gain spatial and temporal information on intracellular processes of single cells. Nanowires (NWs) are gaining more and more interest due to their potential cellular applications, such as delivery of compounds or sensing platforms [l-3]. Here, we interface arrays of vertical indium-arsenide NWs with human embryonic kidney cells and rat embryonic dorsal root ganglion neurons. A selection of critical cell functions and pathways are shown not to be impaired, including cell adhesion, membrane integrity, intracellular enzyme activity, DNA uptake, cytosolic and membrane protein expression and the neuronal maturation pathway. The results demonstrate the low-invasiveness of InAs NW arrays and thereby open up their potential for cellular investigations [4].

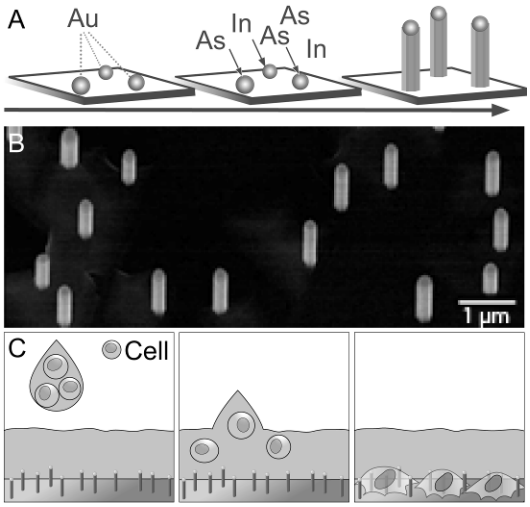


*Fig. 1: Vertical arrays of InAs NWs as a substrate for cell culture. (A) Growth model for NWs. (B) Scanning electron micrograph of an aligned NW array of InAs. (C) Illustration of the gentle method used to interface cells with NW arrays.*

**METHODS:** In this study, we interface cells from the human embryonic kidney cell line (HEK293) and rat embryonic dorsal root ganglion neurons (F11) with vertically aligned indium arsenide (InAs) nanowires (NWs) (figure 1). The results include cross-section images of living cells with embedded NWs and scanning electron micrographs providing information on the interaction between NWs and cells

**RESULTS:** We show for the first time the spontaneous and intimate interaction of arrays of vertically aligned InAs NWs with two relevant cell lines, human embryonic kidney cells (HEK293) and rat embryonic dorsal root ganglion neurons (F11). The interfacing approach is evaluated with respect to the ability of bringing nanowires in contact with the interior of cells and the effect on cell viability.
We report maintained cellular membrane integrity and cytosolic esterase activity, as well as continued functionality of the F11 maturation pathway.
The viability of cells and the cellular machinery are shown not to be impaired even by the presence of NWs. Moreover, we show successful cellular transfection resulting in transcription, translation, and localization of cytosolic- and membrane proteins, despite a close concomitant interaction with InAs NWs [4].

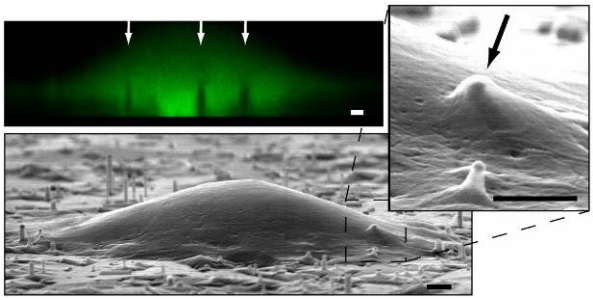

*Fig. 2: Cell cultured on NW array. Confocal fluorescence and scanning electron micrographs of a cell with embedded NW. Scale bars are 1 µm.*

**DISCUSSION & CONCLUSIONS:** These results strongly support the idea that NW arrays can be used, in complement to the traditional methods, as a platform for cellular investigation without interfering with cellular health or function.

**REFERENCES:** [1] W. Kim et al. (2007) *JACS* **129**, 7228 (2007), [2] W. Hällström, et al, (2007) *Nano Lett* **7**, 2960, [3] T. Berthing et al. (2009) *J. Nanoneuroscience.* **1**, 3, [4] T. Berthing et al. *submitted.*

European Cells and Materials Vol. 20. Suppl. 3, 2010 (page 172) ISSN 1473-2262

# Organic electronic materials from oligopeptide-polymer conjugates

Roman Marty[1], Ruth Szilluweit[1], Holger Frauenrath[1*]

[1] *EPFL – STI – IMX – LMOM, Building MXG, Room 040, Station 12, 1015 Lausanne, Switzerland.*

**INTRODUCTION:** Nature's way of self-organizing molecules into materials serves as the role model for the strategy toward hierarchically structured polymers containing semiconducting π-conjugated segments. A good starting point for its development appears to be a look at nanostructures from β-sheet forming oligopeptides as they occur in biological systems, such as amyloid fibrils. [1] Previous investigations in our group had revealed that a precise control of the position, orientation, and reactivity of π-conjugated molecular fragments was achieved by β-sheet-type N-H···O=C hydrogen-bonding. The investigated molecules gave rise to well-defined fibrillar features with a length of several micrometers, and a uniform width of a few nanometers. [2] A similar aggregation behavior is expected for symmetric oligopeptide-polymer conjugates bearing organic semi-conducting segments such as naphthalene-, perylene- or higher rylene bisimides on which we focus in the present investigation (Figure 1). The fibrillar arrangement brings the π-conjugated segments in close contact so that nanowires with a well-defined charge percolation path should be obtained.

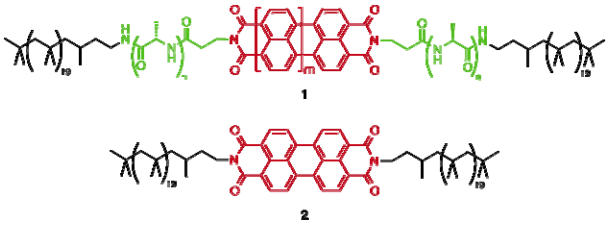

*Fig. 1: Perylene bisimides bearing polymer or oligopeptide-polymer conjugate side-chains.*

**DISCUSSION & CONCLUSIONS:** First, we prepared oligoalanine-polymer conjugates using standard peptide chemistry with PyBOP as the coupling agent, and amine terminated poly(isobutylene) (PIB-$NH_2$) as the polymer. The perylene bisimide derivates **1** (m = 1) with 0–4 hydrogen-bonding sites on each side-chain were synthesized by a condensation reaction of the corresponding oligoalanine-PIB conjugates with perylene bisanhydride. The aggregation behavior was investigated by IR, UV/VIS, and fluorescence spectroscopy. The derivative **2** without any hydrogen-bonding sites is highly soluble in various organic solvents and showed a low tendency to aggregate via π-π-stacking. By contrast, pre-liminary results imply the formation of aggregates in the case of the hydrogen-bonded derivatives that were visualized by AFM techniques.

**REFERENCES:** [1] R. Nelson, M. R. Sawaya, M. Balbirnie, A. Ø. Madsen, C. Riekel, R. Grothe, D. Eisenberg (2005) *Nature* **435**: 773-7. [2] E. Jahnke, N. Severin, P. Kreutzkamp, J. P. Rabe, H. Frauenrath (2008) *Adv. Mater.* **20**: 409-14.

**ACKNOWLEDGEMENTS:** Funding by the Swiss National Science Foundation (SNF Grant 200020-121812/1) and by the European Research Council (ERC Grant 587119) is gratefully acknowledged.

# Bio-transistor for Label Free Living Cell Diagnosis

A.Matsumoto[1], N.Sato[2], R.Yoshida[2], K. Kataoka[2], Y.Miyahara[1]

[1] *National Institute for Materials Science, Tsukuba, Japan.*

[2] *The University of Tokyo, Tokyo, Japan.*

**INTRODUCTION:** Alternation of SA contents on cell surface glycan chains have been implicated in numerous normal and pathological processes including developments, differentiations and tumor metastasis. Most tumor-associated carbohydrate antigens including those clinically approved as tumor markers involve sialic acid (SA), an anionic monosaccharide that frequently occurs at the termini of the glycan chains. Indeed, overexpression of SA on the cell surface has been implicated in the malignant and metastatic phenotypes for many different types of cancers, while decreased SA expression has also been identified in erythrocytes of diabetic mellitus. Techniques to conveniently monitor cell surface SA therefore have great relevance to handy ways of cytology. Ordinarily, cell surface SA density is assessed via multiple enzymatic and labelling procedures, which involve severely invasive, in many cases lethal procedures. Besides, SA residues must be either enzymatically or acid-catalytically cleaved from the glycan chains and then disintegrated into the free forms that can finally be subjected to the quantification. The present work describe a label-free detection of cell surface sialic acid (SA) using a self-assembled monolayer (SAM) of phenylboronic acid (PBA) compound integrated on a field effect transistor (FET) extended gold gate electrode. Due to selective binding between undisassociated PBA and SA at pH 7.4 among other glycan chain constituent monosaccharides, we found that carboxyl anions of SA were exclusively detectable as the change in threshold voltage ($V_T$) of the PBA-modified FET. .

**METHODS:** A self-assembled monolayer (SAM) of 10-carboxy-1-decanethiol was first formed on a gold electrode followed by a condensation reaction with an amino group functionalized PBA (3-aminophenylboronic acid) resulting in the introduction of meta-amide substituted PBA onto the SAM terminal. The electrode was then lined to a field effect transistor (FET) gate for real-time monitoring of the charge density changes taking place on the electrode when binding with anionically charged SA. As for proof-of-principle, erythrocyte was first investigated, for which alternations of SA content (frequently "decline"[3] while conflicting reports also exist)

have been reported in diabetes mellitus. Along with native erythrocytes, those with enzymatically-decreased surface SA (20% remains) were also prepared and used as a control system. The PBA-modified FET was also tested for its ability to assess degree of tumor metastasis. Metastatic murine melanoma cells expressing luciferase (B16-F10-Luc-G5) were utilized for their ability to specifically metastasize to healthy lungs of mice after intravenous injection. Tumoral lung specimens with 15 and 30 % metastases in cell population, respectively, as determined by bioluminescent assays, were subjected to the SA expression analyses using the device along with a healthy pneumocyte as a 0% metastasis model.

**RESULTS & DISCUSSION:** Comparison between the two (native and sialidase-treated rabbit erythrocytes) systems revealed remarkably distinct $V_T$ profiles with correspondence to the altered SA content per cell, suggesting that once a cell number-$V_T$ calibration is determined for a healthy phenotype, the altered SA expressions can directly be monitored in a real-time manner, simply by placing the known-count living cell suspensions onto the electrode. Likewise, remarkably pronounced correlation between the tumoral fraction and the magnitude of $V_T$ shift were obtained. These results provide evidence that an advancement of metastasis in the living tissue is actually assessable using the PBA-modified FET, where, clearly, the increased $V_T$ shift for higher metastases results from a greater SA expression (4-fold as colorimetrically determined, data not shown) on B16-F10-Luc-G5 relative to healthy pneumocyte. These techniques can be readily extended to other primary *vs* tissue systems if their cell number-$V_T$ calibrations are predetermined. Such a capability may serve as a remarkably easy and quantitative adjunct to histological evaluation of tumor malignancy and metastatic potential during intra- or postoperative diagnoses.

**REFERENCES:**

[1] A. Matsumoto, et al. (2009) *Adv Mater* **21**:4372-78. [2] A. Matsumoto, et al (2009) *Chem Commun* **37**:5609-11. [3] A. Matsumoto, et al (2009) *J. Am. Chem. Soc.* 2009, **131**, 12022-12023. [4] A. Matsumoto, et al (2010) *Angew. Chem., Int. Ed.* 2010, in press.

European Cells and Materials Vol. 20. Suppl. 3, 2010 (page 174) ISSN 1473-2262

# A New Aspect of Drug Delivery System in Cancer Therapy

Y. Matsumura

*Investigative Treatment Div, Research Center for Innovative Oncology, National Cancer Center Hospital East, Kashiwa, Japan*

Conventional low molecular weight (LMW) anticancer agents including molecular targeting agents can easily extravasate from normal blood vessels and are distributed throughout the whole body leading to adverse side effects of the drugs.

In order to overcome such off-target effects caused by LMW anticancer agents, a so-called missile therapy was developed in which an anti cancer drug or toxin is conjugated to a cancer cell-specific monoclonal antibody. Such macromolecules are too large to pass through a normal vessel wall but can extravasate from leaky tumor vessels and accumulate selectively in tumor tissue. At first, this strategy of missile therapy was expected to be highly successful.

However, most human solid tumors, possess abundant stroma that hinders the distribution of macromolecules, including anti-cancer agent-conjugated antibodies. This tissue consequently becomes a barrier preventing immunoconjugates from attacking cancer cells

We show the successful development of a new strategy that overcomes this drawback and achieves highly localized concentration of the LMW cytotoxic agent SN-38 by conjugating it to a specially raised antibody to a plentiful component of tumor stroma. These newly developed immunoconjugates selectively extravasated from leaky tumor vessels, bound to the stromal antigen network ensleeving tumor vessels and created a scaffold, from which effective sustained release of the time-dependent anti-cancer agent SN-38 occurred. This released anti-cancer agent subsequently diffused throughout the tumor tissue causing marked arrest of tumor growth associated with damage to tumor vessels and death of cancer cells. Cancer stromal targeting therapy, utilizing a cytotoxic agent conjugated to a monoclonal Ab directed at a specific inert constituent of the tumor stroma is thus validated as a highly effective new modality of oncological therapy, especially for refractory, stromal-rich cancers.

**ACKNOWLEDGMENTS:**

I thank my collaborators, Dr Shino Manabe (Synthetic Cellular Chemistry Laboratory, RIKEN Advanced Science Institute), Dr Masahiro Yasunaga (Investigative Treatment Division, Research Center for Innovative Oncology, National Cancer Center Hospital East), Dr David Tarin (Department or Pathology, University of California).

European Cells and Materials Vol. 20. Suppl. 3, 2010 (page 175) ISSN 1473-2262

# Plasma polymers in biotechnology: power, patterning and PDMS

Sally L McArthur

*Biointerface Engineering Group, IRIS, Faculty of Engineering and Industrial Sciences, Swinburne University of Technology, Hawthorn, VIC Australia*

*smcarthur@swin.edu.au*

The emerging proteomics field has triggered the development of many bioanalytical tools and technologies. Since biological samples are usually present in small quantities and volume, there is a high priority for the analytical tools to be able to process these minute samples creating opportunities for microfluidic devices and assay to be developed. There are significant limitations inherent in the current technologies used in protein extraction and separation for proteomes larger than 3,000 as this represents the upper limit of protein separation using conventional 2D gels. The project aims to investigate novel micro-channel processing schemes that will enable spatio-temporal separation of both soluble and membrane-related proteins that can subsequently be interfaced with mass spectrometry analysis. The ability to control interactions between biomolecules and micro-channel surfaces is an integral component of this project. Plasma polymerisation has been shown to be an attractive method for coating microchannel surfaces with a wide variety of different chemistries (acids, glymes, anhydrides, amines and epoxies). A major advantage in the use of the plasma polymers is that they can be translated to a variety of substrate materials commonly used for microfluidic devices including glass and PDMS. By utilising photolithographic patterning, arrays of different chemistries can be created within channels. This approach has enabled us to both immobilise functional biomolecules (antibodies and trypsin) in specific regions of the devices, as well as establish protein separation techniques (ion metal affinity (IMA) and isoelectric focussing (IEF)). In order to understand how the surface properties of a material influence the organization of biomolecules surface analytical techniques such as X-ray photoelectron spectroscopy (XPS), static secondary ion mass

spectrometry (SSIMS), zeta potential measurement, AFM, mass spectrometry and biological assays have all been utilised to provide a complementary approach for characterizing these complex devices.

European Cells and Materials Vol. 20. Suppl. 3, 2010 (page 176) ISSN 1473-2262

# Phosphatidylserine-containing Phytantriol Cubic-Phase Particles: Influence of Lyotropic Liquid Crystalline Phase Behaviour on Cellular Response

H.H. Shen[1], J.G. Crowston[2], F. Huber[1], K.M. McLean[1], S. Saubern[1], P.G. Hartley[1]

*[1]CSIRO Molecular and Health Technologies, Clayton South, Vic. 3169, Australia. [2] Centre for Eye Research Australia, University of Melbourne, Vic. 8002, Australia.*

**INTRODUCTION:** A number of surfactant and lipid based particle dispersions have been suggested for use in biomedical applications [1-2]. Safe and effective utilisation of such systems requires that they do not result in an adverse biological response. Factors such as particle size, dose and surface characteristics are believed to play key roles in the biological response to these materials [3]. Detailed understanding of the role of these parameters on determining biological response is important for safe future applications of these entities. In this work, we have studied *in vitro* the role of lipid particle phase behaviour and composition in modulating cellular uptake and cytotoxicity of lyotropic liquid crystalline nanoparticles (cubosomes) based on the lipid like surfactant: Phytantriol.

**METHODS:** Cubosomes were co-formulated from phytantriol/Pluronic F-127 and increasing concentration of Di-palmitoyl-phosphatidylserine (DPPS). The structure was characterized using small angle X-ray scattering (SAXS) and Cryo-TEM. The viability of L929 fibroblast cells following exposure to cubosome formulations were studied by a MTT assay and confocal microscopy of fluorescently-labelled cubosomes. Model lipid bilayers were prepared using the vesicle deposition technique and interactions with cubosomes were studied using Quartz-crystal microgravimetry with dissipation.

**RESULTS & DISCUSSION:** SAXS (Fig. 1A) of the dispersed particles with increasing DPPS content resulted in a Pn3m to Im3m cubic phase transition and a concomitant increase in the appearance of vesicles as seen by TEM (Fig. 1B).

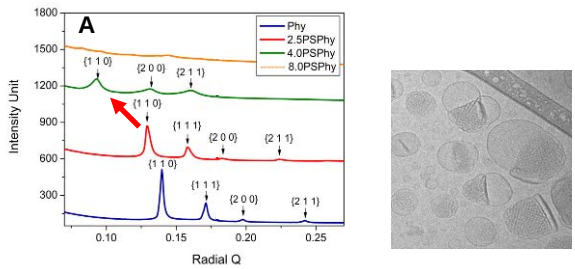


*Fig. 1: (A) SAXS characterisation of phytantriol and DPPS-containing phytantriol cubosomes. (B) Cryo-TEM images of DPPS-containing phytantriol cubosomes showing the presence of vesicles.*

Cell viability in the presence of cubosomes was found to decrease as the cubosome DPPS content was increased. Interactions of fluorescently labelled cubosomes with L929 fibroblast cells were probed using confocal microscopy. Fig. 2 shows that octadecyl rhodamine labelled DPPS-phytantriol dispersions (red) penetrated through the cell membrane and localised in the cytoplasm, DPPS free phytantriol particles, however, mainly aggregated at the cell periphery associated with the external cell membrane.

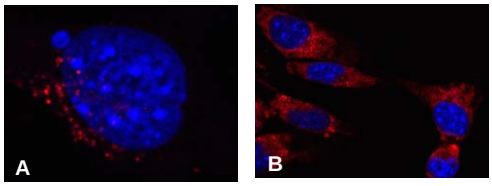


*Fig. 2: Confocal images of L929 cells after 24 hours incubation with octadecyl rhodamine labelled phytantriol (A) and DPPS-containing phytantriol (B) cubosomes. Blue: DAPI*

Furthermore the Quartz-crystal microgravimetry with dissipation data indicates that attachment of DPPS-containing phytantriol dispersions to model lipid membranes is rapid relative to phytantriol-only cubosomes, and that the overall mass increase is higher. We therefore hypothesise that the cytotoxicity of the DPPS-containing dispersions is related to the preferential attachment and cell uptake at the cell membrane surface.

**CONCLUSIONS:** We have demonstrated that addition of DPPS to cubosomes has a marked effect on the phase behaviour which is correlated with differences in cellular uptake and cytotoxicity. This has significant implications for the design and formulation of lipidic dispersions for therapeutic applications such as drug delivery.

**REFERENCES:** [1] P.T. Spicer (2005) *Current Opinion in Colloid & Interface Science* 10(5-6):274-279. [2] W. K. Fong, T. Hanley, B.J. Boyd (2009) *Journal of Controlled Release* 135(3): 218-226. [3] G. Pastorin (2009) Pharmaceutical Research 26(4):746-769.

European Cells and Materials Vol. 20. Suppl. 3, 2010 (page 177) ISSN 1473-2262

# Variation of Surface Functional Groups of Oxide Nanoparticles and their Impact on Protein Interactions

F.Meder[1], T.Daberkow[1], L.Treccani[1], K.Rezwan[1]

[1] *Advanced Ceramics, University of Bremen, Am Biologischen Garten 2, 28359 Bremen, Germany*

**INTRODUCTION:** The rising interest in nanoparticles due to their huge potential application in many different fields goes along with an unknown impact on health and environment. With regard to the unclear toxicity of inorganic nanoparticles and their suitability as biomaterials, the interactions of these materials with biological systems are of great importance.[1, 2]
The adsorption of proteins is one of the first reactions when artificial materials are exposed to biological media. It is known that the interactions are affected by the surface properties of both systems, whereas the bulk material plays a secondarily role.[1,2] How surface properties influence the interactions is not understood in detail yet. In this work, by changing the surface properties of nanoparticles via chemical modifications, we aim to detect and understand the "response" of biomolecules and want to elucidate the adsorption mechanism of proteins on oxide materials.
Interactions of nanomaterials and proteins shape properties like the state of dispersion, surface charges, sizes or the mobility of the nanomaterials in biological systems. In view of their cellular interactions and toxic characteristics this behaviour is believed to be of great importance.[2]

**METHODS:** α-Alumina nanoparticles ($d_{50}$= 150 nm, BET=13 m²/g) were used as model particles. Surface functionalisation was achieved using different silane and phosphate precursors (3-Amino-propyl-triethoxysilane, 3-(Triethoxy-silyl)-propylsuccinic-anhydride, 3-(Trihydroxy-silyl)-1-propane-sulfonic-acid and pyrophosphoric-acid). Particles and particle surfaces before and after functionalisation have been characterised by BET, DLS, HRTEM, zeta potential measurements, water vapour adsorption, FTIR, EDX and photochemical end group assays. Protein adsorption experiments have been carried out with model proteins like Albumin, Lysozyme and ß-Galactosidase under controlled media properties. Detection of protein adsorption has been realized by zeta potential measurements, fluorescence and UV-spectroscopy.

**RESULTS:** The surfaces of α-Alumina particles were functionalised controllably resulting in physical (charge) and chemical (chemical group) modifications. The zeta potential of functionalised particles differed from untreated alumina and indicated a modification of the surface (Fig. 1). Negatively charged BSA adsorbed preferably on positively charged alumina surfaces. On negatively charged surfaces an adsorption of BSA could not be observed at experimental conditions (Fig. 2).

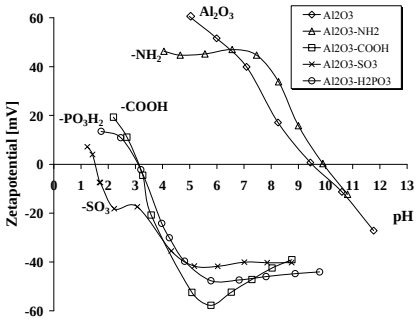


*Fig. 1: Effect of surface functional groups on the zetapotential and isoelectric point of alumina*

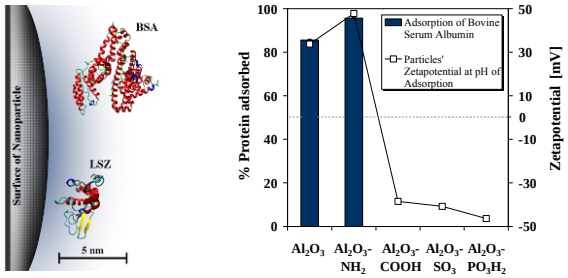


*Fig. 2: Schematic of protein-particle-encounter (left); behaviour of the adsorption of proteins (BSA) on functionalised nanoparticles (right)*

**DISCUSSION & CONCLUSIONS:** From our preliminary results it can be seen that the adsorption of proteins is affected substantially by different functionalisations of alumina. Electrostatic interactions seem to play a major role in the adsorption mechanism for the investigated system considering that hydrophilicities were in comparable dimensions for the different functionalisations. The adjustment of surface properties of the investigated nanoparticles is fundamental for protein adsorption. Therefore we assume that these differently modified surfaces will also have different impacts in cell tests and cytotoxicity studies.

**REFERENCES:** [1]K.Rezwan, L. Meier, L. Gauckler (2005) *Biomaterials* **26**: 4351-4357 [2]A.Nel, L. Mädler, D. Velegol, T. Xia, E. Hoek, P. Somasundaran (2009) *Nat Mater* **8**: 543-557

European Cells and Materials Vol. 20. Suppl. 3, 2010 (page 178) ISSN 1473-2262

# Long-Range SPR sensors integrated in microfluidic device for sensitive detection

R. Mejard, M. Kurkuri, H. Griesser, B. Thierry

*Ian Wark Research Institute, University of South Australia, Mawson Lakes, SA 5095, Australia.*

**INTRODUCTION:** SPR-based biosensing technologies have matured to become an essential tool in biomolecular studies, for instance for the detection of DNA or protein analytes. The ability of conventional SPR sensors to detect the binding of large biological entities such as cells and bacteria remains however limited due to the poor penetration of the evanescent waves in the analyzed medium. Long range surface plasmons (LR-SPR) are coupled surface plasma waves that propagate on opposite sides of a thin noble metal film suspended between two dielectrics with similar refractive indices. The longer propagation lengths of the plasmon waves in the analyzed medium associated with LR-SPR is of high interests and many applications have been proposed, for instance in non-linear optics and biosensing. The intrinsic low loss of LR-SPR is also advantageous as it results in narrower SPR features which offer greater sensitivity to shifts of the resonance angle [1]. A limitation of LR-SPR is the relative difficulty in fabricating with precision multilayered thin films that supports LR-SPR. The preparation of the required dielectric film with a low refractive index is particularly challenging; the most successful approach to date has relied on the spin-coating of Teflon AF™.

The aim of this work is to integrate various LR-SPR based sensors within microfabricated devices towards the immunospecific capture and detection of large biological entities. We also report an alternative method to develop LR-SPR sensors, based on the plasma polymerization of low refractive index nano-porous siloxane films.

**METHODS:** A mixture of Tetramethyldisiloxane (TMDSO) and cyclohexane using argon (200 sccm) and oxygen (80 sccm) as carrier gases was plasma polymerized (2 kW applied power). The resulting thin film coated substrates were annealed in a custom made crucible at 500 $^{o}$C for 2 hrs. LR-SPR sensors were also prepared using Teflon AF and MY133MC, which possess a refractive index of 1.33. Standard soft molding technology was used to integrate the LR-SPR sensors in microfabricated devices. A prism was used to couple the incoming light to the sensing device (Kretschmann configuration). Polydimethylsilane (PDMS) microchannels were coupled to LR-SPR sensors functionalized with epoxy-rich thin films prepared by the pulsed plasma polymerization of allyl glycidyl ether.

**RESULTS:** As shown in Figure 1, the reflectance dips observed with LR-SPR sensors are typically much narrower than those achieved with conventional SPR (cSPR) sensors. Our first approach consisted in the fabrication of nanoporous siloxane thin film with tunable RIs. Addition of carbonaceous compounds such as cyclohexane in the monomer feed during the plasma polymerization of TMDSO enabled the introduction of nanoscaled porogen in the polymer layer; these carbonaceous nanoaggregates were eliminated from the siloxane film by annealing, which resulted in the formation of nanoscale porosity. The nanostructured siloxane films showed significantly lower refractive index in comparison to pure TMDSO films and could be used to create LR-SPR sensors. These novel sensors were compared with those prepared using Teflon AF as well as a novel polymer with low RI, MY133MC.

The LR-SPR sensors could be integrated within microfabricated channels designed to favour the immuno-specific capture of target cells. Epoxy groups introduced on the surface of the sensors could be readily reacted with herceptin, a monoclonal antibody which binds with high affinity to HER2 positive cancer cells.

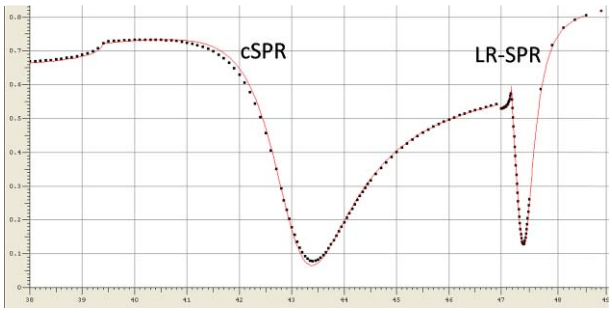


*Fig. 1: Reflectance dips of cSPR and LR-SPR.*

**DISCUSSION & CONCLUSIONS**: Various LR-SPR sensors were integrated in microfabricated devices and used to detect the binding of cancer cells. LR-SPR are more sensitive than conventional ones and the proposed approach is expected to provide improved technology for the detection of rare target cells in biological fluids.

**REFERENCES:** [1] J. Dostalek (2007) et. Al., *Plasmonics* **2**: 97-106.

**ACKNOWLEDGEMENTS:** This project is supported by the ARC (DP0881254).

European Cells and Materials Vol. 20. Suppl. 3, 2010 (page 179) ISSN 1473-2262

# Protein adsorption onto nanopores at the nanometer scale

G.M.L. Messina and G.Marletta

*Laboratory for Molecular Surface and Nanotechnology (LAMSUN) – Dept. of Chemical Sciences – University of Catania and CSGI*

**INTRODUCTION:** Surface nanostructuring of polymeric thin films in two-dimensional (2D) porous substrates is an intriguing strategy for various applications including microelectronics, sensing, catalysis, optics and biomedical science.[1-3] For instance, ordered pore arrays have been shown to be very promising as nanocontainers and/or nanoreactors of protein/oligopeptide molecules for controlled drug delivery and highly efficient catalysis applications.[4,5]

**METHODS:** We present a versatile and simple approach for rapidly fabricating nanopatterned surfaces on micrometer scale. Monodisperse silica nanoparticles were spin-coated onto gold surfaces. Subsequent annealing process leads to the formation of a monolayer of ordered colloidal crystals on substrates. A polymer layer is then deposited on samples, embedding the nanoparticle distribution. Finally, the selective removal of the silica nanospheres leads to the formation of nanostructured micron-sized area. The nanopatterned surfaces consisted of 2D nanopore arrays, having internal area of gold surrounded by polymeric matrix. The nanopores depth can be modulated by using UV-ozone treatment, in particular by increase time treatment, decrease pore depth.

**RESULTS:** This simple and versatile approach is a potentially powerful technique for the fabrication of 2D nanopatterned polymer arrays. Figure 1, shows a typical atomic force microscopy (AFM) image of the 2D nanopores arrays resulting from the spin coated PMMA solution in the interstices of the colloidal crystal. This figure indicates that these polymer nanopores have a diametr about of 100 nm and a depth in the range of 30-40 nm. The nanopores periodicity is consistent with that of colloidal crystals made of monodispersed silica nanoparticles with a diameter of 147 nm.

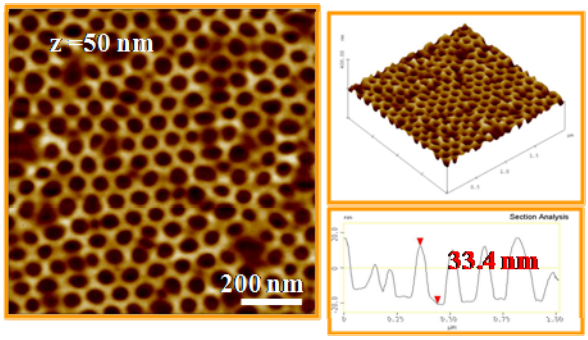


*Fig. 1: AFM height images and corresponding 3D and section analysis curves for nanostructured surface.*

**DISCUSSION & CONCLUSIONS:** The preferential adsorption of Chicken eggs lactoferrin and human lysozyme was investigated onto the nanostructured surfaces prepared from different spin-coated polymers. The adsorption was studied as a function of the pore geometrical features, including volume, aspect ratio and diameter, as well as the chemical contrast. The driving chemical factors were identified in terms of surface free energy gradients and chemical termination of the pore bottom and walls.

**REFERENCES:** [1]J. H. Moon, W. S. Kim, J.-W. Ha, S. G. Jang, S.-M. Yang and J.-K. Park (2005) *Chem. Commun*., 4107-4109. [2]L. S. McCarty, A. Winkleman and G. M. Whitesides (2007) *Angew. Chem., Int. Ed.*, **46**, 206-209. [3]X. Chen, Z. Chen, N. Fu, G. Lu and B. Yang (2003) *Adv. Mater*., **15**, 1413-1417.[4]L. Wang, M. H. Lee, J. Barton, L. Hughes and T. W. Odom (2008) *J. Am. Chem. Soc*., **130**, 2142-2143. [5]J. Yuan, L. Qu, D. Zhang and G. Shi (2004) Chem. Commun., 994-995.

European Cells and Materials Vol. 20. Suppl. 3, 2010 (page 180) ISSN 1473-2262

# Understanding amyloid aggregation by statistical analysis of atomic force microscopy

Jozef Adamcik[1], Jin-Mi Jung[2], Jérôme Flakowski[3], Paolo De Los Rios[3], Giovanni Dietler[4] & Raffaele Mezzenga[1*]

*[1] ETH Zürich, IFNH, Zürich, Switzerland [2]University of Fribourg, Fribourg, Switzerland, [3]EPFL Lausanne, LBS, Lausanne, Switzerland, [4]EPFL Lausanne, LPMV, Lausanne, Switzerland.*

**INTRODUCTION:** Aggregation of proteins is central to many aspects of daily life, ranging from blood coagulation, to eye cataract formation disease, food processing, or prion-related neurodegenerative infections. In particular, the physical mechanisms responsible for amyloidosis, the irreversible fibril formation of various proteins implicated in protein misfolding disorders such as Alzheimer, Creutzfeldt-Jakob or Huntington's diseases, have not yet been fully elucidated. In this work we demonstrate that by performing a statistical polymer physics analysis on the molecular conformations of amyloid fibrils revealed by single molecule AFM, different stages of amyloidal aggregation can be individually resolved [l].

**METHODS:** The β-lactoglobulin fibrils were prepared by the protocol described in our previous reports [2,3]. AFM was operating in tapping mode in air. The contour length of fibrils was measured with Ellipse. The persistence length $l_p$ was determined directly from the AFM images via the bond correlation function for semiflexible polymer in 2D conformation:

$$<\cos\theta(s)> \sim exp(-s/2l_p)$$

**RESULTS:** By performing a statistical analysis on single-molecule AFM images, we were able to demonstrate the analogies among heat-denaturated β-lactoglobulin fibrils and amyloidal fibrils, inferring a general amyloidosis process in both classes of materials. Cross section, persistence length and height periodic fluctuations along the contour length of the fibrils allowed to establish that single filament, double, triple and multi-stranded left-handed helical aggregates all occur under equilibrium conditions and that the most frequent population appears to be the double stranded helices. The resulting morphology of the fibers correspond to that of a multi-stranded twisted ribbon. Fig.1 sketches the hierarchical helical structure emerging from the present study for amyloid-like fibrils.

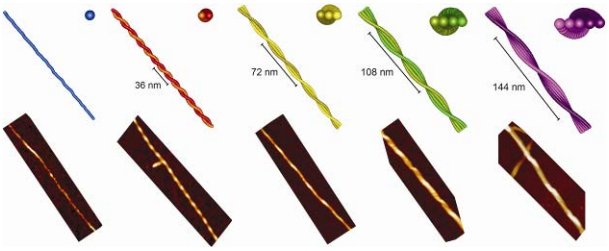


*Fig. 1: AFM images and corresponding coarse-grain molecular dynamics reconstructions of the left-handed helical fibril formation from the twisting of multi-strand ribbons with a number of filaments ranging between 1 and 5.*

**DISCUSSION & CONCLUSIONS:** We present theoretical and numerical arguments supporting a multi-stranded twisted ribbon model with variable helical pitch. Our results illustrate the potential of this approach for investigating fibrillar systems and suggest a possible general model for amyloid fibril assembly. In particular, they demonstrate a strong tendency to inter-fibril aggregation, even for fibrils with very high linear charge density. Thus, strong repulsive electrostatic forces and low ionic strength are not sufficient alone to prevent amyloidal aggregation, and a strong energetic driving force must exist to promote aggregation under these conditions. Once aggregation has occurred, the electrostatic repulsive forces induce a twisting of the observed ribbon. Possible attractive forces might arise from the amphotheric nature of the protein fibrils, in which neutral residues occurring periodically along the contour length of the fibrils can promote strong attractive 'hydrophobic' interactions. The occurrence of a ribbon-like cross-section arises from the balance of hydrophobic attraction and electrostatic long-range repulsion.

**REFERENCES:** [1] J. Adamcik, J.M. Jung, J. Flakowski, P. De Los Rios, G. Dietler and R. Mezzenga (2010) Nat Nanotechnol doi:10.1038/nnano.2010.59. [2] J.M. Jung, G. Savin, M. Pouzot, C. Schmitt and R. Mezzenga (2008) Biomacromolecules **9**:2477-2486. [3] J.M. Jung and R. Mezzenga (2010) Langmuir **26**:504-514.

European Cells and Materials Vol. 20. Suppl. 3, 2010 (page 181) ISSN 1473-2262

# The nanostructure of biological tissues: a scanning X-ray scattering study

B. Müller[1,2], H. Deyhle[1,2], G. Schulz[1], S. Mushkolaj[1], O. Bunk[3]

[1]*Biomaterials Science Center, University of Basel, Basel, Switzerland.*
[2]*School of Dental Medicine, University of Basel, Basel, Switzerland.*
[3]*Paul Scherrer Institut, Villigen, Switzerland.*

**INTRODUCTION:** The human body is composed of functional micro- and nanostructures, which are usually organized in three-dimensional fashion and exhibit preferential orientations. While the microstructures are accessible for example by micro computed tomography, the nanometer-scale features are generally only uncovered on surfaces by means of optical methods or electron microscopy. The present communication demonstrates the power of synchrotron radiation-based scattering by means of a focused X-ray (5 µm × 20 µm) that rasterizes tissue slices. The acquired scattering data yield the abundance and orientation of all components with extension from atomic to sub-micrometer periodicities. This means, all kinds of nanostructures such as hydroxyapatite crystallites or collagen fibrils can be quantitatively gathered. As prominent examples, we show teeth[1], brain, and urethra specimens.[2]

**METHODS:** The data were recorded at the cSAXS beamline of the Swiss Light Source (Paul Scherrer Institut, Villigen, Switzerland) as described previously.[3] The wet tissue slices some hundred micrometer thin were put into polyimide sachets to prevent dehydration. Some specimens were resin-embedded for conventional histology.

**RESULTS:** Fig. 1 shows the scattering intensities of a 380 µm-thin section of an embedded male porcine urethra parallel to the cavity. The images were generated from about 40'000 scattering patterns obtained with an 11.2 keV X-ray beam, scanned along the specimen in 75 and 50 µm steps in x- and y-directions, respectively. The specimen-detector distance was about 7.1 m.

The images of Fig. 1 show the presence of highly oriented nanostructures with extensions between 5 and 300 nm. The colours relate to the preferential orientations according to the wheel on the right, whereas the brightness corresponds to the nanostructure's abundance.

The liquid-like soft urethral tissue consists of epithelium, connective tissue (*lamina propria*) and muscles (*tunica muscularis*). This layered composition is represented on the nanometer scale by the elongated parallel turquoise-coloured features with oriented nanostructures.

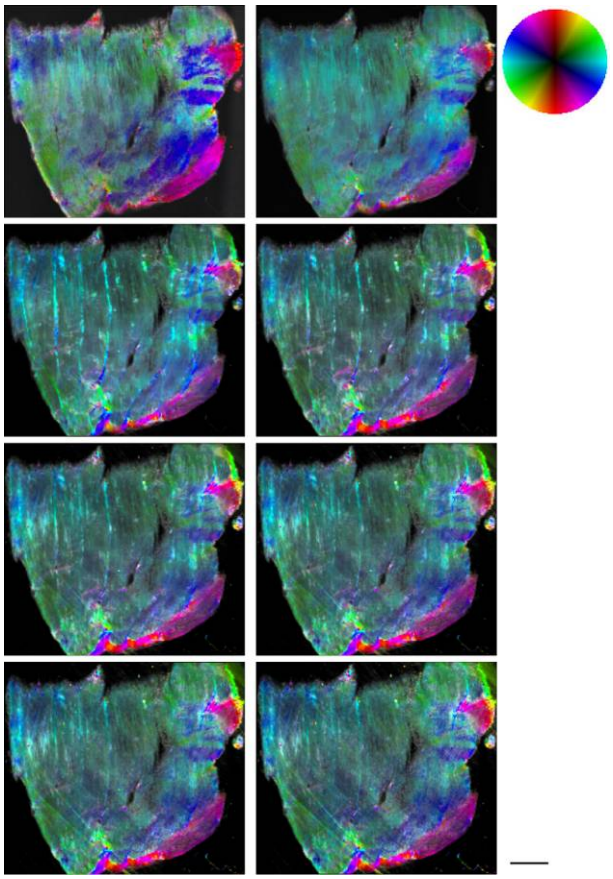

*Fig. 1: The series of scanning SAXS images shows the characteristic anatomy of the urethra. The sagittal images from top-left to bottom-right represents the nanostructures ranging from 5 to 8 nm, 11 to 20 nm, 38 to 57 nm, 76 to 102 nm, 114 to 131 nm, 152 to 176 nm, 200 to 229 nm, and 269 to 305 nm, respectively. The colours are chosen according to the nanostructure's orientations, see colour wheel, their brightness relates to their abundance. The bar corresponds to 2 mm.*

**CONCLUSIONS:** Scanning X-ray scattering provides the abundance and orientation of all nanostructures with micrometer resolution in real space along sections of hard and soft tissues.

**REFERENCES:** [1] H. Deyhle et al (2009) *Proc SPIE* **7401**:74010E. [2] B. Müller et al (2010) *Eur J Clin Nanomed* in press. [3] O. Bunk et al (2009) *New J Phys* **11**:123016.

**ACKNOWLEDGEMENTS:** The valuable work of S. Buser (Basel), M. Imholz (Basel), and A. Morel (Zürich) is gratefully acknowledged.

European Cells and Materials Vol. 20. Suppl. 3, 2010 (page 182) ISSN 1473-2262

# Plasmonic and Nano-photonic Elements for Bio-Sensing Application

M. Roussey, Q. Tan, A. Cosentino, V. Musi, S. Herminjard, H. P. Herzig

*Ecole Polytechnique Fédérale de Lausanne (EPFL), Institut de Microtechniques (IMT), Optics & Photonics Technology Laboratory (OPT), Neuchâtel, Switzerland*

**INTRODUCTION:** Since several years, surface plasmon resonance (SPR) is an attractive method for optical measurements of refractive index variation in gas, liquid or solid environment. In parallel, following the development of nano-fabrication, optical nano-structures [1] have been demonstrated to be powerful and versatile for bio-sensing [2, 3]. We present here an overview of the techniques available at the OPT Lab to measure refractive index variations. Moreover, the possible upgrades that nano-photonics may provide to these methods and how it can be applied to bio-sensing.

**METHODS:** The SPR technique is based on the measurements of the resonance position linked to the refractive index variation of the analyte. The plasmon is exited at the surface of a thin gold layer using the Kretshmann configuration (Fig. 1).

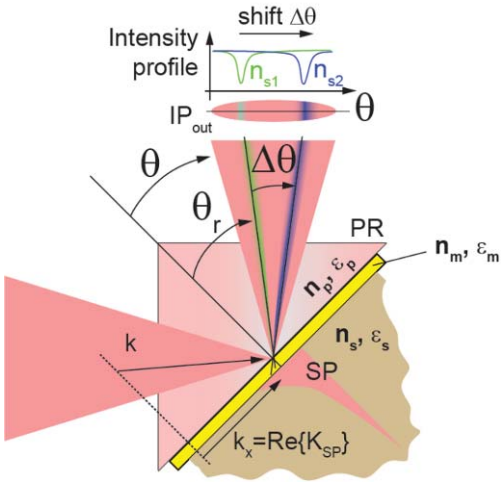


*Fig. 1: Principle of the SPR sensor [4].*

This technique allows a high sensitive measurement of the refractive index variation. However, the integration in compact devices is difficult. An alternative to SPR sensing is the use of nano-structure based devices. An example is presented in Fig. 2. The principle is to place a nano-cavity on an optical waveguide and to detect the perturbation of the response when the environment of the cavity is modified.

**RESULTS:** Using the SPR technique, the detection of $CO_2$ and the measurement of its concentration in $N_2$ has been demonstrated. The results, published in [4], show the ability of the technique to work in the mid infra-red (λ=4.4 μm).

Recently the first tests with biological elements (proteins) have shown promising results.

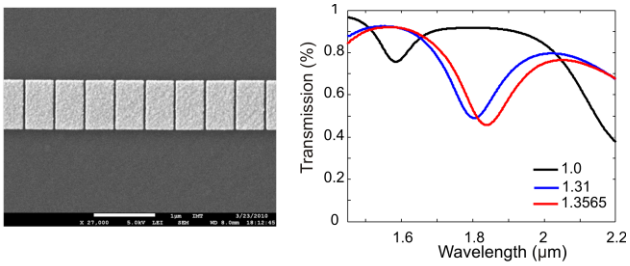


*Fig. 2: SEM image of the nano-sensor (left) and simulated response (right).*

Nevertheless, the problems of the volume of analyte and the integration remain. Theoretical studies have demonstrated that nanostructure based sensors, such as the one presented in Fig. 2 can reach a sensitivity of 800 nm/RIU (refractive index unit). In the particular case of Fig. 2, the structure consists on a classic silicon waveguide on which a 20 nm thick layer of gold has been deposited. This layer presents an array of slits (30 nm width) which allows the confinement of the electromagnetic field at the surface. A droplet of analyte deposited on the active part of the sensor (800 nm x 15 μm) is enough to obtain a measurement of the variation of the refractive index.

**DISCUSSION & CONCLUSIONS:** The two techniques present different aspects (temperature regulation, reproducibility) interesting for bio-sensing with each different advantage: the powerful and well-known SPR technique allows measurements with a high reliability, while nano-sensors offer the prospect of the integration and in-parallel measurements at low cost. Moreover the nanostructure based sensor is selective in wavelength, which can be chosen by changing the geometrical parameter of the cavity.

**REFERENCES:** [1] X. Fan, *et al.* (2008) *Analytica Chimica Acta* **620**:8-26. [2] J. Homola, *et al.* (1999) *Sensors and Actuators B* **54**:3-15. [3] M.E. Stewart, *et al.* (2008) *Chem. Rev.* **108**:494-521. [4] S. Herminjard, *et al.* (2009) *Opt. Exp.* **17**:293-303.

**ACKNOWLEDGEMENTS:** This work is financially supported by the SNF project ELF *n°200021-117930*.

European Cells and Materials Vol. 20. Suppl. 3, 2010 (page 183) ISSN 1473-2262

# Optimization of Carbon Nanotubes PEGylation by Response Surface Methodology

*Hadidi N.[1] , Nafissi-Varcheh N. [2], Kobarfard F.[3], Aboofazeli R.[1]*

*[1] Pharmaceutics Dept., [2]Pharmaceutical Biotechnology Dept. & [3]Medicinal Chemistry Dept., School of Pharmacy, Shaheed Beheshti University of Medical Sciences, Tehran, Iran.*

**INTRODUCTION:** Biomedical applications of carbon nanotubes (CNTs) have attracted much attention in recent years. Their unique intrinsic optical, electromagnetical and physicochemical features, enabling covalent and non-covalent binding of several pharmaceutical entities, have made them interesting in delivery of various therapeutic molecules. Application of CNTs in biological systems depends on their compatibility with hydrophilic environments, and therefore, solubilization of CNTs is essential. Functionalized CNTs with improved water solubility and biocompatibility are able to cross cell membranes as nanoneedles, shuttling a wide range of biologically active molecules into cells. The stealth PEGylated single-walled nanotubes (SWNTs) exhibit much longer blood-circulation half-life in vivo and also a low hepatic uptake, compared to other functionalized CNTs.

**METHODS:** PEGylation of CNTs with phospholipid-polyethylene glycol (PL-PEG 2000 and 5000) is one of the most commonly used protocols for SWNT functionalization. Response Surface Methodology (RSM), consisting of critical parameters such as PL-PEG type and ratio of PL-PEG/SWNT, was used to construct a design space. Optimization was then established based on loading of PEG on the surface of CNTs as well as their water solubility. Stability of PEGylated carbon nanotubes was investigated in phosphate buffer saline and cell medium. The effects of PEGylated SWNTs on the viability of Jurkat cell line (human tumor T lymphocytes) were also evaluated.

**RESULTS:** On the basis of quantitative measurement of free amines (trinitrobenzene sulfonic acid method) and thermogravimetric analysis, the loading of PEG was estimated to be 20-50% with suitable stability in phosphate buffer saline and cell medium. Atomic Force Microscopy and Scanning Electron Microscopy studies also showed a fairly uniform length and diameter and surface PEG coverage. Comparative studies revealed that PEGylated CNTs prepared by this method, are more soluble and biocompatible than pure CNTs and are comparable to marketed PEG-SWNTs.

**DISCUSSION & CONCLUSIONS:** PEGylation of CNTs was selected as a strategy to make these nanostructures more soluble and biocompatible. RSM and 2$^{nd}$ order polynomial equations were applied to investigate how Pl-PEG may influence the solubility of CNTs. Equations were then applied to maximize PEG loading and CNTs' solubility. Finally, optimum combinations of critical factors were gained and practically verified. Compared with other frequently used covalent strategies, our non-covalent functionalization protocol could retain largely the intrinsic optical properties of the nanostructures, which are essential in various biological imaging, biodistribution studies and sensing applications. In this research, an optimized protocol for non-covalent PEGylation of carbon nanotubes was established. These conjugated, soluble and biocompatible CNTs, could be considered as promising nano-vehicles for binding of drug molecules, including anticancers.

**REFERENCES:** [1] Liu Z,Chen K., Davis C., Sherlock S., Cao Q., Chen X., Dai H., (2008) *Cancer Res* ,68: (16) 6652-6660 [2] Liu Z., Tabakman S, Welsher K, Dai H. (2009 ) *Nano Res* (2009) 2: 85 120 [3] Feazell R.P., Nakayama-Ratchford N., Dai H., Lippard S. J. ,(2007) *J. AM. Chem. Soc*., 129, 8438-8439 [4] Liu Z., Tabakman S., Chen Z., Dai H., (2009) *Nature Protocols*, 4(9):1372-1382

**ACKNOWLEDGEMENTS:** This research is being financially supported by Nanomedicine and Tissue Engineering Research Center, Shaheed Beheshti University of Medical Sciences in I.R. of Iran.

European Cells and Materials Vol. 20. Suppl. 3, 2010 (page 184) ISSN 1473-2262

# Magnetic Enrichment of "Smart" Gold Nanoparticle-Antibody Conjugates for High-Sensitivity Diagnostic Immunochromatography

M.A. Nash[1], P. Yager[1], A.S. Hoffman[1], P.S. Stayton[1]

[1]*Department of Bioengineering, University of Washington, Seattle, USA*

**INTRODUCTION:** We present an integrated bioseparation and detection system comprising thermally-responsive nanoparticle mixtures for point-of-care diagnostic immunochromatography. The system allows for labelling of the target biomarker with colloidal gold, followed by magnetic separation/enrichment. Detection by lateral flow immunoassay is then used to visualize the target biomarker at the test line of a nitrocellulose flow strip. The nanoparticle system is composed of a mixture of iron oxide and gold nanoparticles, each with a thermally-responsive poly(N-isopropylacrylamide) (pNIPAm) coating. These "smart" polymers undergo a hydrophilic to hydrophobic phase transition upon heating above the lower critical solution temperature (LCST) of ~32 ºC. Upon raising the temperature, the two particle types co-aggregate, forming magnetic/gold agglomerates. Subsequent application of a magnetic field results in magnetophoresis and separation of the biomarker bound to the gold nanoparticles (AuNPs). Enrichment is achieved upon discarding the supernatant, and dissolving the captured aggregates into a smaller volume of cold carrier fluid. Detection of the enriched gold-labeled biomarker by immunochromatography is shown to be more sensitive than conventional non-concentrating approaches.

**METHODS:** A cationic diblock copolymer was synthesized as described [1]. Homo-poly(NIPAm)-coated iron-oxide nanoparticles (mNPs) were synthesized as described [2]. The diblock was adsorbed to citrate-capped AuNPs, and conjugated to streptavidin (SA) via carbodiimide chemistry. A malaria biomarker (PfHRP2) was spiked into 50% human plasma. Biotinylated anti-PfHRP2 IgG (1 nM) was bound to the PfHRP2 biomarker, followed by addition of AuNP-SA (2 nM), mNPs (1 mg/mL), and free pNIPAm (2 mg/mL). The particles were heated above the LCST, and separated by a magnet within 30 minutes. Captured aggregates were re-dissolved into a 50-fold smaller fluid volume below the LCST, and flowed through a nitrocellulose membrane with surface-immobilized anti-PfHRP2 antibodies. The total assay time was ~40 minutes. Gold colloid absorbance in the capture zone was measured using a flat-bed scanner and image analysis.

**RESULTS:**

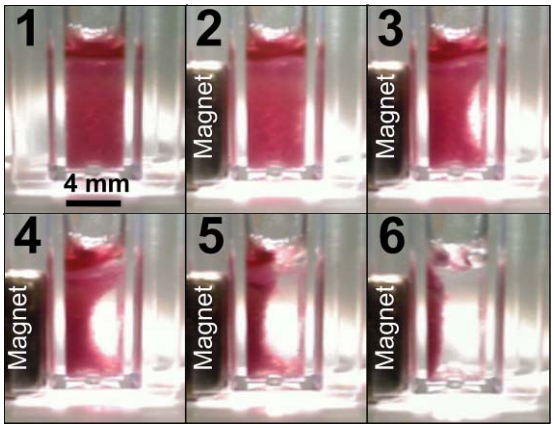


*Figure 1. Time-lapse images showing magnetic separation of AuNPs. (Image 1) A temperature stimulus is applied to the AuNP/ mNP mixture, causing polymer phase transition. (Images 2-6) A magnetic field is applied and the AuNPs are pulled to the side of the cuvette via polymer-induced co-aggregation with mNPs. Capture time=30 min.*

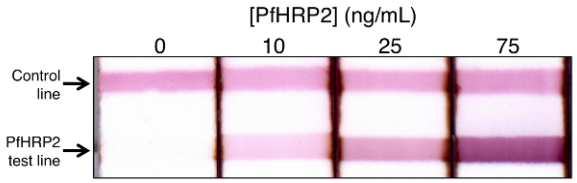


*Figure 2. After separation, the enriched AuNPs are disaggregated and flowed through the capture zone of the flow strip. Absorbance signal at the test line correlated with the amount of PfHRP2 in the samples. Larger enrichment factors were found to boost the signal from clinical samples, while not significantly increasing the background noise.*

**DISCUSSION & CONCLUSIONS:** The new integrated approach for labelling, purifying, and rapidly detecting biomarkers from plasma using "smart" nanoparticle mixtures is advantageous for achieving high-sensitivity detection without the need for complex equipment, with applications in point-of-care immunochromatography.

**REFERENCES:** [1]M.A. Nash, J.J. Lai, A.S. Hoffman, P. Yager, P.S. Stayton (2010) *Nano Lett.* 10(1): 85-91. [2]J.J. Lai, K.E. Nelson, M.A. Nash, A.S. Hoffman, P. Yager, P.S. Stayton (2009) *Lab Chip* 9(14):1997-2002.

**ACKNOWLEDGMENTS:** NSF-GRFP, NIH (Grant EB000252)

European Cells and Materials Vol. 20. Suppl. 3, 2010 (page 185) ISSN 1473-2262

# Nanotoxicology as a Predictive Science: Froms cells to whole animals

André Nel

*Chief, Division of NanoMedicine and the California NanoSystems Institute; Director of the UC Center for the Environmental Impact of Nanotechnology (UC CEIN), UCLA, California, USA*

Predictive toxicology is an essential tool for successful drug development because toxicity is one of the major reasons for product failure. It is essential to identify and exclude new drug candidates with unfavorable safety profiles as early as possible in the development process including the use of high throughput screening (HTS). Predictive toxicology has recently been introduced to industrial chemical toxicity. Both the National Toxicology Program as well as the National Research Council (NRC) in the US National Academy of Sciences (NAS) have recommended that toxicological testing in the 21st-century evolve from a predominantly observational science at the level of disease-specific models to predictive science models focused on broad inclusion of target-specific, mechanism-based biological observations. It was further recommended that the biological testing be based on robust scientific paradigms that can be used to screen multiple toxicants simultaneously instead of costly animal experiments looking at a single toxicant at one time.

While the concept of predictive toxicological modeling is still comparatively novel in the field of nanosafety, a number of attempts have been made to show that in vitro toxicological assessment correlates with in vivo inflammatory effects in the lung. Our own previous research into the adverse health effects of ambient particulate matter has elucidated the utility of abiotic and in vitro cellular studies in assessing the pro-inflammatory effects of ambient ultrafine particles based on oxidant potential. Our work also demonstrated that the cytotoxic effects of cationic particles in macrophages and epithelial cells show correlation to PMN cell counts and increased LDH levels in the BAL fluid of mice. More recently, we have begun to explore the pulmonary toxicity of ZnO, showing important linkage between cellular responses and in vivo toxicological outcomes in zebra fish and the rodent lung lung.

Becher et al. compared in vitro pro-inflammatory responses in macrophages and epithelial cells to PMN cell counts in BAL fluid obtained from rats receiving a series of stone particles intratracheal and demonstrated a correlation between in vitro

and in vivo results. In contrast, Sayes et al failed to demonstrate good correlation between in vitro and in vivo results in which they utilized nano-and micron-size particles (carbonyl iron, crystalline silica, amorphous silica, nano-ZnO and fine-sized ZnO) in a well-designed dose-response study. The in vitro endpoints included the assessment of LDH release, metabolic activity and cytokine production in rat epithelial cells and primary alveolar macrophages. The authors concluded that there was poor correlation between in vitro and in vivo outcomes. However, Oberdörster et al. re-analyzed the Sayes data by converting the particle mass-dose response data to particle surface area-dose response curves and performing the comparisons at the steepest slope of the dose-response relationship. The conclusion was that it was possible to show in vitro to in vivo correlation when using a surface area-normalized response metric. The Oberdorster group also demonstrated through the use of cell-free and cell-based assays that ROS production, LDH release and activation of an IL-8 promoter-luciferase reporter show good correlation with acute pulmonary inflammation in rats being challenged by IT instillation of 7 distinct particle types (Au, nano-TiO2, fine TiO2, NH2-PS, Ag, elemental carbon, Cu). In addition, Dr. Ken Donaldson's laboratory in Edinburgh has recently demonstrated that in vitro screening for IL-8 production in A549 cells exposed to a panel of low toxicity (e.g., TiO2, carbon black) versus highly reactive quartz and metal (e.g., Ni, Co) nanoparticles shows correlation to PMN counts in the BAL fluid of male Wistar rats.

In addition to above research data the talk will cover the use of HTS paradigms in the CEIN to demonstrate how one can utilize in vitro screening efforts to prioritize animal testing that shows coherence as well as differences with the in vitro screening results. Together with the use of compositional and combinatorial nanomaterial libraries and our computerized expert system, we are attempting to develop predictive toxicological paradigms.

European Cells and Materials Vol. 20. Suppl. 3, 2010 (page 186) ISSN 1473-2262

# Cytotoxicity evaluation of boron-doped diamond surfaces obtained by the HFCVD technique in osteoblast-like cells

MA.Neto[1], EL.Silva[1], CMF. Gomes[2], AJS.Fernandes[3], FJ.Oliveira[1], RF.Silva[1]

[1]*CICECO, Dept. of Ceramics & Glass Engineering, University of Aveiro, Aveiro, Portugal.*

[2]*IBILI, Institute of Biophysics/Biomathematics, Faculty of Medicine, University of Coimbra*

[3]*I3N, Dept. of Physics, University of Aveiro, Aveiro, Portugal.*

**INTRODUCTION:** Diamond surfaces obtained by chemical vapour deposition (CVD) techniques are intrinsically biocompatible. After doping with boron these coatings become p-type conductive making them attractive as electrically surfaces in biossensing applications. Former studies have shown that both undoped and boron-doped coatings are highly biocompatible to different cell types, supporting cell adhesion, viability and differentiation and selectively control the cell growth [1-2]. However these studies were done exclusively on nanocrystalline diamond (NCD) coatings grown by the Microwave Plasma Chemical Vapour Deposition (MPCVD) technique. This contribution will focus on the cytotoxicity of boron-doped diamond coatings (both NCD and microcrystalline (MCD) types) using the Hot Filament Chemical Vapour Deposition (HFCVD) technique on osteoblast-like cells. Cellular proliferation and adhesion results are also presented.

**METHODS:** Four sets of diamond coatings were grown using the Hot Filament Chemical Vapour Deposition (HFCVD) technique on silicon substrates. Hydrogen and methane were used as the precursor gases for diamond growth and boron oxide diluted in ethanol and dragged by argon as the dopant. The coatings morphology was varied by adjusting the CH4/H2 ratio. Two sets were prepared using the conditions for MCD growth and two using the conditions of (NCD). These included one set of doped MCD and one of doped NCD coatings.

Osteoblast-like MNNG/HOS cells were seeded at a density of 30.000 cells/well in 24-well plates containing sterile samples of diamond coated silicon substrates. Cells were maintained in culture medium (RPMI+10%FBS) during 5 days in a humidified air atmosphere containing 5% of CO2 at 37ºC. Cell culture on polystyrene wells served as control samples. Cell proliferation was assessed by a colorimetric MTT assay after 5 days of incubation. The values were expressed as percent normalized to control samples.

**RESULTS:** Fig. 1 shows that all diamond coatings support cell adhesion. This observation is more obvious on undoped MCD samples and on boron-doped NCD samples. Fig. 2 illustrates a small decrease in cells proliferation compared to controls (70-80% for the NCD coatings and 62-66% for the MCD coatings).

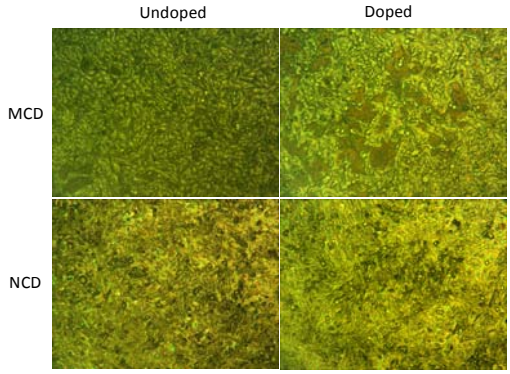


*Fig. 1: Optical microscope images of the diamond coatings with adhered osteoblast-like cells.*

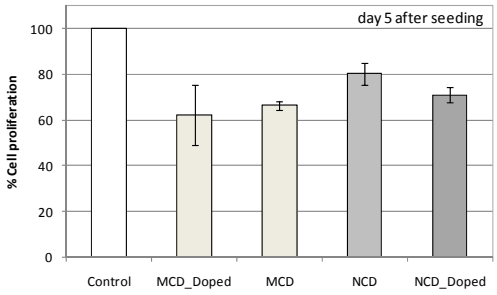


*Fig. 2: Percentage of cells proliferation on the diamond coatings at 5 days incubation.*

**DISCUSSION & CONCLUSIONS:** In this work we have demonstrated that diamond coatings, obtained using the HFCVD technique, are highly biocompatible to osteoblast-like cells. These coatings support cell adhesion and proliferation even with the silicon substrate in contact with the biological culture. The undoped NCD coatings seam to enhance cell colonization.

**REFERENCES:** [1] A. Kromka, L. Grausova, L. Bacakova, et al (2010) *Diam Relat Matet* **19**:190-95. [2] M. Kopecek, L. Bacakova, J. Vacik, et al (2008) Phys Stat Sol (A) **205**:2146-53.

**ACKNOWLEDGEMENTS:** MA. Neto and EL. Silva would like to acknowledge, respectively, the grants SFRH/BPD/45610/2008 and SFRH/BD/ 61675/2009 from FCT - Fundação para a Ciência e a Tecnologia.

# Cadmium Telluride quantum dot nanoparticles cause oxidative stress and apoptosis in mammalian cells

K. Nguyen[1], V. Seligy[1], P. Rippstein[2], and A. Tayabali[1]

[1] *Biotech Lab, Mechanistic studies, EHSRB, HECSB, Health Canada, Ottawa, ON, Canada*
[2] *The University of Ottawa Heart Institute, Ottawa, ON, Canada*

**INTRODUCTION:** Quantum dots are semiconductor nanoparticles and fluorophores with unique electrical and optical properties that make them useful materials in microelectronics and biomedical research [1]. Due to their spectral properties such as broad adsorption, narrow emission and photostability [2], quantum dots based on Cadmium Telluride (CdTe-QDs) offer great potential in these applications, especially in therapeutic targeting and in medical and molecular imaging. While the applications of CdTe-QDs are growing, there is limited information on their toxicity. Toxicity of CdTe-QDs has been proposed to be associated with the generation of reactive oxygen species (ROS) and cadmium ions ($Cd^{2+}$) which are toxic to cells [3,4]. However, the detailed mechanisms that lead to cell death induced by CdTe-QDs remain unclear. In this study, the mechanisms of CdTe-QD toxicity in mouse macrophage and human epithelial cells were investigated, and the results revealed that QDs cause cell death via oxidative stress-induced apoptotic pathways.

**METHODS:** Murine J774A.1 macrophages and human HT29 epithelial cells were exposed to different concentrations of CdTe-QDs ($10^{-7}$-$10^{1}$ug/ml) for different time points (4hr -24hr). After treatment, cells were fixed and processed for transmission electron microscopy (TEM) and confocal microscopy to detect sub-cellular changes and apoptosis. In a parallel set of experiments, cell lysates were screened for total glutathione (GSH) and superoxide dismutase (SOD) using colorimetric/ enzymatic assays. Active caspase-3 level was detected using an ELISA assay. Phosphoprotein levels were measured using multiplex bead-based assays.

**RESULTS:** Transmission electron microscopy (TEM) revealed changes in sub-cellular architecture and enlargement of mitochondria in treated cells. A two-fold decrease in total GSH level and a 2 to 8-fold increase in SOD activity in CdTe-QD-treated cells were observed, suggesting that cells were undergoing oxidative stress. The Annexin V assay using confocal microscopy showed apoptotic cells from CdTe-QD treatment. CdTe-QDs caused increase in phosphorylation of selected proteins such as JNK, Erk-MAP kinase, CREB, and p38, and caused a decrease in IkBa level. CdTe-QD treatment also resulted in an increase in caspase-3 activity in test cells.

**DISCUSSION & CONCLUSIONS:** The results show that CdTe QDs cause mitochondrial dysfunction and affect different signal transduction pathways that are related to the metabolic activity of cells. This study suggests that CdTe-QDs cause cytotoxicity to mammalian cells by inducing oxidative stress and apoptosis. This study provides much needed mechanistic details for understanding toxicity endpoints that might be important for nanoparticle health risk assessment.

**REFERENCES:** [1]Cho, S.J. *et al*. (2007) *Langmuir* **23**: 19971-19980. [2]Gwinn M.R. and Wallyathan, V. (2006) *Environmental Health Perspectives*. **144**: 1818-1825. [3] Lovric, J. *et al* (2005) *Chem Biol* **12**: 1227-1234. [4]Hild W.A. *et al*. (2008) *European Journal of pahrmaceutics and Biopharmaceutics*. **68**: 1 53-168.

**ACKNOWLEDGEMENTS:** The study was supported by Canadian Regulatory System for Biotechnology and Chemical Management Plan Monitoring and Surveillance Grants.

European Cells and Materials Vol. 20. Suppl. 3, 2010 (page 188) ISSN 1473-2262

# QCM-D as a tool for sensing at polymer based nano-biointerfaces

E.Nilebäck[1], Olivia Lindau-Jonsson[1]

[1] *Q-Sense AB, Sweden*

**INTRODUCTION:** In nanobiotechnology, surface-based sensing and characterization of engineered nanostructures for biological or medical applications is often crucial. This creates a need for techniques able to detect events taking place on the nanoscale. Quartz Crystal Microbalance with Dissipation monitoring (QCM-D) is an attractive method to detect such nanoscale events by simultaneously measuring the mass (related to the resonance frequency of the crystal, Δf) and viscoelastic properties (related to the energy dissipation of the crystal oscillation, ΔD) of adlayers forming on the sensor surface. This opens up for a great variety of applications and here three studies will be presented where QCM-D has been used for studying polymer based nano-biointerfaces.

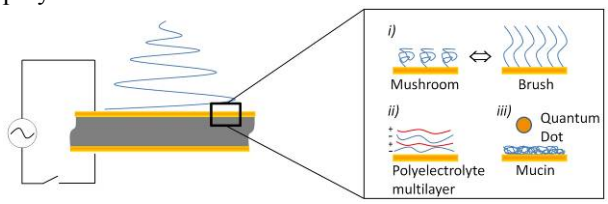


*Fig. 1: Schematic drawing showing the QCM-D principle and illustrations of three application examples.*

## METHODS AND RESULTS:

**Grafted polymer conformation and phase transitions.** Polymers grafted to a surface can adopt several different conformations and the ability to control these transitions increases the applicability of such layers. Zhang and Wu review results from QCM-D investigations of poly(*N*-isopropylacrylamide) and poly(2-dimethylanino)ethyl focused on polymer conformation. [1] They were able to control the conformation of the polymers *in situ* by altering temperature and grafting density and also to identify different phases in the polymer adsorption process.

**Biopolymer polyelectrolyte assemblies.** Polyelectrolyte multilayers (PEMs) were introduced by Decher and co-workers in 1992 and have since attracted extensive attention, because of their extraordinary advantages in a wide range of applications as well as variability regarding rigidity, chemical composition, thickness etc.. Here, Boudou *et al* compared the mechanical properties of poly(L-lysine)/hyaluronan, chitosan/hyaluronan and poly(allylamine hydrochloride)/(poly(L-glutamic acid) PEMs. [2] This study combined results from QCM-D, infrared spectroscopy and atomic force microscopy to extract the differences between the three PEMs regarding the degree of hydration, Young's modulus, molar density, thickness, cross-linking and cross-link distance.

**Nanotoxicology.** The continuous development of engineered nanomaterials in various contexts is potentially hazardous as these novel materials may have adverse effects on biological systems. Therefore it is important to study the physico-chemical properties of engineered nanomaterials. In this study by Wiecinski *et al* the stability in solution of quantum dots with different PEG-coatings was studied in simulated gastric and intestinal fluids, in the absence and presence of pepsin and mucin. [3] These results were complemented by QCM-D experiments where quantum dots were adsorbed to mucin-modified sensors.

**CONCLUSIONS:** QCM-D is a versatile technique for studying biointerfaces and events occurring on the nanoscale. The dissipation enables proper modeling of adsorption and conformation of highly viscoelastic and hydrated layers such as polymers not easily extracted from other techniques. Taken together, QCM-D is an interesting tool for exploring the field of nanobiotechnology.

**REFERENCES:** [1] G. Zhang, C. Wu, Quartz Crystal Microbalance Studies on Conformational Change of Polymer Chains at Interface, (2009) *Macromol. Rapid Commun.* **30**:328-335. [2] T. Boudou, T. Crouzier, Auzély-Velty, K. Glinel and C. Picart, Internal Composition versus the Mechanical Properties of Polyelectrolyte Multilayer Films: The Influence of Chemical Cross-Linking, (2009) *Langmuir* (ACS). **25**:13809-13819**.** [3] P.N. Wiecinski, K.M. Metz, A.N. Mangham, K.H. Jacobson, R.J. Hamers, and J.A. Pedersen, Gastrointestinal biodurability of engineered nanoparticles: Development of an in vitro assay,(2009) *Nanotoxicology.* **3**: 202-214.

European Cells and Materials Vol. 20. Suppl. 3, 2010 (page 189) ISSN 1473-2262

# Integration of functionalised injectable hydrogels for brain tissue engineering

D.R.Nisbet[1,2], D.I.Finkelstein[2], J.S.Forysthe[1]

*[1] Monash University, Clayton, Melbourne, Australia [2] The Mental Health Research Institute of Victoria, Parkville, Melbourne, Australia.*

**INTRODUCTION:** In-order to utilise tissue engineering for the treatment of central nervous system injury or disease, it is essential to control and instruct endogenous cell behaviour using functionalised scaffolds. Here, thermally gelling xyloglucan hydrogel, along with xylogucan-graft-poly-$_D$-lysine (xylo-graft-PDL) was evaluated in a pilot study through implantation into the caudate putamen of adult rats.

**METHODS:** PDL was tethered to xyloglucan using EDC chemistry [1]. Unmodified xyloglucan as well as 90:10, 50:50 and 100% blends were then prepared at 3 wt% in PBS. The scaffolds were then implanted into the caudate putamen of adult Wistar rats at anteroposterior 1.0 mm and lateral 2.5 mm from bregma (depth of 7.5mm) [2]. Animals were perfused at 7 different time points prior to immunohistochemistry, which marked microglia, macrophages, astrocytes, neurons, neurites and laminin [2].

**RESULTS:** The microglia/macrophage response was the same for xyloglucan and the blends, peaking 3 days after implantation before decreasing back to homeostatic levels. No penetration of the microglia was observed, but the cells did accumulate at the interface between the scaffold and the brain tissue. Astrocyte peak activation occurred for a period that extended from 14-21 days post implantation. This reaction subsided more rapidly for the unmodified hydrogel than the blends, however at 60 days post implantation the number of positively mark astrocytes within the brain parenchyma had returned to physiological levels.

Most noteworthy, was the discovery of increased astrocyte and neurite penetration within the hydrogel scaffolds as the concentration of PDL increased. Astrocyte and neurite penetration also coincided with the presence of laminin.

**DISCUSSION & CONCLUSIONS:** Both neurites and astrocytes coexisted in the scaffolds at all time points, which may indicate that astrocytes are cytotrophically supporting neurones. However, it is likely that laminin is responsible for mediating this process also, as it was present with the astrocytes post injury and during their infiltration.

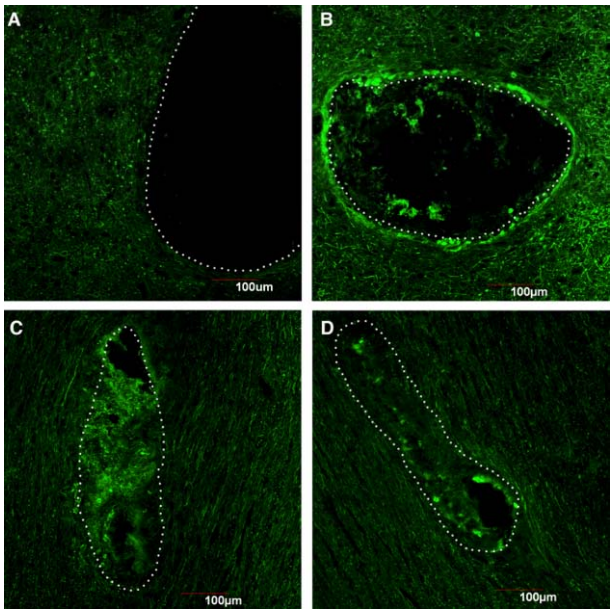


*Figure 1 - Fluorescence images of neurites within the brain parenchyma interacting with xyloglucan scaffolds. Where A) is unmodified xyloglucan; B) a blend of 90:10 xyloglucan and xyloglucan-graft-PDL; C) a blend of 50:50 xyloglucan and xyloglucan-graft-PDL; and D) 100 % xyloglucan-graft-PDL. The white dotted lines indicate the interface between the xyloglucan scaffolds and the brain tissue.*

Astrocytes are known to secrete laminin and this plays an important role in the growth and adherence of neurones. While PDL may be responsible for the attraction of neurites and astrocytes, we believe that it is more likely the laminin, which is secreted by astrocytes that is cytrotropically supporting and/or attracting neurite elongation.

**REFERENCES:** [1] K.E. Crompton, J.D. Goud, R.V. Bellamkonda, et al (2007) *Biomaterials* **28**:441-49. [2] D.R. Nisbet, A.E. Rodda, M.K. Horne, et al (2010) *Tissue Eng.* doi: 10.1089/ten.TEA.2009.0677.

**ACKNOWLEDGEMENTS:** We are grateful to the Australian Research Council Postdoctoral Fellowship (to DRN) and the Australian Research Council Discovery Project (DP0985433) (to DRN and JSF).

European Cells and Materials Vol. 20. Suppl. 3, 2010 (page 190) ISSN 1473-2262

# Conformational Changes of Cytochrome c Oxidase: Varying the Redox State by Electronic Wiring

Christoph Nowak[1], Wolfgang Knoll[1], Renate L. C. Nauman[1]

[1] *Austrian Institute of Technology, AIT, Donau-City Str. 1, 1220 Vienna, Austria*

**INTRODUCTION:** Cytochrome c oxidase (CcO) is the final complex of the respiratory chain. It catalyzes the transformation of the energy of oxygen reduction into a difference of electrochemical potentials of protons across the inner mitochondrial membrane which is then used to generate adenosine triphosphate (ATP). CcO has been the subject of intense research for many years. Oxygen reduction by cytochrome c was shown to proceed along four redox centers, $Cu_A$, heme a, heme $a_3$ and $Cu_B$, and in an intricate mechanism to be coupled to proton transfer. Surface-Enhanced ATR-FTIR-Spectroscopy is a sufficient sensitive method for a detailed kinetic analysis of the Electrontransfer (ET) processes inside CcO. Time–resolved (tr)-ATR-FTIR-spectroscopy was, therefore, used to monitor electron transfer within CcO. Data acquisition of the FTIR spectra of the enzyme was triggered by direct bioelectronic coupling to the electrode, and kinetic constants for internal electron transfer between the metal centers were obtained and then compared to those obtained previously by fast-scan cyclic voltammetry.

**METHODS:** Preparation of the two-layer gold surface and immobilization of the protein were previously described in [1,2].

Spectro-electrochemical measurements: The spectroelectrochemical cell was mounted on top of a trapezoid silicon ATR-crystal required for a single reflection in the ATR mode. The IR beam of the FTIR spectrometer was coupled into the prism at an angle of incidence Q = 60°. The ATR-FTIR setup was equipped with a function generator which triggered the potentiostat of the Autolab as well as the spectrometer. Measurements under anaerobic conditions were performed in a buffer solution flushed with Ar containing $K_2HPO_4$ 0.05 mol/L, KCl 0.1 mol/L, pH=8 and the oxygen trap consisting of glucose (0.3 %w/w), glucose oxidase (75 µg/mL) and catalase (12.5 µg/mL). Electrochemical measurements were taken in a three electrode configuration with gold as the working electrode, a Ag|AgCl,KClsat. reference, and a platinum wire as the counter electrode. All electrode potentials are quoted versus SHE.

**RESULTS:** This system enabled us to observe the sequential electron transfer (eT) within the multi-redox-site membrane protein induced by electronic wiring to the gold surface using time-resolved (tr)-SEIRAS. Conformational transitions concerning a large number of single amino acids and also of secondary structures as a consequence of eT could be seen in a wide range of frequencies from 0.7 Hz to 2 kHz. A high resolution of the spectra was achieved by a combination of Two-Dimensional Infrared (2D IR) Spectroscopy and phase-sensitive detection. Kinetic constants were obtained by applying periodic potential pulses and recording spectral changes as a function of time. Methods were developed to separate these kinetic constants from the contribution due to charging currents.

**DISCUSSION & CONCLUSIONS:** Time resolution in the µs time-scale has been demonstrated in the current work, and this should be sufficient to perform a detailed kinetic analysis of the full enzymatic cycle of the CcO, measured in the presence of oxygen. The present investigation has clearly shown that $Cu_A$ is the initial electron acceptor of the bioelectronic coupling, which is essential to know for further investigations. Furthermore, the current study has shown that time-resolved ATR FTIR can be used to monitor rapid bioelectronic electron transfer processes. Rate constants were determined comparable to those obtained previously by electrochemistry and electrodynamic simulations.

**REFERENCES:** [1]Nowak, C.; Luening, C.; Knoll, W.; Naumann, R.L.C., (2009), *Appl Spectroscopy* **63**, 1068-1074. [2]F. Giess, M. G. Friedrich, J. Heberle, R. L. C. Naumann and W. Knoll, (2004), *Biophys J*, **87**, 3213-3220.

European Cells and Materials Vol. 20. Suppl. 3, 2010 (page 191) ISSN 1473-2262

# Detecting water transport through lipid membranes on a millisecond level using microfluidics and fluorescent dyes

G. Ohlsson[1], S. Tabaei[1] (shared first authors), M. Brändén[1], J. O. Tegenfeldt[2], and F. Höök[1]

[1]*Department of Applied Physics, Chalmers University of Technology, Göteborg, Sweden*

[2]*Department of Physics, University of Gothenburg, Göteborg, Sweden*

**INTRODUCTION:** When an osmotic pressure is induced across the membrane of lipid vesicles, water will first rapidly leak out of the vesicles, resulting in volume shrinkage, followed by vesicle swelling upon solute transport into the vesicles. With the aim to screen aquaporin-controlled water transport reactions on the level of *single lipid vesicles* containing *single membrane proteins*, a microfluidic setup has been designed to enable rapid (sub 10 ms) switching of liquid over a predefined area (Fig. 1). The device has been characterized by studying water and sugar-alcohol transport in single vesicles (Fig. 2) by following changes in the self quenching of dyes encapsulated in lipid vesicles attached to the surface of a microfluidic device. Switching speeds sufficiently fast to probe aquaporin-controlled water transport have been obtained.

**METHODS:** Lipid vesicles (POPC and 1% biotin-modified PE) were made by extrusion through a 200 nm filter in a calcein (30 mM) containing buffer. Surface attachment was controlled by immobilizing the vesicles to a NeutrAvidin modified surface of the microfluidic device. Time resolved changes in fluorescence-emission intensity upon volume-change induced self quenching of calcein were measured in an inverted microscope operated in either EPI or TIRF mode using a camera running at 125 frames/sec. The microfluidic channels were made by soft lithography, with the PDMS structure bonded on top of a thin microscope glass slide using oxygen plasma treatment [1]. A membrane vacuum pump and an electronic valve were used to manage rapid switching of buffer liquids over the measurement area (Figs 1 b and c).

**RESULTS:** To test the performance of the microfluidic switching, the channel was fed with water and a carboxyfluorescein solution and monitored in surface-sensitive TIRF mode. The intensity profile upon switching the liquid flow to one of the outlets is shown in Figure 1 a, demonstrating a time resolution similar to that of the camera (8 ms).

Figure 2 shows the fluorescent intensity profile of *a single surface-bound 200 nm vesicle* during a switch from a water-based buffer to buffer containing glycerol. The first step ($\tau \approx 50$ ms) corresponds shrinkage due to water transport out from the vesicle, followed by a slower ($\tau = 900$ ms) intensity increase upon glycerol transport into the vesicle.

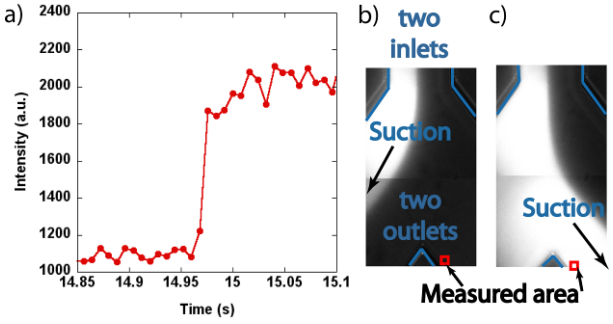


*Fig. 1. (a) The fluorescence intensity measured in TIRF mode on a single vesicle sized area (2x2 pixels) during switching as illustrated in (b) and (c). Time resolution is limited by the frame rate to 8 ms.*

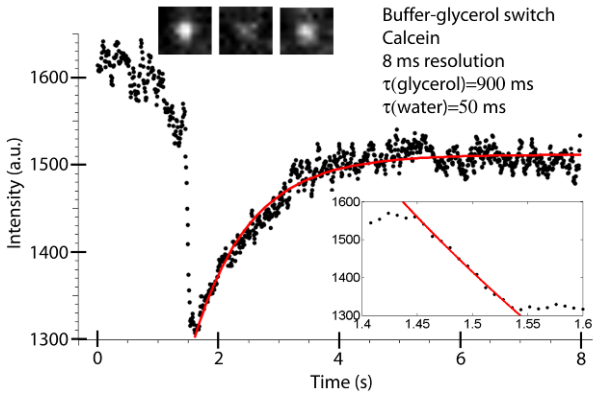


*Fig. 2. A water to glycerol switch over one single calcein-filled vesicle (photos). The initial fast decay is the water transport (inset: zoomed) and the second, slower recovery of the signal corresponds to glycerol transport. Time resolution: 8 ms. EPI mode.*

**DISCUSSION & CONCLUSIONS:** Transport of water and sugar alcohols through cell membranes was measured down to the single vesicle level, offering the potential to probe population dynamics by simultaneous monitoring of multiple vesicles. Current work is focused on screening of inhibitory ligands to water and sugar transporters, in particular aquaporins.

**REFERENCES:** [1] Jo BH et al. (2000) J. Microelectromech S 9:76-81

**ACKNOWLEDGEMENTS:** EU FP7 ASMENA is acknowledged for financial support.

European Cells and Materials Vol. 20. Suppl. 3, 2010 (page 192) ISSN 1473-2262

# Multifunctional nanoparticles for healthcare applications

C.I. Olariu[1], H.P.P. Yiu[1], L. Bouffier[1], T. Nedjadi[2], E. Costello[2], C. M. Halloran[2], M.J. Rosseinsky[1]

[1] *Chemistry Department, University of Liverpool, Liverpool, UK.* [2] *Division of Surgery and Oncology, Royal Liverpool University Hospital, Liverpool, UK*

**INTRODUCTION:** Early stage diagnosis of cancer greatly enhances successful treatment and positive patient prognosis. Sensitive and accurate imaging methods are an important tool for diagnosis. It is possible that specific and precise diagnosis could be achieved using nanoparticles as cancer recognition markers. [1-3] Multifunctional magnetic nanoparticles with several integrated properties provide enormous potential for healthcare applications. Smart surface tailoring methods can be applied to iron oxide nanoparticles in order to functionalize them with organic groups so that multiple entities can be integrated simultaneously in the same nanoparticle in further steps. These entities can be fluorescent markers, drug molecules, targeting agents, DNAs and *si*RNAs. Introducing multiple reactive moieties on the particle surface becomes a critical step in creating a robust 'all-in-one' system for biomedical diagnosis. Cytotoxicity assessment of the nanoparticles after each chemical modification is also essential as the final purpose of the system is *in vivo* applications.

**METHODS:** Iron oxide nanoparticles ranging from 5 nm to 30 nm were prepared using various synthetic methods. Afterwards, the surface of the particles was decorated with multiple reactive moieties by functionalization with organic coupling agents. These functional groups on the surface allowed the simultaneous binding of fluorescent dyes and specific proteins. A schematic representation of these chemical steps is presented in *Figure 1*.

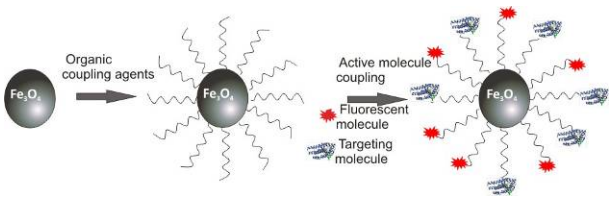


*Fig. 1: Schematic representation of nanoparticles functionalization*

**RESULTS:** A full structural and morphological characterization of multifunctionalized nanoparticles was carried out using elemental analysis, FTIR, zeta potential, TEM and TGA analysis. Fluorescence microscopy was used to confirm the coupling of fluorescent molecules or fluorescently tagged proteins. The multifunctionalized magnetic nanoparticles which were labeled with two different molecules are shown in *Figure 2*. The two colors (red and green) present on the nanoparticles confirm that the fluorescent dye (RITC- red) and fluorescent tagged protein (BSA tagged with FITC- green) are coupled on the nanoparticles.

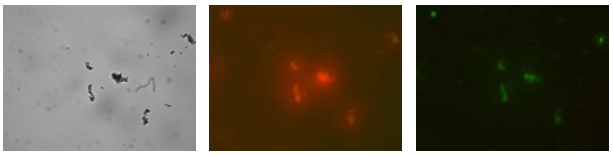

*Fig. 2: Phase contrast and fluorescence images of nanoparticles simultaneously labeled with RITC (red) and BSA tagged with FITC (green).*

Currently the particles are undergoing analysis for specific targeting of pancreatic cancer cells. Results show that tagging these nanoparticles with a specific targeting molecule binding to pancreatic cancer cells.

**DISCUSSION & CONCLUSIONS:** Multiple functional groups on the surface of nanoparticles offer the possibility of labeling the nanoparticles with targeting molecules and for specific recognition of pathologic sites. Labeling with fluorochromes allows monitoring of the fate of the nanoparticles by fluorescence and MRI imaging. This protocol can be applied to diagnosis of other cancers e.g. breast or colon cancer.

**REFERENCES:** [1]O. Veiseh, C. Sun, J. Gunn, et al (2005) *Nano Letters* **5**: 1003-1008. [2]R. Qiao,C. Yang, M. Gao (2009) *J Mater Chem* **19**: 6274-6293. [3]F. Hu, L. Wei, Z. Zhou et al (2006) *Adv Mater* **18**: 2553-2556

**ACKNOWLEDGEMENTS:** EPSRC for funding.

European Cells and Materials Vol. 20. Suppl. 3, 2010 (page 193) ISSN 1473-2262

# Using Tip-Enhanced Raman Spectroscopy for the Nanoscale Chemical Analysis of Cell Membrane-Like Structures

L. Opilik*, T. Schmid, J. Stadler, R. M. Balabin, R. Zenobi

**Department of Chemistry and Applied Biosciences, ETH Zurich, 8093 Zurich, Switzerland*
*opilik@org.chem.ethz.ch; phone +41-44-6334145; fax +41-44-6321292; www.zenobi.ethz.ch*

The biological membrane plays an important role in numerous cellular processes and is linked to various diseases. Many of its biological functions have been shown to depend on local environments with specific compositions.[1] Self-assembled nanoscale compartments enriched in sphingolipids, cholesterol and proteins called "lipid rafts" are believed to be a locus for biochemical reactions taking place on the cell membrane.[2] Investigation of such domains with nanometer resolution is still a very challenging task, especially when it is done in their native environment. Model membrane systems have been developed to study biophysical processes occurring at the cell membrane in a controlled fashion. Solid supported lipid bilayers are a prominent example because of their accessibility for various surface-specific analytical techniques.[3] In this study, tip-enhanced Raman spectroscopy (TERS) is applied to such model lipid bilayers to test its applicability for the nanoscale chemical analysis of the most important membrane constituents.

TERS is a non-destructive analytical technique capable of yielding vibrational spectra of samples with a lateral resolution below 30 nm.[4] It is essentially an apertureless near-field technique where conventional optics are used to illuminate a metal or metalized scanning probe microscopy (SPM) tip. This tip is brought in close proximity to a sample surface leading to a significant enhancement (several orders of magnitude) of the Raman scattering from the molecules located in the small region under the tip apex. Biological materials are in general very weak Raman scatterers due to their non-resonant character. Therefore, their investigation demands a highly optimized TERS setup, especially with respect to tip fabrication.

We are currently working with two different TERS configurations in our laboratory. On one hand, electrochemically etched silver tips are used in scanning tunneling microscopy (STM) feedback for gap-mode TERS investigations on flat gold surfaces (Figure 1a). On the other hand, silver-coated atomic force microscopy (AFM) tips are used for TERS on transparent samples with the option to work in an aqueous environment (Figure 1b).[5]

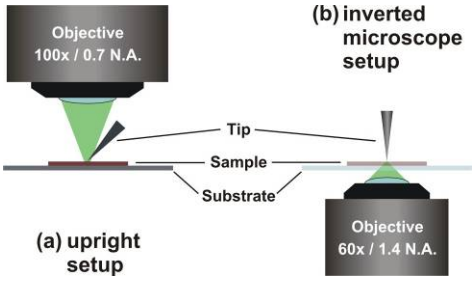


*Fig. 1: Arrangement of SPM tip, sample and objective for the two setups used for TERS investigations: (a) upright setup for opaque and transparent samples and (b) inverted microscope setup for transparent samples equipped with an oil immersion objective.*

TERS was successfully performed on supported lipid bilayers (SLBs) with varying complexity. The data was compared to reference spectra from individual membrane components, which were collected using confocal Raman spectroscopy as well as surface-enhanced Raman spectroscopy (SERS). Raster scans on SLBs provided information on the distribution of certain membrane constituents with nanometer spatial resolution.

Our results pave the way for detailed nanoscale chemical analysis of cell membranes in their natural physiological environment, which will give valuable insights into the working mechanisms of a cell.

**REFERENCES:** [1] S. Semrau, T. Schmidt (2009) *Soft Matter* **5**:3174-86. [2] D. Lingwood, K. Simons (2010) *Science* **327**:46-50. [3] E. T. Castellana, P. S. Cremer (2006) *Surf. Sci. Rep.* **61**:429-44. [4] B. Pettinger, B. Ren, G. Picardi, R. Schuster, G. Ertl (2005) *J. Raman Spectrosc.* **36**:541-50. [5] T. Schmid, B. S. Yeo, G. Leong, J. Stadler, R. Zenobi (2009) *J. Raman Spectrosc.* **40**:1392-99.

European Cells and Materials Vol. 20. Suppl. 3, 2010 (page 194) ISSN 1473-2262

# Particle Shape Effect on Trafficking in Tissue-like Media

S. Orsi[1], G. Romeo[2], D. Guarnieri[1], P.A. Netti[1]

*[1] CRIB and, IIT, Naples, Italy. [2] DIMP, University of Naples Federico II, Naples, Italy.*

**INTRODUCTION:** Understanding how geometrical, physical and chemical parameters influence nano-particle interaction with the biological environment in terms of transport, targeting, adhesion and cellular internalization, is crucial to rationally design functional nano-biomaterials. Size, chemistry and shape non-trivially affect particle trafficking in tissues as a consequence of the structural and chemical complexity of such media. While the effects of both particle size and chemistry have long been investigated, the influence of the shape has received attention only recently. Different studies highlight the importance of the particle shape on cellular uptake and intracellular trafficking[1]. However a fundamental understanding of the mechanisms at the origin of such effect is still lacking. We have used hyaluronic acid (HA), a basic component of the extracellular matrix, as a simple system to study how particle transport mechanisms are affected by particle shape. We realized ellipsoidal nano-particles of different aspect ratios and equal volume starting from spherical ones[2] and measured their diffusivities in semidilute solutions of HA. In particular we find that particle diffusivity is controlled by the ratio of the characteristic length scale of the transient polymer network and particle sizes. Finally we find that such an effect is also reflected on cellular internalization kinetics.

**METHODS:** Fluorescent polystyrene spherical nano-particles (Duke Scientific) were dispersed in PVA water solutions which were subsequently casted to obtain PVA thin films. The films were heated at a temperature above the PS glass transition temperature and then unidirectionally stretched. The final particle aspect ratio was modulated by applying a given stretching ratio. The particles were recovered by dissolving the films in water. To characterize the nano-particles shape and dimensions, we performed scanning electron microscopy (SEM), and polarized and depolarized dynamic light scattering (DLS, DDLS) in dilute water suspensions. The medium in which we measure the nano-particle diffusion is a semidilute water solution of HA 155 KDa (Fidia). The critical HA concentrations values defining the beginning of dilute, semidilute and semidilute entangled regimes were derived by rheology. The diffusivities of the ellipsoidal nano-particles in HA solutions were measured by DLS. Finally, we evaluated the internalization kinetics of nano-particles, in serum free culture condition, in Porcine Endothelial cells (PAE) by performing image analyses of Confocal laser micrographies.

**RESULTS:** By stretching the PVA films containing the spherical nano-particles, we obtain ellipsoids all having the same volume, and with aspect ratios which depend on the stretching ratio in an affine way, as shown in Figure 1.

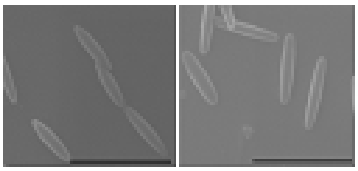

*Fig. 1: SEM images of PS nano-particles obtained by stretching ratios of 2.4 (left) and 3.1 (right). The scale bar is 500 nm.*

We have measured the diffusivities of ellipsoids of different aspect ratios in semidilute solutions of HA at different concentrations. We find that when the dimension of the smaller axis of the ellipsoid is comparable to the mesh size of the polymer network, the particle long time diffusivity is higher than that predicted by the Stokes-Einstein equation for homogeneous fluids with the same viscosities of our HA solutions. In agreement with this result, we find, as shown in Figure 2, that the short-time cellular internalization is more efficient when particle aspect ratio is increased.

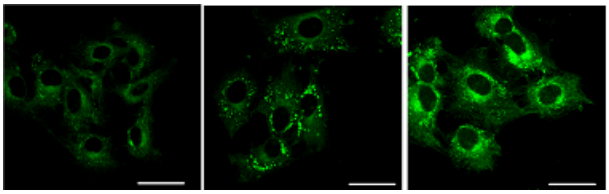

*Fig. 2: CLSM images of PAE cells after 3h incubation period at 37°C with nano-particles obtained by deforming nanospheres of 88nm in diameter with a stretching ratio of 1, 2.4, 3.1 from left to right, respectively. The scale bar is 20μm.*

**DISCUSSION & CONCLUSIONS:** By using a semidilute solution of HA as a model system, we have obtained useful informations about the effect of nano-particle shape on particle trafficking in complex media like tissues.

**REFERENCES:** [1]S. Gratton, P.A. Ropp, P.D. Pohlhaus et al (2008) PNAS **105**: 11613-8. [2]J. Champion, Y. Katare, S. Mitragotri. (2007) PNAS **104; 29**: 11901-4.

European Cells and Materials Vol. 20. Suppl. 3, 2010 (page 195) ISSN 1473-2262

# Replication of nano-pillar array structures for tissue engineering applications

H. Özçelik[1], C. Padeste[2], J. Ziegler[2], A. Schleunitz[2], M. Bednarzik[2], V. Hasırcı[1]

[1]*METU, BIOMAT, Department of Biological Sciences, Ankara 06531, Turkey*

[2]*Lab for Micro- and Nanotechnology, Paul Scherrer Institut, 5232 Villigen PSI, Switzerland*

**INTRODUCTION:** For cell biology and in tissue engineering it is important to understand cell behaviour on the nanoscale. Recently, it became clear that nanotopography can elicit strong and different effects such as changes in migration, adhesion, cytoskeletal organisation and gene regulation, on a range of cell types [1-3]. The technology to produce structures, e.g. in silicon substrates, of dimensions interesting for studying interactions with cells is well established. However, to make such structures attractive for cell growth studies they need to be replicated in high numbers into biologically relevant materials.
Here we present a two-step replication process which allows the reproduction of high aspect ratio nanopillar arrays into biocompatible polymers which are soluble in organic solvents.

**METHODS:** Square millimeter sized arrays of nanopillars of up to 900 nm height and 200 nm diameter and with a pillar-to-pillar distance of 1 µm to 10 µm were produced on a silicon wafer by e-beam lithography and reactive ion etching (Fig. 2). The replication process is schematically shown in Fig. 1. A negative replicate is first formed by polydimethyl-siloxane (PDMS) casting. The final replicates are produced by solvent casting from 1-4% solutions of poly(L-D,L-lactic acid) (PLLA). On the replicated structures human osteosarcoma cell line cells, SaOs-2, as well as Mouse Bone Marrow Stem Cells (BMSCs) were cultured.

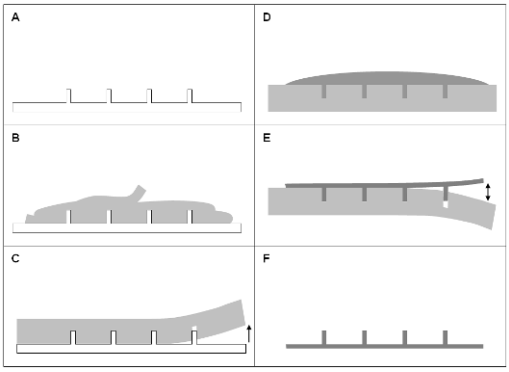


*Fig. 1: Scheme of the replication procedure: Silicon nanopillar arrays (A) are embedded in PDMS (B). After curing the PSMS is separated from the master(C) and covered with a droplet of PLLA solution (D). After slow evaporation of the solvent the replicate is separated from the PDMS (E/F).*

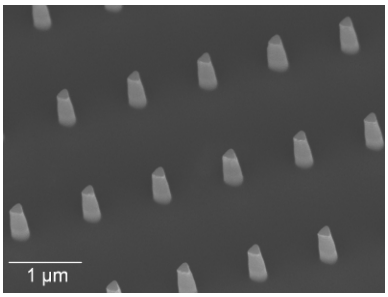


*Fig. 2: Array of nanopillars (900 nm high) dry-etched into silicon.*

**RESULTS & DISCUSSION:** The replication process proved to be suitable for nano-sized pillar structures with aspect ratios as high as 4-5. AFM measurements confirmed the same height of the pillars of the master and the replicates. The flexibility of the PDMS cast facilitates the detachment in both replication steps. Furthermore, a considerable solvent uptake of the PDMS appears beneficial in the second step, resulting in high enough polymer concentration in the cavities to form solid pillars.

In first cell culture experiments it was found that different types of cells react very differently on the surface topography: While BMSC cells appeared to avoid contact with the nanopillar arrays, the SaOs-2 cells tried to adapt to the structured surfaces as they elongated along the axes with the shortest pillar-to-pillar distance (arrows in Fig. 3).

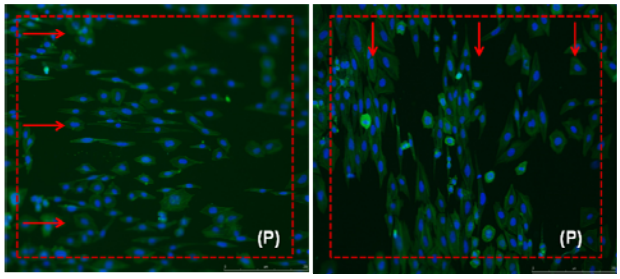


*Fig. 3: SaOs-2 cells positioned and elongated on the nanopillar-patterned areas (P).*

**REFERENCES:** [1] C.J. Bettinger, R. Langer, J.T. Borenstein (2009). *Angew Chem Int Ed* **48**: 5406. [2] E. Martinez, E. Engel, J.A. Planell (2009) *Ann Anat* **191**: 126. [3] L.A. Cyster, K.G. Parker, T.L. Parker, D.M. Grant. (2004) *Biomaterials* **25**: 97.

European Cells and Materials Vol. 20. Suppl. 3, 2010 (page 196) ISSN 1473-2262

# Integration of polarized light-emitting nanostructures for biomarker sensing

S.Pagliara[1,2], A.Camposeo[1], A.A.R.Neves[1], A.Polini[1,2], R.Cingolani[3], D.Pisignano[1,2]

*[1] National Nanotechnology Laboratory of CNR-Istituto Nanoscienze, Distretto Tecnologico, Università del Salento, via Arnesano I-73100, Lecce, Italy. [2] ISUFI, Università del Salento, via Arnesano, I-73100 Lecce, Italy. [3] Italian Institute of Technology, via Morego, 30, Genova, Italy.*

**INTRODUCTION:** Polymer light-emitting nanofibers are particularly attracting as low-cost excitation sources for many μ-TAS applications. The integration of active organic nanostructures in microfluidic devices made by conventional or soft lithographies is relevant for high-sensitivity diagnostic applications, mainly based on highly specific biological affinity reactions. In this context, the exploitation of miniaturized polarized light-sources into lab-on-chips, involving very tiny needed liquid volumes for single reaction, is a very interesting challenge. Moreover the possibility to gently position single light emitting nanofibers within lab-on-a-chip architectures with micrometer accuracy allows photo-excitation of chromophores flowing in very restricted chambers, thus involving low analyte-antigen concentrations.

We review our recent results on realization and characterization of light-emitting polymer nanofibers by electrospinning (ES), and on their integration as polarized light-sources in microfluidic devices for biosensing applications. We optimize the fabrication parameters to enhance the resulting optical anisotropy, thus increasing sensitivity. Fascinating approaches for the careful positioning of single polymer nanofibers include optical trapping and manipulation.

**METHODS:** The light-emitting conjugated polymer poly[2-methoxy,5-(2-ethylhexyloxy)-phenylene-vinylene] -MEH-PPV- is dissolved in dichloroethane and mixed to a thermoplastic host matrices. For ES process, an electrostatic field in the range 0.6-1.3 kV/cm is applied, using a flow rate of 10 μl/min, and the fibers are collected aligned on a patterned copper foil collector. The optical trapping setup is custom-built on an inverted microscope with a high numerical aperture objective, using a CW laser at 800 nm. PDMS microfluidic devices produced by soft lithography are coupled to the light emitted by the fibers. The system is characterized by polarization-dependent absorption, photoluminescence, and excitation in total internal reflection configuration.

**RESULTS:** The alignment of fibers into arrays is evaluated by SEM investigation, finding typical angular distribution described by Gaussian functions. This is correlated to the achievable optical anisotropy as accomplished by comparing

the transmittance of polarized light through aligned arrays and through isotropic non-woven fiber networks. Moreover, the polarized light-emitting arrays are exploited as excitation sources embedded in lab-on-a-chip PDMS architectures. Solution of chromophore molecules are injected in the microchannels, and excited by nanofiber polarized emission almost resonantly to their absorption (Fig. 1). This allows a significant increase of the resulting S/N ratio from the excited microchannels with respect to an unpolarized excitation scheme. For precise positioning and alignment into microfluidic architecture, extensive manipulation experiments are carried out on single polymer nanofibers. Nanofibers could be optically trapped along the optical axis, or oriented along the beam polarization. Constant rotation of a trapped nanofiber could also be obtained by tilting the fiber against a surface, with the rotation controlled by the optical power.

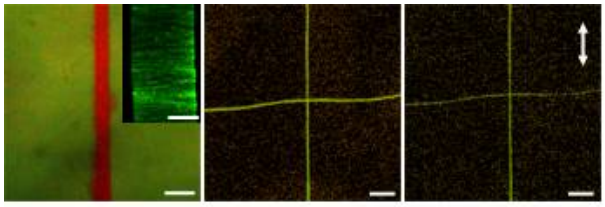

*Fig. 1: (a) Excitation of chromophore red emission by arrays of polarized green light-emitting nanofibers (inset). (b) Light emitted by two single crossed nanofibers and (c) analyzed by a polarizer schematized by the white arrow. Scale bar = 200 (a), 100 (inset in (a)) and 5 (b) and (c) μm.*

**DISCUSSION & CONCLUSIONS:** A few straightforward approaches are proposed as promising tools for the careful embedment of polarized light-emitting nanofibers in lab-on-a-chips, for biological and medical diagnostics.

**REFERENCES:** [1] S. Pagliara, A. Camposeo, A. Polini, R. Cingolani, D. Pisignano (2009) *Lab Chip* **9**: 2851-56. [2] A.A.R. Neves, A. Camposeo, S. Pagliara *et al* (2010) *Opt. Express* **18**: 822-30.

**ACKNOWLEDGEMENTS:** The authors are grateful to the support of the Apulia Regional Strategic Project PS 144.

European Cells and Materials Vol. 20. Suppl. 3, 2010 (page 197) ISSN 1473-2262

# Capacitance-based real time monitoring of Chemosensitivity

R.M. Lee[1], Y.J Park[1], K.-H.Yoo [1, 2*]

[1] *Graduate Program for Nanomedical Science and Technology, Republic of Korea.*
[2] *Department of Physics, Yonsei University, Republic of Korea.*

**INTRODUCTION:** Selection of chemotherapy is based on a broad scale of factors, including a patients' age and tumor characteristics. One potential approach to improve the therapeutic efficacy is to use ex vivo approaches to evaluate the sensitivity to specific chemotherapeutic agents using patients' tumor cells[1]. There are several assays such as MTT assay, ATP-dependent bioluminescence assay, Alamar Blue Assay, to test resistance of tumor cells to chemotherapy by measuring the amount of living cells remaining after exposure to drug doses. However these methods are based on optical measurement requiring optical dye, so we have developed a capacitance sensor. We measure the cell viability in real time without labelling.

**METHODS:** The capacitance sensor array, composed of sixteen sensors with gap areas of 50 μm×7000 μm, was also fabricated on the glass substrate (Fig. 1). An acrylic well with a volume of 300 μl was attached to each sensor with a curing agent (polydimethylsiloxane and toluene mixed at 1:10) for cell culture. The size of array sensors is same as conventional 96 well plate. The capacitance was measured simultaneously from all sixteen sensors with a data acquisition/switching unit (Agilent 34970A) connected to the LCR meter (Agilent 4284A). Data were collected every min for the single capacitance sensor and every 5 min for the capacitance sensor array. For comparison, we carried out the MTT assay**.** SK-BR-3 cells were seeded at a density of $5\times10^4$ per well in 100μl of culture medium into a 96-well plate and incubated overnight for attachment. Cells were treated with different concentrations of DOX (0.25μg/ml, 2.5μg/ml, 10μg/ml, 25μg/ml, 50μg/ml, and 100μg/ml in culture medium 100μl). After 24, 48, and 72 h, the medium is removed and the MTT solution (0.5mg/ml) was added to samples. After 4 h incubation at 37 °C, the MTT solution was removed. DMSO was added to each well. The optical density was measured at 490 nm using a microplate reader. The percentage cell proliferation was calculated as [Optical density (OD) of the sample/OD of the control] × 100.

**RESULTS:** The procedure before DOX treatment is same as MTT assay and after

treatment, measured the capacitance of cell. Fig.1 shows capacitance sensor which used on this experiment. By the sensor, the capacitance value is decrease during cell death[2] (Fig.2). The amount of capacitance change is proportion to DOX treatment.

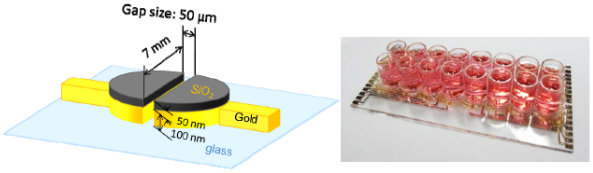


*Fig.1 Schematic diagram of a capacitance sensor array (left) and image of 16 well arrays (right).*

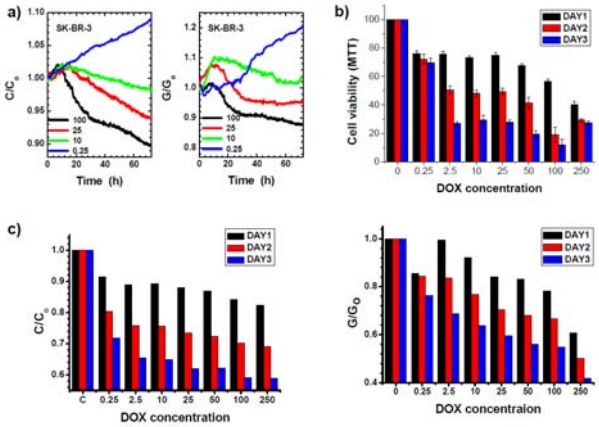


*Fig.2 Viability of SK-BR-3 cells which were exposed to DOX by capacitance sensor (a) and MTT assay (b). c) shows calculated capacitance and conductance normalized by measured values for proliferation for each DOX dose. .*

**DISCUSSION & CONCLUSIONS:** The cell viability obtained by capacitance sensor arrays was in good agreement with MTT assay method. Unlike conventional assay method using dye, which requires an extra step in the assay procedure, capacitance sensor arrays can provide an advantage to the method by allowing a simpler assay procedure.

**REFERENCES:** [1]J. Komen, F. Wolbers (2008) *Biomedical Microdevices*, **10**(5):727-37. [2] Lee et al. (2009) *Biosensors and Bioelectronics*, **25**:1325-32.

**ACKNOWLEDGEMENTS:** This work has been financially supported by Korea Science and Engineering Foundation through National Core Research Center for Nanomedical Technology (Grant No. R15-2004-024-00000-0).

European Cells and Materials Vol. 20. Suppl. 3, 2010 (page 198) ISSN 1473-2262

# Aptamer-based biofunctional layer for thrombin detection

L.Pasquardini, E.Agostini, L.Lunelli, C.Potrich, L.Vanzetti, C.Pederzolli

*FBK-Fondazione Bruno Kessler, Materials and Microsystems Centre, Trento, Italy.*

**INTRODUCTION:** This work focuses on the development and the characterization of a biofunctional layer able to efficiently recognize a target protein. The biofunctional layer is based on a dual-site binding strategy with modified aptamers [1]. Aptamer-based chips present many advantages over antibodies, such as the possibility to operate in a wide variety of sample matrices, including non-physiological buffers, and at a temperature that would denature antibody formulations. The biological model chosen for the present work is the protein thrombin (factor IIa). Two aptamer sequences able to bind to different sites of this protein are used [2]. The first aptamer (ApI), anchored to substrate, specifically immobilizes the target protein to the sensor surface, while the second sequence (ApII), carrying a fluorescent molecule, allows target detection. In this work we focus on the immobilization of ApI molecules on the surface and the characterization both in terms of molecular density and functional interaction with the target protein.

**METHODS:** A silicon oxide surface was functionalized in wet conditions using a functional silane. After a piranha activation, the substrate was placed in a mercaptopropyltrimethoxysilane (MPTMS) toluene solution (1% v/v) at 60°C for 10 minutes. The primary aptamer, carrying a dithiol chemical group at one end was then immobilized on the sensor surface in carbonate/bicarbonate buffer. Whole plane samples were homogeneously treated for surface analysis, while a localized deposition was obtained with a contact spotter (Biodyssey Calligrapher, Biorad). After a washing step, the surface was passivated with 1mM mercaptohexanol for 2 hours. A thrombin solution at 100nM was incubated for 30 minutes, followed by washing steps.

**RESULTS:** The silanization efficacy was evaluated chemically and morphologically by means of XPS (X-ray Photoelectron Spectroscopy) and AFM (Atomic Force Microscopy) measurements. The AFM characterization of MPTMS deposited on $SiO_2$ revealed uniformly distributed features, with a moderate increment in the initial surface roughness. The XPS analysis (Table 1) shows an increase in the carbon content due to the silane aliphatic chain, and a sulphur peak appears. Using a fluorescent derivative of ApI its immobilization on silanized surfaces was also

evaluated in terms of density and homogeneity via spectrofluorimetric and microscopy analysis. Fig 1 reports the evaluation of the immobilized aptamer density with increasing concentrations of the spotting solution, resulting in a range from 0.5 to 7.5 x $10^{12}$ molecules/$cm^2$. Besides fluorescence, XPS analysis confirms successful aptamer immobilization with the appearance of the nitrogen peak and the increase in the carbon content. Incubation of the aptamer-treated surfaces with thrombin induces a further increase in the nitrogen and carbon content in XPS spectra. Immunofluorescence methods were also utilized, confirming the recognition of the target protein by the aptamer layer.

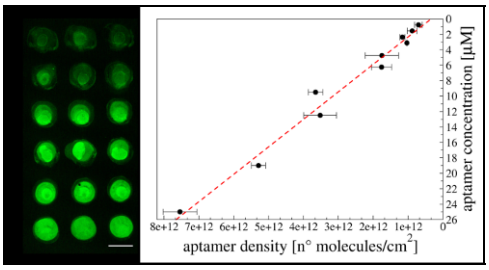


*Fig 1: Fluorescent ApI aptamer array spotted on MPTMS at increasing concentrations (left, scale bar 100µm); density of immobilized molecules (right).*

*Table 1. XPS atomic percentage at 15° tilt angle.*

| surface | O 1s | N 1s | C 1s | S 2p | Si 2p |
|---|---|---|---|---|---|
| activated | 49.2 | - | 16.8 | - | 34.0 |
| silanized | 30.0 | - | 37.3 | 7.2 | 25.6 |
| aptamer | 22.9 | 1.9 | 48.4 | 5.3 | 21.4 |
| thrombin | 22.4 | 4.7 | 50.1 | 6.4 | 16.4 |

**DISCUSSION & CONCLUSIONS:** The characterization of immobilized aptamer layers on MPTMS surfaces suggests that a suitable density of biorecognition molecules is obtained.

**REFERENCES:** [1] S. Song, L. Wang, J. Li, J. Zhao, C. Fan et al (2008) *Trends Anal Chem* **27, 2**:108-117; [2] D.K. Kim , K. Kerman (2008) *Anal Biochem* **379**:1-7.

**ACKNOWLEDGEMENTS:** This work is accomplished in the framework of the NAoMI Project funded by the Province of Trento (http://naomi.science.unitn.it/).

European Cells and Materials Vol. 20. Suppl. 3, 2010 (page 199) ISSN 1473-2262

# Chemical and morphological characterization of polypeptide layers deposited for directed cell attachment

*Cs. B. Pénzes[1], M. Mohai[2], G. Mező[3], I. Szabó[3], Sz. Bősze[3], É. Kiss[1]*

*[1]Laboratory of Interfaces and Nanostructures, Institute of Chemistry, Eötvös Loránd University, Budapest 112, POB 32 H-1518, Hungary e-mail: cspenzes@gmail.com*

*[2]Institute of Materials and Environmental Chemistry, Chemical Research Centre, HAS, Hungary*

*[3]Research Group of Peptide Chemistry, Eötvös L. University, HAS, Budapest, Hungary*

**INTRODUCTION:** Synthetic, polycationic peptides/proteins, such as poly(L/D-lysine) are widely used for coating cell culture dishes or other biosurfaces. Such nonspecific adhesive coatings, however, promote initial cell adhesion with moderate efficiency, may cause abnormal cell-spreading, and might be cytotoxic [1]. Applying such large, substrate-coating molecules as backbones for carrying specific adhesive peptide motifs, however, may provide efficient synthetic adhesion molecules [2]. Branched chain polypeptides with polylysine backbone as carriers [3, 4] might be a good candidates for this purpose. Surface covering property of different branched chain polypeptides developed in our laboratory were investigated. The surface coating efficiency of polypeptides using simple adsorption or covalent bound was compared.

**METHODS:** Polypetides were adsorbed and chemically coupled to the surface of solid substrates. Adsorption was performed from aqueous buffer solutions (pH=7.4) in the range of concentration: 0,01-1 g $dm^{-3}$. The chemical coupling was developed by reacting amino groups of the peptide with the amino functionalized substrate via glutaraldehyde chemistry or using glutaranhydride/EDC system.

**RESULTS:** Both the adsorption and the chemical attachment were followed by detailed X-ray photoelectron spectroscopy (XPS) studies. According to the atomic composition of the surface layer (Table 1) the chemical coupling resulted in higher coverage and thicker layer of all of the polypetides on the glass substrate studied here than the adsorption of the same molecules.

The morphology of the polypeptide nanolayers was characterized by atomic force microscopy (AFM). The substrate surface seemed to be covered by a countinous layer of the polypeptides although the images revealed that the surface structure of the film is highly dependent on the type of polypeptides as the examples in Fig.1 show. The thickness of the surface layer is in the nm range given by AFM study of scratchings.

*Table 1. Atomic composition (%) of the surface layer of polypeptides deposited onto glass substrate by adsorption or chemical coupling applying the peptides at 0.1 g $dm^{-3}$ concentration in both cases determined by XPS analysis*

| adsorbed | N (%) | Si (%) | C (%) |
|---|---|---|---|
| pLys | 3.6 | 18.5 | 35.4 |
| AK | 5.8 | 17.6 | 36.2 |
| EAK | 4.1 | 20.5 | 25.9 |
| SAK | 3.3 | 21.3 | 23.2 |

| coupled | N (%) | Si (%) | C (%) |
|---|---|---|---|
| pLys | 6.1 | 7.6 | 64.0 |
| AK | 7.1 | 8.6 | 59.8 |
| EAK | 5.5 | 10.3 | 59.8 |
| AK | 9.5 | 8.9 | 56.9 |

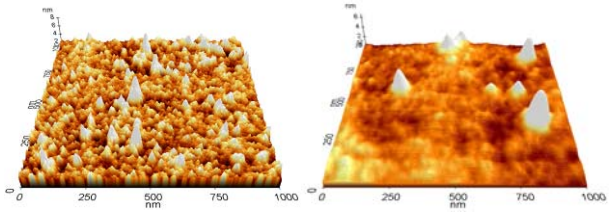


*Fig. 1 AFM images of adsorbed layer of polylysine and cRGD on glass*

The more precise evaluation of the layer thickness is provided by the combination of experimental value measured by AFM technique with a detailed analysis of the XPS data using the MultiQuant program [5] modelling the structure and composition within the surface layer.

**REFERENCES:** [1]Bershadsky, A., *et al.* (1996) *Curr. Biol.* **6**, 1279–1289. [2]Hersel, U., *et al.* (2003) *Biomaterials* 24, 4385–4415. [3]Hudecz, F., *et al.* (1980) *Coll. Czech. Chem. Commun.* **45**, 933-940. [4]Mező G., *et al.* (1997) *Biopolymers* **42**, 719-730.
[5]Mohai M., *XPS MultiQuant*, www.chemres.hu

**ACKNOWLEDGEMENTS:** This work was supported by grants from the National Office for Research and Technology (NKTH BIOSURF_OM00146/2008, OTKA68120, GVOP*3.2.1-2004-04-0099/3.0*)

European Cells and Materials Vol. 20. Suppl. 3, 2010 (page 200) ISSN 1473-2262

# Chitosan-based nanoparticles prepared by template polymerization

P. Pereira [1], FM. Gama [1]

[1] *IBB-Institute for Biotechnology and Bioengineering, Centre for Biological Engineering, Minho University, Campus de Gualtar 4710-057, Braga, Portugal.*

**INTRODUCTION:** Chitosan (CS) /poly(acrylic acid) (PAA) nanoparticles (NPs) have recently been obtained by template polymerization[1]. In this technique, the NPs are produced upon polymerization of an acrylic monomer next to the chitosan backbone. Due to the electrostatic interaction, the negatively charged acrylic monomers align along the chitosan molecules. These physic interactions leads to self-assembled particles. The molecular weight and deacetylation degree of chitosan affect the solubility, size, and stability of the particles.

**METHODS:** The CS/PAA NPs were synthesized by polymerization of AA in a CS solution. The CS was firstly dissolved in 50mL of AA solution (3mmol), in molar ratio of the 1:1, [aminoglucoside units]: [AA], under magnetic stirring until the solution became clear. In order to induce the polymerization of acrylic monomer, an initiator ($K_2S_2O_8$, 0,1mmol) was added to the solution. The pH value of the system was maintained at about 4,0. The mixture was placed at 70ºC, under magnetic stirring and nitrogen atmosphere. After two hours, the solution became opaque and the reaction was stopped in an ice bath. The milky solution was filtered to eliminate any aggregates. To remove the initiator and the acrylic monomers that not reacted, the solution was dialysed against deionised water, in a 12-14KDa cut-off membrane, for three days. The CS/PAA NPs characterization was carried out by dynamic light scattering (DLS) to determine de size distribution and zeta potential, cryo-field emission scanning electron microscopy (Cryo-FESEM) to visualize the size and shape of the particles and size exclusion chromatography (SEC) to verify the extension of the acrylic monomer polymerization.

**RESULTS:** The polymerization of acrylic acid in the presence of chitosan is showed in Fig. 1. The size distribution of the nanoparticles was evaluated with a Malvern Zetasizer instrument, and showed an average size of 360nm (Fig, 2a). The CS/PAA NPs have size stability even after seven months. However, the NPs exhibited a pH-sensitive behaviour and their size increases with increasing of pH. The CS/PAA NPs appeared spherical in Cryo-FESEM micrographs (Fig. 2b).

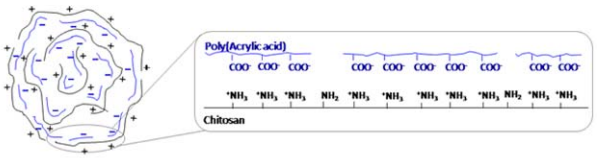


*Fig. 1: Schematic representation of electrostatic interactions that allows the self-assembling.*

The surface charge of the NPs at acid pH is quite positive, about 40mV. However, at pH 7.4 the zeta potential decreases to near neutrality. The average molecular weight of PAA in CS solution, measured using SEC, was about 800Da.

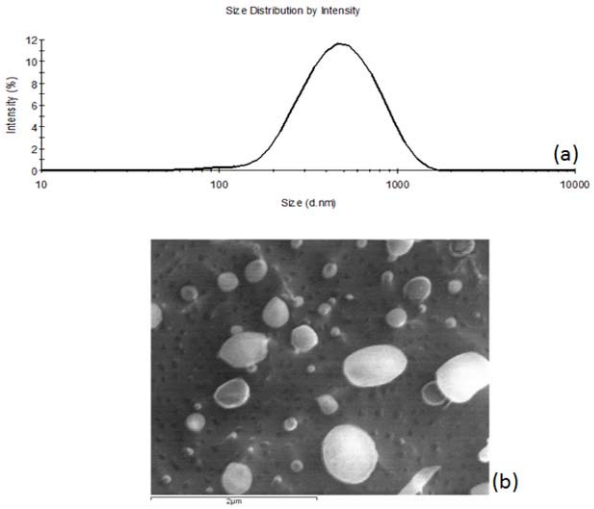


*Fig. 2: Size distribution by intensity (a) and Cryo-FESEM image (b) of CS/PAA NPs.*

**DISCUSSION & CONCLUSIONS:** The electrostatic interaction between poly(acrylic acid), negatively charged, and chitosan backbone with positive charge promotes the self-assembly of NPs. The size profile of CS/PAA NPs observed by Cryo-FESEM was consistent with that measured in the DLS, ranging from 200nm to 1000nm. As the surface charge, at pH 7.4 the zeta potential decreases to near neutrality, because the pka of chitosan is 6.5 and therefore the amines are no longer protonated. In short, these NPs can be successfully produced under very mild conditions.

**REFERENCES:** [1] Y. Hu, X. Jiang, Y. Ding, et al (2002) *Biomaterials* **23:** 3193-201.

**ACKNOWLEDGEMENTS:** Paula Pereira was supported by the grant SFRH/BD/64977/2009, from Fundação para a Ciência e Tecnologia (FCT), Portugal.

European Cells and Materials Vol. 20. Suppl. 3, 2010 (page 201) ISSN 1473-2262

# Investigation of Interaction between Oligonucleotides and Cobalt Ferrite Nanoparticles

A.G. Pershina, V.Yu. Serebrov, A.E. Sazonov

*The Siberian State Medical University, Tomsk, Russia.*

**INTRODUCTION:** The constructions based of superparamagnetic nanoparticles are particularly useful in biomedicine for nucleic acids separation, gene detection, creating gene delivery system, as MRI contrast agent and biosensors, due to they can be effective detecting and controlling magnetically [1-2]. Development of nanostructures for specific problems solution requires deep understanding of interaction between nanoparticles and biomolecules. In the present work the interaction of cobalt ferrite nanoparticles and 18-mer single-stranded oligonucleotides $dG_{18}$, $dT_{18}$, $dA_{18}$, $dC_{18}$ and $dN_{18}$ (3´-gtaaaacgacggccagtg-5´) was investigated.

**METHODS:** Superparamagnetic cobalt ferrite nanoparticles $CoFe_2O_4$ (average diameter 10 nm) were prepared by mechanochemical synthesis [3]. The bionanocomposites were formed by incubating 4 nmol of 18-mer oligonucleotide with 0.1 mg cobalt ferrite nanoparticles in 0.3 mL 10 mM Tris-HCl buffer. Then composites were separated by magnetic precipitation from the mixture and twice washed with $ddH_2O$. The amount of oligonucleotides bound with nanoparticles was determined by UV-spectrophotometry of supernatants. Desorption of DNA from the surface of nanoparticles was carried out for 12 h up to the complete adsorption equilibrium. The $D_2O$ solution infrared spectra were recorded on IR-Fourier spectrometer (Nicolet 6700) by the ATR method on the diamond crystal.

**RESULTS:** UV-spectrophotometric analysis showed that cobalt ferrite particles combine with oligonucleotides in the Tris-buffer and form bionanocomposites. The binding capacity decrease in the order $dG_{18}$ (40 nmol/mg) > $dC_{18}$ (38 nmol/mg) > $dT_{18}$ (30 nmol/mg) > $dA_{18}$ (24 nmol/mg); for $dN_{18}$ this value was 28 nmol per mg nanoparticles. The examine of ionic strength effect showed that forming of oligonucleotide- $CoFe_2O_4$ composites in 0.4 M NaCl contain buffer led to decrease oligonucleotide binding capacity of nanoparticles. It was determined that presence of sodium phosphate salt in the medium prevent from binding of $dT_{18}$ and $dA_{18}$ molecules to nanoparticles surface stronger than binding of $dG_{18}$ and $dC_{18}$. Accordingly, the research of bionanocomposites stability under changes of chemical composition of medium showed that

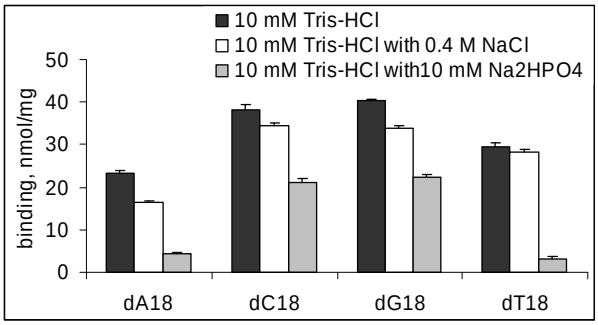


*Fig. 1: Effect of buffer composition on binding of the oligonucleotides with cobalt ferrite nanoparticles.*

$dA_{18}$ and oligod$T_{18}$ molecules during incubation in 20 mM sodium-phosphate buffer were almost completely desorbed of nanoparticles surface, while desorption level for $dG_{18}$ and $dC_{18}$ was much lower and not exceeded 8 and 13 nmol (per mg) respectively.

Study of $CoFe_2O_4$- oligonucleotide composites by FTIR-spectroscopy indicated that heterocyclic ring N7 atom of guanine, the exocyclic carbonyl groups of the purine and pyrimidine bases, and phosphate groups of sugar-phosphate backbone take part in interaction. FTIR data allows one to suppose that the binding was provided by the formation of the coordination bonds between oligonucleotides atoms and transition metal ions on the particles surface.

**DISCUSSION & CONCLUSIONS:** It was suggested that interaction of oligonucleotides with cobalt ferrite nanoparticles depend on nucleotide content. Received data open up possibilities for control binding between the oligonucleotides and nanoparticles and can be used to design specific magnetic DNA-nanoparticles hybrid structures and creating of biosensors.

**REFERENCES:** [1]Q.A. Pankhurst, J. Connolly, S.K. Jones, J. Dobson (2003) *J. Phys. D: Appl. Phys.* **36**:167-185. [2] J.M. Perez, L. Josephson, T.O'Loughlin et al. (2002) *Nature Biotechnology* **20:**816-820. [3] E.P. Naiden, V.A. Zhuravlev, V.I. Itin et al. (2008) *J. Physic of solid body*, **50**: 857-863 (in Russia).

**ACKNOWLEDGEMENTS:** This research was supported by RFBR (grant 06-04-96962, grant 07-04-12170, grant 09-04-99114).

European Cells and Materials Vol. 20. Suppl. 3, 2010 (page 202) ISSN 1473-2262

# Antibacterial Activity of Tigecycline Micro/Nanoparticles under Supercritical Fluids Conditions

L.Pinheiro[1], A.Matos[1], J.Crespo[1], L.Padrela[2], MA.Rodrigues[2], HA.Matos[2], M.Castro[1], A.Durte[1], AJ.Almeida[1], A.Bettencourt[1]

*[1] iMed.UL-Research Institute for Medicines and Pharmaceutical Sciences, Faculty of Pharmacy, University of Lisbon, Av. Prof. Gama Pinto, 1649-003, Lisboa, Portugal. [2] Dep. Chemical and Biological Engineering, Instituto Superior Técnico, Av. Rovisco Pais, 1049-001, Lisboa, Portugal.*

**INTRODUCTION:** Challenges associated with the production of micro/nanoparticles with narrow size distributions for drug delivery can be addressed using supercritical fluids (SCFs) [1,2]. The most common SCF used in pharmaceutical applications is carbon dioxide ($CO_2$) due to its low critical properties and minimal toxicity. Clinicians and hospital infection control always faced the rapid increasing resistance in nosocomial pathogens. Tigecycline, a member of a new class of broad-spectrum antibacterials, the glycylcyclines, overcomes the two major mechanisms of tetracycline resistance (ribosomal protection and efflux pumps). *In vitro*, tigecycline demonstrates activity against a wide range of resistant bacteria, implicated in complicated skin, abdominal and bone tissue infections [3]. The processing of a nano drug delivery system based on tigecycline has been described by Ignjatovic *et al.* [4]. Taking into consideration the possibility of a tigecycline micro/nanoparticulate system production by SCF methodologies, we report the impact of supercritical conditions on this antibiotic antibacterial activity.

**METHODS:** Tigecycline particles were produced by Supercritical Enhanced Atomization (SEA) technique using intense shear atomization by liquid jet dispersion with the assisting supercritical carbon dioxide (SC-$CO_2$), after the antibiotic dissolution in a mixture composed of 50% water and 50% ethanol. This solution was pumped through a coaxial nozzle (allowing the mixing with the compressed SC-$CO_2$) before depressurization into a precipitator vessel. A nozzle setup with a centered orifice of 150 μm diameter was used. Droplets formed during spray atomization were dried inside a temperature controlled precipitator near atmospheric pressure (0.4 MPa) and 323 K. SC-$CO_2$ flow rate was 17 g/min. The $CO_2$ was compressed to an atomization pressure of 8 MPa. The particles were collected from the precipitator walls and from a cyclone. Particle size and surface morphology analysis were performed by scanning electron microscopy (SEM). Particle size distributions were obtained by analysis of SEM images using the Sigma Scan software. Antibacterial activity of tigecycline micro/nanoparticles was evaluated using the Mueller-Hinton agar diffusion method against a collection of

reference antibiotic-susceptible isolates *Escherichia coli* ATCC 25922, *Pseudomonas aeruginosa* ATCC, *Staphylococcus aureus* ATCC 25923 and resistant clinical isolates, namely *Klebsiella pneumoniae* (producing CTX-M-15 beta lactamase), *P. aeruginosa* (producing a metallo beta lactamase IMP-5), *E. coli* (with a class 1 integron carrying the *bla*CTX-M-9 gene), *Acinetobacter baumannii* (the European clone II producing an oxacillinase OXA-40) and methicillin resistant *S. aureus* (MRSA). For each bacterial culture (inoculum size 2 to $3\times10^5$ cells/mL), standard 6 mm paper discs were placed on the surface of the nutrient in Petri plates and 15 μL of a tigecycline stock solution was added. Plates were incubated under anaerobic conditions for 24h at 37 ºC, followed by measuring the diameters of the inhibition zones.

**RESULTS:** Tigecycline micro/nanoparticles were successfully evaluated for the antibiotic antimicrobial activity against all the reference and multidrug resistant isolates analysed. Supercritical conditions do not modified the microbiological stability.

**DISCUSSION & CONCLUSIONS:** The maintenance of the tigecycline bioactivity is a key-step for controlling the efficiency in microbiological terms of the SEA technology. The SCF methodology employed in the production of tigecycline particles proved to be feasible in terms of the impact of supercritical conditions on the antibiotic antibacterial activity.

**REFERENCES:** [1] M.A. Rodrigues, J. Li, L. Padrela et al (2009) *J Supercrit Fluids* **48**:253-60. [2] E. Reverchon, R. Adami, S. Cardea et al (2009) *J Supercrit Fluids* **47**:484-92. [3] P.J. Peterson, A. Ruzin, M. Tuckman, et al (2010) *Diagn Microbiol Infect Dis* **52**:195-201. [4] N.L. Ignjatovic, P. Ninkov, R. Sabetrasekh, et al (2010) *J Mater Sci Mater Med* **21**:231-39.

European Cells and Materials Vol. 20. Suppl. 3, 2010 (page 203) ISSN 1473-2262

# Thermal characterization of Hap/TCP bioceramics with variable phase ratio

L. Pluduma, K. Salma, L. Berzina-Cimdina

*Riga Technical University, Riga Biomaterials Research and Development Centre, Riga, Latvia.*

**INTRODUCTION:** Biphasic calcium phosphate (BCP) bioceramics belong to a group of bone substitute biomaterials that consist of a mixture of hydroxyapatite (HAp), $Ca_{10}(PO_4)_6(OH)_2$), and beta-tricalcium phosphate (β-TCP), $Ca_3(PO_4)_2$ [1]. BCP is obtained when a synthetic calcium-deficient apatite (CDA) is sintered at temperature above 700°C. The Ca-deficiency depends on the method of preparation of HAp including technological parameters such as synthesis pH and temperature [2]. HAp/β-TCP ratio determines the reactivity of BCP bioceramics (as the extent of dissolution in body fluid) [3]. Dissolution of HAp after implantation is too low to achieve the optimal results, but the dissolution rate of β-TCP ceramics is too fast for bone bonding [4].

The aim of this study was to investigate the influence of pH of synthesis media on the degree of Ca-deficiency of powders and characterized the thermal behaviour of HAp/β-TCP bioceramic samples.

**METHODS:** The powders were prepared by wet chemical precipitation method using neutralization reaction between $Ca(OH)_2$ and $H_3PO_4$. Temperature of the suspension during synthesis was maintained constant (45°C). The ending pH value of the suspension was stabilized in the range of 5-7 for 1 h. The suspension was aged for 20 hours at ambient temperature to complete reaction. After aging suspension was filtered; precipitate was dried at 105°C and ground in a mortar. Fourier-transform infrared spectroscopy (FTIR), X-ray diffraction (XRD), field emission scanning electron microscopy (SEM) and differential thermal analysis (DTA) were used to characterize synthesized and calcinated (1000-1300°C) powders.

**RESULTS:** XRD patterns revealed that as-dried powders were poorly crystallized CDAs. After thermal treatment at 1000°C, β-TCP was observed along with HAp. The relative intensity ratios of the HAp/TCP after powders heat treatment at 1000°C were found out with XRD using the semi-quantitative method. Depending on the ending pH of synthesis suspension HAp/TCP ratios were 80/20, 60/40, 40/60 and 20/80. DTA analysis (Fig. 1) shows an endothermic peak from 50 to 200°C that is due to evaporation of physically adsorbed water. The presence of $HPO_4$ group is evident in FTIR spectrum. This indicates CDAs as synthesis product. DTA curve shows that $HPO_4$ decomposes into calcium pyrophosphate at about 340°C. CDA transforms into mixture of two phases (HAp and β-TCP) at 780°C. HAp and β-TCP phases both decompose above 1400°C.

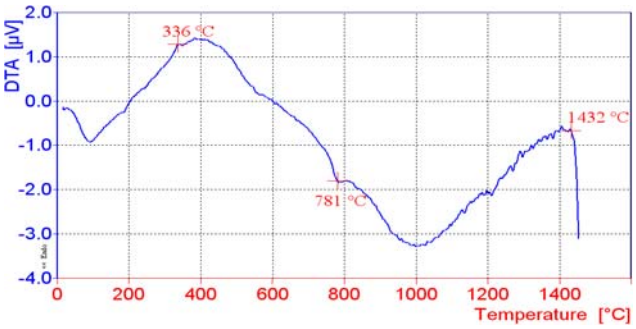


*Fig. 1: DTA curve of BCP with HAp/β-TCP ratio 20/80.*

**DISCUSSION & CONCLUSIONS:** Phase ratio of BCP ceramics depends strongly on the ending pH value of synthesis suspension. Thermal analysis is important characterization method of BCP to investigate transformation and decomposition of CDAs that characterizes thermal stability of bioceramic samples. CDAs transformation temperature depends on ratio of HAp and β-TCP phases in the sample. Transformation temperature indicates a start of sintering process. Bioactivity of BCP depends on sintering temperature that also affects microstructure of bioceramics.

**REFERENCES:** [1] R.Z. LeGeros, S. Lin, et.al. (2003) *J.Mater.Sci.- Mater.Med.* **14**: 201-209. [2] J. Marchi, P. Greil, et.al. (2009) *Int. Appl. Ceram. Technol.* **6** (1): 60-71.[3] G. Daculsi, O. Laboux, et.al. (2003) *J.Mater.Sci.-Mater.Med.* **14**: 195-200.[4] S.H. Kwon, Y.K. Jun, et.al. (2003) *J.Eur.Ceram.Soc.* **23**: 1039-1045.

**ACKNOWLEDGEMENTS:** This work has been supported by the European Social Fund within the project "Multidisciplinary Research in Biomaterials Technology of New Scientist Group",No.2009/0199/1DP/1.1.1.2.0/09/APIA/VIAA/090, (PVS ID 1380).

This work has been partly supported by the European Social Fund within the project "Support for the implementation of doctoral studies at Riga Technical University".

European Cells and Materials Vol. 20. Suppl. 3, 2010 (page 204) ISSN 1473-2262

# Electroanalysis of oseltamivir phosphate using new microsensors based on nanostructured materials

S.-F.Pop 1, R.I. Stefan-van Staden[2], R.-M. Ion[1], J.F. van Staden[2], H.Y. Aboul-Enein

[1]*Valahia University, Targoviste, 18-20 Blvd. Unirii., Targoviste, Romania*

[2]*Laboratory of Electrochemistry and PATLAB Bucharest, National Institute of Research for Electrochemistry and Condensed Matter, 202 Splaiul Independentei Str., 060021, Bucharest, Romania*

**INTRODUCTION:** Oseltamivir phosphate manufactured under the trade name Tamiflu as an ester-type prodrug of the neuraminidase inhibitor (oseltamivir carboxylate), has been developed for the treatment of A and B strains of the influenza virus. This compound is a neuraminidase inhibitor, which mimics the natural sialic acid substrate and binds to the active site, preventing the viral neuraminidase protein from cleaving host-cell receptors, thereby interfering with the release of new virus particles from infected cells. The free base and Zn complex of tetranaphthaloporphyrin possess a strong Q absorption band above 700 nm, a desired property for biological photosensitization. Intersystem crossing to the excited triplet level is efficient and the quantum yield of singlet oxygen production approaches 0.6 in some solvents. The microelectrodes based on metal-porphyrins are well known for their catalytic activity. Their reliable construction will favorize the reliability of the analytical information. Two porphyrins were proposed for the design of diamond and carbon paste based electrodes: zinc-tetranaphthaloporphyrin (ZnTNP) and zinc-5,10,15,20-tetra(4-sulfophenyl)porphyrin (ZnTSPP).[1-2]

**METHODS:** The technique used for direct voltammetric assay was differential pulse voltammetry (DPV) with an applied pulse potential of 25 mV/sec. vs. Ag/AgCl. The modified carbon or diamond paste microelectrode, together with the reference and counter electrodes were dipped into the cell containing the buffered analyte. The peak heights were measured at the following potentials: 830 and -680mV for ZnTNP based diamond (I) and carbon (II) paste electrodes, and 398 and -643mV for ZnTSPP based diamond (III) and carbon paste electrodes (IV).

**RESULTS:** The microsensors proposed for the assay of oseltamivir phosphate were characterized using DPV at the potentials mentioned in the section related with methods. Their sensitivities were: 0.844mA/mol/L (I), 27.8mA/mol/L (II), 36.0mA/mol/L (III), and 67.0mA/mol/L (IV). The working concentration ranges were: $10^{-11}$ – $10^{-7}$mol/L (I), $10^{-9}$ – $10^{-7}$ mol/L (II), $10^{-10}$ – $10^{-8}$ mol/L (III), and $10^{-9}$ –$10^{-7}$ mol/L (IV). The limits of detection are lower than $10^{-9}$mol/L. The response of the microsensors was stable for more than 3 months. A RSD less than 1.0% was recorded during this time. The proposed electrodes covered a large range of concentration with good sensitivities and limits of detection.

**DISCUSSION & CONCLUSIONS:** The proposed microsensors were reliable for more than 3 months when used for the assay of oseltamivir phosphate. Their utilization for the determination of tamiflu in its pharmaceutical compounds simplified the analysis, because the tablet was dissolved in water, buffered and measured using the proposed method.

The design of the microsensors is simple and reliable. Their sensitivities are very good, the best being recorded when ZnTSPP incorporated in carbon paste (IV) was used for microsensor design.

**REFERENCES:** [1] Pop S.-F., Ion R.-M., Neagu M., Constantin C. (2010) *Journal of Materials Science and Engineering USA* **4:**16-21. [2] Pop S.-F., Ion R.-M., *Issue Materials, Methods & Technologies*, (2010) **4**: 112-120.

**ACKNOWLEDGEMENTS:** The authors thank to the Romanian National Programme PN II, Contract Nr. D1 1055/2007, PORFSENS and POSDRU/6/1.5/S/23.

European Cells and Materials Vol. 20. Suppl. 3, 2010 (page 205) ISSN 1473-2262

# Measurement of the changes in the shape and permeability of tethered liposome layers under challenge from an antimicrobial peptide

J. Popplewell[1], M.J. Swann[1], and M. Brändén[2]

[1]*Farfield Group, Farfield House, Southmere Court, Electra Way, Crewe Business Park, Crewe, Cheshire, CW1 6GU, United Kingdom*

[2]*Layerlab, Stena Center 1B, S-412 92 Göteborg, Sweden.*

**INTRODUCTION:** Here for the first time we report simultaneously the changes in shape, permeability and density of a layer of liposomes at a range of applied melittin concentrations. Using the ability of dual polarisation interferometry (DPI) to deconvolute changes in mass at the solid liquid interface into changes in thickness and density, we are able to directly measure the assembly of a layer of tethered liposomes, then report changes to the liposome layer, both in terms of shape and permeability as melittin is added at decreasing lipid:peptide ratios. By directly recording the changes in the liposome parameters as melittin is bound, including the point at which the liposomes became permeable, we are able to directly assign each stage of the mass binding profile to a stage in the multiphasic process of melittin binding, and thus deliver additional mechanistic insight into the process by which antimicrobial peptides disrupt membranes.

**METHODS:** Liposomes of DLPC were formed by extrusion through 50nm pore membranes. These were tethered in a relatively unconstrained way to an optical waveguide sensor surface using a Neutravidin/DNA oligomer tag coupling method[1]. Responses of the liposomes to a range of increasing concentration melittin challenges were monitored using DPI.

**RESULTS:** We observe that at high lipid:peptide ratios (~ 100:1) pores are formed, with a change in the density of the liposome layer but with no change in the radius. At decreased lipid:peptide ratios (~25:1) the liposomes increase in diameter by about 3-4 nm, with little further change in permeability. Then at lower lipid:peptide ratios (<10:1) we observe a rapid, biphasic binding step, shown to include a rapid increase in liposome radius, before wholesale destabilisation of the liposome layer, this is shown in Figure 1. The ability of Dual Polarisation Interferometry to add liposomal structural information to the characteristic biphasic mass change reported by a number of Surface Plasmon Resonsnce based publications makes it considerably easier to convincingly assign the different stages of mass signal to the multiphasic process of peptide induced lysis.

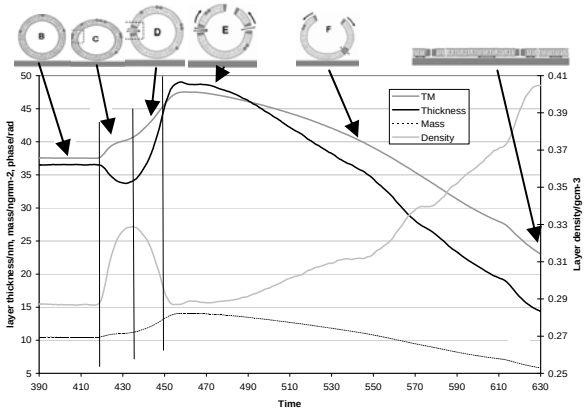


*Fig. 1: Effect of melittin at elevated concentration on a layer of DLPC liposomes.*

**DISCUSSION & CONCLUSIONS:** The additional insight into the mechanism of antimicrobials afforded by DPI, namely the ability to assign each step of the binding signal to a step in the disruption mechanism, DPI and tethered liposome layers offer a powerful route to studying the efficacy of the next generation of antimicrobial candidates.

**REFERENCES: 1,** *ChemPhysChem* Volume **9** Issue 17, Pages 2480 - 2485

**ACKNOWLEDGEMENTS:** The authors would like to acknowledge the EU Framework 7 fund project ASMENA # 214666

European Cells and Materials Vol. 20. Suppl. 3, 2010 (page 206) ISSN 1473-2262

# Building a model 3D immunosensor on gold nanoparticle monolayers

S. Boujday, A.L. Morel and C.M. Pradier
Université Pierre et Marie Curie- Paris 6, UMR CNRS 7197, Laboratoire de Réactivité de Surface, F75005 Paris, France

**INTRODUCTION:** The sensitivity of immunosensors may be significantly improved by building gold nanoparticles (AuNPs) ordered layers on which the IgG receptors are immobilised; both for geometric reason and thanks to the sensitivity of some optical detection techniques, a significant enhancement of the sensor sensitivity is expected on such 3D layers. The challenge is to build an ordered layer of optimal size nanoparticles, and of doing the right chemistry to functionalise them.
Here we built such gold Np layers and evaluated the increase of the number of receptors and of their accessibility brought by such a construction.
**METHODS:** Planar gold chips have been functionalised by amine-terminated self assembled monolayer (SAMs) on which gold NP of 15 or 60 nm diameter were immobilised. Two routes were explored: in a 1st series of experiments, they were grafted right after their synthesis, followed by their functionalisation ; the latter consisted in a covalent binding of protein A to an acid-terminated thiol layer (PrA allows the grafting of antibodies in a well oriented manner); in a second set of experiments, gold Nps were functionalised before their grafting.
The synthesis and deposition of gold nanoparticles, 15 and 60 nm size, were characterised by combining Polarisation Modulation InfraRed Reflexion Absorption Spectroscopy (PM-IRRAS), Photo electron Spectroscopy (XPS) and Surface Enhanced Raman Scattering (SERS), as well as Atomic Force Microscopy (AFM), which all proved the formation of a well dispersed layers of nanoparticles, but with significantly different coverages. The elaboration and bioactivity of the so-built 3D immunosensors were monitored by PM-IRRAS [1], a technique that, in the present case, strictly measures the number of immobilised probes or target molecules, without any optical or electrical enhancement effect.

**RESULTS and DISCUSSION**: Compared to PrA and rIgG immobilised on planar gold samples, the construction of 3D immunosensors increases the number of PrA by a factor of 2 on 60 nm AuNPs, but almost no incresa was observed on 15nm AuNPs. The latter result is explained by the little increase of the available gold area. However, the number of IgG probes was increased whatever the AuNPs size, likely thanks to a decrease of the PrA layer rigidity; overall, the anti-rIgG/rIgG ratio, stating the probe accessibility, was increased by a factor 2 on the larger nanoparticles. The important result is that nanoparticles of 60 nm are preferable for the following reason: they enable to build a denser and well dispersed layer and they increase both the number of receptors (IgGs) and their accessibility.
In the case of gold Np functionalisation in the liquid phase, before immobilisation, similar interesting improvements were observed but with the adventitious formation of AuNPs aggregates on the surface.
**CONCLUSIONS:** This work demonstrates the key role of the number, and of the accessibility of the molecular receptors, which both may be improved by building immunosensors on gold nanoparticles, and choosing the optimal functionalisation method.
Measurements are currently done to test the sensitivity of the anti rIgG detection by Surface Plasmon Resonance on these 3D immunosensors.

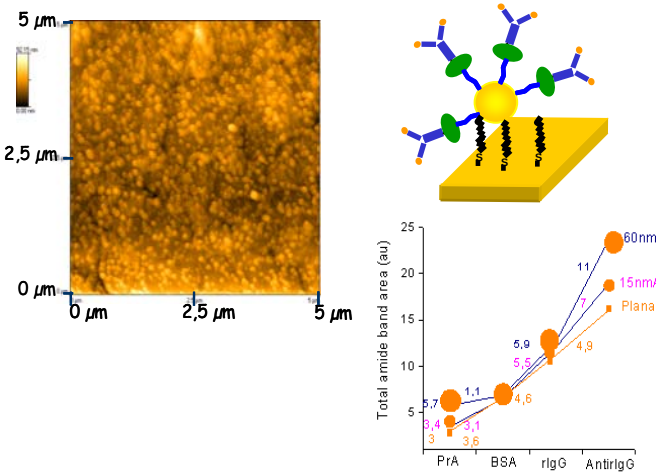


*Fig. 1: A well dispersed layer of 15 nm size gold nanoparticles (left); the scheme of a 3D immunosensor and, amount of grafted proteins, at the successive steps of immunosensor elaboration, on the planar gold , and on 15 and 60nm Np immunosensors.*

**REFERENCES:** [1]S. Boujday, C. Gu, M. Girardot, M. Salmain, and, C.M. Pradier, Talanta, 78, 2009, 165-170. S. Boujday, A-L Morel and C.M. Pradier, Coll. and Surfaces B, 2010, 81, 304-312

European Cells and Materials Vol. 20. Suppl. 3, 2010 (page 207) ISSN 1473-2262

# Biomedical Functionalization of Magnetic Nanoparticles and their uptake into T lymphocytes

E.-M. Prinz [1], E. Eggers [2], H.-H. Lee [3], U. Steinfeld [3], R. Hempelmann [1]

*[1] Universität des Saarlandes, Physikalische Chemie, Saarbrücken, Germany. [2] KIST–Europe Forschungsgesellschaft gem. GmbH, Saarbrücken, Germany. [3] URSAPHARM Arzneimittel GmbH, Saarbrücken, Germany.*

**INTRODUCTION:** The aim of this project is the magnetically controlled drug-positioning of drug loaded magnetic nanoparticles (NPs) in T lymphocytes and a magnetically controlled drug release. These drug loaded NPs are intended for the use in an adoptive cancer immunotherapy. This is a new approach where immune cells will be used as an autonomous highly target specific drug delivery systems. Due to its auto-fluorescence Doxorubicin (Dox) is used as a model chemotherapeutic drug.

**METHODS:** Magnetic NPs with the chemical composition $Mn_{0,8}Zn_{0,2}Fe_2O_4$ (crystallite size is between 10-15nm) are synthesized by the co-precipitation method.[1] The thus synthesized NPs are functionalized with dextran which can be activated via carboxymethyl or aldehyde groups. Carboxymethyl dextran (CMD) is synthesized by esterification of dextran with monochloro acetic acid and polyaldehyde dextran PAD is synthesized by oxidation of the hydroxyl groups via sodium periodate. The attachment of the drug to the CMD coated magnetic NPs leads to an acid amide bond. The bonding of the drug to PAD-NPs is done by reductive amination and leads to an amino bond.

Characterisation of the uncoated, coated and drug loaded NPs is done by X-ray diffraction (XRD), transmission electron microscopy (TEM), dynamic light scattering (DLS), FT-IR-, UV/VIS-, Raman- and fluorescence spectroscopy. The uptake efficiency of these NPs into T cells is investigated by TEM, fluorescence and convocal microscopy and by fluorescence activated cell sorting (FACS).

**RESULTS:** *Fig. 1* shows the fluorescence microscopy pictures of Dox-PAD and Dox-CMD loaded NPs in T cells. The pictures (middle & right) show the red fluorescence in the area or the nucleus of the Dox-CMD-NPs loaded T cells. The nucleus of the Dox-PAD-NPs loaded lymphocytes (left) doesn't show this fluorescence. The uptake of the Dox-CMD-NPs into T cells was successful. The drug intercalates into the DNA of the cell. The Doxorubicin of the Dox-PAD coated particles could not be detected. At present it is not clear whether the NPs are taken up into the nucleus or are just adsorbed on the cell surface.

Another suitable explanation is that Dox-PAD coated NPs are more stable then Dox-CMD coated NPs. Therefore the Doxorubicin could not be removed and doesn't intercalate into the DNA.

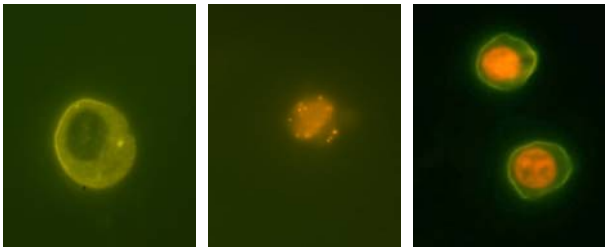

*Fig. 1: Fluorescence microscopy of Dox-CMD (middle & right) and Dox-PAD (left) loaded NPs in T cells, T cells marked with CD45-FITC and incubated with 20 µg/mL drug loaded NPs for about 20 h at 37°C.*

**DISCUSSION & CONCLUSIONS:** We have shown two different ways of bonding the drug to the particles. In the first way the drug bonds to the carboxyl groups of CMD-coated nanoparticles and the other method leads to an amino bond between PAD coated NPs and the drug. It has been shown that the drug loaded NPs are internalized by the cells via TEM- and fluorescence microscopy measurements. TEM pictures of the uptake behaviour of drug functionalized NPs by T cells have demonstrated that both functionalized NPs are taken up by the cells and clustered in membrane surrounded cellular structure.

We also have found different ways of bonding the drug via its keto group to dextran derivates.[2] The measurements for the uptake of these synthesized particles into T cells are still running. Another study is the encapsulation of the drug for a better survival rate of the T lymphocytes.

**REFERENCES:** [1] E. Auzans, D. Zins, E. Blums, R. Massart, *Journal of Materials Science* **1999**, *34*, 1253, [2] E.-M. Prinz *et al* 2010 *J. Phys.: Conf. Ser.* **200** 122009.

**ACKNOWLEDGEMENTS:** We gratefully acknowledge financial support by DFG.

European Cells and Materials Vol. 20. Suppl. 3, 2010 (page 208) ISSN 1473-2262

# Understanding Cooperative Protein Adsorption Events: A Comparison between experiment and Monte Carlo Simulations

M. Rabe*, D. Verdes, S. Seeger

*Universtät Zürich,Physikalisch-Chemisches Institut,*

*Winterthurestrasse 190, Zürich, Switzerland*

**INTRODUCTION:** Cooperative effects have been found to play a major role in protein adsorption events. Unraveling the molecular details behind these effects is of great importance to understand the processes that regulate the activity and function of biological interfaces. In this work, we investigate the microscopic events behind cooperative protein adsorption by means of Monte-Carlo (MC) simulation and scanning fluorescence microscopy.

**METHODS:** To achieve an accurate description of the experimentally kinetics we proposed two independent adsorption pathways[1]. First, there is a non-cooperative adsorption pathway that takes place on empty surface regions. The second pathway describes the cooperative adsorption through a tracking of a protein to the nearest available binding site. A major limit of presenting the cooperative adsorption through rate equations consists of the meaning of the so called parameter α. As it is connected with the coverage level at which the lateral tracking of adsorbing proteins to an available binding site in the vicinity breaks down, α can be considered as an abstract measure for the maximum allowed lateral tracking distance, $r_{coop}$. The correlation between this macroscopically measurable parameter α and the real tracking distance $r_{coop}$ can only be obtained through the microscopic MC simulation. As schematically illustrated in Figure 1 the simulation gives access to the adsorption kinetics and to scan images which both can be compared to experimental data.

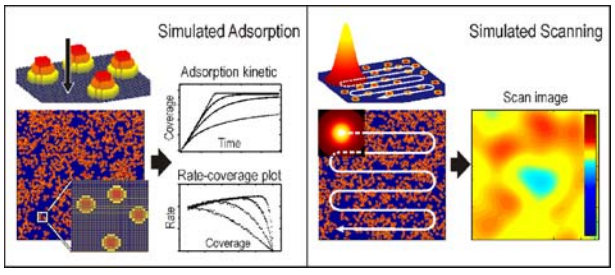


*Fig. 1: Overview of the Monte-Carlo simulation. Adsorption kinetics (left) and scan images (right) are simulated and compared with experimental data.*

**RESULTS:** The implemented algorithm represents our proposed mechanism of cooperative adsorption[2] whose key feature is that a protein approaching the surface in an occupied region is not necessarily rejected like in the classical Langmuir-type adsorption model. Instead, the protein is tracked to the nearest binding site guided by the local electrostatic field arising from the pre-adsorbed charged proteins and the surface. To quantify the correlation between the length of the cooperative radius $r_{coop}$ and the parameter α, the influence of the former on the resulting adsorption kinetics has to be explored. Using experimentally obtained rate constants as input parameters, we are able to correlate macroscopic observations, such as the characteristic adsorption kinetics, with the microscopic tracking distance $r_{coop}$. The simulations reveal why cooperative adsorption leads to inhomogeneous protein density distributions observed experimentally. It is found that the tracking distance may be up to 2.5 times the protein's diameter.

**DISCUSSION & CONCLUSIONS:** From the simulation data we extracted information with regard to the adsorption kinetics and to the self-organization of adsorbed proteins. Since the present study provides a correlation between the parameter α and the tracking distance $r_{coop}$ a microscopic interpretation of experimental data is now possible. Apart from the adsorption kinetics we also explored the self-organization behavior of proteins from a microscopic point of view. It was found that the random adsorption of proteins on a surface causes minute density fluctuations which, under cooperative conditions, evolve into persistent density differences after adsorption. Due to the agreement between macroscopic observations with the simulation we consider this study to highlight the validity of relating cooperative adsorption to the proposed tracking mechanism which has not been formulated in such a straightforward manner before.

**REFERENCES:** [1]M. Rabe, D. Verdes, J. Zimmerman, S. Seeger (2008) *J Phys. Chem. B* **112**: 13971-80, [2]M. Rabe, D. Verdes, S. Seeger (2010) *J Phys. Chem. B,* accepted.

European Cells and Materials Vol. 20. Suppl. 3, 2010 (page 209) ISSN 1473-2262

# Biosilicification studies using amino acids in ionic liquid [BMIM-$BF_4$]

R.Ramanathan[1], S.K.Bhargava[1], V.Bansal[1]

[1] *School of Applied Sciences, RMIT University, Melbourne, Australia.*

**INTRODUCTION:** Biosilicification process in living organisms (e.g. diatoms, plants, etc) proceeds under mild conditions resulting in complex hierarchal structures. In aquatic organisms, the process is believed to be triggered by cationic proteins such as silicateins and polycationic peptides like silaffins that act as a template/scaffold/catalyst for silica synthesis [1-3]. Although significant understanding has been gained from molecular biology on the process of biosilicification, little is known explaining the formation of 3D ornate silica superstructures in nature. Notably, most aforementioned studies were explored in aqueous solvents that do not necessarily mimic natural silicification environment. Ionic liquids (ILs) have recently attracted significant attention as 'green' solvents for synthesis of nanomaterials due to their unique physio-chemical properties [4]. Nonetheless, it is noteworthy that the potential of ILs have not yet been explored to study biosilicification process. We envisage that replacing conventional solvents with ILs might provide certain degree of control over the self-organization process due to interesting properties of ILs such as high viscosity and high ionic strength that can significantly influence the biosilicification process.

In this study, we have explored the potential of IL 1-butyl-3-methylimidazolium-tetrafluoroborate [BMIM-$BF_4$] towards understanding the formation of unique silica superstructures with diatom like morphology using amino acids as catalysts.

**METHODS:** Varying concentrations of 20 different amino acids were added to IL [BMIM] [$BF_4$] containing 1 mM of silica precursor (TEOS) and reaction was allowed to continue for 16 h at 25±0.1 °C under stationary conditions. Following the reaction, the reaction products were washed with acetonitrile to remove viscous IL, and analysed using SEM, XRD and XPS.

**RESULTS:** We demonstrate for the first time the formation of complex hierarchal silica structure formation in the presence of IL where silica precursor was hydrolysed by amino acids. Some representative SEM images confirmed the formation of complex silica morphologies while SAED provided information on the non crystalline nature of the synthesized particles that resemble structures formed in nature [3].

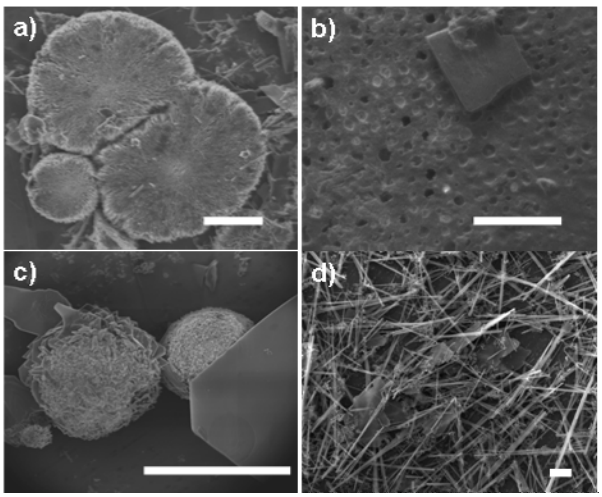


*Fig. 1: SEM images of silica structures synthesized using amino acids (a) lysine (b) arginine (c) histidine and (d) tryptophan. (Scale bars: 50 µm)*

**DISCUSSION & CONCLUSIONS:** As cationic proteins and peptides were responsible for silicification process, cationic amino acids were studied in detail for replication of biosilicification process under in vitro conditions. Concentration dependent studies suggest that controlled aggregation of amino acids acts as a template/scaffold for the formation of silica superstructures. A detailed study of the process using each amino acid, we propose a plausible mechanism for the formation of structures with exquisite morphologies. This provides significant enhancement in our understanding of diatom morphology enabling the replication of silica structures for applications in catalysis, sensing, and surface enhanced Raman scattering (SERS). As a representative case, only cationic amino acids and tryptophan mediated synthesis are shown in the above image. The formation of unique silica structures with close resemblance to diatoms found in nature using all amino acids will be shown during the oral presentation.

**REFERENCES:** [1] V. Bansal, A. Ahmad, M. Sastry (2006) J. Am. Chem. Soc. **128**: 14059-66. [2] V. Bansal, et al (2005) Adv. Mater. **17**: 889-92. [3] F.C. Meldrum, H. Cölfen (2008) *Chem. Rev.* **108**:4332-432. [4] H.J. Ryu, L. Sanchez, H.A. Keul, et al (2008) *Angew. Chem. Int. Ed.* **47**:7639-43.

**ACKNOWLEDGEMENTS:** R.R thanks DEEWR for Australian Postgraduate Award.

European Cells and Materials Vol. 20. Suppl. 3, 2010 (page 210) ISSN 1473-2262

# Sedimentation of Nanoparticles in *in vitro* Toxicity Assays

Hubert Rauscher, Francesca Broggi, Valentina Mariani, Jessica Ponti, François Rossi

*European Commission Joint Research Centre, 21027 Ispra (VA), Italy.*

**INTRODUCTION:** Nanoparticle toxicity assessments face specific challenges because nanoparticles settle, agglomerate and diffuse in liquid media, depending for example on particle size, shape, surface chemistry, and media viscosity. For reliable toxicity assays it is therefore necessary to assess the influence of nanoparticle-specific properties. In this contribution we specifically analyse particle sedimentation and its influence on the effective cellular dose relevant for *in vitro* assays.

**METHODS:** Cobalt ferrite ($CoFe_2O_4$) nanoparticles of different dimensions (reference P601 and P703) were provided by Colorobbia Italia s.p.a. UV-VIS measurements were used to characterize particle sedimentation in cell culture medium without phenol-red. Cyclic UV-VIS spectra were recorded every 30 min, for up to 72 h.

**RESULTS:** We consider the sedimentation of nanoparticles in a liquid column under a gravitational field and assume that the particles move at their terminal velocity in z-direction and that the particle concentration $c$ is a function of $z$ only. The concentration of such particles can be described by the following partial differential equation:

$$\frac{\partial c}{\partial t} = D\frac{\partial^2 c}{\partial z^2} - B\frac{\partial c}{\partial z} \quad . \qquad (1)$$

D is the diffusion coefficient and $B = \frac{2g\delta r^2}{9\eta}$, where δ is the density of the particles minus the density of the liquid, r is the particle radius and n is the liquid viscosity.[1] Assuming an initially homogeneous particle concentration and considering that the particles move at low speed without convection and little turbulence, the analytical solution of equation (1) can be used to calculate the concentration of nanoparticles at any position of the column as a function of time.

Depending on their size and mass particles accumulate with time at the bottom of the liquid column. We show that the sedimentation of $CoFe_2O_4$ nanoparticles of different size, as measured by UV-VIS spectroscopy at different height positions in liquid medium, can be well described with this model. For experiments that use cells attached to the bottom of a culture dish,

e.g., in the colony forming efficiency assay, this can affect the effective dose reaching the cells. Hence, as a consequence of sedimentation the effective concentration of nanoparticles at cell cultures increases with time, and depends on the nature of the particles (size, material) and the specific experiment (type of Petri dish or well, height of the liquid column above the cells). The example in figure 1 shows that for $CoFe_2O_4$ particles the effective nanoparticle concentration $n$ at the bottom of a dish, i.e., at the location of the cells, depends sensitively on the size of the nanoparticles and the duration of the experiment ($n_0$ = initial concentration).

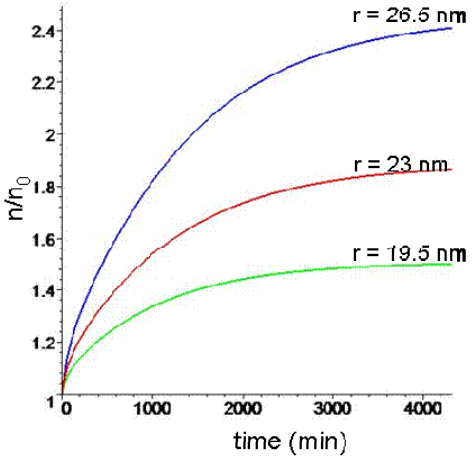


*Fig. 1: Accumulation of nanoparticles at the bottom of a Petri dish for different particle radii r as a function of time.*

**DISCUSSION & CONCLUSIONS:** For *in vitro* assays to study nanoparticle toxicity which use cells located at the bottom of a liquid column, sedimentation effects can considerably increase the nanoparticle concentration reaching the cells. As a consequence, if cell cultures are exposed on a time scale of days to the same nanoparticle-containing test medium, sedimentation effects should be considered in order to get a proper dose-effect relationship.

**REFERENCES:** [1]M. Mason, W. Weaver (1924) *Phys. Rev.* **23**: 412.

European Cells and Materials Vol. 20. Suppl. 3, 2010 (page 211) ISSN 1473-2262

# α- SYNUCLEIN AGGREGATION ON SUPPORTED LIPID BILAYERS

N.P. Reynolds[1]*, M. Rabe[1], D. Verdes[1], A. Soragni[2], E. Liverani[2], R. Riek[2], S. Seeger[1]

*[1]Institute of Physical Chemistry, The University of Zurich, Switzerland [2]Laboratory of Physical Chemistry, ETH Zurich, Switzerland.*

**INTRODUCTION:** α-synuclein (aS) is a small protein, consisting of 140 amino acids, and is expressed predominantly in neural tissues. Its physiological function is still not fully understood, however upon self-aggregation it forms large amyloid fibrillar structures known as Lewy Bodies (LB). The presence of LBs in the substantia nigra of patients is a hallmark pathological feature of Parkinson`s disease (PD). PD is a neurodegenerative disease which over time causes high levels of neuronal damage, severely impairing the motor functions of sufferers. The mechanisms by which LB, or more probably smaller pre-fibrillar aggregates, cause cell death are still largely unknown, but interactions between aS and the cell membrane are though to play an important role. In this work the interactions of WT aS, plus two mutant variants, with supported lipid bilayers (SLB) was studied by surface sensitive Förster resonance energy transfer (FRET).

**METHODS:** All imaging was performed using supercritical angle fluorescence (SAF) microscopy[1]. By employing a parabolic lens SAF collects only the fluorescence emitted above the angle of total internal reflection. The intensity of the emitted fluorescence decays exponentially with increasing distance from the surface; therefore fluorescence that does not arise from within ~ 200 nm from the surface is excluded. The SAF signal is further split into acceptor and donor channels allowing the measurement of surface sensitive FRET. Using donor labelled SLBs, together with aS labelled with spectrally overlapping acceptor fluorophores; it was possible to directly observe the energy transfer, and thereby interactions, between protein and SLB.

**RESULTS:** Aggregates of all 3 protein variants studied (WT, A53T and E57K), show energy transfer when adsorbed to SLBs. The extent of energy transfer was observed to follow the order E57K>A53T ≅WT. Surprisingly it was found that at the concentrations studied (100 – 400 nM) both the A53T and E57K mutants caused an increased concentration of lipids at the points of aggregate adsorption, as seen by an increase in fluorescence intensity in the donor channel. However, no such effect was observed for WT aS.

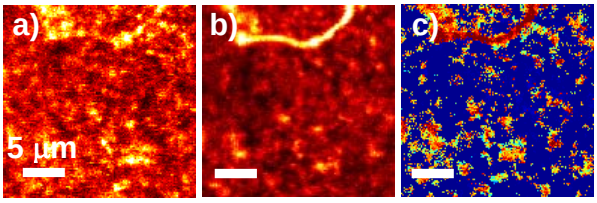


*Fig. 1: SAF microscopy images of aS fibrils adsorbed to SLBs. a) Donor channel, b) acceptor channel, c) FRET efficiencies from which transfer energy was determined.*

**DISCUSSION & CONCLUSIONS:** The observation of energy transfer from the SLB to aS aggregates indicates that upon adsorption aS clusters form close interactions with the lipid molecules in the bilayer. We postulate that the increased concentration of lipids at adsorption sites is due to lipid extraction from the bilayer which form a sheath around the aS aggregates, as previously observed with the amyloid forming protein IAPP[2]. This disruption of the integrity of the membrane may be a contributing factor to the permealisation of the cell membrane, a proposed neurodegenerative mechanism in PD[3]. No equivalent effect was seen for the WT protein in the same concentration range, however at higher concentrations (3 μM) extensive membrane damage was observed. This concentration dependence correlates with evidence showing that the onset of idiopathic PD is caused by a multiplication of the WT aS gene, resulting in an overproduction of the protein[4], whereas inherited PD caused by mutations to the aS shows no such gene multiplication. This work provides evidence that one mechanism of cell death in PD is via the adsorption of aS aggregates which disrupt the bilayer, resulting in the permealisation of the cell membrane.

**REFERENCES:** [1] Enderlein, J. *et. al.* (1998) *App. Opt.* **38**:724-732, Domanov, Y.A., Kinnunen, P.K.A. (2008) *J. Mol. Biol.* **376**:42-54 [3] Lashuel, H.A.D *et. al.* (2002) *Nature* **418**:291 [4] Singleton, A.B. (2003) *Science* **302**:841

European Cells and Materials Vol. 20. Suppl. 3, 2010 (page 212) ISSN 1473-2262

# Multiscale flow simulation of water past a fullerene

K. Ritos[1], E. M. Kotsalis[1], J. H. Walther[1,2],
Y. Ding[1], M. Praprotnik[1,3], P. Koumoutsakos[1]

*[1]Chair of Computational Science, ETH Zurich, Zurich, Switzerland, [2]Department of Mechanical Engineering, Technical University of Denmark, Lyngby, Denmark , [3]Laboratory for Molecular Modeling, National Institute of Chemistry, Ljubljana, Sloveni*

**INTRODUCTION:** We present a three-dimensional multiscale flow simulation of water past a buckyball. We employ the Schwarz alternating method to couple molecular dynamics of liquid water and the $C_{540}$ fullerene with the Lattice-Boltzmann (LB) description of the Navier- Stokes (NS) equations. Our approach allows for studying nanoscale flow phenomena that are out of scope of the pure atomistic simulation.

**METHODS:** The simulation model is shown schematically in Fig.1. We extend the Schwartz domain decomposition scheme [1] by a fully 3D atomistic-continuum coupling.

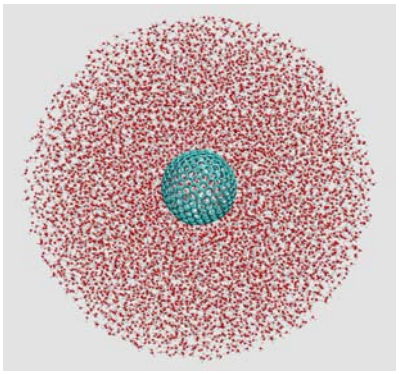

*Fig. 1: Cross section of the water molecules that surround the $C_{540}$ fullerene molecule.*

The computational domain is cubical. Lattice nodes are centered in corresponding cubical MD sampling cells of size α. The spherical MD domain provides the LB method with velocity boundary conditions (BCs). The MD domain has non-periodic force BCs in all three directions in order to maintain the correct mean virial pressure [2]. Furthermore, we use a specular boundary to impose the ideal kinetic part of the system pressure. Liquid water is modeled with the rigid SPC/E water model. The simulations are performed at T = 300K and ρ = 997kg/m$^3$. Force field parameters for the rigid $C_{540}$ fullerene molecule are taken from Refs.[3,4]. Long range electrostatic interactions are treated by the reaction field method with a cutoff of α. In order to correctly describe the hydrodynamics we employ in this study the linear momentum preserving Dissipative Particle Dynamics (DPD) thermostat.

**RESULTS:** The results from the multiscale simulations are compared with full MD reference simulations. In the inset of Fig.2 we monitor the evolution of the convergence rate. In the same figure we plot the x-component of the fluid velocity. In Fig.3 we present the tangential velocity radial profile, which shows that the slip velocity at the surface is not zero.

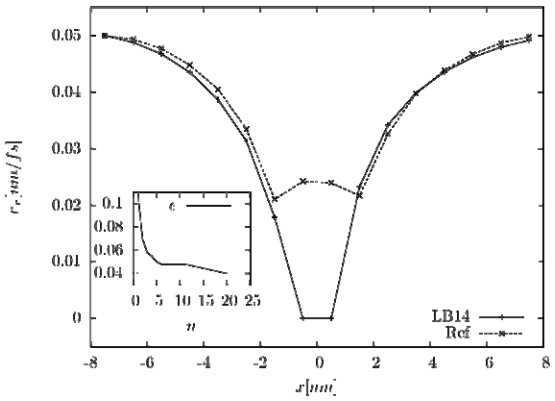


*Fig. 2: The x-component velocity. The inset shows the convergence of the hybrid toward the reference solution.*

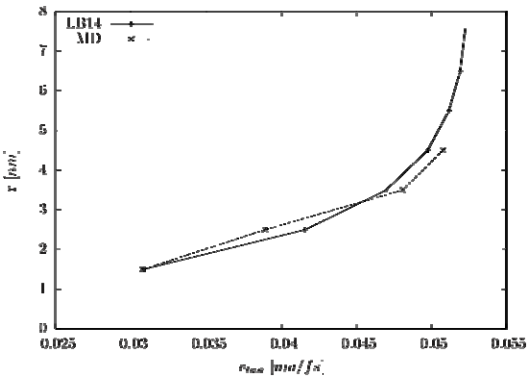


*Fig. 3: The tangential velocity profile in the radial direction from the fullerene.*

**REFERENCES:** [1] E.M. Kotsalis, J.H. Walther, and P. Koumoutsakos (2007) *Phys. Rev. E* **76**:016709. [2] T. Werder, J. H. Walther, R. L. Jaffe, T. Halicioglu, and P. Koumoutsakos (2003) *J. Phys. Chem. B* **107**:1345. [3]T. Werder, J. H. Walther, R. L. Jaffe, T. Halicioglu, and P. Koumoutsakos (2008) *J. Phys. Chem. B* **112**:14090.

European Cells and Materials Vol. 20. Suppl. 3, 2010 (page 213) ISSN 1473-2262

# Intracellular processing of proteins mediated by biodegradable polyelectrolyte capsules

Pilar Rivera Gil[1*], Stefaan De Koker[2], Bruno G. De Geest[3], and Wolfgang J. Parak[1]

*[1] Fachbereich Physik und Wissenschaftliches Zentrum für Materialwissenschaften (WZMW), Philipps Universität Marburg, Renthof 7, 35037 Marburg, Germany. [2] Department of Molecular Biomedical Research, Ghent University, Belgium. [3] Laboratory of Pharmaceutical Technology, Ghent University, 9000 Ghent, Belgium. * pilar.riveragil@physik.uni-marburg.de*

**INTRODUCTION:** Uptake and processing of capsules or particles by cells are important issues with regard to the transport of active agents into the cytoplasm. A recently introduced delivery concept of layer-by-layer assembly of thin planar films [1] or spherical geometries [2] of polyelectrolyte multilayer capsules has emerged as a universal carrier system in which cargo and additional functionalities can be introduced as well in the cavities and in the walls of the capsules [3] [4]. Polyelectrolyte multilayer microcapsules functionalized with nanoparticles are ingested spontaneously by cells [5] [6]. Polyelectrolyte microcapsules are deformed upon the incorporation process due to the mechanical stress caused in the intracellular space. Deformation was dependent on the structure of the capsule walls [7]. Despite deformation, capsules do not lose their cargo even upon compression inside cells. The capsules can be then filled with different bioactive molecules like drugs, antigens or genetic material for different purposes such as disease treatment, vaccination or gene delivery. For example, capsules filled with a pH-sensitive dye are taken up by cells and are able to deliver information about the local concentration of protons inside the cells. Thus, the results suggest that internalized capsules are trapped in acidic vesicles rather than free in the cytosol.

**RESULTS & DISCUSSION:** Polyelectrolyte capsules are made by layer-by-layer assembly of oppositely charged biological charged materials such as dextran and L-arginine, to obtain biocompatible and biodegradable hollow capsules. By encapsulation of DQ-Ovalbumine™, a fluorogenic substrate for proteases the degradation of the capsules can be spectroscopically controlled. After capsule uptake by living cells the walls of the capsules were actively degraded and digested by intracellular proteases. Upon capsule wall degradation intracellular proteases could reach the protein cargo in the cavity of the capsules. Enzymatic fragmentation of the self-quenched fluorescence-labeled protein by proteases led to individual fluorescence-labeled peptides and thus revoked self-quenching of the dye. In this way non-active (non-fluorescent) molecules were converted into active (fluorescent) molecules. The data demonstrate that biodegradable capsules are able to convert non-active molecules (pro-drugs) to active molecules (drugs) specifically only inside cells where appropriate enzymes are at hand. In this way only cargo inside the capsules reaching cells is activated, but not the one in capsules which are remaining extracellularly. The peptide fragments undergo further processing inside the cells, leading ultimately to exocytosis [8].

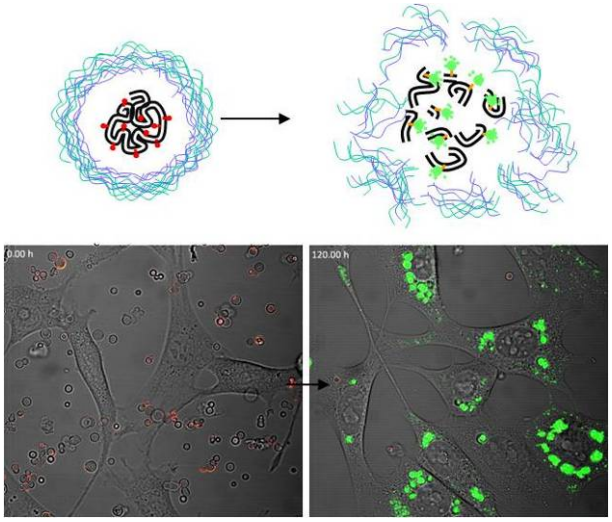


*Fig. 1: Intracellular processing of biodegradable capsules acctivates green fluorescence as model system for intracellular activation of a passive prodrug.*

**REFERENCES:**

[1] Decher, G. *Science*, 1997. **277**: p. 1232-1237. [2]Donath, E., et al., *Angewandte Chemie Int. Ed.*, 1998. **37**(16): p. 2202-2205. [3] De_Geest, et al. *Chemical Society Reviews*, 2007. **36**: p. 636-649. [4] Zebli, B., et al.. *Langmuir*, 2005. 21: p. 4262-4265. [5] Muñoz_Javier, A., et al. *SMALL*, 2006. 2(3): p. 394-400. [6] de_Geest, B.G., et al. *Advanced Materials*, 2006. **18**: p. 1005-1009. [7]Muñoz_Javier, A., et al. *Advanced Materials*, 2008. **20**(22): p. 4281-4287. [8] Rivera Gil, P., et al. *Nanoletters*, 2009.

European Cells and Materials Vol. 20. Suppl. 3, 2010 (page 214) ISSN 1473-2262

# Electrochemical analysis of peptide-functionalized titanium dental implant surfaces

D.Rodríguez[1,2,3], G.Vidal[1], P.Sevilla[2,3], F.J.Gil[2,3]

*1 E.U. Enginyeria Tècnica Industrial de Barcelona, Technical University Catalonia (EUETIB-UPC) C.Urgell,187, 08036-Barcelona (Spain), 2Centre de Recerca en nanoEnginyeria (CRnE), UPC, Barcelona (Spain), 3BiBiTE Group, ETSEIB-UPC, Barcelona (Spain).*

**INTRODUCTION:** The titanium surface of prostheses and implants is a prime target for modification in order to optimise osseointegration of medical devices to the bone. One of the most interesting approaches to this goal is the functionalization of titanium surfaces with peptides. Analysis of the presence, type of bonding or surface density of these peptides is not immediate. This study aims to detect changes in functionalized surfaces with electrochemical techniques, and compares the results with those acquired with much more complex and expensive techniques like XPS, contact angle or FTIR.

**METHODS:** **s**amples of grade 2 commercially pure titanium of 10mm diameter and 2mm width were cut from a bar with a diamond disk cutter, grinded and polished with $Al_2O_3$ particles up to roughness values of $R_a$~15nm and thoroughly cleaned.

Functionalization of the titanium disks followed this protocol: (1) Surface activation of clean titanium samples with oxygen plasma to create OH- groups on $TiO_2$ surface; (2) Immersion in a pentane solution with Diisopropylethylamine (DIEA) and APTES silane, during 1h at room temperature (Ti+APTES samples); (3) The GG**RGD**SGG peptide sequence (RGD: cell adhesion motive) [1], was used to functionalize the silanized titanium surfaces (Ti+APTES+RGD samples). Silanized samples were immersed in the peptide solution (4-Morpholineethanesulfonic acid (MES) buffer, pH 6.0, with EDC NHS) overnight at room temperature. Non-treated titanium samples (Ti samples) and RGD-peptide adsorbed titanium samples (Ti+RGD) were used as control. Replicas were made to allow statistical analysis of data.

Electrochemical characterization of the samples was made with a ParStat 2273 potentiostat (Princeton Applied Research) in a HBSS medium (Sigma-Aldrich) at 37ºC, with a KCl electrode as electrical potential reference and a graphite bar as counterelectrode. Tests included a free potential measurement, cyclic voltammetry and Electrochemical Impedance Spectroscopy (EIS) (range: 64kHz-2mHz, signal: 50mV). Samples were also characterised with XPS, contact angle measurements and FTIR-DR.

**RESULTS:** Results of XPS, contact angle and FTIR-DR confirm that the samples were silanised and functionalised as expected, detecting presence of silane and silane plus peptide, respectively, as shown for XPS in table 1 (presence of Si and N).

*Table 1: XPS measures of surface composition (at%).*

| | Ti | Ti+APTES | Ti+APTES+RGD | Ti+RGD |
|---|---|---|---|---|
| O1s | 43.0 | 43.6 | 44.1 | 39.9 |
| C1s | 36.8 | 34.7 | 28.3 | 38.5 |
| Ti2p | 18.2 | 14.6 | 16.8 | 16.5 |
| Si2p | 0.3 | 3.6 | 3.4 | n/a |
| N1s | 1.7 | 3.5 | 7.4 | 5.1 |

Measured values of free potential showed slight differences (Ti: 0.102V, Ti+APTES: -0.141V, Ti+APTES+RGD: -0.168V). Cyclic voltammetry showed significant differences in current intensity for the Ti+APTES+RGD samples (figure 1) compared to other samples. The different models generated with the EIS data, however, do not provide a significant distinction between functionalised samples and the rest of the samples (data not shown).

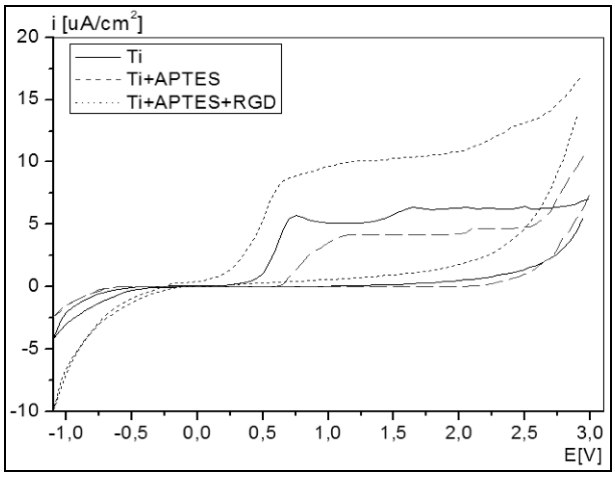


*Figure 1: Cyclic voltammetry of samples.*

**CONCLUSIONS:** the presence of silanes and peptides such as RGD sequences on the surface of titanium can be detected and studied with electrochemical measurements.

**REFERENCES:** [1]C. Chollet, C. Chanseau, M. Remy, et al (2009) *Biomaterials* **30**:711-20.

**ACKNOWLEDGEMENTS:** This study was funded by the Spanish Ministry of Sciences, project MAT 2008-06887-CO3.

European Cells and Materials Vol. 20. Suppl. 3, 2010 (page 215) ISSN 1473-2262

# A brief view into protein kinase A Iα activation process

O.N.Rogacheva

*Sechenov Institute of Evolutionary Physiology and Biochemistry RAS, St.Petersburg, Russia.*

**INTRODUCTION:** Catalytic (C) subunit of protein kinase A (PKA) Iα in its inactive state forms a complex with regulatory (R) subunit. A and B domains of R subunit make contacts with C subunit, however both domains remain capable of cAMP binding [1]. The conformational transition that connects cAMP binding with subunits dissociation remains unclear in spite of intensive study over the last few decades and its great importance in cell functioning and drug design. Here we tried to clarify this process using molecular dynamic (MD) simulations.

**METHODS:** A (G96 – E245) and B (G235 – S376) domains of R subunit were cut from 2QCS PDB structure and minimized. Then Targeted MD (TMD) simulations were performed with each domain in the absence of C subunit. Reference structures were prepared using 1NE6 PDB structure. Forces (elastic force constant was 2 kcal/mol/Å$^2$ per TMD atom) were applied to the backbone atoms of phosphate binding cassette (PBC) only (S197 – V213 for A domain and Y321 – V337 for B domain) or PBC and terminal B/C helices (D225 – E245 for A domain and D349 – S376 for B domain). All simulations lasted for 1-10 ns and were performed in water box using CHARMM27 force field and NAMD program.

**RESULTS:** cAMP-bound (hereafter called "closed") domains prove to be energetically more favorable than C-subunit bound ("open") ones. Moreover, PBCs of A and B domains (in the absence of C subunit) tend to become closed even in the absence of cAMP because closed PBC has α helix with 4 backbone H bonds, and open PBC has $3_{10}$ helix with 3 ones. **A domain:** In agreement with Rehman hypothesis [2] we demonstrated that transition of PBC from open to closed conformation caused B/C helix movement by means of tight hydrophobic contact between the side chains of L203 (PBC) and Y229 (B/C helix). This leads to N3A-motif (D119 – A150) displacement and induction of kink in the B/C helix (all sequential α helix backbone H-bonds from R230(C=O)-M234(N-H) to L233(C=O)-T237(N-H) are broken). Two H-bonds (the side chains of T237 and Y229, and the side chains of R241 and E200) fix newly formed kink. Conformational changes of A domain seem to occur even in the absence of agonist (certainly, when C subunit is removed). **B domain:** B domain behaves similarly to A domain at the beginning of conformational transition: the only force that causes B/C helix movement is the hydrophobic contact L327-F353. However at the latter stages B/C helix movement is mainly guided by formation of critical F374-adenine (cAMP) interaction and further replacement of it by final Y371-adenine contact. These interactions move B/C helix down on cAMP binding site. As a result bulky hydrophobic side chains of I363 and L364, which form hydrophobic contacts with I253 of N3A-motif (T237 – A268), cause N3A-motif displacement. This process is accompanied by kink formation in C helix of A domain (α helix backbone H-bonds K242(C=O)-E246(N-H) and M243(C=O)-F247(N-H) are broken). Our data let us assume that B/C helix "placing" on cAMP binding site and further structural changes are possible only in the presence of agonist.

**DISCUSSION & CONCLUSIONS:** According to our data free R subunit in solution consists of closed A domain combined with partially closed B one. In this structure W260 (which belongs to B domain N3A-motif) is disposed at a distance of 5-6 Å from cAMP-binding site of A domain. So, cAMP binding to A domain caused W260 motion towards adenine and as a result the displacement of B domain N3A-motif. Provided that cAMP occupies B domain binding site, this facilitates correct B/C helix packing. When R subunit is in complex with C one, we deal with inverse process, which begins with F374-adenine contact formation, because A domain is tightly fixed by C subunit. This process was delineated by Kim et al. [3]; however, TMD simulation let us introduce some important changes. Current model is in a good agreement with experimental data [4] that confirm cAMP initial binding to A domain in free R subunit and to B domain in R:C complex.

**REFERENCES:** [1]O.N. Rogacheva, A.V. Popov, E.V. Savvateeva-Popova et al. (2010) *Biochemistry (Moscow)* **75(2)**: 286-96. [2] H.Rehman, Prakash B., Wolf E. et al. (2003) *Nature Structural Biology* **10**(1):26-32 [3] C. Kim, C.Y. Cheng, A. S. Saldanha, and S.S. Taylor (2007) *Cell* **130**:1032-43 [4] D. Ogreid, S.O. Doskeland (1981) *FEBS Letter* **129**:282-286.

European Cells and Materials Vol. 20. Suppl. 3, 2010 (page 216) ISSN 1473-2262

# A sophisticated model of the human epithelial airway barrier to study uptake, cell responses and intracellular distribution of nanoparticles

B. Rothen-Rutishauser, M. Clift, Ch. Brandenberger, A. Lehmann, L. Müller, D. Raemy and P. Gehr

*Institute of Anatomy, Division of Histology, University of Bern, Baltzerstr. 2, 3000 Bern 9*

**INTRODUCTION:** Nanoparticles (NPs <100nm) show promising features for pharmaceutical applications. However, biomedical applications of NPs require a detailed understanding of potential interactions with biological systems. Understanding the intracellular localisation of biomedical nanoparticles (NPs), such as their co-localisation within cellular organells, e.g. endosomes or lysosomes, mitochondria or nuclei, or, alternatively free in the cytosol, can provide essential information in regard to the potential toxicity of NPs. One important route of entry into the body is pulmonary inhalation, therefore we have established a triple-cell co-culture model of the human epithelial airway barrier composed of epithelial cells, monocyte-derived macrophages and dendritic cells to study nanoparticle-lung cell interactions [1].

**METHODS:** Polymer coated iron-platinum and gold NPs with a fluorescent dye embedded in the polymer shell were used to investigate their intracellular localization in lung cells, i.e. epithelial cells, macrophages as well as dendritic cells, and their potential to induce a pro-inflammatory response dependent on concentration and incubation time [2]. In addition, a quantitivate method was used to evaluate the intracellular gold NP distribution [3] by transmission electron microsopy within time (1h, 4h and 24h).

**RESULTS:** By laser scanning microscopy it was shown that the iron-platinum NP were taken up by all three cell types but macrophages and dendritic cells to a higher extent than epithelial cells. In both cell types of the defence system but not in epithelial cells, a particle dose-dependent increase of tumor necrosis factor-α is found. By comparing the iron-platinum- and the gold NPs as well as the shell only it was shown that the cores combined with the shells are responsible for the induction of inflammatory effects and not the shells alone. The quantitative analysis revealed a significant, non-random intracellular gold NP distribution (Fig. 1). No particles were observed in the nucleus, mitochondria, endoplasmatic reticulum or golgi, and the cytosol was not the preferred NP compartment., A significant increased gold NP localization in large vesicles (lysosomes) was found with prolonged post-incubation times, indicating intracellular particle trafficking.

**DISCUSSION & OUTLOOK:** In conclusion, by using sophisticated cell culture and microscopic methods, it is possible to determine if NPs exposed to cultured lung cells can penetrate into these cells, inducing an effect and furthermore, in which intracellular compartments they are subsequently localized (trafficking). We will use this method to compare different sized NPs and particles composed of various materials.

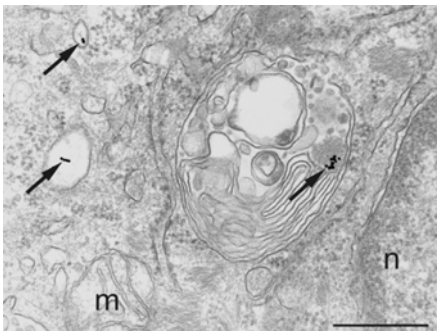


*Fig. 1: Intracellular compartments with plain gold NPs. The particles are localized within vesicles of different size categories (< 150, 150-1000, >1000 nm). (nucleus = n, mitochondria = m, scale bar =500 nm). Adapted from [3].*

**REFERENCES:** [1] Rothen-Rutishauser B, Kiama SG, Gehr P. A three-dimensional cellular model of the human respiratory tract to study the interaction with particles. *Am J Respir Cell Mol.Biol* **32(4)**:281-9 (2005). [2] Lehmann AD, Parak WJ, Zhang F, Zulqurnain A, Röcker C, Nienhaus GU, Gehr P, Rothen-Rutishauser B. Fluorescent-magnetic hybrid nanoparticles induce a dose-dependent increase of the pro-inflammatory response in lung cells in vitro correlated with intracellular localization. *Small* **6(6)**:753-62 (2010). [3] Brandenberger Ch, Mühlfeld Ch, Zulqurnain A, Lenz AG, Schmit O, Parak WJ, Gehr P, Rothen-Rutishauser B. Quantitative evaluation of cellular uptake and trafficking of gold nanoparticles with different surface coatings. *Small* (2010), in press.

**ACKNOWLEDGEMENTS:** This work was supported by the German Research Foundation (DFG SPP 1313), the Swiss National Foundation (Nr. 3100A0_118420), the Doerenkamp Zbinden foundation and the AnimalFreeResearch.

European Cells and Materials Vol. 20. Suppl. 3, 2010 (page 217) ISSN 1473-2262

# 3D microenvironments to control the chondrocyte phenotype

M.Rottmar[1], R.Mhanna[2], M.Wong-Zenobi[2], K.Maniura-Weber[1]

*[1] Empa, Laboratory for Materials-Biology Interactions, St.Gallen, Switzerland. [2] Institute for Biomedical Engineering, Laboratory of Biosensors and Bioelectronics, ETH Zurich, Zurich, Switzerland.*

**INTRODUCTION:** Cells are inherently influenced by their surroundings as they show different morphologies when extracted from their natural site in an organism and cultivated on an extraneous culture substrate[1]. Still, most *in vitro* studies on cell structure and function are carried out on planar glass or plastic substrates with properties being distinctly different from the characteristics of biological surfaces. These stiff, flat substrates impose highly unnatural geometric and mechanical constraints and thus it is well accepted that cells can show a behavior which is different compared to the *in vivo* situation[2]. When cultivated in 2D monolayer culture, chondrocytes lose their characteristic phenotype. Cultivation in 3D environments helps to maintain their chondrogenic phenotype and has even been shown to promote re-differentiation of culture expanded chondrocytes[3].

Our goal is to study a platform which prevents de-differentiation of freshly isolated chondrocytes and induces re-differentiation of culture expanded chondrocytes by studying cell behaviour in engineered 3D microenvironments.

**METHODS:** Bovine articular chondrocytes were isolated from 6 months old calves and cultivated in chondrogenic medium (DMEM + 10%FCS + 1% PSN + 50µg/ml ascorbic acid). When specified, 2µg/ml cytochalasin D were added to the medium. Cells were immunohistochemically stained against collagen II and analyzed by fluorescence microscopy to detect the chondrogenic phenotype. 3D microwells were produced by standard microfabrication technique in silicon followed by thin film replica molding in PDMS (Fig.1). The wells were functionalized with fibronectin whereas the chip surface was passivated to prevent cell attachment[5].

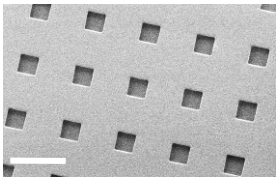

*Fig.1: SEM image of square shaped microwells [scale bar 150µm]*

**RESULTS:** Freshly isolated chondrocytes (passage 0) are round in shape and stain positively for collagen II. After expansion for two passages on 2D tissue culture plastic, the cells flatten, spread and become collagen II-negative (Fig.2). Cultivation of dedifferentiated chondrocytes (p4) in the presence of cytochalasin D causes a round cell shape and cells show a weak signal when stained for collagen II (not shown).

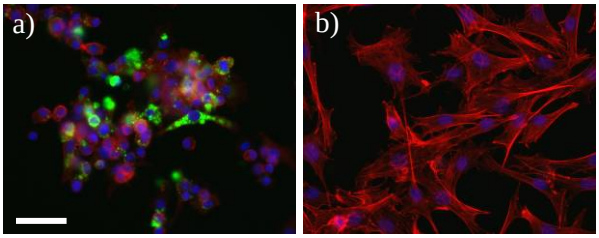


*Fig. 2: Bovine chondrocytes a) freshly isolated (p0) or b) culture expanded (p2) cultivated for 3 days and stained for collagen II (green), actin (red) and nuclei (blue) [scale bar 50µm].*

Cultivation of dedifferentiated chondrocytes in 3D microwells causes a round cell morphology with diffuse actin staining (Fig.3).

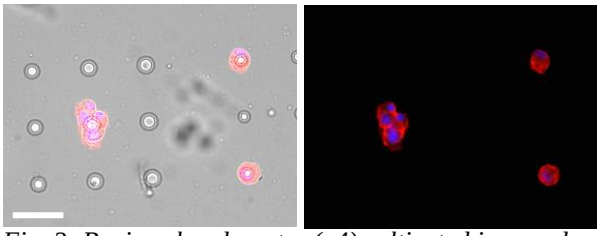

*Fig. 3: Bovine chondrocytes (p4) cultivated in round shaped microwells for 2 days and stained for actin (red) and nuclei (blue) [scale bar 50µm]*

**DISCUSSION & CONCLUSIONS:** In accordance with previous studies, cultivation in 2D monolayer culture was shown to lead to de-differentiation of chondrocytes. Also, disruption of the actin cytoskeleton with cytochalasin D results in re-expression of the chondrogenic marker collagen II (not shown). Initial results cultivating cells in 3D microwells are promising as cell rounding, a hallmark of the chondrogenic phenotype, is achieved by limiting adhesion to the microwell surface.

**REFERENCES:** [1] Weiss P., *Rev Mod Phys* **31**, 11 (1959). [2] Pampaloni F, Reynaud E.G. & Stelzer E.H.K., *Nat Rev Mol Cell Biol* **8**, 839-845 (2007) [3] Benya, P.D., Shaffer, J.D. *Cell* **30** (1982) 215–224 [5] Rottmar M, Håkanson M, Smith M, Maniura-Weber K. *J Mater Sci Mater Med.* 2010 Mar;21(**3**):999-1004.

**ACKNOWLEDGEMENTS:** We thank our collaborators in the CCMX MatLife project on the study of single cells in engineered microenvironments, Prof. Viola Vogel and Prof. Marcus Textor from ETH Zürich.

European Cells and Materials Vol. 20. Suppl. 3, 2010 (page 218) ISSN 1473-2262

# Photophysics of peptoid transporters – From the ensemble down to the single-molecule level

B. Rudat[1,2], S. B. L. Vollrath[1], E. Birtalan[1], H.-J. Eisler[2], U. Lemmer[2], T. S. Balaban[3], S. Bräse[1]

*Karlsruher Institute of Technology: [1]Institute of Organic Chemistry, [2]Light Technology Institute, [3]Institute for Nanotechnology, Karlsruhe, Germany.*

**INTRODUCTION:** Peptoids (oligo-*N*-alkylglycines) with cationic side chains are able to enhance the cellular uptake of targets into mammalian as well as plant cells.[1,2] For analyzing their uptake behavior they are up to now labeled with small organic fluorophores and directly used in cell experiments.

In this work we present the photophysical analysis of these biomolecules, labeled with different dyes, from the ensemble down to the single-molecule level. We measured absorption and fluorescence for micromolar concentrated solutions in water, and photobleaching behavior for single molecules in polymer matrices. The peptoids are compared with data of unbound fluorophores.

**METHODS:** Transporter molecules were synthesized on solid supports and labeled with different fluorescence dyes. We used commercial available ones (like Atto532), as well as fluorophores which we synthesized by our own group (e.g. Pyridinium-derived dyes).

Ensemble absorption spectra of all samples were measured with a Cary 500 Scan (Varian) or Lambda 5 UV/Vis spectrometer (Perkin Elmer), for fluorescence spectra we used a Cary Eclipse Fluorescence Spectrometer (Varian).

In order to perform single-molecule microscopy experiments the samples were dissolved to nanomolar concentrations in poly(methyl methacrylate) (PMMA, Allresist). The solutions were spun onto clean cover slides (900 rpm for 10 s, 4000 rpm for 90 s) and dried. Thereafter, the samples were studied using our home-made confocal setup. For each sample we recorded 2D fluorescence images as well as intensity time traces to analyze the photobleaching behavior.

**RESULTS:** Fig. 1 shows the structure of our standard peptoid transporter.

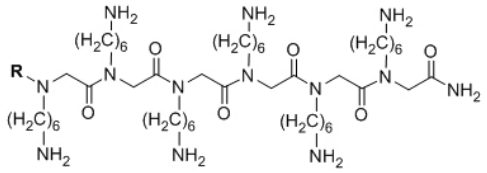

*Fig. 1: Structure of peptoid-carrier system with amine side chains. R: different fluorophores.*

The spectral properties of all fluorophores were only slightly perturbed after coupling to the transporter molecule on solid supports. In contrast, extinction coefficients and quantum yields changed in varying extent for the different fluorescent dyes.

We successfully imaged single dye and peptoid molecules as shown for an Atto532-labeled transporter (Fig. 2, left). Fluorescence intensity traces (Fig. 2, right) gave an indication of single molecule observation and the bleaching times of both free dyes and respective peptoids were almost identical.

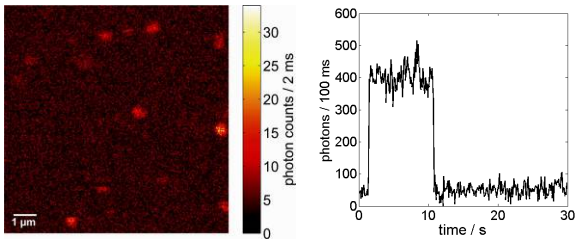


*Fig. 2: Single peptoid molecules (c = 1 nM) imaged in a PMMA matrix (left) and an example of a fluorescence intensity time trace which shows the bleaching of a single peptoid molecule (right).*

**DISCUSSION & CONCLUSIONS:** The decrease of brightness in ensemble measurements indicates that the fluorophores can be quenched by the conjugated peptoid structure. Nevertheless, single-molecule experiments were successful and indicate that further experiments like single-particle tracking should be possible. Accordingly, our next plan is to use this method for analyzing the real-time behavior of fluorescently-labeled peptoids in and on living cells.

**REFERENCES:** [1] T. Schröder, K. Schmitz, N. Niemeier, T. S. Balaban, H. F. Krug, U. Schepers, S. Bräse (2007) *Bioconjugate Chem.* **18**: 342–354. [2] K. Eggenberger, E. Birtalan, T. Schröder, S. Bräse, P. Nick (2009) *ChemBioChem* **10**: 2504–12.

**ACKNOWLEDGEMENTS:** This work is funded by the Center of Functional Nanostructures (CFN, project E1.1, C3.2, C3.5 and A5.5) and the Karlsruher School of Optics and Photonics (KSOP).

European Cells and Materials Vol. 20. Suppl. 3, 2010 (page 219) ISSN 1473-2262

# Electrical energy extraction from human peripheral blood mononuclear cells

M. Sakai[1], X. Wei[1], U. Kübler[2], S. Huber[2], U. Ehlert[2], A. Stemmer[1]

[1] *Nanotechnology Group, ETH Zurich, Switzerland.*

[2] *Department of Clinical Psychology and Psychotherapy, University Zurich, Switzerland.*

**INTRODUCTION:** Mechanisms converting metabolic energy into electricity may be an alternative to conventional batteries in small implants. Glucose is an abundant energy source and its conversion into electrical energy has been demonstrated in bacterial [1] and enzyme-based [2] fuel cells. However, for an implantable device, the former lacks biocompatibility while the latter suffers from the short lifetime of the enzyme catalyst. We have examined the possibility of utilizing transmembrane electron transport of human macrophages to run a biofuel cell, by the use of human host defence. During the immune response, macrophages differentiated from monocytes are activated to initiate phagocytosis, in which macrophages produce reactive oxygen species via electron transport through a membrane-bound protein complex, the NADPH oxidase (nicotinamide adenine dinucleotide phosphate-oxidase) [3]. The electron transfer from activated NADPH oxidase was confirmed to be a source of electrons in a biofuel cell [4]. Here we demonstrate first results obtained from a biofuel cell harvesting electrons from human peripheral blood mononuclear cells (PBMCs).

**METHODS:** For comparison, human monocytic leukemia THP-1 cells were seeded on a gold electrode (anode) and chemically stimulated to differentiate into macrophages. Electrodes were transferred to a two-compartment fuel cell and the NADPH oxidase complex was activated with a chemical stimulus. As a control, the activity of NADPH oxidase was quantified by measuring superoxide anion production via the reduction of water-soluble tetrazolium salts. PBMCs from a healthy adult were isolated by Ficoll-Paque density gradient centrifugation. PBMCs were prepared on a gold electrode as above, and the current flow in the fuel cell was observed.

**RESULTS & DISCUSSION:** The same stimulation to activate NADPH oxidase in THP-1 cells generated the current from PBMCs seeded on the anode. Since the activator triggered the current rise accompanied by superoxide anion production, the activation of NADPH oxidase in PBMCs is most likely the source of the current generation in the biofuel cell. This first demonstration confirms the possibility of extracting electrical energy from human blood cells. Modification of the electrode's surface chemistry may lead to higher performance of the fuel cell.

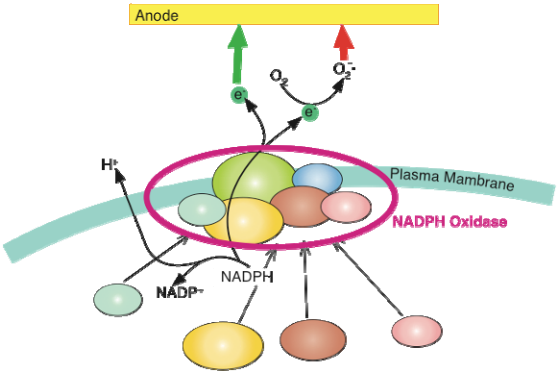


*Fig. 1: Electron transfer from cytosol to an electrode via NADPH oxidase.*

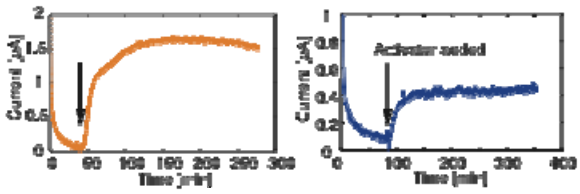


*Fig. 2: Current generation after cell stimulation: one million of THP-1 cells (left) and two millions of isolated PBMCs (right) were seeded on gold electrodes.*

**REFERENCES:** [1] B. Logan and J. Regan (2006) *Environ. Sci. Technol.* **40**:5172-80. [2] E. Katz, A. Shipway and I. Willner (2003) *Handbook of Fuel Cells 1* (Chapter 21), Wiley. [3] A. Cross and A. Segal (2004) *Biochim. Biophys. Acta* **1657**:1-22. [4] M. Sakai, A. Vonderheit, X. Wei, et al. (2009) *Biosens. Bioelectron.* **25**:68-75.

European Cells and Materials Vol. 20. Suppl. 3, 2010 (page 220) ISSN 1473-2262

# Nanoparticle assembly into functional capsules by double emulsion templating

J. Sander, A.R. Studart

*Complex Materials, Department of Materials, ETH Zürich*

**INTRODUCTION:** Encapsulation and controlled release of materials are of great interest in biomedicine, food science and pharmaceutical applications [1]. Due to their tunable permeability, shell thickness and size, hollow capsules made from closely packed colloidal particles in the shell, usually referred to as colloidosomes, are very attractive for these applications. [2, 3] Colloidosomes fabricated using double emulsions as templates allow for highly flexible, efficient loading and capsule formation in a one step process. However, colloidosomes formed by double emulsion templates are currently limited to specially functionalized colloidal silica particles [4]. In this work, we show that the range of materials used to form the capsule shell can be significantly widened by appropriately controlling the surface chemistry of the colloidal nanoparticles and of the oil-water interfaces.

**METHODS:** $Al_2O_3$ (average diameter, d=60 nm), $TiO_2$ (d=25-30 nm), $SiO_2$ (d=250 nm), poly(vinyl difluoride) (PVDF, d=300 nm) and $Fe_3O_4$ (d=5-15 nm) nanoparticles are first suspended in toluene either directly (PVDF) or using the surfactants sorbitan trioleate ($Al_2O_3$, $TiO_2$, $SiO_2$) and oleic acid ($Fe_3O_4$). Water-in-oil-in-water double emulsions are then formed in a glass microfluidic device using the particle-loaded toluene suspension as intermediate oil phase. Since toluene is slightly soluble in water, it can be completely evaporated from the intermediate oil layer, leading to well-controlled colloidosomes. 2% wt polyvinylalcohol (PVA) was used in the innermost and outermost aqueous phases of the double emulsions to stabilize both oil-water interfaces.

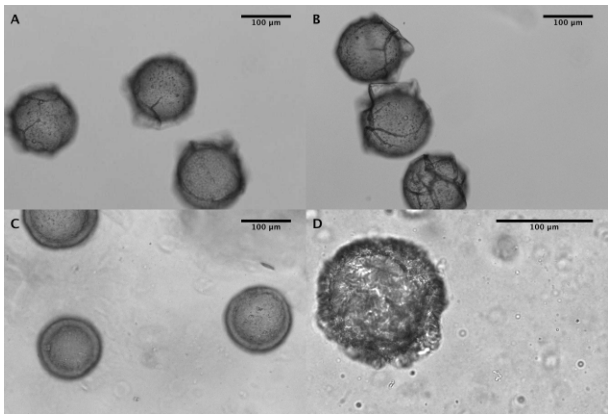


*Fig. 1: Brightfield microscopy images of colloidosomes in water made out of (A) $Al_2O_3$, (B) $TiO_2$, (C) PVDF and (D) $SiO_2$.*

**RESULTS:** Capsules with shells consisting of alumina, silica, poly(vinyl difluoride), magnetite and titania nanoparticles and pore sizes in the range 3-25nm were successfully prepared. Figure 1 shows examples of colloidosomes in the wet state. The size and shell thickness of the colloidosomes can be controlled by tailoring the size of droplets in the double emulsions. Figure 2 shows scanning electron microscopy images of dried capsules.

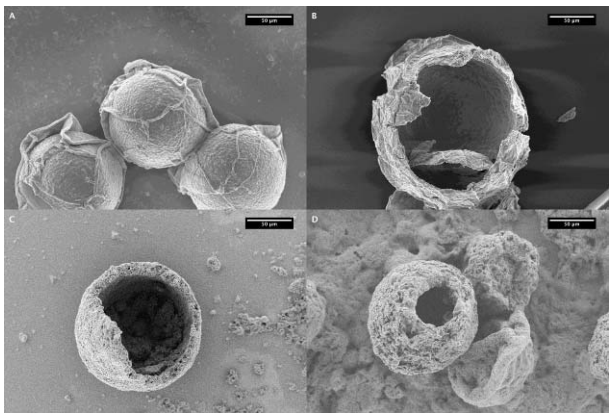

*Fig. 2: SEM images of colloidosomes made out of (A) 60 nm $Al_2O_3$, (B) 30 nm $TiO_2$, (C) 300 nm PVDF, (D) 250 nm $SiO_2$.*

**DISCUSSION & CONCLUSIONS:** Adsorption of PVA on the toluene-water interfaces and the optimum wetting of the nanoparticles in both phases have been identified as crucial for the stability of the colloidosomes. Tailoring of the surface chemistry of the nanoparticles makes them predominantly hydrophobic but still hydrophilic enough to adsorb at the toluene-water interfaces. This prevents the inner water droplets from coalescence with the outermost aqueous phase. Smaller particles lead to more stable colloidosomes due to the stronger effect of interparticle van der Waals attractive forces. Since the surface chemistry can be easily controlled by surfactants, colloidosomes from numerous types of nanoparticles with specific functionalities can be produced using this method.

**REFERENCES:** [1] R. Langer (1998) *Nature* **392**: 5-10. [2] I.Akartuna et al. (2009) *Langmuir* **25**: 12419-12424. [3] AD. Dinsmore et al. (2002) *Science* **298**: 1006-1009. [4] D. Lee, DA. Weitz (2008) *Adv. Mater.* **20**: 3498–3503.

**ACKNOWLEDGEMENTS:** We thank the Swiss National Science Foundation (Grant 200021_126646) for the financial support.

European Cells and Materials Vol. 20. Suppl. 3, 2010 (page 221) ISSN 1473-2262

# Cell-Free Expression of ohe Odorant Receptor OR5 into Artificial Membranes

S. Ritz [1,3], J. Dorn [1], S. Belegrinou [4], M. Nallani [1,2], W. Meier [4], E.-K. Sinner [1,2,3]

*[1] Max Planck Institute for Polymer Research (MPI-P), Mainz, Germany. [2] Institute of Materials Research and Engineering (IMRE), Singapore. [3] Johannes Gutenberg University, Mainz, Germany. [4] University of Basel, Basel, Switzerland*

**INTRODUCTION:** Odorant receptors cover the majority (40-50%) of the pharmaceutically relevant family of seven transmembrane G-protein-coupled receptors (GPCRs) in humans. This reflects their important role in evolution and their ability to perceive a large number of odorants. Today, most of the odorant receptors are still orphan, because the investigation of these receptors in whole organisms is complex. Each olfactory receptor recognizes multiple odorants and each odorant is detected by a specific combination of olfactory receptors. The functional expressing of single odorant receptors in heterologous cells is also difficult, because every receptor needs a suitable, genetically modified amino-terminus for the correct insertion into the plasma membrane. Alternatively, cell-free or in vitro expression systems offer an elegant route for the expression of membrane proteins directly from the genetic template, the complementary DNA (cDNA) into appropriate surfaces.

**METHODS:** Previously, we studied cell-free expression of the olfactory receptor OR5 (*rattus norvegicus*) in a tethered membrane system by Surface Plasmon Resonance Spectroscopy (SPR)/ Surface Plasmon Fluorescence Resonance Spectroscopy (SPFS) [1]. In the present study we show the effect of phospholipids and amphiphilic polymersomes composed of hydroxy poly(butadiene)-poly(ethylene oxid) (PB-PEO-OH) on the cell free expression of OR5. The protein expression and membrane inserted protein-fragments were analyzed by radioactive labelling with with $^{35}$S-methionine and a subsequent Proteinase K digestion.

We also asked if the expression and membrane insertion depend on the origin of the cell-free expression system. Therefore common cell-free expression systems based on bacteria, insects, wheat germ and rabbit reticulocytes were compared by radioactive labelling, and protease digestion.

**RESULTS:** The biocompatibility and successful membrane insertion of OR5 in the block-copolymers (PB-PEO-OH) was shown in comparison to pure DOPC lipid vesicles.

We did extensive studies to distinguish protein insertion in **lipid** and **polymer** vesicles, respectively, from unspecific surface binding. For this, we have inserted methionine with a radioactive isotope from sulfur ($^{35}$S) to label intrinsically the OR5 receptors. After enzymatic digestion, a discrete digestion pattern could be observed, which suggests protein protection by membrane insertion. Three major results are: **i.** The OR5 insertion strongly depends on the expression system (highest yields of OR5 with the insect cell extract but no membrane insertion). **ii.** Supplement of lipids or block copolymers (PB-PEO) enhance the expression and insertion of OR5. **iii.** Vectorial insertion of OR5 (N-terminus outside and C-terminus inside a vesicular or planar lipid membrane surface) leads to a highly organized and highly "active" surface.

**DISCUSSION & CONCLUSIONS:** Our intention is to combine cell-free expression of membrane proteins with matrices mimicking the natural phospholipide membrane. In this context we investigated the insertion of OR5 into artificial phospholipide membranes or amphiphilic block-copolymers assigned as "polymersomes" [2]. The use of synthetic amphiphiles broadens the spectrum of sensor application towards air-born sensors.

**REFERENCES:** [1] R. Robelek (2007) et al., Incorporation of in vitro synthesized GPCR into a tethered artificial lipid membrane system. *Angew Chem Int Ed Engl* **46**, 605-8. [2] S. Belegrinou et al. (2010), Biomimetic supported membranes from amphiphilic block copolymers, *Soft Matter*, **6**, 179-186.

**ACKNOWLEDGEMENTS:** We gratefully acknowledge the EU for financing the FP6 FuSyMem Project 43431.

European Cells and Materials Vol. 20. Suppl. 3, 2010 (page 222) ISSN 1473-2262

# Responsive Polymer Brushes: Functional Platforms for Membrane Protein Assays

M.G. Santonicola, G.W. de Groot, M. Memesa, G.J. Vancso

*Materials Science and Technology of Polymers, MESA+ Institute for Nanotechnology, University of Twente, Enschede, The Netherlands.*

**INTRODUCTION:** There is a growing need for functionalization strategies aimed to improve performance of platforms for pharmaceutical screening. Screening assays for membrane proteins are especially of interest, as these proteins represent more than 50% of all drug targets. In order to selectively probe the functionality of membrane protein ion channels, it would be desirable to have nanoporous supports with controlled ion permeation [1]. Stimulus responsive polymers offer the possibility of achieving rapid and reversible switching between conformations and can be induced locally, which makes them ideal candidates for miniaturized devices with fast response times.

**METHODS:** pH-responsive poly(methacrylic acid) (PMAA) layers were synthesized on silicon surfaces using surface-initiated atom transfer radical polymerization (SI-ATRP). Initiator molecules were immobilized on activated silicon surfaces by vapor-phase deposition and, subsequently, ATRP was carried out in water/methanol mixtures of different ratios at room temperature.

To investigate the dissociation behavior of the responsive polymer brushes, PMAA-grafted substrates were incubated in buffer solutions with different pH values and then characterized by FTIR. FTIR titration curves were used to determine the effective bulk $pK_a$ of the brushes as previously reported [2]. The pH-induced swelling and collapsing of the grafted polymer layers was evaluated *in situ* by null ellipsometry in liquid environment. A multilayer model for a flat film was used for the fitting of both thickness and refractive index of the polymer layer from the experimentally measured ellipsometric angles Ψ and Δ.

**RESULTS:** Grafted layers of PMAA show a strong pH-dependent behavior. The effective $pK_a$ of the bulk polymer brush is 6.2 ± 0.1, which is larger than the effective surface $pK_a$ of the brushes due to ion confinement effects [2]. This value can be controlled by varying the polymer growth conditions, such as the water/methanol ratio of the polymerization medium. The switching behavior

of the PMAA brushes, in terms of both degree of dissociation of carboxylic groups and thickness of the polymer layer, is found to be reversible when changing the pH of the PBS medium between 4 and 8 (Fig. 1). Switching between swollen and collapsed state of the brush is characterized by a swelling factor of 1.6-1.8 and occurs within 1 min.

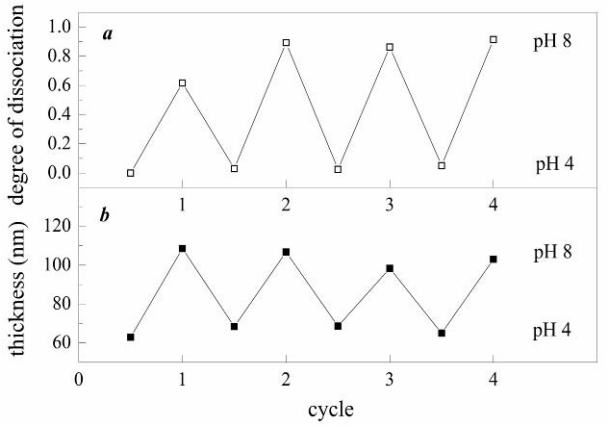


*Fig. 1: Switching behavior of PMAA brushes on silicon surface investigated by FTIR (a) and in situ ellipsometry (b), in response to changes of pH (PBS, 50 mM phosphate).*

**DISCUSSION & CONCLUSIONS:** Polymer brushes synthesized by surface-initiated atom transfer radical polymerization provide a robust and reproducible platform for surface modification. Responsive PMAA brushes grown using surface-initiated ATRP exhibit reversible and rapid switching between conformations, with an effective bulk $pK_a$ of the polymer in the brushes which is shifted to larger values. This is especially relevant for membrane protein assays as switching can be triggered in a pH range closer to physiological conditions where protein functionality is optimal. Grafting of pH-responsive polymer brushes from nanoporous silicon nitride films is also investigated.

**REFERENCES:** [1] E. Reimhult and K. Kumar (2008) *Trends in Biotechnology* **26**(2):82-89. [2] R. Dong, M. Lindau, and C.K. Ober (2009) *Langmuir* **25**(8):4774-4779.

**ACKNOWLEDGEMENTS:** This work is financially supported by the European Commission through the FP7 project ASMENA.

European Cells and Materials Vol. 20. Suppl. 3, 2010 (page 223) ISSN 1473-2262

# Synthesis and characterization of amino-acid funcionalized hydroxyapatite nanoparticles

C.Santos [1,2], M. M Almeida [1], M.E.V. Costa [1]

*[1] Dep Ceramic and Glass Eng, CICECO, University of Aveiro, Portugal. [2] Polytechnical Institute of Setubal, EST, Estefanilha, Setubal, Portugal*

**INTRODUCTION:** Due to its chemical composition similar to that of bone and to its osteoconductivity, nontoxicity and absence of inflammatory effects[1,2] [1]hydroxyapatite (HAP) is a biomaterial with multiple applications. HAP particle surface is prone to chemical modifications thus allowing appropriate biomolecules of interest to be attached to. L-Serine is an aminoacid well recognized for its important role in cell cultures and in cell proliferation[3] which has been coupled to HAP plate like particles[4]. Some demanding applications are now requiring nanosized HAP particles with a biological stability tailored according to a desired specific role. Thus the interest of producing functionalized HAP nanoparticles with pre-defined biomolecules is naturally addressed. The present study is focused on the production of hydroxyapatite nanoparticles in presence of L-Serine. Hydrothermal synthesis is the selected method for obtaining amino acid/HAP nanoparticles using different synthesis times ($t_S$).

**METHODS:** For amino acid/Hap nanoparticles precipitation a calcium phosphate supersaturated solution was prepared as follows: an aqueous citric acid solution (0.6 M) was added with small amounts of $NH_4OH$ (25%) for pH adjustment and then mixed with appropriated amounts of L-serine (0,08 M) and subsequently with $Ca(NO_3)_2$ solutions (0.2 M) and of $(NH_4)_2HPO_4$ solutions (0.2 M). The resulting homogeneous solutions were transferred to a tightly sealed Teflon vessel in a stainless steel autoclave and kept at 180ºC, under different $t_S$ values (0,5; 1; 3; 24 Hours). The precipitated particles were characterized by X-Ray diffraction (XRD) for crystal phase analysis, transmission electron microscopy (TEM) for morphology evaluation, and gas adsorption/desorption (BET and BJH methods) for specific surface area and pore size evaluation. Fourier transform infrared spectroscopy (FTIR) in transmittance mode was used to identify the particle functional groups in the range of 400–4000 $cm^{-1}$, using KBr pellets.

**RESULTS:** The results showed that [amino acid (L-serine)/HAP nanoparticles] were sucessfully synthesized by hydrothermal method. The XRD of the precipitated particles confirmed that all peaks

could be indexed to hydroxyapatite. In addition, it was observed that longer $t_S$ allowed to achieve particles with enhanced crystallinity and larger crystallite sizes. The TEM results revealed the morphology of the obtained particles to be rod like as ilustrated in Fig. 1 for HAP/serine 3H and HAP/serine 24H particles which average lengths are around 70 and 120 nm respectively (fig. 1). Moreover, as compared to HAP nanoparticles synthesized in the absence of L-Serine, higher aspect ratio and larger crystallite sizes are noticed for [HAP/serine] nanoparticles.

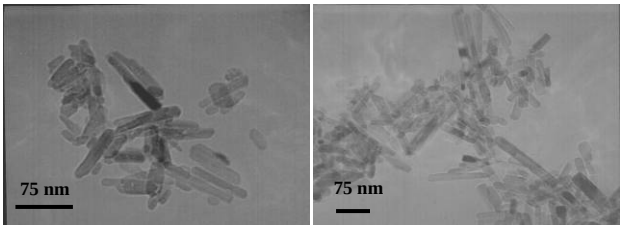


*Fig. 1:Amino-acid(L-serine)/HAP nanoparticles synthesised by hydrothermal method, (a) after 3H of reaction time and (b) after 24H of reaction time.*

FTIR results confirmed that Serine characteristic functional groups were maintained in [HAP/serine] nanoparticles regardless $t_S$.

**DISCUSSION & CONCLUSIONS:** the obtained results reveal a marked influence of $t_S$ on the size, cristalinity, crystallite size and specific surface area of the obtained particles. Consequently the appropriate choice of $t_S$ allows tailoring some properties that are crucial for a particle intended to interact with biological cells and tissues, including its size and solubility. Additionally the longer and thinner particles obtained under L-Serine influence indicate an effective role of L-Serine on HAP growth mechanism. It is thus demonstrated that HAP nanoparticles functionalized with the amino acid L-Serine and displaying a controllable size and crystallinity condition are produced by the hydrothermal synthesis method.

**REFERENCES:** [1]G. Balasudaram et al. (2006) *Biomaterials* **27**:2798-2805; [2]Z. Shi et al. (2009) *Acta Biomaterialia* **5**:338-345; [3]J. Babister et al. (2009) *Biomaterials* **30:**3174-3182.

**ACKNOWLEDGEMENTS:** To FCT for the SFRH/BD/48276/2008 PhD grant.

European Cells and Materials Vol. 20. Suppl. 3, 2010 (page 224) ISSN 1473-2262

# Self-assembled hyaluronic acid nanoparticles: effect of molecular weight and two different chemical approaches

SS. Pedrosa[1], FM. Gama[1]

[1]*IBB-Institute for Biotechnology and Bioengineering, Centre for Biological Engineering, Universidade do Minho, Braga, Portugal*

**INTRODUCTION:** Natural polyssacharides, such as hyaluronic acid (HyA) have been widely used for biomedical and pharmaceutical applications. Hya has multiple functional groups available for chemical conjugation that can convert HyA into nano-sized carriers. We prepared self-assembled HyA nanoparticles by two different chemical derivatization techniques and used two different molecular weights HyA. Our aim was to compare these two techniques and evaluate the influence of molecular weight in the properties of HyA nanoparticles.

**METHODS:** HyA must be rendered soluble in non-aqueous solvents by exchangingthe sodium ion with a lipophilic ion – Tetrabutylammonium - using a cationic exchange resin. One of the chemical derivatization techniques used involve the transesterification of HyA-TBA with glycidyl methacrylate (GMA) in the presence of 4-dimethylaminopyridine (DMAP), as described by Oudshoorn et al [1]. Then, HyA-MA reacts with 1-hexadecanethiol by a Michael addition in the presence of Triethylamine (Fig. 1) [2].

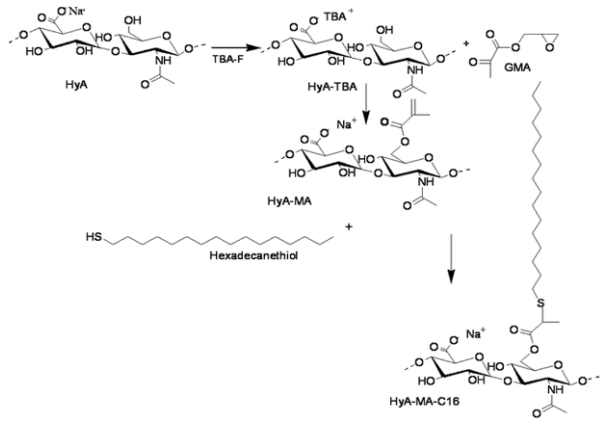


*Fig. 1: Synthesis of Hya-MA-C16.*

The other technique employed for the synthesis of nanoparticles was the chemical conjugation with 1-hexadecylamine in the presence of 1-ethyl-3-(3-dimethylaminopropyl) carbodiimide (EDC) and N-hydroxysuccinime(NHS) (Fig. 2) [3]. In both techniques, the samples were dyalised firstly against a sodium chloride solution to remove the TBA ions and then against deionised water. The two chemical derivatizations were performed using both a low (7460 Da) and a high molecular weight HyA (0.5-2 MDa). The samples obtained were characterized by H-NMR spectroscopy, dynamic light scattering (DLS) and UV-VIS spectroscopy of a hydrophobic compound (curcumin) that asses the existence of hidrofobic moieties.

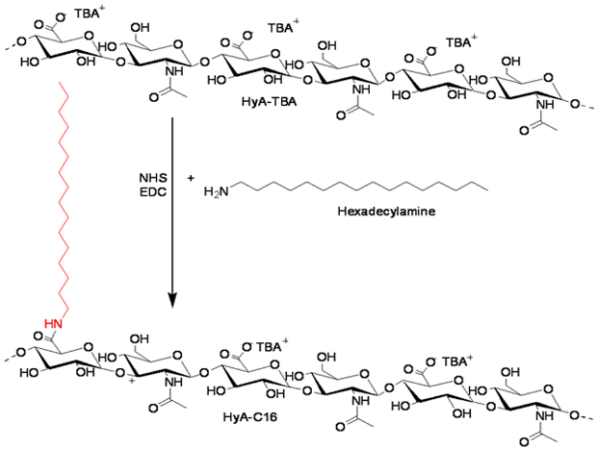


*Fig. 2: Synthesis of HyA-C16*

**RESULTS:** For the synthesis of HyA-MA-C16, we tested different molar ratios of grafting moiety: HMW/LMW and obtained different substitution degrees. Regardless of that, both materials presented good stability in aqueous solution at different pH through a period of nearly two months. The DLS analysis revealed a small difference (170 nm HMW: 140 nm, LMW) in the average size of the nanoparticles. The HMW HyA nanoparticles were able to incorporate a higher percentage of curcumin. A comprehensive characterization of both kinds of nanoparticles will be presented.

**DISCUSSION & CONCLUSIONS:** The chemical conjugation revealed a simpler approach with a more tailored degree of substitution.

**REFERENCES:** [1]M. Oudshroorn, R. Rissmann, Bouwstra, J. et al (2007) *Polymer* **48**: 1915-1920. [2] C. Gonçalves, J. Martins and FM. Gama (2007) *Biomacomolecules* **8**:392-398. [3]KY. Choi, H. Chung, KH., Min, HY. Yoon, et al (2010) *Biomaterials* **31**: 106-114.

**ACKNOWLEDGEMENTS:** Sílvia S. Pedrosa work was supported by the Fundação para Ciência e Tecnologia (FCT) grant SFRH/BD/61516/2009.

European Cells and Materials Vol. 20. Suppl. 3, 2010 (page 225) ISSN 1473-2262

# Enhanced fluorescence at protein-nanostructured ZnO interfaces

C.Satriano[1], M.E.Fragalà[1], Y. Aleeva[2]

[1] *Dipartimento di Scienze Chimiche, Università di Catania. 2 Scuola Superiore Università di Catania, Catania, Italy.*

**INTRODUCTION:** ZnO nanostructured films have been recently proposed as innovative nanoplatforms for biomolecular fluorescence detection. Indeed, ZnO-based nanomaterials may work as excellent signal-intensifying substrates for a wide range of proteins, despite the specific emission wavelength of fluorophores linked to the protein molecules [1-2]. Herein, we report the use of nanoscale ZnO thin films, in the enhanced/quenched fluorescence detection upon interaction with albumin, used as model analyte biomolecule.

**METHODS:** ZnO deposition has been performed either on silicon or glass by MOCVD (at 250°C, 40 min and 400°C, 5 min) using the $Zn(tta)_2$·tmeda metal-organic precursor. The interface between the newly prepared ZnO surfaces and fluorescein-conjugated albumin (FITC-HSA, from Sigma) has been investigated by Confocal Microscopy and FRAP experiments, in terms of ZnO emission spectra change and lateral mobility of the biomolecule in the adlayer, and by XPS, for determining protein surface coverage.

**RESULTS:** The used MOCVD process conditions trigger the formation of extremely thin (< 10 nm) ZnO layers having different thickness, chemical composition (as estimated by XPS) [3] and morphologies (as investigated by AFM and SEM). ZnO films deposited at 250°C show a random distribution of large grains (about 200 nm of average dimension, rms ~ 30 nm) and several spot of thick ZnO islands (Fig.1). On the other hand, those deposited at 400°C exhibit a more uniform coverage of smaller grains (about 80 nm average dimension, rms ~ 10 nm). Such findings are in agreement with a CVD growth model involving, at the low temperature (250°C), a predominant 3D island-like ZnO growth, and a continuous 2D layer formation at the high deposition temperature (400°C).

The fluorescence images and the corresponding emission spectra (Fig.1) evidence different optical response of the two types of ZnO films upon interaction with FITC-HSA. As the 250°C sample, the emission from spot islands (A) is quenched by exposure to albumin, and then partially recovered after copious rinsing with PBS buffer (Fig.1a). The opposite trend, i.e., emission enhancement, is found for both the homogeneous areas of 250 °C sample (B) and the 400°C ZnO sample (Fig. 1b).

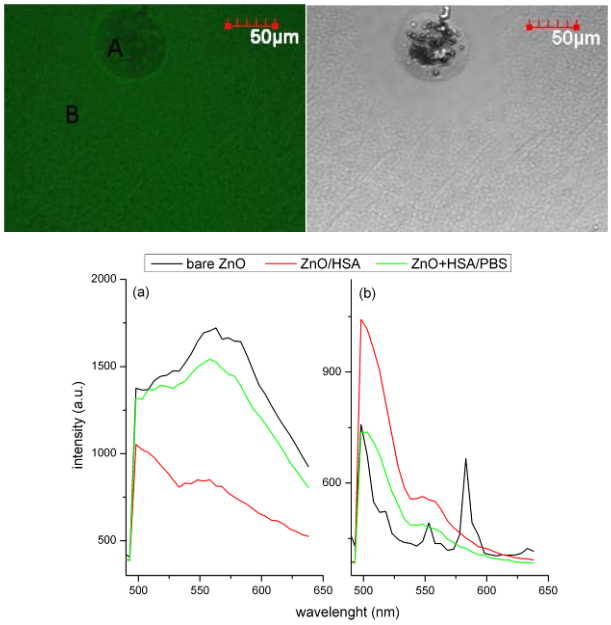


*Fig. 1: Upper: fluorescence (left) and optical mode (right) micrographs of ZnO film (250 °C). Lower: emission spectra corresponding to spot (a) and uniform (b) film areas, before and after interaction with FITC-HSA.*

**DISCUSSION & CONCLUSIONS:** The different ZnO film structures result in the different optical response upon interaction with albumin. In fact the quenching/enhancement of emission is likely related to different binding processes occurring at the interface between ZnO nanostructured thin films and albumin. These results are promising for potential applications in surface bio-engineering of ZnO nanoplatforms with selective response to biological environments.

**REFERENCES:** [1]A. Dorfman, N. Kumar, J. Hahm (2006) *Adv Mater* **18**: 2685–2690. [2] C. D. Corso, A. Dickherber,W. D. Hunt (2008) *Biosens Bioelectr* **24:** 805–811. [3] M. E. Fragalà, C. Satriano, Y. Aleeva, G. Malandrino (2010) *Thin Solid Film* doi: 10.1016/j.tsf.2010.04.005.

**ACKNOWLEDGEMENTS:** The authors acknowledge PRA 2008 (Catania University).

European Cells and Materials Vol. 20. Suppl. 3, 2010 (page 226) ISSN 1473-2262

# Membrane Proteins in Native Membranes Studied by Atomic Force Microscopy: Watching Biological Nano-Machines at Work

I Casuso, N. Buzhynskyy, L. Liu, F. Rico, S. Scheuring

*Institut Curie, U1006 INSERM, 26 Rue d'Ulm, 75248 Paris, France.*

The atomic force microscope (AFM) has become a powerful tool in structural biology allowing the investigation of biological samples under native-like conditions: experiments are performed in physiological buffer at room temperature and under normal pressure. Topographies of membrane proteins can be acquired at a lateral resolution of ~10Å and a vertical resolution of ~1Å. Importantly, the AFM features an extraordinary signal-to-noise ratio allowing imaging of individual membrane proteins in prokaryotic (1) and eukaryotic (2) native membranes that participate in supramolecular assemblies (Fig. 1).

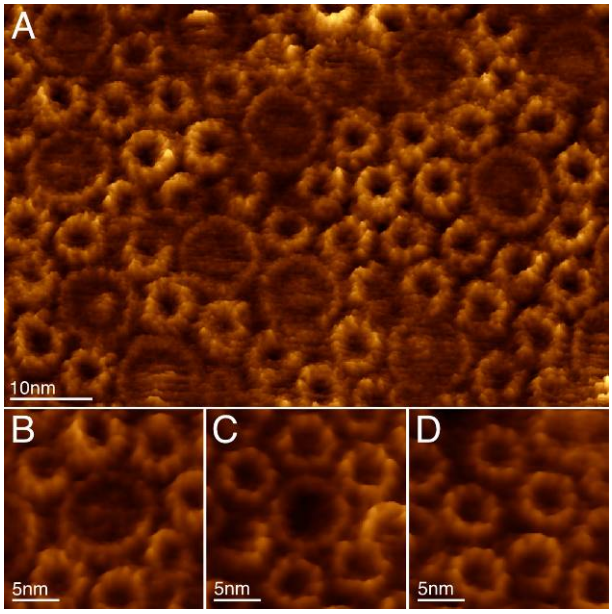


*Figure 1. Structure and supramolecular assembly of photosynthetic complexes in chromatophores of Rsp. photometricum. Containing light-harvesting complexes 2 (LH2), light-harvesting complexes 1 (LH1) and reaction centers (RC). A) High-resolution AFM topograph of the supramolecular assembly of a high-light adapted photosynthetic membrane. B) Core-complex. C) Unknown LH complex with a diameter of ~75Å. D) Nonameric LH2 complexes. Bottom: 'moon-shaped' molecule formed by 6 subunits.*

Imaging techniques in medicine are important for our understanding of pathologies and potential development of cure approaches. It is now clear that many pathologies are based on molecular

disorders – therefore techniques capable to image at a resolution sufficient to observe single molecules and better must be developed and adapted for medical issues. Membrane proteins are involved in many vital processes and their malfunctions often have a serious impact on an organism's state. Nowadays, AFM is a recognized technique able to reveal the structure of supramolecular assemblies of membrane proteins (1). Using AFM as a medical nano-imaging tool, we imaged healthy (2) and cataract affected (3) eye lens membranes at unprecedented resolution. Crucial differences in organization of the two membrane proteins, aquaporin-0 and connexin, are distinguished between healthy and pathological cases.

Most recently, the power of high-speed atomic force microscopy (HS-AFM, (4)) was used to investigate dynamic membrane processes (5). The perspectives of this novel technology to study membrane-mediated protein-protein interactions will be discussed (6) (Fig. 2).

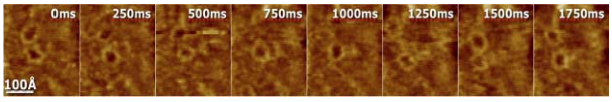


*Figure 2: HS-AFM analysis of dynamic membrane protein dimer interaction. Frame rate: 250ms.*

**REFERENCES:**

[1] S Scheuring & JN Sturgis, *Science*, **309**, 484-487 (2005).

[2] N Buzhynskyy, R Hite, T Walz & S Scheuring, *EMBO Reports*, **8**, 51-55 (2007).

[3] N Buzhynskyy, JF Girmens, W Faigle, & S Scheuring, *JMB*, **374**, 162-169 (2007).

[4] T Ando, N Kodera, E Takai, D Maruyama, K Saito & A Toda, *Proc Nat Amer Soc* **98**: 12468-12472 (2001).

[5] I Casuso, N Kodera, C Le Grimellec, T Ando & S Scheuring, *Biophys J* **97**: 1354-1361 (2009).

[6] I Casuso, P Sens, F Rico & S Scheuring, *Biophys J*, in press (2010).

European Cells and Materials Vol. 20. Suppl. 3, 2010 (page 227) ISSN 1473-2262

# Novel superparamagnetic iron oxide nanoparticles stabilized with chelating amino cellulose

R. Wyrwa[1], N. Michaelis[2], K. Wagner[1], T. Seemann[1], M. Nikolajski[2], J. H. Clement[3], R. Müller[4], T. Heinze[2], M. Schnabelrauch[1]

*[1]Biomaterials Department, INNOVENT e. V., Prüssingstrasse 27 B, D-07745 Jena; Germany. [2] Center of Excellence for Polysaccharide Research, Institute of Organic Chemistry and Macromolecular Chemistry, Friedrich Schiller University of Jena, Humboldtstrasse 10, D-07743 Jena, Germany. [3]Department of Internal Medicine II, University Hospital Jena, Erlanger Allee 101, D-07740 Jena, Germany. [4]Institute of Photonic Technology, Albert-Einstein-Strasse 9, D-07745 Jena, Germany.*

**INTRODUCTION:** Magnetic nanoparticles used in biomedicine are commonly covered with an organic coating to enhance their biocompatibility and prevent rapid agglomeration of the particles. The stabilization is often achieved by rather weak electrostatic interactions between negatively charged shell structures (e. g. carboxymethyl dextran (CMD)) and iron oxide cores bearing a positive partial charge on their surface. However, the stability of those core-shell particles is strongly influenced by the particle concentration and the surrounding medium. The design of ferrofluids with strong interactions between core and shell structures would be therefore desirable to overcome current limitations in the application spectrum of these materials. We report on a strategy to stabilize iron oxide-based nanoparticles by the use of amino cellulose shell structures known for their metal-chelating potential.

**MATERIALS & METHODS:** Iron oxide cores with mean diameters of 10 nm were synthesized by co-precipitation of iron(II) and iron(III) salts [1]. The coating material (Fig. 1), tris(aminoethyl)amino celluose (TAC) with a degree of substitution of 0.63, was prepared from cellulose (Avicel®, DP ~ 250) via tosyl cellulose according to reported procedures [2, 3]. Coating of the nanoparticles was performed in aqueous solution at 45 °C. CMD-coated particles were prepared for comparison. The magnetic fluids were characterized by their chemical composition (content of iron and shell material, Fe(II)/Fe(III) ratio), atomic force microscopy (AFM), magnetometric measurements and photon correlation spectroscopy (PCS). The cytocompatibility of the particles was investigated by a live/dead viability assay using 3T3 fibroblast cells. To study cell-nanoparticle interactions human MCF-7 breast carcinoma cells and leucocytes were incubated with prepared nanoparticles for

different time periods. Magnetically marked cells were separated using a Super MACS (Miltenyi Biotech, Germany).

**RESULTS & DISCUSSION:** Stable magnetic iron oxide nanoparticles could be obtained using the TAC coating. AFM measurements show a mean diameter of 35 nm for the TAC-coated particles measured in the dry state.

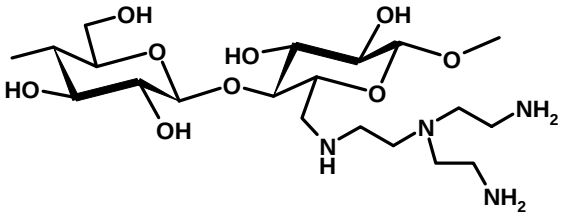


*Fig. 1: Tris(aminoethyl)amino celluose*

In vitro cell culture experiments using 3T3 mouse fibroblasts exhibit no detectable cytotoxic effects of the TAC-coated nanoparticles after a cultivation period of 4 days. In preliminary experiments the interaction of nanoparticles with cells were studied. An intense interaction of both the MCF-7 cells and leukocytes with TAC-coated nanoparticles was observed.

**CONCLUSIONS:** The newly developed TAC shell structures enables the formation of stable magnetic fluids, and in addition, they provide suitable functional groups for the immobilization of further molecules like drugs, markers or contrast agents. The described nanoparticle coating strategy therefore represents an interesting route to design tailored magnetic nanoparticles for biomedical applications.

**REFERENCES:** [1]K. Wagner, A. Kautz, M. Röder et al. (2004) *Appl Organometal Chem* **18**:514-519. [2]K Rahn, M. Diamantoglou, H. Berghmanns et al. (1996) *Angew Makromol Chem* **238**:143-163. [3]A. Jung and P. Berlin (2005) *Cellulose* **12**:67-84.

**ACKNOWLEDGEMENTS:** This work was supported by the BMWi (grant no. VF080018).

European Cells and Materials Vol. 20. Suppl. 3, 2010 (page 228) ISSN 1473-2262

# Local properties of block copolymer thin film based biointerfaces

H. Schönherr, D. Tranchida, E. Sperotto, S. Abdulhussain, E. Wassel

*Universität Siegen, Physical Chemistry, Adolf-Reichwein-Str. 2, 57076 Siegen*

**INTRODUCTION:** Functional biointerfaces in advanced sensors, screening platforms, and devices call for advanced design and preparation in order to match the sophisticated recognition ability of biological systems. This includes the control of chemical composition and mechanical properties on length scales spanning the 100 μm to sub-100 nm regime.

**METHODS & RESULTS:** In recent years we have developed a block copolymer-based platform for the fabrication of functional biointerfaces. Polystyrene-block-poly(tert-butyl acrylate) (PS-b-PtBA) thin films are characterized by their high molecular loading, robustness (due to covalent coupling chemistry), controlled film thickness and reactivity, as well as the possibility to implement topographic patterning and / or chemical patterning by embossing, imprinting and the mentioned unconventional lithographic techniques [1,2]. More recently, these methods were complemented by thermal deprotection strategies [3] that can be expanded by scanning probe lithography to the nanometer scale [4].

In this contribution recent progress in the fabrication and nanoscale analysis of thin PS-b-PtBA films are highlighted. Next to the implementation of specific streptavidin - biotin based conjugation, the passivation of polystyrene-block-poly(tert-butyl acrylate) thin films with poly(ethylene glycol) based on the established grafting-to approach [1, 2] will be compared to the grafting-from approach based on surface initiated atom transfer radical polymerization (ATRP). ATRP with oligo(ethylene glycol methacrylate) (OEGMA) afforded PEG brush covered films with brush thicknesses up to 400 nm. These brushes showed excellent resistance against protein adsorption, comparable to state of the art OEGMA brushes grown from monolayers on gold or silicon. Compared to these brushes the polymer platform show enhanced stability and also offer the possibility to structure the films topographically, e.g. by means of (nano)imprinting [2,3].

For model polymer brushes and chemically modified BCPs the role of entropic contributions to the elastic and elastic-plastic behavior was quantified and unraveled down to individual BCP nanophases (Fig. 1).

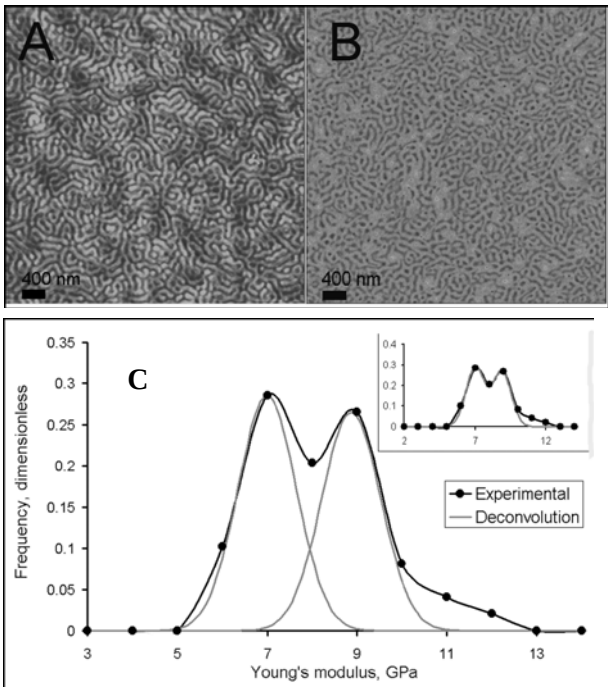


*Fig. 1: Top: AFM (A) topography and (B) phase image of PS-b-PtBA thin film; (C): Distributions of mechanical properties.*

**DISCUSSION & CONCLUSIONS:** For the established BCP platform specific streptavidin - biotin based conjugation was successfully implemented and surface initiated ATRP afforded improved passivation against non-specific protein adsorption. Mechanical properties of single nanophases with typical size in the order of few tens of nanometers were successfully measured by AFM nanoindentation.

**REFERENCES:** [1] C. L. Feng, A. Embrechts, I. Bredebusch, J. Schnekenburger, W. Domschke, G. J. Vancso, Holger Schönherr *Adv. Mater.* 2007, **19**, 286. [2] A. Embrechts, C. L. Feng, C. Mills, M. Lee, I. Bredebusch, J. Schnekenburger, W. Domschke, G. J. Vancso, H. Schönherr *Langmuir* 2008, **24**, 8841. [3] J. Duvigneau, S. Cornelissen, N. Bardají Valls, H. Schönherr, G. J. Vancso *Adv. Funct. Mater.* 2010, **20**, 460. [4] Duvigneau, H. Schönherr, G. J. Vancso *Langmuir* 2008, **24**, 10825.

**ACKNOWLEDGEMENTS:** The authors acknowledge financial support of the Alexander von Humboldt foundation and the University of Siegen.

European Cells and Materials Vol. 20. Suppl. 3, 2010 (page 229) ISSN 1473-2262

# Uptake of 200 nm latex particles and 20 nm quantum dots by the small intestinal mucosa – an intravital two-photon microscopy study in mice

A.Schueth [1], L. Krapf [2], J. Dimitrijevic [3], A. Klinger [1], R.Orzekowsky-Schroeder [2], T. Vossmeyer [3], G. Huettmann [2], H.Weller [3] ,A. Gebert [1]

*1Institute of Anatomy, University of Luebeck, Ratzeburger Allee 160, 23538 Lübeck, Germany*

*2Institute of Biomedical Optics, University of Luebeck, Peter-Monnik-Weg 4, 23562 Lübeck, Germany*

*3Institute of Physical Chemistry, University of Hamburg, Grindelallee 117, 20146 Hamburg, Germany*

**INTRODUCTION:** The mucosa of the small intestine is lined by a columnar epithelium which primarily consists of enterocytes. The Peyer's patches of the small intestine contain M cells which are specialized structures capable of taking up macromolecules and microorganisms for presentation to the gut-associated lymphoid tissue.[1] Since little is known about the transepithelial transport via enterocytes and M cells in vivo, we applied intravital two-photon microscopy to study the kinetics of different sized particle uptake in vivo.

**METHODS:** We employed two-photon laser scanning microscopy [2] (TPLSM) which major advantage is its ability to permit high-resolution and high-contrast imaging from deep within the intact living tissue. This method allows us to repeatedly scan tissue volumes at maximum optical resolution over several hours in anaesthetised mice. We applied carboxylated 200 nm latex particles and 20 nm quantum dots (QD) onto the murine mucosa under nearly physiological conditions and tracked their uptake over hours.

**RESULTS:** Both tailor-made 20 nm carboxylated QD[3] and 200 nm carboxylated latex particles could be detected within the living tissue, and the time kinetics of particle transport into the tissue could be followed in vivo by TPLSM. At 20 min, 20 nm QD were seen in considerable numbers in enterocytes, M cells and dendritic cells in both villus and dome epithelium. 200 nm particles were mainly seen inside the M cells and sub-epithelial dendritic cells of the dome area within a time period of 30–45 min after application. A few 200 nm particles were also found in the villi of the Peyer's patches, but to a far lesser extent.

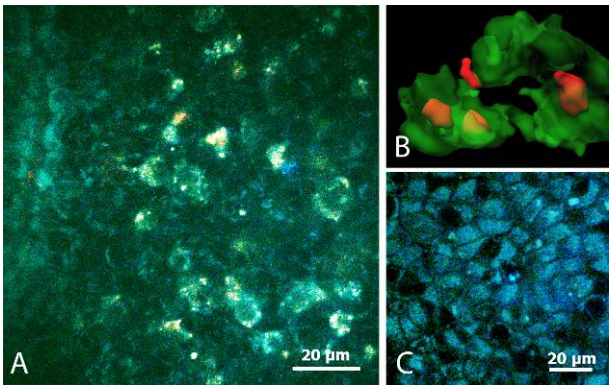


*Fig. 1: Localisation of 200 nm latex particles (blue, A,C) and 20 nm QD (red, A,B) in Peyer's patch domes. Intravital two-photon microscopy.*

**DISCUSSION & CONCLUSIONS:** Our results show that the intact murine mucosa of the small intestine is permeable to nanoparticles and that there is a particle size dependent uptake with 20 nm particles showing significantly greater uptake than 200 nm particles. 20 nm particles are not only ingested by M cells, but also by ordinary intestinal enterocytes of the villi, whereas the uptake of larger particles is restricted to M cells. This setup will be used in further studies to investigate the specific uptake of a variety of nanoparticles displaying different size, charge and functionalisation.

**REFERENCES:**[1] R. Beier, A. Gebert (1998), *Am J Physiol* **275**:G 130- 137. [2] W. Denk, J.H. Strickler, W.W. Webb (1990), *Science* **284**:73- 76. [3] E. Pöselt (2009), *Langmir* **25**:13906.

**ACKNOWLEDGEMENTS:** The project is supported by the Deutsche Forschungsgemeinschaft, GE 647/10-1.

European Cells and Materials Vol. 20. Suppl. 3, 2010 (page 230) ISSN 1473-2262

# Nanogels based on Chitosan: Characterization, Toxicological Evaluation and Applications

C. A. Schütz[1], L. J. Harwood[2], B. Halamoda-Kenzaoui[3], P. Käuper[4]; K. C. McCullough[2], L. Juillerat-Jeanneret[3], C. Wandrey[1]

*[1]Institute of Bioengineering, LMRP, Ecole Polytechnique Fédérale de Lausanne, Lausanne, Switzerland. IBI-LMRP, EPFL, Lausanne, Switzerland. [2]IVI, Mittelhäusern, Switzerland. [3]University Institute of Pathology, CHUV-UNIL, Lausanne, Switzerland. [4]Medipol SA, Lausanne, Switzerland.*

**INTRODUCTION:** Hydrophilic nanogels (Ng) composed of biopolymers have a potential for biomedical and pharmaceutical applications. Although such Ng have been intensely studied during the past decade, comprehensive information about their fate in biological environments is lacking. The evaluation of Ng–cell interactions, including toxicological studies, are a prerequisite for therapeutic applications.

**METHODS:** Chitosan from crustacean and fungal origin were used here to form Ng with alginate (Alg) and/or polyvalent anions. Additional surface decoration with natural polyanions ensured negative surface charge and stabilization in physiological and cell culture conditions[1,2]. Bioactive molecules (proteins, RNAs) can be loaded in the Ng during the entirely water-based formation process. Size distribution, morphology and zeta potential were studied in water, PBS and cell media.

**RESULTS:** Labeled BSA incorporated in the Ng was successfully delivered into porcine monocyte derived dendritic cells[3]. Moreover, proof of uptake was confirmed by using auto-quenched BSA, where fluorescence appears only after proteolytic degradation of the protein inside the endosomes. Fluorecence appearance was delayed in Ng loaded cells compared to free protein in cells.

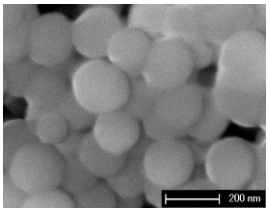


*Fig. 1: Scanning electron microscopy of nanogels.*

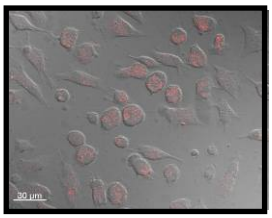

*Fig. 2: Uptake of Ng (red) in MoDCs.*

Toxicological assessment of the Ng in presence of several human cell lines showed cell survival of approx. 95% up to high Ng dose. Oxidative stress, evaluated by reactive oxygen species (ROS) production after incubation with endothelial cells, demonstrated a significant production of ROS at Ng doses above 200 µg/ml.

For antigen delivery purpose, the surface decorating Alg was functionalized to promote targeting towards dendritic cells. Ng loaded with ovalbumin (OVA) were taken up by porcine MoDCs in a dose dependent manner. In vivo, the immune response of mice to OVA-loaded Ng was also dose dependent. Although primary antibody response was less than for controls, a higher memory response was observed for the groups treated with optimized Ng after a second injection.

*Table 1. Hydrodynamic diameter $d_H$, polydispersity index PDI and zeta potential of the hydrophilic nanogels in different media.*

| Ng | $d_H$ (nm) (PDI) | | | zeta potential (mV) |
|---|---|---|---|---|
| | water | PBS | DMEM | water |
| Animal chitosan | | | | |
| Empty | 638 (0.49) | 465 (0.28) | 263 (0.20) | -64 |
| BSA | 513 (0.46) | 371 (0.26) | 310 (0.16) | -62 |
| Fungal chitosan | | | | |
| Empty | 593 (0.53) | 385 (0.32) | | -68 |
| BSA | 492 (0.40) | 358 (0.24) | 273 (0.18) | -66 |

**REFERENCES:** [1]Käuper P., Laue C., 2005, WO2007031812. [2]Schütz C.A. et al., *Chimia* 2009, **63**(4) 220-222. [3]Carrasco C. et al., *Immunology* 2001, **104**, 175.

**ACKNOWLEDGEMENTS:** This research is supported by the Swiss National Science Foundation, grant 404740-117323, and Medipol SA, Ecublens, Switzerland

European Cells and Materials Vol. 20. Suppl. 3, 2010 (page 231) ISSN 1473-2262

# Construction of S-layer cages

David Schuster, Seta Küpcü, Uwe B. Sleytr, Dietmar Pum

*Department of Nanobiotechnology, Universität für Bodenkultur, 1190 Vienna, Austria*

**INTRODUCTION:** The main objective of this project is the fabrication of three-dimensional S-layer protein architectures [1]. Based on the knowledge of coating liposomes and emulsomes with S-layer proteins, micrometer sized hollow spherical, polyhedral and cylindrical morphologies will be created using simple liquid handling procedures. Possible applications of three-dimensional S-layer architectures are the development of artificial viruses, controlled drug targeting and delivery (including hydrophobic substances), affinity matrices, stable foam like structures, to spatially constrained synthesis of nanoparticles [2,3].

**METHODS:** Apart from chemical and liquid handling procedures, TEM, AFM, DLS and fluorescent characterisation methods have been performed.

**RESULTS:** This contribution briefly summarizes the current work and focuses on results like the fabrication of liposomes, emulsomes and calcium carbonate particles as well as their coating with S-layer proteins. Optionally the constructs could be silicified [4]. Finally the scaffolds were dissolved in order to get pure S-layer spheres either cross linked or stabilized with silica layers.

**DISCUSSION & CONCLUSIONS:** Various nanostructures could be formed and investigated. Coating with S-layer protein of the nanoscale scaffolds was successful. Crosslinking of protein coatings and dissolution of subjacent scaffolds generally show a tendency to aggregation and coalescence of the structures. To overcome these challenges is the key to successfully design S-layer cages. New procedures for improving the stability of the S-layer constructs are being developed.

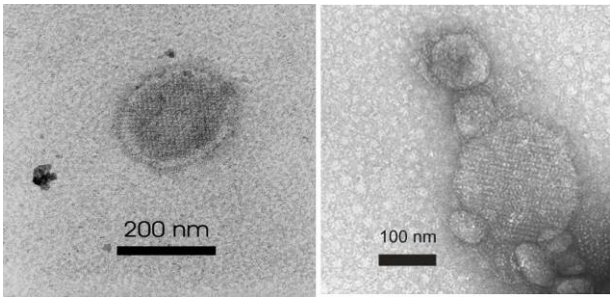


*Fig. 1: Liposome (left) and Emulsomes™ (right) coated with S-layer protein from Geobacillus stearothermophilus PV72/p2, negatively stained.*

**REFERENCES:** [1] U. B. Sleytr, P. Messner, D. Pum, M. Sára (1999) *Angewandte Chemie - International Edition* **38**, 1034-1054. [2] E. M. Egelseer et al. (in press) *The Encyclopedia of Industrial Biotechnology: Bioprocess, Bioseparation, and Cell Technology* (ed M. C. Flickinger) John Wiley & Sons, Inc., Hoboken, USA. [3] U. B. Sleytr et al (2002) *Polyamides and complex proteinaceous materials* (eds I, A. Steinbüchel, S. R. Fahnestock) Wiley-VCH, Weinheim, vol. 1st Ed., pp. 285-338. [4] C. Göbel, B. Schuster, D. Baurecht, U. Sleytr, D. Pum (2010) *Colloids Surf B Biointerfaces* **75**, 565-72.

**ACKNOWLEDGEMENTS:** This project is funded by the AFOSR, Agreement Award Nr.: FA9550-09-0342

European Cells and Materials Vol. 20. Suppl. 3, 2010 (page 232) ISSN 1473-2262

# Vesicular Structures Using Short Amphiphilic Peptides

Th. B. Schuster, D. de Bruyn Ouboter, W. P. Meier

*Department of Chemistry, University of Basel, Basel, Switzerland*

**INTRODUCTION:** Lipid vesicles have been finding medical and cosmetic applications for decades. By way of a comparison, polymeric vesicular systems possess higher stability, greater chemical diversity and thus more potential for functionalisation[1]. As another alternative, purely peptidic systems benefit from their response to environmental stimuli[2] (pH, T, etc.) and degradation by natural pathways.

**METHODS:** Fmoc-based solid-phase peptide synthesis on Rink Amide AM was used, with HCTU/DIPEA as the coupling reagent[3]. Double RP-HPLC with acetonitrile/aq. buffer gradients (0.1% TFA and 2% AcOH) yielded material with purities ≥ 95%. Vesicle formation was induced by dissolving the peptide in ethanol followed by dialysis against water. Transmission and scanning electron microscopy (TEM, SEM) as well as dynamic and static light scattering (DLS, SLS) were used for characterisation.

**RESULTS:** To create an amphiphilic peptide we used gramicidin A (gA) as the hydrophobic contributor and attached a hydrophilic component consisting of either negatively charged glutamic acids (gA-$E_6$-Ac), positively charged lysine (gA-$K_6$-Ac), or unchanged acetylated lysine (X) together with an esterificated (EtO-) C-terminus (EtO-gA-$X_8$-Ac). N-terminal acetylation (Ac) prevented intramolecular charge compensation.

EtO-gA-$X_8$-Ac formed vesicles as shown in TEM (Fig. 1A). In contrast to the ethoxy-free analogue, assembly into a peptide membrane was enabled by the presence of an ethyl-ester-terminus on the hydrophobic component.

Unilamellar vesicle formation was also achieved with the use of the charged gA-$E_6$-Ac system. TEM and SEM showed collapsed, hollow, and egg-shell like structures. The objects exhibited a hydrodynamic radius ($R_h$) of 220 nm and φ ($R_g/R_h$) of 0.9, which is close to the typical value for hollow spheres (1.0).

Mixing negatively charged gA-$E_6$-Ac with positively charged gA-$K_6$-Ac showed no phase separation and allowed the formation of onion like, multilamellar vesicles (Fig. 1B) by means of lateral and perpendicular charge compensation.

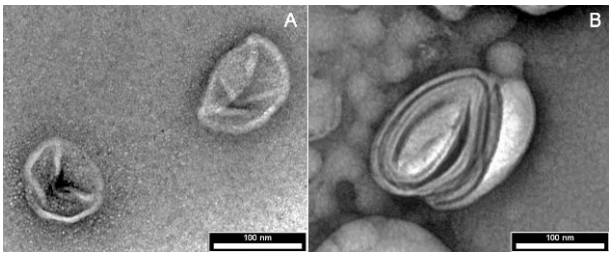


*Fig. 1: TEM images of A) collapsed EtO-gA-$X_8$-Ac vesicles and B) multi lamellar vesicles using a gA-$E_6$-Ac/gA-$K_6$-Ac mixture.*

Point mutation by stepwise replacement of free lysine (K) with acetylated lysine (X) allowed us to create a series of amphiphilic compounds of, in total, ten peptides using gA-$X_8$-Ac and gA-$X_{8-m}K_m$, with m ranging from 0 to 8, with changing hydrophobicity. We observed a change in secondary structure that caused a change in the morphology of the assembly from fibres to micelles when m exceeded 2. Behaviour in aqueous solution stagnated when m was beyond 6.

**DISCUSSION & CONCLUSIONS:** The investigated short amphiphilic peptides possess the ability to form uni- and multilamellar vesicular structures in aqueous solution. Based on the membrane thickness and the theoretical dimensions of the peptides, we suggest a peptidic bilayer, similar to lipids. To our knowledge, this is the first time that short peptides of 22 to 25 amino acids and with a defined secondary structure have formed membranes and vesicles.

Self-assembled morphologies were controllable by defined manipulation of the gA-$X_{8-m}K_m$ sequence.

**REFERENCES:** [1] O. Onaca, R. Enea, D.W. Hughes and W. Meier (2009) *Macromol. Biosci.* **9:**129-139. [2] A. Carlsen and S. Lecommandoux (2009) *Curr. Opin. Colloid Interface Sci.* **14:**329-339. [3] C. Dittrich, D. de Bruyn Ouboter, T.B. Schuster and W.P. Meier (2010) *Biomaterials* submitted.

**ACKNOWLEDGEMENTS:** Financial support by the SNSF and the NCCR Nanosciences is gratefully acknowledged. The authors thank the Zentrum für Mikroskopie (ZMB), Dr. M. Kümin and R. Erdmann (Prof. H. Wennemers), and M. Inglin.

# Multiple Traps Optical Tweezers for Live Cell Force Mapping in Initial Focal Contacts

M.Schwingel, M.Bastmeyer

[1] *Karlsruhe Institute of Technology (KIT), Zoological Institute, Cell and Neurobiology, Karlsruhe, Germany*

**INTRODUCTION:** Since their invention in 1986 by A. Ashkin, optical tweezers have become increasingly valuable tools for research in the biological and physical sciences [1]. Using a focused beam of light to trap and move matter, optical tweezers offer convenient non-invasive access to processes at the mesoscopic scale. Here, we demonstrate the in vitro application of multiple optical tweezers for force mapping in fibroblasts.

Cells exert forces onto their growth substrate during spreading and migration by forming adhesive contacts that connect the cytoskeleton with the extracellular matrix. These forces can be estimated by atomic force microscopy (AFM) or by observing the deformation of micropatterned elastic substrates. Both techniques allow the estimation of adherent forces in the whole cell, but cannot distinguish between single adhesion sites. The application of laser tweezers offers the possibility to study traction forces in specific contact sites.

**METHODS:** Our laser tweezers setup is based on an acousto-optical deflection system (AOD) which allows the independent steering and intensity modulation of a large number of optical traps. The setup is equipped with epifluorescence optics and a live cell imaging chamber to enable force measurements in biological samples.

To examine the initial formation of focal contacts, we expose cells simultaneously to several fibronectin-functionalized beads. These beads are positioned on the apical surface of the cells to mimic new contact sites and are kept in position with forces ranging from 1 pN to 130 pN.

The optical traps are calibrated using the thermal fluctuation method in combination with video microscopy and the linear dependence of trap force on bead displacement

$$F(x) = kx \qquad (1)$$

(x: bead displacement; k: trap stiffness) is utilized to determine the traction force of the cell [3].

**RESULTS:** The multiple trap setting enables force mapping with high spatial and temporal resolution over the whole cell body. Measurements indicate that traction forces are highest in the foremost leading edge and decrease rearwards (Fig1 A to D). Different cell types (B16 cells, MEFs, primary chick fibroblasts) exhibit significant differences regarding traction forces and velocity of retrograde transport, as is depicted in table 1. Furthermore, a dependence of traction forces on bead size is observed: the larger the bead diameter, the stronger the traction force of the fibroblast.

*Table 1. Traction force and retrograde velocity of different cell types.*

| Cell type | Traction Force [pN] | Retrograde velocity [µm/min] |
|---|---|---|
| B16 | 48 ± 10 | 0.1 ±0.05 |
| MEF | 110 ±20 | 0.18±0.03 |
| Prim. C. Fib. | >130pN | 0.5±0.05 |

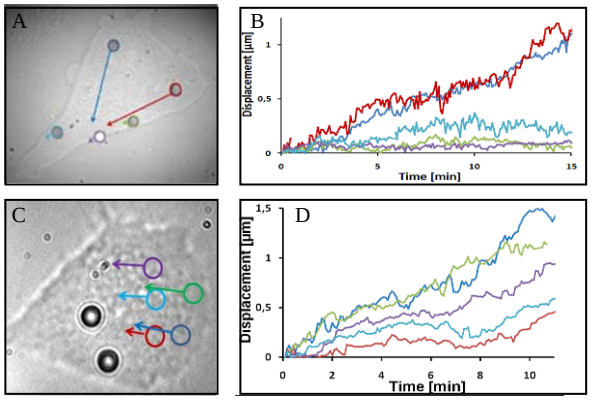


*Fig. 1: A,C) Two different fibroblast with beads placed in the leading edge; arrows indicate the pulling force of the cell; B,D) Bead displacement over time.*

**DISCUSSION & CONCLUSIONS:** The force range accessible with laser tweezers allows studying the development in initial focal contacts in live cells. A dependence of traction force on cell type, bead position and size is observed. The relation between bead size and force will next be examined with respect to the number of adhesion sites it offers to the cell.

**REFERENCES:** [1] A. Ashkin et al (1986) *Optics Let.* **11:**288-290. [2] N. Balaban et al (2001) *Nat. Cell Biol* **3:**466-472. [3] K.C. Neumann, S.M. Block (2004) *Rev Sci Inst* **75**:2787-2809.

**ACKNOWLEDGEMENTS:** The project is funded by the DFG Center for Functional Nanostructures (CFN) and is supported by the Karlsruhe School of Optics and Photonics (KSOP).

European Cells and Materials Vol. 20. Suppl. 3, 2010 (page 234) ISSN 1473-2262

# The Stability and Surface Coverage of Polymer Stabilized Gold Nanoparticles*

KB. Sebby and E. Mansfield

*National Institute of Standards and Technology, Materials Reliability Division, Boulder, CO, USA.*

**INTRODUCTION:** To correlate biological response to material properties, nanoparticle populations need to be thoroughly examined prior to, and subsequent to, biological testing. This research monitors the stability of well characterized gold nanoparticles under biologically relevant conditions and introduces a novel method for quantifying polymer surface coverage that uses less material than alternate techniques.

**METHODS:** Thoroughly characterized, citrate-stabilized 30 nm spherical gold nanoparticles were obtained from NIST (RM 8012). The citrate was replaced with methoxy-polyethylene glycol (PEG) -thiol (MW ~5000 g/mol). The average and distribution of molecular weights of the PEG starting material were determined with NMR spectroscopy and MALDI-TOF mass spectrometry, respectively. The properties of the PEG-stabilized particles were measured and compared to the citrate-stabilized particles with dynamic light scattering (DLS), zeta potential measurements, and spectrophotometry. The surface coverage of PEG was determined with quartz crystal microbalances (QCMs) in a manner analogous to that of thermogravimetic analysis but used 1/1000$^{th}$ of the sample size. Approximately 1 µg of sample was deposited on five QCMs; three QCMs without samples served as controls. The QCMs were heated to successively higher temperatures in a muffle furnace, and changes in the resonant frequencies were measured. Mass changes were calculated from the Sauerbrey equation and adjusted for temperature fluctuations due to heating.

Both citrate- and PEG-stabilized particles were monitored for changes in the presence of dithiothreitol (DTT), and cell culture media (MEM) with and without serum (FBS) by DLS.

**RESULTS:** Changes in light absorption, DLS, and zeta potential measurements were consistent with the addition of a PEG coating to the gold surface. The QCM measurements (Figure 1) showed a decrease in mass of 6.4 % ± 2 % after heating the sample above the PEG decomposition temperature corresponding to a PEG footprint area of 1.3 nm$^2$ ± 0.5 nm$^2$.

DLS measurements (Figure 2) showed increased particle stability after PEGylation. Citrate-stabilized particles flocculated rapidly in MEM and DTT, but were stabilized by the binding of serum proteins from FBS, as priorly assumed [1]. PEG prevented flocculation in MEM and inhibited the binding of serum proteins. Although the PEG-thiol gold bond was susceptible to reduction by DTT, the onset of flocculation began after several hours of incubation time compared to immediate flocculation for the citrate stabilized samples.

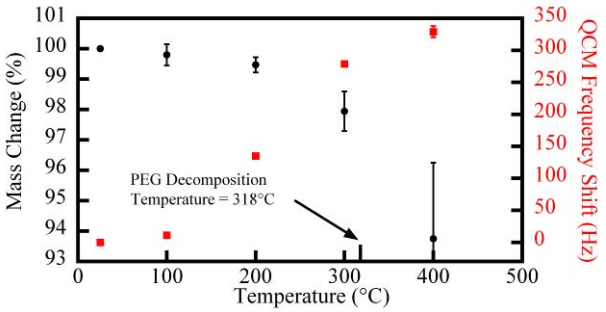


*Fig. 1: The frequency change of QCMs (red) and corresponding mass decrease (black) as a function of temperature.*

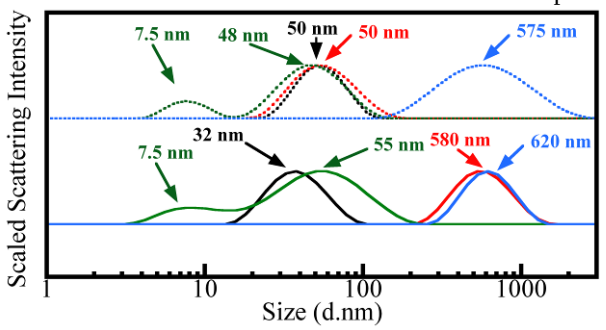


*Fig. 2: DLS size measurements (±2 nm) for citrate- (solid lines) and PEG- (dashed lines) stabilized nanoparticles in water (black), MEM (red), MEM with FBS (green) and 10 mmol/dm3 DTT (blue).*

**DISCUSSION & CONCLUSIONS:** PEG functionalization produces gold nanoparticles with well defined surface chemistry and enhanced stability. Current studies are underway to evaluate the robustness of particle properties post-uptake by HeLa cells, and to substantiate the QCM results with alternate techniques.

**REFERENCES:** [1] P. Nativo, E.A. Prior, M. Brust, (2008) *ACS Nano* **2**:1639-44.

**ACKNOWLEDGEMENTS:** The authors gratefully acknowledge support from the NRC Postdoctoral Fellowship.

European Cells and Materials Vol. 20. Suppl. 3, 2010 (page 235) ISSN 1473-2262

# Cell Sheet Engineering - New Way for Prospective Stem Cell Transplantation

OV. Semenov[1,2], O. Guillaume-Gentil[2], A. Malek[1], K. Maniura[3], M. Ehrbar[1], J. Voros[2], AH. Zisch[1]

*[1] University Hospital Zurich, Zurich, Switzerland. [2] ETH Zurich, Zurich, Switzerland. [3] EMPA, St. Gallen, Switzerland.*

**INTRODUCTION:** Cell sheet engineering has emerged as, versatile method for direct cell transplantation or creation of three-dimensional multilayered thick tissue structures without the need of biodegradable scaffolds. Viable cell sheets from different cell types were successfully harvested from temperature-responsive polymer surfaces and already used for clinical applications [1]. We demonstrate an alternative methodology for assembling and harvesting of stem cell sheets based on applying of electrical potential to conductive indium tin oxide substrates (ITO) functionalized with polyelectrolyte multilayer (PEM) coatings [2].

**METHODS:** We established critical parameters for isolation of placental derived mesenchymal stem cells (PD-MSCs) [3]. Following this we created PD-MSC sheets on ITO substrates functionalized with PEM coatings assembled from 9 alternating layer pairs of cationic poly (allylamine hydrochloride) (PAH) and anionic poly (sodium-4-styrenesulfonate) (PSS). Resulting cell sheets were analyzed for morphology (light and confocal microscopy), viability (life/death stain), vitality (WST-1 assay), phenotypic profile (FACS), and plasticity (mesodermal differentiation). Live, undifferentiated PD-MSC sheets were then harvested from the conductive surface by applying of electrical potential.

**RESULTS:** We showed that conductive ITO substrates functionalized with [PAH-PSS] support adhesion and outgrowth of human mesenchymal stem cells and allow formation of live, dense stem cell sheets. The resulting cell sheets retained their phenotypical profile and could be differentiated towards mesodermal lineage *in vitro* (Figure 1). Moreover, we were able to recover undifferentiated PD-MSC sheets from these functionalized conductive surfaces (Figure 2).

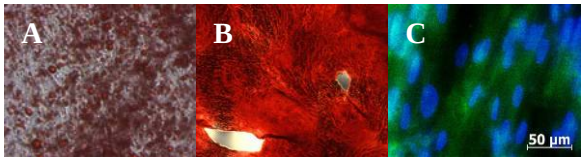


*Fig. 1: Mesodermal differentiation of PD-MSC sheets in vitro on $[PAH\text{-}PSS]_9$ functionalized ITO surfaces: Adipogenic (A), osteogenic (B), and chondrogenic (C ).*

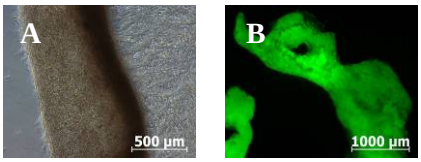


*Fig. 2: Recovering of PD-MSC sheets from $[PAH\text{-}PSS]_9$ functionalized ITO surfaces: PD-MSC sheet recovering (A), live-dead staining of recovered PD-MSC sheet (B).*

**DISCUSSION & CONCLUSIONS:** Conductive ITO substrates functionalized with PEM support formation differentiation and controlled recovering of intact stem cell sheets. Ongoing research is directed towards mesodermal differentiation of harvested stem cell sheets *in vitro* and their differentiation on ITO substrates by co-culture with human adult cell types.

**REFERENCES:** [1] J. Yang, M. Yamato, T. Shimizu, et al (2007) *Biomaterials* **28**:5033-43. [2] O.V. Semenov, A. Malek, AG. Bittermann, et al (2009) *Tissue Engineering Part A* **15(10)**:2977-90. [3] O.V. Semenov, S. Koestenbauer, M. Riegel, et al (2010) *AJOG* **202**:1-13.

**ACKNOWLEDGEMENTS:** This work was funded by a grant of the Competence Center for Materials Science and Technology (CCMX), Switzerland and FP6 grant “Crystal”, European Union.

European Cells and Materials Vol. 20. Suppl. 3, 2010 (page 236) ISSN 1473-2262

# Poly(4-hydroxybutyrate)-*b*-monomethoxy (polyethylene glycol) Copolymer Nanoparticles as a Potential Drug Carriers

M. Shah, MH. Choi and SC. Yoon*

*Nano-Biomaterials Science Laboratory, Division of Applied Life Sciences (BK21), Gyeongsang National University, Jinju 660-701, Republic of Korea.*

**INTRODUCTION:** The copolymers and homopolymers of polyhydroxyalkanoates (PHA) have been widely used as therapeutic agents; however, the in vivo degradation of PHA based materials is very slow. Poly(4-hydroxybutyrate) P(4HB) is more suitable candidate to be utilized in pharmaceutical industries due to its widespread medical applications [1] and rapid in vivo degradation [2]. Modification of a hydrophobic polymer with hydrophilic mPEG stabilizes it and makes it suitable to be used as nontoxic blood compatible candidate for the delivery of drugs [3]. In this paper, P(4HB) was modified with mPEG and used for the preparation of nanoparticles.

**METHODS:** P(4HB)-*b*-mPEG was prepared by transesterification reaction in the presence of bis(2-ethylhexanoate) tin catalyst [4]. The product was characterized using GPC, $^{1}$H-NMR and DSC analysis. Nanoparticles were prepared from the diblock copolymer using emulsification-solvent evaporation technique with sodium deoxycholate emulsifier. The morphology of the nanoparticles was determined by AFM and FE-SEM. DLS and ELS were used to find out the average diameter and surface charge of the nanoparticles. FACS analysis was used to determine the in vitro biocompatibility of the nanoparticles.

**RESULTS:** A novel modified PHA homopolymer based block copolymer, P(4HB)-*b*-mPEG was synthesized by transesterification reaction in the melt. Characterization of the prepared copolymer by GPC showed a relatively unimodal peak and the chemical coupling between the carbonyl carbon of P(4HB) and hydroxyl group of mPEG was confirmed by $^{1}$H-NMR analysis. The diblock copolymer self-assembled into nanostructures with core-shell topology in aqueous solution which was determined by the enzymatic degradation of PHA coupled with mPEG and noncoupled reaction. The morphology of the prepared amphiphilic nanocarriers was observed under AFM and FE-SEM microscope, showing the formation of spherically shaped nanoparticles with smooth surface morphology and relatively uniform distributions. FACS data showed the biocompatibility of the drug loaded nanoparticles.

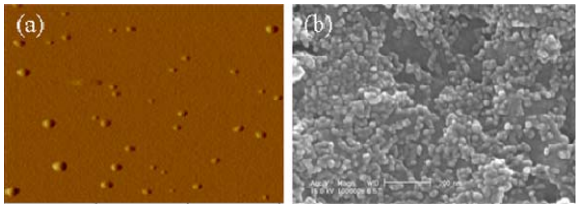


*Fig. 1: Morphology of P(4HB)-b-mPEG nanoparticles: AFM image 3 μm X 3 μm (a) FE-SEM micrograph (b). Scale bar, 200 nm.*

*Table 1. Characterization of p(γ-HB)-b-mPEG nanoparticles.*

| Particle size (nm) | PI | Zeta potential (mV) |
|---|---|---|
| 110 ± 3 | 0.22 ± 0.001 | -19 ± 2 |

**DISCUSSION & CONCLUSIONS:** Amphiphilic block copolymers self-assemble in to nanostructures in aqueous medium, with outer exposed hydrophilic shell and inner concealed hydrophobic polymer core [5]. The amphiphilic nanoparticles preparation from such diblock copolymer is advantageous because it provide a nontoxic core-shell structures in which hydrophobic drugs are entrapped and solubilised in the core hydrophobic domains and the shell providing a concealed nontoxic surface, thus allowing increased bioavailability and safe delivery of hydrophobic drugs.

**REFERENCES:** [1] M. Pötter, and A. Steinbüchel (2005) *Biomacromolecules* **6**:552-560. [2] U. Pieper-Fürst, M.H. Madkour, F. Mayer, et al (1994) *J Bacteriol* **176**:4328-4337. [3] R. Gref, Y. Minamitake, M.T. Peracchia et al (1994) *Science* **263**:1600-1603. F. Ravenelle, and R.H. Marchessault (2002) *Biomacromolecules* **3**:1057-1064. [5] S. Basu, R. Harfouche, S. Soni, et al (2009) *PNAS* **106**:7957-7961.

**ACKNOWLEDGEMENTS:** This study was supported by a grant from the KOSEF/MEST to the Environmental Biotechnology National Core Research Center (R15-2003-012-02001-0) and Korea Science and Engineering Foundation (R01-2000-000-00070-0).

European Cells and Materials Vol. 20. Suppl. 3, 2010 (page 237) ISSN 1473-2262

# Bacterial Toxin for Cytosolic delivery of gold nanoparticles

U.Shaheen, Y.Cesbron and Raphaël Lévy

School of Biosciences University of Liverpool, Liverpool, UK L 69 7ZB

**INTRODUCTION:** Targeted intracellular delivery of biomolecules using nanoparticles has attracted many of the science disciplines. Nanoparticles because of their tuneable size and unique optical properties are emerging not only as imaging probes but also serving as intracellular cargo delivery carriers. Gold nanoparticles are best candidate for all these applications because of their least cytotoxicity and ease of biofunctionalization.

For intracellular delivery application, it is necessary that a carrier is not only has the capacity to carry the biomolecule efficiently but also able to deliver it to the cytosol which is the main site for all physiological and chemical activities inside the cell. It is well documented that on intracellular delivery, bioconjugated gold nanoparticles trapped by endolysosomes where their biomolecular coating degrades eventually. [1]

For avoiding this fate and for gaining access into the cytosol, we used a new approach i.e. toxin assissted delivery of gold nanoparticles. A bacterial toxin Streptolysin-O is a secreted protein of 61 Kda which forms pores in plasma membrane.[2] of host cell for gaining access into the cytosol. It has been used as a simple and rapid mean of transfection for intracellular delivery of oligonucleotides and siRNA.[3]

**METHODS:** We are currently combining fluorescence microscopy (Fig. 1), photothermal microscopy (Fig. 2) and transmission electron microscopy to fully understand the mechanism, localization and fate of gold nanoparticles during SLO assisted uptake.

**RESULTS:** Our results confirm that SLO treated cells showed an increased cellular uptake of Gold nanoparticles then untreated cells. We also studied the effect of poly ethylene glycol (PEG) on SLO assisted cellular uptake by increasing the PEG amount gradually and found that PEG affects the cellular uptake adversely.

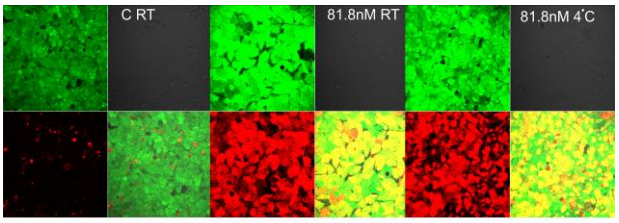


*Fig. 1: HeLa cells treated with 81.8nM SLO and without SLO (C) for 10 minutes and resealed in the presence of serum containing medium at 22oC room temperature (RT) and at 4oC. Cell viability and permeabilisation checked by Fluorecein diacetate FDA (2ng/ml) which gives green fluorescence in live cells only and Propidium iodidePI (1µg/ml) which gives red fluorescence in permeabilised cells and dead cells by staining DNA.*

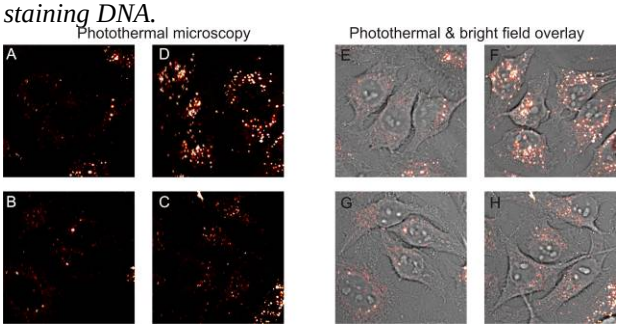


*Fig. 2: 10%CCALNNPEG-90%CALNN GNP inside the HeLa cells treated without SLO (A, E) and with SLO(D,F)20%CCALNNPEG 80%CALNN GNPs inside the HeLa treated without SLO (B, G) and with SLO (C, H) 5nm GNPs and concentration is 600nM.*

**REFERENCES:**

[1] Sée, V. *et al.* Cathepsin L digestion of nanobioconjugates upon endocytosis. *ACS Nano* **3**, 2461-2468 (2009).

[2] Bhakdi, S., Tranumjensen, J. & Sziegoleit, A. Mechanism of membrane damage by streptolysin-O. *Infection and Immunity* **47**, 52-60 (1985).

[3] Spiller, D. G. & Tidd, D. M. Nuclear Delivery of Antisense Oligodeoxynucleotides through Reversible Permeabilization of Human Leukemia-Cells with Streptolysin-O. *Antisense Research and Development* **5**, 13-21 (1995).

# Rheological Properties of Sesame Oil Emulsions

KGH.Silva[1,2,3], RR.Santiago[1,4], KS.Silva[1,4], KCH.Silva[1], EST.Egito[1,2,4]

*[1] Laboratório de Sistemas Dispersos (LASID), Departamento de Farmácia, UFRN, Natal-RN, Brazil. [2] Programa de Pós-graduação em Ciências da Saúde, UFRN, Natal-RN, Brazil. [3] Laboratoire de Physico-Chimie, Pharmacotechnie et Biopharmacie UMR CNRS 8612, Faculté de Pharmacie, Université Paris-Sud XI, Chatenay-Malabry – France. [4] Programa de Pós-graduação em Ciências Farmacêuticas, UFRN, Natal-RN, Brazil.*

**INTRODUCTION:** Oil-in-water (O/W) or water-in-oil (W/O) emulsions used in personal care applications need to satisfy a number of criteria including the right consistency for application, good skin feel, good spreading and good delivery of actives. Therefore, the physical characteristics of the cosmetic or pharmaceutical product, and particularly its rheological properties, play also an important role in the current drug administration. The knowledge of the rheological properties is also important in the processing, the handling, the process design and the product development. This work aims to develop and to analyse a W/O emulsion formulation with potential application in cosmetic industry.

**METHODS:** Pseudo-ternary phase diagrams were constructed at 25°C, for systems containing Sesame oil / surfactants / water. Moreover, rheological studies were performed on a Haake RS600 rheometer equipped with a stainless steel cone/plate measurement device of 35 mm in diameter, a cone angle of 2° and a gap of 105 µm. From the pseudo-ternary phase diagrams (Fig. 1), sevem emulsion formulations (Table 1) were selected and analysed.

Table 1. Sesame oil emulsion formulations (W/W)

| Samples | Sesame oil | Span 80 | Tween 20 | Water |
|---|---|---|---|---|
| **1** | 32.4 | 0 | 8.40 | 19.2 |
| **2** | 25.8 | 1.02 | 9.18 | 24.0 |
| **3** | 35.4 | 1.56 | 6.24 | 16.8 |
| **4** | 32.4 | 1.80 | 4.20 | 21.6 |
| **5** | 31.8 | 2.40 | 3.60 | 22.2 |
| **6** | 32.4 | 3.00 | 3.00 | 21.6 |
| **7** | 34.2 | 2.16 | 1.44 | 22.2 |

**RESULTS:**

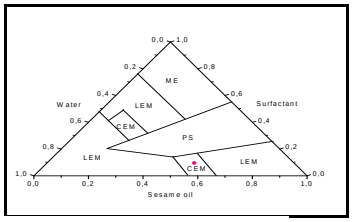


*Fig 1: Pseudo-ternary Phase diagram.*

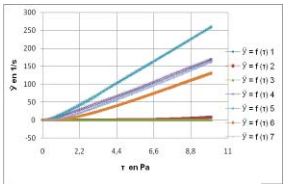

*Fig 2: Rheograms of all formulations.*

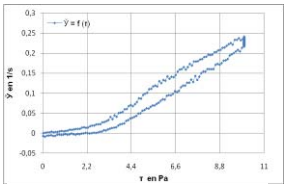

*Fig 3: Sample 2 rheogram.*

**DISCUSSION & CONCLUSIONS:** The rheograms of all emulsions demonstrated pseudo plastic-type behaviour (Fig. 2). For the same shear rate, the emulsions showed an adequate viscosity value, predicting a good topic application. The ascending and descending flow curves of Sample 2 showed hysteresis, usually referred as a 'thixotropic loop'(Fig. 3). Thixotropy is wanted in topical formulations because they are deformed during application and become fluid, then, facilitating the spreading process. The recovery of the initial viscosity after application prevents the product from dripping. Knowledge of rheological properties of topical treatments is essential because the determination of their viscoelastic parameters, critical stress value and hysteresis index is a good technological tool to predict their spreading ability on the skin. The rheological characterization presented in this study is of great relevance for the further development studies on cosmetic products using Sesame oils as oil base. Therefore, in accordance with the intended aim related to the industrial production, to the physical stability, and to the application and/or the cosmetic effect, certain formulations with specific rheological features can be more suitable.

**REFERENCES:** [1] I. Roland, G. Piel, L. Delattre, (2003) *J Pharm* **263**:85-94. [2] S. Tamilvanan (2004) *Prog Lipid Res* **43**:489-533.

**ACKNOWLEDGEMENTS:** Coordenação de Aperfeiçoamento de Pessoal de Nível Superior – CAPES.

# Systematic Development of Emulsions for Formulation Design

KGH.Silva[1,2,3], RR.Santiago[1,4], KS.Silva[1,4], KCH.Silva[1], F.Alexandrino-Júnior[1], EST.Egito[1,2,4]

*[1]Laboratório de Sistemas Dispersos (LASID), Departamento de Farmácia, UFRN, Natal-RN, Brazil. [2]Programa de Pós-graduação em Ciências da Saúde, UFRN, Natal-RN, Brazil. [3]Laboratoire de Physico-Chimie, Pharmacotechnie et Biopharmacie UMR CNRS 8612, Faculté de Pharmacie, Université Paris-Sud XI, Chatenay-Malabry – France. [4]Programa de Pós-graduação em Ciências Farmacêuticas, UFRN, Natal-RN, Brazil.*

**INTRODUCTION:** Emulsions are not only formulated for parenteral and topical administration, but also for oral and ocular routes [1-2]. All emulsions should be first considered as dispersed systems and overall analyzed in terms of stability. Creaming, coalescence, flocculation, phase separation, rupture and Ostwald ripening may occur in emulsified systems leading to numerous instability processes [1]. The development and prediction of the in-time stability of an emulsion are topics of interest for researchers. The aim of this work was to determine which steps and assays should be systematically performed to, efficiently, develop and evaluate the stability and the overall characteristics of an emulsion.

**METHODS:** Formulation design requires at least the construction of a pseudo-ternary phase diagram, a study of the critical hydrophilic-lipophilic balance (cHLB) of the oil and the characterization tests for stability and properties of the emulsions. Additionally, it is of great importance to determine cHLB value in which the larger area of emulsion could be obtained, eleven phase diagrams were constructed. The emulsions (seven formulations) were composed of Sesame oil, surfactant/co-surfactant (Tween® 20/Span® 80) and water. Droplet size evaluation, rheology, microscopic analysis, pH, conductivity measurements, creaming (TurbiScan®), and the investigation of stability under centrifugation and freeze/than cycles were performed.

**RESULTS:**

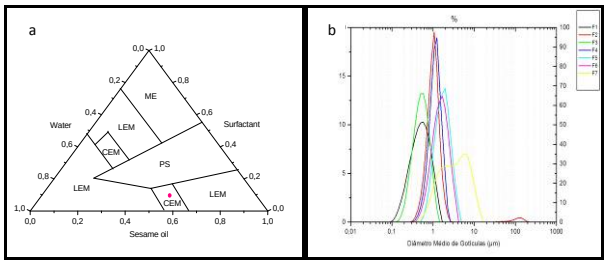


*Fig. 1: a) Pseudo-ternary phase diagram; b) Droplet size evaluation.*

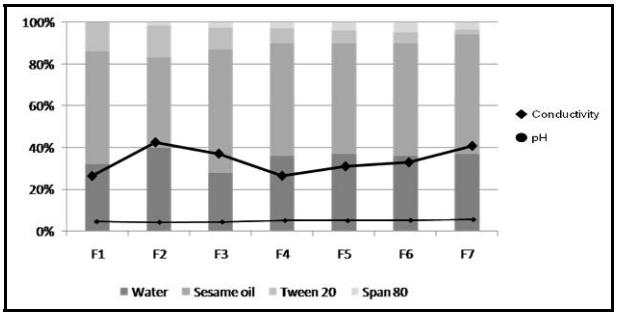


*Fig. 2: pH and conductivity according to each formulation.*

**DISCUSSION & CONCLUSIONS:** The results show that the emulsion area in the psudo-ternary phase diagram, the droplet size and the emulsion type seems to be dependent of the relative amount of surfactants. Rheological studies indicated that the viscosity exhibited two different behaviors, depending on the composition. The TurbiScan® was suitable to evaluate the stability of emulsified systems and gave information about coalescence and size modification. Viscosity, pH and conductivity measurements were useful, especially, in the evaluation of quality assurance. The study under centrifugation gave excellent information about the stability of the system comparing the creaming rates. In fact, it allows the distinction between different emulsions type and HLB determination. The freeze/thaw cycle test was interesting to distinguish some formulations that are similar regarding other stability characteristics, as storage at 45ºC. In conclusion, this work shown that a pattern protocol containing a sequence of steps to predict the unknown cHLB of the oil and the stability of emulsions was mandatory on the development of new emulsion formulations.

**REFERENCES:** [1] I. Roland, G. Piel, L. Delattre, (2003) *J Pharm* **263**:85-94. [2] S. Tamilvanan (2004) *Prog Lipid Res* **43**:489-533.

**ACKNOWLEDGEMENTS:** Coordenação de Aperfeiçoamento de Pessoal de Nível Superior – CAPES.

# How the method of preparation of a Penicillin G Benzathine nanoemulsion interferes on its stability

KGH.Silva[1,2,3], X.Zhang[3], RR.Santiago[1,4], G.Barratt[3], EST.Egito[1,2,4]

*[1]Laboratório de Sistemas Dispersos (LASID), Departamento de Farmácia, UFRN, Natal-RN, Brazil. [2]Programa de Pós-graduação em Ciências da Saúde, UFRN, Natal-RN, Brazil. [3]Laboratoire de Physico-Chimie, Pharmacotechnie et Biopharmacie UMR CNRS 8612, Faculté de Pharmacie, Université Paris-Sud XI, Chatenay-Malabry – France. [4]Programa de Pós-graduação em Ciências Farmacêuticas, UFRN, Natal-RN, Brazil.*

**INTRODUCTION:** Nanoemulsions are fine and non-equilibrium dispersions with droplet size range of 100-600nm[1]. The aim of this work was to study the influence of different methods of preparation of O/W nanoemulsions for parenteral administration of Penicillin G Benzathine (PenGB) on their droplet size and stability. Three methods and their influence on the nanoemulsion properties were evaluated. The investigated methods were: 1. high-energy emulsification (Ultrasound-US), 2. high-pressure homogenization (Ultraturrax-UT) and 3. low-energy emulsification (spontaneous emulsification-SE).

**METHODS:** The US nanoemulsions were prepared using an ultrasonic device (Bioblock Scientific, power 7500 W) during 1 minute at an amplitude of 30%. The UT systems were produced using an Ultraturrax at 13,500 rpm for 3minutes. The SE nanoemulsions were obtained by the spontaneous emulsification process[2]. After the development of the formulation,1mg/mL of PenGB were added to the systems. All formulations had their physicochemical characteristics and parameters evaluated for 30 days. The droplets size was measured using a Light-scattering Particle Size Analyser and the stability study was carried out by a Turbiscan Analyzer.

**RESULTS:**

*Table 1. Particle size (mean and* standard deviation (SD)) *and poly-dispersity index (PdI) of the nanoemulsions.*

| Methods | Size (nm) | | PdI | |
|---|---|---|---|---|
| | Mean | SD | Mean | SD |
| **SE** | 211,3 | 5,214 | 0,088 | 0,01 |
| **US** | 210,9 | 2,108 | 0,359 | 0,018 |
| **UT** | 237 | 2,05 | 0,643 | 0,002 |

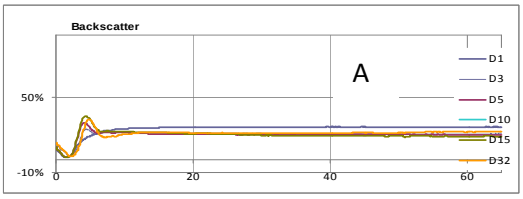


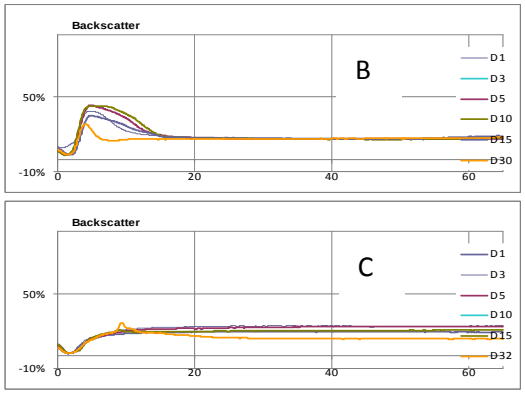


*Fig. 1: Back scattering profiles of Turbiscan analysis of the samples prepared with US (A), UT (B) and SE (C).*

**DISCUSSION & CONCLUSIONS:** After preparation, all formulations presented a milky aspect. From the results of the conductivity (5-50µS/cm), it can be seen that all nanoemulsions were O/W type. The best results of the mean particle size and poly-dispersity index were found for the SE nanoemulsions. In general, poly-dispersity index gives information on the deviation from the average size. Values up to 0.250 are acceptable for parenteral emulsions. Emulsions containing the smallest globules (usually 200–500 nm) tend to be the most physically stable. The Turbiscan analysis reveal that nanoemulsions prepared with SE and US presented best stability after the 30$^{rd}$ day. On the other hand, UT nanoemulsions presented the first phenomena of instability after the 10$^{th}$ day. The US and UT systems were not able to correctly entrap and hold the PenGB. However, the SE method gives the best results with all PenGB entrapped on it. The stability of this refined formulation will be further assessed and the need for optimization will be performed by sequential factorial designs. These results show that the characteristics and properties of these systems depend not only on their composition but also on their preparation method.

**REFERENCES:** [1]Bouchemal, K., et al., *International Journal of Pharmaceutics, 2004.* **280** (1-2): p. 241-251. [2] Egito, E.S. T. et al, S.T.P. *Pharma Sciences,* 1994. 4, 155–162.

# Phase Behavior and Physicochemical Aspects of Sesame Oil Containing Microemulsion Systems

KGH.Silva[1,2,3], RR.Santiago[1,4], G.Barratt[3], EST.Egito[1,2,4]

*[1]Laboratório de Sistemas Dispersos (LASID), Departamento de Farmácia, UFRN, Natal-RN, Brazil. [2]Programa de Pós-graduação em Ciências da Saúde, UFRN, Natal-RN, Brazil. [3]Laboratoire de Physico-Chimie, Pharmacotechnie et Biopharmacie UMR CNRS 8612, Faculté de Pharmacie, Université Paris-Sud XI, Chatenay-Malabry – France. [4]Programa de Pós-graduação em Ciências Farmacêuticas, UFRN, Natal-RN, Brazil.*

**INTRODUCTION:** Sesame, a widely known and important oilseed from *Sesamum indicum*, is considered to have not only nutritional value, but also some medicinal effects. Sesame oil is used in the pharmaceutical, cosmetic, and food industries. Additionally, this oil is of great interest in pharmaceutical formulations and has been used as a solvent in the preparation of sustained-release intramuscular or subcutaneous injections. The advantages of microemulsions over conventional emulsions or other lipid carriers concern its high stability and solubilization properties[1,2,3]. The aim of this work was to investigate the phase behaviour and physicochemical aspects of Sesame oil containing microemulsions systems..

**METHODS:** Aiming to evaluate the microemulsions regions, phase diagram were constructed by titrating surfactants/sesame oil mixtures with water at 25°C. Mixture compositions corresponding to the different types and structure of microemulsions (Table 1) were analysed by polarized light microscopy, pH, rheology behavior, refractive index, stability evaluation, particle size, and transmission electron microscopy.

*Table 1. Microemulsion composition (%).*

| Samples | Water | Sesame oil | Surfactants |
|---|---|---|---|
| **1** | 5 | 5 | 90 |
| **2** | 10 | 10 | 80 |
| **3** | 20 | 20 | 60 |
| **4** | 5 | 20 | 75 |
| **5** | 10 | 20 | 70 |
| **6** | 10 | 30 | 60 |
| **7** | 10 | 40 | 50 |

**RESULTS:**

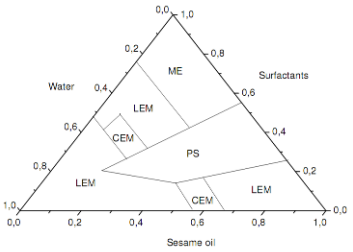


*Fig. 1: Phase diagram (surfactant ratio Tween® 20: Span® 80).*

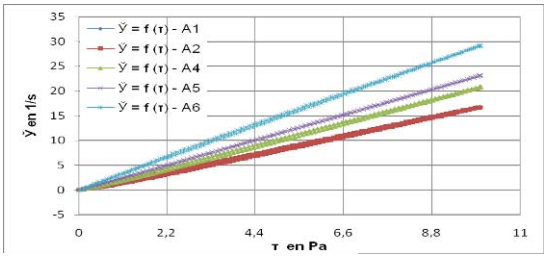


*Fig. 2 : Formulation Rheograms.*

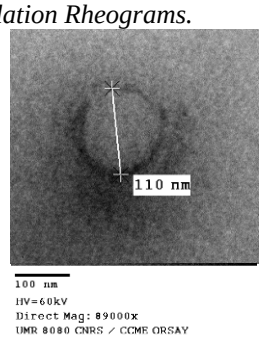


*Fig. 3: Transmission electron microscopy (Sample 4).*

**DISCUSSION & CONCLUSIONS:** The area of existence of O/W microemulsion is represented by the region of the diagrams shown in Figure 1. Rheological studies indicated that all samples exhibited a Newtonian behavior (Fig. 2). The viscosity values of all samples were low and relatively constant at 5 to 10 mPas. The values of pH (around 6.5 for all samples) indicate good biocompatibility. The refractive index (1.453) confirms the transparency of the systems and the isotropy was confirmed by analyses in polarized light microscopy. The particle size and morphology was analyzed by transmission electron microscopy (Fig 3). The samples had revealed stable to 25ºC for more than 6 months, indicating, therefore, adjusted physical stability for pharmaceutical industry. Clearly, a better understanding of the physicochemical property of these systems is necessary in order to optimize their drug transport and its delivery potential.

**REFERENCES:** [1]P. P. Constatinides (1997) *Int. J. of Pharm.* **158**:57-6. [2] S.Tenjarla (1999). *Crit Rev Ther Drug Carrier Syst* 16(5): 461–52. [3]F. Podlogar (2004) *Int. J. of Pharm.* 276: 115–128.

European Cells and Materials Vol. 20. Suppl. 3, 2010 (page 242) ISSN 1473-2262

# Tumor Targeting with a Fusion Toxin derived from an EpCAM-specific Designed Ankyrin Repeat Protein using Polymeric Nanoparticles

Manuel Simon[1,2], Andreas Plückthun[2], Uwe Zangemeister-Wittke[2]

[1]*Institute of Pharmacology, University of Bern, Switzerland,* [2]*Department of Biochemistry, University of Zürich, Switzerland*

**INTRODUCTION:** Targeted delivery of highly potent bacterial protein toxins is of interest for cancer therapy. Using genetically engineered variants of the biotoxin *Pseudomonas* Exotoxin A (ETA) fused to a highly selective cell binding ligand holds promise for tumor targeting [l]. We have recently generated a novel fusion toxin, which is composed of the EpCAM-specific Designed Ankyrin Repeat Protein (DARPin) Ec4 as a highly stable non-IgG cell-binding moiety genetically linked to ETA. Although the fusion toxin Ec4-ETA could be expressed at very high yields and showed promising anti-tumor activity in preclinical experiments *in vivo*, the systemic use of this class of protein therapeutics is limited due to immunogenicity and hepatotoxicity. Encapsulation of the whole fusion toxin into a biodegradable nanopolymer holds promise to provide a new nanomedicine overcoming these limitations.

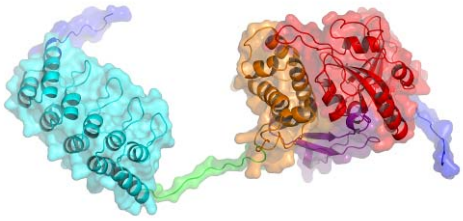

*Fig. 1: Model of the DARPin-exotoxin A fusion toxin Ec4-ETA.*

**METHODS:** Ec4-ETA was encapsulated into polymeric PLGA-PEG nanoparticles using a double-emulsion solvent-evaporation technique. This resulted in fusion toxin-loaded small uniform particles, which were characterized by SEM, photon correlation spectroscopy and zeta potential measurements. The amount of encapsulated fusion toxin was assessed in a microBCA assay. Furthermore, we measured the release kinetic of Ec4-ETA from the PLGA-PEG nanoparticles, and determined its biologic activity in cell binding and viability assays.

**RESULTS:** To improve its pharmacokinetic and safety profile, Ec4-ETA was encapsulated into a polymeric delivery system. To this end, we used the biodegradable polymer PLGA (Poly-lactic-co-glycolic acid) and its PEGylated diblock polymer PLGA-PEG in a w/o/w double emulsion setup, which resulted in high encapsulation efficiencies

(>90%) of the payload. The assembled fusion toxin-loaded nanoparticles were analyzed using SEM and photon correlation spectroscopy, showing a narrow size distribution of small particles (pdi 0.158, d=192.6) and a ζ potential of -12mV. Furthermore, we investigated the drug delivery mechanism of the nanoparticles in a release kinetic study, where, after an initial burst phase, Ec4-ETA was constantly released over a period of 6 days.

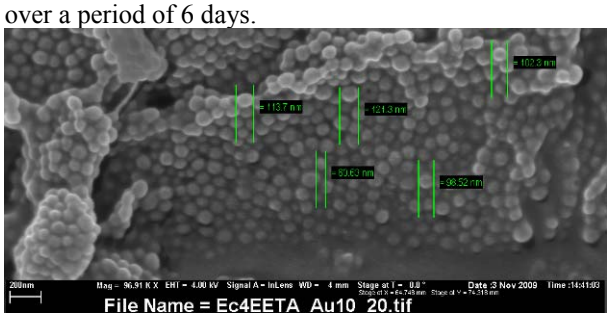


*Fig. 2: SEM image of Ec4-ETA-loaded PLGA-PEG nanoparticles.*

Ec4-ETA released from the particles bound to EpCAM-positive tumor cells through the DARPin moiety, followed by receptor-mediated endocytosis and cell death induction by the biotoxin with an $IC_{50}$ ranging from 3.25 to 0.33 pM. Despite this high potency *in vitro*, however, preliminary experiments in a human tumor xenograft model in mice unveiled that tumor targeting and anti-tumor activity of Ec4-ETA in a nanoparticle were substantially lower than of the free fusion toxin.

**DISCUSSION & CONCLUSIONS:** PLGA-PEG nanoparticles are well suited for encapsulating biotoxins engineered for cancer therapy. However, further investigations *in vivo* are mandatory to improve tumor targeting with PLGA-encapsulated Ec4-ETA and explore its therapeutic potential. In ongoing experiments we are elucidating the most crucial determinants for *in vivo* tumor targeting and efficacy of the Ec4-ETA containing nanomedicine using surface decoration with EpCAM-targeted DARPins or peptides targeting the tumor vasculature. First results from *in vivo* biodistribution and tumor localization experiments with $^{99m}$Tc-labeled preparations will be presented.

**REFERENCES:** [1] Martin-Kilias et al. A Novel Fusion Toxin Derived from an EpCAM-specific Designed Ankyrin Repeat Protein has Potent Antitumor Activity. *Cancer Res.* (submitted)

European Cells and Materials Vol. 20. Suppl. 3, 2010 (page 243) ISSN 1473-2262

# Biocatalysed Peptide Hydrogels: An Investigation of Self-assembly Kinetics using NMR spectroscopy.

Anders B. Sorensen[1], Patrick Hartley[1] and Richard J. Williams[1]

[1]*CSIRO Molecular and Health Technologies, Clayton VIC 3168, Australia*

**INTRODUCTION:** The formation of well defined nano- to micro- scale structures is of interest for many applications in the field of functional materials. The mechanisms used to form these materials range from cross-linking (covalent interactions) to small-molecule self assembly (physical interactions). Recently, research has focussed on the formulation of "smart stimuli-responsive" materials which can change their properties in response to controlled, externally applied stimuli (such as pH, temperature, ionic strength, solvent polarity, biomolecules, and light[1]). One promising method for deriving these materials is via the use of enzymes, which perform a chemical change to the precursor, producing a building block with an increased propensity to interact visualised as a gel-sol response[2]. The self-assembly kinetics have been shown to control the properties of the underpinning structure, and therefore, the mechanical properties of the formed hydrogels. The ability to biofunctionalise these materials and to control their mechanical properties are of interest in biological applications where, for example, substrate modulus has been utilized to direct the differentiation of human mesenchymal stem cells.[3]

However, the direct measurement of the kinetics of self-assembly presents a challenge. Here, we will discuss an NMR methodology which we have developed to investigate the self-assembly kinetics of an enzyme catalysed, peptide self assembly system.

**METHODS:** Self-assembling peptide hydrogels were formed from the self assembly precursor Fmoc-Leucine (L) (20mM) and LL (40mM), using reversed enzymatic hydrolyses catalyzed by the endoprotease Thermolysin[4]. Nuclear Magnetic Resonance (NMR) was used to investigate the formation of hydrogel in real time. The effect of conditions such as pH, substrate concentration and enzyme concentration were investigated.

To investigate the effects of diffusion limitations thermolysin was surface-immobilized on the wall of glass NMR tubes using dopamine.The NMR data was compared to HPLC time course experiments which show the formation of product in contrast to the formation of hydrogel.

**RESULTS and DISCUSSION:** The amount of Fmoc in solution gradually decreases as the enzyme converts Fmoc-L and LL to the self-assembling Fmoc containing tri peptide Fmoc-LLL-OH, which disappears from solution. Fig 1 shows the results of

NMR experiments demonstrating that pH has a marked effect on the self-assembly kinetics. In contrast the enzyme concentration is shown to have little effect as the kinetics seem to be dependent on the design ionisation state of the precursor not the kinetics of the enzyme. The immobilization of the enzyme led to diffusion limitation as the assembly process continued for more then 60 hrs (data not shown).

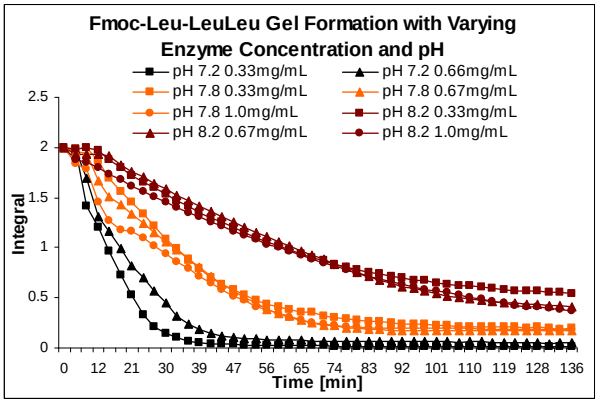


*Fig. 1: NMR time course experiment showing the effect of enzyme concentration (mg/ml) and pH on Fmoc-LLL formation., The integral was referenced to an internal std. and adjusted to a whole integer.*

**CONCLUSIONS:**

We have successfully developed a novel technique to monitor peptide self-assembly kinetics. We are using the insights gained from this technique to develop rationally-designed next generation functional self-assembled peptide based materials.

**REFERENCES:** [1] Mart, R.J. et al (2006) Peptide-based stimuli-responsive biomaterials, *Soft Matter*, **2**, 822. [2] Williams et al. (2010) Exploiting Biocatalysis in peptide self-assembly. *PeptideScience* **94** (1). [3] Engler et al (2005) Substrate elasticity directs adult mesenchymal stem cell differentiation. *Biorheology* **42** (33). [4] Williams et al. (2009) Enzyme-assisted self-assembly under thermodynamic control *Nature Nanotechnology*

European Cells and Materials Vol. 20. Suppl. 3, 2010 (page 244) ISSN 1473-2262

# CAPSOSOMES: AN APPROACH TOWARD CELL MIMICRY

B. Städler[1,2], R. Chandrawati[1], L. Hosta-Rigau[1], F. Caruso[1]

*[1] The University of Melbourne, Melbourne, Australia. [2] current address: Aarhus University, Aarhus, Denmark.*

**INTRODUCTION:** Novel therapeutic approaches rely on the development of nano-engineered vehicles which can mimic lost or missing cellular function. Such artificial cells or organelles, much simpler in design than their biological counterparts, are expected to be a powerful therapeutic tool.[1] Capsosomes, biodegradable polymer capsules with thousands of loaded liposomes as subcompartments, fulfill both requirements: while the polymer capsule provides the structural scaffold with controllable permeability, the liposomes are dividing its interior into sealed subcompartments which are suitable to protect and trap small fragile biomolecules. The data presented in here demonstrate the use of i) cholesterol-modified polymers to maximize and control the loading of liposomes into polymer multilayer films; and ii) a verification of the loading of the liposomes and the loading of liposomes into polymer capsules by demonstrating the functionality of the capsosomes.

**METHODS:** Capsosomes were assembled via the LbL technique. Silica particles were washed and resuspended in a polymer solution to adsorb the precursor layer, washed, suspended in the liposome solution, washed, and then either separation layers and additional liposome layers or a capping layer was adsorbed. Five polymer bilayers (thiolated poly(methacrylic acid) and poly(N-vinyl pyrrolidone) were sequentially adsorbed. The core-shell particles were cross-linked and the template core was removed.

**RESULTS:** *Assembly*: We identified the optimal polymer precursor, separation and capping layer to obtain maximum loading of different types of liposomes. We pioneered a novel approach to anchor multiple layers of liposomes to polymer multilayers based on a non-covalent linker, cholesterol (Schema 1ia and 1ib).[2-4] *Enzymatic assay*: By using the enzyme β-lactamase as the model encapsulate within the liposomes, the enzymatic activity was visualized and quantified by monitoring the conversion of its substrate in a triggered manner.[3,5]

**DISCUSSION & CONCLUSIONS:** Taken all together, capsosomes represent a promising approach to perform enzymatic cascade reactions within a confined environment or to deliver

hydrophobic therapeutics, thereby opening up novel possibilities for constructing artificial cells.

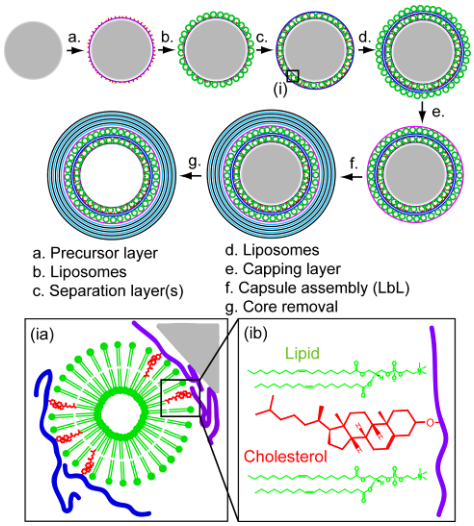


*Schema 1: Capsosome assembly: A template is coated with a polymer precursor layer (a.) followed by a liposome layer (b.). Cholesterol attached to a polymer as non-covalent linker (ia, ib) or electrostatic interactions anchor the liposomes. A number of separation layers (c.) are assembled followed by a second layer of liposomes (d.) and a polymer capping layer (e.). The polymer carrier capsule is assembled via the LbL technique and after dissolving the core, capsosomes (g.) are yielded.*

**REFERENCES:** [1] B. Stadler, A. D. Price, R. Chandrawati, L. Hosta-Rigau, A. N. Zelikin, F. Caruso, (2009) *Nanoscale* **1**, 68-73. [2]R. Chandrawati, B. Stadler, A. Postma, L. A. Connal, S. F. Chong, A. N. Zelikin, F. Caruso, (2009) *Biomaterials* **30**, 5988-98. [3]R. Chandrawati, L. Hosta-Rigau, D. Vanderstraaten, S. A. Lokuliyana, B. Stadler, F. Albericio, F. Caruso, (2010) *ACS Nano* **4**, 1351-61. [4] L. Hosta-Rigau, B. Stadler, Y. Yan, E. C. Nice, J. K. Heath, F. Albericio, F. Caruso, (2010) *Adv. Func. Mater.* **20**, 59-66. [5]B. Stadler, R. Chandrawati, A. D. Price, S. F. Chong, K. Breheney, A. Postma, L. A. Connal, A. N. Zelikin, F. Caruso, (2009) *Angew. Chem.-Int.Edit.* **48**, 4359-62.

**ACKNOWLEDGEMENTS:** This work was supported by Australian Research Council under the Federation Fellowship and Discovery Project schemes.

European Cells and Materials Vol. 20. Suppl. 3, 2010 (page 245) ISSN 1473-2262

# Spin-dependent mechanism of polymerization of nucleotides

V. E. Stefanov, A. A. Tulub

*St. Petersburg State University, St. Petersburg, Russia*

The ion-radical mechanism of decomposition of nucleotides has been theoretically discovered and indirectly confirmed in the experiment [1-2]. It proved much faster than the routine ionic mechanism. According to it nucleoside triphosphate (NTP) decomposes to nucleoside monophosphate (NMP) due to singlet-triplet transition of Mg with subsequent redistribution of electrons between Mg- and NTP-subsystems and formation of ion-radicals $Mg^{+}$ и $\bullet NTP^{3-}$ which generate in solution ion-radical $\bullet NMP^{-}$ within $1.25\times10^{2}$ ps, decomposition stage taking only few ps

$$(H_2O)_6Mg^{2+} + NTP^{4-} \xrightarrow{h\nu(-4H_2O)} [(H_2O)_2Mg^{+}\bullet\text{-}\bullet NTP^{-3}]^{SS} \xrightarrow{unstable} 2PO_3^{-} + O + \bullet Mg^{+}(H_2O)_2 + \bullet NMP^{-} \quad (1)$$

SS denotes spin-separated state with one unpaired electron spin on Mg and the other on NTP. We suggest that the ion-radical pathway can account for the unique capacity of Mg cation to initiate polymerization of nucleotides. In $\bullet NMP^{-}$, atom P is bound with three rather than four oxygen atoms, thus making feasible interaction between $\bullet NMP^{-}$ and $NMP^{2-}$ and, hence, the chain reaction of DNA(RNA) synthesis. We demonstrated that in the presence of inert AMP and water the mechanism of ion-radical polymerization starts from the initial unstable complex $Mg^{2+}(H_2O)_2$-$ATP^{4-}$ in the T-state involving only HO-$C_3$-group of ribose, while HO-$C_2$-group is associated only with ionic mechanism (hydrolysis). We converted starting non-equilibrium structure of the complex from S- to T-state by means of Frank-Compton excitation ($\Delta E^{T-S}$ = 40 kcal/mol). Interaction with AMP was analyzed by molecular dynamics Car-Parinello method [3]. Calculations were performed independently for T and S wave functions (t = 0 ÷ $2\times10^{-6}$ s). The Hamiltonian included interspinal (spin-spin and dipole-dipole) interaction between electrons of radical pairs as well as interspinal (contact and dipole-dipole) interaction between the nuclear, $^{31}P$ (AMP radicals) and $^{1}H$ (all molecules), and electron spins. The obtained results suggest occurrence of the conversion $Mg^{+} \rightarrow Mg^{2+}$, yielding electron to atomic oxygen in the endothermic reaction (1.25 kcal/mol), followed by immediate protonation of $O^{-}$ and subsequent

formation of hydroxyl radical •OH in the exothermic reaction (-2.00 kcal/mol). Hydroxyl radical approaches HO-$C_{3'}$-group of deoxyribose/ribose (spins of •OH and of H atom of HO-$C_{3'}$-group are opposite).

$$\bullet OH + HO\text{-}C_{3'}(AMP) \rightarrow H_2O + \bullet O\text{-}C_{3'}(AMP)$$

Then atom $P_\alpha$ (q = 1.15) of $\bullet AMP^{-}$ attacks oxygen atom O-$C_{3'}$ (q(O) = -0.87) in •AMP, forming dinucleotide AMP-AMP with unpaired spins localized on adenine fragments. The whole process, including formation of $(H_2O)_6Mg^{2+}$ complex, takes $1.2\times10^{3}$ ns. It takes $1.7\times10^{3}$ ns to generate trinucleotide. In evolution the choice between radical and ionic mechanism for polymerization of nucleotides may have taken place at the stage of prebiotic synthesis. Radical mechanism implies transition of Mg to T-state with the energy exceeding that of S-state by ~40 kcal/mol, which is hardly feasible in vitro without external energy input. However, recent X-ray studies [4] showed that in the active site of the enzyme Mg is bound with two Asp residues. In the absence of ATP, subsystem {Mg-$(Asp)_2$} oscillates between T- and S-states, according to our calculations energy of T-state being ~0.003 kcal/mol less than that of S-state. In the interaction of the subsystem with ATP resulting in the formation of quasi-chelate structure, T-state is realized ($\Delta E^{T-S}$ = 1.8 kcal/mol). Thus, the above described scheme of radical polymerization can proceed.

**REFERENCES:** [1]A.A.Tulub, V.E. Stefanov (2004) *J Chem Phys* **121**:11345-50. [2]A. A. Tulub, V. E. Stefanov (2008) *Europ Biophys J* **37**:1309-16. [3]R. Vuilleumier (2006) *Comp Simul Condens Matt Syst* **I**:223-285. [4]L. Yang, K. Arora, W.A. Beard, et al (2004) *J Am Chem Soc* **126**:5441-53

# Cell Signaling with Nanostructures for Regeneration

**Samuel I. Stupp**

*Departments of Chemistry, Materials Science and Engineering, and Medicine*

*Northwestern University*

Our laboratory has developed a superfamily of peptides modified with hydrophobic segments that are programmed to self-assemble into filamentous nanostructures[1-5]. These peptide amphiphiles create high aspect ratio hydrated filaments that are commonly cylindrical, but in some cases are flat, twisted, or tubular in architecture. Their formation is driven by hydrogen bonding, electrostatic interactions, and hydrophobic forces. When filaments are designed to display biological signals on their surfaces they exhibit remarkable bioactivity both *in vitro* and *in vivo*. The supramolecular chemistry of such nanostructures should allow them to interact specifically with cell receptors, extracellular matrix proteins, and intracellular targets. This lecture will describe the development of the self-assembly code that led to these powerful bioactive nanostructures for cell signaling. The lecture will also describe the potential function of these nanoscale filaments in spinal cord injury, Parkinson's disease, growth of blood vessels for ischemic disease, enhacement of cell therapies, and bone growth. A recent demonstration of how they can signal cells operating as *surrogate* growth factors will be illustrated in a model of cartilage regeneration[6]. Future directions with these systems include hierarchical structures that take the form of closed membranes that resemble cells[7], gels with macroscopic monodomains of oriented filaments[8], and crystalline bundles of filaments reminiscent of cytoskeletal structures[9].

[1] Hartgerink, J. D.; Beniash, E.; Stupp, S. I. *Science* **2001**, *294 (5547)*,1684-1688.

[2] Hartgerink, J. D.; Beniash, E.; Stupp, S. I. *PNAS* **2002**, 99 (8), 5133-5138.

[3] Silva, G. A.; Czeisler, C.; Niece, K. L.; Beniash, E.; Kessler, J. A.; Stupp, S. I. *Science* **2004**, 303 (5662), 1352-1355.

[4] Rajangam, K.; Behanna, H. A.; Hui, M. J.; Han, X; Hulvat, J. F.; Lomasney, J. W.; Stupp, S. I. *Nano Letters* **2006,** 6 (9), 2086-2090.

[5] Storrie, H.; Guler, M. O.; Abu-Amara, S. N.; Volberg, T.; Rao, M.; Geiger, B.; Stupp S. I. *Biomaterials* **2007**, 28 (31), 4608-4618.

[6] Shah, R. M.; Shah, N. A.; Del Rosario Lim, M. M.; Hsieh, C.; Nuber, G.; Stupp, S. I. *PNAS* **2010**, 107 (8), 3293-3298.

[7] Capito, R.; Azevedo, H.; Velichko, Y., Mata, A.; Stupp, S. I. *Science* **2008**, 319 (5871), 1812-1816.

[8] Zhang, S.; Greenfield, M. A.; Mata, A.; Palmer, L. C.; Bitton, R.; Mantei, J. R.; Aparicio, C.; de la Cruz, M. O.; Stupp, S. I. *Nature Materials*, **2010**, 9(7), 594-601.

[9] Cui, H.; Pashuck, E. T.; Velichko, Y. S.; Weigand, S. J.; Cheetham, A. G.; Newcomb, C. J.; Stupp, S. I. *Science* **2010**, 327 (5965), 555-559.

# Cell Signaling with Nanostructures for Regeneration

**Samuel I. Stupp**

*Departments of Chemistry, Materials Science and Engineering, and Medicine*

*Northwestern University*

Our laboratory has developed a superfamily of peptides modified with hydrophobic segments that are programmed to self-assemble into filamentous nanostructures[1-5]. These peptide amphiphiles create high aspect ratio hydrated filaments that are commonly cylindrical, but in some cases are flat, twisted, or tubular in architecture. Their formation is driven by hydrogen bonding, electrostatic interactions, and hydrophobic forces. When filaments are designed to display biological signals on their surfaces they exhibit remarkable bioactivity both *in vitro* and *in vivo*. The supramolecular chemistry of such nanostructures should allow them to interact specifically with cell receptors, extracellular matrix proteins, and intracellular targets. This lecture will describe the development of the self-assembly code that led to these powerful bioactive nanostructures for cell signaling. The lecture will also describe the potential function of these nanoscale filaments in spinal cord injury, Parkinson's disease, growth of blood vessels for ischemic disease, enhacement of cell therapies, and bone growth. A recent demonstration of how they can signal cells operating as *surrogate* growth factors will be illustrated in a model of cartilage regeneration[6]. Future directions with these systems include hierarchical structures that take the form of closed membranes that resemble cells[7], gels with macroscopic monodomains of oriented filaments[8], and crystalline bundles of filaments reminiscent of cytoskeletal structures[9].

[1] Hartgerink, J. D.; Beniash, E.; Stupp, S. I. *Science* **2001**, *294 (5547)*,1684-1688.

[2] Hartgerink, J. D.; Beniash, E.; Stupp, S. I. *PNAS* **2002**, 99 (8), 5133-5138.

[3] Silva, G. A.; Czeisler, C.; Niece, K. L.; Beniash, E.; Kessler, J. A.; Stupp, S. I. *Science* **2004**, 303 (5662), 1352-1355.

[4] Rajangam, K.; Behanna, H. A.; Hui, M. J.; Han, X; Hulvat, J. F.; Lomasney, J. W.; Stupp, S. I. *Nano Letters* **2006,** 6 (9), 2086-2090.

[5] Storrie, H.; Guler, M. O.; Abu-Amara, S. N.; Volberg, T.; Rao, M.; Geiger, B.; Stupp S. I. *Biomaterials* **2007**, 28 (31), 4608-4618.

[6] Shah, R. M.; Shah, N. A.; Del Rosario Lim, M. M.; Hsieh, C.; Nuber, G.; Stupp, S. I. *PNAS* **2010**, 107 (8), 3293-3298.

[7] Capito, R.; Azevedo, H.; Velichko, Y., Mata, A.; Stupp, S. I. *Science* **2008**, 319 (5871), 1812-1816.

[8] Zhang, S.; Greenfield, M. A.; Mata, A.; Palmer, L. C.; Bitton, R.; Mantei, J. R.; Aparicio, C.; de la Cruz, M. O.; Stupp, S. I. *Nature Materials*, **2010**, 9(7), 594-601.

[9] Cui, H.; Pashuck, E. T.; Velichko, Y. S.; Weigand, S. J.; Cheetham, A. G.; Newcomb, C. J.; Stupp, S. I. *Science* **2010**, 327 (5965), 555-559.

European Cells and Materials Vol. 20. Suppl. 3, 2010 (page 248) ISSN 1473-2262

# A Gigasealing Lipid Bilayer on a Single Polyelectrolyte Multilayer-filled Nanopore for Ion Channel Sensors

K. Sugihara, J. Vörös, T. Zambelli

*Laboratory of Biosensors and Bioelectronics, Institute for Biomedical Engineering, ETH Zurich, Gloriastrasse 35, CH-8092 Zurich, Switzerland*

**INTRODUCTION:** Ion channels are not only the prime targets for many drugs, but also are used like the one in human's hearts (hERG) for the negative-control test that all drug candidates have to pass. In pharmaceutical industries, "automated patch-clamp"[1] is used for testing drug binding to ion-channels, but the throughput is not sufficient. As such, at present this technology is the bottleneck in the whole screening process. Many alternative systems have been demonstrated: such as black lipid membranes (BLM)[2], where an artificial lipid membrane is painted over a typically 100 μm aperture in a hydrophobic chip; or supported lipid membranes (SLM)[3], where a lipid bilayer is fabricated on a conductive substrate by liposome fusion. Although some ion channels have been investigated in those systems, none of the existing approaches fulfills all the requirements (organic-solvent-free, self-assembling, and long lifetime) to replace the conventional system.

**METHODS:** We fabricated an artificial lipid bilayer on a polymer-filled nanopore (Figure 1a). The bilayer fabrication is organic-solvent free and based on self-assembly. Furthermore, the polymer support enhances the lifetime of the membrane up to a few weeks. The nanopore is filled by spraying polyelectrolytes, and a vesicle solution was added on the polymer-filled nanopore followed by a rinse to form a lipid bilayer.

**RESULTS:** The fluidity of the fabricated bilayer was confirmed by Fluorescent Recovery After Photo-bleaching (FRAP) using Confocal Laser Scanning Microscope (CLSM). The bleached region recovered completely in thirty minutes, proving the standard fluidity of reported PEM-supported-lipid bilayer systems[4]. The electrical resistance of the bilayer was successfully achieved gigaohm, characterized by electrochemical impedance spectroscopy (EIS). To test the membrane protein compatibility, a simple pore-forming peptide melittin was incorporated in the membrane and the channel activities were monitored for two and a half weeks (Figure 1b). The long lifetime of the system allowed us to monitor a time-dependent behavior of the channels, where the channel opening rate increases as time elapses.

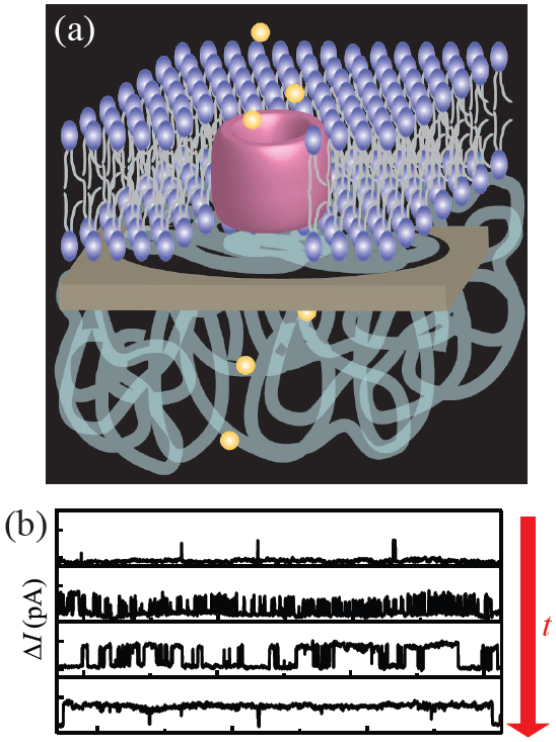


*Fig. 1: (a) Schematic of the sample. (b) Monitoring of Single channel events.*

**CONCLUSIONS:** We developed a gigasealing lipid bilayer by spontaneous vesicle fusion on a PEM-filled nanopore. The system is organic-solvent-free, self-assembling and long lifetime, all properties that potentially make the device higher-throughput than the conventional systems. Single-peptide-channel activities were monitored for a few weeks, proving the membrane-peptide compatibility. The next step toward ion-channel sensoring will be to incorporate target ion channels that do not spontaneously go into lipid membranes by proteoliposome fusion or using cell fragments.

**REFERENCES:**

[1] Dunlop, J., et al., *Nat Rev Drug Discov*, 2008. **7**(4): p. 358-368.

[2] Mueller, P., et al., *Nature*, 1962. **194**(4832): p. 979-980.

[3] Cornell, B.A., et al., *Nature*, 1997. **387**(6633): p. 580-583.

[4] Fischlechner, M., et al., *Soft Matter*, 2008. **4**(11): p. 2245-2258.

European Cells and Materials Vol. 20. Suppl. 3, 2010 (page 249) ISSN 1473-2262

# Folate Targeting Polymeric pH Nanosensors with a Full Dynamic pH Range for Live Cell Measurement

Honghao Sun, Rikke V. Benjaminsen, Kristoffer Almdal, Thomas L. Andresen

*Technical University of Denmark, Department of Micro- and Nanotechnology, Frederiksborgvej 399, 4000 Roskilde, Denmark.*

**INTRODUCTION:** Quantification of H+ concentrations in intracellular compartments is highly important for understanding cellular processes, e.g., the cell internalization pathways and transmembrane H+ gradients in mitochondria. Time resolved measurement of pH in the endocytic pathway of cancer cells is particularly interesting as quantitative information can guide the design of targeted narnodrugs, in which the release of effective thermotherapy molecules are triggered by acid after internalization. However, in current nanosensors drawbacks exist, the most predominant is the narrow measurement range. To broaden the measurement range of pH nanosensors, we constructed new sensors with two conjugated pH sensor fluorophores to a single sensor. Folate was also bound to the sensors to induce folate receptor mediated cellular uptake.

**METHODS:** Polyacrylamide naonoparticles (NPs) was used as matrix, which was prepared by reverse microemulsion polymerization1. In the NP synthesis, 3-amino-propyl-acrylamide was co-polymerized for further functionalization of NPs with folate and fluorescent dyes. Two pH indicator fluorophores, fluorescein (FA) (pKa 6.4, pH5.5~7.5) and Oregon Green (pKa 4.7, pH 3.8~5.7) with complementary pKa and thereby pH measurement range were covalently bound to a same sensor through thiourea bonds. Rhodamine B was bounded to all sensors as reference fluorophore. Folate was conjugated to the sensors via amide bonds, followed by capping excess amine with N-Succinimidyl-N-methylcarbamate (NMC) to give targeting pH nanosensor NPs-Folate-FA-Oregon-Rhb-NMC.).

**RESULTS:** NPs-Folate-FA-Oregon-Rhb-NMC demonstrates a pH measurement range from 4.05 to 7.50. Cellular experiment indicates that the NPs-Folate-FA-Oregon-Rhb-NMC sensor show improved cellular uptake compare to reference sensor NPs-FA-Oregon-Rhb-NMC due to folate receptor medicated internalization. The sensors have a diameter of ~70nm, which was characterized by dynamic light scattering (DLS) and cryogenic Transmission Electron Microscopy .

**DISCUSSION&CONCLUSIONS:** The new NPs-Folate-FA-Oregon-NMC pH nanosensors solves a fundamental problem of previously reported

nonsensors that could only measure a limited pH range. The new sensors offer themselves as an important new tool for measuring pH in intracellular compartments, in particular the acidic endosomes and lysosomes

*Scheme. 1 Synthetic procedure of targeting pH nanosensor.*

*Figure 1. Left, fluorescence intensity spectra of NPs-Folate-FA-Oregon-Rhb-NMC at difference pH; right, Fluorescent intensity ratio of (FA+Oregon)/Rhb is plotted against pH.*

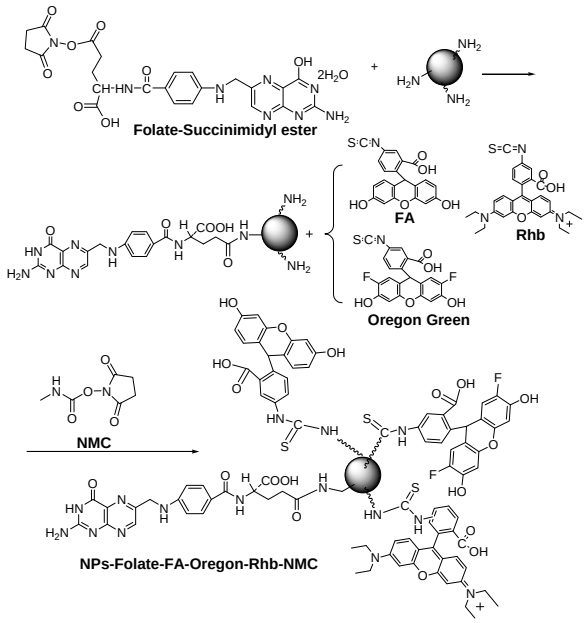


**REFERENCES:** [1]H.H.Sun, T.L. Andresen, R.V. Benjaminsen, K. Almdal. (2009) *Journal of Biomedical Nanotechnology* **5**: 1-7

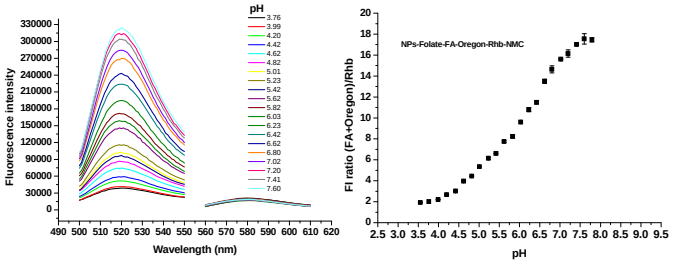


**ACKNOWLEDGEMENTS:** This work was financially supported by Kræftens Bekæmpelse Denmark and NABIIT.

European Cells and Materials Vol. 20. Suppl. 3, 2010 (page 250) ISSN 1473-2262

# Electrical properties of Silsesquioxane Dendrimer (G2-6Ph) LB films with Containing Phenyl Group by STM

Gi-Chan Sung[1], Hyen-Wook Kang[1,2], Burm-Jong Lee[2], Sang-Mok Jang[3], Chungkyun Kim[4] and Young-Soo Kwon[1,*]

*[1]Dept. of Electrical Engineering, Dong-A University, Busan, Korea., [2]Dept. of Chemistry & Institute of Functional Materials, Inje University, Gimhae, Korea, [3]Dept. of Chemical Engineering, Dong-A University, Busan, Korea, [4]Dept. of Chemistry, Dong-A University, Busan, Korea*

**INTRODUCTION:** This research is the application for the nano-device using the electrical properties of G2-6Ph. We investigated the monolayer behavior using the surface pressure-area (π-A) isotherm at the air-water interface. The monolayer was deposited onto highly oriented pyrolytic graphite (HOPG) substrates via the Y-type deposition according to the LB method. We observed the morphological properties and determined the electrical properties of the LB films using STM and STS.

**METHODS:** We have fabricated Langmuir-Blodgett (LB) films of G2-6Ph. We investigated the phase transition by π-A isotherm of G2-6Ph repeatedly five-cycles at the air-water interface. The monolayer was deposited onto highly oriented pyrolytic graphite (HOPG) substrates via Y-type deposition at surface pressure 6 mN/m. We observed the morphology of G2-6Ph LB films using scanning tunneling microscopy (STM). The G2-6Ph image indicated networking form which have cavity at the center. We also investigated an insulating property, conductivity of G2-6Ph by I-V property.

**RESULTS:** A LB thin film of G2-6Ph was fabricated using the LB method. Fig. 1 shows an investigation of the monolayer behavior involving five-cycle π-A isotherms at the air-water interface. We also investigated one-cycle π-A isotherms before studying those of five-cycles. The reduction in surface pressure was not sharp when the barrier was open. Based on these results, we propose that the molecule combination does not break any further, even though the barrier is open. Therefore, we investigated the five-cycle π-A isotherms for a stronger molecule combination. There does not appear to be a collapse point in the five-cycle π-A isotherms. Fig. 2 shows the I-V characteristics of the G2-6Ph LB film. The sample bias voltage was measured from 100 mV to 250 mV by increment of 50 mV. As shown in the I-V characteristics, the conductivity was $1.57\times10^{-13}$, $3.09\times10^{-13}$, $4.55\times10^{-13}$, and $5.58\times10^{-13}$ according to applied sample bias voltages, respectively [1].

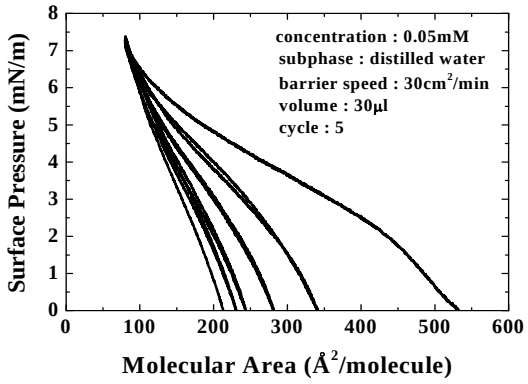


*Fig. 1: 5-cycle π-A isotherm of G2-6Ph.*

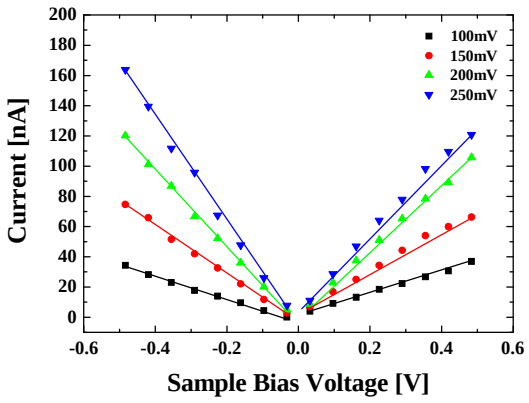


*Fig. 2: I-V Characteristics of G2-6Ph Film.*

**DISCUSSION & CONCLUSIONS:** We have investigated an LB film of G2-6Ph by focusing on its networking form and its electrical properties. According to the I-V characteristics, which show that conductivity increased about increase of sample bias voltage.

**REFERENCES:** [1]J. Y. Lee, G. C. Sung, C. H. Yang, D. S. Shin, C. Kim, Y. S. Kwon (2009) *Thin Solid Films* **518**:834.

# Curcumin Encapsulation Using Biodegradable Polymeric Nanoparticles: Controlled Release, Photostability and Transdermal Skin Penetration

N. Suwannateep[1], S. Wanichwecharungruang[2], J. Lademann[3]

[1] *Program in Biotechnology, Chulalongkorn University, Bangkok, Thailand.*
[2] *Department of Chemistry, Chulalongkorn University, Bangkok, Thailand.*
[3] *Department of Dermatology, Charité -Universitätsmedizin Berlin, Berlin, Germany.*

**INTRODUCTION:** Curcumin, a major yellow pigment from the rhizomes of turmeric (*Curcuma longa* Linn.), lends itself to potential application in medicine and other health related products [1-2]. Nevertheless, very low bioavailability caused by poor absorption, rapid metabolism, fast elimination and fast degradation are well-known problems of this interesting polyphenolic compound [3]. Encapsulation has been used to lessen these problems. However, the encapsulation system is still to be improved in terms of its loading capacity, encapsulation efficiency and curcumin protection capability, and further investigations on the absorption and release of the encapsulated curcumin are required [4].

**METHODS:** Curcumin was encapsulated into four different polymers, namely; methyl ether-terminated poly(ethylene glycol)-4-methoxycinna moylphthaloylchitosan (PCPLC), poly(vinyl-alcohol-co-vinyl-4-methoxycinnamate) with two degrees of 4-methoxycinnamoyl substitution (PB4-I and PB4-II) and ethyl cellulose (EC), by solvent displacement technique. The release of curcumin from nanoparticles was determined. The photostability of the encapsulated curcumin was compared with that of free curcumin. In addition, the transdermal skin penetration of aqueous suspensions of the encapsulated curcumin was investigated.

**RESULTS:**

*Table 1. The encapsulation efficiency (% EE), curcumin loading and photostability of various encapsulated curcumin products.*

| Polymer | % Encapsulation Efficiency | % Loading (w/w) | % Curcumin remained after 4 h sunlight exposure |
|---|---|---|---|
| EC | 96.62 ± 1.11 | 53.94 ± 1.01 | 71.77 ± 1.06 |
| PCPLC | 91.69 ± 1.09 | 50.39 ± 1.19 | 92.91 ± 1.15 |
| PB4-I | 91.22 ± 1.15 | 52.26 ± 1.05 | 78.78 ± 1.08 |
| PB4-II | 90.23 ± 1.08 | 57.28 ± 1.64 | 68.64 ± 1.04 |

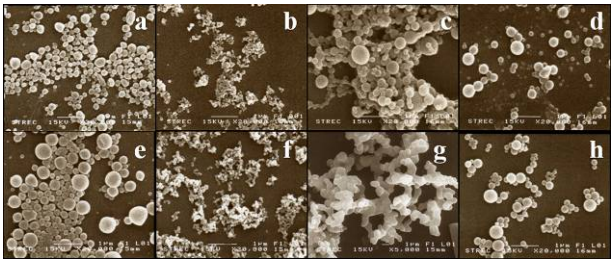


*Fig. 1: SEM photographs of empty (a) EC (b) PCPLC (c) PB4-I (d) PB4-II nanoparticles, curcumin-encapsulated (e) EC (f) PCPLC (g) PB4-I and (h) PB4-II nanoparticles.*

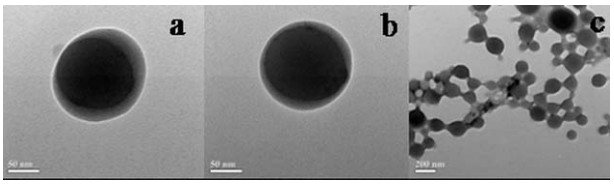


*Fig. 2: TEM photographs of (a) empty EC particles, (b) and (c) curcumin-encapsulated EC particles.*

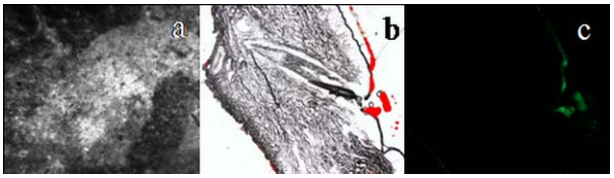


*Fig. 3: Ex vivo transdermal skin penetration photographs of curcumin encapsulated EC particles; LSM photograph (a), transmittance (b) and fluorescence photograph (c).*

**DISCUSSION & CONCLUSIONS:** All four polymers could effectively form curcumin-entrapped spheres with more than 90% encapsulation efficiency at the loading of 1:1 (w/w) polymer to curcumin ratio. The photostability study indicated that the encapsulated curcumin was significantly more stable than free curcumin. *In vitro* experiments suggested a controlled release of curcumin from all nanoparticles at pH 5.5 and pH 7. *An ex vivo* transdermal skin penetration study showed the strongly fluorescent signal of curcumin in the skin tissue. The picture indicated that hair follicle was the main transportation route.

**REFERENCES:** [1] C. H. Hsu and A. L. Cheng (2007) *Adv. Exp. Med. Biol.* **595**: 471–80. [2] M. M. Shishu (2010) *J. Funct. Foods* **2**: 60-5. [3] R. A. Sharma, A. J. Gescher and W. P. Steward (2005) *Eur. J. Cancer* **41**: 1955-68. [4] P. Anand, A. B. Kunnumakkara, R. A. Newman, and B. B. Aggarwal (2007) *Mol. Pharmaceutics* **4**: 807-18.

**ACKNOWLEDGEMENTS:** The authors thank the Office of the Higher Education Commission, NANOTEC and NSTDA, Thailand.

European Cells and Materials Vol. 20. Suppl. 3, 2010 (page 252) ISSN 1473-2262

# Initial Cell Attachment: Events and Kinetics of surface adhesion of NE-4C neural stem cells

I. Székács[1], I. Pál[1], Zs. Környei[1], I. Szendrő[2], E. Madarász[1]

[1] *Institute of Experimental Medicine of Hungarian Academy of Sciences.* [2] *MicroVacuum Ltd. Budapest, Hungary.*

**INTRODUCTION:** The molecular interactions and cell-biological mechanisms behind the adhesive behaviour of cells are not properly understood. By recording material deposition in a narrow layer (100-200 nm above the sensor surface), the OWLS assay provide real-time data on surface – cell membrane contacts, on membrane-derived shred material and compounds secreted by the cells. In order to distinguish between multiple processes of initial cell attachment, novel methods and cell holder cuvettes for OWLS instruments were elaborated.

**METHODS:**

***OWLS:*** The principle of the technique is that a linearly polarized laser light is coupled into the thin, planar waveguide layer by an optical diffraction grating [1]. The actual angle value depends on the complex refractive index of the sensor chip and the deposited material. Varying the angle of incidence of the polarized light, the incoupling angle can be determined with high accuracy, and therefore, the refractive index, thickness and coverage (or mass) of the adsorbed or bound material can be calculated with high sensitivity.

*Cell assays:* Suspensions ($10^6$ cells/ml; 100 µl) of NE-4C neural stem cells [2] in protein free, artificial cerebrospinal fluid were introduced onto the optical grating coupler waveguide sensor (OW 2400) fixed in the temperature-controlled (37°C) cuvette of OWLS 110 instrument (MicroVacuum, Hungary). Cells were allowed to contact the sensor surface, or were separated by "cell-holder membranes". Cell-substrate interactions were monitored up to 120 min.

*Evaluation:* Biosense2.5. program was used to determine the amount (Mass [ng/cm$^2$], distribution (FWHM)) and layer-thickness of deposited material on the sensor surface.

***Analysis on cell shape and motility*:** Modulations in cell shape and surface contacts were followed by time-lapse microscopy and optical sectioning (ApoTome imaging; and confocal microscopy; Zeiss, Olympus).

*Image analyses:* Programs analysing the optical dots given by cell-surface contact points were provided by I. Pál and A. Szabó (Royal Computer Kft., Budapest).

**RESULTS:** Cell sedimentation, contact point formation, spreading, and also cell-derived secreted material lead to alterations in the position and shape of the OWLS resonance peaks [3]. Signals of secretion and immediate cell contacts were distinguished by inserting cell-holder membranes into the OWLS cuvette. The data demonstrated a continuous deposition of secreted material, in contrast to the step-like formation of cell-to surface contacts. The timing of material deposition, contact formation and cell shape changes were compared by relating the OWLS signals to imaging data obtained either on cell-level morphological changes by time-lapse videomicroscopic analyses or on the size and frequency of contact plaques imaged by ApoTome and confocal techniques.

The data outlined a time-table of events of initial cell attachment; At least in case of NE-4C neural stem cells, secretion of extracellular matrix material by suspended cells was shown to precede contact formation. The time course of the above processes is highly determined by both the type of the cell and the adhesive substrate provided for attachment.

**DISCUSSION & CONCLUSIONS:** Combined assays on initial cell attachment demonstrated that monitoring cellular material deposition by OWLS technique provides multiple information, those usable for basic scientific studies and also for designing appropriate adhesive conditions for large-scale (bio-industrial) anchorage of diverse cell types.

**REFERENCES:** [1] www.owls-sensors.com. [2] K. Schlett, E. Madarász (1997) *J Neurosci Res.* **47**:405-415. [3]E. Madarasz, I. Levkovets, K. Erdelyi, I. Szendro (2007) *European Cells and Materials* **14**:100.

**ACKNOWLEDGEMENTS:** This work was supported by the "Bio_Surf" National Technology Program (NKTH, Budapest).

European Cells and Materials Vol. 20. Suppl. 3, 2010 (page 253) ISSN 1473-2262

# Potent Antitumor Effect of NK012 (Polymeric Micelles Incorporating SN-38) Against Hepatic Metastases in a Model of Colorectal Cancer

A.Takahashi[1, 2], N. Ohkohchi[2], T. Kinoshita[1], Y.Matsumura[1]

[1]*National Cancer Center Hospital East, Kashiwa, Japan.*

[2]*University of Tsukuba, Tsukuba, Japan.*

**INTRODUCTION:** Liver metastasis is a major problem in the treatment of colorectal cancer. Chemotherapy is an essential modality in advanced metastasis, and irinotecan hydrochloride (CPT-11) is a key drug in chemotherapy for advanced colorectal cancer. However, chemotherapy- associated liver toxicity, which affects the mortality and morbidity rates of post-chemotherapy hepatectomy, is caused by intensive or prolonged use of CPT-11 [1]. Therefore, a more effective and less toxic drug needs to be developed. We compared the antitumor effects of CPT-11 and NK012, a drug consisting of 7-ethyl-10-hydroxy-camptothecin (SN-38)–incorporating polymeric micelles, on mice with multiple liver metastases of human colon cancer HT-29 cells. In addition, to clarify the behavior of NK012 in the liver parenchyma and metastatic tumors, we investigated in detail the biodisposition of NK012 following intravenous administration.

**METHODS:** NK012 or CPT-11 was intravenously administered three times every 4 days at their respective maximum tolerable doses (NK012: 30 mg/kg, CPT-11: 66.7 mg/kg) to mice bearing liver metastases formed 7 days after portal administration of HT-29 cells (n = 6). *In vivo* antitumor effects were evaluated by bioluminescence imaging and histopathologic observation. Drug biodistribution was analyzed by high-performance liquid chromatography and fluorescence microscopy as described previously [2-3].

**RESULTS:** NK012 abolished the tumors completely in a multiple liver metastatic model of colon cancer. HPLC showed prolonged distribution of NK012 in the tumors, liver, and spleen. Fluorescence microscopy and immunohistochemistry indicated that NK012 penetrated the tumor tissue in the early phase and was distributed near to the tumor vessels in the late phase. NK012 was distributed not in the hepatocytes but in CD68-positive cells such as Kupffer cells in the liver in the early or late phase.

**DISCUSSION & CONCLUSIONS:** NK012 was strongly effective against liver metastases and not harmful to the liver parenchyma, although the drug accumulated for a long time in macrophages such as Kupffer cells. It is speculated that SN-38 released from NK012 stored in normal liver cells is inactivated efficiently by the glucuronyl tranferase in the liver cell.

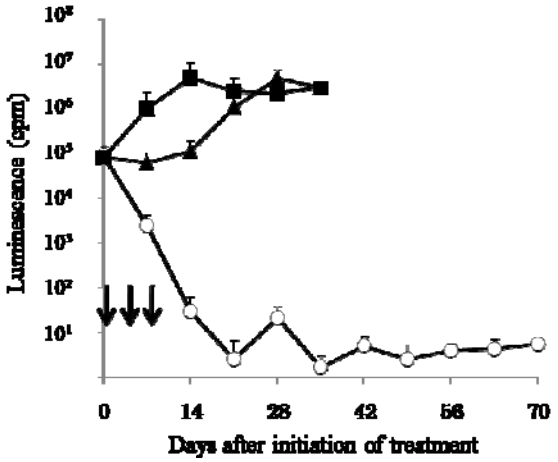


*Fig. 1: Effects of NK012 and CPT-11 in HT-29/Luc liver metastasis mouse models. Each treatment was given on days 0, 4, and 8 (○NK012; 30 mg/kg ×3, ▲CPT-11; 66.7 mg/kg ×3, ■Control; PBS 200 µl ×3, n = 6).*

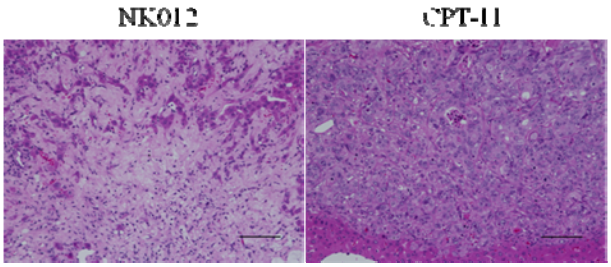


*Fig. 2: H&E sections of metastatic tumor and liver treated with NK012 or CPT-11 (bar, 100 µm). NK012 (30 mg/kg) or CPT-11 (66.7 mg/kg) was administered on days 0, 4, and 8. Metastatic tumors and livers were excised 15 days after initiation of treatment.*

**REFFERECNES:** [1]Fernandez FG, Ritter J, Goodwin JW et al. (2005) *J Am Coll Surg* **200**: 845-53. [2]Koizumi F, Kitagawa M, Negishi T, et al. (2006) *Cancer Res* **66**: 10048-56. [3]Kuroda J, Kuratsu J, Yasunaga M et al. (2009) *Int J Cancer* **124**: 2505-11.

**ACKNOWLEDGEMENTS:** A. Takahashi is an awardee of a research resident fellowship from the Foundation for Promotion of Cancer Research (Japan).

European Cells and Materials Vol. 20. Suppl. 3, 2010 (page 254) ISSN 1473-2262

# Efficient delivery of anti-cancer drugs using functional Poly(Carbonate) micelles stabilized by hydrogen bonding groups

J.P.K. Tan[1], S.H. Kim[2], F. Nederberg[2], K. Fukushima[2], D.J. Coady[2], A. Nelson[2], J.L. Hedrick[2], Y.Y. Yang[1]

[1] *Institute of Bioengineering and Nanotechnology, Singapore.* [2] *IBM Almaden Research Centre, USA.*

**INTRODUCTION:** The administration of lipophilic therapeutics is challenged by water insolubility, *in vivo* instability and non-specific toxicity.[1] Self-assembled micelles formed from amphiphilic block copolymers can be used to solve the aforementioned problems. However, polymeric micelles usually suffered from infinite dilution effect once they enter the blood stream and hydrophobic interactions is insufficient to maintain the self-assembly. We proposed the use of hydrogen bonding to stabilize and improve the drug loading capabilities.

**RESULTS:** For the synthesis of a functional urea carbonate monomer, phenyl isocyanate was reacted with amino alcohols and the phenylurea alcohol formed was then reacted with MTC-acyl chloride. Phenylurea ethanol was obtained from recrystallization (ethyl acetate) in high yields (>90%), and MTC-Urea was purified through a simple flash chromatography procedure in high yields (>85%). MTC-Et monomer was used as a non-functional counterpart to dilute the urea content in the hydrophobic block. Poly(ethylene glycol)-*block*-poly(ethyl-*random*-urea)carbonate PEG-P($E_{1-x}$-$U_x$)C) block copolymer was prepared by using methoxy PEG ($M_n$ of 5000 g/mol) as a macroinitiator for ring-opening polymerization.

PEG-P($E_{1-x}$-$U_x$)C (5k-3k) block copolymers formed nanosized micellar aggregates in 20-40 nm diameters with a narrow size distribution. The critical micellization concentration (cmc) result showed that the stabilized self-association driven by the hydrogen bonding urea lowered the cmc of micelles in an aqueous environment when the urea content was increased from 11.2 ml/L ($x$=0.0) to 2.8 mg/L ($x$=0.4).

The urea-functionalized polymer was used as a drug carrier for doxorubicin (DOX). The urea functionalities increased the drug loading from 6.9 wt% ($x$=0.0) to 10.3 wt% ($x$=0.4). These findings clearly demonstrate the role of hydrogen bonding urea groups in the block copolymer in micelle forming ability, drug loading, and favorable interaction with doxorubicin.

Free DOX exhibited a higher potency than that of micelle bound DOX (Figure 1a). The slightly

lower potency of DOX after being loaded into the micelles was probably due to the slow release of DOX from the micelles and delayed nuclear uptake in the HepG2 cells. The majority of DOX molecules were seen in the nuclei of the cells after 4 h of incubation with free DOX (Fig. 1b). However, DOX molecules were mainly seen in the cytosol of the cells, and only a small portion of DOX molecules were observed in the nuclei when delivered by DOX-loaded micelles due to slow release of DOX and its subsequent diffusion (Fig. 1c and d).

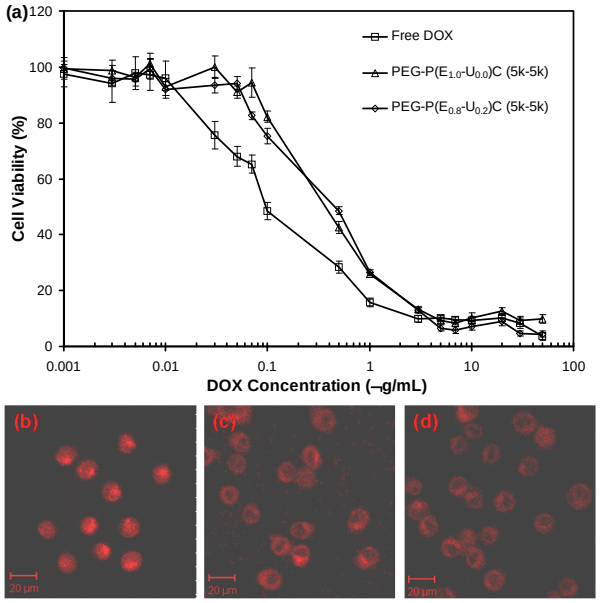


*Fig. 1: (a) Cytotoxicity assay of free DOX and DOX-loaded micelles on HepG2 and confocal images of HepG2 incubated with (b) free DOX, (c) DOX-loaded PEG-P($E_{1.0}$-$U_{0.0}$)C (5k-5k) and (d) DOX-loaded PEG-P($E_{0.8}$-$U_{0.2}$)C (5k-5k).*[2]

**CONCLUSIONS:** The incorporation of urea functionalities facilitated the formation of stable drug-loaded micelles and improved drug loading. These nanosized DOX-loaded micelles produced near complete cancer cell death with the polymeric carriers showing no cytotoxicity.

**REFERENCES:** [1]G.S. Kwon and K. Kataoka (1995) *Adv. Drug Delivery Rev.* **16**:295-309. [2]J.P.K. Tan, S.H. Kim, F.Nederberg et al. (2010) *Macromol. Rapid Commun.* (In Press)

# Deformability of K562 Cells Studied by Optical Tweezers

Z.L. Zhou, B. Tang, A.H.W. Ngan

*Department of Mechanical Engineering, The University of Hong Kong, Pokfulam Road, Hong Kong*

**INTRODUCTION:** Leukaemia is a public health concern worldwide. In this study, the deformability of K562 cell, a type of prominent chronic myelogenous leukaemia (CML) cell line, was investigated by indentation tests performed with a high laser power optical tweezers system.

**METHODS:** Fig. 1 shows the morphology of the K562 cells used in this study.

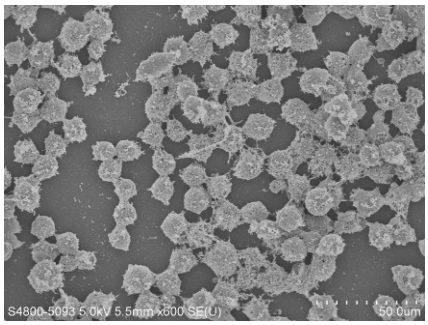


*Fig. 1 SEM image of K562 cells. The cells are spherical.*

Diluted polystyrene microspheres with 5μm in diameter were employed. The indentation procedure is as follow: i) the focus of the microscope was adjusted to overlap with the largest circular section of the cell; ii) a microsphere was trapped by laser of a given power and was pushed to the cell until the laser trapping was lost. The indentation depth was measured based on the microscope observation and the corresponding load can be calculated from the pre-calibrated maximum tapping-force-vs-laser-power relationship (0.1385 pN/mW). For each cell, indentation tests were repeated at different laser powers (1624 mW, 2408 mW and 3216 mW).

**RESULTS:** Fig. 2 shows the microsphere image of indentation tests.

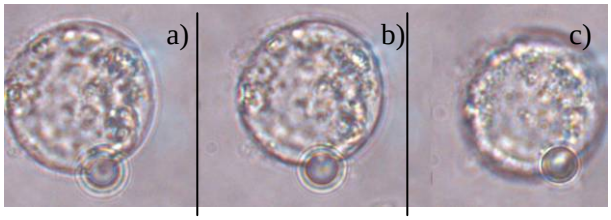


*Fig. 2 Microsphere images of indentation tests performed at a) 1624 mW, b) 2408 mW and c) 3216 mW.*

It was found that for a given cell, the measured indentation depth is linearly proportional to the applied load, as shown in fig. 3. This indicates that the microsphere-cell contact can be treated as approximately linear. The elastic modulus of K562 cells therefore can be calculated with Sneddon's elastic contact equation[1], assuming a constant contact area. The estimated elastic modulus ranges from 65 Pa to 104 Pa.

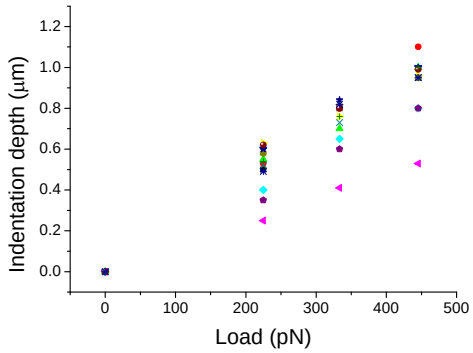


*Fig. 3 Indentation depth and load data recorded from indentation tests performed on different cells.*

**DISCUSSION & CONCLUSIONS:** To our knowledge, the elastic modulus of K562 cells has never been measured before. The elastic modulus of Jurket cells, typical acute myeloid leukaemia (AML) and acute lymphoid leukaemia (ALL) cells measured in previous study are 850 Pa and 48 Pa respectively[2]. The elastic modulus of K562 cells measured here, is larger than that of Jurket cells but is smaller than that of HL60 cells. This agrees with the clinic findings that the leukostasis incidence is in the order AML>CML>ALL[3], because stiffer cells should have a higher ability to obstruct the vasculature.

**REFERENCES:** [1]I.N. Sneddon (1965) *Int J Eng Sci* **3**, 47-57. [2]M.J. Rosenbluth, W.A. Lam and D.A. Fletcher (2006) *Biophysical J* **90**, 2994-03. [3]J.R. Shiber and R.E. Fines (2009) *J Emerg Med*, *in press*..

**ACKNOWLEDGEMENTS:** The presented study was supported by grants from the Research Grants Council (Project No. HKU 716908E)

European Cells and Materials Vol. 20. Suppl. 3, 2010 (page 256) ISSN 1473-2262

# The Glycocalyx of Endothelial Cells under Static and Flow Conditions

S. Tang, H. Hall

*Cells and BioMaterials, Department of Materials, ETH Zurich, Switzerland*

**INTRODUCTION:** Tissues deprived of sufficient blood perfusion often experience ischemia and degeneration leading to complete loss of function. Novel therapeutic agents and methods are being developed to repair damaged blood vessels and stimulate angiogenesis.

The glycocalyx is a layer of membrane-bound macromolecules which covers the luminal surface of endothelial cells which line all vasculature, comprising sulfated proteoglycans, hyaluronan, glycoproteins and binding to plasma proteins [1]. It establishes an exclusion zone between circulating blood in the lumen and the surface of endothelial cells, and plays a pivotal role in permeability functions, inflammatory response as well as mechanotransduction of fluid shear stress to the intracellular cytoskeleton. A functional glycocalyx is essential in maintaining and modulating low occurrences of thrombogeneicity, restenosis and inflammation, especially relevant for cardiovascular diseases [2].

**METHODS:** Human foreskin fibroblasts (hFFs) and human umbilical vein endothelial cells (HUVECs) were cultured on Ibidi μ-slides and subsequently submitted to static and flow conditions. All flow experiments throughout this study were performed using a Reglo Digital® tubing pump (MS-4/12, ISM597D, Ismatec). The cells' viability, elongation, orientation and alignment were analyzed after exposure to 1 and 5.6 ml/min fluid shear stress rates for 24 h. The slides were pre-coated with collagen IV for HUVECs. Cell viability was determined by life and death stain (FDA and Hoechst nuclear stain), and elongation, orientation and alignment were analyzed by ImageJ and MATLAB softwares. The morphological changes due to age (passage number) of endothelial cells were also assessed under flow conditions.

**RESULTS:** HFFs demonstrated little orientation with flow at both flow rates, whereas HUVECs showed good alignment and orientation with flow after 24 hours of exposure to fluid shear stress. Flow application led to the elongation of endothelial cells, and the alignment rate was enhanced by a stronger flow rate. HFFs retained their morphology to a large extent even at high passage numbers, whereas HUVECs displayed a clear morphological change due to increasing age.

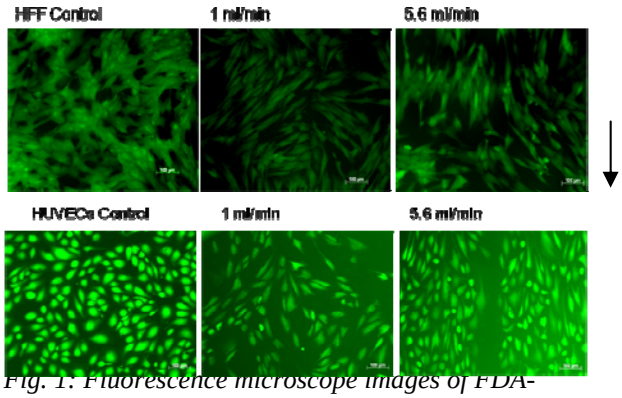


*Fig. 1: Fluorescence microscope images of FDA-stained living hFFs and HUVECs cultivated under static, 1 ml/min, and 5.6 ml/min flow conditions. Arrow indicates the direction of flow.*

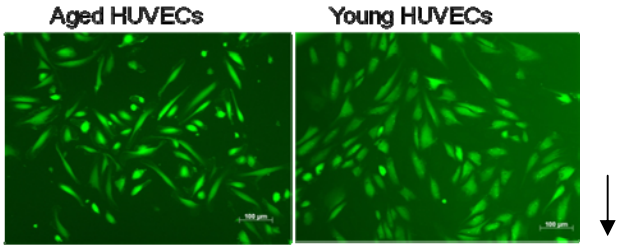


*Fig 2: Comparison of "aged" HUVECs (passage number >5) versus "young" HUVECs (passage number 2-3) in their morphology after 24 hours exposure to 1 ml/min shear stress rate. Living FDA-stained cells are visible.*

**DISCUSSION & CONCLUSIONS:** The morphological changes in endothelial cells induced by application of flow and senescence are significant in characterizing the glycocalyx, which serves as a marker for many diseases. Later an ELISA-type test system will be established for quantification and to determine glycocalyx functionality. It would be valuable to transfer such knowledge on the design of vascular grafts with new surfaces and more favourable surface characteristics, ultimately enhancing their endothelialization.

**REFERENCES:** [1] S. Weinbaum, J.M. Tarbell, E.R. Damiano (2007) *Annu Rev Biomed Eng*, **9**:121-67. [2] Drake-Holland and Noble (2009) *Cardiovas Hematol Disord Drug Targets*, **9**:118-123.

**ACKNOWLEDGEMENTS:** Hall group, Cells and BioMaterials; Vogel group, Biologically Oriented Materials, D-MATL, ETH Zurich

# Nanostructures from oligopeptide-polymer conjugates

Liangfei Tian[1, 2], Ruth Szilluweit[1], Holger Frauenrath[1*]

[1] *EPFL – STI – IMX – LMOM, Building MXG, Room 037, Station 12, 1015 Lausanne, Switzerland.*

[2] *Institute for Polymer Chem., ETH Zurich, Wolfgang-Pauli-Strasse 10, 8093 Zurich, Switzerland.*

**INTRODUCTION:** Supramolecular self-assembly has proven to be a versatile tool for the preparation of nanostructured materials in general.[1] Various examples utilize the self-assembly of β-sheet-forming oligopeptides.[2] Recently, we have demonstrated that oligopeptide-polymer conjugates based on hydrogenated poly(isoprene) and oligo(alanine) are versatile scaffolds for the formation of soluble nanostructures in a "bottom-up" approach.[3] The polymer segment serves as a non-crystalline, flexible, hydrophobic solubilizing group. The simple, short, and monodisperse oligopeptide guides the self-assembly via β-sheet formation. The nanostructure formation can be conveniently controlled at the molecular level, and the inclusion of a diacetylene function in the molecular structure yields supramolecular polymers that can be converted to covalent macromolecules via a topochemical polymerization.[4] Here we report the synthesis of a series of oligopeptide-polymer conjugates, which contain different degrees of polymerization as well as oligo(alanine)s of different lengths. These oligopeptide-polymer-equipped derivatives were further equipped with different conjungated molecules. The stability of the nanostructures and their self-assembly ability with different conjugated molecules was accordingly investigated.

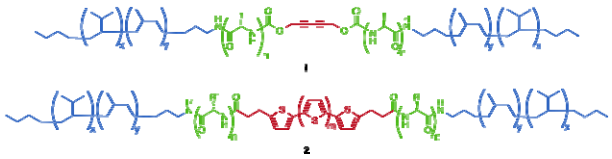

*Fig. 1: Oligopeptide-polymer-equipped derivatives for conjungated molecules.*

**DISCUSSION & CONCLUSIONS:** In the present study, we prepared and investigated a series of diacetylene macromonomers **1** which comprised hydrogenated poly(isoprene) segments with different degrees of polymerization as well as oligo(alanine)s of different lengths. The diacetylene functions served as a sensitive probe for the internal structure and the degree of order of the self-assembled aggregates. The resulting nanostructures were visualized by AFM, and their stability as well as polymerizability were investigated by solution phase IR and UV-vis

spectra. Our investigations showed that the stability of the nanostructures in solution and their polymerizability was strictly determined by both the length of the attached polymers and the number of N-H···O=C hydrogen bonds.

The lessons learned from the diacetylene conjungates were then transferred to oligopeptide-polymer-equipped derivatives of other conjungated molecules such as tetra(thiophene)s **2**. A systematic investigation of UV–vis, CD, fluorescence and IR spectra as well as AFM images revealed that oligopeptide-polymer conjugates were versatile scaffolds for reproducible formation of one-dimensional aggregates, i.e. nanowires, of conjugated molecules.

**REFERENCES:** [1] (a) J.-M. Lehn (2002) *Science* **295**: 2400-03; (b) G. M. Whitesides, B. Grzybowski (2002) *Science* **295**: 2418-21. [2] (a) O. S. Makin, L. C. Serpell (2004) *J Mol Biol* **335**: 1279-88; (b) J. Hentschel, E. Krause, H. G. Börner (2006) *J Am Chem Soc* **128**: 7722-23. [3] (a) E. Jahnke, J. Weiss, S. Neuhaus, T. N. Hoheisel, H. Frauenrath (2009) *Chem Eur J* **15**: 388-404; (b) E. Jahnke, I. Lieberwirth, N. Severin, J. P. Rabe, H. Frauenrath (2006) *Angew Chem Int Ed* **45**: 5383-86. [4] E. Jahnke, P. Kreutzkamp, N. Severin, J. P. Rabe, H. Frauenrath (2008) *Adv Mater* **20**: 409-14.

**ACKNOWLEDGEMENTS:** L.T. acknowledges Dr. Xiangyang Zhang in Laboratory of Organic Chemistry at ETH Zurich for the assistance with mass spectra. Funding from ETH Zurich (Projekt TH-2007-1), and European Research Council (ERC Grant 587119) are gratefully acknowledged.

European Cells and Materials Vol. 20. Suppl. 3, 2010 (page 258) ISSN 1473-2262

# Structural properties and dynamics of linker-histone H1 binding to DNA

R. Dootz[1], A. C. Toma[2], T. Pfohl[1.,2]

*[1] MPI for Dynamics and Self-Organization, Göttingen, Germany. [2] Chemistry Department, University of Basel, Basel, Switzerland.*

**INTRODUCTION:** Despite the key role of the linker-histone H1 in chromatin dynamics, its interactions with nucleosomal DNA are not fully understood. In this work we have used the combination of *in situ* microfluidics and small angle X-ray microdiffraction. It was thus possible to analyze the real-time dynamics and structural evolution of assemblies resulted from the binding of linker-histones H1 to DNA. Our results indicate that the mechanism of H1 interactions with DNA is a two-step process: at first H1 binds non-specifically to DNA and secondly the protein molecules rearrange inside the formed self-assemblies, distorting the DNA conformation.

**METHODS:** *Microfluidic devices*: X-ray compatible microfluidic devices have been used. Crossed microchannels with a depth of 300 µm and a width of 150 µm have been spark eroded in a stainless steel plate and sealed by two Kapton foils.[1] The DNA and H1 solutions were injected into the channels with the help of custom-made syringe pumps, such that the DNA solution is hydrodynamically focused by the H1 solutions (laminar flow conditions).

*Polarized light microscopy*: Direct imaging of H1 induced DNA compaction was monitored by the birefringence signal detected at the interface between the H1 and DNA solutions.

*Microfocused Small angle X-Ray scattering (µ-SAXS)*: The µ-SAXS experiments were performed at the ID10b beamline at ESRF, France. The X-ray beam was focused by beryllium compound refractive lenses (CRL) down to a diameter of 20 µm. 2D scattering patterns have been collected using a CCD detector. Using microfluidics, multiple data points were acquired in a single device with minimal concerns for X-ray radiation damage.[2]

**RESULTS:** Diffusively driven H1/DNA self-assembly was easily monitored by the change in the birefringence signal at the interface between solution streams (Fig. 1, down). µ-SAXS has given information about the H1/DNA assembly's structural evolution at different experimental conditions within the microfluidic channel (higher degree of H1 diffusion represents higher +/- charge ratios). The diffraction peak intensity

profiles are composed by two superposed peaks at positions $q_1$ and $q_2$, corresponding to two different structural arrangements. The position and width of these peaks was found to be dependent on the charge ratio +/- .

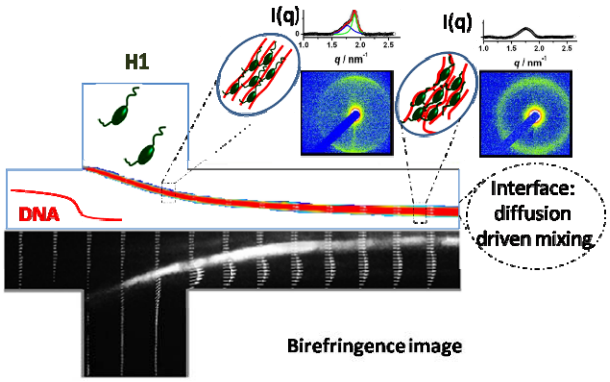


*Fig. 1: Dynamics of structural evolution of H1 induced DNA compaction. (Up) Schematic representation of H1/DNA assemblies combined with 2D diffraction images. Above each diffraction image the corresponding radially averaged scattering intensities are plotted as a function of the scattering vector q. (Down) Half of the birefringence micrograph representing the DNA stream hydrodynamically focused by the H1 side streams.*

**DISCUSSION & CONCLUSIONS:** Combining µ-SAXS with microfluidics we found that the binding of linker-histone H1 to DNA forms two types of mesostructures. In the first type H1 molecules bind unspecifically to DNA, maintaining their extended tail conformation. In the second type the DNA is bended by the H1 folded tails, significantly decreasing the size of H1/DNA mesostructures. Furthermore, from our study, information about the local arrangement of DNA molecules within these dense phases emerges.

**REFERENCES:** [1]A. Otten, S. Köster, B. Struth, A. Snigirev and T. Pfohl (2005) *J Synchrotron Radiat* **12**: 745-50. [2]T. Pfohl et al (2007) *Biomacromolecules* **8**: 2167-72.

**ACKNOWLEDGEMENTS:** We acknowledge ESRF for the allocated beam time on the ID10b line. This work was supported by the DFG (PF 375/2 and SFB 755, B1).

European Cells and Materials Vol. 20. Suppl. 3, 2010 (page 259) ISSN 1473-2262

# Solid-supported biomimetic block copolymer membranes

S.Toughraï, WP.Meier[1]

[1] *Department of Chemistry, University of Basel, Klingelbergstrasse 80, CH-4056 Basel, Switzerland.*

**INTRODUCTION:** The functionalization of surfaces through biomimetic block copolymer membranes aims at developing smart surfaces for biotechnological applications such as biosensing. Amphiphilic block copolymer membranes were chosen instead of lipid membranes as mimics of biological membranes because of their properties, such as thickness, chemical and mechanical stability, lower permeability, fluidity, mobility, etc. Upon insertion of membrane proteins, these systems could allow for the preparation of mechanically and chemically robust and air-stable biosensor devices.

**METHODS:** Surface-initiated atom transfer radical polymerization (ATRP) provides a good control of the brush thickness by controlling polymer molecular weight and by initiating polymerization of a second monomer from the chain end of the first. Poly(2-hydroxyethyl methacrylate)-b-poly(n-butyl methacrylate)-b- poly(2-hydroxyethyl methacrylate), PHEMA-b-PBMA-b-PHEMA block copolymers were synthesized with the first PHEMA block anchored to a self-assembled monolayer on the gold surface while the other PHEMA block exposed to the outer surface. To this end, a self-assembled monolayer of (BrC-$(CH_3)_2COO(CH_2)_{11}S)_2$) initiator was formed through a covalent binding of disulfides to gold. Then, HEMA monomer was polymerized by ATRP. The first PHEMA block initiated the polymerization of BMA. Subsequently, the second PBMA block again initiated HEMA polymerization, thus resulting in a triblock copolymer membrane anchored to the gold substrate. Block copolymer brushes were prepared with different block lengths and characterized both on the gold surfaces and − after detaching from the solid support, − in solution.

**RESULTS[1]:** To test the solvent response behaviour of the triblock copolymer, block-selective solvent as well as a good common solvent for the triblock system were used for swelling experiments. Ethanol was chosen as a good solvent for the triblock copolymer chains, whereas hexane and water selectively swell the PBMA and PHEMA blocks, respectively. The PHEMA blocks swell considerably in water, whereas the hydrophobic PBMA block tends to avoid contacting the aqueous surrounding. However, the

phase segregation was reversible because the reimmersion of the sample into one of three tested solvents resulted in reproducible morphologies. Figure 1(a) shows the 3D topography image of the wet copolymer chains on the gold surface. After drying, the sample acquired a nanodomain topography of the surface [Fig. 1(b)].

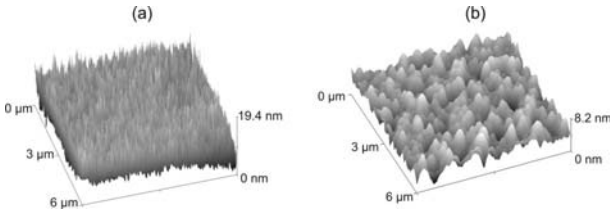


*Fig. 1: Contact mode AFM analysis of the amphiphilic triblock copolymer membrane in water (a) and after sample drying (b).*

**DISCUSSION & CONCLUSIONS:** Upon swelling in water, the brush-like structure of the macromolecules conforms to a stretched conformation of the PHEMA chains. Drying most probably causes a collapse of the polymer brushes and thus formation of nanodomains. The reversibility of the phase segregation proves the covalent attachment of the block copolymer layer and shows the potential use of these block copolymer membranes as responsive surfaces. The amphiphilic character of the triblock copolymer brushes provided a responsive surface that showed a solvent dependent arrangement of the block copolymer chains, which was also reflected in the morphologies of the dried films. The polymer brushes with a hydrophilic-hydrophobic-hydrophilic sequence can be regarded as the first example of solid supported, biomimetic block copolymer membranes prepared by a "grafting-from" approach.

**REFERENCES:** [1] E. Rakhmatullina, et al. (2009) *J. Polym. Sci. A* **47**:1-13.

**ACKNOWLEDGEMENTS:** The authors thank Serena Belegrinou, Dr. Nico Bruns and Dr. Raffaello Masciadri for helpful discussions on the synthesis and characterization of the triblock copolymer brushes. This work is supported by the Swiss National Science Foundation.

European Cells and Materials Vol. 20. Suppl. 3, 2010 (page 260) ISSN 1473-2262

# Encapsulation and study of fibrillar networks in microfluidic droplets

R. Urbani[1], H. M. Evans[2], T. Pfohl[1, 2]

[1] *Chemistry Department, University Basel, Switzerland,* [2] *Max Planck Institute for Dynamics and Self-Organization, Göttingen, Germany*

**INTRODUCTION:** In this project, we study the behaviour and properties, such as elasticity, of fibrillar networks under different conditions. Our focus hereby lies on mechanical impacts such as squeezing and stretching of the networks.

Fibrin network formation is an important part of the human blood coagulation process. Fibrinogen proteins are converted to fibrin by enzyme thrombin, and cross-linked to 3D networks by the enzymatic factor XIII [1].

**METHODS:** Microfluidic devices are produced by negative soft lithography of photoresist SU-8 on silicon wafers. PDMS replica are made out of these wafers and glued on glass slides to form the microdevice. The channels within the devices have sizes of 30μm in width and of 20μm in height.

Human fibrinogen and human α-thrombin are prepared in water and diluted with the according buffers. For microscopy purposes, a fluorescent fibrinogen Alexa Fluor 546 conjugate is also prepared and mixed with human fibrinogen.


*Fig. 1: Scheme of the microfluidic device with three droplet-building aqueous (grey) and one oil (black) inlet, droplets are stored in the large part for network formation*

Subnanoliter-droplets of these aqueous solutions are formed in an oil phase, using a device showed in Fig. 1. To avoid network formation before droplets are formed, the different water solutions are mixed just before the junction. In order to stabilize the generated emulsion, a non-ionic surfactant is added to the oil phase. Droplet sizes and concentrations of the individual solutions can be varied by the flow rates of the different aqueous and of the oil phase. The droplets are formed and then stored in the device until the networks are fully developed.

For analysis of the elastic properties, the network-containing droplets flow through a channel with alternating widths (Fig. 2a). In the wider areas, the

droplets are in a relaxed state (Fig. 2b), while they are squeezed in the narrower parts (Fig 2c). The formation and deformation of the fibrillar networks is imaged by fluorescence microscopy. The recorded images are processed by ImageJ software and custom-made Matlab macros.

**RESULTS:** Fig. 2b shows that fibrillar network are formed in the droplets. *In situ* dynamics of network deformation can be observed (Fig. 2b, c). The network is stretched in one direction while it is squeezed in the other (Fig. 2c). This stands for the high elasticity of the network.

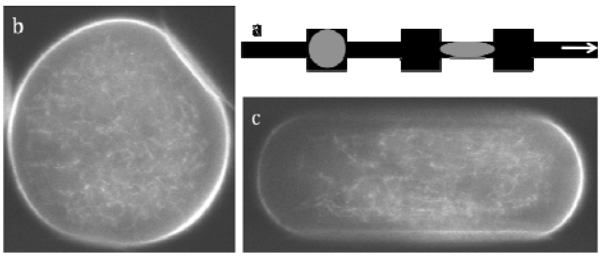


*Fig. 2: Scheme of the analyzing part (a), fibrin networks in relaxed (b) and deformed (c) stages [2]*

**DISCUSSION & CONCLUSIONS:** We are able to encapsulate fibrillar networks in subnanoliter droplets. Studies of the mechanical properties using special microfluidic devices are successfully established. In the future we want to test other parameters like the dependance of network formation and its behaviour on buffer and enzyme concentrations and combine the microscopical imaging with small angle X-ray scattering and diffraction.

**REFERENCES:** [1] L. Muszbek et al., The Involvement of Blood Coagulation Factor XIII in Fibrinolysis and Thrombosis, *Cardiovasc Hematol Agents Med Chem*., 2008, **6**(3), 190-205, [2] H. Evans et al., *In situ* formation, manipulation, and imaging of droplet-encapsulated fibrin, *Lab Chip*, 2009, **0**, 1933-1941,

**ACKNOWLEDGEMENTS:** We gratefully acknowledge SNF and AvH (Alexander von Humboldt foundation, H.M.E.) for financial support. We also thank E. Surenjav, C. Priest, S. Herminghaus and R. Seemann for a fruitful collaboration.

European Cells and Materials Vol. 20. Suppl. 3, 2010 (page 261) ISSN 1473-2262

# Polymeric Micro-Cantilever Arrays for Sensing

P. Urwyler[1,4], O. Haefeli[2], H. Schift[1], J. Gobrecht[1,2], F. Battiston[3], B. Müller[4]

[1]*Paul Scherrer Institute, Villigen, Switzerland.* [2]*University of Applied Sciences Northwestern Switzerland, Windisch, Switzerland.* [3]*Concentris GmbH, Basel, Switzerland.* [4]*Biomaterials Science Center, University of Basel, Switzerland*

**INTRODUCTION:** In the field of biomedicine, silicon-based micro-cantilevers are applied, but are often too expensive for single use. Polymer materials offer tailored physical and chemical properties, including biocompatibility. We have established the injection molding technique to fabricate different polymer cantilever arrays with dimensions in the micrometer range to be functionalized and calibrated for applications in biomedicine.

**METHODS:** The development and fabrication of disposable polymeric micro-cantilever arrays is based on standard thermal injection molding using precisely machined, laser ablated metal molds. The injection molding well established on the millimeter scale and above, is adapted to the molds with extended micro cavities.

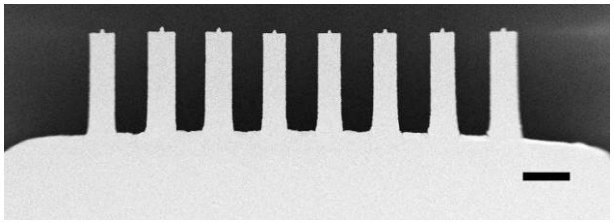

*Fig. 1: SEM micrograph of injection molded PP micro-cantilever array. Scale bar 200 µm.*

*Table 1. Micro-cantilever resonance frequencies. Calculated 30µm – 58.6 kHz, 40µm – 78.2 kHz.*

| Beam No | Measured (kHz) 30 µm thick | | Measured (kHz) 40 µm thick | |
|---|---|---|---|---|
| | Air | Water | Air | Water |
| PVDF 1 | 79.42 | 41.12 | 79.99 | 61.15 |
| PVDF 2 | 54.7 | 41.12 | 77.58 | 61.16 |
| PVDF 3 | 59.86 | 41.12 | 79.99 | 61.12 |
| PVDF 5 | 61.99 | 41.12 | 80.86 | 61.37 |
| PVDF 6 | 47.04 | 41.12 | 74.91 | 61.16 |
| PVDF 7 | 68.93 | 41.20 | 70.69 | 61.43 |
| PVDF 8 | 76.5 | 41.12 | 77.61 | 61.47 |

**RESULTS:** Micro-cantilever arrays (Fig. 1) made of cyclic olefin copolymers (COC), polyoxy-methylen copolymers (POM-C), polypropylene (PP), and polyvinylidenfluorid (PVDF) were successfully injection molded. High performance polymers such as polyetheretherketone (PEEK) are conceivable, but require special processing conditions. The micro-cantilevers were characterized using the Cantisens® Research system. The resonance frequencies of the selected polymeric cantilevers in both air and water are summarized in Table 1. The bimetallic effect was demonstrated both in air (Fig. 2) and water with the heat tests. Deflections in the range of 10 nm – 15 nm have been detected in the thiol binding tests. The successful heat and thiol tests imply that the micro-cantilevers are mechanically compliant for use in biochemistry and biomedicine.

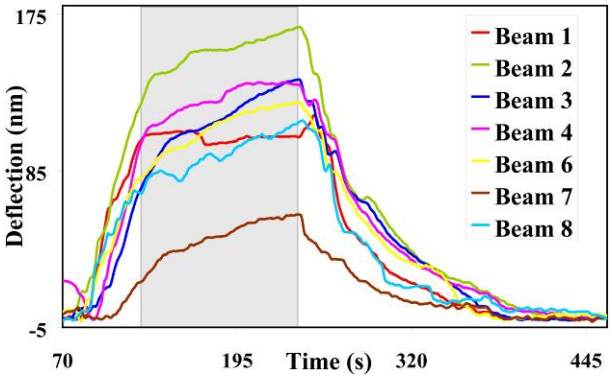


*Fig. 2: Heat test (25°C to 35 °C) with 30 µm IM PVDF cantilevers in air. (Grey area- 35°C).*

**DISCUSSION & CONCLUSIONS:** The resonance frequencies of the polymeric micro-cantilevers are better suited for gas sensing. The polymeric cantilevers can be functionalized to mimic implant surfaces and biocompatible substrates. The measurement of contractile cell forces as described earlier, [1] can also be applied to the functionalized polymeric cantilevers. Thus, the disposable cantilever array sensors will support the selection of advanced surface-modified substrates and medical implant surfaces.

**REFERENCES:** [1] J. Köser, J. Gobrecht, U. Pieles, B. Müller (2008) *Eur. Cells Mater* **16**:38.

**ACKNOWLEDGEMENTS:** Funding by the Swiss Nanoscience Institute is greatly acknowledged. We thank the members from the LMN-PSI, INKA, FHNW (IKT, IPPE), EMPA (K. Jefimovs), BMC, Concentris GmbH, KATZ for their technical assistance.

European Cells and Materials Vol. 20. Suppl. 3, 2010 (page 262) ISSN 1473-2262

# A New One Step Biomolecule Immobilization Strategy using Atmospheric Pressure Plasma Technology

A.Van Hoeck[1], S. Paulussen[1], B. Sels[2]

[1] *VITO, Materials Technology, Boeretang 200, 2400 Mol, Belgium*
[2] *KuLeuven, Centre for Surface Chemistry and Catalysis, 3001 Heverlee Belgium*

**INTRODUCTION:** The deposition of ultra thin bio-functional coatings is of great interest for the fabrication of highly functional and added-value material surfaces. Research efforts on bioactive surfaces for e.g. intelligent packaging, bio-mimicking, biosensors or labs on a chip are therefore increasing. While some methodologies are readily applicable in industrial processes, a simple and fast single step immobilization protocol would offer a cost effective alternative for straightforward production.

Because plasma is the most energetic state of matter, plasma coating technology has been recognized as an attractive technology for surface treatment of materials [1]. From an economical point of view, atmospheric plasma processes are considered as inexpensive, easy to operate and allow to reduce solvent use substantially. In this context, the most remarkable feature of non-equilibrium atmospheric pressure plasmas is the low temperature (max 60°C) which leads to a high preservation of polymer functional groups and a minimum damage to native biomolecule structures [2,3].

However, this work aims at the development of a new, direct immobilization strategy for biomolecules. By feeding the atmospheric plasma discharge zone simultaneously with an polymer precursor and an enzyme solution, it is possible to fabricate a bio-functional layer where the enzymes become entrapped into the polymer matrix. As such, a one-step immobilization process is achieved. Furthermore, the bandwidth of applications can be widened significantly by using other biomolecules like nucleotides or anti-bodies.

**EXPERIMENTAL:** The atmospheric pressure dielectric barrier discharge plasma reactor, shown schematically in Figure 1, was home built. It consists of two parallel plate electrodes of 80 by 145 mm each covered by a glass dielectric of 3 mm thickness, separated by 3 mm spacers. A constant gas flow rate of 6 SLM $N_2$ and an enzyme solution of 0.5 mg/ml were fed to the plasma zone at atmospheric pressure and evacuated at the reactor end.

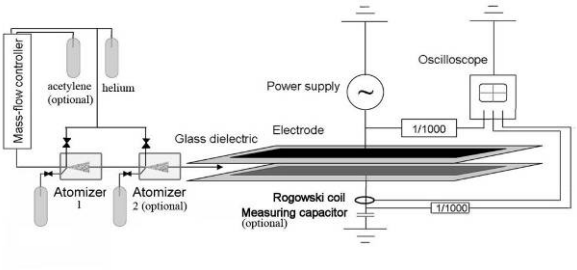


*Figure 1: Schematic representation of the plasma reactor*

**RESULTS:** In this assay, a dielectric barrier discharge was employed at atmospheric pressure and ambient temperature to deposit organic coatings containing immobilized fluorescent proteins or enzymes. Glucose oxidase was administered to the gas flow and afterwards, the distribution and resulting activity of the immobilized enzymes on the electrodes after plasma deposition was evaluated. The coatings were analyzed in depth by FT-IR, XPS and laser scanning confocal microscopy with fluorescent labeled BSA. These analyses provide a clear view on the activity of the immobilized enzymes, their distribution and the chemical composition of the organic matrix.

**CONCLUSION:** An entirely new, single step technology has been developed that enables fast immobilization of biomolecules while retaining their bioactivity on a large scale to surfaces of any kind. The immobilized biomolecules retain their native structure and are homogeneously distributed within the polymer coating. Due to a better reproducibility, higher flexibility, broader applicability and the possibility of in-line treatment this process offers several advantages compared to conventional multi-step immobilization methods.

**REFERENCES:** [1]A. Bogaerts (2002) *Spectrochimica Acta Part B-Atomic Spectroscopy* **57**: 609-658. [2]P. Heyse (2007) *Plasma Processes Polym.* **4**: 145-157. [3]P. Heyse (2008) *Plasma Processes Polym.* **5**: 186-191.

European Cells and Materials Vol. 20. Suppl. 3, 2010 (page 263) ISSN 1473-2262

# Characterization of Bone Graft Substitutes Prepared by Transformation of β-Tricalcium Phosphate to Hydroxyapatite in Aqueous Environment

L.Vecbiskena[1], Z.Irbe[1], K.Salma[1], L.Berzina-Cimdina[1]

[1]*Riga Technical University, Riga Biomaterials Innovation and Development Centre, Riga, Latvia.*

**INTRODUCTION:** Calcium phosphate bone graft substitutes such as calcium phosphate bone cements are materials successfully used for bone repair. There still are potential of improvements on β-tricalcium phosphate (β-TCP) based bone cements. These cements have been described in a few works [1, 2]. These cements set by recrystallization of β-TCP to HAp in aqueous environment. The preparation of β-TCP for use as a starting material for apatite cement is time consuming and complicated (for example milling for 24 h [2]). In this work an alternative method to synthesize β-TCP for use as starting material for apatite cement (bone graft substitute) has been investigated. The transformation of β-TCP to HAp after initial setting of the cement has also been studied.

**METHODS:** Two β-TCP synthesis methods were compared – more explored high temperature synthesis (1) and wet chemical precipitation of calcium deficient HAp with following calcination in temperatures under 1000°C (2).

In high temperature synthesis of β-TCP, a mixture of $CaCO_3$ and $CaHPO_4 \cdot 2H_2O$ (molar ratio – 1:2) was heated for 1h at 1000°C.

In wet chemical precipitation method (described in detail in [3]) calcium deficient HAp was precipitated by gradually adding $H_3PO_4$ solution to $Ca(OH)_2$ suspension. Precipitated calcium deficient HAp was dried and calcined.

Both kinds of synthesized β-TCP were milled in planetary ball mill for various periods to prepare for use as starting material for calcium phosphate cement. Isopropanol was used as milling media.

Sodium phosphate buffer solutions with pH 7 and 0.5M phosphate ion concentration were used as liquid phase for cements.

Phase composition of obtained materials was determined using X-ray diffraction and Fourier-transform infrared spectroscopy.

**RESULTS:** High temperature synthesis yielded well crystallized β-TCP. To obtain bone graft substitutes – cements – with high degree of conversion of β-TCP to HAp from high temperature β-TCP it has to be milled for prolonged periods – 25 h and more.

Calcination of precipitated calcium deficient HAp yielded less crystalline β-TCP with grain size 200 nm and less (Fig.1.). Calcium deficient HAp transformed to β-TCP in temperatures between 650 and 700°C. To obtain starting material for cement, β-TCP had to be milled for less than 10 h.

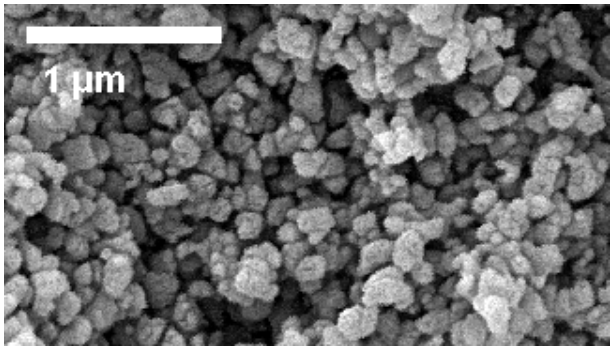


*Fig. 1: FE-SEM micrograph of β-TCP particles formed after calcination of calcium deficient HAp at 700°C for 1 h.*

**DISCUSSION & CONCLUSIONS:** The calcination of precipitated calcium deficient HAp is more effective to prepare β-TCP as starting material for apatite cement – a bone graft substitute. Less milling was required to obtain β-TCP with low crystallinity and the same degree of conversion to HAp after setting of cement.

**REFERENCES:** [1] T.J. Brunner, R.N. Grass, M. Bohner et al (2007) *J Mater Chem* **17**: 4072–78. [2] U. Gbureck, O. Grolms, J.E. Barralet, at al (2003) *Biomaterials* **24**: 4123–31. [3] K. Salma, N. Borodajenko, L. Berzina-Cimdina (2010) *Processing and Application of Ceramics*, **4 [1]**: 45–51.

**ACKNOWLEDGEMENTS:** This work has been supported by the European Social Fund within the project „Support for the implementation of doctoral studies at Riga Technical University".

This work has been partly supported by the European Social Fund within the project "Multidisciplinary Research in Biomaterials Technology of New Scientist Group", No.2009/0199/1DP/1.1.1.2.0/09/APIA/VIAA/090, (PVS ID 1380).

European Cells and Materials Vol. 20. Suppl. 3, 2010 (page 264) ISSN 1473-2262

# New Block Copolymer Nanoparticles for Gene Delivery

D. Velluto, S.Thomas, M. Swartz, J.A. Hubbell

*Institute of Bioengineering and Institute of Chemical Science and Engineering, Ecole Polytechnique Federal de Lausanne, CH-1015 Lausanne, Switzerland*

**INTRODUCTION:** The common method to deliver DNA is the use of viral vectors, but numerous problems exist. Based on this, we prepared new polymeric micelles as non-viral vectors for DNA/RNA which showed to be much less toxic in vitro and in vivo respect to many of the commercial vectors and highly efficient in complexing, stabilizing and delivering the nucleic acids. Aim of this project is to show the effect of micelles-DNA and micelles-siRNA delivery on the tumor growth using B16F10 murine melanoma as model.

**METHODS:** PEG-PPS telechelic thiolate was synthesized as previously reported[1]. From this reactive intermediate, stable PEG-b-PPS (**AB**) was formed by reaction with 2,2'-dithiodipyridine. In order to form the PEG-b-PPS-b-PEI triblock-copolymer, the PEG-PPS telechelic thiolate was conjugated by a thiol-disulfide exchange reaction with a linear poly(2-ethyl-2-oxazoline) telechelic pyridyl disulfide block, which had been synthesized as reported in the literature[2]. Following conjugation, the poly(2-ethyl-2-oxazoline) block was deprotected by acid hydrolysis to yield the triblock copolymer containing the poly(ethylene imine) (PEI) block (**ABC**). When suspended in water, the ABC block copolymer easily self-aggregates to form micelles of different diameters, between 100 and 250 nm. If, instead, mixed micelles of AB and ABC block copolymers are suspended in water, the size is dramatically decreased (30 nm). Both of the platforms were high efficiently conjugated with DNA and siRNA without dramatic changes in the size of the micelles. Particularly both micelle systems were conjugated with GFP plasmid or with nucleolin siRNA and the complexes have been transfected into B16F10 cells and MDA cells respectively. GFP expression has been evaluated after 48hr by mean of fluorescent microscope and Flow Cytometry. Nucleolin knockdown was determined by rtPCR. *In vivo* gene delivery was tested by intratumoral injections of micelles-pOVA (encoding ovalbumin plasmid) in melanoma bearing mice, being the mice previously immunized against ovalbumin. Not immunized mice containing melanoma tumor were injected instead with micelles-siRNA, being nucleolin, one of the most important player in tumor proliferation, the target. In both of the cases, injections were repeated every day and the tumor volume was monitored every day as well.

**RESULTS:** Both the micelle systems have shown high transfection efficiency *in vitro*, being 70% the amount of GFP positive cells in B16F10 (figure 1a). The tumor treatment in pre-immunized mice with OVA-plasmid carried by micelles, have shown highly reduction of tumor growth respect to the control group (figure 1b). Up to 80% of nucleolin knockdown was obtained *in vitro* by micelles-siRNA transfection in MDA cells; *in vivo* siRNA micelles delivery caused strong inhibition of tumors growth (figure 1c).

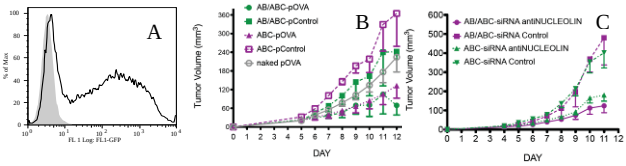


*Fig. 1. Flow Cytometry analysis (A) of GFP expression in B16F10 mediated by AB-ABC micelles. B) Effect of OVA-plasmid (B) and nucleolin siRNA (C) intratumoral delivery and mediated by ABC and AB/ABC micelles on tumor growth in mice.*

**DISCUSSION AND CONCLUSIONS:** The DNA and siRNA delivery mediated by ABC and AB-ABC block copolymers has been observed *in vitro* and *in vivo*, being different mouse's organs and tissues targeted by different ways of administration. Among those, interesting results have been obtained in melanoma tissues

**REFERENCES:**

[1] Velluto, D., Demurtas, D. & Hubbell, J.A, *Mol. Pharm.* **5**, 632-642 (2008).

[2] Hsiue, G.-H., Chiang, H.-Z., Wang, C.-H. & Juang, T.-M, *Bioconj. Chem.* **17**, 781-786 (2006).

European Cells and Materials Vol. 20. Suppl. 3, 2010 (page 265) ISSN 1473-2262

# Monitoring of Gene Expression of Single Mammalian Cells in a Multilayer Microfluidic Device

C.Vollrath, PS.Dittrich

*Department of Chemistry and Applied Biosciences, ETH Zurich, Switzerland*

**INTRODUCTION:** The investigation of cellular response to external, soluble factors is of high interest for the understanding of cellular interactions with the surrounding environment and cell-cell communication. Therefore, a precise control and change of the microenvironment around cells is an important requirement for systematic analyses. Here, a multilayer microfluidic device is proposed, which allows addressing and analysing cells with high temporal and spatial resolution. [1-3] Herein, we report on the investigation of the gene expression in mammalian cells that is induced by tetracycline.

**METHODS:** To monitor the stimulation of gene expression in single mammalian cells (HEK 293) a multilayer microchip with integrated cell traps was designed (Fig. 1). This device enables the positioning and culturing of cells as well as the supply of soluble effectors. Due to the separated channel systems the supply of the soluble factor, and hence, induction of gene expression, is only possible by its diffusion through an intermediate nanoporous membrane. An inducible gene expression system (T-REx$^{TM}$, Invitrogen) is used that can be controlled by tetracycline as external effector. The model gene of interest of this work encodes a destabilized mutant of the Green Fluorescent Protein (GFP). Therefore, gene expression can be monitored online by time-lapse fluorescence microscopy.

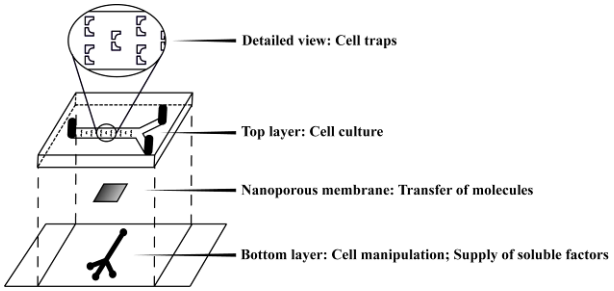


*Fig. 1: Sketch of a multilayer mircofluidic device. The top layer is used for culturing cells, the bottom layer for the supply of soluble effectors. These chemicals are transported with high temporal and spatial resolution to the cells, by diffusion through an intermediate nanoporous membrane. The detailed view shows the design of the cell traps for a defined cell pattern.*

**RESULTS:** For time-lapse fluorescence microscopy experiments, mammalian cells are trapped within the microcages in the top channel, while the bottom channel is filled with tetracycline. Fluorescence imaging revealed the increase of intracellular GFP within 200 min after cell seeding in the microfluidic device. Two typical traces are given in Fig. 2.

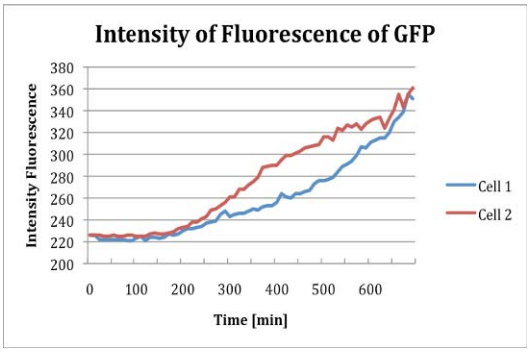


*Fig. 2: Time-lapse fluorescence microscopy to monitor induced GFP expression over time in single mammalian cells.*

**DISCUSSION & CONCLUSIONS:** The microfluidic device facilitates positioning of large cell numbers and hence, parallel cell analyses. The introduction of a second fluidic layer in the microfluidic device allows a supply of the stimulating reagents independent from the (constant) culture medium. By use of the described inducible gene expression system the parameters for titration can be established. In future work the time and spatial resolution of stimulation will be improved to achieve e.g. pulsed stimulation of few cells.

**REFERENCES:** [1] S. Hardt, F. Schönfeld. (eds), (2007) *Microfluidic Technologies for Miniaturized Analysis Systems*, Springer. [2] J. El-Ali, P.K. Sorger, K.F. Jensen (2006) *Nature* **442**: 403-11. [3] P.S. Dittrich, A. Manz (2006) *Nature Rev Drug Disc* **5**: 210-18.

**ACKNOWLEDGEMENTS:** The financial support from the European Research Council (ERC Starting Grant No. 203428, nμ-Lipids) and from the Novartis Doctoral Fellowship 2010 is gratefully acknowledged.

European Cells and Materials Vol. 20. Suppl. 3, 2010 (page 266) ISSN 1473-2262

# Perspectives of Novel Poly(D,L-lactide-*co*-glycolide)/Hydroxyapatite Core-shell Nanoparticles as Carriers of Antibiotics

M. Vukomanović[1,2], S. D. Škapin[2], I. Šarčev[3], N. Ignjatović[1], D. Uskoković[1]

[1] *Institute of Technical Sciences of the Serbian Academy of Sciences and Arts, Belgrade, Serbia.*

[2] *Advanced Materials Department, Jožef Stefan Institute, Ljubljana, Slovenia.* [3] *Medical Faculty, Novi Sad, Serbia.*

**INTRODUCTION:** Local drug delivery for the treatment of infectious bone tissue diseases is a high-importance topic in the field of biomedicine for a last two decades. [1] In general, some of the main problems related to controlled drug delivery of antibiotics are: (i) high initial burst effect with toxic outcome and (ii) low concentration of released drug during extended period of time with possibility for development of resistant spaces.[2] There are some examples suggesting that core-shell particles applied as carriers of drug are able to provide high control over the process of drug release and to prevent burst effect.[3,4] Therefore, the main goal of our work is to design material which will be able to provide these characteristics.

**METHODS:** Loading of the drug within poly(D,L-lactide-*co*-glycolide/hydroxyapatite (PLGA/HAp) was performed by modified ultrasonic processing method.[5] Cell responses were analyzed using MRC-5 cell line by standardized methods.

**RESULTS:** PLGA/HAp particles with loaded antibiotic showed morphology of nanostructured core-shells (Fig. 1a). Characteristics of the surface of material obtained after 24h in medium with MRC-5 cells provided their attachment onto the material (Fig 1b). Histological analyses showed absence of the changes in the shape and texture of vital cells and they had high affinity for interaction with material (Figs. 1c and 1d). According to the testes based on the mitochondrial activity (MTT) and compactness of the cells' membrane (DET), after cells interactions with PLGA/HAp with different contents of antibiotic during first 24h, high percents of survival were obtained (Table 1). Agar test showed no detectable zone of decoloration around the samples and no observable signs of cell lysis indicating 0/0 cell response meaning absence or very low cytotoxicity effect (Table 1).

**DISCUSSION & CONCLUSIONS:** PLGA/HAp core-shells gave satisfied outcome during their interaction with human-like MRC-5 cells showing high level of compatibility and bioactivity of material which opened interesting field for the future *in vivo* research. Concerning biodegradable PLGA shell able to control process of drug release and osteoconductive HAp core able to promote bone reparation process so far this material showed promising properties for delivery of antibiotics.

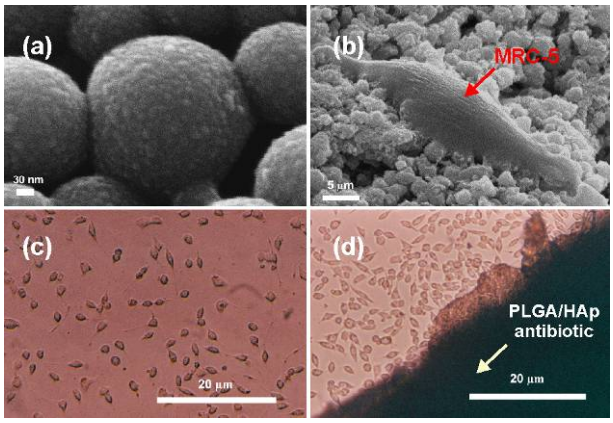


*Fig. 1: PLGA/HAp/antibiotic core-shells (a); cell attachment onto the surface of material (b); histological analysis of cells responses: control (c) and PLGA/HAp/antibiotic (d).*

*Table 1. MRC-5 cell line responses obtained after 24h of incubation with PLGA/HAp/antibiotic.*

| Antibiotic (wt. %) | MTT (survival %) | DET (survival %) | Agar test |
|---|---|---|---|
| 0 | 92.9±1.2 | 93.6±2.3 | 0/0 |
| 1 | 80.9±0.3 | 91.2±5.0 | 0/0 |
| 5 | 74.1±2.9 | 89.6±2.8 | 0/0 |
| 10 | 68.8±1.4 | 85.3±2.4 | 0/0 |

**REFERENCES:** [1]S. K. Nandi, et al (2009) *Mater. Sci. Eng. C* **29:** 2478-2485. [2] J. G. E. Hendiks, et al (2004) *Biomaterials* **25**: 545-56. T. H. [3] Lee, et al (2002) *J. Control. Release* **83**: 437-452. [4] Y. -H. Lee, et al (2010) *J. Control. Release* doi:10.1016/j.jconrel.2010.03.014. [5] M. Jevtić, et al (2009) *Acta Biomater.* **5**: 208-218.

**ACKNOWLEDGEMENTS:** This research was supported by The Ministry of Science and Environmental Protection of the Republic of Serbia and Serbian-Slovenian Bilateral Scientific Collaboration.

European Cells and Materials Vol. 20. Suppl. 3, 2010 (page 267) ISSN 1473-2262

# Biomimetic, Large-Area, Layered Composites with Superior Properties

Andreas Walther[1], Lars Berglund[2], Olli Ikkala[1]

[1]*Molecular Materials, Department of Applied Physics, Aalto University (formerly Helsinki University of Technology), PO 15100, FIN-00076 Aalto (Finland) – andreas.walther@hut.fi*

[2]*Wallenberg Wood Science Center and Department of Fiber and Polymer Technology, Royal Institute of Technology, SE10044 Stockholm (Sweden)*

**INTRODUCTION:** The hierarchical inorganic/ organic hybrid structures of nature allow inspiration for materials that combine superior mechanical properties with lightweight construction. Both factors are essential to promote sustainability and reduce energy consumption e.g. in constructions and transportation, which are increasingly relevant for future societies. Nacre with its alternating mesoscale inorganic platelets and nanoscale protein layers is a perfect example and has inspired considerable efforts towards biomimetic structures. Excellent properties have recently been reached in laboratory scale model materials. However, the preparations have either remained inherently excessively time-consuming and laborious for larger scale applications due to the sequential layer depositions, or they require tremendous energy during the freezing (-80°C) and sintering (1500°C) processing of ceramic components. Therefore a transfer to major applications is difficult to foresee based on such routes. Thus to promote these structures into true 21st century biomimetic materials with advanced properties, we have to conceive of other innovative strategies.

Herein, we will show how to overcome many obstacles and how to create large-area brick-and-mortar nacre-mimics (Figure 1) with sub-millimeter thicknesses and potentially unlimited lateral dimensions via continuous roll-to-roll processes. One of the key steps is the large scale generation of polymer-coated clay particles with intrinsic core-shell hard/soft character.1

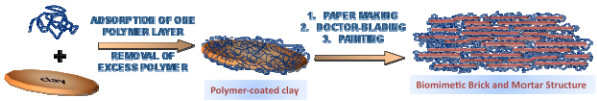


*Figure 1. Two-Level Self-Assembly toward nacre mimics via hard/soft building blocks.*

**RESULTS:** The resulting materials show a highly ordered layered arrangement of the platelet-shaped inorganic nanoparticles, surrounded by an organic polymer matrix. (Figure 2) Due to the utilization of well-defined building blocks, the structures are composed of an optimized hard/soft ratio and a majority fraction of hard reinforcing material.

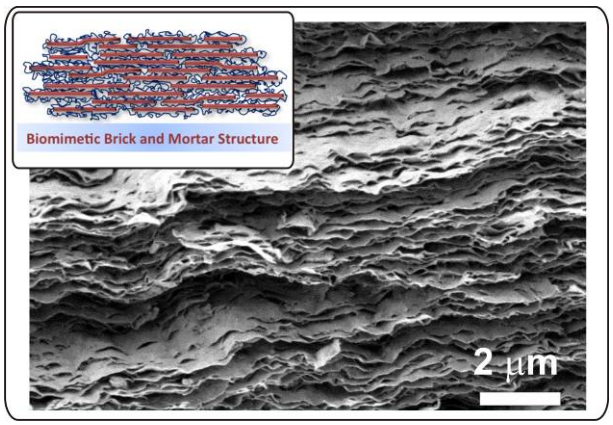


*Figure 2. Layered nacre-mimetic composite exhibiting a brick and mortar architecture.*

Hence, the resulting material properties demonstrate outstanding stiffness and strength, partly surpassing the values of natural nacre. At best we can reach 45 GPa in Young's modulus and 250 MPa as stress at break.

We will also show how the mechanical characteristics can be improved via chemical and physical crosslinking.

**DISCUSSION & CONCLUSIONS:** As main advantages, these techniques combine robustness and time-efficiency to allow scale-up. They are also environmentally friendly as well as energy-efficient and economic. The materials display excellent gas barrier properties, optical translucency and extraordinarily shape-persistent fire-resistance. The strength of the approach is that surprisingly commonplace materials and processes can be used in a novel way. The observations open new avenues towards advanced 21st century biomimetic materials from laboratories to larger scale technology.

**REFERENCES:** [1]A. Walther, I. Bjurhager, J.M. Malho (2009) *Nano Letters* asap doi: 10.1021/nl1003224.

**ACKNOWLEDGEMENTS:** We acknowledge funding from the Finnish Academy and the Wallenberg Foundation as well as J. Ruokolainen, I. Bjurhager and J.M. Malho for their contributions.

European Cells and Materials Vol. 20. Suppl. 3, 2010 (page 268) ISSN 1473-2262

# Investigating the Interactions between Proteins and thermosensitive Microgels

N. Welsch [1,2], M. Ballauff [1, 3]

*[1] Soft Matter and Functional Materials, Helmholtz-Zentrum Berlin für Materialien und Energie GmbH, Berlin, Germany. [2] Humboldt University Berlin, Berlin, Germany. [3] Department of Physics, Humboldt University Berlin, Berlin, Germany.*

**INTRODUCTION:** The interface of materials and biology is emerging as a major research focus and especially nanomaterials in medicine and biotechnology are expected to address many medical and biological problems. On this way, new nanoparticles might be designed which are well-suited as intelligent enzyme supports, drug-delivery systems and biosensors. As particles based on poly(N-isopropylacrylamide) (PNiPA) thermally respond close to the body temperature, functionalized temperature-sensitive microgels has received considerably attention as smart systems in this area of research. For receiving a deeper insight into the interactions between proteins and PS-PNiPA core-shell microgels the adsorption of various proteins as well as the remaining activity of adsorbed enzymes is investigated. In particular, a quantitative study of the activity of physically immobilized *β*-D-glucosidase from *almonds* was performed in detail.

**METHODS:** The PS-core and the cross-linked PNiPA shell were synthesized by standard seed and emulsion polymerization. The immobilization of proteins and the kinetic analysis of free and adsorbed enzyme molecules was performed in the same manner as described in Ref.[1]. The analysis of the secondary structure of native and adsorbed proteins was performed using a FT-IR spectroscopy setup developed for protein analytics (Bruker Optik Confocheck) along lines given previously.[2]

**RESULTS:** We determined the adsorption capacity of PS-PNiPA particles by investigating the efficiency of immobilization at different protein concentrations below 32°C, the critical solution temperature (LCST) of the polymeric carrier.[1] In this case the adsorption behaviour can be described by a Langmuir-type model:

$$\tau_{ads} / \tau_{ads,M} = K\, c_{sol} / (1 + K\, c_{sol}) \qquad (1)$$

The high loading of the microgel with *β*-D-glucosidase from *almonds* indicates strong interactions between both species. Temperature-dependent Michaelis-Menten kinetics show that the immobilization of this enzyme leads to a remarkable enhancement of its hydrolytic activity. This change can be explained by the formation of hydrogen bonds between the amide groups of the PNiPA network and the protein backbone which is supported by Fourier-transform infrared (FT-IR) spectroscopy experiments in absorption mode.

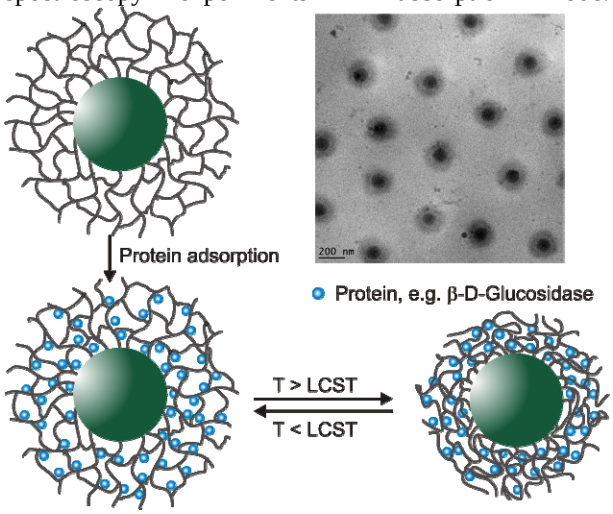


*Fig. 1: Top left and bottom: Schematic representation of the adsorption of proteins on PS-PNiPA microgel particles. Top right: Cryo-TEM image of these particles in the swollen state.*

**DISCUSSION & CONCLUSIONS:** PNiPA based core-shell systems serve as superior carriers for the adsorption of various proteins and enzymes. In contrast to other systems immobilizing biomolecules on these designed carrier particles does not involve any loss of their function but even an increase of activity. In order investigate the spatial distribution of the adsorbed proteins within the polymeric network and to clarify the thermodynamics of the adsorption process Small Angle X-Ray Scattering (SAXS) and Isothermal Titration Calorimetry (ITC) are the most appropriate methods to be applied. On this way we believe to gain a deeper understanding for the interaction of biomolecules with nanoparticles which is essential for new applications to evolve.

**REFERENCES:** [1] N. Welsch, A. Wittemann and M. Ballauff (2009) *J Phys Chem B* **113**:16039-16045. [2] A. Wittemann and M. Ballauff (2004) *Anal Chem* **76**:2813-2819.

**ACKNOWLEDGEMENTS:** Financial support by the Deutsche Forschungsgemeinschaft, Schwerpunkt “Hydrogele“, and by the SFB 481, Bayreuth, is gratefully acknowledged.

# Multiple Optical Tweezers Combined with Microfluidics as a Tool for Single Cell Studies

M.Werner[1], F.Merenda[2], R.Salathé[2] and H.Vogel[1]

[1]*Laboratory of Physical Chemistry of Polymers and Membranes (LCPPM)*

[2]*Advanced Photonics Laboratory (APL)*

*Swiss Federal Institute of Technology Lausanne (EPFL), CH-1015 Lausanne, Switzerland*

**INTRODUCTION:** Optical tweezers use the forces of laser radiation to trap micron-sized particles. Since the first report in 1986 by Ashkin [1] optical tweezers have attracted an ever-growing interest as a tool for manipulating living cells. Here we present an experimental platform based on the combination of multiple optical tweezers with microfluidic devices and fluorescence microscopy, for highly parallel analysis of single cells (fig. 1).

**METHODS:** Multiple optical tweezers were generated by splitting the output beam of an Ytterbium fiber laser (10W, 1064 nm) into a multitude of single beamlets using microlens arrays [2]. Each beamlet was tightly focused into the sample through a high NA objective, collectively forming a hexagonal array of optical traps with a regular spacing of ~6 µm. A steerable optical trap controlled by a galvanometric mirror was implemented in the setup allowing manipulation of individual cells. Three laser lines (488nm, 532nm and 633nm, respectively) were available for fluorescence excitation. All experiments were conducted in a specially designed microfluidic chip.

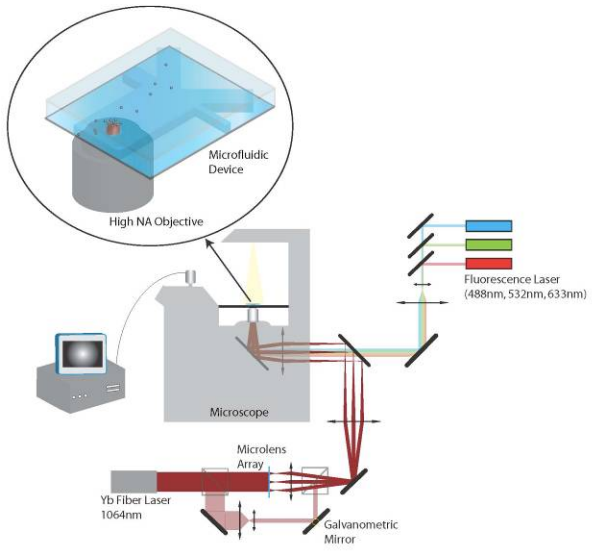


*Fig.1: Illustration of the experimental platform*

**RESULTS:** Cells injected in the microfluidic chip were optically trapped in an array remaining immobilized at typical flowrates of ~100 µm/s (fig. 2). By translating the microfluidic chip relative to the optical axis the particles could be laterally moved to specific locations of the chip. This opened up the possibility to expose the cell array to reagents in a controlled manner and to analyze the cellular responses upon chemical stimuli in a highly parallel format. Applicability of the experimental platform to single cell analysis was demonstrated by monitoring the dynamical response of the intracellular pH of yeast cells following glucose exposure. A method was developed to sort cells in the microfluidic chip for further analysis or incubation. Cells of interest were captured by the steerable optical trap, moved against the flow and released in a separate channel.

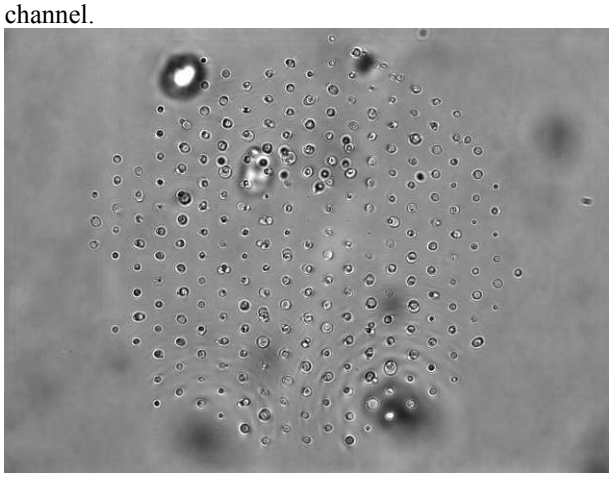

*Fig.2: Transmission micrograph showing multiple optical trapping of yeast cells.*

**DISCUSSION & CONCLUSIONS:** We developed an experimental platform allowing to manipulate and temporarily immobilize individual living cells in an array (> 150 particles simultaneously). Microfluidics provided spatiotemporal control of reagent exposure of the trapped cells and cellular dynamics could be investigated with single cell resolution while only small amounts of material were consumed.

**REFERENCES:** [1] A. Ashkin, J.M. Dziedzic, J.E. Bjorkholm, et al (1986) *Opt Lett* **11**: 288-290. [2] F. Merenda, J. Rohner, et al (2007) *Proc. SPIE* **6644**: 66440P1-66440P10.

European Cells and Materials Vol. 20. Suppl. 3, 2010 (page 270) ISSN 1473-2262

# Human Placenta: An Efficient Barrier for Nanomaterials?

P. Wick[1], A. Malek[2], P.A. Diener[3], A. Zisch[2], H.F. Krug[1], U. von Mandach[2]

[1] *Empa, St. Gallen, Switzerland.* [2] *University Hospital Zurich, Switzerland.*
[3] *Kantonsspital, St. Gallen, Switzerland.*

**INTRODUCTION:** Humans have been exposed to fine and ultrafine particles throughout their history. Since the Industrial Revolution, sources, doses, and types of nanoparticles have changed dramatically. In the last decade, the rapidly developing field of nanotechnology has led to an increase of engineered nanoparticles with novel physical and chemical properties. Regardless of whether this exposure is unintended or not, a careful assessment of possible adverse effects is needed. A large number of projects have been carried out to assess the consequences of combustion-derived or engineered nanoparticle exposure on human health. In recent years there has been a growing concern about the possible health influence of exposure to air pollutants during pregnancy, hence an implicit concern about potential risk for nanoparticle exposure *in utero*. Previous work has not addressed the question of whether nanoparticles may cross the placenta.

**METHODS:** The placental perfusion technique was originally developed by Panigel et al (1967)[1] and was further improved by Schneider et al (1972)[2] and Malek et al (2009)[3](Fig. 1). Intact placentae were obtained from uncomplicated pregnancies either after vaginal or cesarean section. To perfuse the placenta, the arteries and veins of a suitable cotyledon were cannulated resulting in two independent perfusion circuit. Fully characterized fluorescent polystyrene beads of varying size (50 - 500nm) were used as model particles and applied to the perfusion system.

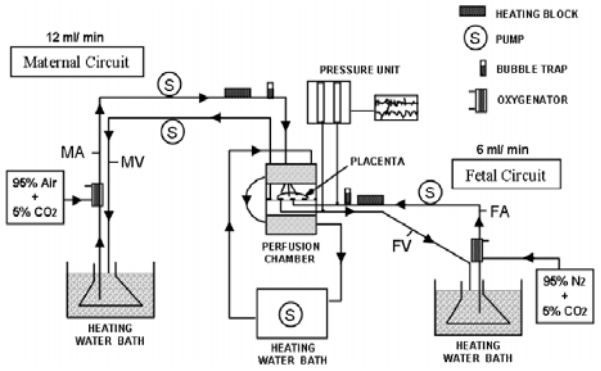


*Fig. 1: Schematic illustration of the human placenta perfusion model FA: fetal artery; FV: fetal vein; MA: maternal artery; MV: maternal vein.*

**RESULTS:** We showed that fluorescent polystyrene particles with diameter up to 240 nm were taken up by the placenta (Fig.2) and were able to cross the placental barrier without affecting the viability of the placental explant[4].

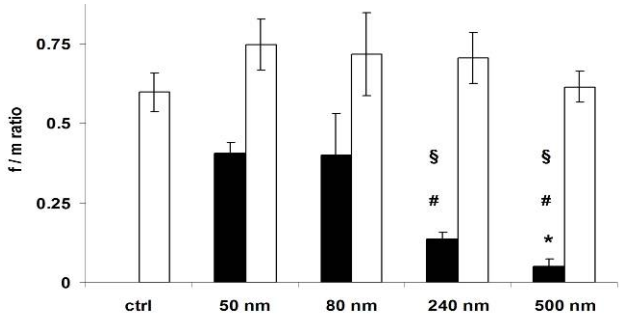


*Fig. 2: Perfusionrates of PS beads with different sizes after 3h of perfusion. The ratios between fetal (f) and maternal (m) concentration of $^{14}$C-antipyrine (open bars) and PS beads (black bars) were calculated after 3h of perfusion. The $^{14}$C-antipyrine values remain unchanged, whereas the perfusion rate of the beads showed size dependence. Data represent mean ± SE of at least four independent experiments.*

**DISCUSSION & CONCLUSIONS:** Our results confirmed the translocation of polystyrene beads through the placenta up to a diameter of 240 nm. Translocation was observed without reducing the viability of the placenta or changes in tissue morphology. This suggests that most nanomaterials have the potential for transplacental transfer and underlines the need for further nanotoxicological studies on this important organ system.

**REFERENCES:** [1] M. Panigel, M. Pascaud, et al (1967) *J Physiol (Paris)***59**(1suppl):277. [2] H. Schneider, M. Panigel, et al (1972) *Am J Obstet Gynecol* **144**(6):822-828. [3] A. Malek, Obrist C, et al (2009) *Reprod Biol Endocrinol* **7**:61-70. [4] P. Wick, A. Malek, et al (2010) *Environ Health Perspect* **118**(3):432-436.

**ACKNOWLEDGEMENTS:** This work was financially supported by an Empa internal grant and by the Medical Faculty Research of the University of Zurich.

European Cells and Materials Vol. 20. Suppl. 3, 2010 (page 271) ISSN 1473-2262

# Gold Nanoparticle Chemiresistors – Towards a Universal (Bio) Chemical Sensor System

L.Wieczorek, B.Raguse, E.Chow, K-H.Müller, J.S.Cooper, L.Hubble

*Future Manufacturing Flagship, Wealth from Ocean Flagship,*

*CSIRO Materials Science and Engineering, Lindfield, NSW 2070, Australia.*

Chemiresistors are sensing devices fabricated of materials that, when exposed to analyte molecules, change their electrical resistance. One of the most attractive classes of materials for chemiresistors are self-assembled monolayer (SAM) capped gold nanoparticles films.[1] The versatility of the SAM chemistry makes tuning the chemical properties of the materials a relatively simple task. The SAM molecules can be, for instance, polar or non-polar, hydrophilic or hydrophobic, and even designed specifically for an analyte molecule of interest.

The electrical resistance of the gold nanoparticle chemiresistors depends exponentially on the distance between the gold nanoparticles and on the tunneling properties of the molecules between the nanoparticles. This property makes the material a very sensitive sensor system with reported detection limits down to parts per billion.[2,3]

Until recently, gold nanoparticle chemiresistor were applied for the detection of volatile analyte molecules in a gas phase.[1-3] We demonstrated that through careful design of devices one can operate the chemiresistors in an aqueous phase.[4]

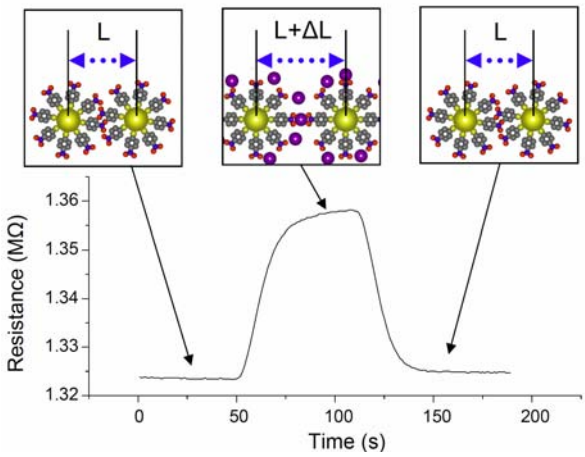


*Figure 1. Typical response of a gold nanoparticle chemiresistor sensor exposed to an aqueous solution of 10 ppm toluene from t = 50 s to t = 110 s. The schematics above depict nanoparticles with an initial separation distance L shifting to a new separation distance L + ΔL due to the infiltration of the analyte and then returning to their initial state with the analyte's egress.*

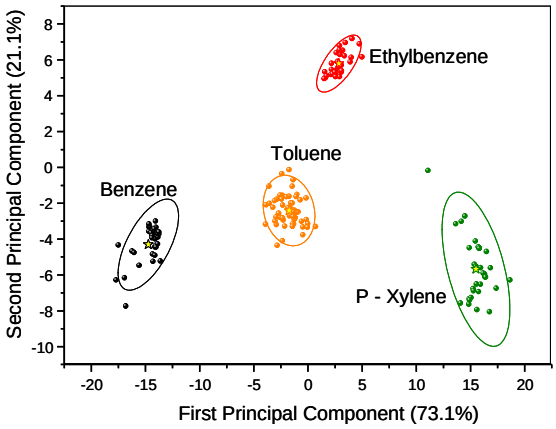


*Figure 2. Principal component plot generated from discriminant analysis of the chemiresistor sensor arrays response to water samples spiked with common organic pollutants.*

Yet the most promising implementation of chemiresistors is to use them in an array configuration, with each of the chemiresistors having nanoparticles functionalized with a different SAMs. The sensor array approach coupled with chemometrics, such as principal component analysis, provides a very powerful chemical analysis system, as already was demonstrated in the detection of lung cancer [5], and hydrocarbon fuels in water. [6]

We envisage this sensor system to be deployed in the discrimination of ions, small and large molecules, amino acids and carbohydrates, with possible applications in metabolomics[7] and other areas of life sciences.

## REFERENCES

[1] Wohltjen, H. and Snow, A., Anal. Chem., 1998, 70(14), pp. 2856-2859. [2] Joseph, Y., Guse, B., Yasuda A., Vossmeyer, T., *Sens. and Actuat. B,* 2004, **98**; pp. 118-195. [3] Zong, Q., Steinecker, W.H., Zellers, E.T., Analyst, 2009, 132 (20), pp.283-293. [4] Raguse, B., Chow E., Barton C.S., Wieczorek L., *Anal. Chem.*, 2007. **79**(19), pp. 7333-9. [5] Peng, G., Tisch, U., Adams, O., et al., Nature Nanotechnology 2009, **4**(10), pp.669-673. [6] Cooper, J.S., Raguse B., et al., *Anal. Chem*., 2010, **82**, pp. 3788-3795.[7] Madsen, R., Lundstedt, T., Trygg J., *Anal. Chim. Acta*, 2010, **659**, pp. 23-33.

European Cells and Materials Vol. 20. Suppl. 3, 2010 (page 272) ISSN 1473-2262

# Functional Biomolecule Nanostructures for Sensing, Catalysis and Circuitry

I. Willner

*Institute of Chemistry, The Hebrew University of Jerusalem, Jerusalem 91904, Israel*
(willnea@vms.huji.ac.il)

The coupling of biomolecules such as enzymes, nucleic acids and antigens/antibodies with metallic or semiconductor nanoparticles or carbon nanotubes provide hybrid materials that combine the unique recognition and catalytic properties of biomolecules with the unique electronic, optical and catalytic properties of nano-objects. These hybrid systems hold great promise for sensor, nanocircuitry and nano-device applications.[1,2] Also, the information encoded in the base-sequence of nucleic acids provides instructive information for the formation of functional DNA nanostructures acting as sensors and DNA machines, and allowing the self-assembly of organized nanostructures.[3]

The electrical contacting of redox enzymes with electrodes is a basic pre-requisite for designing amperometric biosensors and biofuel cells. The reconstitution of apo-enzymes on cofactor-functionalized metallic nanoparticles[4] or carbon nanotubes[5] provides a means to electrically contact redox enzymes with electrodes. Also, the conjugation of biomolecules with semiconductor quantum dots (QDs) enables the development of different optical sensors. This will be exemplified with the construction of QDs-based biosensors to analyze telomerase,[6] kinases,[7] phosphatases[7] and intracellular metabolic processes.[8] Finally, the assembly of metallic nanoparticles on protein templates provides catalytic nanostructures for the synthesis of metallic nanowires and nano-transporters.[9]

The base-sequence encoded in nucleic acids (NAs) allows the design of NAs with specific recognition features (aptamers) and catalytic functions (DNAzymes). The use of aptamers for the amplified detection of cocaine will be described,[10] and the development of molecular machines for the amplified detection of DNA using DNAzymes as catalytic labels will be exemplified.[11] Also, programmed DNA nanostructures enable the design of DNA machines. The construction of DNA "tweezers"[12], "bi-pedal walker", "gear" and "crane" nanodevices will be described. Similarly, the base-sequence of NAs and the tethered chemical functionalities provide instructive information for the self-organization of nanostructures such as catenated DNA chains,[13] DNA strips,[14] and DNA tubes.[15] The resulting

DNA nanostructures provide templates for the precise positioning of enzymes, and for the activation of enzyme cascades.

**References:**

1. E. Katz and I. Willner, *Angew. Chem. Int. Ed.*, **43**, 6042-6108 (2004).
2. I. Willner, R. Baron and B. Willner, *Biosens. Bioelectron.*, **22**, 1841-1852 (2007).
3. a) I. Willner, B. Shlyahovsky, M. Zayats and B. Willner, *Chem. Soc. Rev.*, **37**, 1153-1165 (2008); b)
4. Y. Xiao, F. Patolsky, E. Katz, J.F. Hainfeld and I. Willner, *Science*, **299**, 1877-1881 (2003).
5. F. Patolsky, Y. Weizmann and I. Willner, *Angew. Chem. Int. Ed.*, **43**, 2113-2117 (2004).
6. F. Patolsky, R. Gill, Y. Weizmann, T. Mokari, U. Banin and I. Willner, *J. Am. Chem. Soc.*, **125**, 13918-13919 (2003).
7. R. Freeman, T. Finder, R. Gill and I. Willner, *Nano Lett.*, **10**, 2192-2196 (2010).
8. R. Freeman, R. Gill, I. Shweky, M. Kotler, U. Banin and I. Willner, *Angew. Chem. Int. Ed.*, **48**, 309-313 (2009).
9. F. Patolsky, Y. Weizmann and I. Willner, *Nature Mater.*, **3**, 692-695 (2004).
10. a) B. Shlyahovsky, D. Li, Y. Weizmann, R. Nowarski, M. Kotler and I. Willner, *J. Am. Chem. Soc.*, **129**, 3814-3815 (2007); b) R. Freeman, E. Sharon, R. Tel-Vered and I. Willner, *J. Am. Chem. Soc.*, **131**, 5028-5029 (2009). Addition/Correction: *J. Am. Chem. Soc.*, **131**, 6886-6886 (2009).
11. Y. Weizmann, M. Beissenhirtz, Z. Cheglakov, R. Nowarski, M. Kotler and I. Willner, *Angew. Chem. Int. Ed.*, **45**, 7384-7388 (2006).
12. J. Elbaz, Z.-G. Wang, R. Orbach and I. Willner, *Nano Lett.*, **9**, 4510-4514 (2009).
13. Y. Weizmann, A.B. Braunschweig, O.I. Wilner, Z. Cheglakov and I. Willner, *Proc. Natl. Acad. Sci., USA*, **105**, 5289-5294 (2008).
14. O.I. Wilner, Y. Weizmann, R. Gill, O. Lioubashevski, R. Freeman and I. Willner, *Nature Nanotechnol.*, **4**, 249-254 (2009).
15. O.I. Wilner, A. Henning, B. Shlyahovsky and I. Willner, *Nano Lett.*, **10**, 1458-1465 (2010).

European Cells and Materials Vol. 20. Suppl. 3, 2010 (page 273) ISSN 1473-2262

# Polyethylenimine/DNA Coated Gold Nanoparticles for Gene Delivery

BarbaraWindschiegl, Thomas L. Andresen

*Technical University of Denmark, Department of Micro- and Nanotechnology, Frederiksborgvej 399, 4000 Roskilde*

**INTRODUCTION:** The cationic polymer polyethylenimine (PEI) exhibits a strong DNA compaction capacity and an intrinsic endosomolytic activity and has been widely used in gene delivery. The major challenge in the field is to elucidate the mechanism of the endosomal escape and intracellular trafficking, in order to improve its transfection efficiency and lower the associated cytotoxicity. Most studies were performed with random self-assembled aggregates between PEI and nucleic acid. These nanoparticles are heterogeneous in size which complicates the interpretation of experimental results. Recently uniform gold nanoparticles (AuNPs) were coated with PEI and siRNA using the layer-by-layer (LbL)-technique resulting in an efficient transfection system[1,2]. In our study we design AuNPs containing layers of PEI and DNA and a targeting shell with well defined surface properties in order to perform transfection studies with particular focus on how nanoparticle size influences cellular uptake and transfection efficiency. We furthermore address the intracellular behaviour of these highly uniform particles, i.e. intracellular trafficking and AuNP, PEI, and DNA dissociation.

**METHODS:** Gold nanoparticles (AuNPs) were coated using the layer-by-layer technique. The 50 nm spheres were functionalized and stabilized by the addition of 11-mercaptoundecanoic acid (11-MUA). Layers of polyethylenimine (PEI), DNA and hyaluronic acid (HA) were successive assembled around the AuNPs due to electrostatic interaction of the oppositional charged molecules. We characterized the size, surface charge and shape of the AuNPs by means of dynamic light scattering (DLS), zeta potential (ZP) measurements, UV-vis absorbance spectra and atomic force microscopy (AFM). For cellular uptake studies HeLa and HepG2 cells were used. Confocal laser scanning microscopy (CLSM) was performed to visualize the location of the gold particles and their dissociated compounds.

**RESULTS:** Gold Nanoparticles were successfully coated with PEI, DNA and hyaluronic acid. Uniform particles with controlled size, shape and surface charge were obtained, which was confirmed by DLS, ZP measurements, UV-vis absorbance and AFM. A change in the sign of the

zeta potential indicates efficient coating of each layer. Cellular uptake of the NPs into cells and successful transfection was observed by means of CLSM.

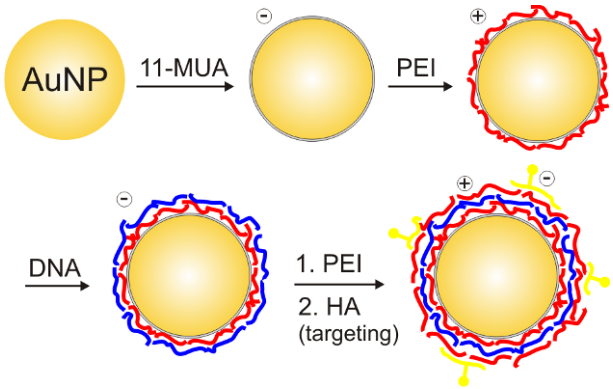


*Fig. 1: Schematic Drawing of gold nanoparticles (AuNPs) coated with PEI, DNA and HA by means of the layer-by-layer technique.*

**DISCUSSION & CONCLUSIONS:** AuNPs can be used as a promising scaffold in gene delivery. PEI/DNA coated particles with controlled size and surface properties (e.g. zeta potential) constitute an optimal tool for a systematic investigation of the mechanism of PEI based transfection. Especially the liberation of the coated compounds and their location in cells enable us to obtain some interesting insights into the cellular effect of PEI. A better understanding of the molecular basis of PEI/DNA transfection is essential in order to create new and non-toxic gene transfection systems for successful gene delivery.

**REFERENCES:** [1] A. Elbakry, A. Zaky, R. Liebl, R. Rachel, A. Goepferich, M. Breunig (2009) *Nano Lett* **9** (5):2059-206. [2] WJ Song, JZ. Du, TM. Sun, PZ. Zhang, J. Wang (2010) *small* **6** (2):239-246.

**ACKNOWLEDGEMENTS:** The Danish Strategic Research Council – NABIIT and the Technical University of Denmark is gratefully acknowledged for funding.

European Cells and Materials Vol. 20. Suppl. 3, 2010 (page 274) ISSN 1473-2262

# Synthesis of Glyco-DNA-Gold Nanoparticle Conjugates

K. G. Witten[1], C. Rech[2], T. Eckert[3], L. Elling[2], W. Richtering[3], U. Simon[1]

*[1] Institute of Inorganic Chemistry, RWTH Aachen University, Germany, [2]Institute of Biotechnology and Helmholtz-Institute for Biomedical Engineering, RWTH Aachen University, [3]Institute of Physical Chemistry, RWTH Aachen University, Germany*

**INTRODUCTION:** DNA-functionalized gold nanoparticles (Au NP-DNA) have been studied in numerous studies over the last decade. Mirkin and co-workers presented the use of Au NP-DNA as intracellular gene regulation agents [1]. The application of Au NP as actuators for the photothermal reversible melting of DNA in Au NP networks was demonstrated by Reismann et al. [2]. Carbohydrate functionalized nanoparticles which imitate the multivalent presentation of carbohydrates on cells have received attention to study specific carbohydrate interactions [3].

We present a new system of Au NP which are functionalized with both, DNA and carbohydrates. Thereby *N*-Acetyl-D-Glucosamine (GlcNAc) modified DNA (GlcNAc-DNA) is bound to Au NP-DNA by Watson Crick base pairing. The GlcNAc-DNA functionalized Au NP then are able to self assemble by specific interaction with *Griffonia Bandeiraea simplicifolia* lectin II (Lectin GS-II) which has four carbohydrate recognition domains. These assemblies can be dissociated by two independent stimuli: temperature induced DNA duplex melting and competition of the Au NP with an excess of free GlcNAc (Fig. 1 a).

**METHODS:** Au NP-DNA [2] and amino- modified GlcNAc [4] were synthesized as described in literature. GlcNAc-DNA was synthesized by coupling thiol-modified ssDNA with amino-modified GlcNAc using 4-*N*-(Maleimidomethyl)-cyclohexanecarboxylic acid *N*-hydroxy-succinimide ester. Au NP assemblies were analyzed by optical spectroscopy, dynamic light scattering (DLS), electron microscopy and small angle X-ray scattering.

**RESULTS:** The addition of Lectin GS-II and complementary GlcNAc-DNA to a solution of AuNP-DNA lead to Au NP self assembly resulting in a red shifted plasmon resonance and an increasing hydrodynamic diameter ($D_h$). A temperature increase resulted in the melting of the DNA duplex linkers and consequently in the dissociation of the networks observable in a decreasing $D_h$. The melting process was fully reversible in a temperature range up to 40°C (Fig. 1 b). On the other hand the addition of an excess of GlcNAc to a solution of growing Au NP networks resulted also in network disassembly which was measured by a decrease of $D_h$ up to values of single particles (Fig. 1 c).

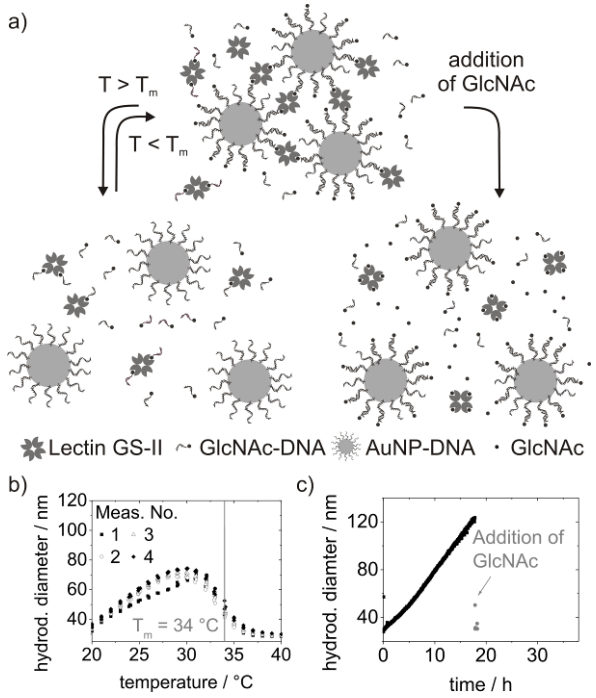


*Fig. 1: Illustration (a) and results from DLS measurements of the disassembly of Lectin GS-II–GlcNAc–DNA-Au NP networks by DNA duplex melting (b) or competition with free GlcNAc (c).*

**DISCUSSION & CONCLUSIONS:** We think that the presented system could be transferable to other biological relevant glycan structures and could have potential for specific targeting of cells as for the use as photothermal actuators and gene regulation agents.

**REFERENCES:** [1]N. L. Rosi, D. A. Giljohann, C. S. Thaxton, A. K. R. Lytton-Jean, M. S. Han, C. A. Mirkin (2006) *Science* **312***:*1027-1030. [2]M. Reismann, J. C. Bretschneider, G. von Plessen, U. Simon (2008) *Small* **4**:607-610. [3]J. M. de la Fuente, S. Penadés (2006) *Biochim. Biophys. Acta* **1760**:636–651. [4]B. Sauerzapfe, K. Křenek, J. Schmiedel, W. W. Wakarchuk, H. Pelantová, V. Křen, L.Elling (2008) *Glycoconjugate J.* **26**:141–159.

**ACKNOWLEDGEMENTS:** We thank the DFG Graduate School "Biointerface" (No. 1035) and the RWTH Aachen Excellence initiative for financial support.

European Cells and Materials Vol. 20. Suppl. 3, 2010 (page 275) ISSN 1473-2262

# High throughput Metal organic framework materials for use as MRI contrast agents

P. P. Wyss[1], D. F. Kennedy[1], J. Mardel[1], J. Kimpton[2], M. Hill[3], C. Drummond[3]

*[1]CSIRO Molecular and Health Technologies, Clayton VIC 3168, Australia. [2]Australian Synchrotron, Clayton VIC, 3168Australia, [3]CSIRO Materials Science and Engineering, Clayton VIC 3168, Australia.*

**INTRODUCTION:** Best described as hybrid materials, metal-organic frameworks (MOFs) consist of metal centers or metal clusters bridged by rigid organic linkers. [1] This generates a 3D material with periodic porosity on the sub nanometer scale. MOFs are known for their huge surface areas, up to 6000$m^2$/g, which makes them ideal candidates for gas adsorption.[2] Because of their high surface areas they have recently attracted a great deal of research interest and have found application in many different areas including gas storage, gas separation and catalysis.

The use of MOFs is not limited to gas storage devices. Recently, preliminary work showed that MOFs had potential as gadolinium (Gd) based magnetic resonance imaging (MRI) contrast agents.[3] Gd is the most effective metal for use as a contrast agent and is already in use in the clinic. Gd(III) is strong paramagnetic ion, since it has the maximum number of unpaired f-shell electrons. This attribute alters the relaxation time of nearby protons of water molecules providing contrast which makes it possible to distinguish the different tissues more accurately. MOFs are excellent potential candidates as in addition they are highly porous and water can infiltrate the pores also affecting the rotational component of the relaxation and the framework structure sequesters the otherwise toxic Gd ions.

**METHODS:** MOFs are produced mostly by hydrothermal or solvothermal techniques, where crystals are slowly grown from a hot solution of metal salt and organic ligands. Despite the large research interest into MOFs, their synthesis remains poorly understood. The reaction conditions required for the successful preparation of crystalline MOFs vary wildly according to the specific system.Therefore, there are scores of different conditions which need to be investigated in order to produce viable materials. To achieve this we have employed a Chemspeed™ robotic synthesis platform for the high throughput synthesis of new MOF materials. Using careful experimental design we are able to identify the optimal conditions for the formation of the MOF within a minimum number of experiments.

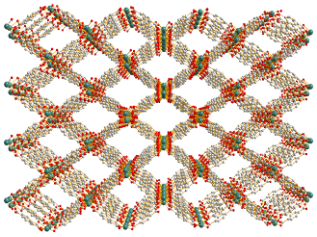

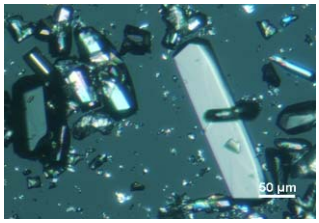


*Fig. 1: (left) Crystal structure of Gd-(benzenedicarboxylate) MOF solvent molecules and hydrogen atoms have been removed for clarity. [4], (right): Microscope picture of Gd-(benzenedicarboxylate) MOF crystals*

**RESULTS:** A variety of novel Gd MOFs have been produced. In order to identify the materials produced in the different experiments, a high-throughput powder X-ray diffraction stage was employed on the powder diffraction beam line at the Australian Synchrotron to quickly obtain the XRD patterns.

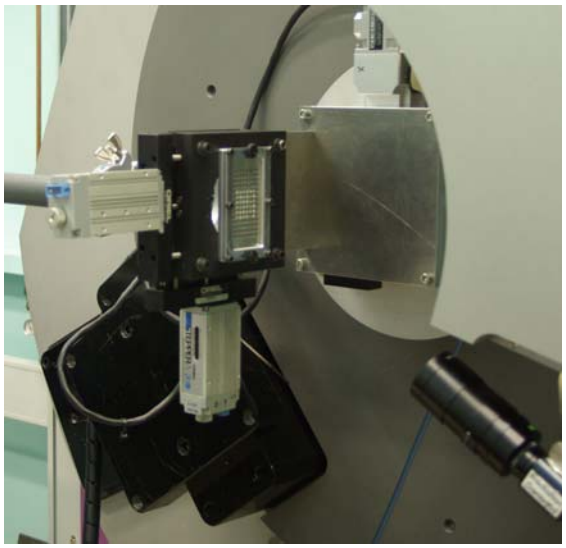

*Fig. 2: High throughput XRD stage at the Australian synchrotron.*

**DISCUSSION & CONCLUSIONS:**

We report the identification of several MOFs which may be employed as MRI contrast agents.

**REFERENCES** [1] Batten, S. R.; Neville, S. M.; Turner, D. R., *Coordination Polymers: Design, Analysis and Application*. Royal Soc. of Chem., Thomas Graham House, Science Park, Milton Road, Cambridge CB4 0WF, UK: 2008. [2] Li, Y.; Yang, R. T., *Langmuir* **2007,** 23, (26), 12937. [3] Rieter, W. J.; Taylor, K. M. L.; An, H. Y.; Lin, W. L.; Lin, W. B., *J. Amer. Chem. Soc.* **2006,** 128, (28), 9024. [4]Poulsen, R.D.; Overgaard, J.; Chevallier, M. A.; Clausen, H. F.; Iversen, B. B. A*cta Cryst. E*, **2005,** 61, M1337-M1339.

# Site-specific immobilization of JAGGED1 on glass substrates for ex vivo expansion of a bone marrow cell population containing hematopoietic stem cells

H. Toda, M. Yamamoto, H. Kohara, Y. Tabata

*Department of Biomaterials, Institute for Frontier Medical Sciences, Kyoto University, Kyoto, Japan.*

**INTRODUCTION:** Ex vivo expansion of hematopoietic stem cells (HSC) is practically necessary to obtain the number of HSC enough for successful treatment of leukemic patients. Recent advance of stem cell biology has demonstrated that Notch signaling is a key pathway to regulate the proliferation and differentiation of HSC [1]. To activate the Notch signaling pathway, a direct binding between a Notch ligand and the receptor via the cell-cell contact is required [2]. In this study, based on the site-specific interaction between protein A and Fc domain, the site-specific immobilization of a Notch ligand was designed to achieve the efficient ligand-receptor binding. The ex vivo expansion of a bone marrow cell population containing HSC was evaluated with the Notch ligand-immobilized substrates.

**METHODS:** A recombinant chimeric protein of Jagged1 and Fc domain (Jagged1-Fc) was employed for the site-specific immobilization. Briefly, protein A was immobilized on *N*-hydroxysuccinimide ester-conjugated glass substrates. To avoid non-specific binding of Jagged1-Fc to substrates, fibronectin was pre-coated on the protein A-immobilized glass substrate. Then, the protein A-immobilized glass substrate was exposed to the solution of Jagged1-Fc chimeric protein to fabricate Jagged1-immobilized substrates. As a control, Jagged1-Fc was coated non-specifically on the fibronetin-coated glass substrate without the protein A immobilization. Mouse lineage negative cells (Lin negative) were isolated from mouse bone marrow through the negative selection of CD3e, CD8a, NK1.1, Ly6G, and B220 by magnetic-activated cell sorting and maintained in serum free X-VIVO media supplemented with stem cell factor and thrombopoietin.

**RESULTS:** The amount of Jagged1-Fc on the glass substrates was changed by altering that initially added, irrespective of the substrate fabrication methods. The cell culture experiment was performed for different substrates with the same Jagged1-Fc amount. Figure 1 shows the ex vivo expansion profile of the cell population with c-kit positive, Sca-1 positive, Lin negative, and CD34 negative (KSL CD34 negative cells) upon being analyzed by a flow cytometry. Apparently,

KSL CD 34 negative cells significantly increased on the Jagged1-immobilized substrates after 6 days of culture, whereas Jagged1-coated substrates and Jagged1-immobilized substrates with a Notch signaling inhibitor did not.

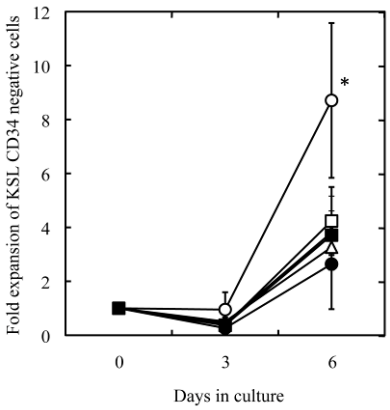


*Fig. 1: The ex vivo expansion of KSL CD34 negative cells after 3 and 6 days of culture in different conditions.*
*( ) Jagged1-immobilized substrates, ( ) Jagged1-immobilized substrates with a Notch signaling inhibitor, ( ) Jagged1-coated substrates, ( ) fibronectin-coated substrates with soluble Jagged1, ( ) fibronectin-coated substrates, and ( ) unmodified substrates. *p<0.05; significance against the fold expansion of KSL CD34 negative cells in other culture conditions.*

**DISCUSSION & CONCLUSIONS:** This result suggests that immobilization of Jagged1-Fc chimeric protein through a specific binding between proteinA and Fc domain enabled Jagged1 to increase the binding efficiency for the Notch receptors and consequently enhance the activation of Notch signaling, which leads to the promoted expansion of a cell population containing HSC ex vivo.

**REFERENCES:** [1] J.M. Butler et al (2010) *Cell Stem Cell* **6**:251-264. [2] R. Kopan et al (2009) *Cell* **137**:216-233.

**ACKNOWLEDGEMENTS:** This research was supported by Grants-in-Aid for "Young Scientist A" and "Challenging Exploratory Research" from the Japan Society for the Promotion of Science (JSPS).

European Cells and Materials Vol. 20. Suppl. 3, 2010 (page 277) ISSN 1473-2262

# Fabrication of Biodegradable Hydrogels with Controlled Vascular Networks

Hiroaki Yoshida, Michiya Matsusaki, Mitsuru Akashi

*Department of Applied Chemistry, Graduate School of Engineering, Osaka University, 2-1 Yamada-oka, Suita 565-0871, JAPAN.*

**INTRODUCTION:** Construction of thick and vascularized complex tissues such as heart and liver is an important issue in tissue engineering. In order to introduce blood vessels into engineered tissues or biodegradable scaffolds, 3-dimensional (3D) cell culture of endothelial cells (EC) in scaffolds or with engineered tissues has been investigated. However, it is difficult to control the position, density and size of the obtained blood vessels. Therefore, if vascular networks with arbitrary position, density and size can be fabricated, we would create thick engineered tissues with desired vascular networks suitable for target tissues and organs.

Herein, we present a novel technique for fabricating biodegradable hydrogels with spatially-controlled multilayered vascular networks. We first prepared poly(γ-glutamic acid) (γ-PGA) hydrogels with arbitrary pore structures, by using silica capillaries as a porogen. Then, in order to incorporate multilayered blood vessels onto the pore surface, we focused on 3D-cell assembly technique, developed by our group recently [l]. Briefly, by preparing nano-sized artificial extracellular matrices (nano-ECM) onto a cell monolayer, which allows 2nd layer of cells, layered architectures can be easily constructed. After formation of vascular smooth muscle cell (SMC) monolayer onto the hydrogel's pore and the following preparation of the nano-ECM onto the monolayer, multilayered blood vessels were successfully constructed inside the gels by co-culturing vascular endothelial cells. This strategy would become a promising technique for vascularization of engineered tissues and implantable devices as well as biodegradable scaffolds.

**METHODS:** Poly(γ-glutamic acid) was crosslinked with cystamine in the presence of water soluble carbodiimide [2]. Then, the reacting solution was transferred into glass plates with 2 mm silicon spacer and arranged silica capillaries (outer diameter: 620 μm). After 3 hours of gelling reaction, the silica was softly extracted, and the gels was washed with ultrapure water for 2 days to remove the remaining compounds. The gels with 1 cm of the pore length were used for the following cell culture. Human umbilical artery smooth muscle cells (UASMC) were injected into the pore of the hydrogels and cultured to form the monolayer. Then, human umbilical vein endothelial cells (HUVEC) were laminated onto the UASMC monolayer via preparation of fibronectin and gelatin (FN-G) nano-ECM by layer-by-layer assembly technique. UASMC and HUVEC were labelled with cell tracker green and PKH26. The structures of the obtained engineered tissues were confirmed by fluorescent microscopy.

**RESULTS & DISCUSSION:** The pore diameter of the obtained γ-PGA hydrogels with capillary pores was 720 μm, almost the same as that of the silica used. After cell culture of UASMC onto the pore, homogeneous green fluorescence inside the pore was observed. Then, by co-culturing HUVEC onto UASMC via the FN-G nano-ECM, bi-layered architecture was constructed, suggested by two colours of layered fluorescence. Using this approach, various types of vascular networks would be fabricated in engineered tissues and scaffolds.

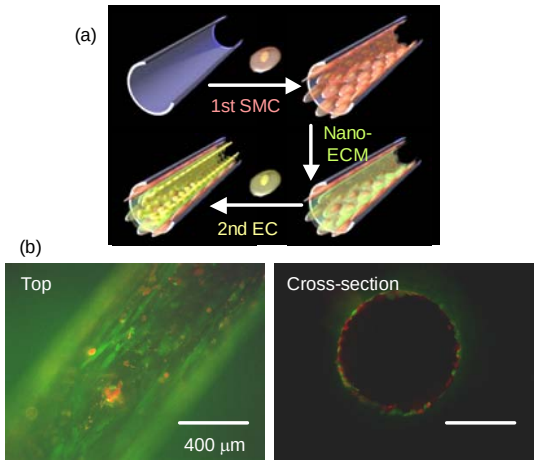


*Fig. 1: (a) Fabrication of biodegradable hydrogels with multilayered blood vessels. (b) Confocal fluorescent images of (above) UASMC monolayer and (below) bilayer blood vessels composed of UASMC and HUVEC.*

**CONCLUSIONS:** The novel strategy in this report would be a new concept for vascularized engineered tissues.

**REFERENCES:** [1] M. Matsusaki, K. Kadowaki, Y. Nakahara, et al (2007) *Angew Chem Int Ed* **46**:4689-92. [2] H. Yoshida, M. Matsusaki, M. Akashi (2009) *Adv Funct Mater* **19**:1001-07.

European Cells and Materials Vol. 20. Suppl. 3, 2010 (page 278) ISSN 1473-2262

# Ring-shaped trap as a template for the formation of silver nanoparticles

J. O. Yu[1], J. R. H. Tame[2], C. Addy[2], and J. G. Heddle[1*]

[1]*Advanced Science Institute, RIKEN, Wako, Japan*

[2]*Protein Design Laboratory, Yokohama City University, Yokohama, Japan*

**INTRODUCTION:** TRAP (trp RNA-binding attenuation protein) is a nanometric ring-shaped protein found in species of *Bacillus*. Mutations of residues in the central cavity of the ring allow it to capture gold nanoparticles in solution.[1] It was speculated that the introduction of glutamate residues in the centre of wild type *Bacillus subtilis* TRAP (*Sub.* TRAP A66E) would capture silver ions in solution, and template their formation into silver nanoparticles. Glutamate residues were previously and successfully used in this way by Belcher and co-workers, who found that virus capsids containing repeating glutamate units were able to mineralize silver.[2] *Bacillus stearothermophilus* TRAP has previously been engineered to produce a self-assembled protein nanotube.[3] It is proposed that the tunnel within the protein tube can also be utilized for mineralization, and possibly nanowire construction. Efficient methods to encourage silver biomineralization within the protein tube will be examined.

**METHODS:** *Bacillus subtilis* TRAP protein was mutated to change residue Arg66 to Glu. using a Quikchange mutagenesis kit (Stratagene) according to manufacturers' protocol. The protein was purified as previously described.[4] The biomineralization reaction consisted of incubating TRAP (200 μL, 1.4 mg/mL,) with $AgNO_3$ (13.4 μL, 1 M, $H_2O$) at 4° C for approx. 18 hours. $NaBH_4$ (6.7 μL, 1 M) was subsequently added, and the resultant mixture allowed to incubate for 2 hours at 4° C. The resulting solution was concentrated via Amicon spin column. Protein solution was applied to a carbon-coated copper grid and stained with 3% phosphotungstic acid. TEM was carried out using a H9500SD (HITACHI, Tokyo) operated at 200 kV.

**RESULTS:** Initial studies using TEM indicates the presence of silver particles constrained within the TRAP protein's cavity (Figure 1). The identity of the silver in the centre of the ring was confirmed by energy dispersive X-ray analysis.

**DISCUSSION & CONCLUSIONS:** We have successfully demonstrated that a modified TRAP protein is able to mineralize silver from solution to produce protein filled with silver nanoparticles. Initial results suggest that the closely related TRAP from *B. stearothermophilus* is unable to carry out this reaction. Further studies will be required to confirm the result and assess the ability of *B. subtilis* TRAP lacking the glutamate mutation to also mineralize silver. Methods to increase the efficiency of the reaction and to find ways of separating mineralized protein from both unmineralized protein and protein-free silver nanoparticles are also being investigated.

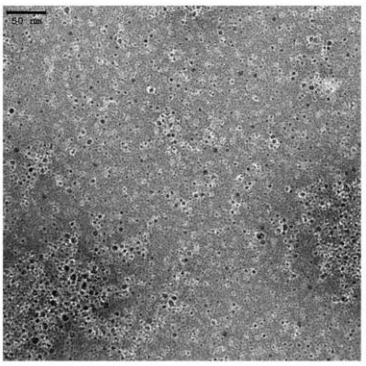

*Figure 1. High resolution TEM micrograph of Bacillus subtilis TRAP A66E with silver nanoparticles in the centre of the rings. The scale bar is 50 nm. Grid is negatively stained with 3% PTA.*

**REFERENCES:** [1]J. G. Heddle, I. Fujiwara, H. Yamadaki, S. Yoshii, K. Nishio, C. Addy, I. Yamashita, J. R. H. Tame, (2007) *Small* **3**, 1950. [2]Y. J. Lee, H. Yi, W. –J. Kim, K. Kang, D. S. Yun, M. S. Strano, G. Ceder, A. M. Belcher, (2009) *Science* **324**, 1051. [3]F. F. Miranda, K. Iwasaki, S. Akashi, K. Sumitomo, M. Kobayashi, I. Yamashita, J. R. H. Tame, J. G. Heddle, (2009) *Small* **5**, 2077. [4]J. G. Heddle, T. Yokoyama, I. Yamashita, S. -Y. Park, J. R. H. Tame, (2006) *Structure* **14**, 925.

**ACKNOWLEDGEMENTS:** J.O.Y. was supported by a JSPS Foreign Postdoctoral Fellowship, J.R.H.T. was supported by grants-in-aid from MEXT and J.G.H was supported by a MEXT Grant-in-Aid for Young Scientists (WAKATE B-20710083) from the ministry of Education, Culture, Sports, Science and Technology, Japan.

European Cells and Materials Vol. 20. Suppl. 3, 2010 (page 279) ISSN 1473-2262

# Temperature Controlled Encapsulation and Release Using Partially Biodegradable Thermo-magneto-sensitive Self-rolling Tubes

S.Zakharchenko, N.Puretskiy, G.Stoychev, M.Stamm, L.Ionov

*Leibniz Institute of Polymer Research Dresden e.V., Dresden, Germany.*

**INTRODUCTION:** Development of approaches for controlled delivery of drugs and cells in living organisms is very important for medicine and regenerative therapy. Stimuli-responsive polymers were demonstrated to be particularly promising for these applications due to their ability to reversibly change physical and chemical properties in response to environmental signal. To date, several approaches based on polymers sensitive either to pH or to temperature signals have been developed and tested. For example, small drug molecules can be delivered using stimuli-responsive hydrogel particles and releases from them due to stimuli-induced contraction. On the other hand, cells can be delivered and released in controlled manner using polymer systems able to undergo sol-gel transition.

**RESULTS & DISCUSSION:** Here we report a new approach for controlled encapsulation and release of microparticles, cells and drugs using thin bilayer films of thermoresponsive and biodegradable polymers, which are able to form self-rolling tubes [1-2].

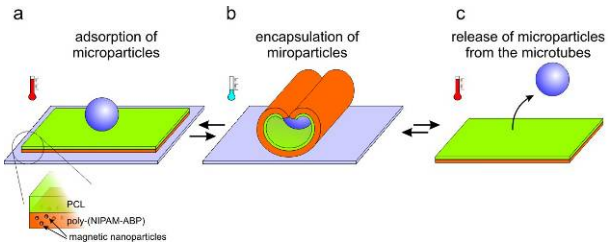


*Fig. 1: Scheme of capture and release of microparticles by self-rolling microtubes. Thin film of poly-(N-isopropilacrylamide-co-4-acrylobenzophenone) (poly-NIPAM-ABP) and polycaprolactone with admixed magnetic particles (a) is able to form self-rolling tube and to encapsulate microparticles at reduced temperature (b). The particle can be released at elevated temperature when the microtube is unrolled (c). Reprinted with permission from ref 2, Copyright Royal Chemical Society.*

In our approach, two polymers – one thermoresponsive poly-(N-isopropylacrylamide)-based copolymer and hydrophobic polycaprolactone (PCL) are used. Small amount of photocrosslinker – benzophenone derivatives – was added to both polymers in order to provide

sensitivity to UV light. The microtubes were produced using photolithography.

We found that bilayer films remain undeformed at T > 28°C and start to roll and form tubes when the temperature decreases below the LCST of poly-(NIPAM-ABP). The following heating affects the morphology of the formed microtube. In particular, the microtubes produced by single revolution are able to unroll almost completely at elevated temperatures when the poly-(NIPAM-ABP) is collapsed. Meanwhile tubes formed by multiple revolutions shrink at elevated temperature and are unable to unroll.

We also tested the possibility to manipulate particle-loaded microtubes using magnetic field. For this, we prepared microtubes containing $Fe_3O_4$ nanoparticles in the thermoresponsive layer and loaded them with microparticles. We found that the freely flowing particle-loaded microtubes start to move in the direction of the magnet when it is applied The direction of the microtubes flow can be immediately switched by changing the position of the magnet, thus demonstrating the possibility to manipulate the microtubes using magnetic field.

**CONCLUSIONS:** Since simple methods such as dipcoating and photolithography were used, the reported method can be easily scaled up for production of large quantities of microtubes. Comparing to the other methods for drug and cell delivery such as hollow capsules, gel particles and vesicles, the presented approach give opportunity of controlled release of large objects such cells by stimuli-induced unrolling of tubes. The suggested approach can be successfully implemented for controlled delivery of drugs and cells in living organisms as well as to design scaffolds for tissue engineering.

**REFERENCES:** [1] V. Luchnikov, O. Sydorenko and M. Stamm (2005) *Advanced Materials* **17**:1177-+. [2] S. Zakharchenko, N. Puretskiy, G. Stoychev, M. Stamm and L. Ionov (2010) *Soft Matter* accepted.

**ACKNOWLEDGEMENTS:** DFG (Grant IO 68/1-1) and Volkswagen Foundation are acknowledged for financial support.

European Cells and Materials Vol. 20. Suppl. 3, 2010 (page 280) ISSN 1473-2262

# Porous bioceramic bone grafts for drug immobilization

V.Zalite, D.Loca, J.Locs, L. Berzina-Cimdina

*Riga Technical University, Riga Biomaterials innovation and Development centre, Latvia*

**INTRODUCTION:** With the recent progress in pharmaceutical industry and biotechnology new drug delivery systems (DDS) are developed. DDS based on the porous hydroxyapatite (HA) ceramics have been extensively studied past two decades due to their potential use in the hard tissue replacement, treatment and regeneration [1-2]. Such properties as porosity, interconnection of pores, drug release profile and mechanical strength of porous bioceramic bone grafts are highly dependent on the intended target [3-4].
In this study an attempt was made to prepare the porous HA scaffolds with sufficient mechanical strength, pore size and sustained drug release.

**METHODS:** HA powder used for bone grafts preparation was synthesized by wet precipitation reaction between calcium hydroxide and phosphoric acid. The dried precipitate was milled to obtain a fine powder. Hydroxyapatite was mixed with an organic additive (polyol) to obtain a highly viscous/plastic mixture. As pore foaming agent $H_4NHCO_3$ was added to the plastic mass. To obtain ceramics the green bodies were sintered at 1150$^{o}$C for two hours.
The porosity was determined with Archimed method, microstructure was investigated using scanning electon microscopy (SEM) and compressive strength was determined using Instron 4301.
Lidocaine hydrochloride was used as a model drug for DDS preparation. Lidocaine and polyvinyl alcohol in porous scaffolds was incorporated using vacuum infiltration. Release of lidocaine was determined using HPLC - UV method.

**RESULTS:** Modifying amount of foaming agent it was possible to obtain ceramic samples with porosity ranging from 36.9% to 55.6% and compressive strength of 10-21MPa. As it is seen from SEM images prepared ceramic scaffolds contain interconnected pores where pore sizes are in range from 20μm to 300μm (see Fig 1.).

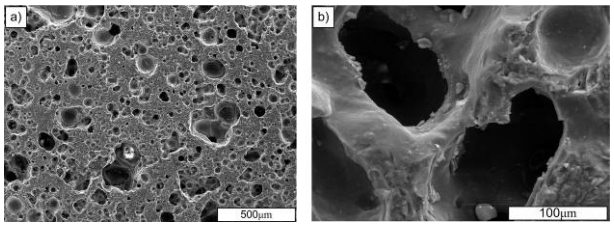


*Fig. 1: SEM images: a)surface microstructure of bioceramic bone grafts; b)pore microstructure.*

The lidocaine release rate was evaluated and compared between HA/lidocaine composites with and without polyvinyl alcohol coating (see Fig. 2.).

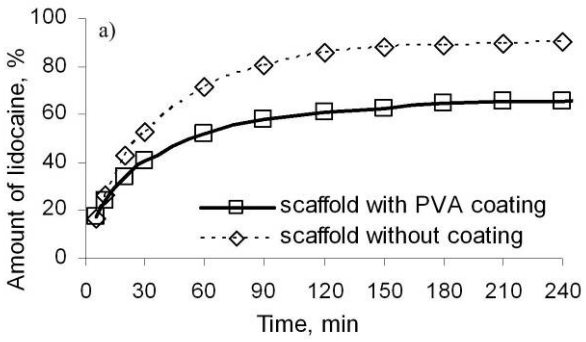


*Fig. 2: Lidocaine release rate from HA/lidocaine composites*

**DISCUSSION & CONCLUSIONS:**

The results of this study indicate that prepared porous HA scaffolds has perspective in such applications as templates for bone tissue ingrowths due to their pore size and structure. High mechanical strength of the samples makes them attractive in dentistry and maxillofacial surgery.
Drug release rate can be sustained for two hours in the case of uncoated composites. PVA coating effectively decreased the lidocaine release rate to more than 4 hours.

**REFERENCES:** [1]E. Chevalier, M.Viana, S. Cazalbou, L. Makein, J. Dubois, D. Chulia (2010) *Acta Biomater* **6**:266-274. [2]R. Yoshida, K. Sakai, T. Okano and Y. Sakurai (2002) *Adv Drug Delivery Rev* **11**:85-108. [3]A. Krajewska. A. Ravaglioli, E. Roncari, P. Pinasco (2000) *J Mater Sci-Mater M* **12**:763-771. [4]H. Yoshikawa, A. Myoui (2005) *J. Artif. Organs* **8**:131-136.

**ACKNOWLEDGEMENTS:** This work has been supported by the European Social Fund within the project "Multidisciplinary Research in Biomaterials Technology of New Scientist Group",No.2009/0199/1DP/1.1.1.2.0/09/APIA/VIAA/090, (PVS ID 1380).

European Cells and Materials Vol. 20. Suppl. 3, 2010 (page 281) ISSN 1473-2262

# Tuning of the silver ion release from antibacterial nanocomposite coatings

V. Zaporojtchenko[1*], T. Hrkac[1], T. Strunskus[1], V. S. K. Chakravadhanula[1], N. Alissawi[1], R. Podschun[2], C. Röhl[3], D. Garbe-Schönberg[4] and F Faupel[1]

*Christian-Albrechts-University, Kiel, Germany.*

*[1] Institut für Materialwissenschaft - Materialverbunde, [2]Institut für Infektionsmedizin, [3]Insitute of Toxicology and Pharmacology for Natural Scientists, [4]Dept. of Geology/ ICPMS Lab*

**INTRODUCTION:** Different nanocomposite antibacterial materials consisting of silver nanoparticles dispersed in a polymer or ceramic matrix have been studied in last decade as material for preventing microbial adhesion. However, most approaches like impregnation of silver in the bulk material lead to ineffective use of the expensive impregnated noble metal particles and decrease of the antibacterial efficiency because of the longer diffusion lengths in the bulk materials. Moreover, the controllable kinetic of the silver ion release plays a decisive role in the medical and environmental application requirements.

**METHODS:** To control the silver release from antibacterial nanocomposites we developed a coating process based on plasma polymerization as well as a vapor phase co-deposition of noble metals and polymers or ceramics to protect a surface against growth of bacteria by depositing a thin nanocomposite film [1-3]. These methods allowed preparing not only nanocomposites with a defined nanoparticle size and concentration but also with a different depth profile of the nanoparticle distribution. The silver release was monitored by ICP-MS. Also particle surface plasmon resonance and radiotracer technique were used to control silver long-term release

**RESULTS**: Influence of the host material, the concentration as well as the particle distribution on the release of biocidal silver ions and antibacterial efficiency were investigated. It was found, that formation of the percolating nanoparticle chains is very important for the long-term silver ion release. Also the influence of the surface barrier layers as well as trace amounts of gold on the silver release were investigated (Fig 1). This was used to create composite coatings with the ability to tune the release of biocidal metal ions, thus, also minimizing possible human toxicity. Antimicrobial activity of nanocomposite coatings can be achieved either by release of metal ions into the external milieu thereby also killing bacteria located in distance to the coated surface or by ions immobilized in/on the nanocomposite preventing microbial biofilm formation on the surface. Direct visualization of growth of bacteria on the surface was also shown by fluorescence microscopy of test specimen after treatment with fluorescent stains.

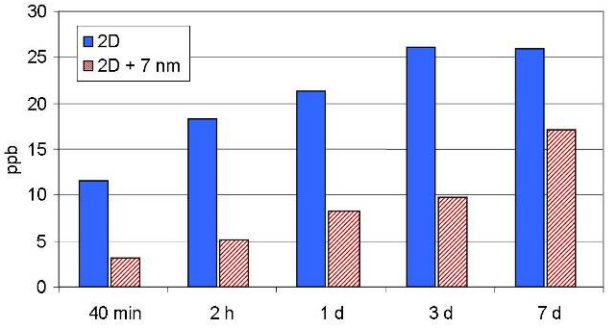


*Fig. 1: Release of Ag from a layer of 2D Ag nanoparticles with and without a 7 nm $TiO_2$-barrier layer. The figure shows the amount of Ag in ppb from 40 min to 7 days treatment in water.*

**DISCUSSION & CONCLUSIONS:** The present tunable antibacterial coating allows a flexible control over the nanostructure of the composites and the kinetics of the silver release. A silver load was found which completely inhibits bacterial colonization by *E.coli* but allows adhesion and spreading of human fibroblast cells. The coatings can be used in a number of applications where optimal kinetic parameters of the silver release are essential to prevent growth of bacteria.

**REFERENCES:**[1]F.Faupel,V.Zaporojtchenko,et.al *Contribut.plasma.Physics* (2007) **47**, *537* [2] V. Zaporojtchenko, R. Podschun, F. Faupel, Nanotechnology (2006) **17**, 4904-4908 *Y .Mishra ,V.Chakravadhanula, et al* J of Nanoscience and Nanotechnology (2010) **10**, 2833–2837

**ACKNOWLEDGEMENTS:** The authors are grateful to the German Research Foundation (DFG) and the World Gold Council (WGC) for the financial support of this work.

European Cells and Materials Vol. 20. Suppl. 3, 2010 (page 282) ISSN 1473-2262

# Fabrication of ZnO structures as templates for interaction with microorganisms

E. S. Zarie, S. Kaps, X. Jin, S. Wille, Y.K. Mishra, R. Adelung

[1] *Functional Nanomaterials, Institute for Materials Science, University of Kiel, Kaiser Str.2, 24143, Kiel, Germany*

**Email: ess@tf.uni-kiel.de**

**INTRODUCTION:** Synthesis of different drugs in solid form for targeted drug delivery is currently a focus of immense research interest in the field of biomedical engineering. Rapid developments in nanotechnology in last decade have been proven to the boon for bioscience, currently known as Nanobiotechnology. Biocompatible nanostructures can be used as suitable drug carrier into the body. Mostly biomedical researchers have used different solvents and toxic materials to formulate the different active pharmaceutical ingredients. However use of nano-micro structures as an alternative of the solvents can be better option with improved anti-microbial activity in this regards [1]. Moreover, those nano and microstructures could be used as a template for 3D cell growth or used as shuttles in drug delivery. In this work we report the synthesis of different (1D, 2D and 3D semiconductor (ZnO) nanostructures by modified vapour liquid solid approach. Preliminary experiments with anti-microbial activity of ZnO nanostructures coated with nipasol have been performed and will be discussed.

**METHODS:** 1D, 2D and 3D nanostructures were synthesized by modified vapour liquid solid approach. Structures of synthesized nanostructures were confirmed by scanning electron microscopy (200kV, Philips). As preliminary tests, these nano-microstructures were coated with pharmaceutical drugs by a novel solvent free technique, they are also used for anti-microbial tests and for the biocompatibility, these nanostructures were also employed for test with different cells and viruses at University of Kiel in Germany and at the Western University of Health Sciences in Pomona, USA.

**RESULTS:** Scanning electron microscopy (SEM) images of synthesized ZnO nanostructures are shown in figure 1. Using modified-VLS approach we synthesize the whole family of nanostructures like nanoparticles, nanorods, nanowires, nanotubes, nanotetrapods, nanoseaurchins, nanosails and nanonails etc. in a homogeneous manner over large areas. The shape and size of nanostructures can be controlled by temperature and annealing time in M-VLS approach.

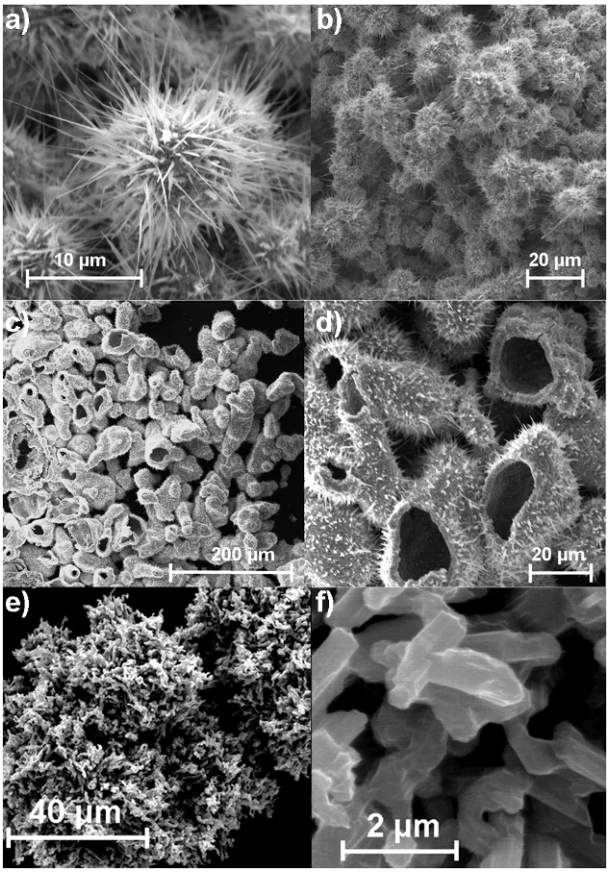


***Fig. 1(a to f):*** *SEM micrographs showing the family of nanostructures that can be produced on large areas in the M-VLS approach.*

**CONCLUSIONS:** Under various conditions, we have successfully performed the controlled growth of different varieties of ZnO nano-microstructures over large area surfaces. Preliminary experiments testing these nanomaterials with microorganisms showed effects that depended on the nanostructure. These effects could be on the one hand antiviral and antibacterial and on the other hand compatible with cell growth.

**REFERENCES:** [1] P. J. Ginty et al., Materials Today 8(2005)42-48.

**Acknowledgement:** We thank S. Rehders for outstanding technical support. ESZ thanks the support grand from Government of Egypt. YKM thanks the Humboldt foundation and RA the DFG for a Heisenberg Professorship.

European Cells and Materials Vol. 20. Suppl. 3, 2010 (page 283) ISSN 1473-2262

# Label-free Chemical Nanoanalysis of Biological Samples using Tip-Enhanced Raman Spectroscopy (TERS)

Renato Zenobi

*Departmenf of Chemistry and Applied Biosciences, ETH Zürich*

*CH-8093 Zürich, Switzerland zenobi@org.chem.ethz.ch*

**INTRODUCTION:** The concept of tip-enhanced Raman spectroscopy (TERS) is based on localized surface plasmons, which lead to a local electric field enhancement if a metal nanostructure is illuminated by a light beam in resonance with the plasmon. The intensity of Raman scattering of molecules in close proximity to such a nanostructure will scale approximately with the $4^{th}$ power of the electric field enhancement factor, and the light confinement by the nanostructure provides the spatial resolution (≈ 20 nm). In practice, TERS is done by dipping an STM tip or a metallized AFM tip into the focus of the excitation laser of a Raman microscope. In certain configurations, TERS can result in the enhancement of Raman scattering by a factor of > $10^7$ [1], resulting in single molecule sensitivity. Thus, TERS provides both exquisite spatial resolution as well as chemical information for the analysis of nanostructures.

**METHODS:** We have been developing TERS for chemical imaging of biological nanostructures [2, 3]. There are numerous hurdles to overcome: The intense local field can cause decomposition of sensitive biomolecules. This problem can be alleviated by short exposure times and rapid scanning. It has also recently become possible to perform TERS experiments in aqueous environments [4], which of course opens the door to study biological samles in their native environment.

**RESULTS:** The presentation will give an overview of the applicability of TERS and related methodologies to study a variety of biological specimens. It was, for example, possible to use highly spatially resolved Raman data to study biomineralization on the nanometer scle [5]. In another application, we showed that TERS is able to detect protein vibrational features in cytochrome C that are not related to the heme chromophore. This is in contrast to all other Raman / SERS studies on cytochrome C that lack the spatial resolution: in this case, the vibrational spectra are swamped by heme related bands [6]. The presentation will end with an outlook [7], including a discussion of the possibility to use

TERS for label-free study of the nanoscale organization of biological and model membranes (Fig. 1).


*Fig. 1: Cartoon of the interaction of a TERS tip with a biological membrane*

**REFERENCES:** [1] W. Zhang, B.-S. Yeo, T. Schmid, and R. Zenobi, J. Phys. Chem. C **111**, 1733-1738 (2007). [2] T. Schmid, J. Burkhard, B.-S. Yeo, W. Zhang, and R. Zenobi, *Anal. Bioanal. Chem.* **391**, 1899 - 1905 (2008). [3] T. Schmid, A. Messmer, B.-S. Yeo, W. Zhang, and R. Zenobi,, *Anal. Bioanal. Chem.* **391**, 1907 – 1916 (2008). [4] T. Schmid, B.-S. Yeo, G. Leong, J. Stadler, and R. Zenobi, *J. Raman Spectroscopy* (Special issue on "Tip-enhanced Raman Spectroscopy") **40**, 1392 – 1399 (2009). [5] M. Sánchez-Román, C. Vasconcelos, T. Schmid, J. A. McKenzie, M. Dittrich, R. Zenobi and M. A. Rivadeneyra, *Geology* **36**, 879 – 882 (2008). [6] B.-S. Yeo, S. Mädler, T. Schmid, W. Zhang, and R. Zenobi, J. Phys. Chem. C **112**, 4867-4873 (2008). [7] B.-S. Yeo, J. Stadler, T. Schmid, and R. Zenobi, *Chem. Phys. Lett.* **472**, 1 – 13 (2009), invited "Fontiers" article.

European Cells and Materials Vol. 20. Suppl. 3, 2010 (page 284) ISSN 1473-2262

# Surface biofunctionalization with Polyelectrolyte Multilayers – Scaffolds for Neural Tissue Engineering

K.Zhou[1], D.Nisbet[1], G.Sun[2], ,C.Bernard[2], G.Thouas[3] J.S. Forsythe[1]

[1] *Department of Materials Engineering Monash University, Australia.* [2] *Monash Immunology and Stem Cell Laboratories Monash University*

[3] *Melbourne University, Australia.*

**INTRODUCTION:** Layer-by-Layer (LbL) deposition of bioactive polyelectrolytes provides an effective means to biofunctionalize 3D nanofibrous scaffolds with micro- size interconnected pores. Polyelectrolyte multilayers (PEMs) have alternating surface properties and can be built up with nanometer scale precision [1]. PEMs can be designed to interact with cells to control the cell adhesion, migration and differentiation. This can be achieved by using different polyelectrolyte materials that build up PEMs and also by fine tuning them by changing pH, ionic strength, layer number etc. This is used to not only control the thickness, but also the roughness and morphology of the PEMs, which consequently influence the cellular response.

**METHODS:** Compression moulded poly-ε-caprolactone (PCL) was used as a simplified 2D substrate model for the LbL deposition. Polyethylenimine treated PCL substrates were soaked alternatively in heparin (H) and PLL (P) solutions followed by a PBS wash after each deposition step. PEMs with different terminating layers were collected and then characterized with water contact angle measurements (CA), X-ray photoelectron spectroscopy (XPS), and quartz crystal microbalance (QCM) to confirm the PEM formation. *In vitro* culture of neural progenitor cells were also performed on the crosslinked PEMs from P4 to H6 (where the number corresponds to polyelectrolyte bilayer number).

**RESULTS:** CA measurements on PEMs showed an alternating step change, which was consistent with alternating atomic sulphur concentration determined using XPS. The total thickness of the PEMs was 125nm for 15 polyelectrolyte layers based on QCM studies. Culture of neural progenitor cells showed improved cell-surface adhesion compared with the unmodified PCL surface. PLL terminating layers also promoted neurite outgrowth, which was significantly different ($P<0.05$) in terms of neurite density to the heparin terminating layer. Results also showed differences in cell morphology, as cells tended to form clusters on PLL terminating layers compared to those on the PLL coated coverslips.

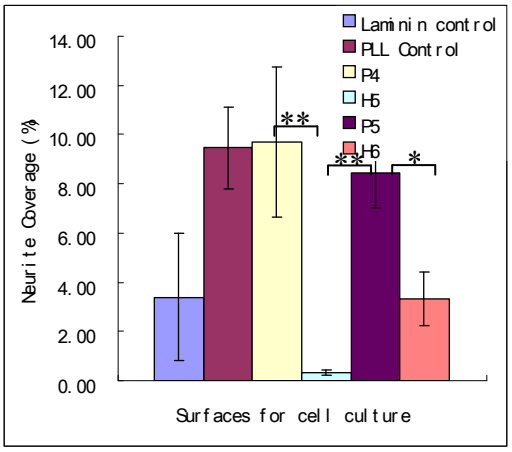


*Fig. 1: Neurite density of neural progenitor cells cultured on laminin, PLL coated glass coverslip control and PEM surfaces. The PCL substrate and negative controls are omitted since few cell attached. *** $p<0.001$, ** $p<0.01$, * $p<0.05$*

**DISCUSSION & CONCLUSIONS:** PEM formation was confirmed by CA measurements. The formation of relative uniform PEM structures from P3 was revealed by XPS and QCM measurements. *In vitro* culture on PLL terminating layers showed the improved cell attachment compared with unmodified PCL substrates. By switching to a heparin terminating layer, we are able to present a surface with a non-adherent property to cultured neural progenitor cells, while cells that did were probably interacting with PLL chains that had penetrated from the underlying layer. This chain interpenetration between adjacent layers also caused the cell clustering on heparin terminating layers.

**REFERENCES:** [1] Bertrand, P., A. Jonas, et al. (2000) Macromolecular Rapid Communications 21(7): 319-348.

**ACKNOWLEDGEMENTS:** This work is supported by grants from the Australian Research Council (DP0985433) the Baker Foundation, Bellberry Ltd, the National Health and Medical Research Council of Australia and the National Multiple Sclerosis Society of New York.

European Cells and Materials Vol. 20. Suppl. 3, 2010 (page 285) ISSN 1473-2262

# Surface-bound DNA self-assembly or enzymatic reactions toward the PCR-free amplification of nucleic acids biosensor signals

G. Zuccheri, A. Vinelli, M. Onofri, B. Samorì

*Department of Biochemistry, University of Bologna, Italy.*

**INTRODUCTION:** Single-molecule sensitivity can be nowadays achieved when trying to characterize minute amounts of macromolecules n in a research laboratory setting. The sensitivity is significantly worse when working in the field and trying to assess the presence of a pollutant or a pathogen as quickly as possible. Point-of-care testing is the realm of biosensors and the trend of research is towards simplicity of use, low cost, reliability and, last but not least, sensitivity.

In the detection of nucleic acids, the hybridization of an oligonucleotide probe with its poly-nucleotidic target is monitored by changes in physico-chemical properties of an interface, commonly induced by the use of a specific label. The probe, often bound to an oligonucleotide itself, can be a fluorescent dye, an enzyme, an electroactive moiety or other functional element. Such probes impart specificity and sensitivity to the assay, but make it drift far from simplicity of use (and low cost).

**METHODS AND RESULTS:** Recently, label-free techniques are developing in which the presence of the analyte macromolecule itself can induce detectable physico-chemical changes. The struggle is to make such techniques sufficiently sensitive and specific. In our work, we are trying to implement DNA-based surface-bound amplification strategies that can serve to amplify the read-out signal of DNA hybridization in a label-free biosensor, such as those measuring the electrochemical properties of an electrode interface.

The 'hybridization chain reaction' [1] is an isothermal enzyme-free strategy to trigger polymerization of oligonucleotides into a long double-stranded DNA. We have demonstrated that the 'hybridization chain reaction' can be also implemented (making use of available software tools [2]) in a surface-bound configuration, leading to the self-assembly of many copies of oligonucleotides on a target DNA bound on an oligonucleotide self-assembled monolayer.

In another attempt, we have shown that terminal transferase (a template-free DNA polymerase) can be used to build a long polynucleotide out of the target DNA that is bound to its immobilized oligonucleotide probe.

The Rolling Circle Amplification reaction is a very promising strategy to produce large amounts of DNA without the need of thermal cycling or of an accurate control of temperature. Preliminary evaluations on the *Primer-Generation* RCA [3] show its interest as an additional strategy to increase the amount of target DNA response from a biosensor surface.

**DISCUSSION & CONCLUSIONS:** All these strategies will lead to the accumulation of nucleic acids at the solid-liquid interface when triggered by the probe-target recognition. This produces an amplification of the signal of a label-free biosensor. Even though the amplification factors of these implementations are still as low as 10, their further development is still possible, with the hope of avoiding or reducing the need of polymerase chain reaction in the detection of low concentrations of nucleic acids.

**REFERENCES:**

[1]Dirks, R. M. and N. A. Pierce (2004). "Triggered amplification by hybridization chain reaction." *Proc Natl Acad Sci U S A*, **101**(43): 15275-8. [2]Goodman, P. (2005). "NANEV: a program employing evolutionary methods for the design of nucleic acid nanostructures" *BioTechniques*, **38**(4): 548–550. [3]Murakami, Sumaoka and Komiyama (2009) "Sensitive isothermal detection of nucleic-acid sequence by primer generation–rolling circle amplification" *Nucleic Acids Research*, 2009, **37**, e19.

**ACKNOWLEDGEMENTS:** This work was supported by Framework Programme 6 Integrated Project DINAMICS. .

European Cells and Materials Vol. 20. Suppl. 3, 2010 (page 286) ISSN 1473-2262

# Enzymatic Cascade Reactions in Microchannels: Monolayer Patterning & Reversible Embedding of DNA-Enzyme Hybrids

TuHa Vong,[1,2] Jurjen ter Maat,[1] Sanne Schoffelen,[2] Jan van Hest,[2] Teris van Beek,[1] Han Zuilhof[1]

*[1] Laboratory of Organic Chemistry, Wageningen University, Dreijenplein 8, 6703 HB Wageningen, The Netherlands. [2] Institute of Molecules and Materials, Radboud University Nijmegen, Tournooiveld 1, 1111 AA Nijmegen, The Netherlands.*

E-mail: Han.Zuilhof@wur.nl

**INTRODUCTION:** Because microchips are expensive, it is desirable to have a system that be reused or changed according to one's needs. Typically, biofunctional materials have a shorter active lifetime than the glass substrates. Therefore the goal of this project was to a) provide local and reversible biofunctionalization of glass micro-channels, and b) use this approach to induce enzymatic cascade reactions within a single microchannel, via the use of DNA-linked enzyme hybrids, that can be positioned and removed via DNA hybridization/dehybridization.

**RESULTS & DISCUSSION:** We have developed a novel site-specific surface modification method (patterning by UV irradiation), which leaves a functional linker on the inside wall of a glass microchannel (typical inner diameter: 10 – 100 μm). This local attachment is based on the light-induced reaction of a ω-COOH-functionalized-1-alkene with an acid-washed glass surface.[1] The available linker is then used to covalently couple an amino-terminated oligo-DNA. This thus yields a general platform for the reversible binding of a complementary ssDNA-conjugate strand (e.g. DNA-enzyme).[2]

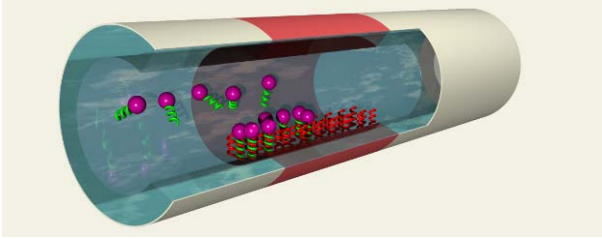

*Figure 1: Local and covalent attachment of oligoDNA within a microchannel provides a general supramolecular platform for the reversible functionalization with (bio-)hybrids.*

Such a reversible attachment is especially attractive in the case of components that have an active lifetime that is significantly shorter than that of the glass chip, such as is the case for many enzymes. Therefore DNA-enzyme constructs were prepared, subsequently attached within the microchannel, and their activity optimized.

Next, an enzymatic cascade reaction was performed within the microchannel, by local attachment of DNA-hybrids of CalB and Horse Radish Peroxidase. It should be noted that after the initial local prefunctionalization with two different oligo-DNA strands flowing the microchannel with a solution containing a mixture of CalB and HRP allows the CalB and HRP to find their own position via specific DNA hybridization. Finally the cascade reaction was shown to work, and the dependence on flow rate, length of functional moieties and specifics of the initial attachment reaction investigated systematically.

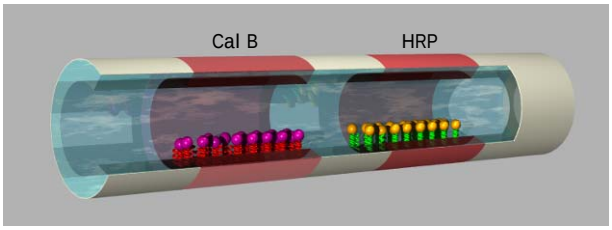


*Fig. 2: Local positioning of DNA-hybrids of CalB and Horse Radish Peroxidase allows an enzymatic cascade reaction within the microchannel.*

**REFERENCES:**

1) J. ter Maat, R. Regeling, M. Yang, M.N. Mullings, S.F. Bent and H. Zuilhof ˛ Photochemical Covalent Attachment of Alkene-Derived Monolayers onto Hydroxyl-Terminated Silica *Langmuir* **2009,** *25*, 11592.

2) T.H. Vong, J. ter Maat, T.A. van Beek, B. van Lagen, M. Giesbers, J.C.M. van Hest and H. Zuilhof - Site-Specific Immobilization of DNA in Glass Microchannels via Photolithography *Langmuir* **2009**, *25*, 13952.

**ACKNOWLEDGEMENTS:** The authors thank NWO-ACTS (PoaC project 053.65.002) and NanoNed (project WMM.6975), both funded by the Dutch Ministry of Economic Affairs, for financial support.

European Cells and Materials Vol. 20. Suppl. 3, 2010 (page 287) ISSN 1473-2262

# Reproducibility evaluation of stearylamine containing nanoemulsions for Gene Therapy

L.M.Verissimo[1], F.Alexandrino-Júnior[1], A.L.Silva[1], A.S.Martins[1], K.G.H.Silva[1], G.C.Silva[1], L.F.Agnez-Lima[1], E.S.T.Egito[1]

[1] *UFRN – Universidade Federal do Rio Grande do Norte - Brazil*

**INTRODUCTION:** Cationic lipid-based emulsions (CLEs) have been investigated as a non-viral gene carrier in therapeutic gene delivery due to the disadvantages related to the use of viral vectors (scale-up control, immunogenicity, oncogenicity and the limited size of nucleic acid that can be packed) (1). The CLEs are systems consisting of two immiscible liquids containing an oil core (natural or semi-synthetic) stabilized by co-surfactants and cationic surfactants, which are responsible for the positive charge in the droplet surface. The presence of cationic surfactants allows the complexation with the negatively charged DNA via electrostatic interactions, resulting in DNA compaction and consequently nanocomplexes formation of emulsion/DNA (2). Achieving reproducibility of pharmaceutical systems production is a crucial step in the development of a new pharmaceutical product. The aim of this work was to evaluate the reproducibility of a stearylamine containing emulsion as a possible carrier for gene therapy.

**METHODS:** Two groups of similar formulation were prepared in different days using the sonication method. Briefly, aqueous phase components were weighed and mixed with distilled water. The mixture was sonicated until clear using a probe sonicator at 10W (Sonicator Ultra Processor XL 2020 from Heat System Inc., EUA) in an ice–water bath. This phase was added to the oil phase and sonicated for 4 min in an ice–water bath and stored at 4ºC. The emulsions were prepared in triplicate. Table 1 shows the final composition of the formulation.

*Table 1. Stearylamine emulsions composition*

| Component | Stearylamine emulsion |
|---|---|
| ***Oil Phase*** | |
| Captex® 355 (MCT) | $5\%_{(w/w)}$ |
| Spam 80® | $0.8\%_{(w/w)}$ |
| ***Aqueous Phase*** | |
| Stearylamine | $0.16\%_{(w/w)}$ |
| Tween 80® | $1.2\%_{(w/w)}$ |
| Distilled water qsp. | 100% |

The mean particle size and zeta potential of each group of emulsions were measured by Dynamic Light Scattering (DLS) and Phase Analysis Light

Scattering, respectively using one of these equipments: Brookhaven ZetaPALS, USA (Nano 1) and Zetasizer, Malvern (Nano 2). The results were compared by the Wilcoxon Test using a significance level of 95%.

**RESULTS:** The result of Wilcoxon Test for the two groups of emulsions showed a P value of 0,2500 e 0,1000 for the mean particle size and zeta potential, respectively (Figure 1).

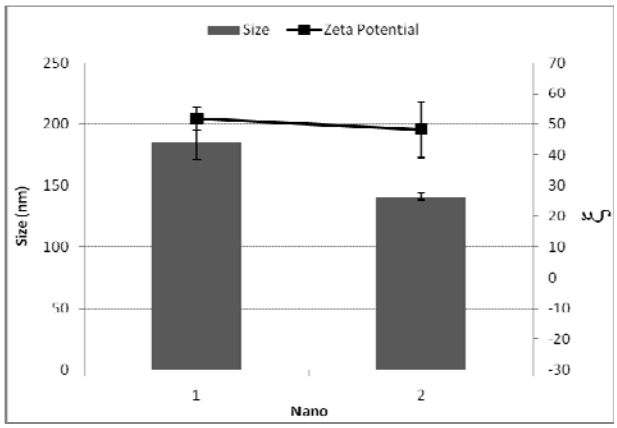


*Fig. 1: Comparison of mean particle size (histogram) and zeta potential (points) of Nano 1 and Nano 2.*

**DISCUSSION & CONCLUSIONS:** The high P values obtained by the comparison of mean particle size and zeta potential of Nano 1 and 2 demonstrate that they do not present any significant difference. Therefore, the nanoemulsion systems used in this study are reproducible and eligible for further studies as gene carriers.

**REFERENCES:**

1. Verissimo LM, Agnez Lima LF, Monte Egito LC, de Oliveira AG, do Egito ES. Pharmaceutical emulsions: a new approach for gene therapy. *J Drug Target.* 2009 Dec 3.

2. Nam HY, Park JH, Kim K, Kwon IC, Jeong SY. Lipid-based emulsion system as non-viral gene carriers. *Archives of Pharmacal Research.* 2009;**32(**5):639-46.

**ACKNOWLEDGEMENTS:** This template was supported by CAPES.

European Cells and Materials Vol. 20. Suppl. 3, 2010 (page 288) ISSN 1473-2262

# High Resolution Atomic Force Microscopy of MG63 Cells on Composite Substrates

Igor Bdikin[1], Filipa Marques[2], Virgília S. Silva[2], Paula P. Gonçalves[2], Monoj K. Singh[1], Jose Gracio[1]

*[1] TEMA & Department of Mechanical Engineering, University of Aveiro, Aveiro, Portugal. [2]CESAM & Department of Biology, University of Aveiro, Aveiro, Portugal.*

**INTRODUCTION:** Precise prediction of chemical and physical behaviour of multicomponent structures at different dimensional scales is one of the most contributing factors to the success in surgical and regenerative techniques using implants [1]. In the past decade, atomic force microscope emerged as one of the most powerful tools for probing mechanical properties (i.e. adhesion and friction forces, elasticity and stiffness) of cell-substrate and cell-cell interactions at subnanometer resolution [2,3]. We challenged the mechanical properties of engineered nanosystems during cell response to composite substrates by Atomic Force Microscopy (AFM).

**METHODS:** AFM measurements were performed with a commercial setup a commercial AFM (DI, Nanoscope IIIA) with. A commercial Si tip-cantilever system with the spring constant of 0.1-10 N/m and typical tip radius less than 10 nm were used. Experiments were carried out in physiological saline solution utilized a liquid cell (Veeco). Imaging was performed in contact modes with scanning velocity 1-50 μm/s and applied force from 10 nN up to 55.0 μN. Deformation of the cell was determined relative to the substrate, based on pattern recognition using a cross-correlation algorithm. Force-loaded cell image was under minimum force-loaded condition (Fig.1) using friction mode. Substrates of composites (carbon nanotubes (CNTs) and polymethyl methacrylate/hydroxyapatite (PMMA/HA)) were prepared by Freeze-granulation technique.

**RESULTS:** AFM surface analyses reveal that the MG63 cells grown onto glass and composite substrate exhibit different shapes with approximate length of 10-30 mm and height of 1-3 mm. Surface roughness for substrates were determined: RMS = 6.8 nm (glass), RMS = 0.1-1 μm (CNTs/PMMA/HA). Deformation of the cell was determined relative to the substrate. AFM friction images were obtained under minimum force-loaded condition (Fig.1). Average compressive stress was calculated by averaging the absolute values of lateral stress vector onto substrate surface. The friction force $F_f$ on the sample is:

$$F_f = \mu(N + F_{ad}), \quad (1)$$

where μ - friction constant, N - local normal force) for a smooth surface if the friction mechanism does not change and $F_{ad}$ - adhesion force. From friction images are possible to determine moment of start of displacement of the cell and magnitude of the applied lateral force exactly at the beginning of cell moving.

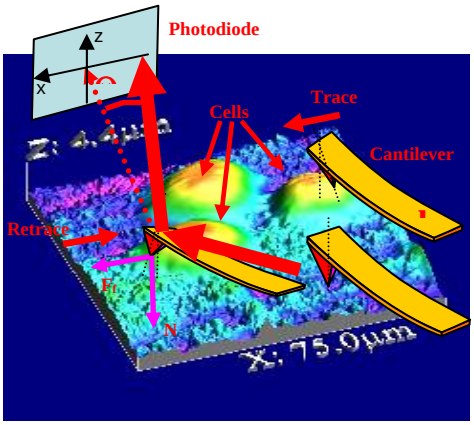


*Fig. 1: Schematic setup of the AFM (friction mode). The torsion of the cantilever is reflects by (a), (b), (c) positions correspond to scanning direction and friction force.*

**DISCUSSION & CONCLUSIONS:** Strong mechanical interactions (adhesion force = 0.4 μN) between fixed MG63 cells and CNTs/PMMA/HA substrate were found. Application of normal force to living cells in physiological saline solution was also accompanied by increased lateral force. Additionally, AFM images revealed that cell height decreased monotonically. In conclusion high roughness and porosity of the CNTs/PMMA/HA appears to favour strong adhesion and penetration of cells into the body of the substrate.

**REFERENCES:** [1]D.A. Lauffenburger and Alan Wellsy (2003) *Biophysical Journal* **84**: 3499–3500. [2]S. Munevar, Yu-li Wang and Micah Dembo (2001) *Biophysical Journal* **80**: 1744–1757. [3]N.Wang, K.Naruse, D.Stamenovic, *et al* (2001) *Biophysics* **98**: 7765–7770.

European Cells and Materials Vol. 20. Suppl. 3, 2010 (page 289) ISSN 1473-2262

# Nanostructured Bioceramic Coatings obtained by Plasma Spray Technique

K.Brinkiene, R.Kezelis, V.Mecius, J.Cesniene

*Lithuanian Energy Institute, Materials Research and Testing Laboratory, Kaunas, Lithuania*

**INTRODUCTION:** In recent years, considerable research was done to deposition of biocompatible coatings in order to protect the medical implant surfaces and to increase the lifetime of various orthopaedic implants [1]. Hydroxyapatite-based ceramic (HA) coatings are largely applied on metallic components of prostheses due to its bioactive properties and chemical structure closed to the structure of natural bone, but the mechanical properties and adherence of these coatings are not good [2]. Therefore, bioinert ceramic coatings are used as bondcoat for HA coatings [3]. Plasma-spraying technique is one of primary methods used commercially to produce ceramic coatings on metallic implants [1]. Alumina/ zirconia composite ceramics can be used as bioinert bondcoat due to good biocompatibility, corrosion resistance and high wear resistance of the materials.

**METHODS:** Ceramic coatings were deposited on stainless steel substrates employing atmospheric plasma spray technique [4]. Texture and structural investigations were performed by scanning electron microscopy. Phase composition and crystallinity was investigated by XRD. Surface roughness was evaluated by surface profilometry. The microhardness measurements were performed by Vickers method at 100 g load. Adhesion was evaluated by scratch test. Tribological characteristics were examined using reciprocated ball-on-plate sliding test (load 30 N, total sliding distance 108 m). Three groups of zirconia coatings with different amount of alumina – 0 (Z100), 15 (ZA15) and 85 wt.% (ZA85) were plasma processed on the polished substrates using alumina and yttria stabilized (5.3 wt.%) zirconia powders (spraying power ~50 kW, spray distance 70 mm).

**RESULTS:** Morphology of all coatings is quite similar and is determined by the parameters of plasma spraying. Uniform and equal-sized grains are dominated in the structure of the deposits (Fig. 1). The distribution of structural elements in the microstructure of plasma sprayed coatings is homogeneous. The thickness of deposits is quite uniform and depends on spray duration. It is in the range of 30-60 μm, when spray duration is 30 and 60 s, respectively.

By XRD, the sprayed coatings are nanocrystalline. The averaged crystallite size, determined by the Scherrer equation is 30 nm for Z100 coating.

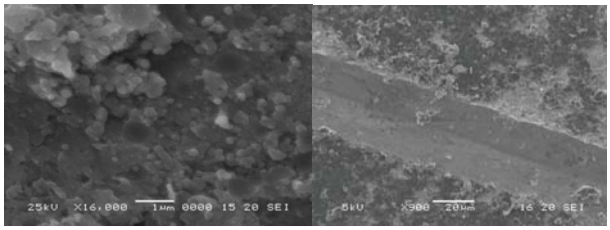

*Fig. 1: SEM images of as-sprayed ZA85 coating (left) and of worn surface of ZA85 sample with wear track at a load of 100 g (right).*

Surface roughness, Vickers microhardness and wear rate of the coatings are presented in Table 1. It was noticed that alumina addition increases the microhardness of zirconia based ceramic coatings.

*Table 1. Characteristics of the deposited coatings.*

| Parameter | Z100 | ZA15 | ZA85 |
|---|---|---|---|
| Ra, μm | 1.14 | 1.36 | 0.8 |
| HV, GPa | 4.67 | 5.74 | 7.25 |
| Wear, $10^{-5}$ $mm^3$/Nm | 3.1 | 2.8 | 2.2 |
| Identified phases * | M, T | M, T, α | M, T, α |

* M – monoclinic, T – tetragonal, $\alpha$ – alfa-alumina

**DISCUSSION & CONCLUSIONS:** The results of these experiments indicated, that wear properties of the coatings are determined by the composition of the material. Addition of alumina to zirconia reduces wear rate of sprayed samples and can improve the tribological properties of the coatings. Plasma sprayed coating doped with 85 wt. % alumina is characterized by lower value of wear rate (2.2 $10^{-5}$ $mm^3$/mN) and higher microstructural homogeneity. Microscopic examination of worn surfaces indicated that abrasion is dominant mechanism in initial stage of wear process.

**REFERENCES:** [1] H. Liang et al. (2004) *Vacuum 73*, pp 317-326. [2] M.F. Morks, A. Kobayashi (2007) *Applied Surface Science* **253**, pp 7136–7142. [3] B.-Y. Chou, E. Chang (2002) *Journal of Materials Science: Materials in Medicine* **11**(6), pp 529-620. [4] K. Brinkiene, R. Kezelis et al. (2006) *Materials Science.* ISSN 1392-1320 **12**(4), pp 300-304.

**ACKNOWLEDGEMENTS:** The work was done by COST 533 Action programme and supported the Agency for Int. Science and Technology Development Programmes in Lithuania.

European Cells and Materials Vol. 20. Suppl. 3, 2010 (page 290) ISSN 1473-2262

# Carbon Nanotube-base Dual Mode Biosensor for Electrical and Surface Plasmon Resonance measurements

Young Wook Chang[1], Jeseung Oh[1], Seunghwan Yoo[2], Dong Jun Kim[3], Seongil Im[2], Young June Park[4], Donghyun Kim[3], and Kyung-Hwa Yoo[1, 2]

*[1] Nanomedical Graduate Program, [2] Department of Physics, [3] School of Electrical Engineering, Yonsei University, Korea, [4] School of Electrical Engineering, Seoul National University, Korea.*

**INTRODUCTION:** Recently, carbon nanotube (CNT)-based biosensors with a field effect transistor (FET) structure have attracted considerable attention because of their merits. Various biological interactions have been monitored by measuring the conductance change. In spite of these successful demonstrations, however, there are several problems to be solved for real applications, such as sensor to sensor variation, unspecific binding, etc. To overcome the above problems, we have proposed a dual mode biosensor that enables the detection of biological events by simultaneously measuring both changes in electrical conductance and surface plasmon resonance (SPR).

**METHODS:** To obtain CNT-MESFET structure (Fig. 1), SWNTs were grown by patterned catalyst growth technique. Electrical measurements were carried out using a semiconductor parameter analyzer. The top gate was fabricated by depositing Cr/Au only on the middle of the semiconducting CNT. The CNT-MESFET was fabricated on the quartz substrate for a dual mode biosensor. Since the large top gate was necessary for SPR measurements, ultra-long SWNTs were grown on the quartz substrate by thermal CVD.[1] Au/Cr electrodes were prepared for electrical measurement. The Au top gate was fabricated in the middle of the CNTs for SPR measurement.

**RESULTS:** Fig. 2 is the SEM image of CNT-MESFET dual mode biosensor. The $I_{SD}$-$V_{SD}$ curves measured after DNA immobilization and hybridization are shown in Fig. 3(a). The conductance was reduced by immobilization of probe ssDNA on the surface of the top gate and further reduced by subsequent hybridization, even though several CNTs were connected between the source and drain electrodes.[2] The SPR curves, which were simultaneously measured with the $I_{SD}$-$V_{SD}$ curves (Fig.3(a)), are presented in Fig. 3(b). Immobilization of probe ssDNA molecules on the Au top gate led to an angle displacement of 0.12° in SPR reflectance minimum. After hybridization caused by addition of a 1 $\mu M$ solution of target ssDNA molecules, the SPR angle was further shifted by 0.10°.

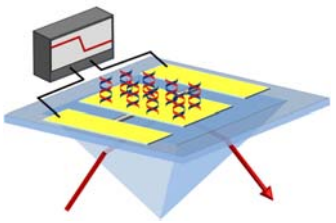

*Fig.1: A Schematic diagram of a dual mode CNT-MESFET biosensor.*


*Fig.2: SEM image of dual mode CNT-MESFET biosensor.*

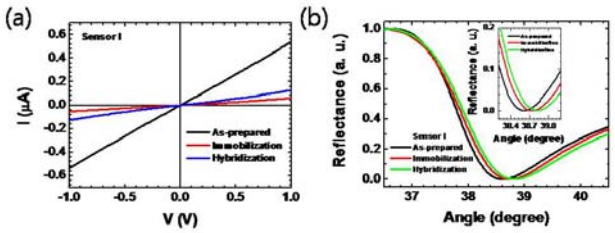


*Fig. 3:(a )$I_{SD}$-$V_{SD}$ curves measured for the CNT-MESFET on the quartz substrate. (b) SPR curves measured for the CNT-MESFET on the quartz substrate.*

**DISCUSSION & CONCLUSIONS:** We have fabricated the CNT-based biosensor with the MESFET structure to develop a dual mode biosensor for electrical and SPR measurements. DNA hybridization on the Au top gate resulted in the shift in SPR reflectance minimum as well as the decrease in $I_{SD}$.

**REFERENCES:** [1] Hong, B. H.; Lee, J. Y.; Beetz, T.; Zhu, Y. M.; Kim, P.; Kim, K. S. J. Am. Chem. Soc. 2005, 127, 15336. [2] Dong, X. C.; Lau, C. M.; Lohani, A.; Mhaisalkar, S. G.; Kasim, J.; Shen, Z. X.; Ho, X. N.; Rogers, J. A.; Li, L. J. *Adv. Mater.* **2008**, 20, 2389.

**ACKNOWLEDGEMENTS:** This work was supported by NRF through National Core Research Center for Nanomedical Technology
(R15-2004-024-00000-0)

European Cells and Materials Vol. 20. Suppl. 3, 2010 (page 291) ISSN 1473-2262

# Modelling of nano-carriers for improved alpha radiotherapy

L.Thijsen[1], D.R.Schaart[1], A.G.Denkova[1]

[1] *Radiation, Radionuclides & Reactors, Delft University of Technology, Mekelweg 15, 2629 JB Delft, The Netherlands*

**INTRODUCTION:** Radiopharmaceuticals are used in the field of nuclear medicine for both treatment and diagnosis of numerous diseases such as cancer. Ideally, the radiopharmaceuticals should be transported to, and retained at the diseased site without causing damage to healthy tissue. This is especially true in the case of alpha emitting radionuclides. Alpha radiotherapy is considered to have great potential for the treatment of cancer due to the very efficient cell destruction of the alpha particles. However, the daughter recoil atoms formed during the alpha decay have significant energy and break loose from any chemical bond.[1] This implies that there is no control over their bio-distribution in vivo. Additionally, most of these radionuclides accumulate at the bone and can induce significant radiotoxic effects. Therefore, the retention of the daughter recoil atoms is of great importance. In this work we use a modelling approach to engineer polymersomes in such a way that they can retain the daughter recoil nuclides and therefore limit adverse effects commonly associated with alpha radiotherapy.

**METHODS:** Monte Carlo simulations in Geant4 were used to calculate the penetration range of the recoil radionuclides which is related to their energy. The decay, diffusion, nuclear and electronic stopping in polymersomes with different dimensions and composed of the block copolymer poly(ethylene oxide)-b-poly(butadiene) (PEO-PB) were simulated. In some cases nano-particles were added to the block copolymer to evaluate the influence of metal nano-particles on the ranges of the recoiling radionuclides.

The simulations were carried out for both single decay and for multiple decay steps, i.e. the radionuclide decays to another alpha emitter, which decays as well, and so on until a stable isotope is reached.

**RESULTS:** The recoil range of recoiling daughter thorium-226 ($^{226}$Th) of the decay of uranium-230 ($^{230}$U) is shown in Figure 1 for several materials. In water, the mean recoil range is around 100 nm. Figure 2 shows the recoil atoms escaping a polymersome in the case of the complete decay series of $^{230}$U consisting of 5 recoiling daughters.

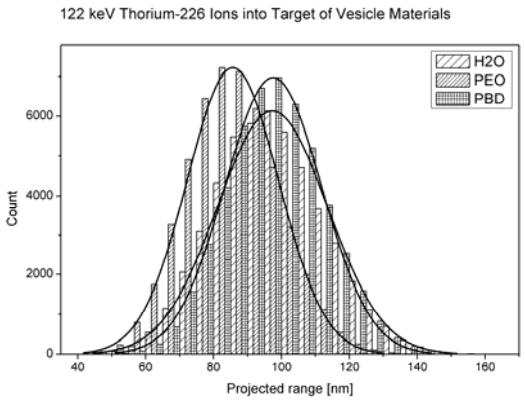


*Fig. 1 Range distribution of 122 keV $^{226}$Th atom in water, poly(ethylene oxide) and poly(butadiene) target.*

Figure 2 depicts the influence on the recoil range of metal nano-particles incorporated in the bilayer of the polymersomes.

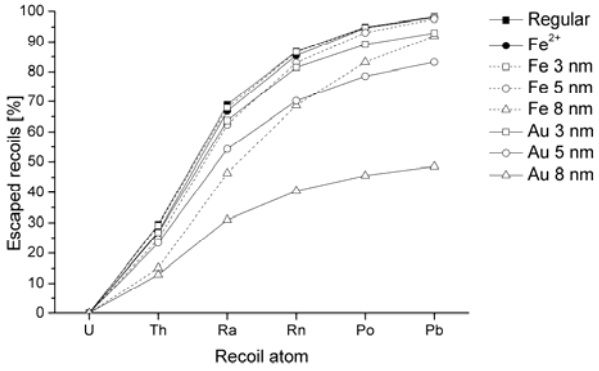


*Fig. 2 Recoil atoms escaping a multilayer polymersome with radius of 150 nm in the presence and absence of nano-particles. The escaped recoils are given as a percentage of the total number of uranium decays, cumulatively.*

**DISCUSSION & CONCLUSIONS:** Metal nano-particles incorporated in polymersomes reduce the penetration range of the recoiling atoms. Polymersomes with dimensions of 150 nm can retain up to 70% single recoil atoms. In the case of series of recoiling atoms larger vesicles need to be used.

**REFERENCES:** [1] S. Stavroula, B. J. Kappel, J. S. Jaggi, M. R. McDevitt, D. A. Scheinberg, G. Sgouros (2007) *Bioconjug Chem.* **18**: 2061–2067.

European Cells and Materials Vol. 20. Suppl. 3, 2010 (page 292) ISSN 1473-2262

# Ferroelectric Properties of Dried Rat Embryonic Neurons from the *Substantia nigra* by the Piezoresponse Force Microscopy

Alejandro Heredia[1], Igor Bdikin[2], Graça Baltazar[3], Andrei Kholkin[1]

*[1] CICECO & Department of Ceramics and Glass Engineering, University of Aveiro, Aveiro, Portugal. [2] TEMA & Department of Mechanical Engineering, University of Aveiro, Aveiro, Portugal. Portugal. [3] Faculdade de Ciências da Saúde, Departamento de Ciências Médicas, Universidade da Beira Interior, Beira Interior, Portugal.*

**INTRODUCTION:** Ferroelectricity is the spontaneous polarization of molecules by applying an external electric field. It is well known in inorganic materials and in some biological assemblies of lipids, macromolecules as microtubules and it is discussed in voltage-gated ion channels in cell membranes. Till now there is no direct evidence in biological functions or active mechanisms [1, 2]. Biological membranes have an anisotropic electrostatic behavior supporting biological functions. Electrostatic interactions inside/near the membrane originate from three potentials: 1) The transmembrane potential, is the driving force for ion transport through channels 2) the surface potential, regulates the cytosolic/ environmental factors with cell membranes. These two membrane potentials are well known to have clear membrane functions. However, there is a third membrane potential with rather unclear functions, the dipole potential. It is a relatively large positive potential barrier at the membrane midplane created the most probably by phospholipid molecular dipoles at the interfacial planes. Although studied for decades, it is among the least understood aspects of biological membranes [3].

**METHODS:** Images were performed by the piezoresponse force microscopy (PFM) in a commercial scanning force microscope (Ntegra Aura, NT-MDT, Moscow, Russia) [4]. PFM signals were acquired in the form $A\cos\theta$, where A is the amplitude of the piezoelectric vibrations and $\theta$ is the phase shift between the driving and detected signals. In this way, domains with opposite polarities exhibit different contrasts.

**RESULTS:** Lipids and voltage-gated ion channels are common molecules in neurons and other excitable cells, having a potential for the occurrence of bio-ferroelectricity. The first condition for ferroelectric behavior is the alignment of dipole moments as occurs experimentally in microtubules (34,000 Debye at 2_1 × 105 V/m and 2MHz) [1] and in other cellular components such as lipids.

The organizations of lipids in dopaminergic neurons, the order in some voltage-gated membrane proteins and cytoskeleton elements might be coordinated in the whole cells and potentially produce an electromechanical behavior.

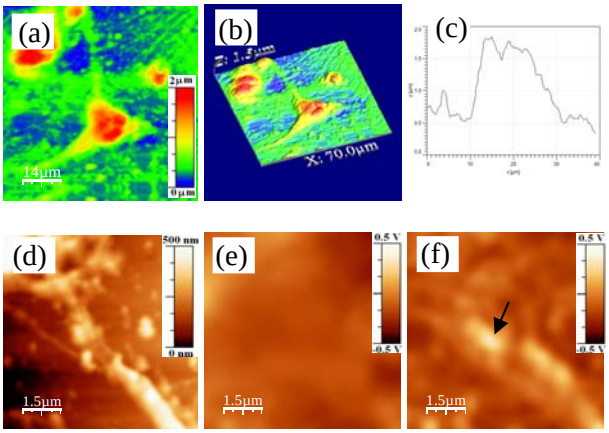


*Fig. 1: (a) Topography and (b) three dimensional image of the topography of a neuron. In (c) height profile. (d) topography, (e) before and (f) after poling (+ 30 V, 10 s) PFM images of neuron. Arrow in (c) shows the point where the local poling was performed*

**DISCUSSION & CONCLUSIONS:** Here, we directly measure the electromechanical properties of dried rat embryonic neurons from the *Substantia nigra* by the PFM. Our preliminary results indicate that ferroelectric behaviour in those neurons is probably caused by the ordering, purity and dipole arrangement of molecules in the membrane and cytosol. This research contributes to understand the electrical properties of nerve cells that up to now, due to the imprecise knowledge of the dipole coupling in cellular systems, remain unknown. The biological function of the interfacial field associated with the dipole potential is one of many questions in the rapidly emerging view that the lipid environment contributes significantly to membrane functions and to the resting potential

**REFERENCES:**

[1]K. J. Böhm, N. E. Mavromatos, A. Michette, R. Stracke, E. Unger, (2005) **24**:319 - 330.[2]H. R.Leuchtag, Voltage-Sensitive Ion Channels: Biophysics of Molecular Excitability, Springer, 2007, p. 532.[3]Y. Yang, K. M. Mayer, N. S. Wickremasinghe, J. H. Hafner, (2008) 95 5193-5199.[4]A.Kholkin,I.Bdikin, D.Kiselev, V. Shvartsman, S. H. Kim, (2007) *Journal of Electroceramics* **19** 83-96.

# Application of Nano-$TiO_2$ Sol in Crop Diseases Control

H. Cui*, J. Jiang, P. Zhang, W. Gu, Q. Liu

*Institute of Environment and Sustainable Development in Agriculture, Chinese Academy of Agricultural Sciences, Beijing 100081, China*

**INTRODUCTION**: Nano-$TiO_2$ has shown to be potential for agricultural application because of its photocatalytic disinfection and photobiological effects [1,2]. Our group has conducted experimental researches on biological effects of nano-$TiO_2$ [3-5]. This paper reported the biological effects of $TiO_2$ sol on crop production.

**METHODS**: $TiO_2$ sol was prepared according to the way mentioned by Ichinose [2]. Photocatalytic bactericidal effects of $TiO_2$ were evaluated by inoculated with P. s. pv. lachrymans and X. vesicatoria. Cucumber was chosen as experimental crop. Cucumber leaves in treated blocks were sprayed with $TiO_2$ sol. Control experiments were conducted by spraying water. Photosynthetic rates of cucumber leaves were measured, and the contents of chlorophyll of leaves were analyzed.

**RESULTS:** The results of composition analysis and characteristics of $TiO_2$ sol were shown in Table 1.

*Table 1: Characteristics of $TiO_2$ sol*

| $TiO_2$(%) | pH | Crystal type | Particle size(nm) |
|---|---|---|---|
| 1.6 | 7.8 | Anatase | 52.9 |

The photocatalytic bactericidal effects of $TiO_2$ were shown in Table 2. The relative bactericidal rate of nano-$TiO_2$ sol to *P. s. pv. lachrymans* and *X. vesicatoria* were 99.9% and 100%, respectively.

*Table2: Bactericidal rate of $TiO_2$ sol*

| Pathogens | Treatments | Survival (CFU) | Bactericidal rate(%) |
|---|---|---|---|
| *P. s. pv. lachrymans* | Control | 1944±45.6A | - |
| | $TiO_2$-treated | 1.6±0.5B | 99.9 |
| *X. vesicatoria* | Control | 1393.7±37A | - |
| | $TiO_2$-treated | 0B | 100 |

The effects of $TiO_2$ sol on cucumber diseases, *P. s. pv. lachrymans* and *P. cubensis* , were investigated and the results were shown in Table3 and Fig.1.

*Table 3: Effects of $TiO_2$ sol on preventing from cucumber diseases*

| Plant diseases | Treatment | Disease incidences | Disease indexes | Control efficiency |
|---|---|---|---|---|
| *P. s. pv. lachrymans* | Control | 68.3 a | 14.5 a | |
| | $TiO_2$-treated | 42.7 b | 6.3 b | 68.6% |
| *P. cubensis* | Control | 76.2a | 39.2 a | |
| | $TiO_2$-treated | 26.8b | 7.8 b | 90.6% |


*Fig.1: Field test of $TiO_2$ sol for the control of Pseudoperonospora cubensis*

**DISCUSSION & CONCLUSIONS**: This study confirmed that $TiO_2$ sol owns following biological effects: (1) forming a successive, adhesive and transparent film on the surface of leaves, which causes photocatalytic and photobiological effects. (2) possessing powerfully bactericidal effects to plant pathogens. (3) blocking and inhibiting bacterial and fungal diseases of crops .

**REFERENCES:** [1] T. Matsunaga, R. Tomoda, T. Nakajima, et al (1985) *Fens Microbiol Lett* **29**: 211-14. [2] H. Ichinose, A. Kawahara, and H. Katsuki (1996) *J Ceram Soc JPN* **104**: 914-17. [3] L.L. Li, H.X. Cui, and P. Zhang (2008) *Trans CSAE* **24**: 223-26. [4] P. Zhang, H.X. Cui, L.L. Li (2008) *J Inorg Mater* **23**: 55-60. [5] P. Zhang, H.X. Cui, N. Song, et al (2006) *Trans CSAE* **22**: 13-16.

**ACKNOWLEDGEMENT**: This work was supported by national 863 program (Grant No. 2006AA10A203, and Grant No. 2007AA021808).

European Cells and Materials Vol. 20. Suppl. 3, 2010 (page 294) ISSN 1473-2262

# Transfection of Pig Somatic Cells using Magnetic nanoparticle as Gene Carrier

W.Gu[1], H.Cui[1], J Cui[1], Q Liu[1], Y Lu[1], H Ren[2], K Li[2]

[1]*Institute of Environment and Sustainable Development in Agriculture* [2]*Institute of Animal Sciences Academy of Agricultural Sciences, Beijing, P.R. China*

**INTRODUCTION:** Transgenic animals with a stable incorporation of foreign DNA in the germ line are of great value for both research and commercial purposes [1]. Effective gene delivery into mammalian somatic cells is an essential step in reproductive cloning using somatic cell nuclear transfer technique. One of the fundamental limitations to non-viral gene delivery is the low vector concentration next to the cell surface due to the diffusion barrier of vector accumulation. However, this barrier could be overcome by magnetic nanoparticle aided gene delivery which is termed as magnetofection. To investigate the potential of magnetofection in transgenic animal production, magnetofection was employed to transfer reporter gene into somatic cells and the transfection efficiency was examined in this study. Specifically, green fluorescent protein (GFP) or red fluorescent protein (RFP) was used as a marker gene, and porcine kidney epithelial cells (PK15 cells) were used as donor somatic cells. Moreover, the feasibility of magnetofection of PK15 cells with multiple genes was investigated.

**METHODS:** Transfection of PK 15 cells with EGFP plasmid was performed using PolyMAG magnetic nanoparticles according to manufacture's protocol (Chemicell, German). After 24h incubation, PK15 cells were qualitatively assayed for GFP expression through fluorescence activated cell sorting (BD Biosciences, Canada). The possibility of simultaneous transfection of multiple genes into PK15 cells by magnetofection was tested next by co-transfecting pEGFP and DsRed2 plasmids into PK 15 cells at 1:1 weight ratio. Fluorescent imaging of GFP and RFP expression in PK15 cells was performed with an inverted confocal laser scanning microscope (LSM510-META, Zeiss, German)

**RESULTS:** Strong expression of the GFP was found in roughly 25% of PK15 cells at 24h post magnetofection (Fig. 1A). In addition to GFP, a second plasmid, DsRed2 was co-transfected with PK15 cells and expression of RFP in PK15 cells was observed as well (Fig. 1B). Moreover, co-expression of GFP and RFP in PK 15 cells (appeared as yellow in Fig. 1C) was well demonstrated. However, RFP expression could only be detected in a subpopulation of GFP expressing cells due to a weaker expression.

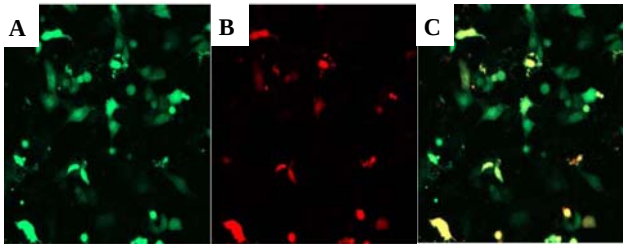


*Fig. 1: Fluorescence images of expression of (A) GFP and (B ) RFP in PK15 cells 24h after co-transfection of pEGFP and DsRed2 plasmids by magnetofection.(C) the overlap of A and B.*

**DISCUSSION & CONCLUSIONS:** PolyMag is fabricated by surface modification of $Fe_3O_4$ nanoparticles with 25 kDa branched polyethylenimine (PEI) [2]. The positively charged PEI polymers are capable of binding to negatively charged DNA plasmid and enable the DNA/polyMAG complex to respond to an external magnetic force which speeds up the sedimentation of gene to the cell surface and shortens the time span of gene delivery within minutes. The rapid accumulation of complex at cell surface significantly improves the dose–response profile. Consequently, a minimal DNA dose is sufficient to achieve high transfection levels [3]. The findings of this study revealed that mangetofection led to a reproducible and efficient transfection of PK15 cells. Furthermore, simultaneous expression of GFP and RFP in PK15 cells was achieved by magnetofection. Such efficient transfection and simultaneous expression of multiple genes in somatic cells thereby validate the potential of magnetofection as a non-viral transfection technique for somatic cell nuclear transfer.

**REFERENCES:** [1] J.M. Robl, Z. Wang, P. Kasinathan, Y. Kuroiwa (2007) *Theriogenology* **67**:127-33. [2] F. Scherer, M. Anton, U. Schillinger, et al (2002) *Gene Ther.* **9**:102-09. [3] O. Mykhaylyk, Y.S. Antequera, D. Vlaskou, et al (2007) *Nat. Protoc.* **2**:2391-11.

**ACKNOWLEDGEMENTS:** We thank the National Transgenic Major Program (No.2009ZX08010-006B) for the financial support of this work.

European Cells and Materials Vol. 20. Suppl. 3, 2010 (page 295) ISSN 1473-2262

# Large Scale Separation of Metallic and Semiconducting Single-Walled Carbon Nanotubes using Magnetic Nanoparticles; Application to Carbon Nanotubes based Biosensor

Hyung Joon Kim[1], Eun-Kyung Lim[2], Seungjoo Haam[2], Kyung-Hwa Yoo[1,3,*]

*[1] Graduate Program for Nanomedical Science, [2] Department of Chemical and Biomolecular Engineering, and [3] Department of Physics, Yonsei University, Seoul, South Korea.*

**INTRODUCTION:** Recently, carbon nanotube (CNT)-based biosensors with a field effect transistor (FET) structure have attracted considerable attention because of their merits, such as their label-free detection, real-time monitoring, ultra-high sensitivity, and simplicity of apparatus. However, since SWNTs are always grown as the bundles of metallic and semiconducting tubes, it is extremely important to separate metallic and semiconducting SWNTs in high yields for real applications. To overcome this problem, we have developed the separation method using magnetic nanoparticles (MNPs) functionalized with polycationic tri-aminated polysorbate 80 (TP80) [1]. Using separated SWNTs, we fabricated CNT network biosensors and found that most devices exhibited a p-type semiconducting behavior.

**METHODS:** To obtain a well-dispersed SWNT solution, acid-treated SWNTs were added to 0.01 M SDS dissolved in DI water and sonicated at room temperature. The dispersed SWNT solution was centrifuged to remove nondispersible SWNT and the resulting supernatant solution was carefully decanted. Subseqeuntly, MNPs-T80 suspended in deionized (DI) water was added to the dispersed SWNT solution (1:10, v/v) and then sonicated at room temperature. To collect SWNTs functionalized with MNPs-T80, a permanent magnet was placed at the bottom of vial containing the mixture of SWNT solution and MNPs-T80 solution. After four day, the upper part (SWNTs-up) was carefully decanted with the magnet placed at the bottom of vial. Then, to detect of DNA hybridization, separated semiconducting SWNTs based on field effect transistor was fabricated. The SWNTs surface was modified with a linker (1-Pyrenebutyric acid N-hydroxysuccinimide ester) [2]. After introducing the linker, probe DNA solutions were incubated. The electrical properties of the SWNTs-FET devices during the introducing of the target DNA were measured by a semiconductor characterization system.

**RESULTS:** To investigate electrical transport properties of separated SWNTs, we fabricated field effect transistor (FET) devices using pristine SWNTs, SWNTs-bm, and SWNTs-up on Si substrates with thermally grown 300 nm-thick $SiO_2$

layer. The I-$V_G$ of SWNTs-bm device exhibited a p-type semiconducting behavior, while the current of SWNTs-up device was not barely modulated by applying $V_G$, where the highly doped Si substrate was used as a bottom gate (Fig. 1). The real time measurement of DNA hybridization can be conducted using the semiconducting network-SWNTs FET (Fig. 2).

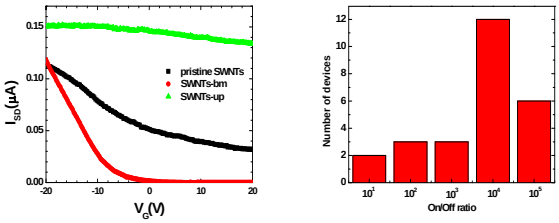


*Fig. 1: Drain current vs gate voltage for the pristine, bottom and upper SWNTs devices measured at a drain voltage of 1 V (left). Histogram of distribution of $I_{on}/I_{off}$ ratios (right).*

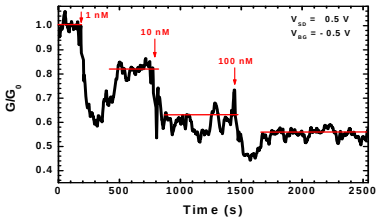


*Fig. 2: Real time monitoring of various concentration of target DNA at $V_{SD}$ = 0.5 V and $V_{BG}$ = - 0.5 V during DNA hybridization in PBS.*

**DISCUSSION & CONCLUSIONS:** We have demonstrated SWNT separation using MNPs-TP80. We also measured the conductance change after DNA hybridization using semiconducting network-SWNTs FET.

**REFERENCES:** [1] E.-K. Lim, J. Yang, J.-S. Suh, Y.-M. Huh and S. Haam (2009) *J.Mater.Chem.* **19**:8958. [2] R. J. Chen, Y. Zhang, D. Wang, H. Dai (2001) *J. Am. Chem. Soc*. **123**: 3838.

**ACKNOWLEDGEMENTS:** This work was supported by NRF through National Core Research Center for Nanomedical Technology.
(R15-2004-024-00000-0)

# Monte Carlo Simulation of Gold Nanoparticle-Enhanced Radiation Therapy

C.Park[1], S.Asadi[2], JK.Kim[1]

*[1] Kookmin University, Seoul Korea. [2] K.N. Toosi University of Technology, Tehran Iran.*

**INTRODUCTION:** Radiation therapy is one of the important treatment methods for cancer patients along with surgery and chemotherapy. To improve the therapeutic ratio of radiation therapy, many kinds of radiosensitizer are under study. Most researches about cancer nanotechnology use nanoparticles as diagnostic probes or drug-delivery vehicles because they can penetrate deep into tumours. There is little report about clinical application of synthetic nanoparticles combined with radiation therapy. A limited number of computational studies demonstrated that the brachytherapy with gold nanoparticles enhanced selectivity during treatment [1-3]. In this study, we simulated dose enhancement effect of the gold nanoparticles using MCNP-4C code for both high dose rate (HDR) source ($^{192}$Ir) and low dose rate (LDR) source ($^{125}$I) in brachytherapy. We also compared the difference between water and tissue phantoms.

**METHODS:** The composition of the tissue and tumour phantom was same with the 4-component tissue defined by the International Commission on Radiation Units and Measurements (ICRU 1989). When we added gold nanoparticles to the tumour phantom, we recalculated the composition considering the weight of gold nanoparticles. We used two commonly used brachytherapy sources, $^{192}$Ir and $^{125}$I. Fig. 1 shows the schematic diagram of MCNP model geometry for dose calculation. Elements included in the model were the source, tumour phantom, tissue phantom and voxel for calculating the dose.

**RESULTS:** We computed the dose enhancement factor (DEF) in the tumours having gold nano-particles of 0, 7, 18 and 30 mg using MCNP-4C code. Fig. 2 shows the calculated DEFs for HDR source varying with distance from tumour. DEFs in tumour with gold nanoparticles are higher than 1, and enhanced with increasing amount of gold nanoparticles. In contrast, DEFs in tissue have nearly constant value of 1, indicating that the gold nanoparticles enhance the selectivity of brachytherapy.

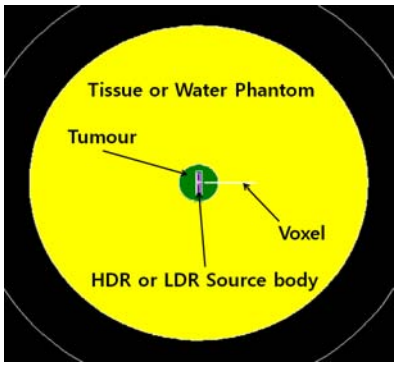


*Fig. 1: MCNP model geometry for dose calculation.*

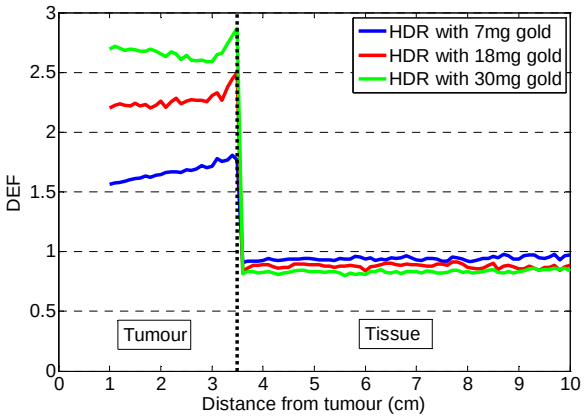


*Fig. 2: Calculated dose enhancement factor (DEF) for HDR source $^{192}$Ir vs. distance from tumour.*

**DISCUSSION & CONCLUSIONS:** Simulations with MCNP-4C code were done to evaluate the dose enhancement effect of the gold nanoparticles for both HDR and LDR sources in brachytherapy. Distinct difference in dose was found between water phantom and tissue phantom in HDR source. Gold nanoparticles enhanced the selectivity of brachytherapy during radiation treatment. We are involved in an interdisciplinary research group developing functional nanoparticles to enhance the radiation effect and investigating their radio-sensitizing effect in mouse tumour models. Uptake and distribution of gold nanoparticles in tumours are under study to develop optimized gold nano-particles that can maximize radiosensitizing effect. In addition, proper administration of gold nano-particles and radiation energy will be investigated to form the foundation of future clinical study.

**REFERENCES:** [1] S.H. Cho (2005) *Phys Med Biol*, **50**:N163-N173. [2] S.H. Cho, B.L. Jones, and S. Krishnan (2009) *Phys Med Biol* **54**:4889-4905. [3] A. Piermattei, A. Fidanzio, L. Azario, et al (2002) *Phys Med Biol* **47**:4205-4221.

**ACKNOWLEDGEMENTS:** This work was supported by the KOSEF grant funded by the Korea government (MEST). (R01-2008-000-20581-0).

European Cells and Materials Vol. 20. Suppl. 3, 2010 (page 297) ISSN 1473-2262

# Local Delivery of Drug and Heat using Multifunctional Nanoparticles and Their Synergistic Anticancer Activities

Sun-Mi Lee[1], Huiyul Park[2], Kyung-Hwa Yoo[1,2]

*[1] National Core Research Center forNanomedical Technology, Yonsei University, Seoul 120-749, Korea. [2] Department of Physics, Yonsei University, Seoul 120-749, Korea.*

**INTRODUCTION:** Various near-infrared (NIR) resonant nanomaterials such as gold (Au) nanoshell particles, Au nanocages, Au nanorods, and single-walled carbon nanotubes have been widely studied because they strongly absorb NIR light and produce localized cytotoxic heat upon NIR irradiation [1]. However, if the photothermal treatment is combined with chemotherapy, a therapeutic efficacy is expected to be significantly improved since the cytotoxicity of some chemotherapeutic agents is enhanced at elevated temperatures. Thus, we have developed doxorubicin (DOX)-loaded poly(ethylene glycol)-poly(lactic-*co*-glycolic acid)-Au half-shell nanoparticles (DOX-loaded PEG-PLGA-Au H-S NPs) to facilitate the combined treatments.

**METHODS:** Au was deposited onto a DOX-loaded PEG-PLGA NPs monolayer prepared [1], leading to a half-shell structure (Fig. 1), and the Au surface was functionalized with thiol-terminated methoxy-PEG. We prepared tumor-bearing mice by implanting A431 human epidermoid carcinoma cells into the Balb/C nude mouse and then investigated the therapeutic efficacy of DOX-loaded PEG-PLGA-Au H-S NPs. We also measured time-lapse *in vivo* NIR images of NPs and fluorescence images of release of DOX from the NPs.

**RESULTS:** The large amounts of intratumorally injected NPs were found to be localized in the tumor site and to remain in the tumor region over 72 h (Fig. 1). When the tumor site was irradiated by NIR light for 10 min, red fluorescence was emitted from the tumor site in contrast only autofluorescence was observed before NIR irradiation (Fig. 1). The mice treated only with DOX (10 mgkg$^{-1}$) or DOX-loaded PEG-PLGA NPs (0.35 mg·kg$^{-1}$ for DOX) exhibited tumor volume increases of 160 or 130% over 28 days, respectively. On the other hand, for the mice treated with PEG-PLGA-Au NPs (200 μg) and exposed to 2.56 Wcm$^{-2}$ NIR light for 10 min, the tumor volume was reduced by NIR irradiation and further decreased by about 70% until 14 days. After 14 days, however, the tumor began to grow again, implying that incomplete destruction of tumor cells by the photothermal treatment can induce a recurrence of the tumor. Finally, we

injected DOX-loaded PEG-PLGA-Au H-S NPs (0.25 mg·kg$^{-1}$ for DOX) intravenously or intratumorally, and then irradiated the tumor region with NIR light (2.56 Wcm$^{-2}$, 10 min) at 24 h post-injection. The tumor volume was more rapidly reduced and completely destroyed at 7 days and no recurrences of the tumors were found (Fig 1). These results demonstrated that the combined DOX and photothermal treatments were more cytotoxic than chemotherapy or photothermal treatment alone.

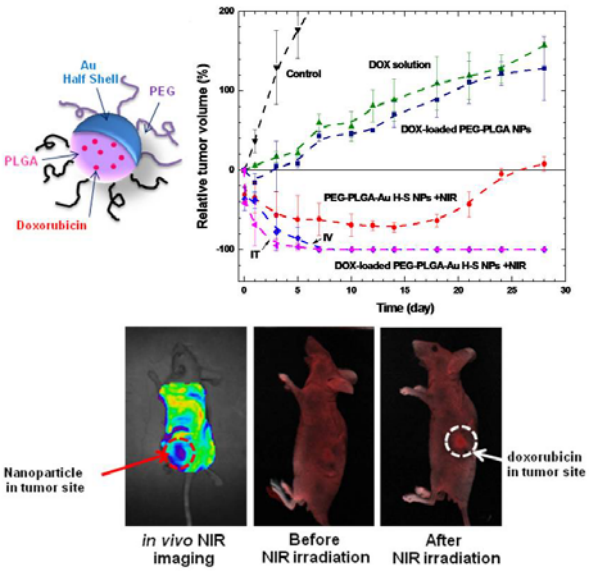


*Fig. 1: The structure, multifunctional properties and in vivo imaging of DOX-loaded PEG-PLGA Au H-S NPs.*

**DISCUSSION & CONCLUSIONS:** DOX-loaded PEG-PLGA-Au half-shell nanoparticles provide multifunctions, such as photothermal treatment, photothermally controlled drug delilvery, and *in vivo* optical imaging. In addition, the combined doxorubicin and photothermal treatments using these multifunctional nanoparticles show synergistic therapeutic effects.

**REFERENCES:** [1] H. Park, J. Yang, J. Lee, et al (2009) *ACS Nano*, **3**:2919-2926.

**ACKNOWLEDGEMENTS:** This work has been financially supported by NRF through National Core Research Center for Nanomedical Technology (Grant No. R15-2004-024-00000-0).

European Cells and Materials Vol. 20. Suppl. 3, 2010 (page 298) ISSN 1473-2262

# Ultra stable block copolymer assemblies for nuclear imaging and therapy

C.M.A. Streng[1], D. S. Escalante[1], A.G. Denkova[1], E. Mendes[2]

*[1] Radiation, Radionuclides & Reactors, Delft Univ. of Technology, Mekelweg 15, 2629 JB Delft, The Netherlands. [2] NanoStructured Matarials, Dept Chem Eng., Delft Univ. of Technology, Julianalaan 136, 2628 BL Delft, The Netherlands.*

**INTRODUCTION:** In nuclear medicine, radiopharmaceuticals for both treatment and diagnosis of several diseases (e.g. cancer, PET, SPECT, etc.) have to be transported to and retained at the diseased site without causing damage to healthy tissue. Contrary to other drug controlled delivery strategies, safe deposition of the radioactive substance at the tumor site requires a stable carrier. This is needed to ensure no dissociation or leakage of the radionuclide during transportation. Block copolymer micelles are expected to be ideal nano-carriers for this purpose, provided that they are stable enough via, for instance, cross-linking of the hydrophobic micellar core.

**METHODS:** Spherical micelles assembled of Poly(ethylene oxide)-Poly(propylene oxide)-Poly(ethylene oxide) tri-block copolymers were stabilized using a hydrophobic cross-linking agent that accumulates in the core of the micelles (pentaerythritol tetraacrylate, PETA) [1]. Aqueous solutions containing 5wt% of the tri-block copolymer Pluronic P123 [$(EO)_{20}(PO)_{70}(EO)_{20}$] were prepared. PETA solutions dissolved in ethanol with different concentrations were prepared. The PETA solutions were added to the P123 micelless in the ratio 1:100. The total solutions was then degassed for 1 hour with $N_2$, and cross-linked [CL] using γ-radiation from a $^{60}$Co-source (2.5 kGy/h).

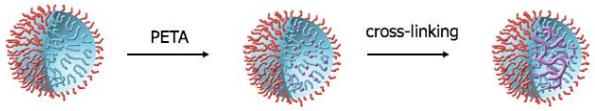


*Fig. 1. Schematics of the cross-linking method.*

The micelle sizes in solution were investigated by dynamic light scattering (DLS), a technique that allows one to measure the autocorrelation function $g^{(2)}(t)$ of the scattered light intensity fluctuations detected in a small volume of the solution up to the microsecond time range. The autocorrelation function is used for the determination of the diffusion coefficient of the measured species that is related tot the hydrodynamic size of the micelles. Cross-linking efficiency was checked by diluting the cross-linked samples in a good solvent for both, hydrophilic and the hydrophobic blocks (ethanol) in which no micelles are formed.

**RESULTS & DISCUSSION:** The correlation function shows that net intensity and correlation time increases with radiation time (i.e. radiation dose) (Fig. 2). This graph has been obtained after dilution of the samples in ethanol. The data suggests that 15 min of gamma radiation is sufficient to induce cross-linking of the micelles. Micelles that have not been cross-linked (NC) have poor correlation function. Additionally the cross-linked micelles exhibit very good stability at higher temperatures and when exposed to ultra sound. The resulting hydrodynamic radii are displayed in Fig. 3.

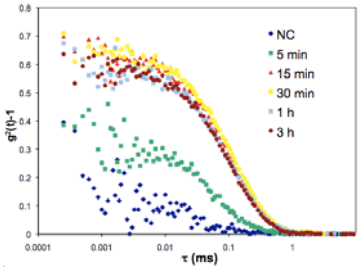


*Fig. 2: Correlation function $g^{(2)}(t)$ as function of γ-irradiation time.*

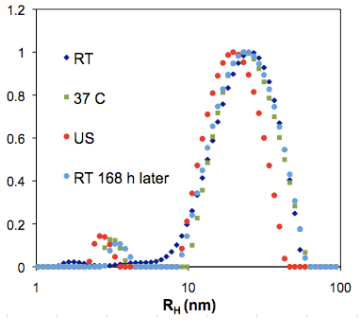


*Fig. 3: Distribution of micelle sizes after cross-linking and dilution in ethanol, at room temperature (RT), at 37ºC, after one hour in ultrasound bath (US) and after ageing at room temperature for 168 hours.*

**CONCLUSIONS:** Pluronic P123 micelles can be permanently cross-linked with γ-radiation when PETA is used as a cross-linking agent.

**REFERENCES:** [1]F.Li, T.Ketelaar, A.T.M. Marcelis, F.A.M. Leermakers, M.A.Cohen Stuart, and E.J.R. Sudhlter (2007) *Macromolecules*, **40** (2): 329-333

# Local Infused A-MCP-1 Nanoparticles to Inhibit Rabbit Intimal Hyperplasia

Jing Yang[1#] Yong Zeng[2#] Wenling Zhu[2] Cunxia Song[1*]

*1. Institute of Biomedical Engineering, Chinese Academy of Medical Sciences, Tianjing, 300192, China*

*2. Department of Cardiology, Peking Union Medical College Hospital, Beijing 100730, China*

#These authors contributed equally to this work; *Corresponding author

**INTRODUCTION:** Percutaneous transluminal coronary angioplasty (PTCA) is one of the most effective treatments for atherosclerosis diseases, but long-term curative effect is greatly affected by restenosis. Antisense monocyte chemotactic protein-1 (A-MCP-1) play an important role in restenosis process. In our study, polylactic- polyglycolic acid (PLGA) co-polymer was used as carrier matrix, to study the effects of local infusion of A-MCP-1 NPs.

**METHODS:** PLGA nanoparticles loaded with A-MCP-1 plasmid were prepared by an emulsification-solvent evaporation technique. Male New Zealand White rabbits (3.5 to 4.0 Kg) were generally anesthetized with sodium pentobarbital (50 mg/kg IV). 15 rabbits were performed the carotid artery injury and divided into 3 groups (5/each group), local infused different solution, including Antisense MCP-1- nanoparticles group, empty nanoparticles group, control group. The animals were killed 14 days after treatment for further analysis. Part of samples of the treated artery segment was reserved for RNA and DNA analysis, while the rests were used for histology analysis. The anesthetized rabbit was perfused with PBS (1 minute) and saline to clear intravascular system. And the aorta total DNA was isolated and integrity of antisense MCP-1 gene was determined by polymerase chain reaction (PCR). PCR reactions were performed using the primers 5′ -CAGGTGGGGTCTTTCATTCC-3′and 5′ -CGTGTGTTCTTGGGTTGTGG-3′.

Amplification was performed in a Rapid Cycle for 30 cycles with denaturation at 94C for 60 s, annealing at 62C for 60 s, and extension at 72C for 90 s. PCR products were analyzed by electrophoresis on a 1% agarose gel. Total RNA was isolated from arteries homogenized in Trizol reagent (Life Technologies). Northern analyses were used to assess the MCP-1 and antisense MCP-1 mRNA expression. All results are expressed as mean±SD and compared by ANOVA and 2-tailed unpaired Student t test, with a significance level of $P<0.05$.

**RESULTS:** Shown as Figure 1, there is a specific segment in gene NPs group, while there are not in control group and Empty Nps group, result suggesting that nanoparticle can make integrity of antisense MCP-1 into vessel wall.

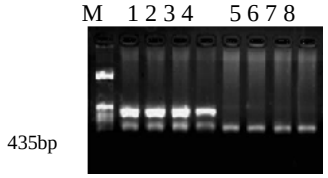


Fig 1. A-MCP-1 DNA integrity in artery tissues. From left to right,1-4：Gene NPs group；5-6：Control group; 7-8: Empty Nps group

**DISCUSSION & CONCLUSIONS:**In conclusion, these results well demonstrated that gene NPs directly delivered into artery lumen through a conventional defusing catheter were uptake by vascular wall at the targeted site and was capable of inducing local transfection and long-term site-specific gene expression. Antisense MCP-1 expression can inhibit endogenous MCP-1 expression, influence growth factors expression and also inhibit intima hyperplasia after angioplasty.

**ACKNOWLEDGEMENTS:** These studies were supported in part by projects from (Tianjin Natural Science Fund 08JCYBJC11200 ) and the NSFC of China (30800225,50830106).

**REFERENCES:**[1] Labhasetwar V, Song C, Humphrey W, et al(1998). Arterial uptake of biodegradable nanoparticles: Effect of surface modification. *J Pharm Sci* **87**(10), 1229-34.